UNIVERSITY OF CALIFORNIA

Santa Barbara

Development of New Methods Towards Actinide-Carbene Fragments

A dissertation submitted in partial satisfaction of the

requirements for the degree Doctor of Philosophy

in Chemistry

by

Greggory T. Kent

Committee in charge:

Professor Trevor W. Hayton, Chair

Professor Peter C. Ford

Professor Gabriel Ménard

Professor Lior Sepunaru

June 2022

The dissertation of Greggory T. Kent is approved.

Professor Peter C. Ford

Professor Gabriel Ménard

Professor Lior Sepunaru

Professor Trevor W. Hayton, Committee Chair

June 2022

Development of New Methods Towards Actinide-Carbene Fragments

by

Greggory T. Kent

Acknowledgements

I would like to begin by thanking the person who inspired my passion for the sciences, Dr. Karen Nieto-Chaney, without her I likely would have never ventured down this path. Secondly, I would like to thank my undergraduate mentor Dr. Weiming Wu for inspiring me to attend graduate school and helping me learn how to think like a scientist. To the Wu group members, especially Daniel Blackburn and Kristen McGraw, your help and presence in my undergraduate career was instrumental in crafting the soft skills that I still use today.

I came into UCSB not having even taken an inorganic chemistry course, however with the unparalleled support and patience of Prof. Trevor Hayton I was able to find success. Trevor, I cannot begin to thank you for your help throughout these years and for remaining patient while I slowly grew into an independent scientist. I hope to be as supportive a mentor to future chemists as you were to me. My committee, Prof. Peter Ford, Prof. Gab Ménard, and Prof. Lior Sepunaru were instrumental throughout my graduate career, especially during the beginning when I had no idea what I was doing, thank you. I would also like to thank all my various collaborators from throughout the years, Prof Skye Fortier and Dr. Jesse Murillo for collecting a number of crystal structures for me, Prof Jochen Autschbach and Dr. Xiaojuan Yu for all their quick computational work. A special thank you to Dr. Guang Wu who was critical to me successfully learning X-ray crystallography. I would also like to thank Prof. Ram Seshadri and Prof. Tony Cheetham for allowing me to learn about inorganic materials science from them.

To the Hayton lab members, both former and current, you all made this experience truly enjoyable and memorable. Dr. Mikiyas Assefa, you were the person who taught me how to use

a glovebox and so many other things, thank you. Dr. Selena Staun, you kept lab fun, lighthearted and listened to me complain about being tired all the time, thank you. Current Haytonians Miguel “Fingerguns” Baeza Cinco, Phoebe Hertler, Thien Nguyen, and Osvaldo Ordonez, you all made these last few years manageable with your company and insight, it was an honor and I know you will all find success.

I would like to thank my parents who have never stopped loving and supporting me. I would have never found all my success and happiness without my parents, nor would I be the person I am today, I owe them everything. Last and most importantly, to my fiancé Katie, you have been with me through the highs and lows of this entire process and constantly pushed me to be the best chemist I possibly could, I am so happy you are in my life and I am forever grateful.

Vita of Greggory T. Kent

Education

University of California Santa Barbara, Santa Barbara, CA **2017-Present**

Doctor of Philosophy (Expected)
Advisor: Prof. Trevor W. Hayton

San Francisco State University – San Francisco, CA **2012-2016**

Bachelor of Science, Biochemistry

Professional Employment

University of California Santa Barbara **2017-2020**

Teaching Assistant, Department of Chemistry

San Francisco State University **2016**

Teaching Assistant, Department of Chemistry

Publications

Kent, G. T.; Yu, X.; Wu, G.; Autschbach, J.; Hayton, T. W., Ring-opening of a Thorium Cyclopropenyl Complex Generates a Transient Thorium-bound Carbene. *Chem. Commun.* **2022** *Accepted*.

Kent, G. T.; Yu, X.; Wu, G.; Autschbach, J.; Hayton, T. W., Synthesis and Electronic Structure Analysis of the Actinide Allenylidenes, $[\{(NR_2)_3\}An(CCCPh_2)]^-$ (An = U, Th; R = $SiMe_3$). *Chem. Sci.* **2021** 12, 14383-14388. DOI: 10.1039/D1SC04666G

Kent, G. T.; Yu, X.; Wu, G.; Autschbach, J.; Hayton, T. W., Synthesis of Parent Acetylide and Dicarbide Complexes of Thorium and Uranium and an Examination of Their Electronic Structures. *Inorg. Chem.* **2021** 60, 15413–15420. DOI: 10.1021/acs.inorgchem.1c02064

Staun, S. L.; **Kent, G. T.**; Alejandra Gomez-Torres, Wu, G.; Fortier, S.; Hayton, T. W., Reductive Coupling of Xylyl Isocyanide Mediated by Low-Valent Uranium *Organometallics* **2021** 40, 2934-2938 DOI: 10.1021/acs.organomet.1c00365

Kent, G. T.; Cook, A.W.; Damon, P. L.; Lewis, R. A.; Wu, G.; Hayton, T. W., Synthesis and Characterization of Two "Tied-back" Lithium Ketimides and Isolation of a Ketimide-bridged $[Cr_2]^{6+}$ Dimer with Strong Antiferromagnetic Coupling. *Inorg. Chem.* **2021** 60, 4996-5004. DOI: 10.1021/acs.inorgchem.1c00052

Kent, G. T.; Murillo, J.; Wu, G.; Fortier, S.; Hayton, T. W., Coordination of Uranyl to the Redox-Active Calix[4]pyrrole Ligand. *Inorg. Chem*. **2020** 59, 8629-8634. DOI: 10.1021/acs.inorgchem.0c01224

Sergentu, D. C.; **Kent, G. T.**; Staun, S. L.; Yu, X.; Cho, H.; Autschbach, J.; Hayton, T. W., Probing the Electronic Structure of a Thorium Nitride Complex by Solid-State ^{15}N NMR Spectroscopy. *Inorg. Chem.* **2020** 59, 10138-10145. DOI: 10.1021/acs.inorgchem.0c01263

Kent, G. T.; Wu, G.; Hayton, T. W., Synthesis and Crystallographic Characterization of the Tetravalent Actinide-DOTA Complexes [$An^{IV}(\kappa^8$-DOTA)(DMSO)] (An = Th, U). *Inorg. Chem.* **2019** 58, 8253-8256. DOI: 10.1021/acs.inorgchem.9b00736

Tang, K. G.; **Kent, G. T.**; Erden, I.; Wu, W., cis-β-Bromostyrene derivatives from cinnamic acids via a tandem substitutive bromination-decarboxylation sequence. *Tetrahedron Lett.* **2017** 58, 3894–3896. DOI: 10.1016/j.tetlet.2017.08.069

Kent, G. T.*; McGraw, K. M.*; Gonzalez, J. R.; Erden, I.; Wu, W., Competitive, substrate-dependent reductive debromination/dehydrobromination of 1,2-dibromides with triethylamine. *Tetrahedron Lett.* **2017** 58, 1973-1975. *Authors contributed equally DOI: 10.1016/j.tetlet.2017.04.024

Blackburn, D. J.; **Kent, G. T.**; Wu, W., Regiospecific synthesis of 6-halouridine derivatives: An effective method for coupling sterically hindered pyrimidine bases to ribose. *Tetrahedron Lett.* **2017** 58, 1348-1350. DOI: 10.1016/j.tetlet.2017.02.063

Kent, G. T.; Blackburn, D. J.; Gonzalez, J. R.; Mayer, M. L.; Wu W., Convenient synthesis of phosphonohydrazines from arylamines. *Tetrahedron Lett.* **2016** 57, 2097-2099. DOI: 10.1016/j.tetlet.2016.03.111

Presentations

Kent, G. T.; Yu, X.; Pauly, C.; Wu, G.; Autschbach, J.; Hayton, T. W. "Synthesis and Characterization of Actinide Parent Acetylide Complexes" ACS Fall Meeting. Atlanta, GA, Oral Presentation, August **2021**

Kent, G. T.; Wu, G.; Hayton, T. W. "Coordination of Macrocyclic Ligands to the Actinides" Southern California Organometallics Meeting. USC, Oral Presentation, February **2019**.

Awards & Mentorship

- Department of Chemistry and Biochemistry Chair's Fellow. **2021**
- NSF Graduate Research Fellowship Program - *Honorable Mention*. **2019**
- Future Leaders in Advanced Material Mentor. University of California-Santa Barbara. **2019** & **2020**
- Eureka Fellowship Mentor. University of California-Santa Barbara. **2018**
- David and Lola Bjorkquist Scholarship for Undergraduate Chemistry and Biochemistry Majors. San Francisco State University, May **2016**.

Field of Study

Major Field: Synthetic Inorganic Chemistry
Studies in *f*-element Organometallic Chemistry and their Electronic Structures with Professor Trevor W. Hayton, University of California Santa Barbara

Abstract

Development of New Methods Towards Actinide-Carbene Fragments

by

Greggory T. Kent

The reaction of UCl_4 or $ThCl_4(DME)_2$ with 1,4,7,10-tetrazacyclodecane-1,4,7,10-tetraacetic acid (H_4DOTA), and 6 equiv of trimethylamine, in DMSO results in the formation of $[An^{IV}(\kappa^8\text{-}DOTA)(DMSO)]$ (An = U, Th), which can be isolated in moderate yields after work-up. Both Complexes are the first structurally characterized actinide DOTA complexes to feature the κ^8 binding mode for the DOTA ligand. In addition, we isolated a few crystals of $[U(\kappa^4\text{-}H_2DOTA)(DMSO)_4][Cl]_2$. Crystallographic characterization of this material reveals that the $[H_2DOTA]^{2-}$ ligand in $[U(\kappa^4\text{-}H_2DOTA)(DMSO)_4][Cl]_2$ is only coordinated to U^{4+} by its four carboxylate arms, generating an overall κ^4 binding mode. Similar complexes have been previously proposed as intermediates of H_4DOTA complexation pathway, but this intermediate had not been structurally characterized until now.

Reaction of $[Li(THF)]_4[L]$ (L = Me_8-calix[4]pyrrole]) with 0.5 equiv of $[U^{VI}O_2Cl_2(THF)_2]_2$ results in formation of the oxidized calix[4]pyrrole product, $[Li(THF)]_2[L^{\Delta}]$, concomitant with formation of reduced uranium oxide by-products. $[Li(THF)]_2[L^{\Delta}]$ can also be generated by reaction of $[Li(THF)]_4[L]$ with 1 equiv of I_2. I hypothesize that formation of $[Li(THF)]_2[L^{\Delta}]$ proceeds via formation of a highly oxidizing cis-uranyl intermediate, $[Li]_2[cis\text{-}U^{VI}O_2(calix[4]pyrrole)]$. To test this hypothesis, I explored the reaction of $[Li(THF)]_2[L^{\Delta}]$ with either 0.5 equiv of $[U^{VI}O_2Cl_2(THF)_2]_2$ or 1 equiv of $[U^{VI}O_2(OTf)_2(THF)_3]$, which affords the isostructural uranyl complexes, $[Li(THF)][U^{VI}O_2(L^{\Delta})Cl(THF)]$ and

[Li(THF)][$U^{VI}O_2(L^{\Delta})$(OTf)(THF)], respectively. In the solid state, [Li(THF)][$U^{VI}O_2(L^{\Delta})$Cl(THF)] and [Li(THF)][$U^{VI}O_2(L^{\Delta})$(OTf)(THF)] feature unprecedented uranyl-η^5-pyrrole interactions, making them rare examples of uranyl organometallic complexes. In addition, [Li(THF)][$U^{VI}O_2(L^{\Delta})$Cl(THF)] and [Li(THF)][$U^{VI}O_2(L^{\Delta})$(OTf)(THF)]exhibit some of the smallest O−U−O angles reported to date (162.0(7) and 162.7(7)°; 164.5(5)°, respectively). Importantly, the O−U−O bending observed in these complexes suggests that the oxidation of $[Li(THF)]_4[L]$ does indeed occur via an unobserved cis-uranyl intermediate.

The reaction of $[AnCl(NR_2)_3]$ (An = U or Th; R = $SiMe_3$) with NaCCH and tetramethylethylenediamine (TMEDA) results in the formation of $[An(C{\equiv}CH)(NR_2)_3]$ (An = U, Th), which can be isolated in good yields after work-up. Similarly, reaction of 3 equiv of NaCCH and TMEDA with $[AnCl(NR_2)_3]$ results in the formation of [Na(TMEDA)][$An(C{\equiv}CH)_2(NR_2)_3$] (An = U, Th), which can be isolated in fair yields after work-up. Reaction of $[U(C{\equiv}CH)(NR_2)_3]$ with 2 equiv of KC_8 and 1 equiv of 2.2.2-cryptand in THF results in formation of the U(III) acetylide complex, [K(2.2.2-cryptand)][$U(C{\equiv}CH)(NR_2)_3$]. Thermolysis of $[U(C{\equiv}CH)(NR_2)_3]$ or $[Th(C{\equiv}CH)(NR_2)_3]$ results in formation of the bimetallic dicarbide complexes, $[\{An(NR_2)_3\}_2(\mu,\eta^1{:}\eta^1\text{-}C_2)]$ (An = U, Th), whereas reaction of $[U(C{\equiv}CH)(NR_2)_3]$ with $[Th\{N(R)(SiMe_2)CH_2\}(NR_2)_2]$ results in formation of $[U(NR_2)_3(\mu,\eta^1{:}\eta^1\text{-}C_2)Th(NR_2)_3]$. The ^{13}C NMR chemical shifts of the α-acetylide carbons in $[Th(C{\equiv}CH)(NR_2)_3]$, [Na(TMEDA)][$Th(C{\equiv}CH)_2(NR_2)_3$], and $[\{Th(NR_2)_3\}_2(\mu,\eta^1{:}\eta^1\text{-}C_2)]$ exhibit a characteristic spin-orbit induced downfield shift, due to participation of the 5f orbitals in the Th-C bonds. Magnetism measurements demonstrate that

[{U(NR$_2$)$_3$}$_2$(μ,η^1:η^1-C$_2$)] displays weak ferromagnetic coupling between the U(IV) centers (J = 1.78 cm^{-1}).

The reaction of [AnCl(NR$_2$)$_3$] (An = U, Th, R = SiMe$_3$) with *in situ* generated lithium-3,3-diphenylcyclopropene results in the formation of [{(NR$_2$)$_3$}An(CH=C=CPh$_2$)] (An = U, Th) in good yields after work-up. Deprotonation of [{(NR$_2$)$_3$}U(CH=C=CPh$_2$)] or [{(NR$_2$)$_3$}Th(CH=C=CPh$_2$)] with LDA/2.2.2-cryptand results in formation of the anionic allenylidenes, [Li(2.2.2-cryptand)][{(NR$_2$)$_3$}An(CCCPh$_2$)] (An = U, Th). The calculated ^{13}C NMR chemical shifts of the C$_\alpha$, C$_\beta$, and C$_\gamma$ nuclei in [{(NR$_2$)$_3$}Th(CH=C=CPh$_2$)] and [Li(2.2.2-cryptand)][{(NR$_2$)$_3$}Th(CCCPh$_2$)] nicely reproduce the experimentally assigned order, and exhibit a characteristic spin-orbit induced downfield shift at C$_\alpha$ due to involvement of the 5f orbitals in Th–C bonds. Additionally, the bonding analyses for [Li(2.2.2-cryptand)][{(NR$_2$)$_3$}U(CCCPh$_2$)] and [Li(2.2.2-cryptand)][{(NR$_2$)$_3$}An(CCCPh$_2$)] show a delocalized multi-center character of the ligand π orbitals involving An. While a single-triple-single-bond resonance structure (e.g., An-C≡C-CPh$_2$) predominates, the An=C=C=CPh$_2$ resonance form contributes, as well, more so for uranium analog.

I also report the synthesis, characterization, and reactivity of the bis(diisopropylamino)cyclopropenylidene (BAC) adducts of [M(NR$_2$)$_3$] (M = Ce, U; R = SiMe$_3$), namely, [(NR$_2$)$_3$M(BAC)] (M = Ce, U). Photolysis of [(NR$_2$)$_3$Ce(BAC)] with a 365 nm LED source results in formation of the methylenecyclopropene species, [(^{i}Pr$_2$N)$_2$C$_3$C(N^{i}Pr$_2$)(CCN^{i}Pr$_2$)], via the formal dimerization and rearrangement of two BAC fragments. [(^{i}Pr$_2$N)$_2$C$_3$C(N^{i}Pr$_2$)(CCN^{i}Pr$_2$)] can also be generated under catalytic conditions by performing the photolysis of BAC in the presence of 10 mol% [Ce(NR$_2$)$_3$]. Whereas heating

[$(NR_2)_3U$(BAC)] results in the formation of [$(NR_2)_2U${N(R)($SiMe_2$)(2,3-(N^iPr_2)-C(H)C=CC(H))}], via the formal ring opening and insertion of the BAC ligand.

The reaction of [Cp_3ThCl] with *in situ* generated lithium-3,3-diphenylcyclopropene results in the formation of [Cp_3Th(3,3-diphenylcyclopropenyl)], in good yields. Thermolysis of [Cp_3Th(3,3-diphenylcyclopropenyl)] results in isomerization to the ring-opened product, [Cp_3Th(3-phenyl-1H-inden-1-yl)] via a hypothesized carbene intermediate. By comparison, reaction of [Cp_3UCl] with *in situ* generated lithium-3,3-diphenylcyclopropene results in the formation of [$Cp_2U(\eta^2$-triphenylethylene)] via a hypothesized U(VI)-carbyne intermediate. Furthermore, reaction of [Cp_3U(THF)] with 2 equiv 3,3-diphenylcyclopropene results in the formation of [Cp_3U(3,3-diphenylcyclopropyl)], via formal hydrogen atom abstraction. These transformations represent several new modes of reactivity of 3,3-diphenylcyclopropene with the actinides, improving our ability to use this reagent as a carbene source. A combined DFT and $^{13}C\{^1H\}$ NMR analysis of [Cp_3Th(3,3-diphenylcyclopropenyl)] shows a spin–orbit induced downfield shift at C_α due to participation of the 5f orbitals in the Th–C bond.

Table of Contents

List of Figures

List of Schemes

List of Tables

List of Abbreviations

°	degree
°C	degree Celsius
ε	extinction coefficient
Δ	difference
δ	chemical shift, ppm
η^n	hapticity of order n
κ^n	denticity of order n
μ	micro or denotes bridging atom
ν	stretching frequency, cm^{-1}
χ_M	Molar Magnetic Susceptibility
Å	angstrom, 10^{-10} m
acac	acetylacetonate
An	Actinide
av.	average
BAC	Bisdiisopropylaminocyclopropylidene
BDE	bond dissociation energy
bpdc	2,2'-bipyridine-6,6'-dicarboxylic acid
$(Bpin)_2$	Bis(pinacolato)diboron
br	broad
Bu	butyl
calcd.	calculated
$^{13}C\{^1H\}$	Carbon-13 proton decoupled
ca.	circa
CCD	charge-coupled-device
chp	6-chloro-2-hydroxypyridinate
COSY	Homonuclear Correlation Spectroscopy
cot	1,3,5,7-cyclooctatetraene
Cp'	1,2,4-^{t}Bu$_3$C$_5$H$_2$
Cp^*	η^5-C_5Me_5
Cp	η^5-C_5H_5
cm^{-1}	wavenumber
12-crown-4	1,4,7,10-tetraoxacyclododecane
18-crown-6	1,4,7,10,13,16-hexaoxacyclooctadecane
2,2,2-cryptand	4,7,13,16,21,24-hexaoxa-1,10-diazabicyclo[8.8.8]hexacosane
CSM	Continuous Shape Measure
CV	cyclic voltammetry
Cy	Cyclohexyl
cyclam	1,4,8,11-tetraazacyclotetradecane
d	doublet *or* day(s)
d_n	deuterated in *n* positions
DFT	Density Functional Theory
Dipp	2,6-diisopropylphenyl
DME	1,2-dimethoxyethane
DMF	Dimethylformamide

DMSO	Dimethylsulfoxide
DOTA	1,4,7,10-tetraazacyclododecane-N,N′,N″,N‴-tetraacetic acid
$E_{1/2}$	average wave potential, $(E_{p,a} + E_{p,c})/2$
$E_{p,a}$	anodic half-wave potential
$E_{p,c}$	cathodic half-wave potential
e^-	electron
eq	equation
emu	electromagnetic unit
EPR	Electron Paramagnetic Resonance
equiv	equivalent
Et	ethyl
Et_2O	diethyl ether
Fc	ferrocene
g	gram(s)
GOF	goodness of fit
^1H	Hydrogen-1
h	hour(s)
H_2(1,8-DMC),	1,8-dimethyl-1,4,8,11-tetraazacyclotetradecane
H_2NTClPP	5,10,15,20-tetrakis[(4-*tert*-butyl)phenyl]porphyri
H_2TBPP	5,10,15,20-tetrakis(4-chlorophenyl)porphyrin
$^HN_4$	2,11-diaza[3,3(2,6) pyridinophane
HOMO	Highest Occupied Molecular Orbital
Hz	Hertz
$i_{p,a}$	anodic half-wave current
$i_{p,c}$	cathodic half-wave current
^{i}Pr	isopropyl
IR	infrared
ITI	Inverse Trans Influence
J	NMR coupling constant
J	Joule
K	Kelvin
K_f	Formation Constant
L	liter *or* ligand
LDA	Lithium diisopropylamide
LED	Light Emitting Diode
^{7}Li{^{1}H}	Lithium-7 proton decoupled
Ln	lanthanide
M	Molar *or* Mega
m	meter *or* multiplet *or* medium
m	meta
Me	methyl
MeCN	Acetonitrile
$^{Me}N_4$	*N,N*-dimethyl-2,11-diaza[3,3(2,6) pyridinophane
min	minute(s)
mL	milliliter(s)
mmol	millimole(s)

MO	Molecular Orbital
mol	mole(s)
NBO	natural bond order
^{n}Bu	n-butyl
NHE	Normal Hydrogen Electrode
NIR	near infrared
NLMO	Natural Localized Molecular Orbital
NMR	nuclear magnetic resonance
Np	neopentoxide
o	ortho
OEP	octaethylporphyrin
omtaaH_2	dibenzooctamethyltetraazaannulene
ORTEP	Oak Ridge Thermal Ellipsoid Program
OTf	trifluoromethylsulfonate
p	para
Ph	phenyl
phen	phenanthroline
pip	piperidine
Pn*	Permethylpentalene
ppm	parts per million
py	pyridine
q	quartet
QTAIM	Quantum Theory of Atoms-in-Molecules
redox	reduction-oxidation
RT	room temperature
s	singlet *or* strong *or* second(s)
sh	shoulder
SOC	Spin orbit coupling
SQUID	Superconducting Quantum Interference Device
T	Tesla
t	triplet
TPB	Tributylphosphate
^{t}Bu	*tert*-butyl
THF	tetrahydrofuran
TIP	Temperature Independent Paramagnetism
TMEDA	*N,N,N',N'*-tetramethylethylenediamine
tmtaaH_2	dibenzotetramethyltetraaza[14]annulene
tol	toluene
trop	tropolonate
UV	ultraviolet
V	Volt
vis	visible
vs	very strong *or* versus
vw	very weak
w	weak
WBI	Wiberg Bond Index

WFT	Multi-configurational Wavefunction Theory
XAS	X-ray Absorption Spectroscopy
XPS	X-ray Photoelectron Spectroscopy

Just Keep Swimming

-Dory

Chapter 1. Investigation of f-Element Bonding for Enhanced Nuclear Waste Processing

1.1 Nuclear Energy and Closing the Nuclear Waste Cycle

As the effects of climate change grow and the production of fossil fuels dwindles there is an increasing demand for non-fossil fuel energy alternatives which can be quickly constructed.[1] Nuclear power has found renewed interest as a popular carbon-free energy alternative for many countries, due to both its scalability and energy production density.[2] The use of nuclear power differs from country to country, but it accounts for approximately 10% of global energy production and 28% of non-fossil fuel-based energy production. [2] For instance, nuclear power accounts for approximately 20% of all the electricity generated in the United States, whereas in France this number is 71%.[3] Despite the evidence of nuclear power's appeal as a non-fossil fuel alternative, opponents of its use cite concerns over safety issues related to operating power plants, and the generation of radioactive waste.

One of the greatest challenges associated with the development of new and existing nuclear power plants is the handling of spent nuclear fuel.[4] Over time, the conversion of fissile fuel into fission products, such as the lanthanides, which "quench" neutrons required for nuclear fission, result in reactor fuel in with a decreased efficiency.[5, 6] Consequently, the now spent fuel must be replaced periodically. The spent fuel is comprised of mostly uranium (95.6%), stable fission products (2.9%), such as lanthanides and transition metals, and minor actinides that are formed from neutron capture by uranium and plutonium.[5] The minor actinides(e.g., Np, Am, Cm, Bk, Cf, etc.), which account for only <0.1% of the spent fuel, contribute to much of the nuclear waste's long-term radiotoxicity.[7] Thus efficient separation of the minor actinides from the remainder of spent fuel would greatly reduce the amount of highly radioactive waste needed to be safely stored in the long term. Furthermore, enhanced separation techniques

would also permit better separation and recycling of uranium and plutonium into mixed oxide fuels for fast neutron reactors, which do not produce as much minor actinide waste.[8]

Traditionally there have been two methods for spent fuel handling, the first is the 'once-through' method wherein spent fuel is removed, allowed to cool, then sealed in casks and stored in underground mines. [9-11] Not only does this method produce significantly higher amounts of waste but the probability of leaks and environmental contamination is also high (see section 1.4).[12] The second 'multi-use' method involves similar removal and cooling but instead of being put into storage is entered into a separation process whereby uranium and plutonium are separated from the remainder of nuclear waste and recycled back into usable nuclear fuel.[9] This process, known as PUREX or Plutonium Uranium Redox Extraction, exploits differences in the redox chemistry between uranium/plutonium and the remainder of minor actinides/lanthanides for efficient separation.[13]

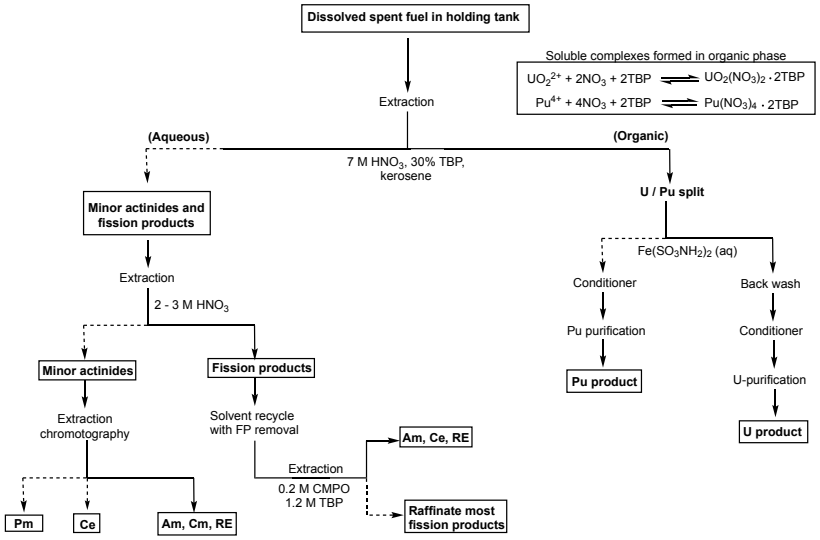

Scheme 1.1. Flowchart showing spent fuel separation using the PUREX method, including aqueous phase separation. Adapted from Ref 13.

In the PUREX method uranium and plutonium are fully separated from the remainder of the nuclear fuel via an extraction into organic media using the extractant tri-*n*-butyl phosphate (TBP). Unfortunately, TBP is not efficient at separating the minor actinides from the minor fission products due to similar electronic properties.[14, 15] Since the minor actinides account for much of the long-term radiotoxicity it would be valuable to develop better separation methods which can differentiate and separate the minor actinides from the remaining nuclear fuel waste.

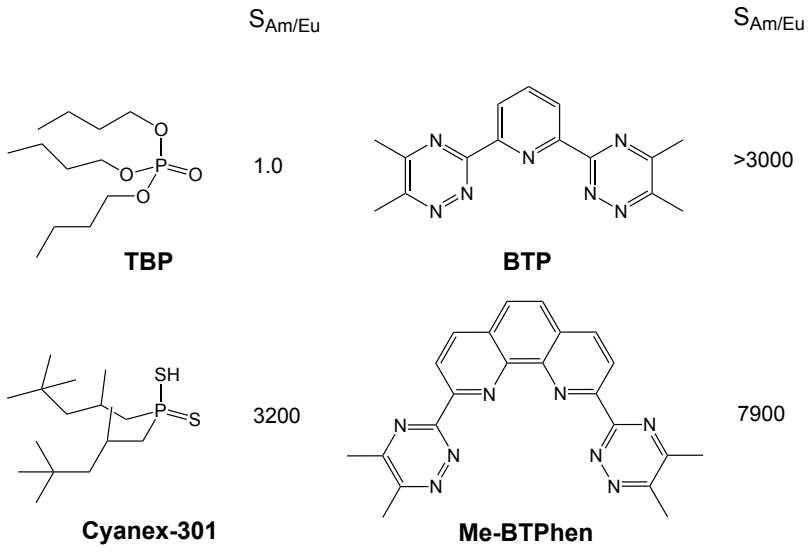

Figure 1.1. Exploitation of 'soft' ligand donor for selective separation of Am^{3+} vs. Eu^{3+}. Adapted from Refs 19 and 20.

The challenges associated with separation of the minor actinides from the lanthanides stem from their similar 'hard' chemistry and preferred trivalent charge. However, research into the chemical differences between the lanthanides and minor actinides has shown that the minor actinides engage in slightly more covalent interactions compared to their 4f congeners.[14, 16, 17] Indeed these differences have been previously exploited by many,[18, 19] including Zhu and co-workers who investigated the use of bis(2,2,4-trimethylpentyl)dithiophosphinic acid for

selective separation of Am^{3+} from Eu^{3+}.[20] By exchanging the hard oxygen donor in TBP, with a soft donor ligand (i.e., more covalent), such as sulfur, and optimizing the geometry of the ligand scaffold, separation between americium and europium increased by 5000 times (Figure 1.1). While these results are incredibly promising, the continued development of better extractants will require detailed investigation into the fundamental differences between the actinides and lanthanide bonding interactions.

1.2 f-orbital Bonding and Covalency in Actinide-Ligand Bonding

Traditional practice and theory have treated the actinides as hard metal ions, where, like the lanthanides, their chemistry is governed mostly by their charge and ionic radii.[21, 22] The lanthanides and actinides share similar ionic radii between congeners leading to similar chemical behavior.[23] More recently, research into the chemistry of these elements has confirmed that the actinides, most notably the early actinides, do in fact bond differently compared to the lanthanides, resulting in diverging reactivities between each other.[24-29] This can be rationalized by relativistic effects, which afford better shielding of the actinide's valence electrons, and results in better overlap between actinide and ligand frontier orbitals (Figure 1.2). [21, 28]

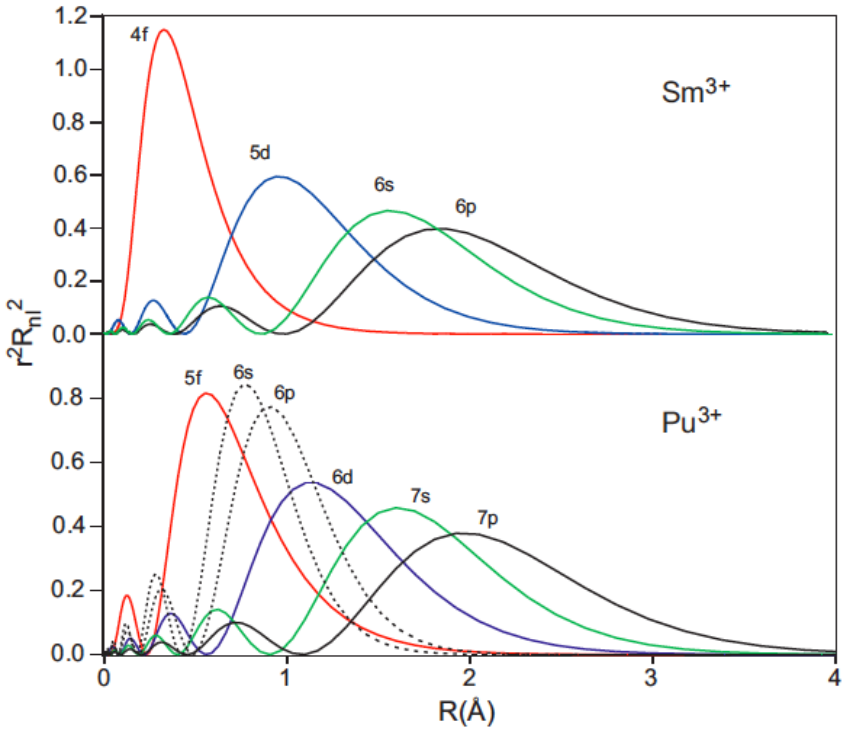

Scheme 1.2. Radial distribution seen in 4f (Sm^{3+}) versus 5f (Pu^{3+}) orbitals. Taken from Ref 28.

Given the potential to exploit the differences between actinide and lanthanide covalent interactions for selective nuclear waste extraction, there has been a renewed interest in studying their differing bonding properties.[30] Typically, these studies have been caried out using synchrotron-based X-ray techniques. X-ray absorption spectroscopy (XAS) is a common technique which has been widely used to probe the differences between actinide and lanthanide bonding.[31-34] For instance, Kozimor and co-workers used Cl K-edge XAS to examine the covalent interactions of several isostructural metal-chloride complexes, including $[(C_5Me_5)_2MCl_2]$ (M = Ti, Zr, Hf, Th, and U)and $[MCl_6]^{2-}$ (M = Ti, Zr, Hf, and U). [35] Their results found slight decreases in orbital mixing as the principal quantum number of the metal center increased, though substantial metal character was still observed for the actinides. In

another example, Shuh and co-workers used C K-edge XAS to examine 5f and 6d orbital participation in $[(C_8H_8)_2An]$. These results highlighted both actinide 5f and 6d orbital participation in the An-C bonds, as well as the scope of this technique.[36]

Unfortunately, a systemic issue with XAS techniques is the requirement of synchrotron beam time, which limits the number of studies that may be performed. As a result, there is an emerging need for the development of new low cost and accessible techniques for covalency studies. One such method that the Hayton group and others have recently pioneered is the use of NMR spectroscopy coupled with DFT calculations to quantify the amount of 5f and 6d participation in An–L bonding.[37-42] Simply put, NMR chemical shifts are highly sensitive to heavy atom spin-orbit coupling (SOC) effects.[43-46] These spin-orbit effects result in deshielding (typically) of the directly-bound NMR active nuclei through the fermi contact mechanism (Figure 1.3).[47] Through density functional theory (DFT) calculations the amount shielding/deshielding due of spin-orbit coupling can be quantified and the orbital participation deconvoluted.

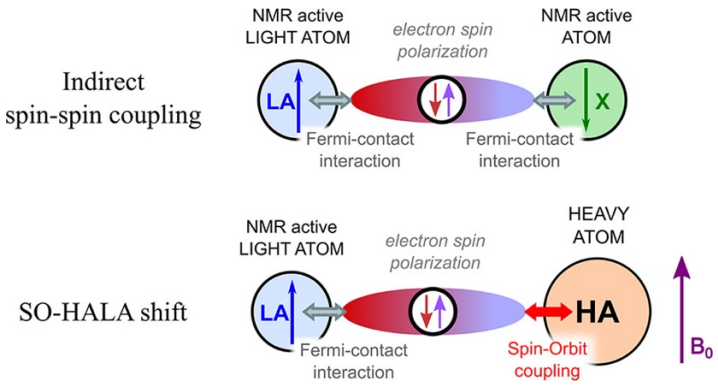

Figure 1.3. Schematic representing an analogy between indirect spin-spin coupling and the SOC induced heavy atom-light atom shift via a Fermi-contact mechanism. Taken from ref 47.

A variety of nuclei have been employed for this purpose, including ^{77}Se, ^{125}Te, and ^{15}N.[37, 39, 41, 48] This analysis has also been applied to a variety of organometallic actinide and lanthanide complexes, including those containing alkyl, aryl, carbene, and acetylide ligands.[40, 42, 49-54] For instance, Hayton and co-workers reported the synthesis and characterization of a thorium(IV) nitride, $[K(18\text{-crown-6})(THF)_2][(R_2N)_3Th(\mu\text{-}^{15}N)(Th(NR_2)_3]$ (**A**, R = $SiMe_3$), and the parent thorium amide complex, $[Th(NR_2)_3(^{15}NH_2)]$ (Figuer 1.4, **B**).[48] Since thorium(IV) is a diamagnetic metal center with a directly bound ^{15}N-containing ligand, the ^{15}N NMR spectra were recorded and examined using DFT calculations. SOC effects were found to cause a net 35 ppm downfield shift of $[K(18\text{-crown-6})(THF)_2][(R_2N)_3Th(\mu\text{-}^{15}N)(Th(NR_2)_3]$ 15N resonance vs $[Th(NR_2)_3(^{15}NH_2)]$ 15N resonance, suggesting greater covalent interactions between thorium and the nitride moiety. Their results were further corroborated by natural localized molecular orbital calculations (NLMO). These results not only found a substantial amount of covalency in $[K(18\text{-crown-6})(THF)_2][(R_2N)_3Th(\mu\text{-}^{15}N)(Th(NR_2)_3]$ but also revealed relatively equal amounts of 6d and 5f orbital participation in the Th–N π-interactions.

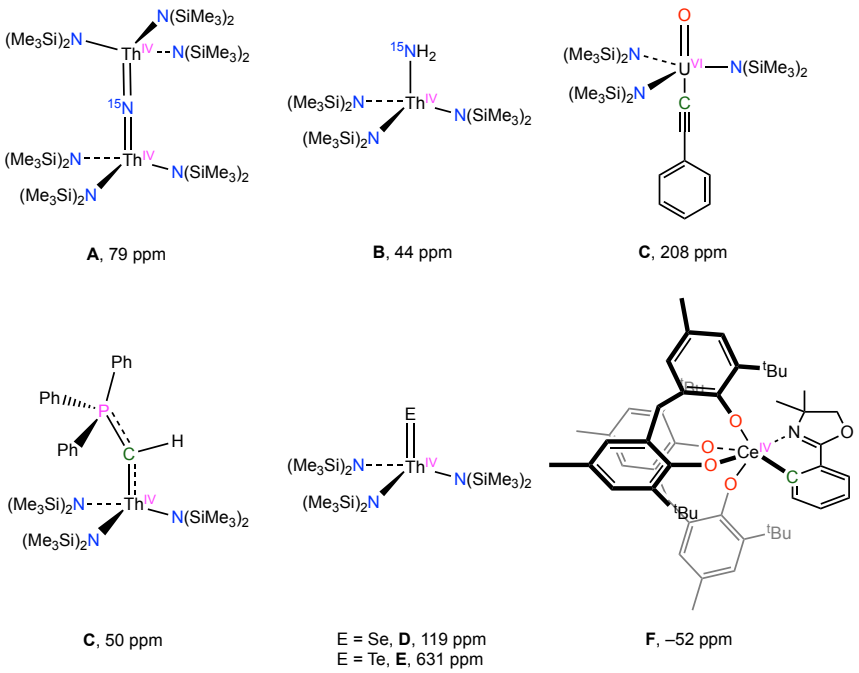

Figure 1.4. Some previously reported f-element complexes with their respective Δ SOC chemical shift. Adapted from Refs 39, 40, 48, 49, 52 and 53.

Schelter and co-workers have also used ^{13}C NMR spectroscopy to investigate the covalent interactions of a range of U(VI) phenyl-acetylide complexes $[U^{VI}(O)(C{\equiv}C{-}C_6H_4{-}R)(N(SiMe_3)_2)_3]$ (R = NMe_2, OMe, Me, Ph, H (**C**), Cl, Figure 1.4).[52, 53] Their results found a very covalent U–C bond, where the large downfield shift of the C_α acetylide resonances and U–C bond distances are correlated with the electron donating ability of the *para*-phenyl substituent. Indeed, DFT calculations found between 29% to 28% U(IV) metal character and between 62% to 60% 5f character, underscoring the highly covalent 5f interactions found in U(IV) organometallics. These results, and others,[39-41, 48-50, 53, 55] highlight the use of NMR spectroscopy in combination with DFT calculations as an emerging technique which provides an economical alternative to synchrotron-based X-ray techniques. This

techniques will enhance our ability to quickly assess the covalent interaction of a wide library of actinide and lanthanide complexes with NMR active nuclei.

1.3 f-Element-Ligand Multiple Bonds

Within inorganic coordination chemistry, the pursuit of novel complexes featuring metal-ligand multiple bonds has yielded critical advancements in both energy and materials sciences.[56-61] By studying the electronic structures of metal-ligand multiple bonds chemists and materials scientists have been able to tailor both reactivity and electronic properties to enhance their utility.[62-65] While weaker interactions, such as single bonds or donor pair interactions, are easier to generate, the enhanced covalency of metal-ligand multiple bonds makes their fundamental electronic structures easier to study. By comparison to the transition metals, the study of f-element ligand multiple bonds with main group elements remains in its adolescence.[30, 66-68]

While f-element metal oxo,[69-72] imido,[73-75] chalcogenido,[39, 76-80] and nitrido complexes[30, 41, 48, 81-84] have become increasingly well documented in recent years, a large gap between our understanding of transition metal-multiple bonds and f-element-multiple bonds remains.[30] This knowledge gap can be further emphasized by the non-existence of Schrock-type carbenes, which do not rely on heteroatom support or stabilization, and f-element carbynes. The paucity of f-element Schrock-type carbenes and carbynes can be rationalized by an energetic mismatch between the 'hard' actinide and lanthanide f orbitals with the 'soft' sp^2 or sp hybridized carbon ligand. Thus, all examples of f-element carbenes are either supported by ancillary chelators or require the use of hetero atom stabilization (Figure 1.5).[40, 42, 85-94] For example, the first actinide-carbene complex, $[Cp_3U(CHP(Me)_2R)]$ (**G**, R = Ph and Me), reported by Gilje and

co-workers in 1981 relies on a β-phosphorous atom to help dissipate the high partial negative charge at the carbene site.[95] In 2018, Liddle and co-workers reported the synthesis of the uranium silyl-phosphino-carbene complex [U{C(SiMe$_3$)(PPh$_2$)}(BIPMTMS)(Cl)][Li(2,2,2-cryptand)] (**H**) which utilizes a P(III) substituent to help stabilize the An=C interaction, instead of a P(III/V) substituent.[96]

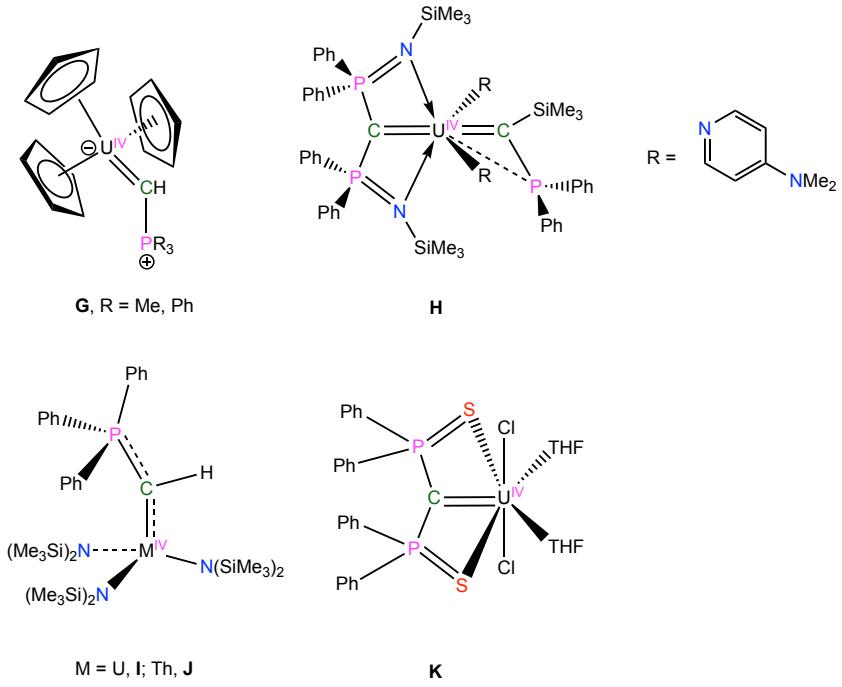

Figure 1.5. Representative examples of previously reported f-element carbon multiple bonds. Adapted from Refs 40, 88, 85, 95, and 96.

Despite the advances in carbene and f-element multiple bond chemistry, an unsupported Schrock-type carbene does not exist, likewise no f-element carbynes exist either. The synthesis and examination of these motifs' covalent interactions would provide the fundamental information required for the development of better separation techniques.

1.4 Actinide Chelation with Polydentate Ligands

Separation and immobilization of the actinides from aqueous solution is another important facet of closing the nuclear waste cycle. The hexavalent uranyl ion (*trans*-UO_2^{2+}) is the most common nuclear waste fragment found in aqueous solution (>95% abundant).[97] Unfortunately, the uranyl ion is also incredibly water soluble making it a potent groundwater and seawater contaminant.[98] Since leaching of uranium waste, from both mining and fuel storage, into ground water is a frequently encountered problem,[99-101] the development of new methods for the separation and stabilization of uranium from aqueous solution are critical.

Several aspects of *trans*-uranyl are well established: (1) uranyl adopts a rigid *trans* geometry (2) the uranium center is surprisingly difficult to reduce, given its 6+ oxidation state (3) the U–O bond is chemically inert.[56, 102-104] These aspects can be well illustrated by the U–O bond dissociation enthalpy (604 kJ/mol),[105] which 72 kJ/mol greater than the BDE for the C–O bond in carbon dioxide (532 kJ/mol).[106]

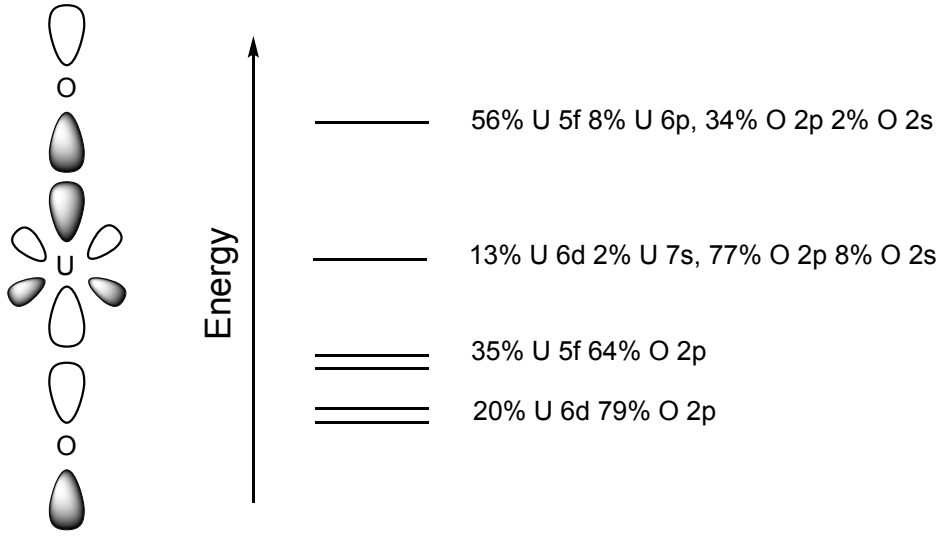

Figure 1.6 *trans*-uranyl U–O bonding molecular orbitals. Adapted from Ref 109.

Careful examination of the energy landscape of uranyl isomerization has found that the *cis* isomer of $[UO_2(OH)_4]^{2-}$ is approximately 18.0 kcal/mol higher in energy than the trans isomer.[107] The energy penalty for isomerization can be rationalized by changes in electronic structure.[107, 108] Computational studies of *trans*-uranyl's frontier orbital participation have found that there are two σ-interactions and four π-interactions, leading to an overall U–O bond order of three (Figure 1.6).[109] While it is generally agreed upon that these bonding interactions predominately consist of oxygen based σ_u, σ_g, π_u, and π_g orbitals, the ordering of these interactions is still contested.[102, 103, 105, 110-118] One study using Kohn-Sham DFT methods suggested an energetic ordering of $\pi_g < \pi_u < \sigma_g << \sigma_u$ (Figure 1.6).[109] Examination of the σ_u HOMO found a 64% uranium contribution and a small but significant amount of $6p_z$ participation (8%). The large uranium contribution and involvement of $6p_z$ orbitals in the U–O bonds helps explain their strong covalent nature and observed *trans* geometry.

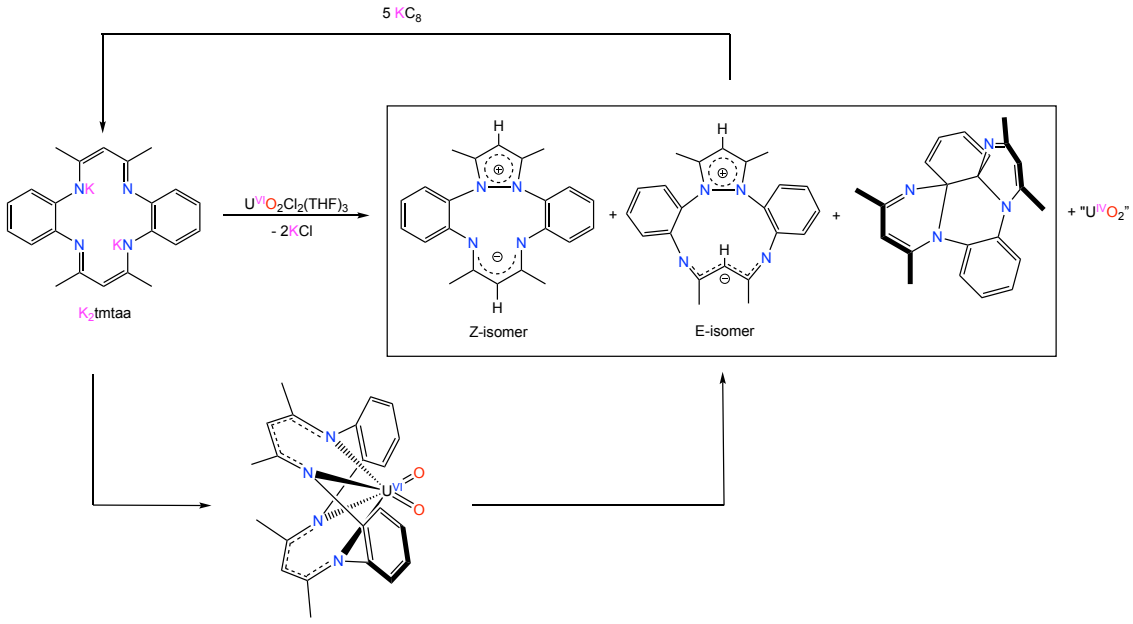

Scheme 1.2 Previous example of an attempted uranyl trans/cis isomerization using $[tmtaa]^{2-}$ as the co-ligand. Adapted from Ref 127.

Given our understanding of the uranyl ion it has been suggested that careful ligand design could facilitate isomerization of trans-uranyl through electronic and/or steric interactions.104 While slight deviations from uranyl's trans geometry are uncommon, they are not completely unknown.119-123 Pedrick and co-workers first demonstrated that uranyl bending was possible when they showed that reaction of either 2,11-diaza[3,3](2,6) pyridinophane or N,N′-dimethyl-2,11-diaza[3,3](2,6) pyridinophane with either $[UO_2Cl_2(THF)_2]_2$ or $UO_2(OTf)_2(THF)_3$ results in bent uranyl complexes with O–U–O angles ranging between 168.2(3)° to 161.7(5)°.[124] More recently, Ikeda-ono and co-workers utilized commercially available phenanthroline to enforce an O–U–O angle of 161.8(1)° where the deviation from linearity is rationalized by shared steric effects and π-π stacking of adjacent phenanthroline ligands in the solid state.[125] In an another attempt to isomerize *trans*-uranyl, Hayton and co-workers chose to chelate uranyl with the bulky macrocyclic dibenzotetramethyltetraaza[14]annulene (tmtaa) ligand (Scheme 1.2).[126] Instead of chelation, ligand oxidation and uranyl reduction to uranium oxide was observed to occur through a hypothesized *cis*-uranyl complex, *cis*-$[UO_2(tmtaa)]$. Interestingly, reduction of the uranyl ion by two electrons to water insoluble uranium oxides would offer an attractive option for selective uranyl immobilization and separation. These results suggest that, by using a sterically bulky and redox-active macrocyclic chelator, an electrocatalytic uranyl reduction cycle could be developed (Scheme 1.3). Such a model system would aid in the development of new methods of uranyl immobilization and stabilization.

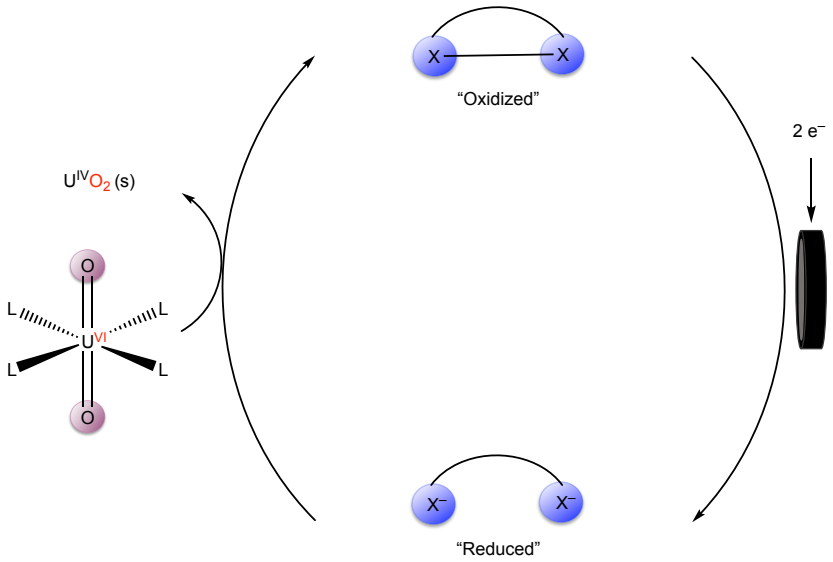

Scheme 1.3. Possible model system for electrocatalytic uranyl reduction via a *cis*-uranyl intermediate.

1.5 General Remarks

This thesis is divided into six chapters and covers two main areas of research: 1) Synthesis of f-element-carbon multiple bonds and 2) Use of macrocyclic chelators to manipulate and stabilize actinides in aqueous solution. The goal of the research described herein is to develop a better understanding of f-element bonding through the synthesis of new organometallic complexes, for potential applications in nuclear waste clean-up, medicine, and redox catalysis.

Chapter 2 describes the synthesis and characterization of the first structurally characterized actinide-DOTA complexes to feature the κ^8 binding mode for the DOTA ligand. Crystallographic studies find anomalously long An-N bond lengths, I believe the hard An^{4+} ions are not well suited to coordination by the relatively soft N atoms of the cyclen ring, suggesting that DOTA may not be the optimal chelator for the An^{4+} ions. These results are

significant because several applications, such as targeted alpha therapy, will require the development of extremely potent actinide chelators.

Chapter 3 details the reaction of the well-known macrocyclic ligand, [Me_8-calix[4]pyrrole], with the uranyl ion, results in ligand oxidation through a hypothesized highly-oxidizing *cis*-uranyl intermediate. Reaction of the oxidized ligand with an additional equivalent of the uranyl ion results in the isolation of a rare bent uranyl complex. I also propose that redox active macrocyclic ligands could have potential uses in homogenous uranyl reduction and immobilization.

Chapter 4 explores the coordination of the parent acetylide ligand (–C≡CH) to the actinides. In this chapter I outline the synthesis and characterization of new thorium(IV) and uranium(IV/III) acetylide complexes. I go on to describe the thermal decomposition of the An(IV) parent acetylide complexes to actinide bridging dicarbides as well as the synthesis of a mixed uranium/thorium dicarbide. These complexes are also explored by DFT calculations and a discussion of their electronic structure is given.

Chapter 5 describes a method for the synthesis of An(IV)-allenyl and An(IV)-allenylidene complexes, using lithium-diphenycyclopropene as the allenyl/allenylidene source. The An(IV)-allenylidene complexes represent the first non-heteroatom stabilized carbenes of the actinides. X-ray crystallography, ^{13}C NMR spectroscopy, IR spectroscopy, and DFT calculations are all used to probe the electronic structure of these complexes and a discussion of the results is given.

Chapter 6 investigates the coordination and reactivity of the potential carbon atom transfer reagent bis(diisopropylamino)cyclopropenylidene (BAC) with isostructural U(III) and Ce(III) complexes. In the case of cerium(III) I find that photolysis of a BAC solution with 10 mol% Ce(III) results in catalytic ring opening of a BAC ligand and coupling to an additional equivalent of BAC to yield a new methylenecyclopropene species. I also find that thermolysis of the uranium(III)·BAC adduct results in ring opening and formation of a uranium(IV) dienyl-metalacyclic complex.

Chapter 7 explores the role of supporting ligands in the synthesis of the An(IV)-allenyl complexes from chapter 5. By changing the supporting ligand from the bulky silylamide ligand ($N(SiMe_3)_2$) to the less bulky cyclopentadienide (Cp) ligand, I find diverging reactivities in their products. In the case of thorium(IV) ortho C–H activation of a ligand phenyl substituent to form a thorium(IV)-indenyl complex is observed. Whereas in the case of uranium(IV) I find that the ring opened cyclopropene inserts itself into a Cp ligand, yielding a triphenylethylene dianion. To explain the diverging reactivity, I propose that a transient An-carbenoid is formed which, in the case of uranium, can form a highly reactive U(VI)-carbyne that inserts into the Cp ligand.

1.6 References

1. *IAEA Annual Report* **2020**.
2. IEA, World Energy Outlook 2019. World Energy Outlook. **2009**.
3. *World energy outlook*. OECD International Energy Agency: 2021.
4. OECD, *Actinide and Fission Product Partitioning and Transmutation.* OECD Publishing.
5. Choppin, G.; Liljenzin, J.-O.; Rydberg, J.; Ekberg, C., Chapter 21 - The Nuclear Fuel Cycle. In *Radiochemistry and Nuclear Chemistry (Fourth Edition)*, Choppin, G.; Liljenzin, J.-O.; Rydberg, J.; Ekberg, C., Eds. Academic Press: Oxford, 2013; pp 685-751.

6. Hill, C., Ion exchange and Solvent Extraction. Press, C. R. C., Ed. 2009; p 119.

7. Madic, C.; Lecomte, M.; Baron, P.; Boullis, B., Separation of long-lived radionuclides from high active nuclear waste. *Comptes Rendus Physique* **2002**, *3*, 797-811.

8. Agency, O. N. E., *Management of recyclable fissile and fertile materials*. Nuclear Energy Agency, Organisation for Economic Co-Operation and Development: 2007.

9. EIA, The Nuclear Fuel Cycle.

10. NRC, Radioactive Waste. **2017**.

11. Crowley, K. D.; Ahearne, J. F., Managing the Environmental Legacy of US Nuclear-Weapons Production: Although the waste from America's arms buildup will never be" cleaned up," human and environmental risks can be reduced and managed. *American Scientist* **2002**, *90*, 514-523.

12. Vartabedian, R., Nuclear accident in New Mexico ranks among the costliest in US history. *LA Times* **2016**, *22*.

13. NEA, Spent Nuclear Fuel Reproccessing Flowsheet.

14. Nash, K. L., A review of the basic chemistry and recent developments in trivalent f-elements separations. *Solvent Extr. Ion Exch.* **1993**, *11*, 729-768.

15. Wenzel, U.; Branquinho, C.; Herz, D.; Ritter, G., Separation of Long-Lived α-Emitters from Highly Radioactive Solutions in the Thorium-Uranium Fuel Cycle. In *Actinide Seperations*, ACS Publications: 1980.

16. Dam, H. H.; Reinhoudt, D. N.; Verboom, W., Multicoordinate ligands for actinide/lanthanide separations. *Chem. Soc. Rev.* **2007**, *36*, 367-377.

17. Ionova, G.; Ionov, S.; Rabbe, C.; Hill, C.; Madic, C.; Guillaumont, R.; Krupa, J., Mechanism of trivalent actinide/lanthanide separation using bis (2, 4, 4-trimethylpentyl) dithiophosphinic acid (Cyanex 301) and neutral O-bearing co-extractant synergistic mixtures. *Solvent Extr. Ion Exch.* **2001**, *19*, 391-414.

18. Kolarik, Z., Complexation and separation of lanthanides (III) and actinides (III) by heterocyclic N-donors in solutions. *Chem. Rev.* **2008**, *108*, 4208-4252.

19. Bhattacharyya, A.; Ansari, S. A.; Gadly, T.; Ghosh, S. K.; Mohapatra, M.; Mohapatra, P. K., A remarkable enhancement in Am^{3+}/Eu^{3+} selectivity by an ionic liquid based solvent containing bis-1,2,4-triazinyl pyridine derivatives: DFT validation of experimental results. *Dalton Trans.* **2015**, *44*, 6193-6201.

20. Zhu, Y.; Chen, J.; Jiao, R., Extraction of Am (III) and Eu (III) from nitrate solution with purified Cyanex 301. *Solvent Extr. Ion Exch.* **1996**, *14*, 61-68.

21. Kaltsoyannis, N.; Scott, P., *The f elements*. Oxford University Press: New York, 1999.

22. Katz, J. J.; Morss, L. R.; Seaborg, G. T., *The Chemistry of the Actinide Elements.* 2nd ed.; 1986.

23. Choppin, G. R., Comparison of the solution chemistry of the actinides and lanthanides. *J. less-common met.* **1983**, *93*, 323-330.

24. Ingram, K. I.; Kaltsoyannis, N.; Gaunt, A. J.; Neu, M. P., Covalency in the f-element–chalcogen bond: computational studies of [M(N $(EPH_2)_2)_3$](M= La, U, Pu; E= O, S, Se, Te). *J. Alloys Compd.* **2007**, *444*, 369-375.

25. Gaunt, A. J.; Reilly, S. D.; Enriquez, A. E.; Scott, B. L.; Ibers, J. A.; Sekar, P.; Ingram, K. I. M.; Kaltsoyannis, N.; Neu, M. P., Experimental and Theoretical Comparison of Actinide and Lanthanide Bonding in $M[N(EPR_2)_2]_3$ Complexes (M = U, Pu, La, Ce; E = S, Se, Te; R = Ph, ^{i}Pr, H). *Inorg. Chem.* **2008**, *47*, 29-41.

26. Ingram, K. I.; Tassell, M. J.; Gaunt, A. J.; Kaltsoyannis, N., Covalency in the f Element− Chalcogen Bond. Computational Studies of $M[N(EPR_2)_2]_3$ (M= La, Ce, Pr, Pm, Eu, U, Np, Pu, Am, Cm; E= O, S, Se, Te; R= H, ^{i}Pr, Ph). *Inorg. Chem.* **2008**, *47*, 7824-7833.

27. Jones, M. B.; Gaunt, A. J.; Gordon, J. C.; Kaltsoyannis, N.; Neu, M. P.; Scott, B. L., Uncovering f-element bonding differences and electronic structure in a series of 1: 3 and 1: 4 complexes with a diselenophosphinate ligand. *Chem. Sci.* **2013**, *4*, 1189-1203.

28. Neidig, M. L.; Clark, D. L.; Martin, R. L., Covalency in f-element complexes. *Coord. Chem. Rev.* **2013**, *257*, 394-406.

29. Choppin, G. R., Covalency in f-element bonds. *J. Alloys Compd.* **2002**, *344*, 55-59.

30. Liddle, S. T., The Renaissance of Non-Aqueous Uranium Chemistry. *Angew. Chem. Int. Ed.* **2015**, *54*, 8604-8641.

31. Solomon, E. I.; Hedman, B.; Hodgson, K. O.; Dey, A.; Szilagyi, R. K., Ligand K-edge X-ray absorption spectroscopy: covalency of ligand–metal bonds. *Coord. Chem. Rev.* **2005**, *249*, 97-129.

32. Altman, A. B.; Pacold, J. I.; Wang, J.; Lukens, W. W.; Minasian, S. G., Evidence for 5d-σ and 5d-π covalency in lanthanide sesquioxides from oxygen K-edge X-ray absorption spectroscopy. *Dalton Trans.* **2016**, *45*, 9948-9961.

33. Daly, S. R.; Keith, J. M.; Batista, E. R.; Boland, K. S.; Clark, D. L.; Kozimor, S. A.; Martin, R. L., Sulfur K-edge X-ray Absorption Spectroscopy and Time-Dependent Density Functional Theory of Dithiophosphinate Extractants: Minor Actinide Selectivity and Electronic Structure Correlations. *J. Am. Chem. Soc.* **2012**, *134*, 14408-14422.

34. Löble, M. W.; Keith, J. M.; Altman, A. B.; Stieber, S. C. E.; Batista, E. R.; Boland, K. S.; Conradson, S. D.; Clark, D. L.; Lezama Pacheco, J.; Kozimor, S. A.; Martin, R. L.; Minasian, S. G.; Olson, A. C.; Scott, B. L.; Shuh, D. K.; Tyliszczak, T.; Wilkerson, M. P.; Zehnder, R. A., Covalency in Lanthanides. An X-ray Absorption Spectroscopy and Density Functional Theory Study of $LnCl_6^{x-}$ (x = 3, 2). *J. Am. Chem. Soc.* **2015**, *137*, 2506-2523.

35. Kozimor, S. A.; Yang, P.; Batista, E. R.; Boland, K. S.; Burns, C. J.; Clark, D. L.; Conradson, S. D.; Martin, R. L.; Wilkerson, M. P.; Wolfsberg, L. E., Trends in Covalency for d- and f-Element Metallocene Dichlorides Identified Using Chlorine K-Edge X-ray Absorption Spectroscopy and Time-Dependent Density Functional Theory. *J. Am. Chem. Soc.* **2009**, *131*, 12125-12136.

36. Minasian, S. G.; Keith, J. M.; Batista, E. R.; Boland, K. S.; Clark, D. L.; Conradson, S. D.; Kozimor, S. A.; Martin, R. L.; Schwarz, D. E.; Shuh, D. K.; Wagner, G.

L.; Wilkerson, M. P.; Wolfsberg, L. E.; Yang, P., Determining Relative f and d Orbital Contributions to M–Cl Covalency in MCl_6^{2-} (M = Ti, Zr, Hf, U) and $UOCl^{5-}$ Using Cl K-Edge X-ray Absorption Spectroscopy and Time-Dependent Density Functional Theory. *J. Am. Chem. Soc.* **2012**, *134*, 5586-5597.

37. Du, J.; Seed, J. A.; Berryman, V. E. J.; Kaltsoyannis, N.; Adams, R. W.; Lee, D.; Liddle, S. T., Exceptional uranium(VI)-nitride triple bond covalency from ^{15}N nuclear magnetic resonance spectroscopy and quantum chemical analysis. *Nat. Chem.* **2021**, *12*, 5649.

38. Wu, W.; Rehe, D.; Hrobárik, P.; Kornienko, A. Y.; Emge, T. J.; Brennan, J. G., Molecular Thorium Compounds with Dichalcogenide Ligands: Synthesis, Structure, ^{77}Se NMR Study, and Thermolysis. *Inorg. Chem.* **2018**, *57*, 14821-14833.

39. Smiles, D. E.; Wu, G.; Hrobárik, P.; Hayton, T. W., Use of ^{77}Se and ^{125}Te NMR Spectroscopy to Probe Covalency of the Actinide-Chalcogen Bonding in $[Th(E_n)\{N(SiMe_3)_2\}_3]^-$ (E = Se, Te; n = 1, 2) and Their Oxo-Uranium(VI) Congeners. *J. Am. Chem. Soc.* **2016**, *138*, 814-825.

40. Smiles, D. E.; Wu, G.; Hrobárik, P.; Hayton, T. W., Synthesis, Thermochemistry, Bonding, and ^{13}C NMR Chemical Shift Analysis of a Phosphorano-Stabilized Carbene of Thorium. *Organometallics* **2017**, *36*, 4519-4524.

41. Sergentu, D.-C.; Kent, G. T.; Staun, S. L.; Yu, X.; Cho, H.; Autschbach, J.; Hayton, T. W., Probing the Electronic Structure of a Thorium Nitride Complex by Solid-State ^{15}N NMR Spectroscopy. *Inorg. Chem.* **2020**, *59*, 10138-10145.

42. Rungthanaphatsophon, P.; Huang, P.; Walensky, J. R., Phosphorano-Stabilized Carbene Complexes with Short Thorium(IV)– and Uranium(IV)–Carbon Bonds. *Organometallics* **2018**, *37*, 1884-1891.

43. Autschbach, J.; Zurek, E., Relativistic Density-Functional Computations of the Chemical Shift of ^{129}Xe in $Xe@C_{60}$. *J. Phys. Chem. A* **2003**, *107*, 4967-4972.

44. Autschbach, J., Analyzing NMR shielding tensors calculated with two-component relativistic methods using spin-free localized molecular orbitals. *J. Chem. Phys.* **2008**, *128*, 164112.

45. Wolff, S. K.; Ziegler, T.; Lenthe, E. v.; Baerends, E. J., Density functional calculations of nuclear magnetic shieldings using the zeroth-order regular approximation (ZORA) for relativistic effects: ZORA nuclear magnetic resonance. *J. Chem. Phys.* **1999**, *110*, 7689-7698.

46. Ballard, C. C.; Hada, M.; Kaneko, H.; Nakatsuji, H., Relativistic study of nuclear magnetic shielding constants: hydrogen halides. *Chem. Phys. Lett.* **1996**, *254*, 170-178.

47. Vícha, J.; Novotný, J.; Komorovsky, S.; Straka, M.; Kaupp, M.; Marek, R., Relativistic Heavy-Neighbor-Atom Effects on NMR Shifts: Concepts and Trends Across the Periodic Table. *Chem. Rev.* **2020**, *120*, 7065-7103.

48. Staun, S. L.; Sergentu, D.-C.; Wu, G.; Autschbach, J.; Hayton, T. W., Use of ^{15}N NMR spectroscopy to probe covalency in a thorium nitride. *Chemical Science* **2019**, *10*, 6431-6436.

49. Panetti, G. B.; Sergentu, D.-C.; Gau, M. R.; Carroll, P. J.; Autschbach, J.; Walsh, P. J.; Schelter, E. J., Isolation and characterization of a covalent Ce^{IV}-Aryl complex with an anomalous ^{13}C chemical shift. *Nat. Commun.* **2021**, *12*, 1713.

50. Ordoñez, O.; Yu, X.; Wu, G.; Autschbach, J.; Hayton, T. W., Synthesis and Characterization of Two Uranyl-Aryl "Ate" Complexes. *Chem. Eur. J.* **2021**, *27*, 5885-5889.

51. Seaman, L. A.; Hrobárik, P.; Schettini, M. F.; Fortier, S.; Kaupp, M.; Hayton, T. W., A Rare Uranyl(VI)–Alkyl Ate Complex $[Li(DME)_{1.5}]_2[UO_2(CH_2SiMe_3)_4]$ and Its Comparison with a Homoleptic Uranium(VI)–Hexaalkyl. *Angew. Chem. Int. Ed.* **2013**, *52*, 3259-3263.

52. Lewis, A. J.; Carroll, P. J.; Schelter, E. J., Stable Uranium(VI) Methyl and Acetylide Complexes and the Elucidation of an Inverse Trans Influence Ligand Series. *J. Am. Chem. Soc.* **2013**, *135*, 13185-13192.

53. Mullane, K. C.; Hrobárik, P.; Cheisson, T.; Manor, B. C.; Carroll, P. J.; Schelter, E. J., ^{13}C NMR Shifts as an Indicator of U–C Bond Covalency in Uranium(VI) Acetylide Complexes: An Experimental and Computational Study. *Inorg. Chem.* **2019**, *58*, 4152-4163.

54. Kent, G. T.; Yu, X.; Pauly, C.; Wu, G.; Autschbach, J.; Hayton, T. W., Synthesis of Parent Acetylide and Dicarbide Complexes of Thorium and Uranium and an Examination of Their Electronic Structures. *Inorg. Chem.* **2021**, *60*, 15413-15420.

55. Kent, G. T.; Yu, X.; Wu, G.; Autschbach, J.; Hayton, T. W., Synthesis and electronic structure analysis of the actinide allenylidenes, $[\{(NR_2)_3\}An(CCCPh_2)]^-$ (An = U, Th; R = $SiMe_3$). *Chem. Sci.* **2021**, *12*, 14383-14388.

56. Gordon, G.; Taube, H., The exchange reaction between uranyl ion and water in perchloric acid solution. *J. Inorg. Nucl. Chem.* **1961**, *19*, 189-191.

57. Chauvin, Y., Olefin Metathesis: The Early Days (Nobel Lecture). *Angew. Chem. Int. Ed.* **2006**, *45*, 3740-3747.

58. Grubbs, R. H., Olefin-Metathesis Catalysts for the Preparation of Molecules and Materials (Nobel Lecture). *Angew. Chem. Int. Ed.* **2006**, *45*, 3760-3765.

59. Schrock, R. R., Multiple Metal–Carbon Bonds for Catalytic Metathesis Reactions (Nobel Lecture). *Angew. Chem. Int. Ed.* **2006**, *45*, 3748-3759.

60. Yandulov, D. V.; Schrock, R. R., Catalytic Reduction of Dinitrogen to Ammonia at a Single Molybdenum Center. *Science* **2003**, *301*, 76-78.

61. Yandulov, D. V.; Schrock, R. R.; Rheingold, A. L.; Ceccarelli, C.; Davis, W. M., Synthesis and Reactions of Molybdenum Triamidoamine Complexes Containing Hexaisopropylterphenyl Substituents. *Inorg. Chem.* **2003**, *42*, 796-813.

62. Yandulov, D. V.; Schrock, R. R., Reduction of Dinitrogen to Ammonia at a Well-Protected Reaction Site in a Molybdenum Triamidoamine Complex. *J. Am. Chem. Soc.* **2002**, *124*, 6252-6253.

63. Cardin, D. J.; Cetinkaya, B.; Lappert, M. F., Transition metal-carbene complexes. *Chem. Rev.* **1972**, *72*, 545-574.

64. Yandulov, D. V.; Schrock, R. R., Studies Relevant to Catalytic Reduction of Dinitrogen to Ammonia by Molybdenum Triamidoamine Complexes. *Inorg. Chem.* **2005**, *44*, 1103-1117.

65. Nugent, W. A.; Mayer, J. M., *Metal-Ligand Mulitple Bonds.* John Wiley & Sons: New York, NY, 1988.

66. Hayton, T. W., Metal–ligand multiple bonding in uranium: structure and reactivity. *Dalton Trans.* **2010**, *39*, 1145-1158.

67. Hayton, T. W., Recent developments in actinide–ligand multiple bonding. *Chem. Commun.* **2013**, *49*, 2956-2973.

68. Zhu, Q.; Zhu, J.; Zhu, C., Recent progress in the chemistry of lanthanide-ligand multiple bonds. *Tetrahedron Lett.* **2018**, *59*, 514-520.

69. Dutkiewicz, M. S.; Goodwin, C. A. P.; Perfetti, M.; Gaunt, A. J.; Griveau, J.-C.; Colineau, E.; Kovács, A.; Wooles, A. J.; Caciuffo, R.; Walter, O.; Liddle, S. T., A terminal neptunium(V)–mono(oxo) complex. *Nat. Chem.* **2022**, *14*, 342-349.

70. Fortier, S.; Hayton, T. W., Oxo ligand functionalization in the uranyl ion (UO_2^{2+}). *Coord. Chem. Rev.* **2010**, *254*, 197-214.

71. Kiernicki, J. J.; Harwood, J. S.; Fanwick, P. E.; Bart, S. C., Reductive silylation of Cp*UO_2(^{Mes}PDI^{Me}) promoted by Lewis bases. *Dalton Trans.* **2016**, *45*, 3111-3119.

72. Coughlin, E.; Bart, S. C., Reductive silylation of uranyl mediated by iminosemiquinone ligands. *Polyhedron* **2019**, *170*, 783-787.

73. Kiplinger, J. L.; Morris, D. E.; Scott, B. L.; Burns, C. J., Enhancing the reactivity of uranium(vi) organoimido complexes with diazoalkanes. *Chem. Commun.* **2002**, 30-31.

74. Cheisson, T.; Kersey, K. D.; Mahieu, N.; McSkimming, A.; Gau, M. R.; Carroll, P. J.; Schelter, E. J., Multiple Bonding in Lanthanides and Actinides: Direct Comparison of Covalency in Thorium(IV)- and Cerium(IV)-Imido Complexes. *J. Am. Chem. Soc.* **2019**, *141*, 9185-9190.

75. Moreau, L. M.; Lapsheva, E.; Amaro-Estrada, J. I.; Gau, M. R.; Carroll, P. J.; Manor, B. C.; Qiao, Y.; Yang, Q.; Lukens, W. W.; Sokaras, D.; Schelter, E. J.; Maron, L.; Booth, C. H., Electronic structure studies reveal 4f/5d mixing and its effect on bonding characteristics in Ce-imido and -oxo complexes. *Chem. Sci.* **2022**, *13*, 1759-1773.

76. Smiles, D. E.; Wu, G.; Hayton, T. W., Synthesis of Uranium–Ligand Multiple Bonds by Cleavage of a Trityl Protecting Group. *J. Am. Chem. Soc.* **2014**, *136*, 96-99.

77. Smiles, D. E.; Wu, G.; Hayton, T. W., Synthesis of Terminal Monochalcogenide and Dichalcogenide Complexes of Uranium Using Polychalcogenides, $[E_n]^{2-}$ (E = Te, n = 2; E = Se, n = 4), as Chalcogen Atom Transfer Reagents. *Inorg. Chem.* **2014**, *53*, 10240-10247.

78. Smiles, D. E.; Wu, G.; Hayton, T. W., Reversible Chalcogen-Atom Transfer to a Terminal Uranium Sulfide. *Inorg. Chem.* **2014**, *53*, 12683-12685.

79. Smiles, D. E.; Wu, G.; Kaltsoyannis, N.; Hayton, T. W., Thorium–ligand multiple bonds via reductive deprotection of a trityl group. *Chem. Sci.* **2015**, *6*, 3891-3899.

80. Smiles, D. E.; Wu, G.; Hayton, T. W., Synthesis, Electrochemistry, and Reactivity of the Actinide Trisulfides [K(18-crown-6)][An(η^3-S_3)(NR_2)$_3$] (An = U, Th; R = $SiMe_3$). *Inorganic Chemistry* **2016**, *55*, 9150-9153.

81. King, D. M.; Tuna, F.; McInnes, E. J.; McMaster, J.; Lewis, W.; Blake, A. J.; Liddle, S. T., Synthesis and structure of a terminal uranium nitride complex. *Science* **2012**, *337*, 717-720.

82. King, D. M.; Liddle, S. T., Progress in molecular uranium-nitride chemistry. *Coord. Chem. Rev.* **2014**, *266*, 2-15.

83. Falcone, M.; Poon, L. N.; Fadaei Tirani, F.; Mazzanti, M., Reversible dihydrogen activation and hydride transfer by a uranium nitride complex. *Angew. Chem. Int. Ed.* **2018**, *130*, 3759-3762.

84. Staun, S. L.; Wu, G.; Lukens, W. W.; Hayton, T. W., Synthesis of a heterobimetallic actinide nitride and an analysis of its bonding. *Chem. Sci.* **2021**, *12*, 15519-15527.

85. Cantat, T.; Arliguie, T.; Noël, A.; Thuéry, P.; Ephritikhine, M.; Floch, P. L.; Mézailles, N., The U=C Double Bond: Synthesis and Study of Uranium Nucleophilic Carbene Complexes. *J. Am. Chem. Soc.* **2009**, *131*, 963-972.

86. Cooper, O. J.; Mills, D. P.; McMaster, J.; Moro, F.; Davies, E. S.; Lewis, W.; Blake, A. J.; Liddle, S. T., Uranium–Carbon Multiple Bonding: Facile Access to the Pentavalent Uranium Carbene [U{$C(PPh_2NSiMe_3)_2$}$(Cl)_2$(I)] and Comparison of U^V=C and U^{IV}=C Bonds. *Angew. Chem. Int. Ed.* **2011**, *50*, 2383-2386.

87. Ren, W.; Deng, X.; Zi, G.; Fang, D.-C., The Th=C double bond: an experimental and computational study of thorium poly-carbene complexes. *Dalton Trans.* **2011**, *40*, 9662-9664.

88. Fortier, S.; Walensky, J. R.; Wu, G.; Hayton, T. W., Synthesis of a Phosphorano-Stabilized U(IV)-Carbene via One-Electron Oxidation of a U(III)-Ylide Adduct. *J. Am. Chem. Soc.* **2011**, *133*, 6894-6897.

89. Ma, G.; Ferguson, M. J.; McDonald, R.; Cavell, R. G., Actinide Metals with Multiple Bonds to Carbon: Synthesis, Characterization, and Reactivity of U(IV) and Th(IV) Bis(iminophosphorano)methandiide Pincer Carbene Complexes. *Inorg. Chem.* **2011**, *50*, 6500-6508.

90. Cooper, O. J.; Mills, D. P.; McMaster, J.; Tuna, F.; McInnes, E. J. L.; Lewis, W.; Blake, A. J.; Liddle, S. T., The Nature of the U=C Double Bond: Pushing the Stability of High-Oxidation-State Uranium Carbenes to the Limit. *Chem. Eur. J.* **2013**, *19*, 7071-7083.

91. Gregson, M.; Wooles, A. J.; Cooper, O. J.; Liddle, S. T., Covalent Uranium Carbene Chemistry. *Comments Inorg. Chem.* **2015**, *35*, 262-294.

92. Seed, J. A.; Sharpe, H. R.; Futcher, H. J.; Wooles, A. J.; Liddle, S. T., Nature of the Arsonium-Ylide $Ph_3As=CH_2$ and a Uranium(IV) Arsonium–Carbene Complex. *Angew. Chem. Int. Ed.* **2020**, *59*, 15870-15874.

93. Maity, A. K.; Ward, R. J.; Rupasinghe, D. M. R. Y. P.; Zeller, M.; Walensky, J. R.; Bart, S. C., Organometallic Uranyl Complexes Featuring a Carbodicarbene Ligand. *Organometallics* **2020**, *39*, 783-787.

94. Boronski, J. T.; Seed, J. A.; Wooles, A. J.; Liddle, S. T., Fragmentation, catenation, and direct functionalisation of white phosphorus by a uranium(IV)–silyl–phosphino–carbene complex. *Chem. Commun.* **2021**, *57*, 5090-5093.

95. Cramer, R. E.; Maynard, R. B.; Paw, J. C.; Gilje, J. W., A uranium-carbon multiple bond. Crystal and molecular structure of $(\eta^5\text{-}C_5H_5)_3UCHP(CH_3)_2(C_6H_5)$. *Journal of the American Chemical Society* **1981**, *103*, 3589-3590.

96. Lu, E.; Boronski, J. T.; Gregson, M.; Wooles, A. J.; Liddle, S. T., Silyl-Phosphino-Carbene Complexes of Uranium(IV). *Angew. Chem. Int. Ed.* **2018**, *57*, 5506-5511.

97. Park, B. H.; Gao, F.; Kwon, E.-h.; Ko, W. I., Comparative study of different nuclear fuel cycle options: quantitative analysis on material flow. *Energy Policy* **2011**, *39*, 6916-6924.

98. Gorman-Lewis, D.; Burns, P. C.; Fein, J. B., Review of uranyl mineral solubility measurements. *J. Chem. Thermodyn.* **2008**, *40*, 335-352.

99. Letman, M. M.; Drage, J.; Ryan, A.-M.; Lake, C.; Jamieson, R., Development of a leaching procedure to assess the risk of uranium leaching due to construction and demolition waste disposal. *Waste Manage. (Oxford)* **2018**, *78*, 144-150.

100. Park, G.-I.; Lee, H.-K., The Leaching Behavior of Unirradiated $ UO_2 Pellets in Wet Storage and Disposal Conditions. *Nucl. Eng. Technol.* **1996**, *28*, 349-358.

101. Baik, M.-H.; Cho, H.-R., Roles of uranyl silicate minerals in the long-term mobility of uranium in fractured granite. *J. Radioanal. Nucl. Chem.* **2022**, *331*, 451-459.

102. Wadt, W. R., Why uranyl ion (2+) is linear and isoelectronic thorium dioxide is bent. *J. Am. Chem. Soc.* **1981**, *103*, 6053-6057.

103. Dyall, K. G., Bonding and bending in the actinyls. *Mol. Phys.* **1999**, *96*, 511-518.

104. Hayton, T. W., Understanding the origins of O_{yl}–U–O_{yl} bending in the uranyl (UO_2^{2+}) ion. *Dalton Trans.* **2018**, *47*, 1003-1009.

105. Denning, R. G., Electronic Structure and Bonding in Actinyl Ions and their Analogs. *J. Phys. Chem. A* **2007**, *111*, 4125-4143.

106. Gibson, J. K.; Haire, R. G.; Santos, M.; Marçalo, J.; Pires de Matos, A., Oxidation Studies of Dipositive Actinide Ions, An^{2+} (An = Th, U, Np, Pu, Am) in the Gas Phase: Synthesis and Characterization of the Isolated Uranyl, Neptunyl, and Plutonyl Ions UO_2^{2+}(g), NpO_2^{2+}(g), and PuO_2^{2+}(g). *The Journal of Physical Chemistry A* **2005**, *109*, 2768-2781.

107. Schreckenbach, G.; Hay, P. J.; Martin, R. L., Theoretical Study of Stable Trans and Cis Isomers in $[UO_2(OH)_4]^{2-}$ Using Relativistic Density Functional Theory. *Inorg. Chem.* **1998**, *37*, 4442-4451.

108. Mullane, K. C.; Lewis, A. J.; Yin, H.; Carroll, P. J.; Schelter, E. J., Anomalous One-Electron Processes in the Chemistry of Uranium Nitrogen Multiple Bonds. *Inorg. Chem.* **2014**, *53*, 9129-9139.

109. Kaltsoyannis, N., Computational Study of Analogues of the Uranyl Ion Containing the −NUN− Unit: Density Functional Theory Calculations on UO_2^{2+}, UON^+, UN_2,

$UO(NPH_3)^{3+}$, $U(NPH_3)_2^{4+}$, $[UCl_4\{NPR_3\}_2]$ (R = H, Me), and $[UOCl_4\{NP(C_6H_5)_3\}]$. *Inorg. Chem.* **2000**, *39*, 6009-6017.

110. Denning, R. G., Electronic structure and bonding in actinyl ions. In *Complexes, Clusters and Crystal Chemistry*, Springer Berlin Heidelberg: Berlin, Heidelberg, 1992; pp 215-276.

111. Dekock, R. L.; Baerends, E. J.; Boerrigter, P. M.; Snijders, J. G., On the nature of the first excited states of the uranyl ion. *Chem. Phys. Lett.* **1984**, *105*, 308-316.

112. Pyykko, P.; Laaksonen, L., Relativistically parameterized extended Hueckel calculations. 8. Double-.ζ parameters for the actinoids thorium, protactinium, uranium, neptunium, plutonium, and americium and an application on uranyl. *J. Phys. Chem.* **1984**, *88*, 4892-4895.

113. Jørgensen, C. K., Can the highest occupied molecular orbital of the uranyl ion be essentially 5f? *Chem. Phys. Lett.* **1982**, *89*, 455-458.

114. Zhang, Z.; Pitzer, R. M., Application of relativistic quantum chemistry to the electronic energy levels of the uranyl ion. *J. Phys. Chem. A* **1999**, *103*, 6880-6886.

115. Pyykkoe, P.; Li, J.; Runeberg, N., Quasirelativistic pseudopotential study of species isoelectronic to uranyl and the equatorial coordination of uranyl. *J. Phys. Chem.* **1994**, *98*, 4809-4813.

116. Pepper, M.; Bursten, B. E., The electronic structure of actinide-containing molecules: a challenge to applied quantum chemistry. *Chem. Rev.* **1991**, *91*, 719-741.

117. Cornehl, H. H.; Heinemann, C.; Marçalo, J.; de Matos, A. P.; Schwarz, H., The "Bare" Uranyl (2+) Ion, UO. *Angew. Chem. Int. Ed.* **1996**, *35*, 891-894.

118. Tatsumi, K.; Hoffmann, R., Bent cis d_0 MoO_2^{2+} vs. linear trans d_0f_0 UO_2^{2+}: a significant role for nonvalence 6p orbitals in uranyl. *Inorg. Chem.* **1980**, *19*, 2656-2658.

119. Wilkerson, M. P.; Burns, C. J.; Morris, D. E.; Paine, R. T.; Scott, B. L., Steric Control of Substituted Phenoxide Ligands on Product Structures of Uranyl Aryloxide Complexes. *Inorg. Chem.* **2002**, *41*, 3110-3120.

120. Sarsfield, M. J.; Helliwell, M., Extending the Chemistry of the Uranyl Ion: Lewis Acid Coordination to a U=O Oxygen. *J. Am. Chem. Soc.* **2004**, *126*, 1036-1037.

121. Maynadié, J.; Berthet, J.-C.; Thuéry, P.; Ephritikhine, M., The first cyclopentadienyl complex of uranyl. *Chem. Commun.* **2007**, 486-488.

122. Jones, G. M.; Arnold, P. L.; Love, J. B., Oxo–Group-14-Element Bond Formation in Binuclear Uranium(V) Pacman Complexes. *Chem. Eur. J.* **2013**, *19*, 10287-10294.

123. Kiernicki, J. J.; Cladis, D. P.; Fanwick, P. E.; Zeller, M.; Bart, S. C., Synthesis, Characterization, and Stoichiometric U–O Bond Scission in Uranyl Species Supported by Pyridine(diimine) Ligand Radicals. *J. Am. Chem. Soc.* **2015**, *137*, 11115-11125.

124. Pedrick, E. A.; Schultz, J. W.; Wu, G.; Mirica, L. M.; Hayton, T. W., Perturbation of the O–U–O Angle in Uranyl by Coordination to a 12-Membered Macrocycle. *Inorg. Chem.* **2016**, *55*, 5693-5701.

125. Schöne, S.; Radoske, T.; März, J.; Stumpf, T.; Patzschke, M.; Ikeda-Ohno, A., $[UO_2Cl_2(phen)_2]$, a Simple Uranium(VI) Compound with a Significantly Bent Uranyl Unit (phen=1,10-phenanthroline). *Chem. Eur. J.* **2017**, *23*, 13574-13578.

126. Assefa, M. K.; Pedrick, E. A.; Wakefield, M. E.; Wu, G.; Hayton, T. W., Oxidation of the 14-Membered Macrocycle Dibenzotetramethyltetraaza[14]annulene upon Ligation to the Uranyl Ion. *Inorg. Chem.* **2018**, *57*, 8317-8324.

Chapter 2. Synthesis and Crystallographic Characterization of the Tetravalent Actinide-DOTA Complexes, [An^{IV}(κ^8-DOTA)(DMSO)] (An = Th, U)

Portions of this work were published in:

Greggory T. Kent, Guang Wu, Trevor W. Hayton Synthesis and Crystallographic Characterization of the Tetravalent Actinide-DOTA Complexes, [An^{IV}(κ^8-DOTA)(DMSO)] (An = Th, U). *Inorg. Chem.* **2019**, 58, 8253-8256.

2.1 Introduction

H_4DOTA (1,4,7,10-tetraazacyclododecane-1,4,7,10-tetraacetic acid) and its derivatives form strong chelate interactions with the f elements.[1] The resulting complexes have been used for a wide variety of applications, including MRI imaging and nuclear medicine.[2-5] While lanthanide DOTA chemistry has been studied for decades,[6-10] the synthesis and characterization of actinide DOTA complexes is not well established. H_4DOTA has previously been explored as a chelator for ^{225}Ac,[11, 12] specifically for the generation of an alpha-particle therapeutic.[13, 14] The resulting complex was characterized by ITLC-GC and its stability was probed in vitro.[15] In addition, the chelation of An^{3+} by H_4DOTA has been probed by ESI-MS (An = Pu, Am),[16] as well as UV-vis spectroscopy and EXAFS (An = Pu, Am).[17] The binding constants of H_4DOTA with Am^{3+} and Cm^{3+} have also been measured,[18] and the ^{1}H NMR spectrum of [Th(DOTA)] has been recorded.[19] In contrast, only a few actinide DOTA complexes have been structurally characterized.[20] For example, only one structurally characterized Th(DOTA) complex is known, a bimetallic aquo complex: $[Th_2(H_2O)_{10}(\kappa^4\text{-}H_2DOTA)_2][NO_3]_4$,[20] while just two DOTA-containing uranium complexes are known: the U(IV) cluster, $[U_6(\mu\text{-}OH)_4(\mu\text{-}O)_4(H_2O)_8(HDOTA)_4]$, and the 2D uranyl-coordination polymer, $[(UO_2)_2(H_2DOTA)(C_2O_4)(H_2O)_2]$.[20, 21] Notably, in all three of these examples, the DOTA ligand does not bind to the metal ion via all eight of its donor atoms. In fact, to the best of my knowledge, there are no structurally characterized actinide complexes where DOTA coordinates in its κ^8 binding mode. Critically, the structural characterization of more An(DOTA) complexes would allow us to evaluate the suitability of DOTA (and its variants) for use as a chelator in targeted alpha therapy.

In the research reported herein, I report the synthesis and crystallographic characterization of [An^{IV}(κ^8-DOTA)(DMSO)] (An = U, Th). I also report the crystallographic characterization of [U(κ^4-H_2DOTA)(DMSO)$_4$][Cl]$_2$, which is an intermediate formed along the H_4DOTA complexation pathway.

2.2 Results and discussion

Scheme 2.1. Synthesis of Complexes **2.1** and **2.2**.

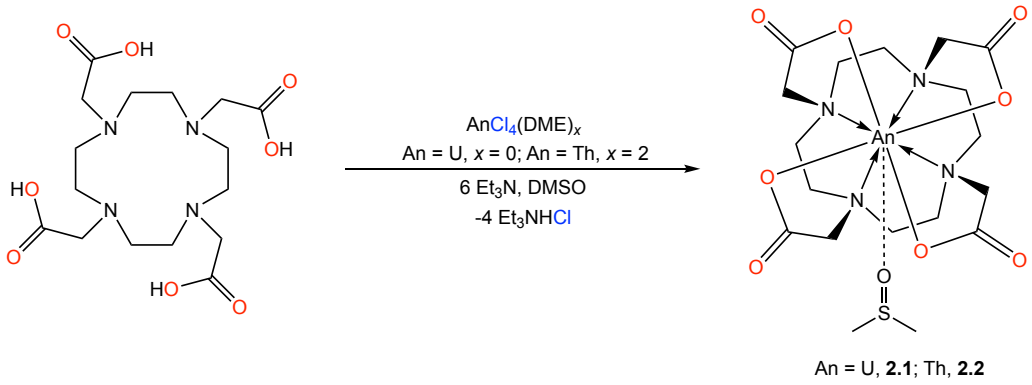

Addition of one equiv of H_4DOTA and 6 equiv of NEt_3 to a lime-green DMSO solution of UCl_4 results in a gradual color change to turquoise over the course of 1 h (Scheme 2.1). Work-up of the reaction mixture, followed by crystallization from DMSO/toluene results in isolation of [U^{IV}(κ^8-DOTA)(DMSO)] (**2.1**), as green-blue blocks in 47% yield. [Th^{IV}(κ^8-DOTA)(DMSO)] (**2.2**) can be made similarly, using $ThCl_4(DME)_2$ in place of UCl_4. It can be isolated in 53% yield as a white microcrystalline solid after recrystallization from hot DMSO. More recently, Moisey and co-workers have shown that the modification of this synthesis can yield both [U^{IV}(κ^8-DOTA)(H_2O)], [Na][U^{IV}(κ^8-DOTA)(OH)], and [Na][U^{IV}(κ^4-DOTA)(F)].[22] The rapid complexation of An^{4+} by H_4DOTA under anhydrous conditions is notable. In acidic aqueous solutions, by contrast, complexation of Ln^{3+} by H_4DOTA can take days to weeks.[23]

The successful isolation of **2.1** and **2.2** requires that the DMSO and H_4DOTA be relatively dry. If the H_4DOTA contains occluded water, I have found that the reaction results in formation of a sticky, intractable solid, which is presumably a hydroxide-bridged coordination polymer. The synthesis of the related U(IV) complex, $[U(DO3A)(DMSO)_2][Br]$ (DO3A = [4,7,10-tris-carboxymethyl-1,4,7,10-tetraazacyclododec-1-yl]-acetic acid) also requires water-free conditions.[24]

Complexes **2.1** and **2.2** are air- and water-stable. Complex **2.1** is soluble in DMSO and DMF, and modestly soluble in H_2O, while complex **2.2** is only sparingly soluble in DMSO, but modestly soluble in H_2O. They are both insoluble in CH_2Cl_2, THF, pyridine, alkanes, and aromatic solvents. Their insolubility in CH_2Cl_2 is beneficial because it permits the removal of any residual $[NEt_3H][Cl]$, should it present in the isolated material.

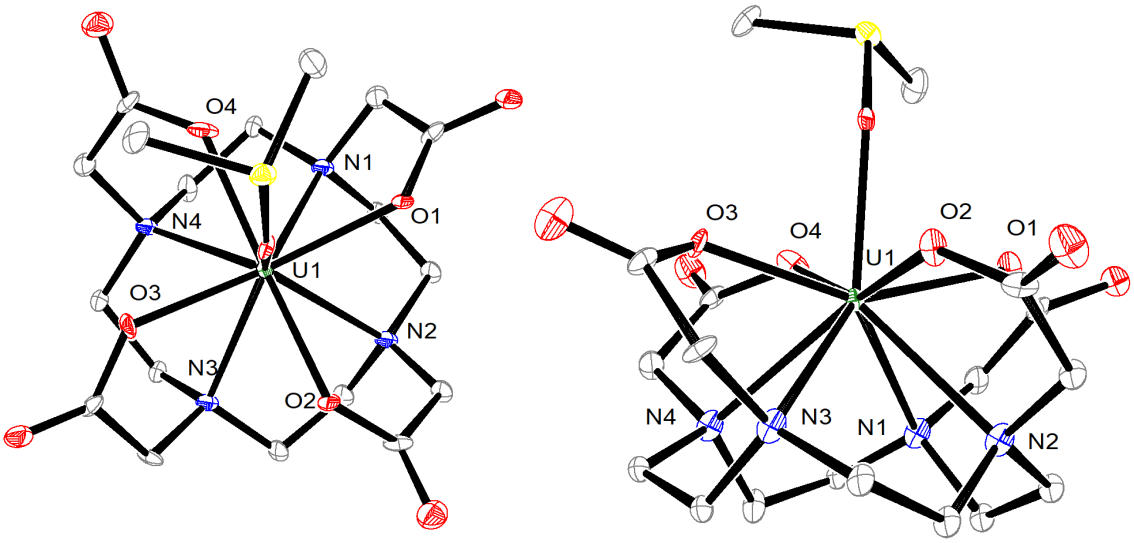

Figure 2.1. ORTEP diagrams of one independent molecule of $[U(\kappa^8\text{-DOTA})(DMSO)]\cdot DMSO$ (**2.1·DMSO**), with 50% probability ellipsoids. Hydrogen atoms and solvate molecules omitted for clarity.

Complexes **2.1** and **2.2** are isomorphous: they crystallize in the monoclinic $P2_1$ space group as DMSO solvates with two independent molecules in the unit cell. The solid-state molecular structure of one independent molecule of **2.1·DMSO** is shown in Figure 2.1. The $[DOTA]^{4-}$ ligand in **2.1** binds to the U^{4+} center with an octadentate coordination mode. A single DMSO ligand also coordinates to the U^{4+} center, resulting in an overall 9-coordinate geometry. The twist angles between the N_4 and O_4 faces that are formed upon DOTA coordination are 40(1)° and 38(1)° for **2.1** and **2.2**, respectively. These values are close to the ideal value of 45° expected for a capped square antiprism (SAP). Comparable values have been observed for several other $[Ln(DOTA)]^-$ complexes.[1] The average $An{-}O_{carboxylate}$ distances for **2.1** and **2.2** are 2.30 Å (range = 2.27(2) to 2.33(2) Å) and 2.36 Å (range = 2.33(2) to 2.38(2) Å), respectively. The average An−N distances for **2.1** and **2.2** are 2.72 Å (range = 2.67(2) to 2.74(2) Å) and 2.75 Å (range = 2.73(2) to 2.78(2) Å), respectively (Table 2.1). While no An(κ^8-DOTA) complexes have been characterized by X-ray crystallography, $[An(\kappa^8\text{-DOTA})(H_2O)]^-$ (An = Pu, Am) has been characterized by EXAFS.[17] The reported An-O (Pu-O = 2.43 ± 0.02 Å, Am-O = 2.44 ± 0.02 Å) and An-N (Pu-N = 2.67 ± 0.02 Å, Am-N = 2.68 ± 0.02 Å) distances are comparable to those observed in **2.1** and **2.2**. For further comparison, the average M-O and M-N distances in [Zr(DOTA)] are 2.13 and 2.42 Å, respectively.[25] Finally, the $An\text{-}O_{DMSO}$ distances for **2.1** and **2.2** are 2.38(2)/2.39(2) and 2.40(2)/2.39(2) Å, respectively. These distances are consistent with previously reported $An\text{-}O_{DMSO}$ distances.[24]

Table 2.1. Selected Metrical Parameters for **2.1** and **2.2** (Å)

Complex	**2.1**	**2.2**
av. An−O	2.30	2.36
av. An−N	2.72	2.75
An-O_{DMSO}	2.38(2), 2.39(2)	2.40(2), 2.39(2)
An−O_{plane}	0.565(7)	0.555(8)
An−N_{plane}	1.72(1)	1.75(1)
Twist angle (°)	40(1)	38(1)

The room temperature ^{1}H NMR spectrum of **2.1** in D_2O exhibits six paramagnetically shifted proton environments between 38.54 and -55.61 ppm (Figure 2.2). The sharp singlets at 21.74 and -55.61 ppm are assigned to the two acetate proton environments. I made these assignments by comparison with the NMR spectral data reported for $[Eu(DOTA)(H_2O)]^-$.[26] The four remaining peaks are assignable to the four unique proton environments of the cyclen ring. Three of these peaks, at 38.54, 19.32, and 5.76 ppm, are doublets with J_{HH} = 15 Hz, while the fourth (0.76 ppm) is a singlet. The presence of six peaks of equal intensity makes it appear that complex **2.1** is in the slow-exchange regime at this temperature.[6] Inspection of the ^{1}H NMR spectrum of [Zr(DOTA)] suggests that it is also in the slow-exchange regime.[25]

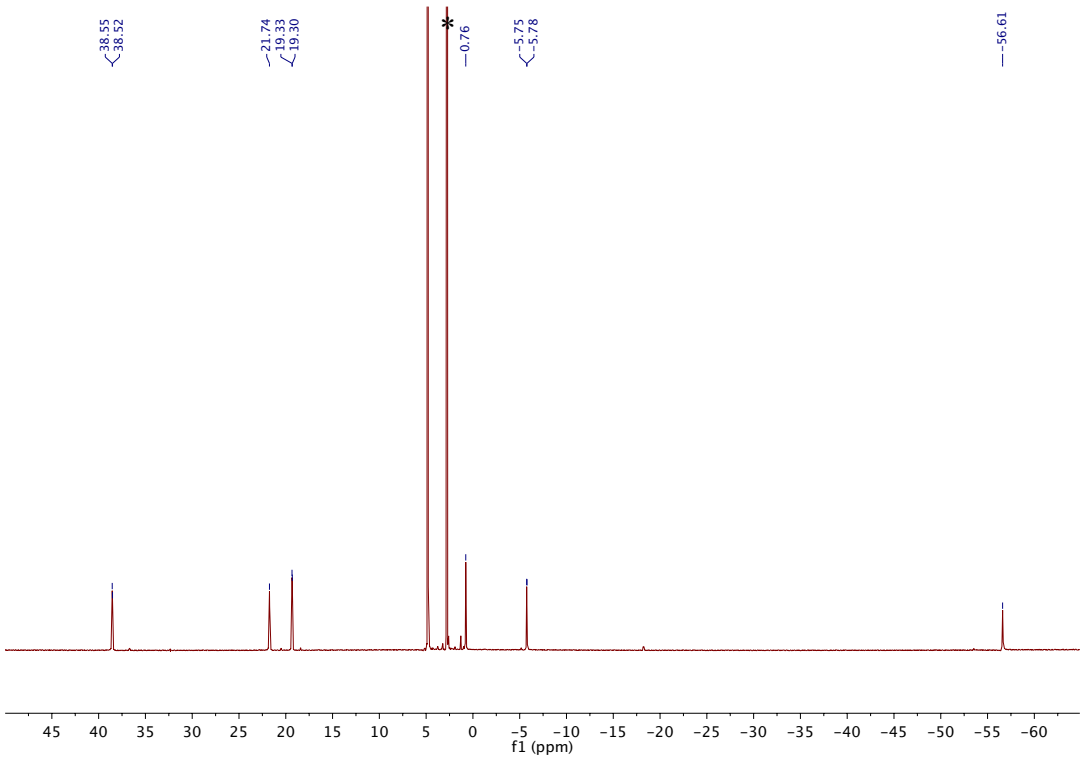

Figure 2.2. ^{1}H NMR spectrum of [U(κ^{8}-DOTA)(DMSO)] (**1**) in D_2O at room temperature. (*) indicates the resonance assignable to dimethyl sulfoxide.The room temperature ^{1}H NMR spectrum of **2.2** in D_2O exhibits five very broad resonances, ranging from 3.87 ppm to 2.84 ppm, suggestive of a fluxional system. Consistent with this hypothesis, upon heating this sample to 65 °C, these five resonances transform into three broad resonances, at 4.23, 3.77, and 3.33 ppm. These values are in good agreement with those previously reported for [Th(κ^{8}-DOTA)(H_2O)] generated *in situ*.[19] Similar behavior was observed for [La(DOTA)(H_2O)]$^{-}$, and was explained by invoking the inversion of the cyclen ring.[6] The ^{13}C{^{1}H} NMR spectra of **2.2** also features evidence of fluxionality. At room temperature, its ^{13}C{^{1}H} NMR spectrum features resonances at 55.22 and 57.09 ppm, which are assignable to two unique cyclen methylene environments (Figure A2.3). Upon warming to 45 °C, the two methylene resonances coalesce into a single peak (Figure A2.4). Using the two-site exchange

approximation, the activation barrier ($\Delta G_c^{\ddagger}$) for ring inversion was calculated to be 61 kJ/mol.[27] For comparison, $\Delta G_c^{\ddagger}$ = 61 kJ/mol and 64 kJ/mol for cyclen ring inversion in [La(DOTA)(H_2O)]$^-$ and [Eu(DOTA)(H_2O)]$^-$, respectively.[26, 28]

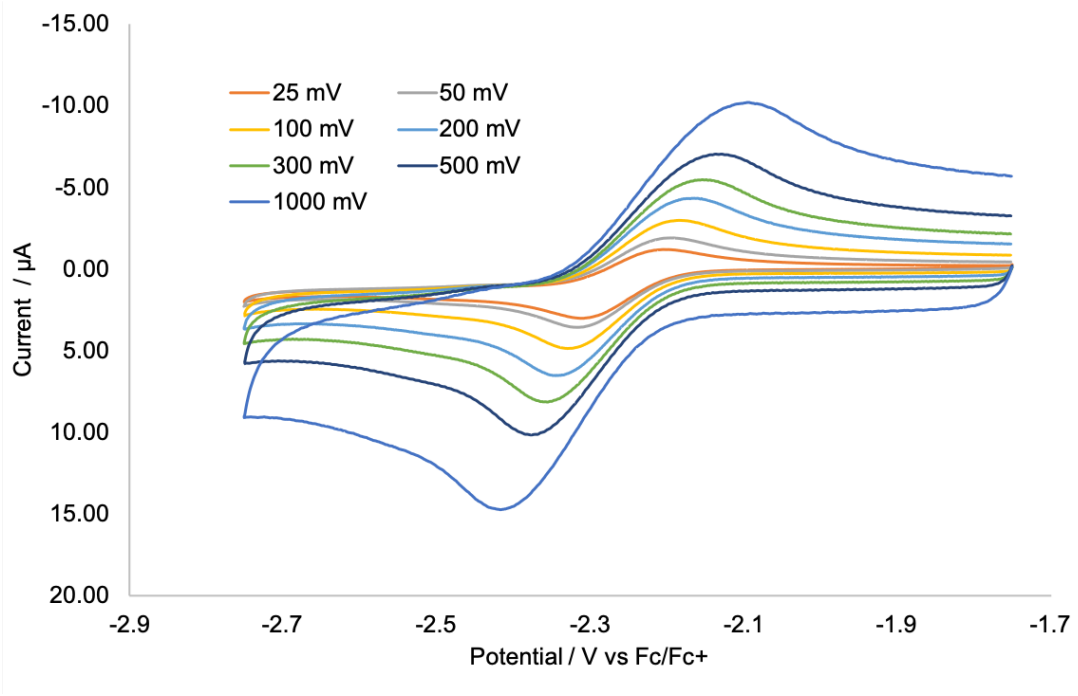

Figure 2.3. Scan rate dependent cyclic voltamogram of complex **2.1** (vs. Fc/Fc^+). Measured in DMSO with 0.1 M [NBu_4][BPh_4] as the supporting electrolyte.

I also recorded the cyclic voltammogram of complex **2.1** in DMSO at a variety of scan rates, using either [NBu_4][PF_6] or [NBu_4][BPh_4] as supporting electrolyte. The cyclic voltammogram (with [NBu_4][BPh_4] as supporting electrolyte) features a reversible redox feature with $E_{1/2}$ = -2.26 V (vs. Fc/Fc^+) (Figure 2.3). I have assigned this feature to a U(IV)/U(III) reduction event. Not surprisingly, this value is much decreased from the reported reduction potential of -0.58 V (vs. SHE) for U^{4+}(aq),[29, 30] highlighting the ability of strongly chelating macrocyclic ligands to stabilize the An^{4+} state.[31] Using [NBu_4][PF_6] as supporting

electrolyte, I observe the presence of a quasi-reversible feature at +0.44 V (vs. Fc/Fc^{+}) (Figure A2.8). This feature becomes increasingly reversible with increasing scan rates and has been assigned as a U(IV)/U(V) oxidation event.[30] For further comparison, Moisy and co-workers recorded the cyclic voltammogram of $[Na][U^{IV}(\kappa^8\text{-DOTA})(F)]$ in a 0.2 M acetate buffer and found two reversible redox waves, assignable to U^{V}/U^{IV} (1.29 V vs. SHE) and U^{IV}/U^{III} (-1.38 V vs. SHE) couples.[22] The potentials of these two features, as well as the potential difference ($\Delta E_{1/2}$ = 2.7 V) are similar to those observed for **1** ($\Delta E_{1/2}$ = 2.77 V).

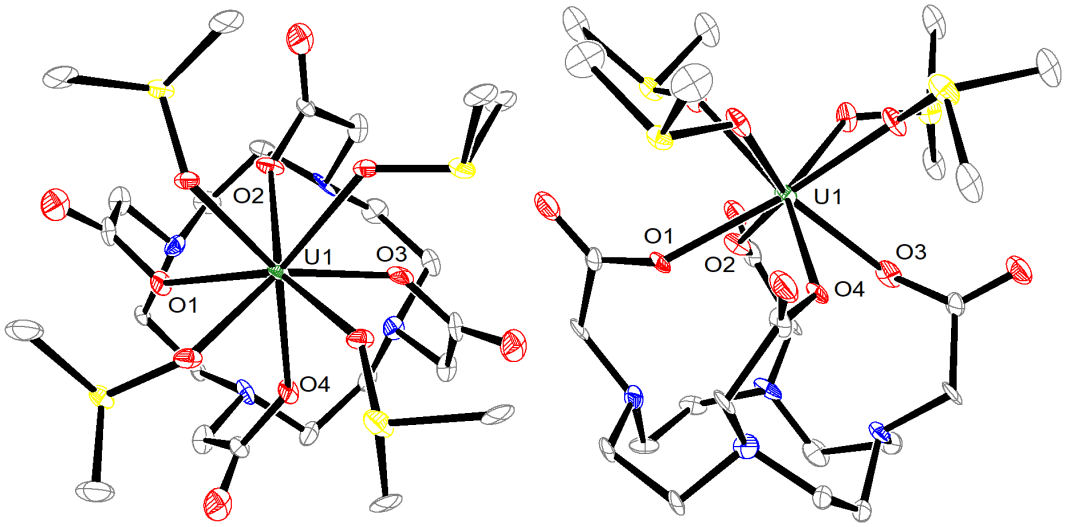

Figure 2.3. ORTEP diagrams of $[U(\kappa^4\text{-}H_2DOTA)(DMSO)_4][Cl]_2$ (**2.3·5DMSO**), with 50% probability ellipsoids. Hydrogen atoms, chloride counterions, and solvent molecules have been omitted for clarity. Selected bond distances (Å): U1−O1 = 2.39(1), U1−O2 = 2.27(1), U1−O3 = 2.36(1), U1−O4 = 2.29(1), av. $U-O_{DMSO}$ = 2.37.

In one instance, during an attempt to crystallize **2.1** I grew a few green-brown blocks. An X-ray crystallographic analysis of these crystals revealed them to be $[U(\kappa^4\text{-}H_2DOTA)(DMSO)_4][Cl]_2$ (**2.3**). Complex **2.3** crystallizes in the orthorhombic $P2_12_12$ space

group as a DMSO solvate, **2.3·5DMSO**, and its solid-state structure is shown in Figure 2.3. Complex **2.3** features a square antiprismatic geometry with a twist angle of 44.5(3)° between the DMSO and DOTA O_4 planes. The $[H_2DOTA]^{2-}$ ligand is coordinated in a κ^4 fashion via all four carboxylate arms. Four DMSO ligands are also coordinated to the uranium center. Two outer sphere Cl^- ions, required to maintain charge balance, are also found in the structure. The average $U\text{-}O_{carboxylate}$ distance is 2.33 Å (range: 2.27(1) - 2.39(1) Å) and the average $U\text{-}O_{DMSO}$ distance is 2.37 Å (range: 2.32(1) to 2.42(1) Å). While the two labile DOTA protons could not be located in the difference Fourier map, in the calculated structures of the related complexes, $[M(\kappa^4\text{-}H_2DOTA)(H_2O)_5]^+$ (M = Nd, Pu, Am), the four carboxylate arms are deprotonated and two nitrogen atoms are protonated.[17] Significantly, the κ^4 binding mode observed for the DOTA fragment in **2.3** has been proposed as an intermediate binding mode along the DOTA complexation pathway.[32-35] This binding mode has been detected by a variety of spectroscopies,[23] but the observation of **2.3** represents the first time that it has been characterized by X-ray crystallography. That said, it should be noted that this binding mode has been observed for a handful of DOTA derivatives, including 1,4,7,10-tetraazacyclododecane-1,4,7,10-tetrakis[methylene(2-carboxyethyl)phosphinic acid] (DOTPI) and 1,4,7,10-tetrakis(carbamoylmethyl)-1,4,7,10-tetraazacyclododecane (DOTAM).[36, 37]

2.3 Summary

In summary, I have synthesized and structurally characterized the first An^{IV}(DOTA) complexes that feature a κ^8 binding mode of the DOTA ligand. Moreover, isolation and characterization of **2.3** represents the first crystallographic confirmation of the previously proposed κ^4 intermediate formed during DOTA complexation. The lack of any other

crystallographically-characterized κ^8-bound actinide DOTA complexes is surprising, given the long f element history of this ligand. In this regard, I attribute my success to use of non-aqueous reaction and crystallization conditions, which results in fast metal complexation and the inhibition of hydrolysis. Ultimately, I believe this work will accelerate the development of potent An^{4+} chelators, which will be required for a variety of applications, including targeted alpha therapy.[14, 38, 39]

2.4 Experimental

2.4.1 General. All reactions and subsequent manipulations were performed under anaerobic and anhydrous conditions under an atmosphere of nitrogen. Toluene was dried using a Vacuum Atmospheres DRI-SOLV Solvent Purification system and stored over 3Å sieves for 24 h prior to use. Triethylamine, Dimethyl sulfoxide (DMSO), and dichloromethane (CH_2Cl_2) were degassed and dried over 3Å molecular sieves for 72 h prior to use. [$ThCl_4(DME)_2$] and UCl_4 were synthesized according to previously reported literature procedures.[40, 41] 1,4,7,10-tetraazacyclododecane-1,4,7,10-tetraacetic acid (H_4DOTA) was purchased from TCI Chemicals and dried under vacuum at room temperature for 24 h prior to use. All other reagents were purchased from commercial suppliers and used as received.

All NMR spectra were recorded on a Varian UNITY INOVA 500 spectrometer. ^{1}H and $^{13}C\{^1H\}$ NMR spectra were referenced to external $SiMe_4$ using the residual protio solvent peaks as internal standards.[42, 43] IR spectra were recorded on a Nicolet 6700 FT-IR spectrometer with a NXR FT Raman Module. Elemental analyses were performed by the Microanalytical Laboratory at University of California (Berkeley, CA).

2.4.2 Cyclic Voltammetry Measurements. CV experiments were performed with a CH Instruments 600c Potentiostat, and the data were processed using CHI software (version 6.29). All experiments were performed inside the glovebox using a 20 mL glass vial as the cell. The working electrode consisted of glassy carbon (2 mm diameter), the counter electrode was a platinum wire, and an Ag/AgCl wire was used as a reference electrode. Solutions employed for CV studies were typically 1 mM in analyte and 0.1 M in $[NBu_4][PF_6]$ or $[NBu_4][BPh_4]$. Ferrocene was used to reference all experiments.

2.4.3 Synthesis of [U(κ^8-DOTA)(DMSO)] (2.1). A colorless solution of 1,4,7,10-Tetraazacyclododecane-1,4,7,10-tetraacetic acid (H_4DOTA) (51.0 mg, 0.126 mmol) and triethylamine (76.6 mg, 0.757 mmol) in DMSO (1 mL) was slowly added to a lime-green, stirring solution of UCl_4 (48 mg, 0.126 mmol) in DMSO (1 mL). The resulting solution was allowed to stir for 1 h, whereupon the solution turned from lime-green to turquoise. This solution was then layered with toluene (6 mL) and subsequent storage of this solution for 24 h at room temperature resulted in the deposition of a turquoise solid. The supernatant was decanted away and the remaining solid was rinsed with dichloromethane (3 × 3 mL) to remove any remaining $[NEt_3H][Cl]$. The solid was then dried *in vacuo* to afford a green-blue powder. The powder was transferred to a 4 mL scintillation vial, DMSO (1.5 mL) was then added, and the mixture was gently heated to 80 °C. After dissolution of the solid, the 4 mL scintillation vial was placed inside a 20 mL scintillation vial and toluene (5 mL) was added to the outer vial. Storage of this two vial system for 24 h at room temperature resulted in the deposition of turquoise blocks of **2.1**. Yield 42.6 mg, 47%. In one instance, the attempted crystallization of **2.1** resulted in the deposition of a few green-brown blocks of **2.3**. These were subsequently isolated and analyzed by X-ray crystallography. ^{1}H NMR (500 MHz, 25 °C, D_2O): δ 38.54 (d,

J_{HH} = 15 Hz, H_{ax}, 4H), 21.74 (s, H_{ac}, 4H), 19.32 (d, J_{HH} = 15 Hz, H_{eq}, 4H), 2.74 (s, DMSO, 6H), 0.76 (s, H_{eq}, 4H), 5.77 (d, J_{HH} = 15 Hz, H_{ax}, 4H), -56.61 (s, H_{ac}, 4H). IR (KBr pellet, cm^{-1}): 2981 (w), 2883 (w), 2862 (w), 1651 (vs), 1458 (m), 1400 (m), 1306 (s), 1292 (s), 1236 (m), 1153 (w), 1080 (s), 1009 (m), 1003 (s), 931 (vs), 903 (m), 839 (m), 800 (m), 710 (s), 684 (w), 646 (w), 565 (w), 499 (w), 455 (w), 401 (w).

2.4.4 Synthesis of [Th(κ^8-DOTA)(DMSO)] (2.2). A colorless solution of H_4DOTA (54.5 mg, 0.134 mmol) and triethylamine (81.8 mg, 0.809 mmol) in DMSO (1 mL) was slowly added to a colorless solution of [$ThCl_4(DME)_2$] (74.7 mg, 0.134 mmol) in DMSO (1 mL). This solution was allowed to stir for 1 h, which resulted in the deposition of a white powder. This solid was isolated on a medium porosity glass frit, rinsed with dichloromethane (3 × 1 mL), transferred to a 20 mL scintillation vial and dried *in vacuo*. The powder was then transferred to a 4 mL scintillation vial, DMSO (1.5 mL) was added, and the mixture was gently heated to 60 °C. After dissolution of the solid, the solution was allowed to cool slowly to room temperature, which resulted in the deposition of **2.2** as colorless crystalline blocks. Yield 51.7 mg, 54%. Anal. Calcd for $C_{18}H_{30}N_4O_9STh$: C, 30.43; H, 4.26; N, 7.82. Found; C, 30.24; H, 4.40; N, 7.82. ^{1}H NMR (500 MHz, 3 °C, D_2O): δ 3.72 (d, J_{HH} = 15 Hz, H_{ac}, 4H), 3.57 (d, J_{HH} = 15 Hz, H_{ac}, 4H), 3.54 (s, H_{ax}, 4H), 2.87 (s, $H_{ax/eq}$, 8H), 2.64 (d, J_{HH} = 15 Hz, H_{eq}, 4H), 2.53 (s, DMSO, 6H). ^{1}H NMR (500 MHz, 13 °C, D_2O): δ 3.79 (s, H_{ac}, 4H), 3.67 (s, H_{ac}, 4H), 3.63 (s, H_{ax}, 4H), 2.98 (s, $H_{ax/eq}$, 8H), 2.73 (d, J_{HH} = 15 Hz, H_{eq}, 4H), 2.64 (s, DMSO, 6H). ^{1}H NMR (500 MHz, 23 °C, D_2O): δ 3.87 (s, H_{ac}, 4H), 3.78 (s, H_{ac}, 4H), 3.68 (s, H_{ax}, 4H), 3.06 (s, $H_{ax/eq}$, 8H), 2.84 (s, H_{eq}, 4H), 2.73 (s, DMSO, 6H). ^{1}H NMR (500 MHz, 35 °C, D_2O): δ 3.96 (s, H_{ac}, 8H), 3.78 (br s, $H_{ax/eq}$, 8H), 3.14 (br s, $H_{ax/eq}$, 8H), 2.86 (s, DMSO, 6H). ^{1}H NMR (500 MHz, 42 °C, D_2O): δ 4.02 (s, H_{ac}, 8H), 3.80 (br s, $H_{ax/eq}$, 8H), 3.15 (br s, $H_{ax/eq}$, 8H), 2.93 (s, DMSO,

6H). ^{1}H NMR (500 MHz, 45 °C, D_2O): δ 4.06 (s, H_{ac}, 8H), 3.78 (br s, $H_{ax/eq}$, 8H), 3.18 (br s, $H_{ax/eq}$, 8H), 2.96 (s, DMSO, 6H). ^{1}H NMR (500 MHz, 55 °C, D_2O): δ 4.14 (s, H_{ac}, 8H), 3.67 (br s, $H_{ax/eq}$, 8H), 3.27 (br s, $H_{ax/eq}$, 8H), 3.05 (s, DMSO, 6H). ^{1}H NMR (500 MHz, 65 °C, D_2O): δ 4.20 (s, H_{ac}, 8H), 3.74 (br s, $H_{ax/eq}$, 8H), 3.33 (br s, $H_{ax/eq}$, 8H), 3.14 (s, DMSO, 6H). $^{13}C\{^{1}H\}$ NMR (126 MHz, 3 °C, D_2O): δ 181.41 (CO_2^-), 66.74 (CH_2^{ac}), 57.36 (CH_2^{et}), 55.37 (CH_2^{et}). $^{13}C\{^{1}H\}$ NMR (126 MHz, 12 °C, D_2O): δ 181.31 (CO_2^-), 66.70 (CH_2^{ac}), 57.32 (CH_2^{et}), 55.38 (CH_2^{et}). $^{13}C\{^{1}H\}$ NMR (126 MHz, 23 °C, D_2O): δ 181.20 (CO_2^-), 66.64 (CH_2^{ac}), 57.22 (CH_2^{et}), 55.36 (CH_2^{et}). $^{13}C\{^{1}H\}$ NMR (126 MHz, 35 °C, D_2O): δ 181.04 (CO_2^-), 66.56 (CH_2^{ac}), 57.18 (CH_2^{et}), 55.70 (CH_2^{et}). $^{13}C\{^{1}H\}$ NMR (126 MHz, 42 °C, D_2O): δ 180.94 (CO_2^-), 66.51 (CH_2^{ac}), 56.52 (CH_2^{et}), 55.37 (CH_2^{et}). $^{13}C\{^{1}H\}$ NMR (126 MHz, 45 °C, D_2O): δ 180.89 (CO_2^-), 66.49 (CH_2^{ac}), 56.65 (CH_2^{cylcen}). $^{13}C\{^{1}H\}$ NMR (126 MHz, 55 °C, D_2O): δ 180.75 (CO_2^-), 66.42 (CH_2^{ac}), 56.19 (CH_2^{cylcen}). $^{13}C\{^{1}H\}$ NMR (126 MHz, 65 °C, D_2O): δ 180.60 (CO_2^-), 66.35 (CH_2^{ac}), 55.99 (CH_2^{cylcen}). IR (KBr pellet, cm^{-1}): 2987 (w), 2926 (w), 2914 (w), 2860 (w), 1653 (vs), 1471 (w), 1466 (w), 1400 (w), 1336 (s), 1300 (s), 1234 (w), 1151 (w) 1080 (s), 1030 (s), 939 (m), 931 (s), 899 (m), 837 (m), 800 (m), 708 (s), 646 (w), 563 (w), 498 (w), 453 (w).

2.4.5 X-ray Crystallography. Data for **2.1**, **2.2**, and **2.3** were collected on a Bruker KAPPA APEX II diffractometer equipped with an APEX II CCD detector using a TRIUMPH monochromator with a Mo Kα X-ray source (α = 0.71073 Å). The crystals were mounted on a cryoloop under Paratone-N oil, and data was collected at 100(2) K for **2.1** and **2.2** and at 105(2) K for **2.3**, using an S3 Oxford nitrogen gas cryostream. Frame exposures of 10 s were used for both **2.1** and **2.3**. Frame exposures of 20 s were used for **2.2**. Data collection and cell parameter determinations were conducted using the SMART program.[44] Integration of the data frames and final cell parameter refinements were performed using SAINT software.[45] Absorption

corrections of the data were carried out using the multi-scan method SADABS.[46] Subsequent calculations were carried out using SHELXTL. Structure determination was done using direct or Patterson methods and difference Fourier techniques. All hydrogen atom positions were idealized and rode on the atom of attachment. Structure solution, refinement, graphics, and creation of publication materials were performed using SHELXTL.[47]

The unit cells of complexes **2.1** and **2.2** both lack mirror or glide plane symmetry; therefore, the space group $P2_1$ was chosen over $P2_1/c$ or $P2_1/n$. Confirmation of my choice of space group was made by running the Addsym feature in Platon, which suggested no additional symmetry. This result was further confirmed by solving the structure of **2.2** in P1, and then running the Addsym feature in Platon, which suggested $P2_1$ as the correct space group. Both **2.1** and **2.2** also crystallize as racemic twins. For both structure refinements, I applied the TWIN and BASF commands in SHELX. The refined BASF values are 0.55 and 0.52 for complex **2.1** and **2.2**, respectively. In addition, the EADP command was used to constrain the anisotropic displacement parameters of pseudo-symmetry related atoms. For complex **2.3**, the EADP command was used to constrain the anisotropic displacement parameters of the non-hydrogen DOTA ligand atoms. Two of the DMSO solvates in **2.3** also contained positional disorder. The positional order was addressed by modeling these DMSO solvates over two positions, each with half occupancy, using the SADI then EADP commands. Hydrogen atoms were not assigned to disordered DMSO solvates, nor were positions assigned to the two labile hydrogen atoms of the $[H_2DOTA]^{2-}$ ligand, as they could not be located using the difference Fourier map.

Table 2.2. Crystallographic details for complexes **2.1·DMSO**, **2.2·DMSO**, and **2.3·5DMSO**.

	2.1·DMSO	**2.2·DMSO**	**2.3·5DMSO**
Formula	$C_{20}H_{36}N_4O_{10}S_2U$	$C_{20}H_{36}N_4O_{10}S_2Th$	$C_{34}H_{80}Cl_2N_4O_{17}S_9U$
Crystal Habit, Color	Block, Green-blue	Block, Colorless	Block, Green-Brown
Crystal Size (mm)	0.2 × 0.15 × 0.05	0.15 × 0.1 × 0.05	0.2 × 0.1 × 0.05
MW (g/mol)	794.68	788.69	1414.49
crystal system	Monoclinic	Monoclinic	Orthorhombic
space group	$P2_1$	$P2_1$	$P2_12_12$
a (Å)	8.606(4)	8.621(7)	13.4985(7)
b (Å)	34.594(15)	34.68(3)	41.320(5)
c (Å)	9.192(5)	9.216(8)	10.3457(5)
α (°)	90	90	90
β (°)	108.443(10)	108.333(13)	90
γ (°)	90	90	90
V (Å^3)	2596(2)	2616(4)	5770.4(5)
Z	4	4	4
T (K)	100(2)	100(2)	105(2)
λ (Å)	0.71073	0.71073	0.71073
GOF	0.890	0.951	1.436
Density (calcd) (Mg/m^3)	2.033	2.003	1.628
Absorption coefficient (mm^{-1})	6.474	5.921	3.294
F_{000}	1552	1544	2872
Total no Reflections	11520	19259	33597
Unique Reflections	7715	10469	11711
Final R indices*	$R_1 = 0.0582$	$R_1 = 0.0686$	$R_1 = 0.0705$
	$wR_2 = 0.1193$	$wR_2 = 0.1211$	$wR_2 = 0.1577$
Largest Diff. peak and hole (e$^-$ A^{-3})	2.490, -2.783	2.490, -2.783	5.248, -3.044

* $[I > 2\sigma(I)]$

2.5 Appendix

2.5.1 NMR Spectra

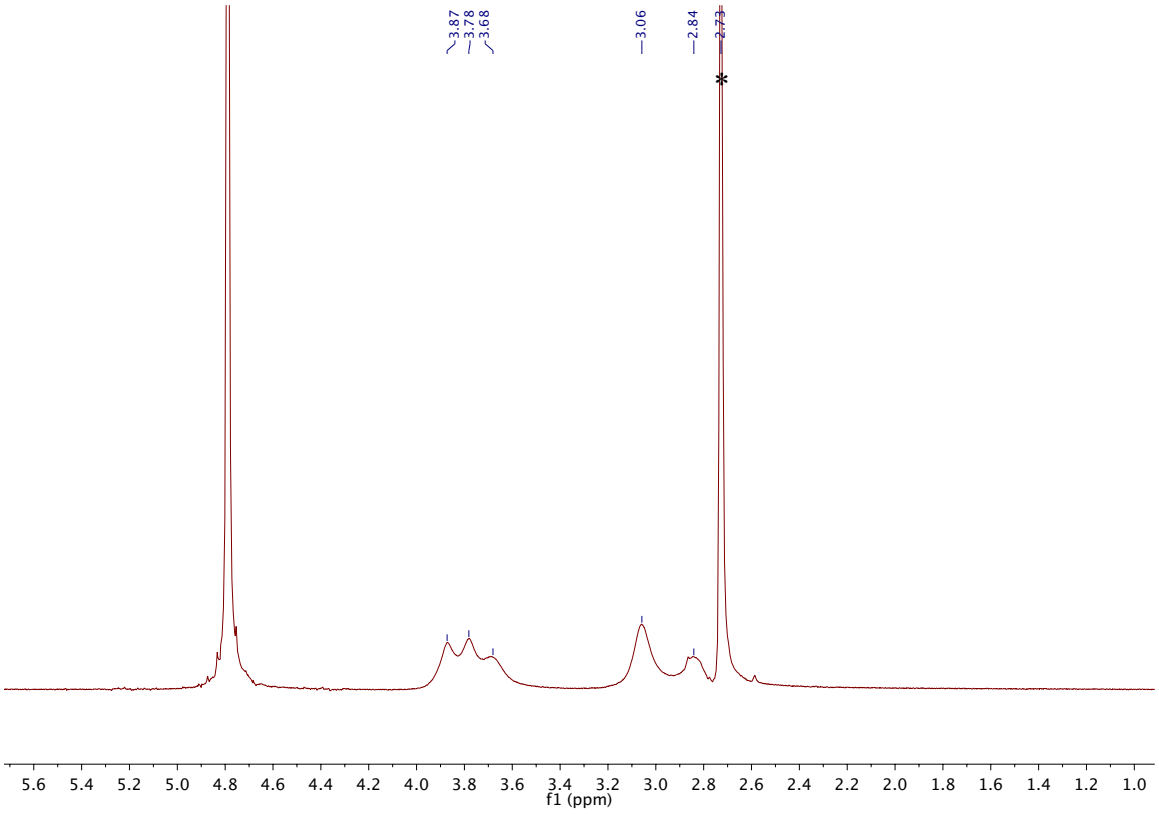

Figure A2.1. ^{1}H NMR spectrum of [Th(κ^{8}-DOTA)(DMSO)] (**2.2**) in D_2O at room temperature. (*) indicates the resonance assignable to dimethyl sulfoxide.

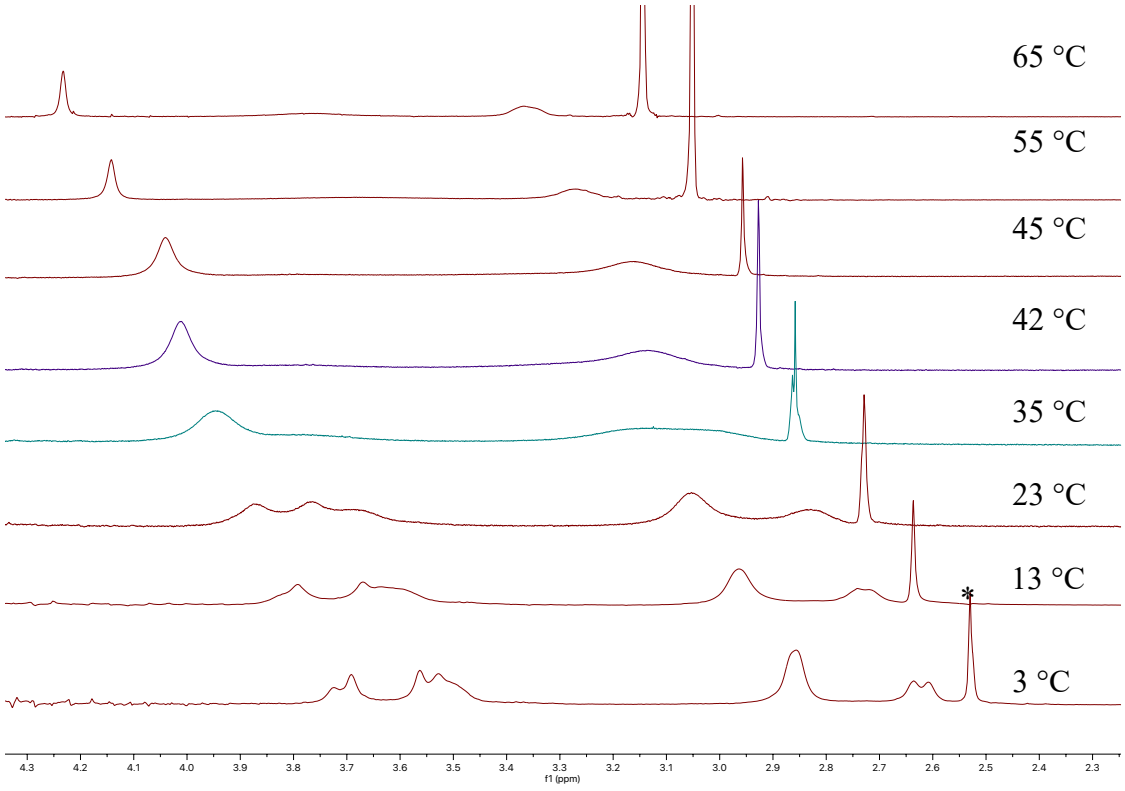

Figure A2.2. Variable temperature ^{1}H NMR spectra of [Th(κ^{8}-DOTA)(DMSO)] (**2.2**) in D_2O from 3 °C (bottom) to 65 °C (top). (*) indicates the resonance assignable to dimethyl sulfoxide.

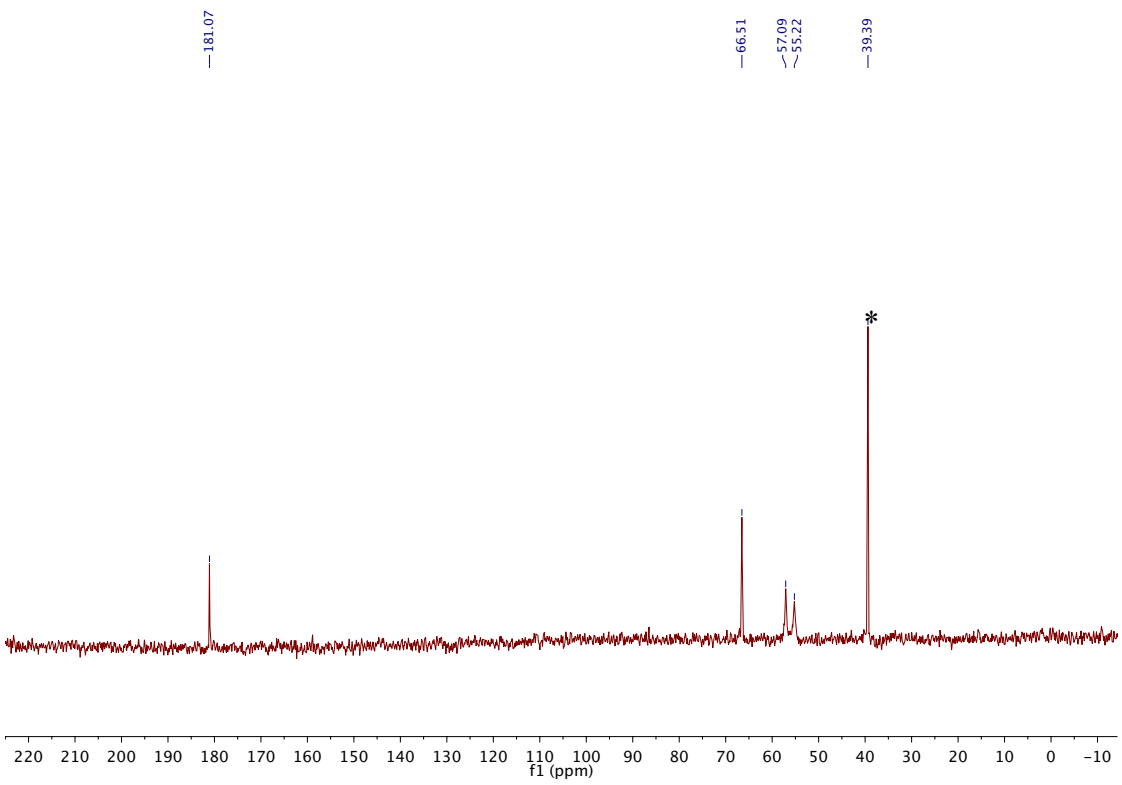

Figure A2.3. $^{13}C\{^{1}H\}$ NMR spectrum of [Th(κ^8-DOTA)(DMSO)] (**2.2**)in D_2O at room temperature (23 °C). (*) indicates the resonance assignable to dimethyl sulfoxide.

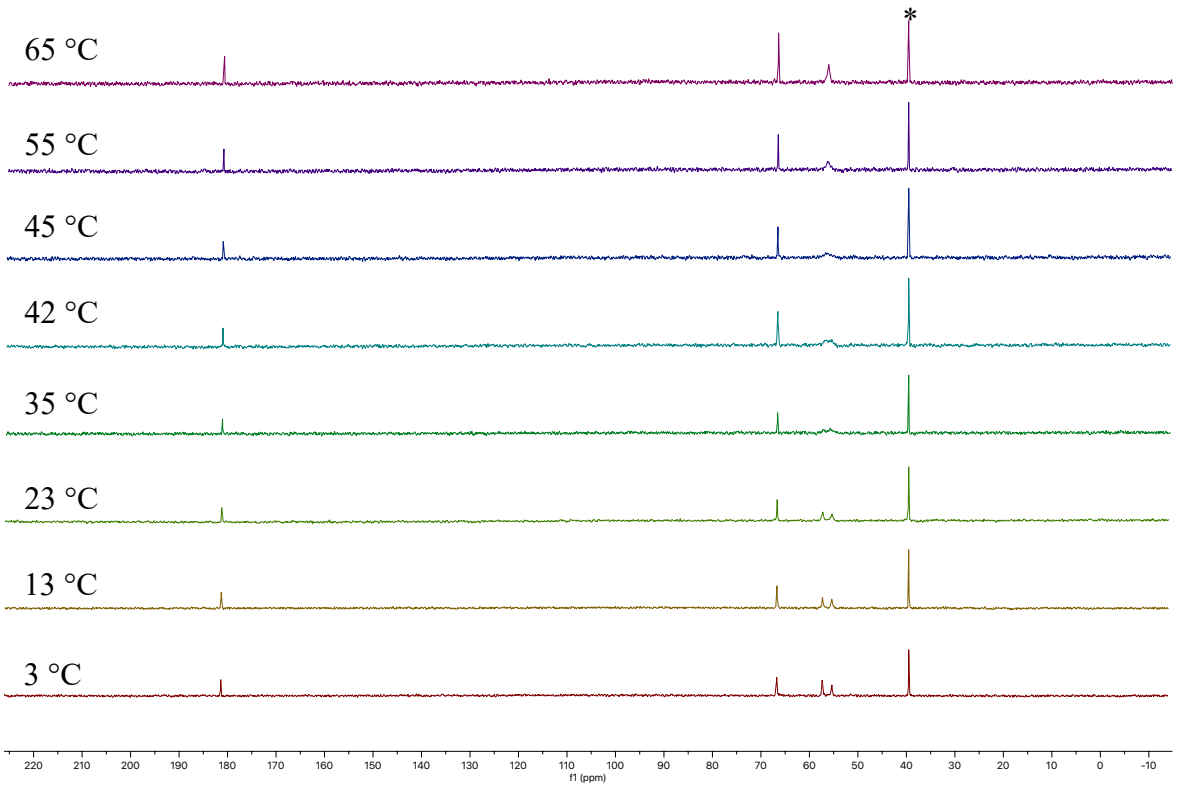

Figure A2.4. Variable temperature $^{13}C\{^{1}H\}$ NMR spectra of [Th(κ^8-DOTA)(DMSO)] (**2.2**) in D_2O from 3 °C (bottom) to 65 °C (top) . (*) indicates the resonance assignable to dimethyl sulfoxide

2.5.2 IR Spectra

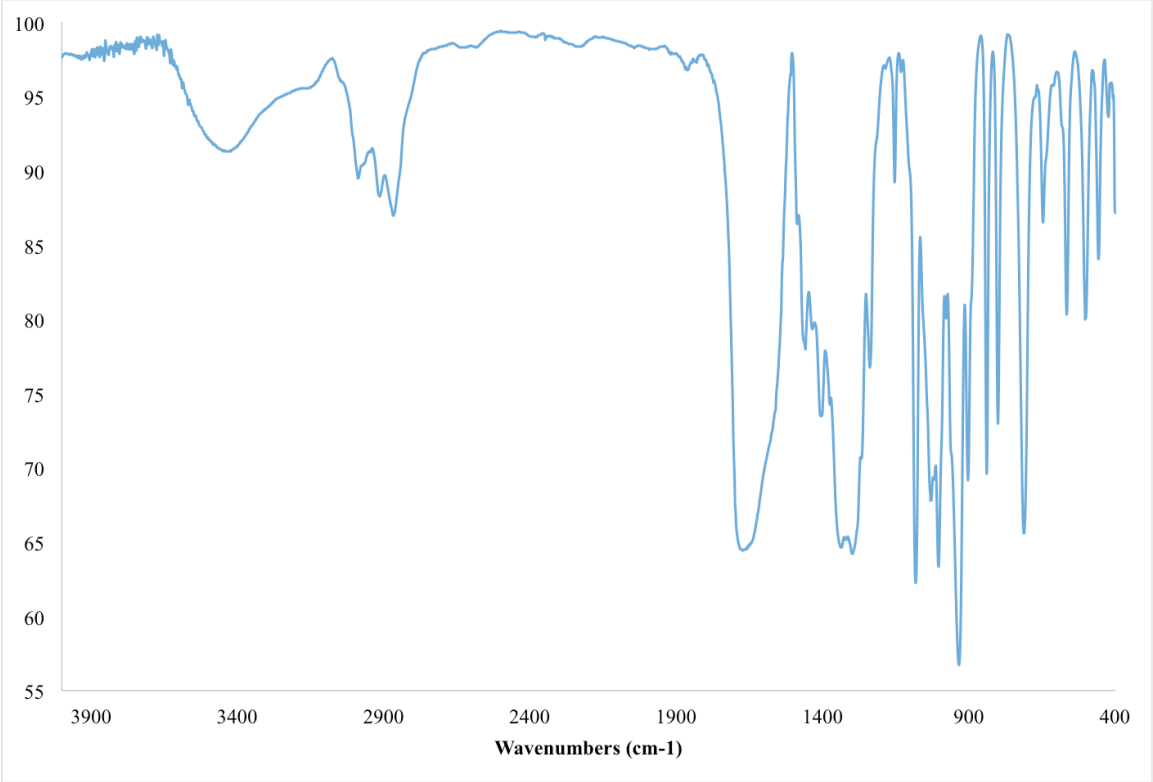

Figure A2.5. IR spectrum of [U(κ^8-DOTA)(DMSO)]·DMSO (**2.1·DMSO**) (KBr Pellet).

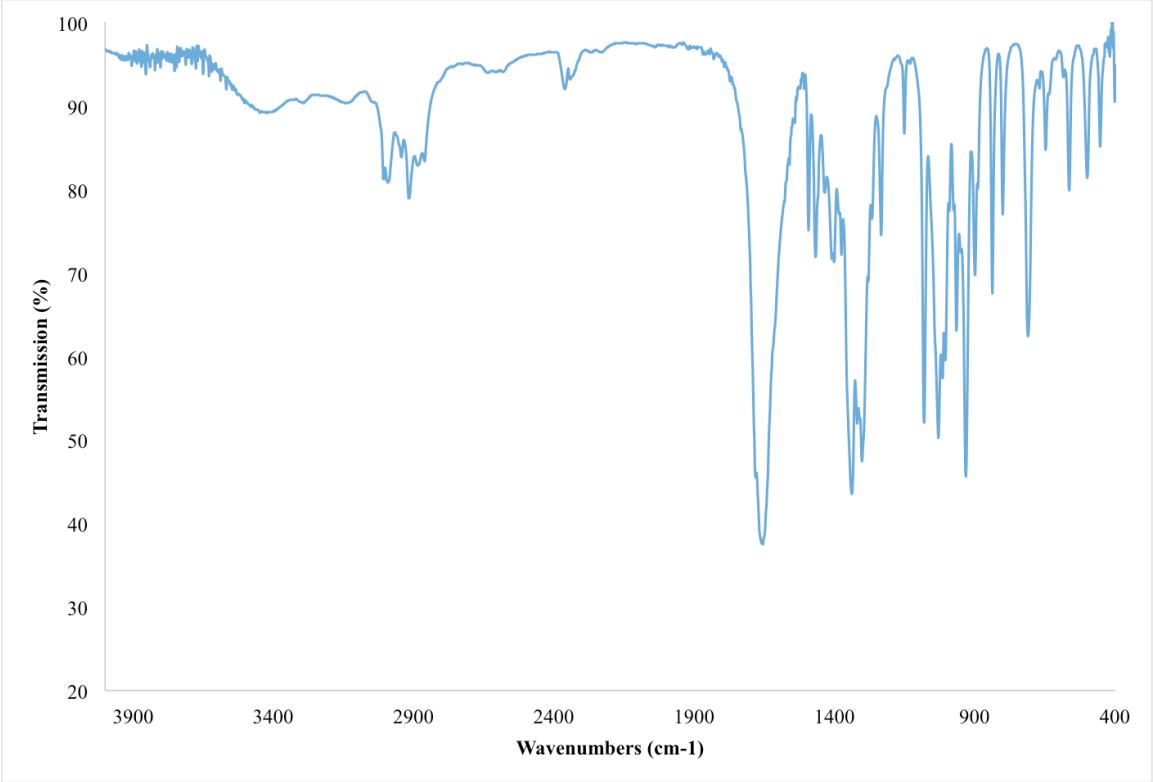

Figure A2.6. IR spectrum of [Th(κ^8-DOTA)(DMSO)]·DMSO (**2.2·DMSO**) (KBr Pellet).

2.5.3 Cyclic Voltammetry

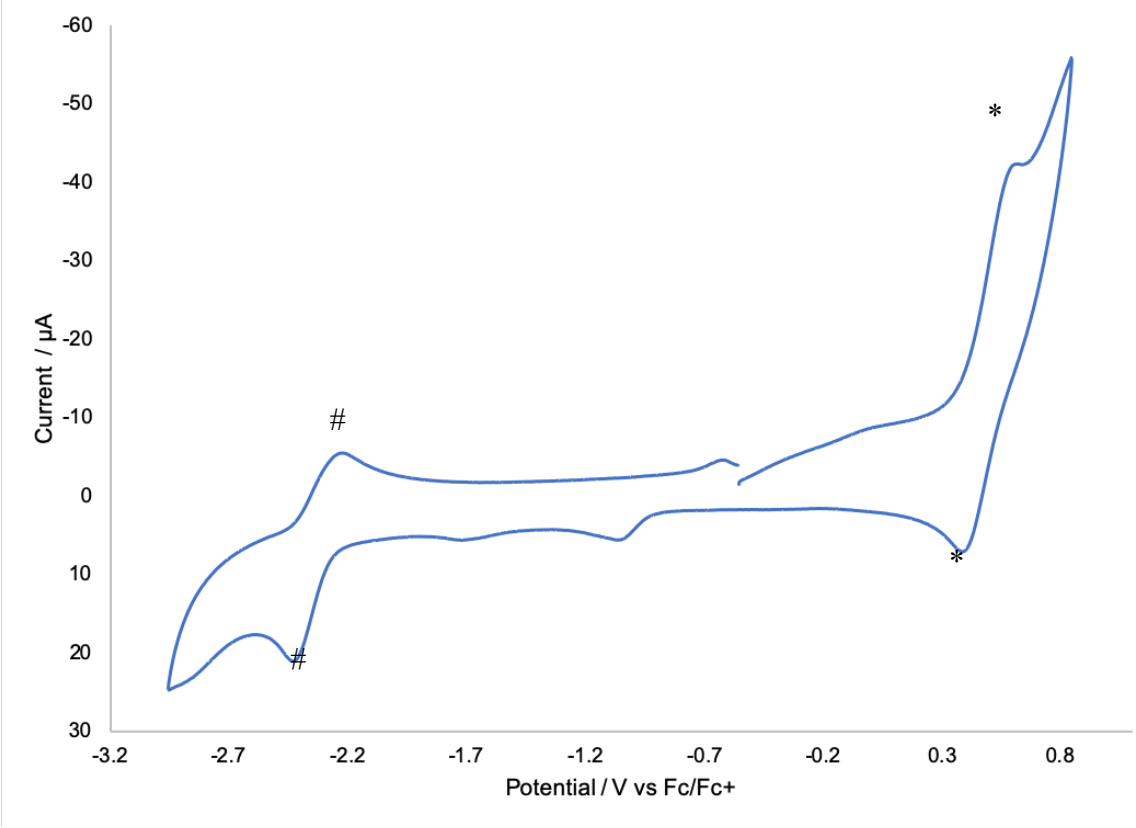

Figure A2.7. Cyclic voltammogram of complex **2.1** (200 mV/s scan rate, vs. Fc/Fc^{+}). Measured in DMSO with 0.1 M $[NBu_4][PF_6]$ as the supporting electrolyte. (*) is assignable to the quasi-reversible U(V)/U(IV) redox feature. (#) is assignable to the reversible U(III)/U(IV) redox feature.

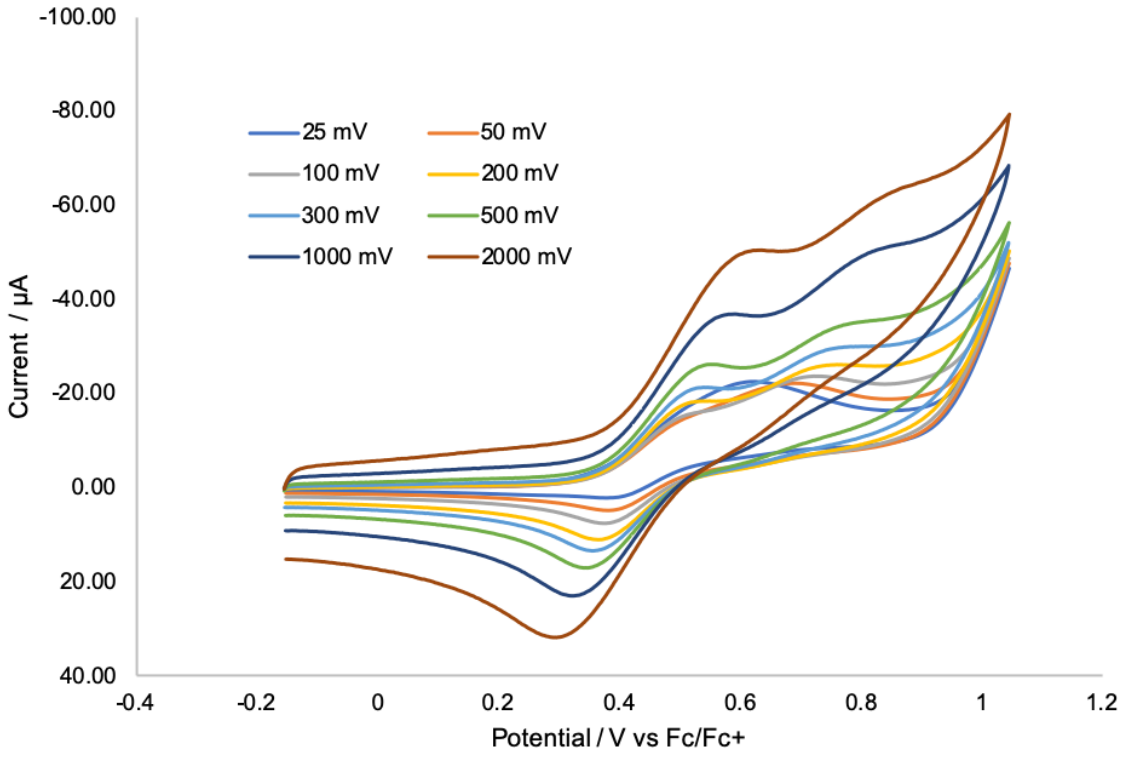

Figure A2.8. Partial cyclic voltammogram of the U(V)/U(IV) redox feature of [U^{IV}(κ^8-DOTA)(DMSO)] (**2.1**) measured in DMSO with 0.1 M [NBu_4][PF_6] as the supporting electrolyte.

Table A2.1. Electrochemical parameters for the U(IV/V) feature of [U^{IV}(κ^8-DOTA)(DMSO)] (**2.1**) in DMSO with 0.1 M [NBu_4][PF_6] as the supporting electrolyte (vs. Fc/Fc^+).

Oxidation Feature	Scan rate, V/s	$E_{p,c}$, V	$E_{p,a}$, V	$\Delta E_p{}^a$	$i_{p,a}/i_{p,c}$
	0.025	0.381	0.549	0.168	2.78
	0.050	0.383	0.480	0.097	1.67
	0.100	0.377	0.488	0.111	1.68
	0.200	0.365	0.501	0.136	1.51
	0.300	0.355	0.512	0.157	1.48
	0.500	0.346	0.520	0.174	1.41
	1.000	0.322	0.542	0.220	1.34
	2.000	0.307	0.578	0.271	1.23

$\Delta E_p{}^a$ is defined as the potential difference between the anodic wave and the cathodic wave generated after the change in sweep direction.

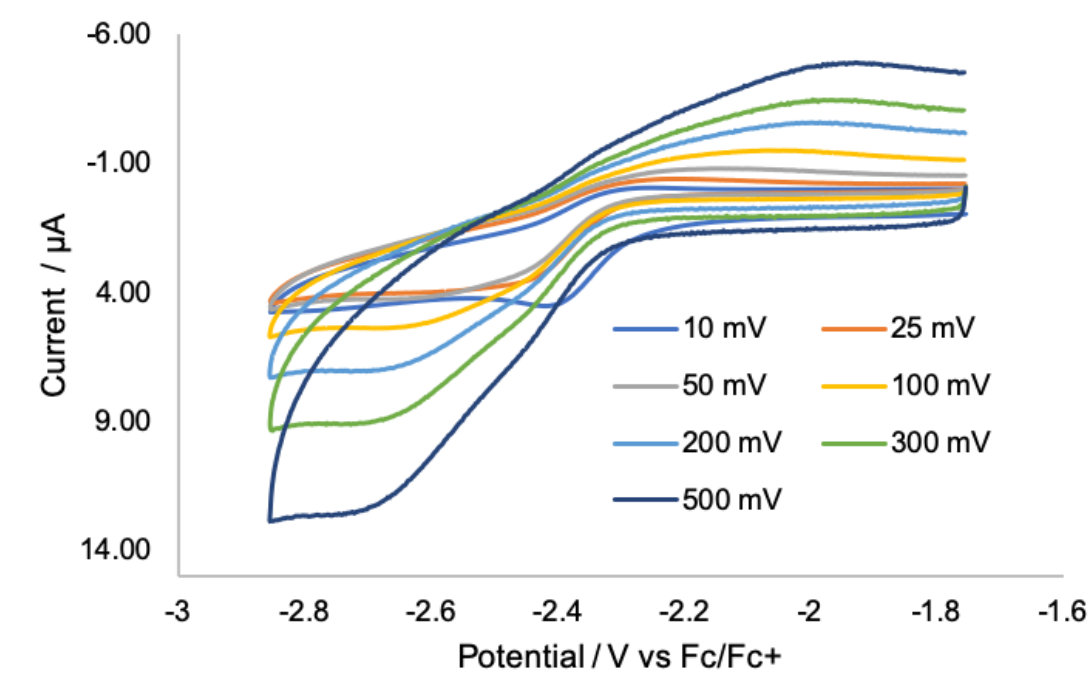

Figure A2.9. Partial cyclic voltammogram of the U(IV)/U(III) redox feature of [U^{IV}(κ^8-DOTA)(DMSO)] (**2.1**) measured in DMSO with 0.1 M [NBu_4][PF_6] as the supporting electrolyte.

Table A2.2. Electrochemical parameters for the U(III/IV) feature of [U^{IV}(κ^8-DOTA)(DMSO)] (**2.1**) in DMSO with 0.1 M [NBu_4][PF_6] as the supporting electrolyte (vs. Fc/Fc^+).

Oxidation Feature	Scan rate, V/s	$E_{p,c}$, V	$E_{p,a}$, V	ΔE_p^a	$i_{p,c}/i_{p,a}$
	0.025	-2.45	-2.31	0.140	2.80
	0.050	-2.53	-2.29	0.234	2.93
	0.100	-2.55	-2.25	0.309	1.67
	0.200	-2.60	-2.12	0.481	1.27
	0.300	-2.63	-2.10	0.523	1.19
	0.500	-2.66	-2.06	0.602	1.01
	1.000	-2.69	-2.02	0.679	1.07
	2.000	-2.75	-1.94	0.812	1.14

ΔE_p^a is defined as the potential difference between the anodic wave and the cathodic wave generated after the change in sweep direction.

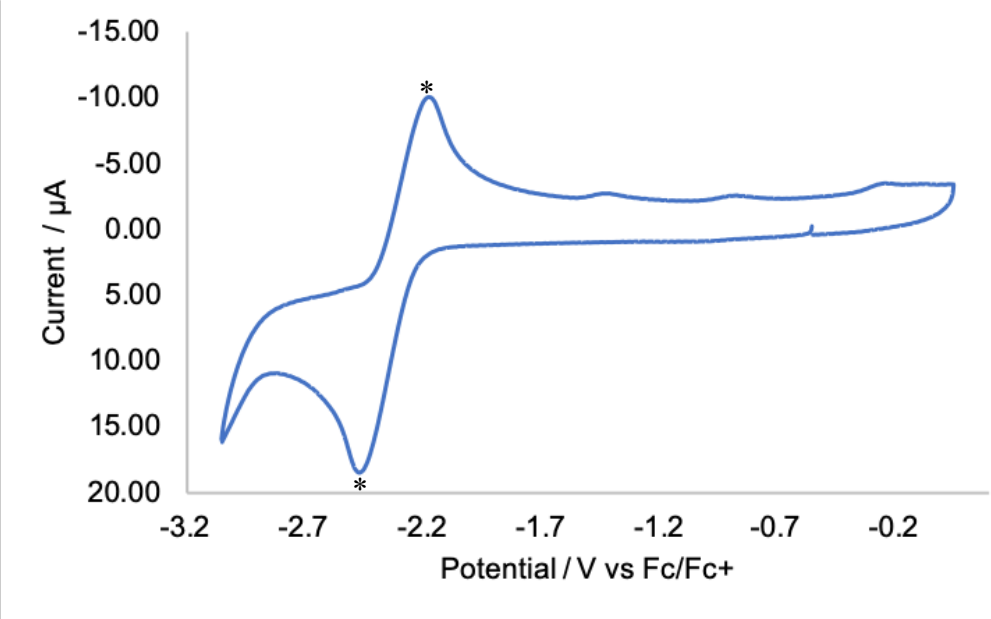

Figure A2.10. Cyclic voltammogram of complex **2.1** (200 mV/s scan rate, vs. Fc/Fc^{+}). Measured in DMSO with 0.1 M $[NBu_4][BPh_4]$ as the supporting electrolyte. (*) is assignable to the reversible U(III)/U(IV) redox feature.

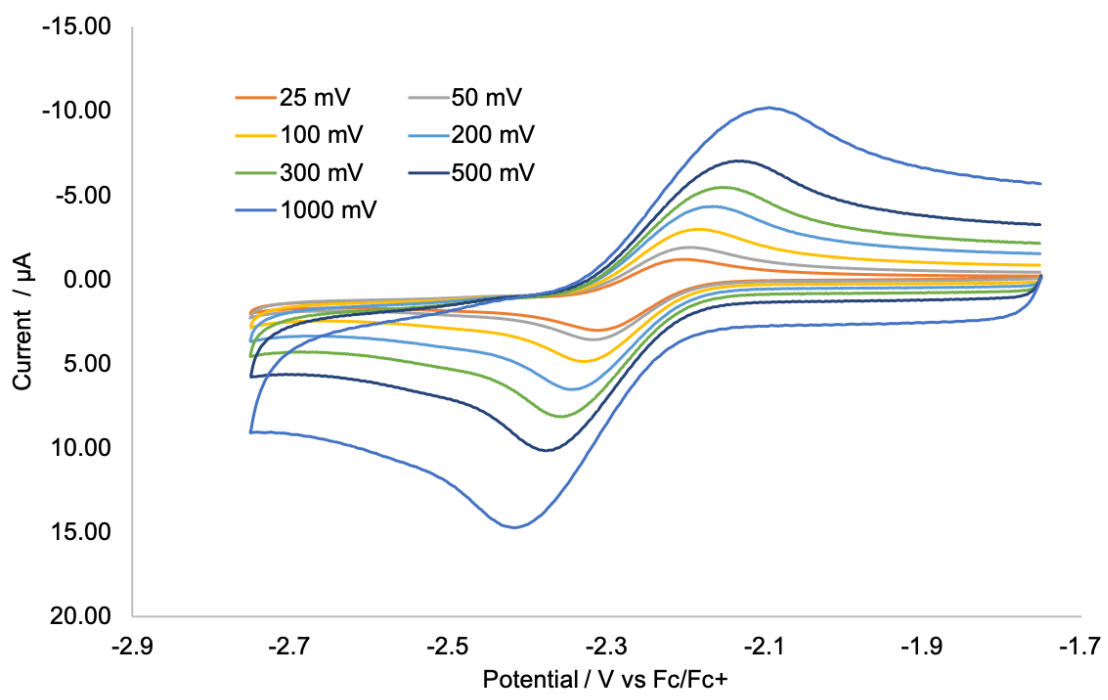

Figure A2.11. Partial cyclic voltammogram of the U(IV)/U(III) redox feature of [U^{IV}(κ^8-DOTA)(DMSO)] (**2.1**) measured in DMSO with 0.1 M [NBu_4][BPh_4] as the supporting electrolyte.

Table A2.3. Electrochemical parameters for the U(III/IV) feature of $[U^{IV}(\kappa^8\text{-DOTA})(DMSO)]$ (**2.1**) in DMSO with 0.1 M $[NBu_4][BPh_4]$ as the supporting electrolyte (vs. Fc/Fc^+).

Oxidation Feature	Scan rate, V/s	$E_{p,c}$, V	$E_{p,a}$, V	$\Delta E_p{}^a$	$i_{p,c}/i_{p,a}$
	0.025	-2.31	-2.21	0.108	1.37
	0.050	-2.32	-2.19	0.125	1.25
	0.100	-2.33	-2.18	0.147	1.21
	0.200	-2.34	-2.17	0.174	1.17
	0.300	-2.36	-2.15	0.202	1.17
	0.500	-2.38	-2.14	0.241	1.25
	1.000	-2.42	-2.11	0.307	1.14
	2.000	-2.47	-2.06	0.407	1.09

$\Delta E_p{}^a$ is defined as the potential difference between the anodic wave and the cathodic wave generated after the change in sweep direction.

2.6 References

1. Viola-Villegas, N.; Doyle, R. P., The coordination chemistry of 1,4,7,10-tetraazacyclododecane-N,N′,N″,N‴-tetraacetic acid (H_4DOTA): Structural overview and analyses on structure–stability relationships. *Coord. Chem. Rev.* **2009**, *253*, 1906-1925.

2. Volkert, W. A.; Hoffman, T. J., Therapeutic Radiopharmaceuticals. *Chem. Rev.* **1999**, *99*, 2269-2292.

3. Kostelnik, T. I.; Orvig, C., Radioactive Main Group and Rare Earth Metals for Imaging and Therapy. *Chem. Rev.* **2019**, *119*, 902-956.

4. Caravan, P.; Ellison, J. J.; McMurry, T. J.; Lauffer, R. B., Gadolinium(III) Chelates as MRI Contrast Agents: Structure, Dynamics, and Applications. *Chem. Rev.* **1999**, *99*, 2293-2352.

5. Wahsner, J.; Gale, E. M.; Rodríguez-Rodríguez, A.; Caravan, P., Chemistry of MRI Contrast Agents: Current Challenges and New Frontiers. *Chem. Rev.* **2019**, *119*, 957-1057.

6. Aime, S.; Botta, M.; Ermondi, G., NMR study of solution structures and dynamics of lanthanide(III) complexes of DOTA. *Inorg. Chem.* **1992**, *31*, 4291-4299.

7. Spirlet, M. R.; Rebizant, J.; Desreux, J. F.; Loncin, M. F., Crystal and molecular structure of sodium aqua(1,4,7,10-tetraazacyclododecane-1,4,7,10-tetraacetato)europate^{III} tetrahydrate $Na^+(EuDOTA{\cdot}H_2O)^-{\cdot}4H_2O$, and its relevance to NMR studies of the conformational behavior of the lanthanide complexes formed by the macrocyclic ligand DOTA. *Inorg. Chem.* **1984**, *23*, 359-363.

8. Sherry, A. D.; Brown, R. D.; Geraldes, C. F. G. C.; Koenig, S. H.; Kuan, K.-T.; Spiller, M., Synthesis and characterization of the gadolinium^{3+} complex of DOTA-propylamide: a model DOTA-protein conjugate. *Inorg. Chem.* **1989**, *28*, 620-622.

9. Magerstädt, M.; Gansow, O. A.; Brechbiel, M. W.; Colcher, D.; Baltzer, L.; Knop, R. H.; Girton, M. E.; Naegele, M., Gd(DOTA): An alternative to Gd(DTPA) as a $T_{1,2}$ relaxation agent for NMR imaging or spectroscopy. *Magn. Reson. Med.* **1986**, *3*, 808-812.

10. Cacheris, W. P.; Nickle, S. K.; Sherry, A. D., Thermodynamic study of lanthanide complexes of 1,4,7-triazacyclononane-N,N',N"-triacetic acid and 1,4,7,10-tetraazacyclododecane-N,N',N",N'"-tetraacetic acid. *Inorg. Chem.* **1987**, *26*, 958-960.

11. McDevitt, M. R.; Ma, D.; Lai, L. T.; Simon, J.; Borchardt, P.; Frank, R. K.; Wu, K.; Pellegrini, V.; Curcio, M. J.; Miederer, M.; Bander, N. H.; Scheinberg, D. A., Tumor Therapy with Targeted Atomic Nanogenerators. *Science* **2001**, *294*, 1537-1540.

12. Miederer, M.; Scheinberg, D. A.; McDevitt, M. R., Realizing the potential of the Actinium-225 radionuclide generator in targeted alpha particle therapy applications. *Adv. Drug Deliv. Rev.* **2008**, *60*, 1371-1382.

13. Thiele, N. A.; Brown, V.; Kelly, J. M.; Amor-Coarasa, A.; Jermilova, U.; MacMillan, S. N.; Nikolopoulou, A.; Ponnala, S.; Ramogida, C. F.; Robertson, A. K. H.; Rodríguez-Rodríguez, C.; Schaffer, P.; Williams, C.; Babich, J. W.; Radchenko, V.;

Wilson, J. J., An Eighteen-Membered Macrocyclic Ligand for Actinium-225 Targeted Alpha Therapy. *Angew. Chem. Int. Ed.* **2017**, *56*, 14712-14717.

14. Deblonde, G. J. P.; Lohrey, T. D.; Booth, C. H.; Carter, K. P.; Parker, B. F.; Larsen, Å.; Smeets, R.; Ryan, O. B.; Cuthbertson, A. S.; Abergel, R. J., Solution Thermodynamics and Kinetics of Metal Complexation with a Hydroxypyridinone Chelator Designed for Thorium-227 Targeted Alpha Therapy. *Inorg. Chem.* **2018**, *57*, 14337-14346.

15. McDevitt, M. R.; Ma, D.; Simon, J.; Frank, R. K.; Scheinberg, D. A., Design and synthesis of ^{225}Ac radioimmunopharmaceuticals. *Appl. Radiat. Isot.* **2002**, *57*, 841-847.

16. Audras, M.; Berthon, L.; Martin, N.; Zorz, N.; Moisy, P., Investigation of actinides(III)-DOTA complexes by electrospray ionization mass spectrometry. *J. Radioanal. Nucl. Chem.* **2015**, *303*, 1897-1909.

17. Audras, M.; Berthon, L.; Berthon, C.; Guillaumont, D.; Dumas, T.; Illy, M.-C.; Martin, N.; Zilbermann, I.; Moiseev, Y.; Ben-Eliyahu, Y.; Bettelheim, A.; Cammelli, S.; Hennig, C.; Moisy, P., Structural Characterization of Am^{III}- and Pu^{III}-DOTA Complexes. *Inorg. Chem.* **2017**, *56*, 12248-12259.

18. Thakur, P.; Conca, J. L.; Choppin, G. R., Complexation studies of Cm(III), Am(III), and Eu(III) with linear and cyclic carboxylates and polyaminocarboxylates. *J. Coord. Chem.* **2011**, *64*, 3214-3236.

19. Jacques, V.; Desreux, J. F., Kinetically and thermodynamically stable isomers of thorium chelates of polyaza polycarboxylic macrocycles. *J. Alloys Compd.* **1994**, *213-214*, 286-289.

20. Tamain, C.; Dumas, T.; Hennig, C.; Guilbaud, P., Coordination of Tetravalent Actinides (An=Th^{IV}, U^{IV}, Np^{IV}, Pu^{IV}) with DOTA: From Dimers to Hexamers. *Chem. – Eur. J.* **2017**, *23*, 6864-6875.

21. Thuéry, P., The first crystal structure of an actinide complex of the macrocyclic ligand DOTA: a two-dimensional uranyl–organic framework. *CrystEngComm* **2008**, *10*, 808-810.

22. Dovrat, G.; Illy, M.-C.; Berthon, C.; Lerner, A.; Mintz, M. H.; Maimon, E.; Vainer, R.; Ben-Eliyahu, Y.; Moiseev, Y.; Moisy, P.; Bettelheim, A.; Zilbermann, I., On the Aqueous Chemistry of the U^{IV}–DOTA Complex. *Chem. Eur. J.* **2020**, *26*, 3390-3403.

23. Moreau, J.; Guillon, E.; Pierrard, J.-C.; Rimbault, J.; Port, M.; Aplincourt, M., Complexing Mechanism of the Lanthanide Cations Eu^{3+}, Gd^{3+}, and Tb^{3+} with 1,4,7,10-Tetrakis(carboxymethyl)-1,4,7,10-tetraazacyclododecane (dota)—Characterization of Three Successive Complexing Phases: Study of the Thermodynamic and Structural Properties of the Complexes by Potentiometry, Luminescence Spectroscopy, and EXAFS. *Chem. – Eur. J.* **2004**, *10*, 5218-5232.

24. Natrajan, L. S., The first structural and spectroscopic study of a paramagnetic 5f DO3A complex. *J. Chem. Soc., Dalton Trans.* **2012**, *41*, 13167-13172.

25. Pandya, D. N.; Bhatt, N.; Yuan, H.; Day, C. S.; Ehrmann, B. M.; Wright, M.; Bierbach, U.; Wadas, T. J., Zirconium tetraazamacrocycle complexes display extraordinary

stability and provide a new strategy for zirconium-89-based radiopharmaceutical development. *Chem. Sci.* **2017**, *8*, 2309-2314.

26. Desreux, J. F., Nuclear magnetic resonance spectroscopy of lanthanide complexes with a tetraacetic tetraaza macrocycle. Unusual conformation properties. *Inorg. Chem.* **1980**, *19*, 1319-1324.

27. Kost, D.; Carlson, E. H.; Raban, M., The validity of approximate equations for k_c in dynamic nuclear magnetic resonance. *J. Chem. Soc. D* **1971**, 656-657.

28. Blahut, J.; Hermann, P.; Tošner, Z.; Platas-Iglesias, C., A combined NMR and DFT study of conformational dynamics in lanthanide complexes of macrocyclic DOTA-like ligands. *Phys. Chem. Chem. Phys.* **2017**, *19*, 26662-26671.

29. Bard, A. J.; Parsons, R.; Jordan, J.; International Union of, P.; Applied, C.; International Association of Chemical, S., *Standard potentials in aqueous solution*. 1st ed.. ed.; New York : M. Dekker: New York, 1985.

30. Bratsch, S. G., Standard Electrode Potentials and Temperature Coefficients in Water at 298.15 K. *J. Phys. Chem. Ref. Data* **1989**, *18*, 1-21.

31. Deblonde, G. J. P.; Sturzbecher-Hoehne, M.; Rupert, P. B.; An, D. D.; Illy, M.-C.; Ralston, C. Y.; Brabec, J.; de Jong, W. A.; Strong, R. K.; Abergel, R. J., Chelation and stabilization of berkelium in oxidation state +IV. *Nat. Chem.* **2017**, *9*, 843–849.

32. Wu, S. L.; Horrocks, W. D., Kinetics of Complex Formation by Macrocyclic Polyaza Polycarboxylate Ligands: Detection and Characterization of an Intermediate in the Eu^{3+}-dota System by Laser-Excited Luminescence. *Inorg. Chem.* **1995**, *34*, 3724-3732.

33. Burai, L.; Fábián, I.; Király, R.; Szilágyi, E.; Brücher, E., Equilibrium and kinetic studies on the formation of the lanthanide(III) complexes, $[Ce(dota)]^-$ and $[Yb(dota)]^-$ (H_4dota = 1,4,7,10-tetraazacyclododecane-1,4,7,10-tetraacetic acid). *J. Chem. Soc., Dalton Trans.* **1998**, *0*, 243-248.

34. Brücher, E.; Laurenczy, G.; Makra, Z. S., Studies on the kinetics of formation and dissociation of the cerium(III)-DOTA complex. *Inorg. Chim. Acta* **1987**, *139*, 141-142.

35. Jang, Y. H.; Blanco, M.; Dasgupta, S.; Keire, D. A.; Shively, J. E.; Goddard, W. A., Mechanism and Energetics for Complexation of ^{90}Y with 1,4,7,10-Tetraazacyclododecane-1,4,7,10-tetraacetic Acid (DOTA), a Model for Cancer Radioimmunotherapy. *J. Am. Chem. Soc.* **1999**, *121*, 6142-6151.

36. Stenson, P. A.; Thompson, A. L.; Parker, D., Structural characterisation of a diprotonated ligand lanthanide complex—a key intermediate in lanthanide ion association and complex dissociation pathways. *J. Chem. Soc., Dalton Trans.* **2006**, 3291-3293.

37. Šimeček, J.; Hermann, P.; Havlíčková, J.; Herdtweck, E.; Kapp, T. G.; Engelbogen, N.; Kessler, H.; Wester, H.-J.; Notni, J., A Cyclen-Based Tetraphosphinate Chelator for the Preparation of Radiolabeled Tetrameric Bioconjugates. *Chem. – Eur. J.* **2013**, *19*, 7748-7757.

38. Pham, T. A.; Xu, J.; Raymond, K. N., A Macrocyclic Chelator with Unprecedented Th^{4+} Affinity. *J. Am. Chem. Soc.* **2014**, *136*, 9106-9115.

39. Pham, T. A.; Altman, A. B.; Stieber, S. C. E.; Booth, C. H.; Kozimor, S. A.; Lukens, W. W.; Olive, D. T.; Tyliszczak, T.; Wang, J.; Minasian, S. G.; Raymond, K. N., A Macrocyclic Chelator That Selectively Binds Ln^{4+} over Ln^{3+} by a Factor of 10^{29}. *Inorg. Chem.* **2016**, *55*, 9989-10002.

40. Kiplinger, J. L.; Morris, D. E.; Scott, B. L.; Burns, C. J., Convenient Synthesis, Structure, and Reactivity of $(C_5Me_5)U(CH_2C_6H_5)_3$: A Simple Strategy for the Preparation of Monopentamethylcyclopentadienyl Uranium(IV) Complexes. *Organometallics* **2002**, *21*, 5978-5982.

41. Cantat, T.; Scott, B. L.; Kiplinger, J. L., Convenient access to the anhydrous thorium tetrachloride complexes $ThCl_4(DME)_2$, $ThCl_4(1,4\text{-dioxane})_2$ and $ThCl_4(THF)_{3.5}$ using commercially available and inexpensive starting materials. *Chem. Commun.* **2010**, *46*, 919-921.

42. Harris, R. K.; Becker, E. D.; De Menezes, S. M. C.; Granger, P.; Hoffman, R. E.; Zilm, K. W., Further Conventions for NMR Shielding and Chemical Shifts (IUPAC Recommendations 2008). *Magn. Reson. Chem.* **2008**, *46*, 582-598.

43. Harris, R. K.; Becker, E. D.; Cabral de Menezes, S. M.; Goodfellow, R.; Granger, P., NMR nomenclature: nuclear spin properties and conventions for chemical shifts. IUPAC Recommendations 2001. International Union of Pure and Applied Chemistry. Physical Chemistry Division. Commission on Molecular Structure and Spectroscopy. *Magn. Reson. Chem.* **2002**, *40*, 489-505.

44. *SMART Apex II*, Version 2.1 ed.; Bruker AXS Inc.: Madison WI, 2005.

45. *SAINT Software User's Guide*, Version 7.34a ed.; Bruker AXS Inc.: Madison, WI, 2005.

46. Sheldrick, G. M., *SADABS*, the Siemens Area Detector Absorption Correction; University of Göttingen: Göttingen, Germany, 2005.

47. *SHELXTL PC*, Version 6.12 ed.; Bruker AXS Inc.:Madison, WI, 2005.

Chapter 3. Coordination of Uranyl to the Redox-Active Calix[4]pyrrole Ligand

Portions of this work were published in:

Greggory T. Kent, Jesse Murillo, Guang Wu, Skye Fortier, Trevor W. Hayton. Coordination of Uranyl to the Redox-Active Calix[4]pyrrole Ligand. *Inorg. Chem.* **2020**, 59, 8629–8634.

3.1 Introduction

The ability to manipulate the uranyl ($U^{VI}O_2^{2+}$) oxidation state has potential use in nuclear fuel processing, immobilization of uranyl contamination in groundwater, and uranium extraction from seawater.[1-6] Control of actinyl redox also has implications for the SANHEX process, which has been proposed as a method to separate Am and Cm from spent fuel.[7, 8] Because of these potential applications, the redox chemistry of uranyl has come under increased scrutiny in recent years.[9, 10] For example, in 2008 the Hayton group reported the formation of $[U^{V}O_2(Ar_2nacnac)(Ph_2MePO)_2]$ ($Ar_2nacnac$ = (2,6-$^{i}Pr_2C_6H_3$)*N*C(Me)CHC(Me)*N*(2,6-$^{i}Pr_2C_6H_3$)) by reduction of $[U^{VI}O_2(Ar_2nacnac)(Ph_2MePO)_2][OTf]$ with Cp_2Co.[11] In this case, they argued that the normally unstable $U^{V}O_2^{+}$ ion was stabilized by the coordination of the strongly donating and sterically bulky $Ar_2nacnac$ ligand to the uranyl equatorial plane. Similarly, Mazzanti reported that reduction of $[U^{VI}O_2(dpaea)]$ ($dpaeaH_2$ = bis(pyridyl-6-methyl-2-carboxylate)-ethylamine) with Cp^*_2Co lead to formation of water-stable $[Cp^*_2Co][U^{V}O_2(dpaea)]$.[12] Another means of uranyl reduction, developed by us and others,[13-25] is 'reductive silylation'.[17, 18] This technique has emerged as a reliable and general method for converting UO_2^{2+} to U^{5+} in non-aqueous environments – a transformation that is normally quite challenging.[10]

More recently, Bart and co-workers have shown that redox-active ligands can also mediate uranyl reduction and functionalization.[25-28] For example, treatment of the uranyl iminosemiquinone complex, $[(^{dipp}isq)_2U^{VI}O_2(THF)]$ (^{dipp}iq = 4,6-di-*tert*-butyl-2-[(2,6-diisopropylphenyl)imino]quinone) with pivaloyl chloride results in isolation of the U(IV)

chloro complex, $[(^{dipp}iq)_2U^{IV}Cl_4]$, along with pivalic anhydride.[29] In this example, the 2 electrons required to convert U(VI) to U(IV) come from the iminosemiquinone ligand, which is converted to its neutral quinone form during the transformation. Similarly, Dr. Mikiyas Assefa reported that reaction of K_2(tmtaa) (tmtaaH_2 = dibenzotetramethyltetraaza[14]annulene) with $[U^{VI}O_2Cl_2(THF)_2]_2$ resulted in formation of the $2e^-$ oxidation products of $(tmtaa)^{2-}$ (Scheme 3.1).[30] Also formed in the reaction is the reduced uranium oxide, U_4O_9. In this case, Dr. Assefa hypothesized that the reaction products were formed upon decomposition of the unobserved *cis*-uranyl intermediate, *cis*-$[U^{VI}O_2$(tmtaa)], which undergoes a facile intramolecular redox reaction. However, the hypothesized *cis*-uranyl intermediate has yet to be observed, which has limited the understanding of the role that uranyl structural changes play in mediating this redox chemistry. Moreover, this method of uranyl manipulation is still restricted to only a handful examples.[30-32]

Scheme 3.1. Oxidation of $[tmtaa]^{2-}$ via the proposed *cis*-uranyl intermediate, *cis*-$[U^{VI}O_2$(tmtaa)]

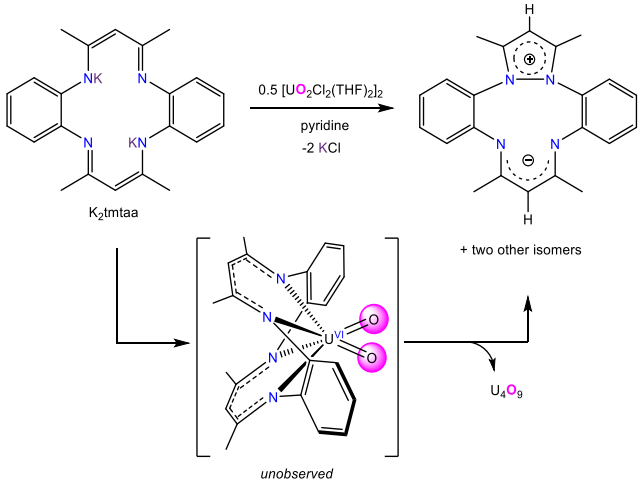

In an effort to further develop this under-explored method of uranyl redox manipulation, I endeavored to study the ligation of other redox-active macrocycles to the uranyl ion. In this regard, the [calix[4]pyrrole]$^{4-}$ family of porphyrinogen macrocycles may be suitable candidates.[33, 34] This ligand framework can exist in three different oxidation states, $[L]^{4-}$, $[L^{\Delta}]^{2-}$, and $L^{\Delta\Delta}$ (L = [Me$_8$-calix[4]pyrrole]$^{x-}$) (Chart 3.1).[33-36] Moreover, these three states can be reversibly interconverted via chemical and electrochemical methods.[34] Given these past results, I hypothesized that ligation of $[L]^{4-}$ to uranyl would also result in metal reduction,[37, 38] concomitant with ligand oxidation.

Chart 3.1. Chemical structures of $[L]^{4-}$, $[L^{\Delta}]^{2-}$, and $L^{\Delta\Delta}$

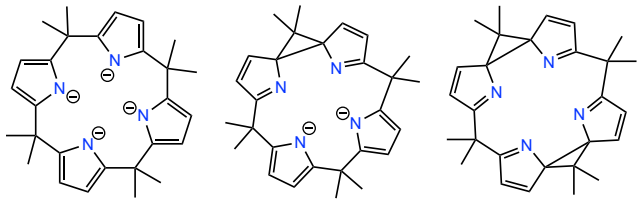

3.2 Results and discussion

Addition of 2 equiv of [Li(THF)]$_4$[L], as a colorless THF solution, to a THF solution of $[U^{VI}O_2Cl_2(THF)_2]_2$ results in an immediate color change from yellow to deep brown. Work-up of the reaction mixture results in isolation of $[Li(THF)]_2[L^{\Delta}]$ (**3.1**) as orange blocks in 40% yield. Also formed in the reaction is a deep brown powder, which is likely uranium(IV) oxide on the basis of Dr. Assefa's past results with the $(tmtaa)^{2-}$ ligand (Scheme 3.2).[30] Complex **3.1** is the product of the 2e$^-$ oxidation of $[calix[4]pyrrole]^{4-}$ by $[U^{VI}O_2Cl_2(THF)_2]_2$. As Dr. Mikiyas Assefa hypothesized for his tmtaa chemistry,[30] I suggest that the reduction of uranyl to UO_2 proceeds via an unobserved, highly oxidizing *cis*-uranyl intermediate $[Li]_2[cis$-

$U^{VI}O_2$(calix[4]pyrrole)], which subsequently oxidizes the [calix[4]pyrrole]$^{4-}$ ligand. Similar results are observed upon reaction of $[Li(THF)]_4[L]$ with $[U^{VI}O_2Cl_2(Ph_3PO)_2]$ (see further discussion below).

Scheme 3.2. Oxidation of $[Li(THF)]_4[L]$ with $[U^{VI}O_2Cl_2(THF)_2]_2$ or I_2

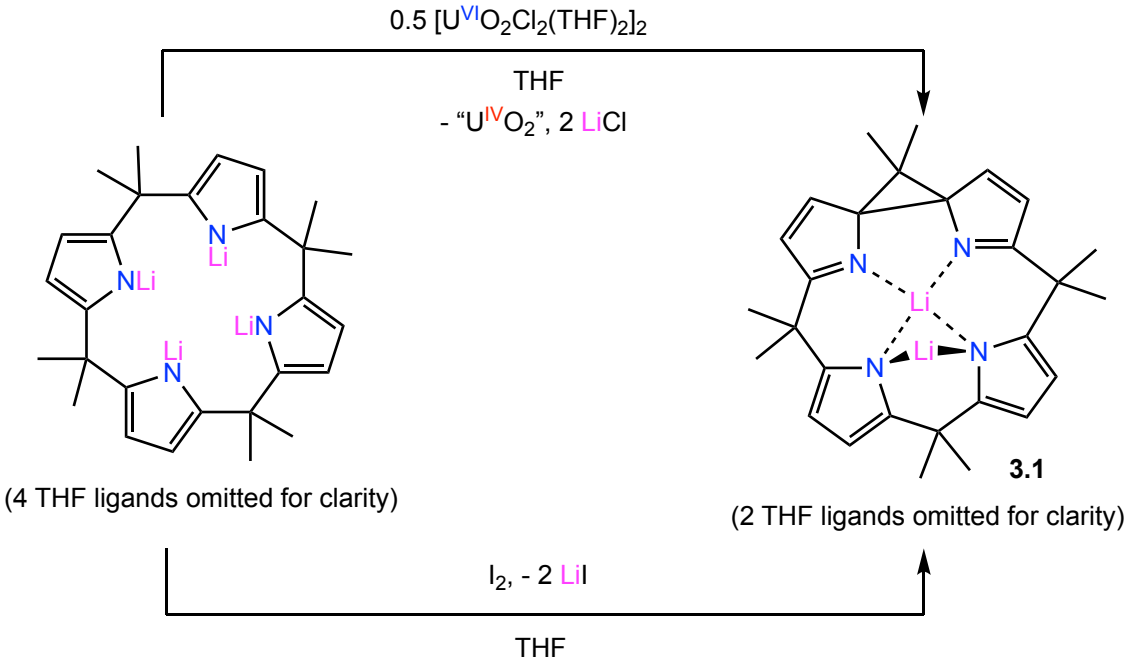

X-ray quality crystals of **3.1** were grown by storage of a concentrated Et_2O solution for 24 h at -25 °C. When grown in this fashion, one of the coordinated THF molecules is partially replaced with a diethyl ether molecule, generating a material with the formula $[Li(THF)][Li(THF)_{0.58}(Et_2O)_{0.42}][L^A]\cdot 0.5Et_2O$ (Figure 3.1). Its solid-state molecular structure reveals the formation of a new carbon-carbon bond between two pyrrole rings (C15-C14 = 1.591(5) Å), resulting in the generation of a cyclopropyl ring. This structural change is further evidenced by the contraction of the oxidized dipyrrole subunit N-N distance (N3-N4 = 2.702(4) Å) relative to the reduced dipyrrole subunit N-N distance (N1-N2 = 2.887(4) Å). The oxidation

state is further confirmed by the presence of only two lithium cations in the solid state structure. One lithium cation is found in the inner cavity of the ring, bound to all four pyrrole nitrogen atoms and one molecule of THF, while the other lithium cation is found outside of the inner cavity and bound to two nitrogen atoms. Its third coordination site is occupied by a mixture of THF and Et_2O. The metrical parameters of **3.1** are in good agreement with those reported for other oxidized calix ligands, such as $[Li]_2[L'^{\Delta}]$ (L′ = Et_8-calix[4]pyrrole, i.e., the octaethyl-substituted analogue of the calix[4]pyrrole ligand)[35] and $[L^{\Delta}Zn]$.[34]

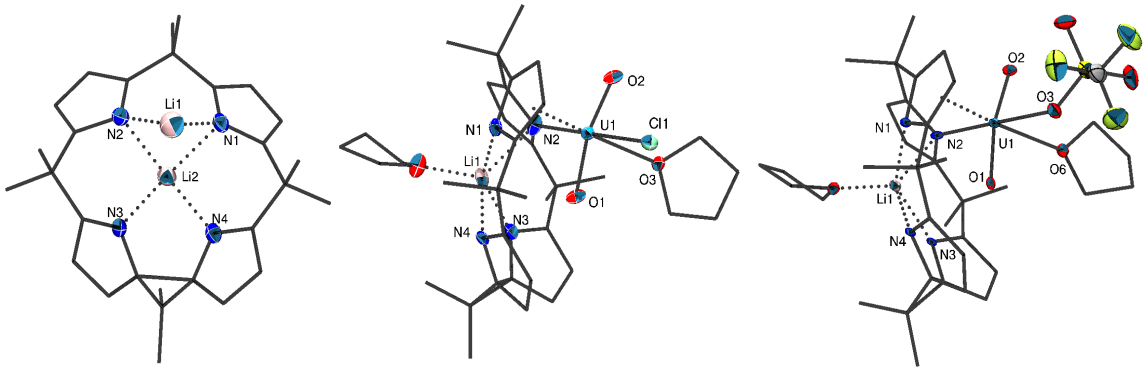

Figure 3.1. Solid state molecular structures of complexes $[Li(THF)][Li(THF)_{0.58}(Et_2O)_{0.42}][L^{\Delta}]\cdot 0.5Et_2O$ (**3.1**, left), $[Li(THF)][U^{VI}O_2(L^{\Delta})Cl(THF)]\cdot C_7H_8$ (**3.2**$\cdot C_7H_8$, middle), and $[Li(THF)][U^{VI}O_2(L^{\Delta})(OTf)(THF)]$ (**3.3**, right), respectively, with 50% probability ellipsoids shown for non-carbon atoms. Hydrogen atoms, solvate molecules, and coordinated Et_2O/THF molecules in $[Li(THF)][Li(THF)_{0.58}(Et_2O)_{0.42}][L^{\Delta}]\cdot 0.5Et_2O$ omitted for clarity.

Complex **3.1** can also be accessed by reaction of $[Li(THF)]_4[L]$ with 1 equiv of I_2 in THF (Scheme 3.2). When synthesized in this fashion it can be isolated in 73% yield after work-up. Its ^1H NMR spectrum in THF-d_8 at -60 °C features four pyrrole and six methyl environments,

consistent with the C_s symmetry observed in the solid state (Figure A3.2). Curiously, upon warming to room temperature the six methyl resonances coalesce into three broad, overlapping resonances, suggesting that the saddle structure of **3.1** undergoes rapid inversion at room temperature (Figure A3.1). Finally, the room temperature $^{7}Li\{^{1}H\}$ NMR spectrum of **3.1** exhibits two broad resonances at 0.79 and -1.09 ppm, in a 1:1 ratio, which is also consistent with the solid state structure (Figure A3.4).

In an effort to isolate a model structure of the proposed $[Li]_2[cis\text{-}U^{VI}O_2(\text{calix[4]pyrrole})]$ intermediate, I explored the ligation of **3.1** to the uranyl fragment. I rationalize that, despite its increased rigidity due to the presence of the cyclopropyl ring, it should still be capable of binding to uranyl, and also provide a good approximation of the $[\text{calix[4]pyrrole}]^{4-}$ coordination environment. Moreover, because of its reduced oxidation potential relative to $[Li(THF)]_4[L]$,[34] I should not observe further uranyl redox chemistry. Thus, reaction of $[U^{VI}O_2Cl_2(THF)_2]_2$ with 2 equiv of **3.1**, in THF at -25 °C, quickly results in a color change from yellow to deep green (Scheme 3.3). Work-up of the reaction mixture, followed by crystallization from hexanes/toluene affords $[Li(THF)][U^{VI}O_2(L^{\Delta})Cl(THF)]$ (**3.2**), as deep green needles in 49% yield. Similarly, reaction of $[U^{VI}O_2(OTf)_2(THF)_3]$ with **3.1** in THF and at -25 °C, quickly results in a color change from yellow to deep green. Work-up of the reaction mixture, followed by crystallization from THF, affords the analogous triflate complex, $[Li(THF)][U^{VI}O_2(L^{\Delta})(OTf)(THF)]$ (**3.3**), as deep green needles in 30% yield (Scheme 3.3). I attribute the lower yield of **3.3** to the formation of the fully oxidized calix fragment, $L^{\Delta\Delta}$, which I observe in the ^{1}H NMR spectra of the crude reaction mixtures (Figure A3.15).[34] The oxidation of $[L^{\Delta}]^{2-}$ to $L^{\Delta\Delta}$ during the reaction suggests that $[U^{VI}O_2(OTf)_2(THF)_3]$ is a better oxidant than

$[U^{VI}O_2Cl_2(THF)_2]_2$, which consistent with weaker donor ability of $[OTf]^-$ vs. $[Cl]^-$. Consistent with this hypothesis, $L^{\Delta\Delta}$ is not observed in crude reaction mixtures of **3.2**.

Scheme 3.3. Synthesis of Complexes **3.2** and **3.3**

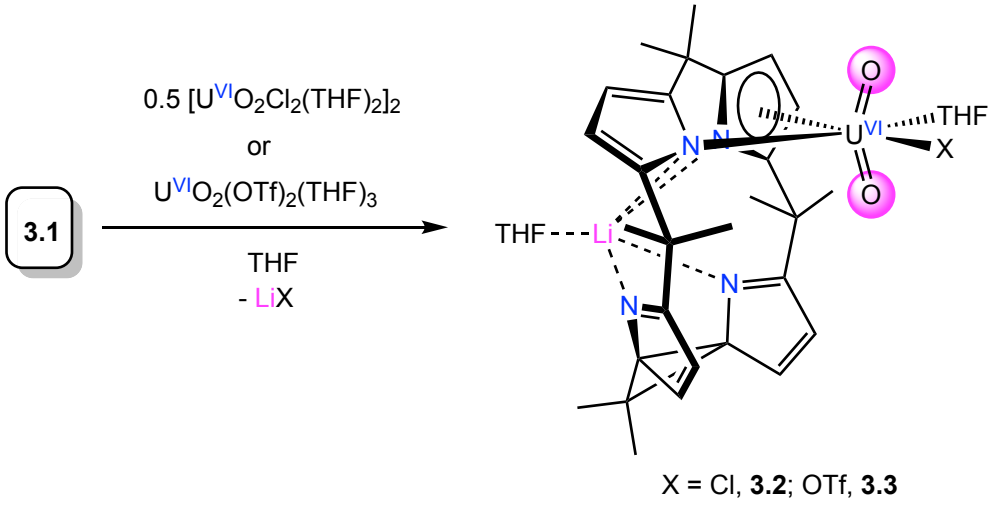

X = Cl, **3.2**; OTf, **3.3**

Complex **3.2** crystallizes in the triclinic space group *P*-1 as the toluene solvate, **3.2**·C_7H_8, with two independent molecules in the asymmetric unit, while complex **3.3** crystallizes in the monoclinic space group $P2_1/n$ (Figure 3.1). Due to poor crystal quality complex **3.3**'s solid state structure was determined using a Bruker Kappa Apex III instrument at the University of Texas at El Paso by Drs. Fortier and Murillo . Complexes **3.2** and **3.3** are isostructural: both feature distorted octahedral geometries about the uranium center; however, **3.3** bears an κ^1-triflate group in place of the chloride ligand in **3.2**. The calix ligand in both complexes features a mixed η^1/η^5-binding mode to uranium, wherein the calix ligand binds to uranium via one pyrrole ring in an η^1-fashion and a second pyrrole ring in an η^5-fashion. A similar mixed-hapticity binding mode was observed in the U(III) complex, [(Et_8-calix[4] pyrrole)U^{III}(dme)][K(dme)].[39] Complexes **3.2** and **3.3** have U-centroid distances of 2.54(1)

(U1-C4 = 2.716(19), U1-N1 = 2.771(16), U1-C3 = 2.836(18),U1-C1 = 2.84(2), U1-C2 = 2.871(19) Å) and 2.53(1) Å (U1-C2 = 2.690(6), U1-C3 = 2.771(6), U1-N1 = 2.792(5), U1-C4 = 2.870(6), U1-C5 = 2.923(6) Å), respectively. For comparison, the η^5-pyrrole interaction observed in **3.2** and **3.3** is reminiscent of the η^5-cyclopentadienyl interaction observed in $[NEt_4]_2[U^{VI}O_2(\eta^5\text{-}C_5Me_5)(CN)_3]$ and $(\eta^5\text{-}C_5Me_5)U^{VI}O_2(^{Mes}PDI^{Me})$ ($^{Mes}PDI^{Me}$ = 2,6-(2,4,6-Me_3-C_6H_2-N=CMe)$_2C_5H_3N$). These two complexes feature similar U-centroid distances of 2.598(3) and 2.582 Å, respectively.[25, 40]

The average U=O bond lengths in **3.2** and **3.3** are 1.77 and 1.76 Å, respectively, which is typical of the *trans*-uranyl fragment.[11, 41, 42] However, the O−U−O angles in **3.2** (162.0(7)/162.7(7)°) and **3.3** (164.5(5)°) are substantially reduced from the 180° expected for this fragment, and are among the smallest reported to date (Table 3.1).[43, 44] I attribute the O−U−O bending to the close approach of the ligand backbone to the O_{yl} atoms (**3.2**: O1···C25 = 2.82 Å and O2···C3 = 2.95 Å; **3.3**: O1···C9 = 2.84 Å and O2···C3 = 2.89 Å). Significantly, the O−U−O bending observed upon ligation of **3.1** to uranyl appears to confirm my hypothesis that the initial oxidation of [calix[4]pyrrole]$^{4-}$ does, indeed, occur via a *cis*-uranyl intermediate. For comparison, the uranyl pyridinophane complexes, $[U^{VI}O_2(OTf)_2(^{H}N4)]$ and $[U^{VI}O_2(OTf)(THF)(^{Me}N4)][OTf]$ ($^{H}N4$ = 2,11-diaza[3,3](2,6) pyridinophane, and $^{Me}N4$ = *N*,*N*′-dimethyl-2,11-diaza[3,3](2,6) pyridinophane) feature O-U-O angles of 162.8(3)° and 161.7(5)°, respectively.[45] Similarly, the uranyl 1,10-phenanthroline (phen) complexes, $[U^{VI}O_2(phen)_2(2,4,6\text{-}X_3C_6H_2CO_2)_2]$ (X = F, Cl, Br), feature O−U−O angles ranging from 164.9(2)° to 162.2(2)°.[46] For further comparison, $[NEt_4]_2[U^{VI}O_2(\eta^5\text{-}C_5Me_5)(CN)_3]$ and $(\eta^5\text{-}C_5Me_5)U^{VI}O_2(^{Mes}PDI^{Me})$, which feature similar η^5-bound rings, adopt O−U−O angles of 168.40(9)°,[40] and 168.3(2)°,[25] respectively. In all cases, bending can be rationalized by the

steric constraints imposed by coordination of the ligand to the uranium center.[43] Finally, the lithium cations in both **3.2** and **3.3** are each coordinated to four N atoms of the calix ligand, as well as one THF molecule. This binding mode is reminiscent of the K^+ binding mode in [(Et_8-calix[4]tetrapyrrole)U^{III}(dme)][K(dme)],[39] and the Li^+ binding mode in $[Li(THF)]_2[U^{VI}O_2(N(SiMe_3)_2)_2$(tmtaa)].[47]

Table 3.1. Selected Metrical Parameters for **3.2** and **3.3** (Å and °).

Complex	**3.2**	**3.3**
U=O	1.77(1)/1.78(1)	1.765(4)/
	1.77(2)/1.78(2)	1.762(4)
U−cent.	2.53(1)/2.54(1)	2.53(1)
U-O_{THF}	2.42(1)/2.45(2)	2.402(4)
U−X	2.739(5)/	2.441(5)
X = Cl or OTf	2.736(4)	
U−N	2.54(1)/2.54(2)	2.494(5)
O−U−O (°)	162.0(7)/162.7(7)	164.5(5)

The ^{1}H NMR spectrum of **3.2** in THF-d_8 at -30 °C reveals 8 doublets between 6.0 and 7.5 ppm, assignable to 8 unique pyrrole environments, as well as 8 singlets between 1.0 and 2.5 ppm, which are assignable to 8 unique methyl environments (Figure A3.7), consistent with the C_1 symmetry seen in the solid state. However, upon warming **3.2** to 25 °C the 8 pyrrole and 8 methyl environments coalesce and broaden significantly. This observation suggests that, at room temperature, the ligand fragment in **3.2** is rapidly exchanging its η^1- and η^5-bound pyrrole rings, while the uranium-coordinated THF and $[Cl]^-$ ligands also likely undergo exchange. These parallel exchange processes result in an averaged structure that adequately rationalizes the room temp ^{1}H NMR spectrum. Similar dynamic behavior is observed for complex **3.3** (Figure A3.11). In addition, the ^{19}F{^{1}H} NMR spectrum of **3.3** features a sharp

singlet at 78.43 ppm, assignable to the $[OTf]^-$ ligand (Figure A3.13), while the $^7Li\{^1H\}$ NMR spectrum of **3.3** features a broad peak at 0.02 ppm (Figure A3.12), which is assignable to the lone Li^+ environment. The $^7Li\{^1H\}$ NMR spectrum of **3.2** is essentially identical to that of **3.3** (Figure A3.9).

Finally, in an effort to probe the suitability of $[Li(THF)]_4[L]$ as a catalyst for uranyl reduction, I explored the chemical reversibility of the $[Li(THF)]_4[L]$ to **3.1** conversion. To that end, I monitored the reaction of $[Li(THF)]_4[L]$ with $[U^{VI}O_2Cl_2(Ph_3PO)_2]$ in THF-d_8 by ^1H NMR spectroscopy. This reaction results in an immediate color change from yellow to deep-brown, while no precipitate is observed to form. The ^1H NMR spectrum of the reaction mixture after 5 minutes revealed the presence of **3.1**, along with a small amount of H_4L. These two species are present in a 10:2 ratio. Subsequent addition of excess Li^0 to this sample resulted in complete disappearance of **3.1** and reformation of $[Li(THF)]_4[L]$ over the course of 10 h. The ratio of $[Li(THF)]_4[L]$:H_4L in this sample is 10:2.5 (Scheme 3.4 and Figure A3.16). On standing for 24 h, a deep-brown solid slowly began to deposit in the reaction mixture, which I ascribe to uranium(IV) oxide. Note that Floriani and co-workers previously reported reduction of $[Li]_2[L'^{\Delta}]$ with 2 equiv of Li^0 results in formation of $[Li]_4[L']$.[35] Overall, the reversibility of the $[Li(THF)]_4[L]$ oxidation suggest that it could be employed in the catalytic reduction of uranyl. However, its high water sensitivity renders it impractical for use in real-world systems. Nonetheless, my results represent an important proof-of-principle toward the development of a practical system.

Scheme 3.4. Reversible Redox Chemistry of **3.1**

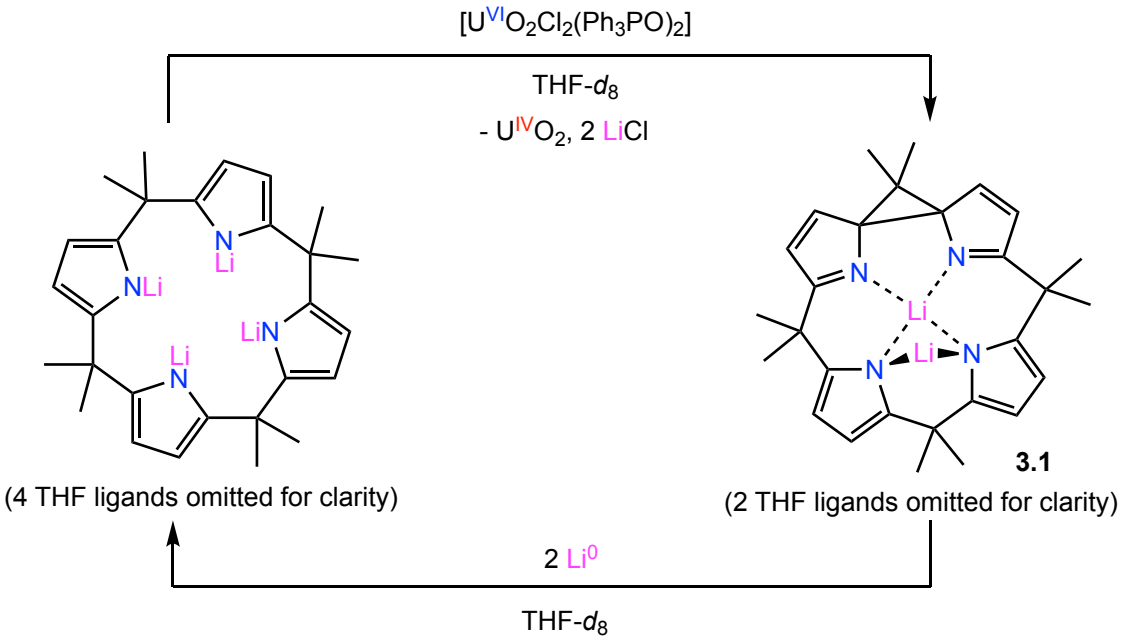

3.3 Summary

In summary, I have explored the reactivity of the well-known macrocyclic ligand, $[Li(THF)]_4[Me_8$-calix[4]pyrrole], with the uranyl ion. This reaction results in oxidation of the [calix[4]pyrrole]$^{4-}$ fragment, forming of the oxidized calix ligand, $[Li(THF)]_2[L^{\Delta}]$ (**3.1**), concomitant with reduction of the uranyl ion. I hypothesize that this reaction proceeds through a highly-oxidizing *cis*-uranyl intermediate, $[Li]_2[cis\text{-}U^{VI}O_2(L)]$. In an effort to test this hypothesis, I explored the reaction of **3.1** with uranyl salts, which results in the isolation of $[Li(THF)][U^{VI}O_2(L^{\Delta})Cl(THF)]$ (**3.2**) and $[Li(THF)][U^{VI}O_2(L^{\Delta})(OTf)(THF)]$ (**3.3**). Significantly, complexes **3.2** and **3.3** are the first η^5-pyrrole complexes of the uranyl ion. As such, they represent rare examples of organometallic uranyl complexes.[25, 40, 48-55] Moreover, the O-U-O bending observed in the solid state for these two complexes supports my hypothesis

that reduction of uranyl by [Li(THF)]$_4$[Me$_8$-calix[4]pyrrole] occurs via a *cis*-uranyl intermediate. My results present the most detailed picture yet of the structural changes that occur to uranyl upon coordination to a macrocycle, and provide further support that O-U-O bending in the uranyl ion renders it a strong oxidant. In addition, this transformation represents a rare example of the controlled reduction of uranyl by ligation to a redox-active ligand. Going forward, I plan to develop this method of uranyl manipulation into an electro-catalytic uranyl reduction process.

3.4 Experimental

3.4.1 General. All reactions and subsequent manipulations were performed under anaerobic and anhydrous conditions under an atmosphere of dinitrogen. Diethyl ether (Et_2O), toluene, and hexanes were dried using a Vacuum Atmospheres DRI-SOLV Solvent Purification system and stored over 3Å sieves for 24 h prior to use. Tetrahydrofuran (THF) was distilled over calcium hydride followed by distillation over sodium benzophenone, collected, and stored over 3Å sieves for 24 h prior to use. THF-d_8 and C_6D_6 were stored over 3Å sieves for 24 h prior to use. $[UO_2Cl_2(THF)_2]_2$,[41] $[UO_2Cl_2(Ph_3PO)_2]$,[27] $[UO_2(OTf)_2(THF)_3]$,[56] H_4L (L = Me$_8$-calix[4]pyrrole),[57] and [Li(THF)]$_4$[L][33] were synthesized according to previously reported literature procedures.

All NMR spectra were recorded on a Varian UNITY INOVA 500 spectrometer or an Agilent Technologies 400-MR DD2 400 MHz spectrometer. ^{1}H and ^{13}C{^{1}H} NMR spectra were referenced to external $SiMe_4$ using the residual protio solvent peaks as internal standards. The ^{7}Li and ^{19}F{^{1}H} NMR spectra were referenced indirectly with the ^{1}H resonance of $SiMe_4$ at 0 ppm, according to IUPAC standard.[58, 59] IR spectra were recorded on a Nicolet 6700 FT-

IR spectrometer with a NXR FT Raman Module. Elemental analyses were performed by the Microanalytical Laboratory at University of California (Berkeley, CA).

3.4.2 Synthesis of [Li(THF)]$_2$[L^A] (3.1). To a colorless stirring solution of [Li(THF)]$_4$[L] (530 mg, 0.716 mmol) in THF (10 mL) was slowly added I_2 (181.6 mg, 0.716 mmol). This resulted in a rapid color change to deep orange. No solid was observed in the reaction mixture. After 5 min, the volatiles were removed in vacuo to provide a deep orange solid. The solid was suspended in cold (-25 °C) THF (3 mL), and the resulting suspension was filtered through a medium porosity glass frit to provide an orange powder and a pale orange supernatant. The orange powder was subsequently rinsed with 2 mL of cold THF to afford [Li(THF)]$_2$[L^A] (**3.1**) as an orange powder. Yield: 304 mg, 73%. Anal. Calcd for $C_{36}H_{48}N_4Li_2O_2$: C, 74.21; H, 8.30; N, 9.62. Found: C, 73.84; H, 8.04; N, 9.32. ^{1}H NMR (500 MHz, 25 °C, THF-d_8): 7.60 (br s, H_{pyr}, 2H), 6.83 (br s, H_{pyr}, 2H), 5.67 (br s, H_{pyr}, 4H), 1.53 (br s, CH_3, 15H), 1.42 (br s, CH_3, 6H), 1.29 (br s, CH_3, 3H). (500 MHz, 0 °C, THF-d_8): 7.62 (br s, H_{pyr}, 2H), 6.84 (br s, H_{pyr}, 2H), 5.67 (br s, H_{pyr}, 4H), 1.63 (s, CH_3, 3H), 1.59 (s, CH_3, 6H), 1.51 (s, CH_3, 6H), 1.42 (s, CH_3, 6H), 1.29 (s, CH_3, 3H). ^{1}H NMR (500 MHz, -20 °C, THF-d_8): δ 7.63 (d, J = 4.7 Hz, H_{pyr}, 1H), 6.84 (d, J = 4.9 Hz, H_{pyr}, 1H), 5.67 (s, H_{pyr}, 2H), 5.63 (s, H_{pyr}, 2H), 1.63 (s, CH_3, 3H), 1.61 (s, CH_3, 3H), 1.58 (s, CH_3, 3H), 1.51 (s, CH_3, 6H), 1.42 (s, CH_3, 6H), 1.29 (s, CH_3, 6H). ^{1}H NMR (500 MHz, -40 °C, THF-d_8): δ 7.64 (d, J = 4.5 Hz, H_{pyr}, 2H), 6.84 (d, J = 4.8 Hz, H_{pyr}, 2H), 5.66 (d, J = 2.4 Hz, H_{pyr}, 2H), 5.62 (d, J = 2.7 Hz, H_{pyr}, 2H), 1.64 (s, CH_3, 6H), 1.56 (s, CH_3, 3H), 1.51 (s, CH_3, 6H), 1.42 (s, CH_3, 6H), 1.31 (s, CH_3, 3H). ^{1}H NMR (500 MHz, -60 °C, THF-d_8): δ 7.65 (d, J = 5.0 Hz, H_{pyr}, 2H), 6.83 (d, J = 4.8 Hz, H_{pyr}, 2H), 5.66 (d, J = 2.7 Hz, H_{pyr}, 2H), 5.61 (d, J = 2.6 Hz, H_{pyr}, 2H), 1.67 (s, CH_3, 3H), 1.63 (s, CH_3, 3H), 1.54 (s, CH_3, 2H), 1.51 (s, CH_3, 6H), 1.42 (s, CH_3, 6H), 1.33 (s, CH_3, 3H). ^{1}H NMR (500 MHz, -80 °C,

THF-d_8): δ 7.65 (d, J = 4.9 Hz, H_{pyr}, 2H), 6.82 (d, J = 4.9 Hz, H_{pyr}, 2H), 5.65 (d, J = 2.5 Hz, H_{pyr}, 2H), 5.60 (d, J = 2.1 Hz, H_{pyr}, 2H), 1.70 (s, CH_3, 3H), 1.64 (s, CH_3, 3H), 1.52 (s, CH_3, 3H), 1.50 (s, CH_3, 6H), 1.41 (s, CH_3, 6H), 1.36 (s, CH_3, 3H). ^{7}Li NMR (155 MHz, 25 °C, THF-d_8): δ 0.79 (s, 1Li), -1.09 (s, 1Li). $^{13}C\{^1H\}$ NMR (126 MHz, -30 °C, THF-d_8): δ 187.59 (**6**), 150.88 (**5**/**4**), 150.06 (**5**/**4**), 144.17 (**12**), 128.35 (**11**), 101.75 (**10**), 99.00 (**9**), 87.53 (**3**), 68.39 (THF), 47.50 (**13**), 41.81 (**7**), 39.26 (**2**), 37.27 (**14**), 31.53 (**1**), 30.61 (**8**), 30.23 (**8**), 26.58 (THF). IR (KBr pellet, cm^{-1}): 3089 (m), 3076 (m), 2962 (s), 2926 (s), 2866 (s), 1576, (s), 1460, (s), 1367 (m), 1350 (s), 1277 (m), 1244 (w), 1203 (m), 1155 (m), 1126 (w), 1092 (m), 1047 (s), 1022 (m), 916 (m), 895 (m), 800 (s), 802 (s), 741 (w), 725 (s), 609 (m), 577 (w), 557 (vw), 536 (vw), 499 (vw), 445 (m), 436 (m), 417 (s).

3.4.3 Isolation of [Li(THF)][Li(THF)$_{0.58}$(Et$_2$O)$_{0.42}$][L^A]. To a stirring yellow solution of $[UO_2Cl_2(THF)_2]_2$ (69.9 mg, 0.0717 mmol) in THF (2 mL) was added slowly a THF solution (2 mL) of $[Li(THF)]_4[L]$ (106.3 mg, 0.143 mmol). This resulted in a rapid color change to deep brown. The mixture was allowed to stir for 30 min before the volatiles were removed *in vacuo*, which afforded a brown-orange solid. The brown-orange residue was extracted into Et_2O (3 × 3 mL) and filtered through a Celite column supported on glass wool (0.5 cm × 2 cm). This yielded a brown-orange filtrate and left a brown-black solid on the Celite column. The volume of this solution was reduced *in vacuo* to 5 mL. Storage of this solution for 24 h at -25 °C resulted in the deposition of X-ray quality orange blocks of [Li(THF)][Li(THF)$_{0.58}$(Et$_2$O)$_{0.42}$][L^A], which were isolated by decanting off the supernatant and drying *in vacuo*. Yield 33.4 mg, 40%. ^{1}H NMR (500 MHz, 25 °C, THF-d_8) δ 7.59 (br s, H_{pyr}, 2H), 6.83 (br s, H_{pyr}, 2H), 5.67 (br s, H_{pyr}, 4H), 3.54 (s, THF, 4H), 3.35 (q, J = 7.0 Hz,

Et_2O, 4H), 1.69 (s, THF, 4H), 1.54 (s, CH_3, 12H), 1.50 (s, CH_3, 3H), 1.42 (s, CH_3, 6H) 1.26 (s, CH_3, 3H), 1.08 (t, J = 7.0 Hz, Et_2O, 6H).

3.4.4 Synthesis of [Li(THF)][$UO_2(L^A)Cl$(THF)] (3.2). To a stirring, -25 °C solution of $[UO_2Cl_2(THF)_2]_2$ (90.1 mg, 0.0929 mmol) in THF (2 mL) was added dropwise a -25 °C solution of **1** (108.2 mg, 0.186 mmol) in THF (2 mL). This addition resulted in an immediate color change from yellow to deep green. As soon as the addition was complete, the volatiles were removed *in vacuo* and the resulting solids were triturated with pentane (2 × 2 mL), affording a deep green solid. This solid was then extracted into toluene (6 mL) and filtered through a Celite column supported on glass wool (0.5 cm × 2 cm). This yielded a deep green solution. The volume of this solution was reduced *in vacuo* to 3 mL, filtered through a Celite column supported on glass wool (0.5 cm × 2 cm), and layered with hexanes (8 mL). Storage of the solution at -25 °C for 48 h resulted in the deposition of deep green needles of [Li(THF)][$UO_2(L^A)Cl$(THF)] (**3.2**), which were isolated by decanting off the supernatant (yield 80 mg, 49%). Anal. Calcd for $C_{36}H_{48}N_4LiClO_4U$: C, 49.07; H, 5.49; N, 6.36. Found: C, 49.44; H, 5.63; N, 6.12. ^{1}H NMR (500 MHz, 25 °C, THF-d_8): δ 7.50 – 6.00 (br m, H_{pyr}, 8H), 1.92 (br s, CH_3, 6H), 1.86 (br s, CH_3, 3H), 1.69 (br s, CH_3, 3H), 1.65 (br s, CH_3, 6H), 1.46 (s, CH_3, 3H), 1.39 (s, CH_3, 3H). ^{1}H NMR (500 MHz, 10 °C, THF-d_8): δ 7.50 – 5.93 (br m, H_{pyr}, 8H), 1.94 (br s, CH_3, 6H), 1.85 (s, CH_3, 3H), 1.69 (br s, CH_3, 3H), 1.64 (br s, CH_3, 6H), 1.47 (s, CH_3, 3H), 1.39 (s, CH_3, 3H). ^{1}H NMR (500 MHz, 0 °C, THF-d_8): δ 7.17 (br s, H_{pyr}, 1H), 6.95 (br s, H_{pyr}, 1H), 6.89 (br s, H_{pyr}, 1H), 6.74 (br s, H_{pyr}, 1H), 6.56 (br s, H_{pyr}, 1H), 6.30 (br s, H_{pyr}, 2H), 6.04 (br s, H_{pyr}, 1H), 2.01 (br s, CH_3, 3H), 1.85 (s, CH_3, 6H), 1.69 (s, CH_3, 3H), 1.64 (br s, CH_3, 6H), 1.47 (s, CH_3, 3H), 1.39 (s, CH_3, 3H). ^{1}H NMR (500 MHz, -10 °C, THF-d_8): δ 7.21 (s, H_{pyr}, 1H), 6.95 (s, H_{pyr}, 1H), 6.90 (s, H_{pyr}, 1H), 6.76 (s, H_{pyr}, 1H), 6.57 (s, H_{pyr}, 1H), 6.30 (s,

H_{pyr}, 1H), 6.26 (s, H_{pyr}, 1H), 6.04 (s, H_{pyr}, 1H), 2.02 (br s, CH_3, 3H), 1.84 (s, CH_3, 6H), 1.70 (s, CH_3, 3H), 1.66 (br s, CH_3, 3H), 1.62 (br s, CH_3, 3H), 1.47 (s, CH_3, 3H), 1.38 (s, CH_3, 3H). ^{1}H NMR (500 MHz, -20 °C, THF-d_8): δ 7.22 (d, J = 4.9 Hz, H_{pyr}, 1H), 6.97 (d, J = 4.7 Hz, H_{pyr}, 1H), 6.91 (s, H_{pyr}, 1H), 6.78 (d, J = 4.9 Hz, H_{pyr}, 1H), 6.58 (s, H_{pyr}, 1H), 6.30 (d, J = 3.3 Hz, H_{pyr}, 1H), 6.26 (d, J = 4.8 Hz, H_{pyr}, 1H), 6.04 (d, J = 3.1 Hz, H_{pyr}, 1H), 2.03 (s, CH_3, 3H), 1.83 (s, CH_3, 6H), 1.70 (s, CH_3, 3H), 1.66 (s, CH_3, 3H), 1.61 (s, CH_3, 3H), 1.47 (s, CH_3, 3H), 1.38 (s, CH_3, 3H). ^{1}H NMR (500 MHz, -30 °C, THF-d_8): δ 7.24 (d, J = 5.0 Hz, H_{pyr}, 1H), 6.98 (d, J = 4.9 Hz, H_{pyr}, 1H), 6.91 (d, J = 2.8 Hz, H_{pyr}, 1H), 6.80 (d, J = 4.9 Hz, H_{pyr}, 1H), 6.59 (d, J = 2.8 Hz, H_{pyr}, 1H), 6.30 (d, J = 3.0 Hz, H_{pyr}, 1H), 6.25 (d, J = 4.9 Hz, H_{pyr}, 1H), 6.03 (d, J = 3.1 Hz, H_{pyr}, 1H), 2.03 (s, CH_3, 3H), 1.82 (s, CH_3, 6H), 1.69 (s, CH_3, 3H), 1.66 (s, CH_3, 3H), 1.61 (s, CH_3, 3H), 1.48 (s, CH_3, 3H), 1.38 (s, CH_3, 3H). ^{1}H NMR (500 MHz, -40 °C, THF-d_8): δ 7.25 (d, J = 4.8 Hz, H_{pyr}, 1H), 6.99 (d, J = 4.7 Hz, H_{pyr}, 1H), 6.92 (d, J = 2.8 Hz, H_{pyr}, 1H), 6.82 (d, J = 4.7 Hz, H_{pyr}, 1H), 6.59 (d, J = 2.8 Hz, H_{pyr}, 1H), 6.30 (d, J = 3.1 Hz, H_{pyr}, 1H), 6.26 (d, J = 4.9 Hz, H_{pyr}, 1H), 6.03 (d, J = 3.1 Hz, H_{pyr}, 1H), 2.03 (s, CH_3, 3H), 1.82 (s, CH_3, 6H), 1.69 (s, CH_3, 3H), 1.66 (s, CH_3, 3H), 1.61 (s, CH_3, 3H), 1.48 (s, CH_3, 3H), 1.38 (s, CH_3, 3H). ^{1}H NMR (500 MHz, -50 °C, THF-d_8): δ 7.27 (d, J = 4.9 Hz, H_{pyr}, 1H), 7.01 (d, J = 4.9 Hz, H_{pyr}, 1H), 6.92 (d, J = 2.8 Hz, H_{pyr}, 1H), 6.84 (d, J = 4.9 Hz, H_{pyr}, 1H), 6.60 (d, J = 2.8 Hz, H_{pyr}, 1H), 6.30 (d, J = 3.1 Hz, H_{pyr}, 1H), 6.26 (d, J = 4.9 Hz, H_{pyr}, 1H), 6.03 (d, J = 3.1 Hz, H_{pyr}, 1H), 2.04 (s, CH_3, 3H), 1.82 (s, CH_3, 6H), 1.68 (s, CH_3, 3H), 1.66 (s, CH_3, 3H), 1.60 (s, CH_3, 3H), 1.48 (s, CH_3, 3H), 1.37 (s, CH_3, 3H). ^{13}C{^{1}H} NMR (126 MHz, -30 °C, THF-d_8): δ 187.77, 187.14, 166.01, 163.74, 152.40, 151.72, 149.91, 146.21, 130.65, 127.67, 127.05, 118.16, 108.73, 108.56, 105.73, 88.25, 47.00, 42.70, 40.69, 40.01, 39.84, 39.54, 34.26, 30.85, 30.70. ^{7}Li{^{1}H} NMR (155 MHz, 25 °C, THF-d_8): δ -0.18 (s). IR (KBr pellet, cm^{-1}): 3097 (w),

3080 (w), 2962 (s), 2920 (s), 2875 (m), 1570 (s), 1493 (w), 1464 (m), 1381 (w), 1362 (w), 1352 (m), 1265 (m), 1244 (w), 1207 (m), 1178 (w), 1155 (m), 1134(w), 1113 (w), 1101 (m), 1051 (s), 1034 (w), 1011 (w), 984 (w), 974 (w), 891 (vs), 858 (s), 810 (s), 795 (s), 752 (m), 731 (m), 696 (w), 673 (w), 606 (m), 501 (w).

3.4.5 Synthesis of [Li(THF)][$UO_2(L^A)$(OTf)(THF)] (3.3). To a stirring -25 °C solution of [$UO_2(OTf)_2(THF)_3$] (121.2 mg, 0.155 mmol) in THF (2 mL) was added dropwise a -25 °C solution of **3.1** (114.8 mg, 0.155 mmol) in THF (2 mL). This addition resulted in an immediate color change from yellow to deep green. As soon as the addition was complete, the deep green-brown solution was filtered through a Celite column supported on glass wool (0.5 cm × 2 cm). This yielded a deep green-brown solution. Layering of this solution with hexanes (8 mL) followed storage of the solution at -25 °C for 24 h resulted in the deposition of copious amounts of a brown solid, which I have tentatively ascribed to $L^{\Delta\Delta}$ (Figure A3.14). Filtration of this solution and further storage at -25 °C for 24 h resulted in the deposition of deep green needles of [Li(THF)][$UO_2(L^A)$(OTf)(THF)] (**3.3**), which were isolated by decanting off the supernatant (yield 35.1 mg, 30%). Anal. Calcd for $C_{37}H_{48}F_3LiN_4O_7SU$: C, 44.67; H, 4.86; N, 5.63. Found: C, 44.13; H, 4.58; N, 5.27. ^{1}H NMR (500 MHz, 25 °C, THF-d_8): δ 7.32 – 5.87 (br m, 8H), 1.98 (s, 3H), 1.83 (br s, 6H), 1.73 (s, 6H), 1.68 (s, 3H), 1.48 (s, 3H), 1.42 (s, 3H). ^{1}H NMR (500 MHz, 10 °C, THF-d_8): δ 7.19 (br s, H_{pyr}, 1H), 6.95 (br s, H_{pyr}, 1H), 6.85 (br s, H_{pyr}, 1H), 6.72 (br s, H_{pyr}, 1H), 6.63 (br s, H_{pyr}, 1H), 6.22 (br s, H_{pyr}, 2H), 6.05 (br s, H_{pyr}, 1H), 1.97 (s, CH_3, 6H), 1.74 (s, CH_3, 3H) 1.72 (s, CH_3, 6H), 1.64 (br s, CH_3, 3H), 1.48 (s, CH_3, 3H), 1.41 (s, CH_3, 3H). ^{1}H NMR (500 MHz, 0 °C, THF-d_8): δ 7.21 (s, H_{pyr}, 1H), 6.96 (s, H_{pyr}, 1H), 6.86 (s, H_{pyr}, 1H), 6.75 (s, H_{pyr}, 1H), 6.64 (s, H_{pyr}, 1H), 6.23 (s, H_{pyr}, 1H), 6.21 (s, H_{pyr}, 1H), 6.05 (s, H_{pyr}, 1H), 1.97 (s, CH_3, 6H), 1.74 (s, CH_3, 3H), 1.73 (s, CH_3, 6H), 1.63 (s, CH_3, 3H), 1.48 (s, CH_3,

3H), 1.41 (s, CH_3, 3H). ^{1}H NMR (500 MHz, -10 °C THF-d_8): δ 7.22 (d, J = 4.9 Hz, H_{pyr}, 1H), 6.97 (d, J = 4.9 Hz, H_{pyr}, 1H), 6.87 (s, H_{pyr}, 1H), 6.76 (d, J = 4.9 Hz, H_{pyr}, 1H), 6.65 (s, H_{pyr}, 1H), 6.24 (s, H_{pyr}, 1H), 6.20 (d, J = 4.8 Hz, H_{pyr}, 1H), 6.04 (s, H_{pyr}, 1H), 1.97 (s, CH_3, 3H), 1.96 (s, CH_3, 3H), 1.73 (s, CH_3, 3H), 1.72 (s, CH_3, 6H), 1.63 (s, CH_3, 3H), 1.48 (s, CH_3, 3H), 1.41 (s, CH_3, 3H). ^{1}H NMR (500 MHz, -20 °C, THF-d_8): δ 7.23 (d, J = 5.0 Hz, H_{pyr}, 1H), 6.98 (d, J = 5.0 Hz, H_{pyr}, 1H), 6.87 (d, J = 2.8 Hz, H_{pyr}, 1H), 6.78 (d, J = 5.0 Hz, H_{pyr}, 1H), 6.65 (d, J = 3.1 Hz, H_{pyr}, 1H), 6.24 (d, J = 3.1 Hz, H_{pyr}, 1H), 6.20 (d, J = 5.0 Hz, H_{pyr}, 1H), 6.04 (d, J = 3.1 Hz, H_{pyr}, 1H), 1.98 (s, CH_3, 3H), 1.96 (s, CH_3, 3H), 1.75 (s, CH_3, 3H), 1.74 (s, CH_3, 3H), 1.72 (s, CH_3, 3H), 1.62 (s, CH_3, 3H), 1.49 (s, CH_3, 3H), 1.41 (s, CH_3, 3H). ^{1}H NMR (500 MHz, -30 °C, THF-d_8): δ 7.24 (d, J = 5.0 Hz, H_{pyr}, 1H), 7.00 (d, J = 4.9 Hz, H_{pyr}, 1H), 6.88 (d, J = 2.8 Hz, H_{pyr}, 1H), 6.80 (d, J = 5.0 Hz, H_{pyr}, 1H), 6.67 (d, J = 2.7 Hz, H_{pyr}, 1H), 6.24 (d, J = 3.0 Hz, H_{pyr}, 1H), 6.20 (d, J = 5.0 Hz, H_{pyr}, 1H), 6.04 (d, J = 3.1 Hz, H_{pyr}, 1H), 1.98 (s, CH_3, 3H), 1.95 (s, CH_3, 3H), 1.75 (s, CH_3, 3H), 1.74 (s, CH_3, 3H), 1.72 (s, CH_3, 3H), 1.62 (s, CH_3, 3H), 1.49 (s, CH_3, 3H), 1.41 (s, CH_3, 3H). ^{1}H NMR (500 MHz, -40 °C, THF-d_8): δ 7.26 (d, J = 4.9 Hz, H_{pyr}, 1H), 7.02 (d, J = 4.9 Hz, H_{pyr}, 1H), 6.89 (d, J = 2.8 Hz, H_{pyr}, 1H), 6.83 (d, J = 5.0 Hz, H_{pyr}, 1H), 6.69 (d, J = 2.8 Hz, H_{pyr}, 1H), 6.25 (d, J = 3.0 Hz, H_{pyr}, 1H), 6.21 (d, J = 5.0 Hz, H_{pyr}, 1H), 6.04 (d, J = 3.0 Hz, H_{pyr}, 1H), 1.99 (s, CH_3, 3H), 1.94 (s, CH_3, 3H), 1.75 (s, CH_3, 3H), 1.74 (s, CH_3, 3H), 1.72 (s, CH_3, 3H), 1.61 (s, CH_3, 3H), 1.49 (s, CH_3, 3H), 1.40 (s, CH_3, 3H). ^{1}H NMR (500 MHz, -50 °C, THF-d_8): δ 7.27 (d, J = 4.9 Hz, H_{pyr}, 1H), 7.03 (d, J = 5.0 Hz, H_{pyr}, 1H), 6.89 (d, J = 2.8 Hz, H_{pyr}, 1H), 6.85 (d, J = 5.0 Hz, H_{pyr}, 1H), 6.70 (d, J = 2.8 Hz, H_{pyr}, 1H), 6.25 (d, J = 3.1 Hz, H_{pyr}, 1H), 6.21 (d, J = 4.9 Hz, H_{pyr}, 1H), 6.04 (d, J = 3.0 Hz, H_{pyr}, 1H), 1.99 (s, CH_3, 3H), 1.93 (s, CH_3, 3H), 1.74 (s, CH_3, 3H), 1.73 (s, CH_3, 3H), 1.71 (s, CH_3, 3H), 1.61 (s, CH_3, 3H), 1.49 (s, CH_3, 3H), 1.40 (s, CH_3, 3H). ^{7}Li NMR (155 MHz, 25°C,

THF-d_8): δ 0.02 (s). $^{19}F\{^1H\}$ NMR (376 MHz, 25 °C, THF-d_8): δ −78.43. (s). IR (KBr pellet, cm^{-1}): 3105 (w), 3080 (w), 2966 (s), 2927 (s), 2872 (m), 1572 (m), 1462 (m), 1381 (w), 1338 (w), 1327 (s), 1288 (m), 1261 (m), 1236 (s), 1207 (s), 1171 (m), 1111 (w), 1097 (w), 1028 (m), 1018 (s), 985 (w), 972 (w), 912(s), 854 (m), 800 (m), 783 (m), 760 (w), 733 (w), 634 (s), 604 (w), 571 (w), 515 (w), 498 (w), 451 (w), 426 (w).

3.4.6 Reversible Oxidation of [Li(THF)]$_4$[L] (3.1). An NMR tube fitted with a J-Young valve was charged with [Li(THF)]$_4$[L] (23.6 mg, 0.031 mmol) and THF-d_8 (0.5 mL). A ^1H NMR spectrum was recorded (Figure A3.16). ^1H NMR (400 MHz, 25 °C, THF-d_8): δ 5.72 (s, H_{pyr}, 8H), 1.46 (s, CH_3, 24H). The NMR tube was brought back inside the glovebox and a pale yellow slurry of [$UO_2Cl_2(Ph_3PO)_2$] (28.6 mg, 0.031 mmol) in THF-d_8 (0.5 mL) was added. The color of the solution quickly turned very deep-brown, but no precipitate was observed. A ^1H NMR spectrum was re-recorded, which revealed the presence of **3.1** and H_4L in a 10:2 ratio (Figure A3.16). ^1H NMR (400 MHz, 25 °C, THF-d_8): δ 7.53 (br d, *o*-C_6H_5, 6H) 7.47 (t, *p*-C_6H_5, 3H), 7.32 (t, *m*-C_6H_5, 6H), 6.83 (br s, H_{pyr} **3.1**, 2H), 5.67 (br s, H_{pyr}, **3.1**, 4*H*), 5.63 (s, H_{pyr}, H_4L, 8H), 1.79 (s, H_4L, CH_3, 24H), 1.54 (br s, CH_3, **3.1** 6H), 1.53 (br s, CH_3, **3.1**, 9H), 1.46 (br s, CH_3, **3.1**, 6H), 1.34 (br s, CH_3, **3.1**, 3H). The NMR tube was brought back inside the glovebox and Li^0 metal was added to the tube as a silvery solid (0.6 mg, 0.073 mmol, 2.3 equiv). The sample was agitated by shaking once per hour, over the course of 10 h, and a ^1H NMR spectrum was re-recorded at 10 h, which revealed the absence of **3.1**, along with the presence of [Li(THF)]$_4$[L] and H_4L, in a 10:2.5 ratio. ^1H NMR (400 MHz, 25 °C, THF-d_8): δ 7.53 (br d, *o*-C_6H_5, 6H) 7.47 (t, *p*-C_6H_5, 3H), 7.32 (t, *m*-C_6H_5, 6H) 5.72 (s, H_{pyr}, [Li(THF)]$_4$[L], 8H), 5.63 (s, H_{pyr}, H_4L, 8H), 1.79 (s, CH_3, H_4L, 24H), 1.46 (s, CH_3, [Li(THF)]$_4$[L], 24H). On

standing for 24 h, a deep-brown precipitate had formed on the walls of the NMR tube, consistent with formation of UO_2.

3.4.7 X-ray Crystallography. Data for **3.1** and **3.3** were collected on a Bruker KAPPA APEX II diffractometer equipped with an APEX II CCD detector using a TRIUMPH monochromator with a Mo Kα X-ray source (α = 0.71073 Å). Data for **3.2** was collected on Bruker KAPPA APEX III diffractometer equipped with an APEX III CCD detector using a TRIUMPH monochromator with a Mo Kα X-ray source (α = 0.71073 Å). The crystals were mounted on a cryoloop under Paratone-N oil, and data was collected at 100(2) K for **3.1**, **3.2**, and **3.3** using an S3 Oxford nitrogen gas cryostream. Frame exposures of 10 s were used for **3.1**, **3.2**, and **3.3**. Data collection and cell parameter determinations were conducted using the SMART program.[49] Integration of the data frames and final cell parameter refinements were performed using SAINT software.[60] Absorption corrections of the data were carried out using the multi-scan method SADABS for **3.1** and **3.3** and TWINABS for **3.2**.[61, 62] Subsequent calculations were carried out using SHELXTL. Structure determination was done using direct or Patterson methods and difference Fourier techniques. All hydrogen atom positions were idealized and rode on the atom of attachment. Structure solution, refinement, graphics, and creation of publication materials were performed using SHELXTL.[54]

For complex **3.1**, one of the solvent ligand sites of Li1 is occupied by a mixture of THF and Et_2O in a 58:42 ratio. As a result of this disorder, the positions of these coordinated Et_2O and THF molecules were constrained with the SADI command and refined isotropically. In addition, a diethyl ether solvate in **3.1** is disordered over two positions, in a 50:50 ratio. As a

result, C100, C101, C103, C104, and O3 were constrained using the SADI command and refined isotropically. Hydrogen atoms were not assigned to these disordered carbon atoms.

The toluene solvate in complex **3.2** exhibited unresolved positional disorder. As a result, its carbon atoms were refined isotropically.

Table 3.2. Crystallographic details for complexes [Li(THF)][Li(THF)$_{0.58}$(Et$_2$O)$_{0.42}$][L$^{\Delta}$]·0.5Et$_2$O, **3.2·C$_7$H$_8$**, and **3.3**.

	[Li(THF)][Li(THF)$_{0.58}$(Et$_2$O)$_{0.42}$][L$^{\Delta}$]·0.5Et$_2$O	**3.2·C$_7$H$_8$**	**3.3**
Formula	$C_{38}H_{48.84}N_4O_{2.5}Li_2$	$C_{79}H_{104}N_8O_8Cl_2Li_2U_2$	$C_{37}H_{48}N_4O_7SF_3LiU$
Crystal Habit, Color	Block, Orange	Needle, Dark-Green	Needle, Dark-Green
Crystal Size (mm)	0.2 × 0.15 × 0.05	0.2 × 0.05 × 0.03	0.25 × 0.05 × 0.03
MW (g/mol)	615.52	1854.54	994.82
crystal system	Monoclinic	Triclinic	Monoclinic
space group	C2/c	P-1	P2$_1$/n
a (Å)	23.649(4)	14.900(1)	10.174(1)
b (Å)	19.253(3)	16.145(1)	19.791(1)
c (Å)	19.371(6)	19.041(1)	18.883(2)
α (°)	90	65.066(2)	90
β (°)	124.753(8)	89.891(2)	94.163(5)
γ (°)	90	70.221(2)	90
V (Å^3)	7247(3)	3855.0(4)	3792.1(5)
Z	8	2	4
T (K)	100(2)	100(2)	100(2)
λ (Å)	0.71073	0.71073	0.71073
GOF	1.191	0.951	1.017
Density (calcd) (Mg/m^3)	1.128	1.598	1.743
Absorption coefficient (mm^{-1})	0.070	4.324	4.404
F_{000}	2647	1844	1968
Total no Reflections	14163	13600	21756
Unique Reflections	6094	10303	6442
Final R indices*	R_1 = 0.0776	R_1 = 0.0999	R_1 = 0.0372
	wR_2 = 0.1962	wR_2 = 0.2549	wR_2 = 0.0744
Largest Diff. peak and hole (e$^-$ A^{-3})	0.744, -0.437	7.045, -5.775	1.681, -1.039

* [I > 2σ(I)]

3.5 Appendix

3.5.1 NMR Spectra

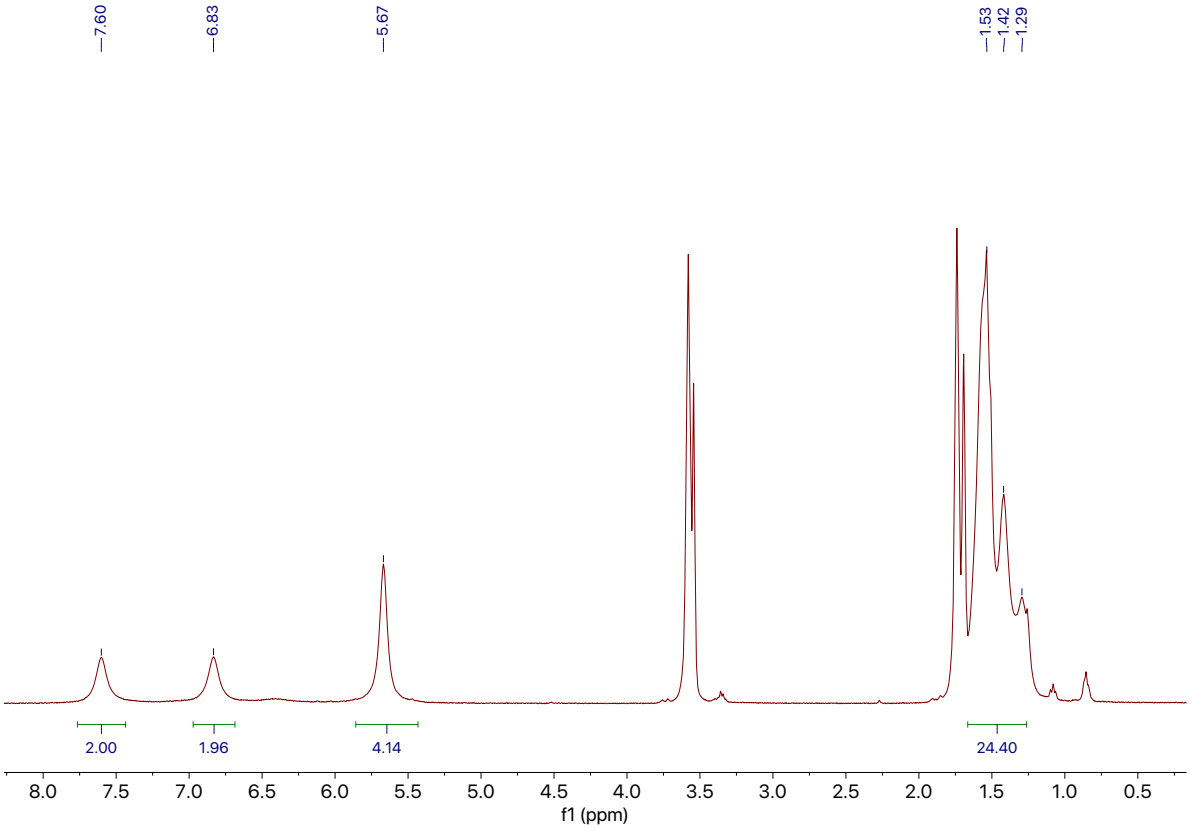

Figure A3.1. ^{1}H NMR spectrum of $[Li(THF)]_2[L^{\Delta}]$ (**3.1**) in THF-d_8 at room temperature.

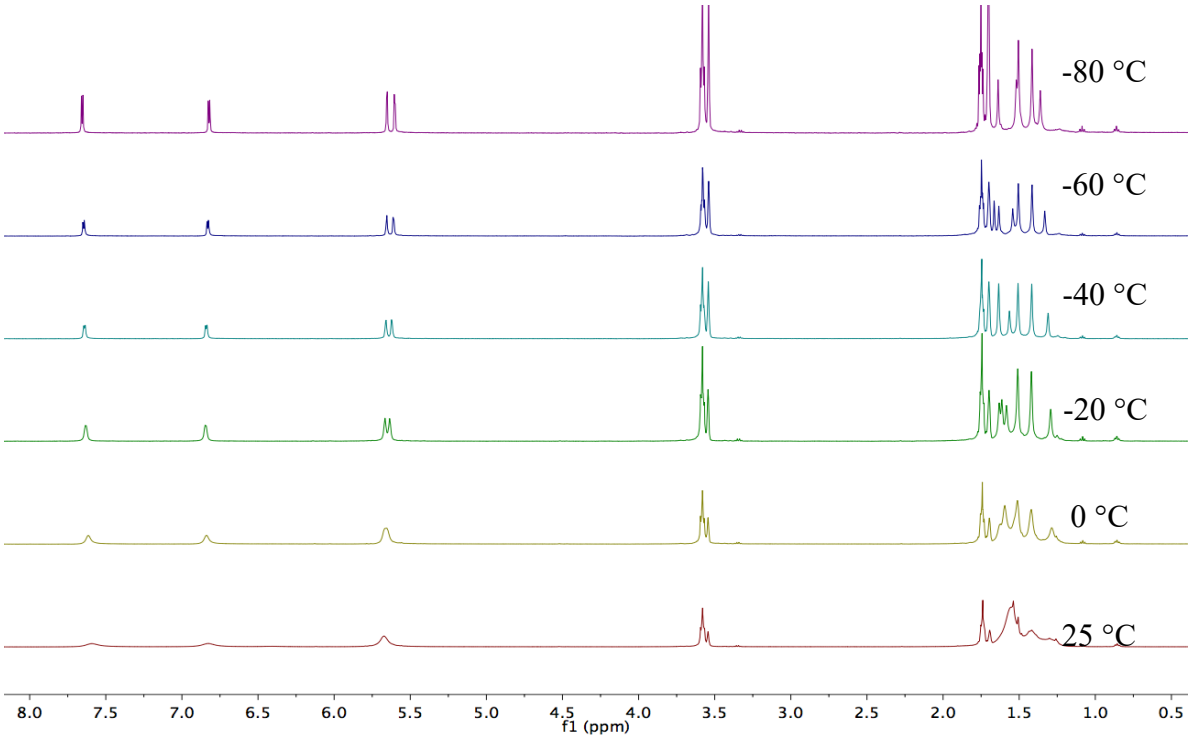

Figure A3.2. Variable temperature ^{1}H NMR spectra of $[Li(THF)]_2[L^{\Delta}]$ (**3.1**) in THF-d_8 from 25 °C (bottom) to -80 °C (top).

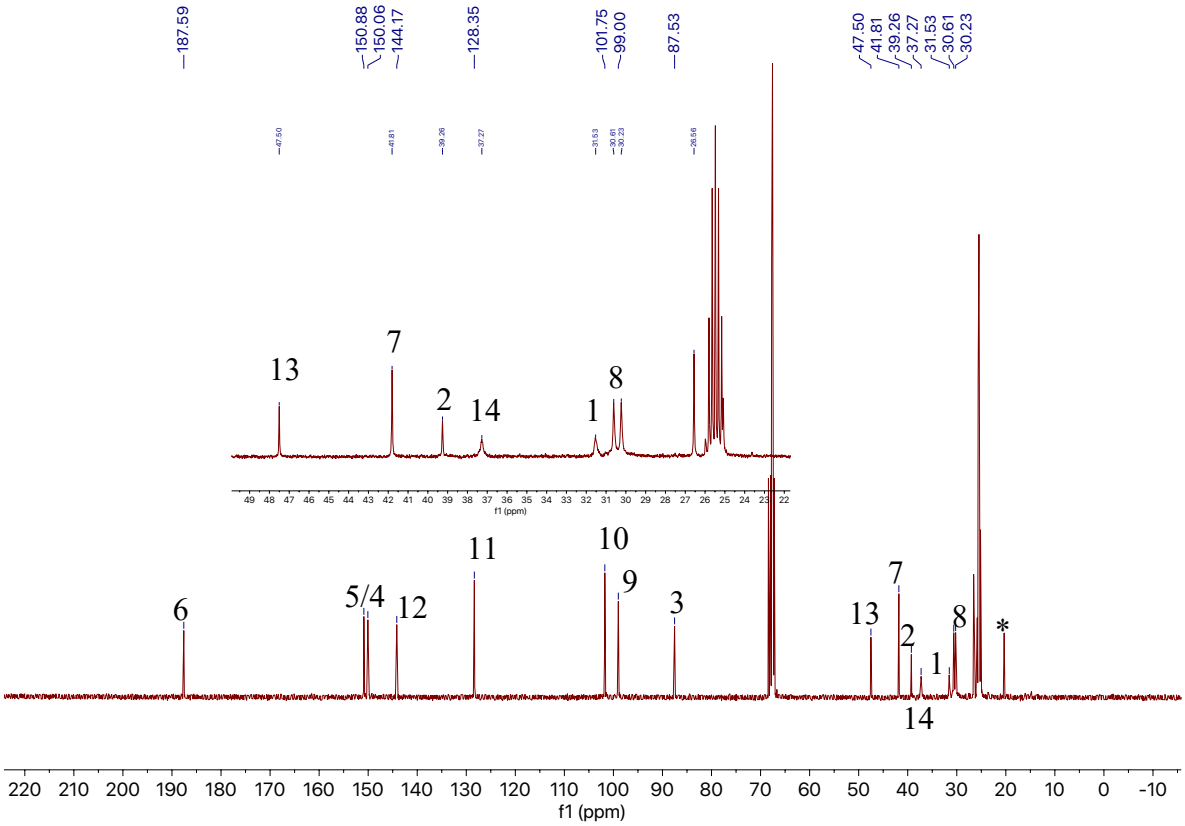

Figure A3.3. $^{13}C\{^{1}H\}$ NMR spectrum of $[Li(THF)]_2[L^A]$ (**3.1**) in THF-d_8 at -30 °C. (*) indicates and unidentified impurity.

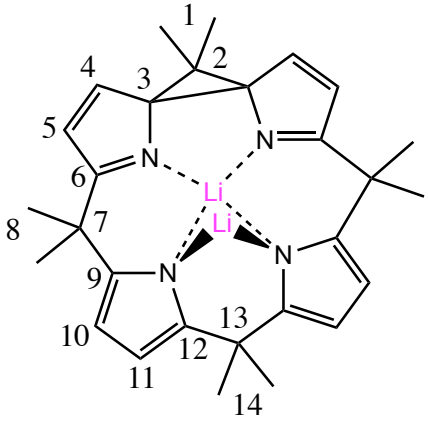

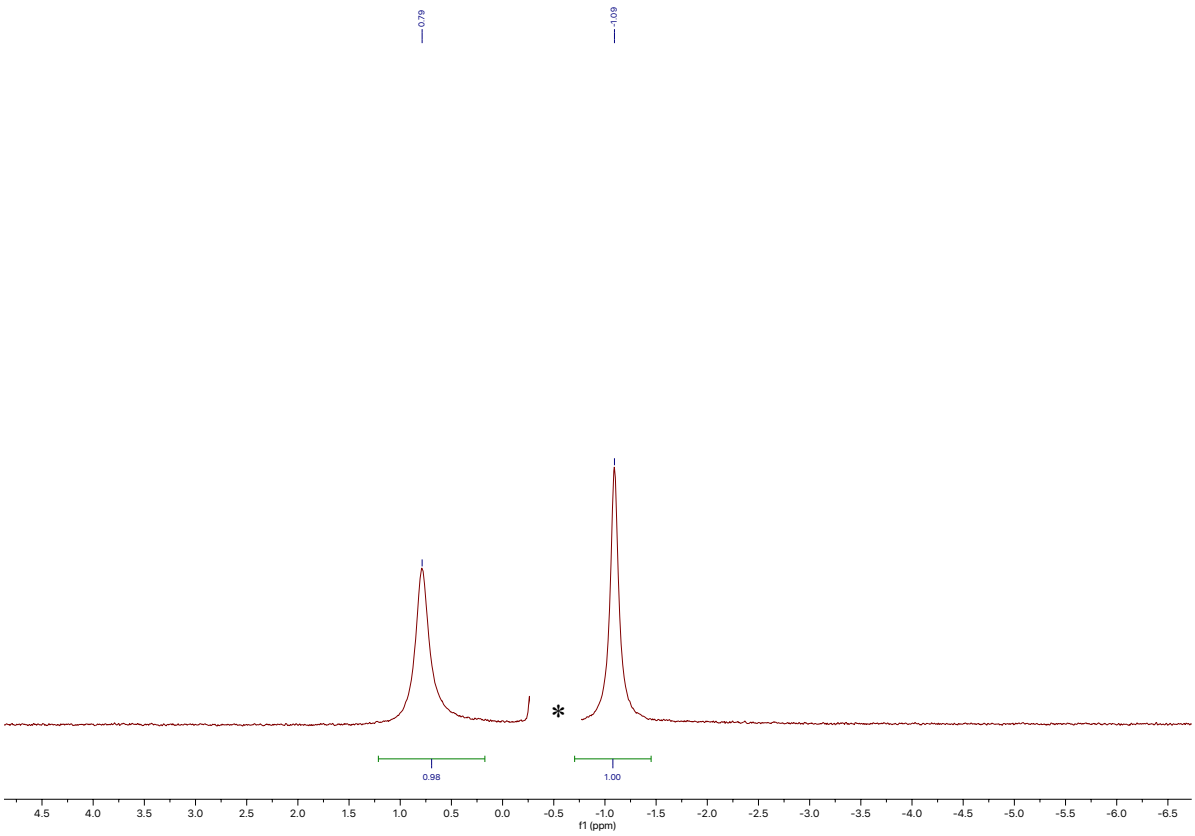

Figure A3.4. ^{7}Li NMR spectrum of $[Li(THF)]_2[L^{\Delta}]$ (**3.1**) in THF-d_8 at room temperature. (*) indicates the resonance assignable to LiI.

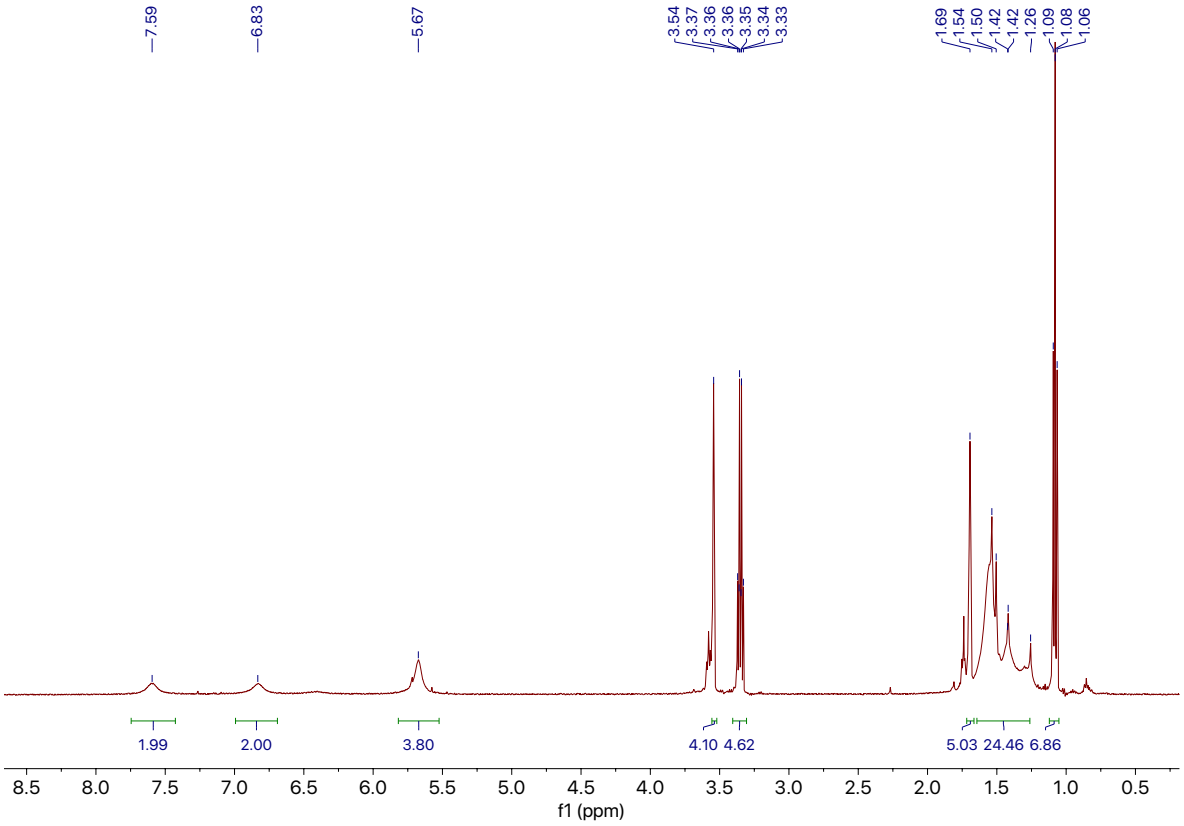

Figure A3.5. ^{1}H NMR spectrum of isolated crystalline material of $[Li(THF)][Li(THF)_{0.58}(Et_2O)_{0.42}][L^{\Delta}]$ in THF-d_8 at room temperature.

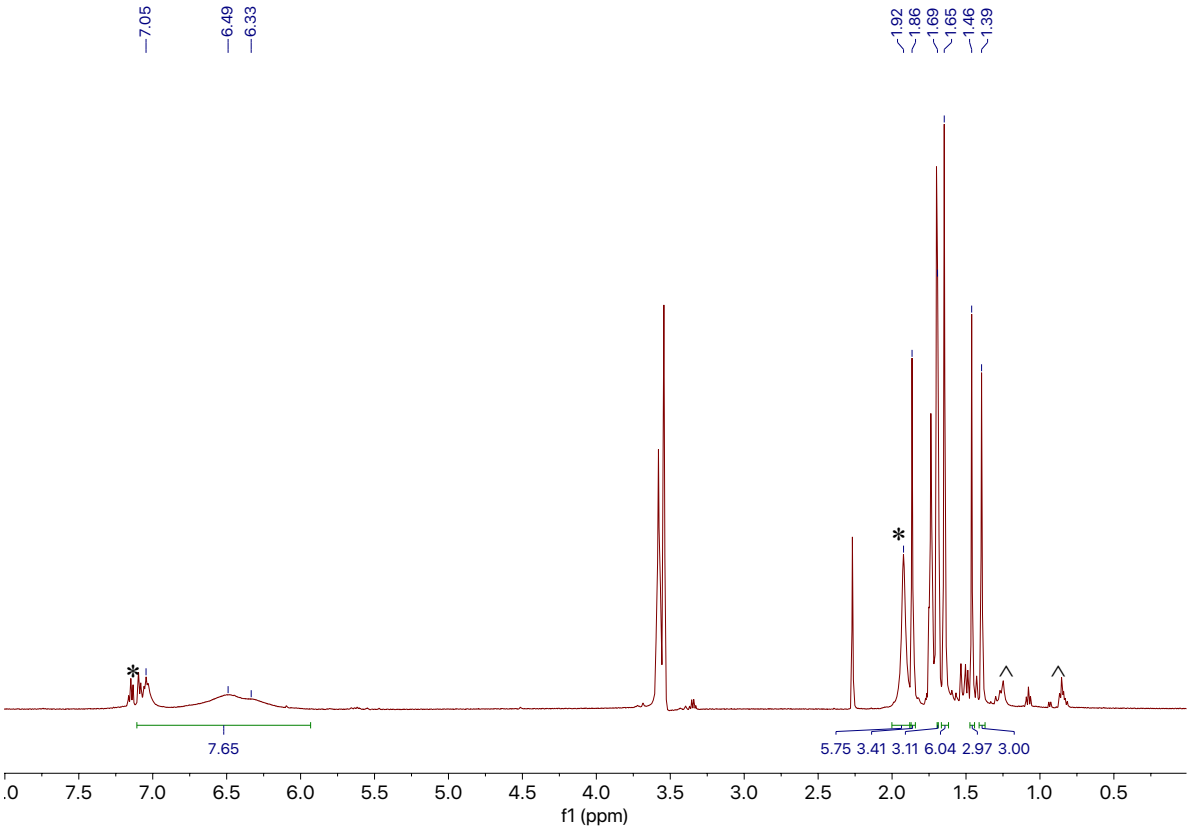

Figure A3.6. ^{1}H NMR spectrum of [Li(THF)][UO_2(L^{Δ})Cl(THF)] (**3.2**) in THF-d_8 at room temperature. (*) indicates resonances assignable to toluene, (^) indicates resonances assignable to hexanes.

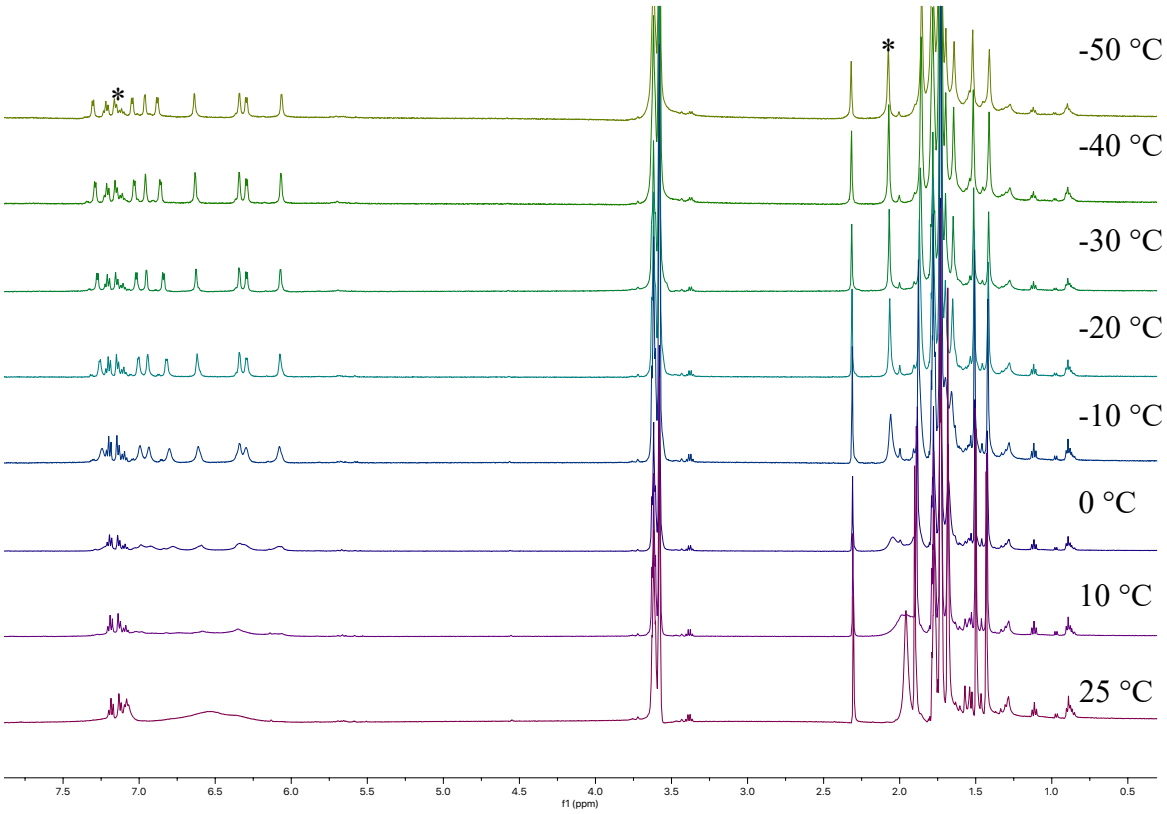

Figure A3.7. Variable temperature ^{1}H NMR spectra of [Li(THF)][UO_2(L^{Δ})Cl(THF)] (**3.2**) in THF-d_8 from 25 °C (bottom) to -50 °C (top). (*) indicates the resonances assignable to toluene.

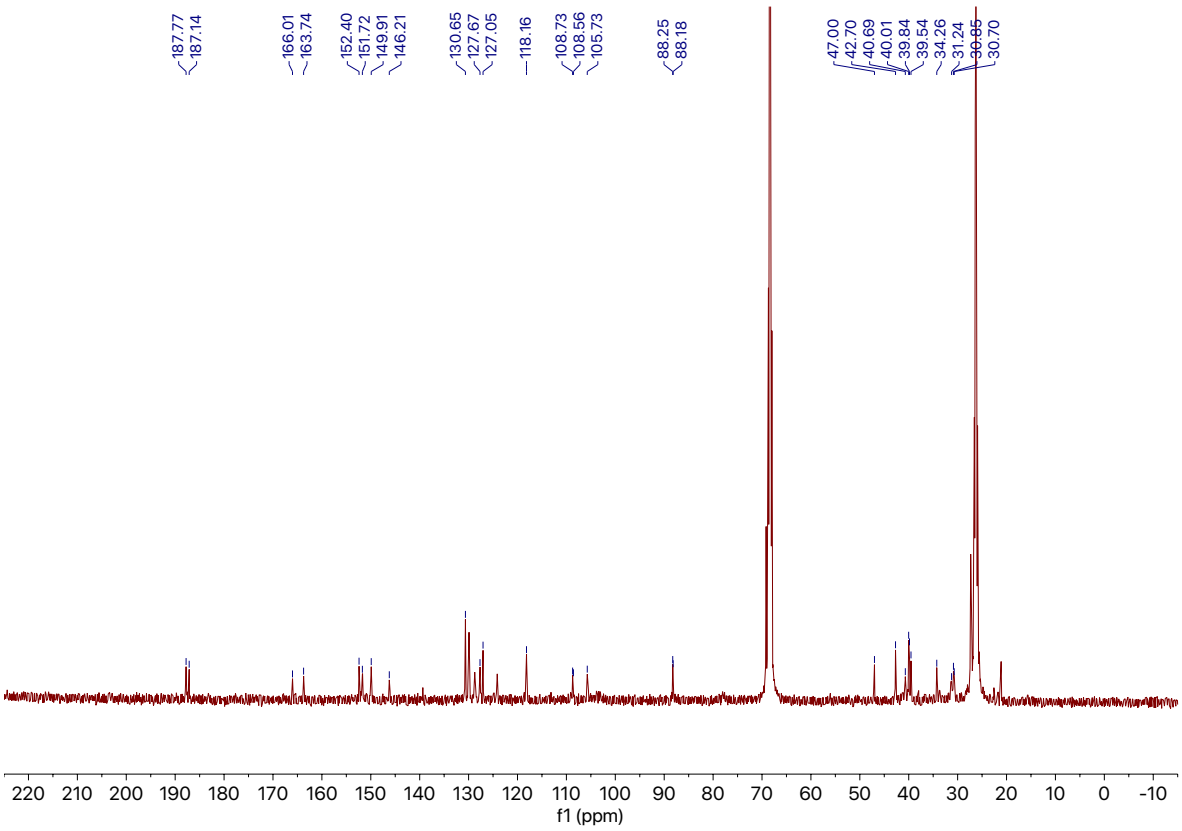

Figure A3.8. $^{13}C\{^{1}H\}$ NMR spectrum of [Li(THF)][$UO_2(L^{\Delta})Cl$(THF)] (**3.2**) in THF-d_8 at -30 °C.

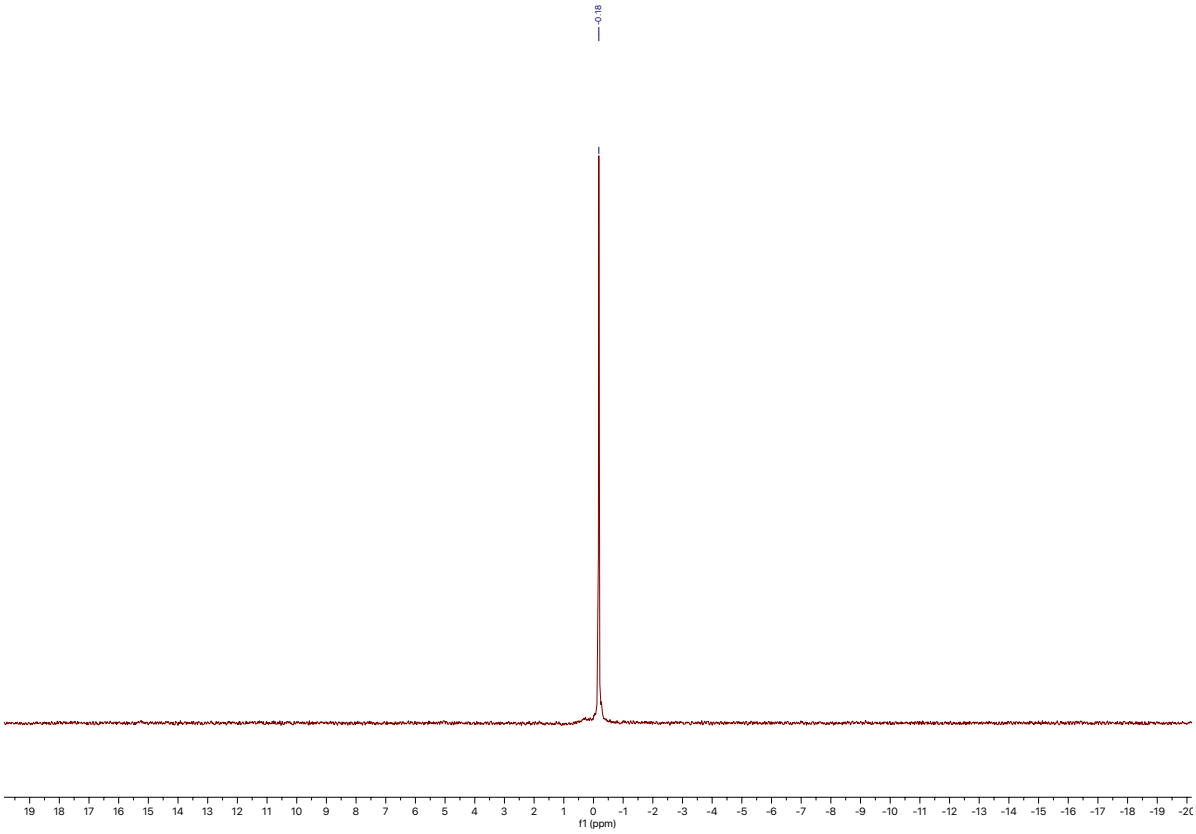

Figure A3.9. ^{7}Li NMR spectrum of [Li(THF)][UO_2(L^A)Cl(THF)] (**3.2**) in THF-d_8 at room temperature.

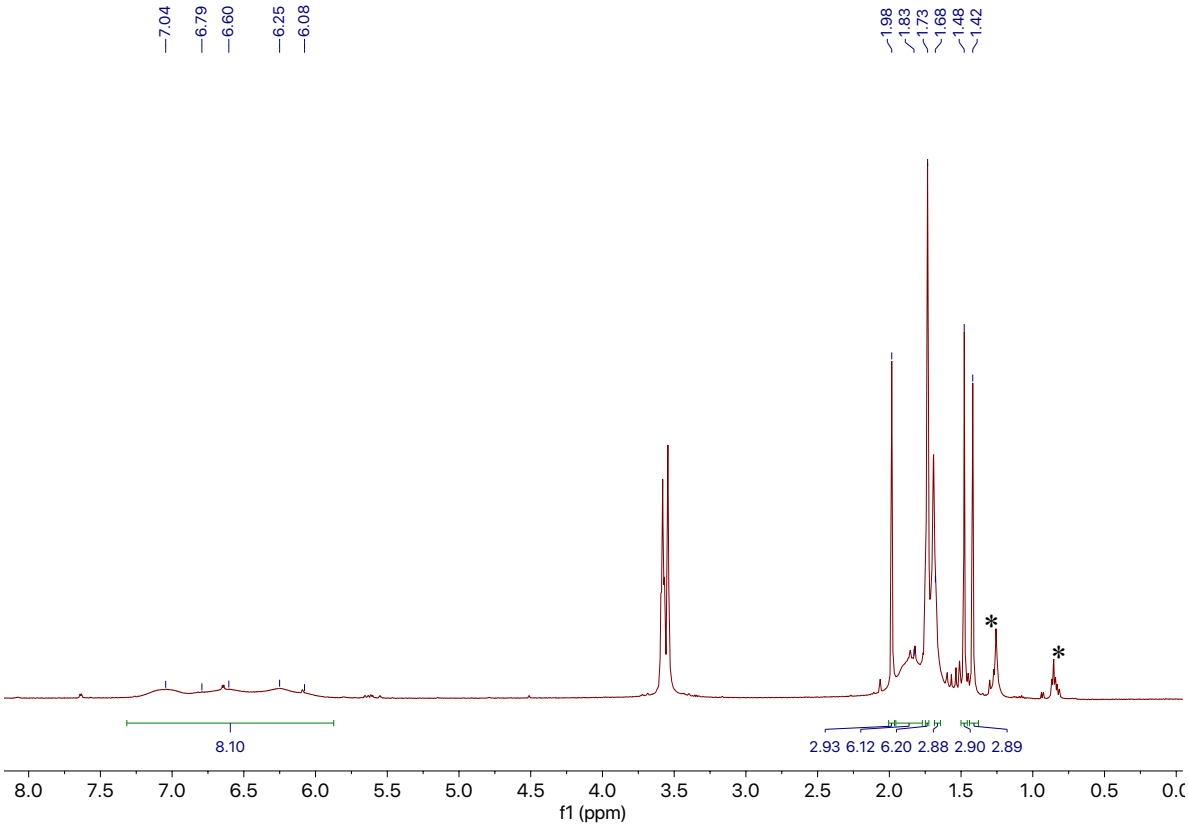

Figure A3.10. ^{1}H NMR spectrum of [Li(THF)][UO_2(L^{Δ})(OTf)(THF)] (**3.3**) in THF-d_8 at room temperature. (*) indicates resonances assignable to hexanes.

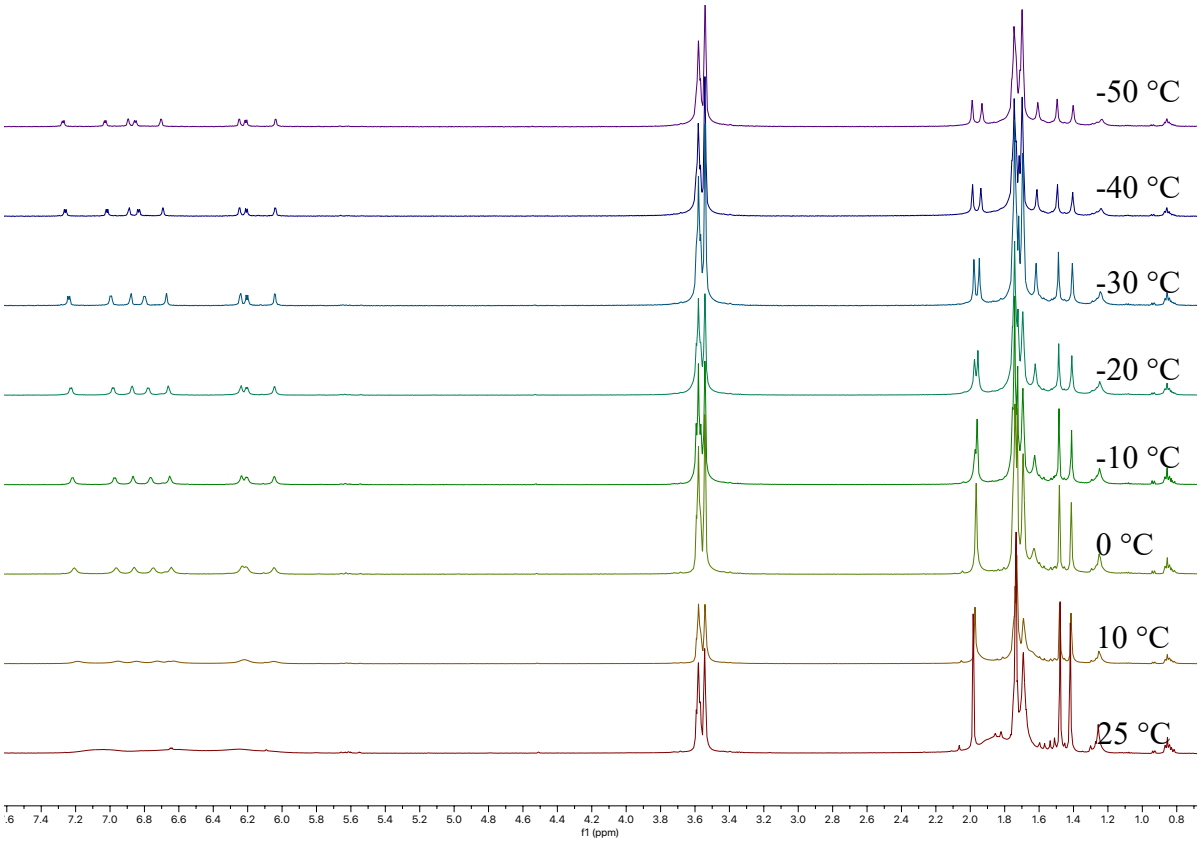

Figure A3.11. Variable temperature ^{1}H NMR spectra of [Li(THF)][UO_2(L^A)(OTf)(THF)] (**3.3**) in THF-d_8 from 25 °C (bottom) to -50 °C (top).

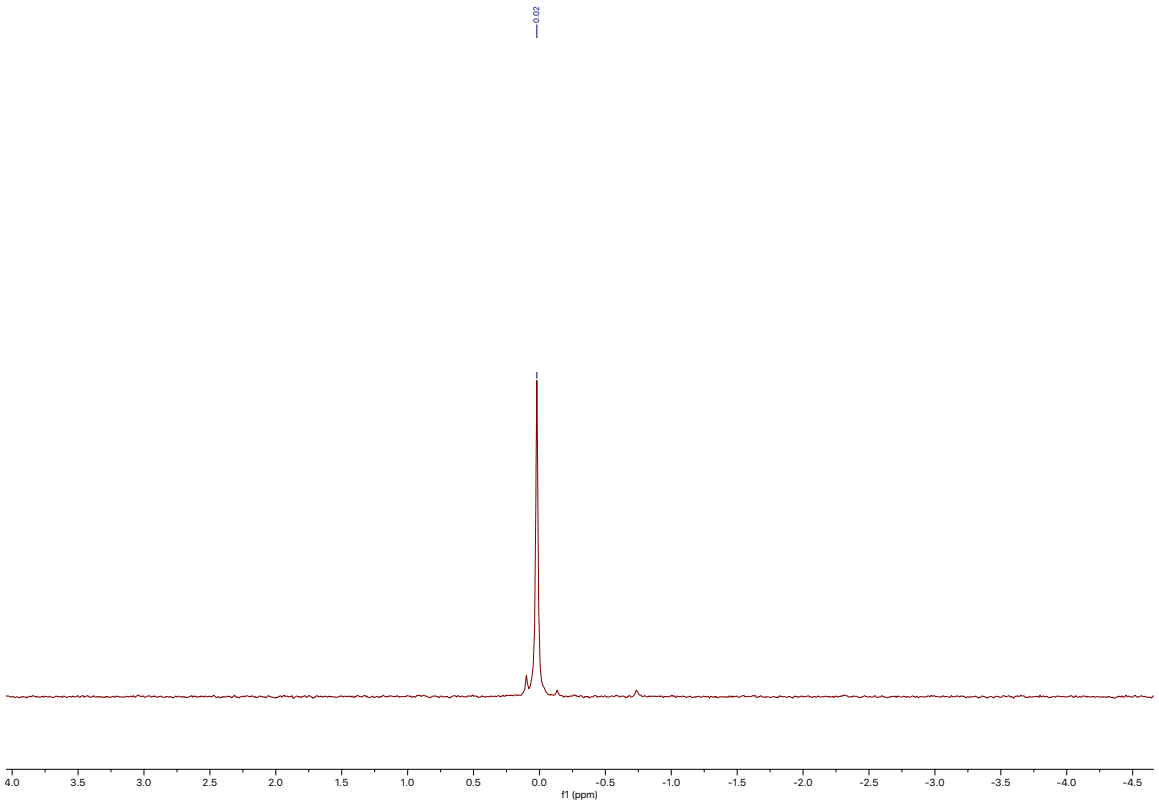

Figure A3.12. ^{7}Li NMR spectrum of [Li(THF)][UO_2(L^A)(OTf)(THF)] (**3.3**) in THF-d_8 at room temperature.

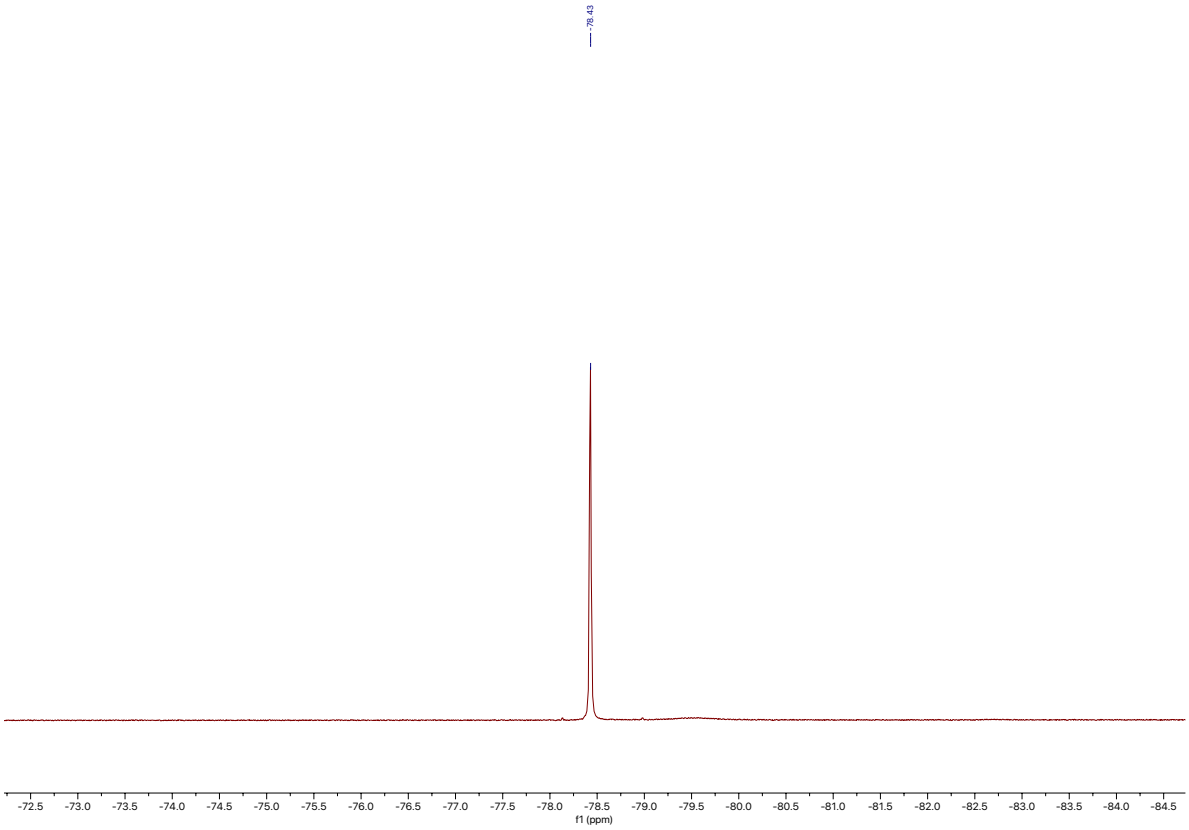

Figure A3.13. $^{19}F\{^{1}H\}$ NMR spectrum of [Li(THF)][UO_2(L^{Δ})(OTf)(THF)] (**3.3**) in THF-d_8 at room temperature.

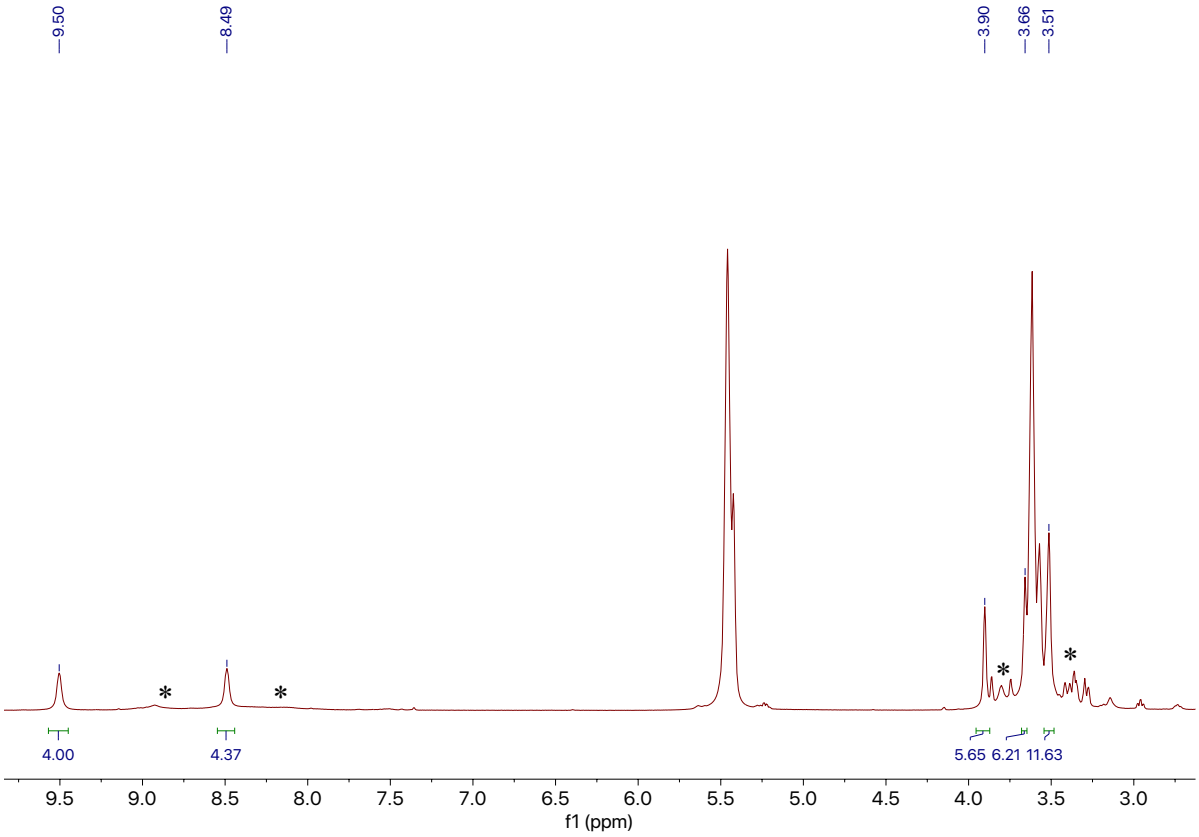

Figure A3.14. ^{1}H NMR spectrum of the brown solid isolated during the work up of [Li(THF)][UO_2(L^A)(OTf)(THF)] (**3.3**) in THF-d_8 at room temperature. (*) indicates resonances assignable to **3.3**. Resonances with integrations are assigned to $L^{\Delta\Delta}$.[13, 14]

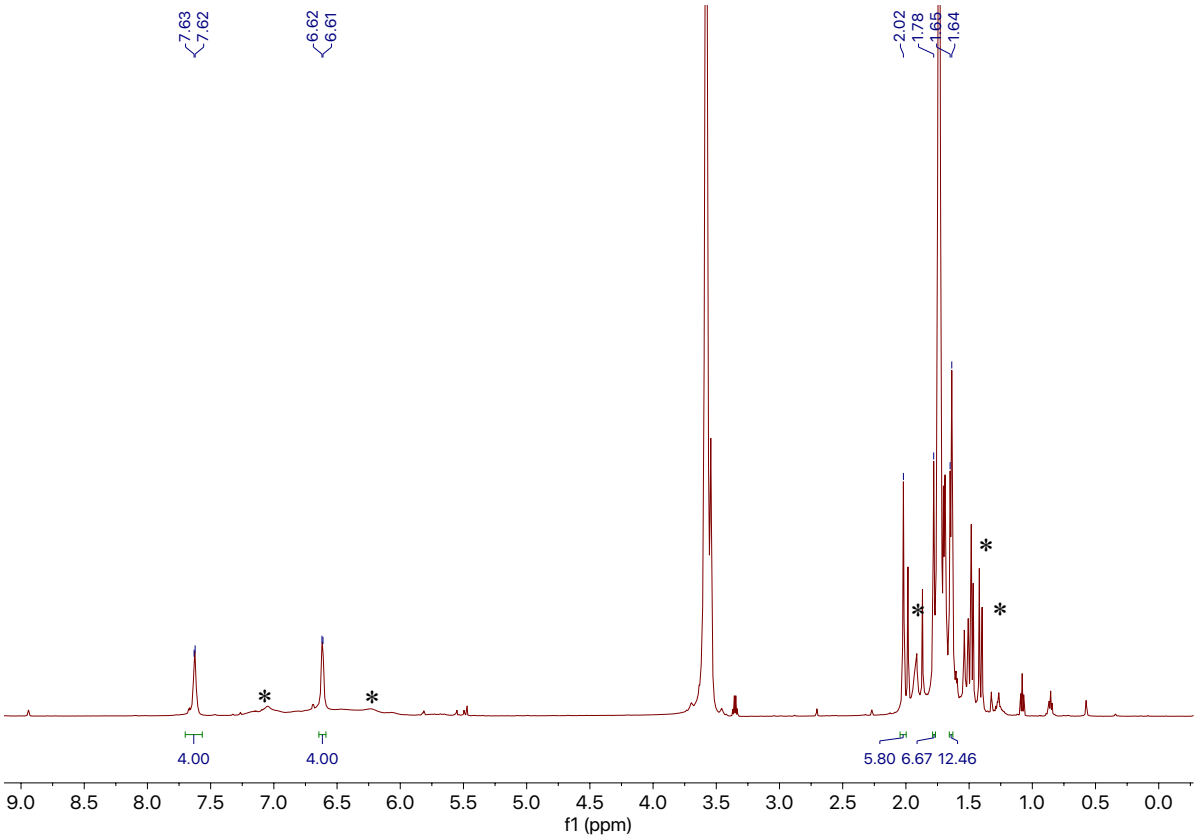

Figure A3.15. ^{1}H NMR spectrum of a crude reaction mixture of $[UO_2(OTf)_2(THF)_3]$ with **3.1** in THF-d_8 at room temperature. Resonances with integrations are assigned to $L^{\Delta\Delta}$.[34, 36] Also present in the spectrum is $[Li(THF)][UO_2(L^{\Delta})(OTf)(THF)]$ (**3.3**), indicated by (*).

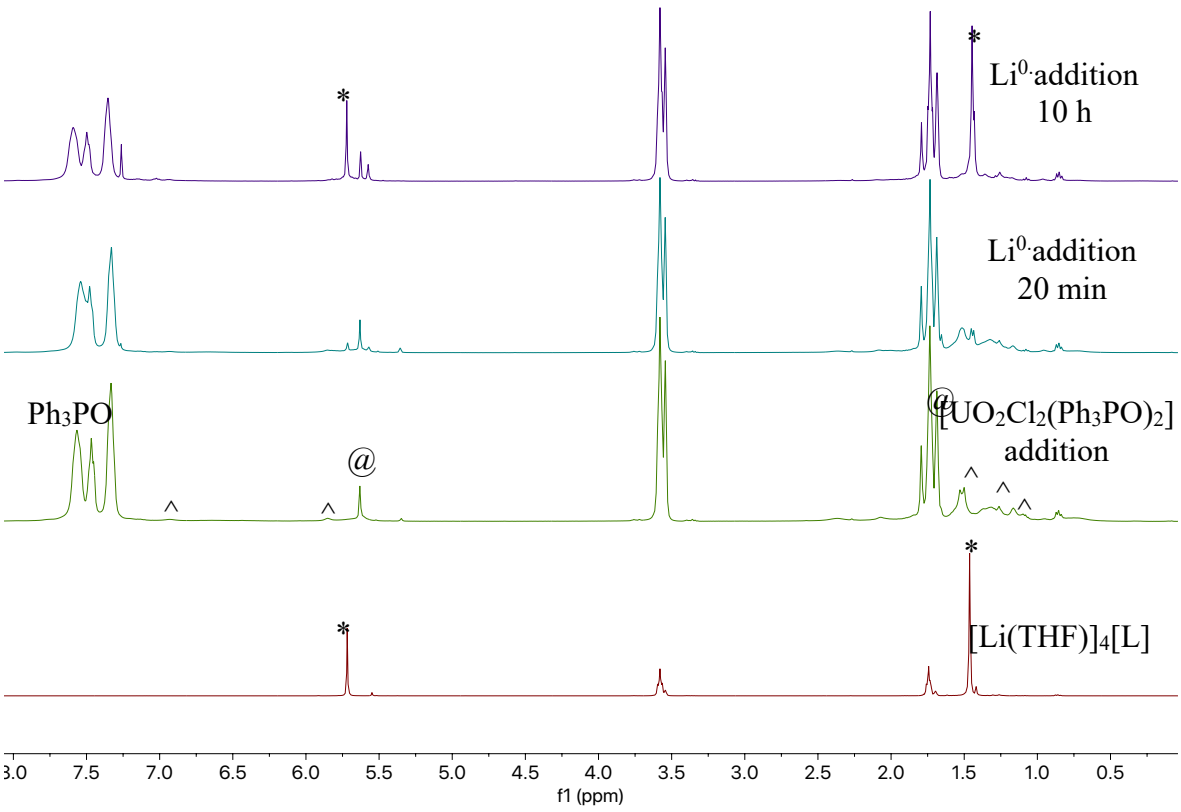

Figure A3.16. ^{1}H NMR spectra of a reaction of $[Li(THF)]_4[L]$ with $[UO_2Cl_2(Ph_3PO)_2]$ followed by reaction with Li^0 metal in THF-d_8 at room temperature. (*) indicates resonances assignable to $[Li(THF)]_4[L]$, (^) indicates resonances assignable to **3.1**, (@) indicates resonances assignable to H_4L.

3.5.2 IR Spectra

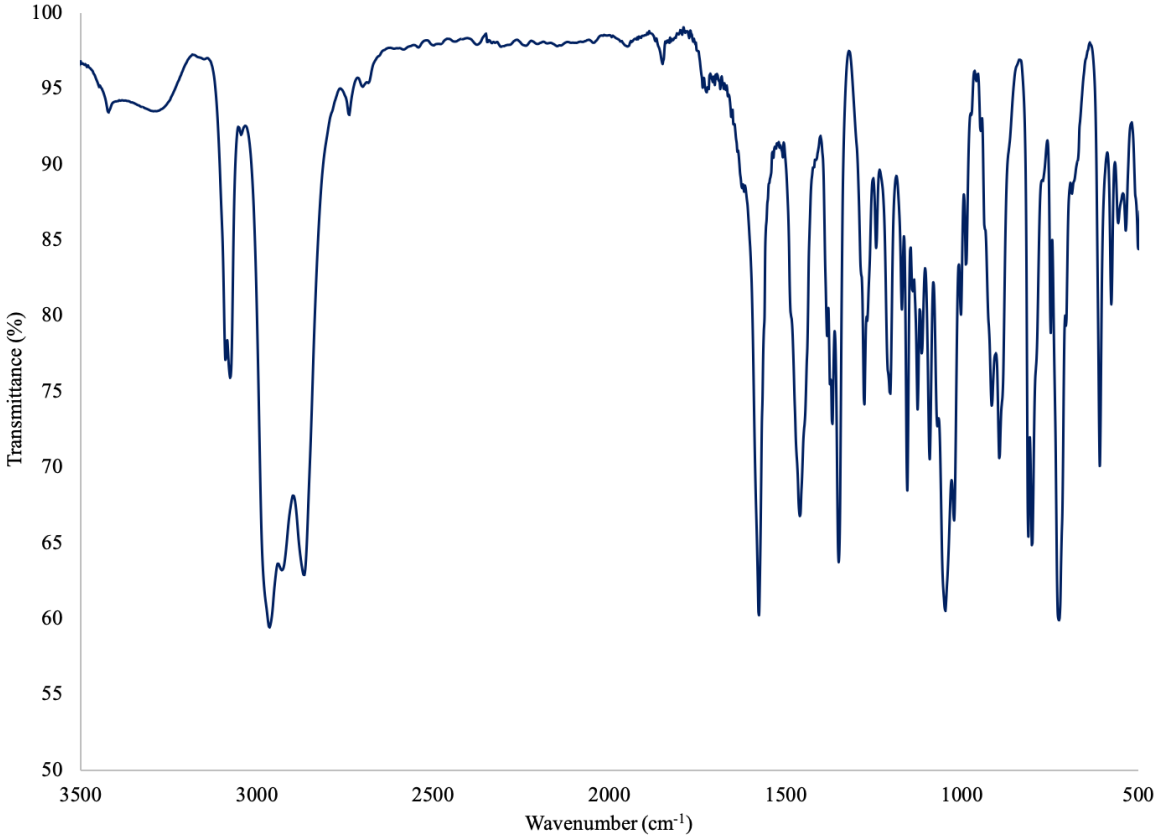

Figure A3.17. IR spectrum of $[Li(THF)]_2[L^A]$ (**3.1**) (KBr Pellet).

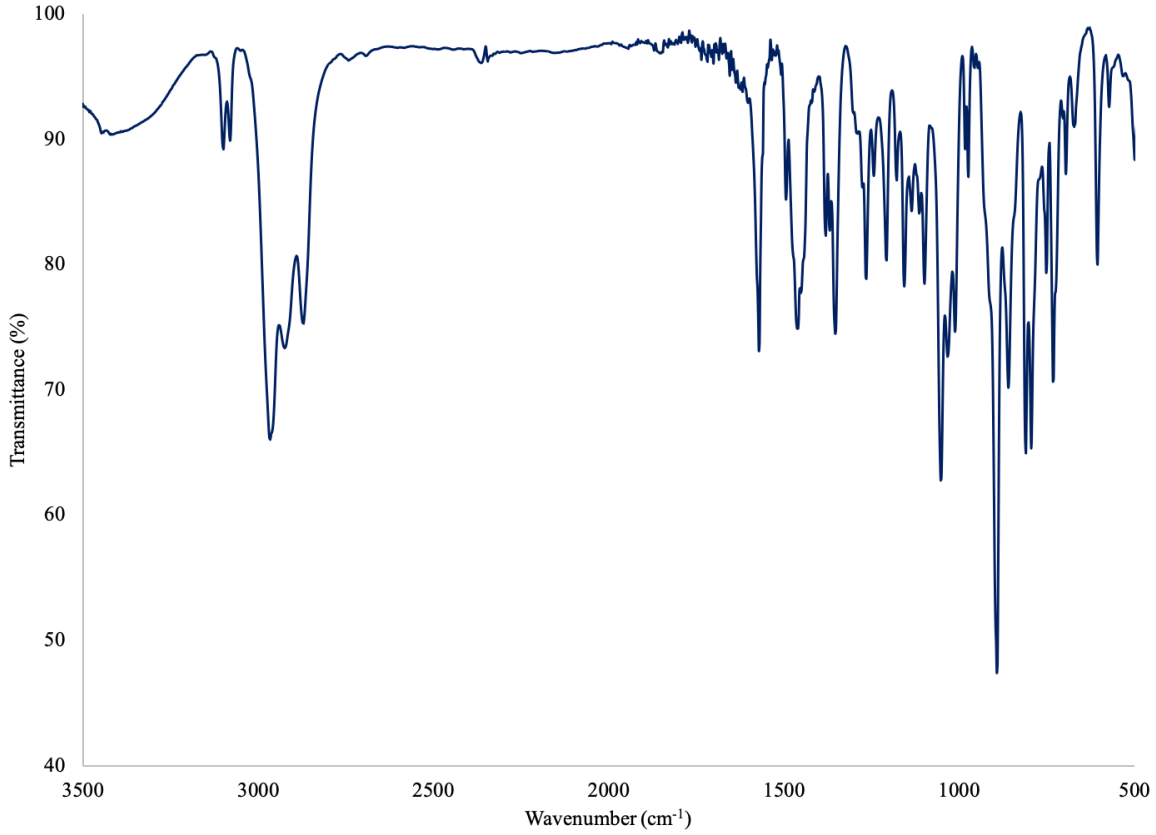

Figure A3.18. IR spectrum of [Li(THF)][UO_2(L^A)Cl(THF)] (**3.2**) (KBr Pellet).

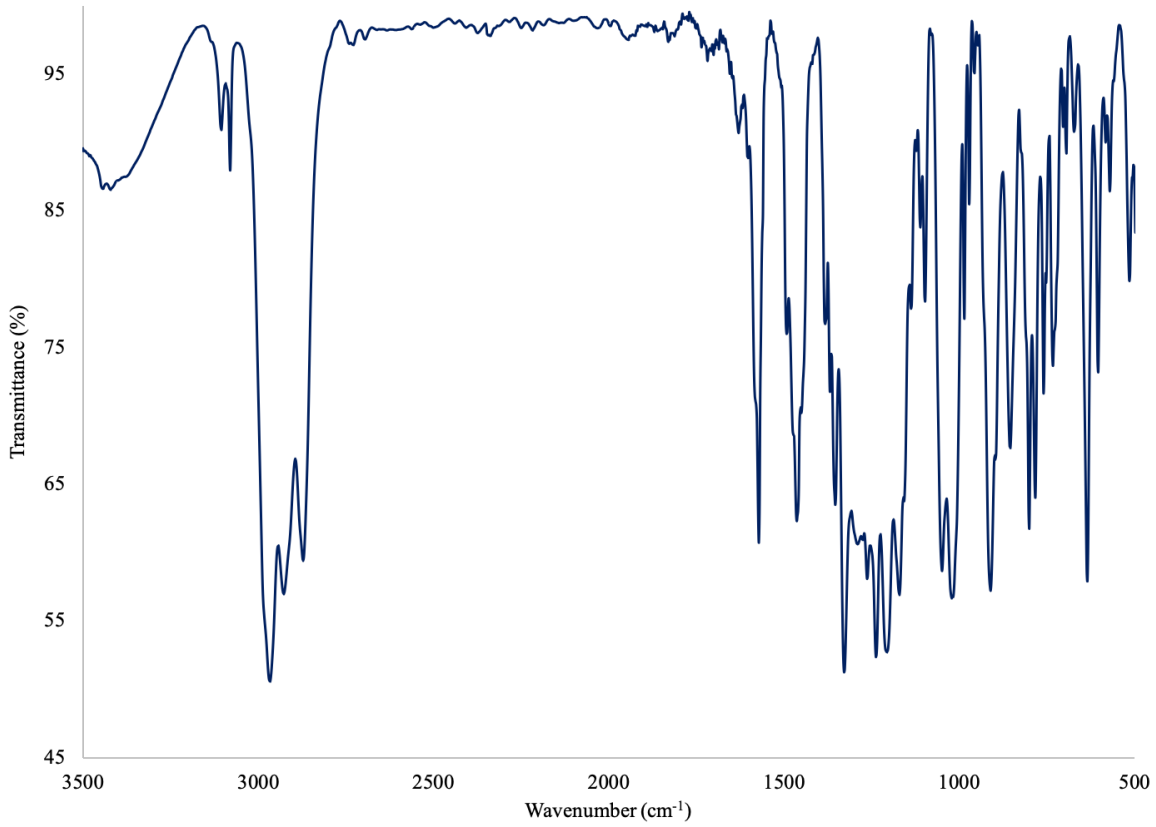

Figure A3.19. IR spectrum of [Li(THF)][$UO_2(L^A)$(OTf)(THF)] (**3.3**) (KBr Pellet).

3.6 References

1. Morris, D. E., Redox Energetics and Kinetics of Uranyl Coordination Complexes in Aqueous Solution. *Inorg. Chem.* **2002**, *41*, 3542-3547.

2. Morrison, S. J.; Metzler, D. R.; Carpenter, C. E., Uranium Precipitation in a Permeable Reactive Barrier by Progressive Irreversible Dissolution of Zerovalent Iron. *Environ. Sci. Technol.* **2001**, *35*, 385-390.

3. Lovely, D. R.; Phillips, E. J. P.; Gorby, Y. A.; Landa, E. R., Microbial Reduction of Uranyl. *Nature* **1991**, *350*, 413-416.

4. Noubactep, C.; Meinrath, G.; Dietrich, P.; Merkel, B., Mitigating Uranium in Groundwater: Prospects and Limitations. *Environ. Sci. Technol.* **2003**, *37*, 4304-4308.

5. Liu, C.; Hsu, P.-C.; Xie, J.; Zhao, J.; Wu, T.; Wang, H.; Liu, W.; Zhang, J.; Chu, S.; Cui, Y., A half-wave rectified alternating current electrochemical method for uranium extraction from seawater. *Nat. Energy* **2017**, *2*, 17007.

6. Xu, Y.; Zondlo, J. W.; Finklea, H. O.; Brennsteiner, A., Electrosorption of uranium on carbon fibers as a means of environmental remediation. *Fuel Process. Technol.* **2000**, *68*, 189-208.

7. McCann, K.; Brigham, D. M.; Morrison, S.; Braley, J. C., Hexavalent Americium Recovery Using Copper(III) Periodate. *Inorg. Chem.* **2016**, *55*, 11971-11978.

8. McCann, K.; Mincher, B. J.; Schmitt, N. C.; Braley, J. C., Hexavalent Actinide Extraction Using *N*,*N*-Dialkyl Amides. *Ind. Eng. Chem. Res.* **2017**, *56*, 6515-6519.

9. Arnold, P. L.; Love, J. B.; Patel, D., Pentavalent uranyl complexes. *Coord. Chem. Rev.* **2009**, *253*, 1973 - 1978.

10. Cowie, B. E.; Purkis, J. M.; Austin, J.; Love, J. B.; Arnold, P. L., Thermal and Photochemical Reduction and Functionalization Chemistry of the Uranyl Dication, $[U^{VI}O_2]^{2+}$. *Chem. Rev.* **2019**, *119*, 10595-10637.

11. Hayton, T. W.; Wu, G., Synthesis, Characterization, and Reactivity of a Uranyl β-Diketiminate Complex. *J. Am. Chem. Soc.* **2008**, *130*, 2005-2014.

12. Faizova, R.; Scopelliti, R.; Chauvin, A.-S.; Mazzanti, M., Synthesis and Characterization of a Water Stable Uranyl(V) Complex. *J. Am. Chem. Soc.* **2018**, *140*, 13554-13557.

13. Berthet, J.-C.; Siffredi, G.; Thuéry, P.; Ephritikhine, M., Controlled Chemical Reduction of Uranyl Salts into $UX_4(MeCN)_4$ (X = Cl, Br, I) with Me_3SiX Reagents. *Eur. J. Inorg. Chem.* **2007**, *2007*, 4017-4020.

14. Arnold, P. L.; Jones, G. M.; Odoh, S. O.; Schreckenbach, G.; Magnani, N.; Love, J. B., Strongly coupled binuclear uranium–oxo complexes from uranyl oxo rearrangement and reductive silylation. *Nat. Chem.* **2012**, *4*, 221-227.

15. Arnold, P. L.; Pécharman, A.-F.; Love, J. B., Oxo Group Protonation and Silylation of Pentavalent Uranyl Pacman Complexes. *Angew. Chem. Int. Ed.* **2011**, *50*, 9456-9458.

16. Yahia, A.; Arnold, P. L.; Love, J. B.; Maron, L., The Effect of the Equatorial Environment on Oxo-Group Silylation of the Uranyl Dication: A Computational Study. *Chem. Eur. J.* **2010**, *16*, 4881-4888.

17. Arnold, P. L.; Pecharman, A.-F.; Hollis, E.; Yahia, A.; Maron, L.; Parsons, S.; Love, J. B., Uranyl oxo activation and functionalization by metal cation coordination. *Nat. Chem.* **2010**, *2*, 1056-1061.

18. Arnold, P. L.; Patel, D.; Wilson, C.; Love, J. B., Reduction and selective oxo group silylation of the uranyl dication. *Nature* **2008**, *451*, 315-318.

19. Schnaars, D. D.; Wu, G.; Hayton, T. W., Silylation of the Uranyl Ion Using $B(C_6F_5)_3$-Activated Et_3SiH. *Inorg. Chem.* **2011**, *50*, 9642-9649.

20. Schnaars, D. D.; Wu, G.; Hayton, T. W., Borane-Mediated Silylation of a Metal-Oxo Ligand. *Inorg. Chem.* **2011**, *50*, 4695-4697.

21. Brown, J. L.; Mokhtarzadeh, C. C.; Lever, J. M.; Wu, G.; Hayton, T. W., Facile Reduction of a Uranyl(VI) b-Ketoiminate Complex to U(IV) Upon Oxo Silylation. *Inorg. Chem.* **2011**, *50*, 5105-5112.

22. Pedrick, E. A.; Wu, G.; Hayton, T. W., Oxo Ligand Substitution in a Cationic Uranyl Complex: Synergistic Interaction of an Electrophile and a Reductant. *Inorg. Chem.* **2015**, *54*, 7038-7044.

23. Pedrick, E. A.; Wu, G.; Kaltsoyannis, N.; Hayton, T. W., Reductive Silylation of a Uranyl Dibenzoylmethanate Complex: An Example of Controlled Uranyl Oxo Ligand Cleavage. *Chem. Sci.* **2014**, *5*, 3204-3213.

24. Pedrick, E. A.; Wu, G.; Hayton, T. W., Reductive Silylation of the Uranyl Ion with Ph_3SiOTf. *Inorg. Chem.* **2014**, *53*, 12237–12239.

25. Kiernicki, J. J.; Cladis, D. P.; Fanwick, P. E.; Zeller, M.; Bart, S. C., Synthesis, Characterization, and Stoichiometric U–O Bond Scission in Uranyl Species Supported by Pyridine(diimine) Ligand Radicals. *J. Am. Chem. Soc.* **2015**, *137*, 11115-11125.

26. Kiernicki, J. J.; Harwood, J. S.; Fanwick, P. E.; Bart, S. C., Reductive silylation of $Cp^*UO_2(^{Mes}PDI^{Me})$ promoted by Lewis bases. *Dalton Trans.* **2016**, *45*, 3111-3119.

27. Kiernicki, J. J.; Zeller, M.; Bart, S. C., Facile Reductive Silylation of UO_2^{2+} to Uranium(IV) Chloride. *Angew. Chem. Int. Ed.* **2017**, *56*, 1097-1100.

28. Coughlin, E.; Bart, S. C., Reductive silylation of uranyl mediated by iminosemiquinone ligands. *Polyhedron* **2019**, *170*, 783-787.

29. Coughlin, E. J.; Qiao, Y.; Lapsheva, E.; Zeller, M.; Schelter, E. J.; Bart, S. C., Uranyl Functionalization Mediated by Redox-Active Ligands: Generation of O–C Bonds via Acylation. *J. Am. Chem. Soc.* **2019**, *141*, 1016-1026.

30. Assefa, M. K.; Pedrick, E. A.; Wakefield, M. E.; Wu, G.; Hayton, T. W., Oxidation of the 14-Membered Macrocycle Dibenzotetramethyltetraaza[14]annulene upon Ligation to the Uranyl Ion. *Inorg. Chem.* **2018**, *57*, 8317-8324.=

31. Duval, P. B.; Burns, C. J.; Clark, D. L.; Morris, D. E.; Scott, B. L.; Thompson, J. D.; Werkema, E. L.; Jia, L.; Andersen, R. A., Synthesis and Structural Characterization of the First Uranium Cluster Containing an Isopolyoxometalate Core. *Angew. Chem. Int. Ed.* **2001**, *40*, 3357-3361.

32. Cantat, T.; Graves, C. R.; Scott, B. L.; Kiplinger, J. L., Challenging the Metallocene Dominance in Actinide Chemistry with a Soft PNP Pincer Ligand: New Uranium Structures and Reactivity Patterns. *Angew. Chem. Int. Ed.* **2009**, *48*, 3681-3684.

33. De Angelis, S.; Solari, E.; Floriani, C.; Chiesi-Villa, A.; Rizzoli, C., Solvent-dependent forms of lithiated 5,5,10,10,15,15,20,20-octaethylporphyrinogen in solution and in the solid state and reaction with tetrahydrofuran. *J. Chem. Soc., Dalton Trans.* **1994**, 2467-2469.

34. Bachmann, J.; Nocera, D. G., Multielectron Chemistry of Zinc Porphyrinogen: A Ligand-Based Platform for Two-Electron Mixed Valency. *J. Am. Chem. Soc.* **2004**, *126*, 2829-2837.

35. Jubb, J.; Floriani, C.; Chiesi-Villa, A.; Rizzoli, C., Redox chemistry of meso-octaethylporphyrinogen: formation and opening of a cyclopropane ring. *J. Am. Chem. Soc.* **1992**, *114*, 6571-6573.

36. Piarulli, U.; Solari, E.; Floriani, C.; Chiesi-Villa, A.; Rizzoli, C., Redox Chemistry Associated with the Complexation of Vanadium(V) and Tungsten(VI) by meso-Octaethylporphyrinogen: Formation and Cleavage of Cyclopropane Units Functioning as Shuttles of Two Electrons. *J. Am. Chem. Soc.* **1996**, *118*, 3634-3642.

37. Burn, A. G.; Nash, K., Electrochemical behavior of uranyl in anhydrous polar organic media. *Radiochim. Acta* **2017**, *105*, 513-522.

38. Martinot, L.; Gubbels, F.; Michaux, C.; Nemeeger, C., Electrochemical Properties of Uranium in Acetonitrile and ββ′ Oxydipropionitrile: Kinetics and Electrodeposition. *Radiochim. Acta* **1992**, *57*, 119-124.

39. Korobkov, I.; Gambarotta, S.; Yap, G. P. A., A Highly Reactive Uranium Complex Supported by the Calix[4]tetrapyrrole Tetraanion Affording Dinitrogen Cleavage, Solvent Deoxygenation, and Polysilanol Depolymerization. *Angew. Chem. Int. Ed.* **2002**, *41*, 3433-3436.

40. Maynadié, J.; Berthet, J.-C.; Thuéry, P.; Ephritikhine, M., The first cyclopentadienyl complex of uranyl. *Chem. Commun.* **2007**, 486-488.

41. Wilkerson, M. P.; Burns, C. J.; Paine, R. T.; Scott, B. L., Synthesis and Crystal Structure of $UO_2Cl_2(THF)_3$: A Simple Preparation of an Anhydrous Uranyl Reagent. *Inorg. Chem.* **1999**, *38*, 4156-4158.

42. Copping, R.; Jeon, B.; Pemmaraju, C. D.; Wang, S.; Teat, S. J.; Janousch, M.; Tyliszczak, T.; Canning, A.; Grønbech-Jensen, N.; Prendergast, D.; Shuh, D. K., Toward Equatorial Planarity about Uranyl: Synthesis and Structure of Tridentate Nitrogen-Donor $\{UO_2\}^{2+}$ Complexes. *Inorg. Chem.* **2014**, *53*, 2506-2515.

43. Hayton, T. W., Understanding the origins of O_{yl}–U–O_{yl} bending in the uranyl (UO_2^{2+}) ion. *Dalton Trans.* **2018**, *47*, 1003-1009.

44. Schöne, S.; Radoske, T.; März, J.; Stumpf, T.; Patzschke, M.; Ikeda-Ohno, A., $[UO_2Cl_2(phen)_2]$, a Simple Uranium(VI) Compound with a Significantly Bent Uranyl Unit (phen=1,10-phenanthroline). *Chem. Eur. J.* **2017**, *23*, 13574-13578.

45. Pedrick, E. A.; Schultz, J. W.; Wu, G.; Mirica, L. M.; Hayton, T. W., Perturbation of the O–U–O Angle in Uranyl by Coordination to a 12-Membered Macrocycle. *Inorg. Chem.* **2016**, *55*, 5693-5701.

46. Carter, K. P.; Kalaj, M.; Kerridge, A.; Ridenour, J. A.; Cahill, C. L., How to Bend the Uranyl Cation via Crystal Engineering. *Inorg. Chem.* **2018**, *57*, 2714-2723.

47. Pedrick, E. A.; Assefa, M. K.; Wakefield, M. E.; Wu, G.; Hayton, T. W., Uranyl Coordination by the 14-Membered Macrocycle Dibenzotetramethyltetraaza[14]annulene. *Inorg. Chem.* **2017**, *56*, 6638-6644.

48. Schettini, M. F.; Wu, G.; Hayton, T. W., Synthesis and reactivity of a uranyl-imidazolyl complex. *Chem. Commun.* **2012**, *48*, 1484-1486.

49. Seaman, L. A.; Hrobárik, P.; Schettini, M. F.; Fortier, S.; Kaupp, M.; Hayton, T. W., A Rare Uranyl(VI)–Alkyl Ate Complex $[Li(DME)_{1.5}]_2[UO_2(CH_2SiMe_3)_4]$ and Its Comparison with a Homoleptic Uranium(VI)–Hexaalkyl. *Angew. Chem. Int. Ed.* **2013**, *52*, 3259-3263.

50. Maity, A. K.; Ward, R. J.; Rupasinghe, D. M. R. Y. P.; Zeller, M.; Walensky, J. R.; Bart, S. C., Organometallic Uranyl Complexes Featuring a Carbodicarbene Ligand. *Organometallics* **2020**, *39*, 783-787.

51. Tourneux, J.-C.; Berthet, J.-C.; Cantat, T.; Thuéry, P.; Mézailles, N.; Ephritikhine, M., Exploring the Uranyl Organometallic Chemistry: From Single to Double Uranium−Carbon Bonds. *J. Am. Chem. Soc.* **2011**, *133*, 6162-6165.

52. Arnold, P. L.; Casely, I. J.; Turner, Z. R.; Carmichael, C. D., Functionalised Saturated-Backbone Carbene Ligands: Yttrium and Uranyl Alkoxy–Carbene Complexes and Bicyclic Carbene–Alcohol Adducts. *Chem. Eur. J.* **2008**, *14*, 10415-10422.

53. Oldham, J. W. J.; Oldham, S. M.; Scott, B. L.; Abney, K. D.; Smith, W. H.; Costa, D. A., Synthesis and structure of -heterocyclic carbene complexes of uranyl dichloride. *Chem. Commun.* **2001**, 1348-1349.

54. Sarsfield, M. J.; Helliwell, M.; Collison, D., The first uranyl–methine carbon bond; a complex with out-of-plane uranyl equatorial coordination. *Chem. Commun.* **2002**, 2264-2265.

55. Mungur, S. A.; Liddle, S. T.; Wilson, C.; Sarsfield, M. J.; Arnold, P. L., Bent metal carbene geometries in amido N-heterocyclic carbene complexes. *Chem. Commun.* **2004**, 2738-2739.

56. Oldham, S. M.; Scott, B. L.; Oldham Jr, W. J., Reaction of the N-heterocyclic carbene, 1,3-dimesityl- imidazol-2-ylidene, with a uranyl triflate complex, $UO_2(OTf)_2(thf)_3$. *J. Appl. Organomet. Chem.* **2006**, *20*, 39-43.

57. Jacoby, D.; Floriani, C.; Chiesi-Villa, A.; Rizzoli, C., Zirconium meso-octaethylporphyrinogen as a carrier for sodium hydride in toluene: zirconium-sodium bimetallic hydride and alkyls. *J. Am. Chem. Soc.* **1993**, *115*, 3595-3602.

58. Harris, R. K.; Becker, E. D.; De Menezes, S. M. C.; Granger, P.; Hoffman, R. E.; Zilm, K. W., Further Conventions for NMR Shielding and Chemical Shifts (IUPAC Recommendations 2008). *Magn. Reson. Chem.* **2008**, *46*, 582-598.

59. Harris, R. K.; Becker, E. D.; Cabral de Menezes, S. M.; Goodfellow, R.; Granger, P., NMR nomenclature: nuclear spin properties and conventions for chemical shifts. IUPAC Recommendations 2001. International Union of Pure and Applied Chemistry. Physical Chemistry Division. Commission on Molecular Structure and Spectroscopy. *Magn. Reson. Chem.* **2002**, *40*, 489-505.

60. *SAINT Software User's Guide*, Version 7.34a ed.; Bruker AXS Inc.: Madison, WI, 2005.

61. Sheldrick, G. M., *SADABS*, the Siemens Area Detector Absorption Correction; University of Göttingen: Göttingen, Germany, 2005.

62. Sheldrick, G. M., *TWINABS*, the Siemens Area Detector Absorption Correction; University of Göttingen: Göttingen, Germany, 2005.

Chapter 4. Synthesis of Parent Acetylide and Dicarbide Complexes of Thorium and Uranium and an Examination of Their Electronic Structures

Portions of this work were published in:

Greggory T. Kent, Xiaojuan Yu, Christophe Pauly, Guang Wu, Jochen Autschbach, Trevor W. Hayton Synthesis of Parent Acetylide and Dicarbide Complexes of Thorium and Uranium and an Examination of Their Electronic Structures. *Inorg. Chem.* **2021**, 60, 15413–15420.

4.1 Introduction

Actinide acetylide complexes have drawn increasing attention for their use in catalysis,[1-11] and more recently for their ability to reveal unique information about actinide electronic structure.[12, 13] For example, Shores and co-workers discovered ferromagnetic communication in a series of bimetallic U(IV) acetylide complexes, such as [{(NN'$_3$)U}$_2$(1,3-(CC)$_2$C$_6$H$_4$)] and [{(NN'$_3$)U}$_2$(1,4-(CC)$_2$C$_6$H$_4$)] (NN'$_3$ = [N(CH$_2$CH$_2$NSi^{t}BuMe$_2$)$_3$]), which they rationalized using Hund's rule.[12] Similarly, Schelter and co-workers probed the covalency of the U–C bond in [U(O)(C≡C−C$_6$H$_4$−*p*−R){N(SiMe$_3$)$_2$}$_3$], (R = NMe$_2$, OMe, Me, Ph, H, Cl) using ^{13}C NMR spectroscopy and density functional theory (DFT).[14, 15] Their results demonstrated extensive 5f orbital participation in the U–C bond. Indeed, the use of NMR spectroscopy to study covalency is emerging as a valuable technique for probing the electronic structure of f-element-ligand bonds. A variety of nuclei have been employed for this purpose, including ^{77}Se, ^{125}Te, and ^{15}N.[16-19] This analysis has also been applied to a variety of organometallic actinide and lanthanide complexes, including those containing alkyl, aryl, and carbene ligands.[20-25]

Despite these recent advancements in actinide acetylide chemistry, the synthesis and reactivity of actinide parent acetylide complexes, e.g., An–C≡CH, remains underexplored. To my knowledge, only one actinide parent acetylide complex is known, [Cp$_3$U(C≡CH)], which was reported by Gebala and co-workers in 1976.[26] In addition, only one actinide dicarbide complex is known, namely, [(μ,η^1:η^1–C$_2$){U(N[*t*-Bu]Ar)$_3$}$_2$], formed by reaction of UI(N[*t*-Bu]Ar)$_3$ with NaCCH.[27] These complexes are intriguing targets, both because of the insights they could give into actinide electronic structure, but also because of the potential for enhanced

reactivity relative to alkyl- or aryl-substituted acetylide complexes. However, the synthetic chemistry to access actinide parent acetylides is not well established.

Herein, I report the synthesis of a family of actinide parent acetylide and dicarbide complexes, including [An(C≡CH)$(NR_2)_3$] (**4.1**, An = U; **4.2**, An = Th), [Na(TMEDA)][An$(C{\equiv}CH)_2(NR_2)_3$] (**4.4**, An = U; **4.5**, An = Th), and [{An$(NR_2)_3$}$_2$(μ,η^1:η^1-C_2)] (**4.6**, An = U; **4.7**, An = Th). These complexes were characterized by a variety of techniques, including ^{13}C NMR spectroscopy, DFT, and SQUID magnetometry, with the goal of understanding the nature of their An–C bonds.

4.2 Results and discussion

4.2.1 Synthesis and Characterization

During his time as a visiting researcher at UCSB, Christophe Pauly found that slow addition of 1.1 equiv of sodium acetylide and 1.1 equiv of tetramethylethylenediamine (TMEDA) in a mixture of xylenes and THF to a cold stirring THF solution of [UCl$(NR_2)_3$] (R = $SiMe_3$) results in an immediate color change from pink to light brown (Scheme 4.1). Work-up and crystallization of the reaction mixture affords [U(C≡CH)$(NR_2)_3$] (**4.1**) as a red-purple solid in 81% yield. Christophe also discovered that complex **4.1** can also be accessed by reaction of U$(NR_2)_3$ (R = $SiMe_3$) with acetylene in THF (See general section for experimental details). When synthesized in this fashion **4.1** can be isolated in 35% yield after work-up (Scheme 4.2). I later found that the thorium analogue, [Th(C≡CH)$(NR_2)_3$] (**4.2**) could be prepared similarly, via the reaction of [ThCl$(NR_2)_3$] with 1.1 equiv of sodium acetylide and TMEDA in cold THF/xylenes. Work-up and crystallization of the resulting reaction mixture affords **4.2** as colorless blocks in 78% yield (Scheme 4.1).

Scheme 4.1. Syntheses of Complexes **4.1**, **4.2**, **4.4**, and **4.5**

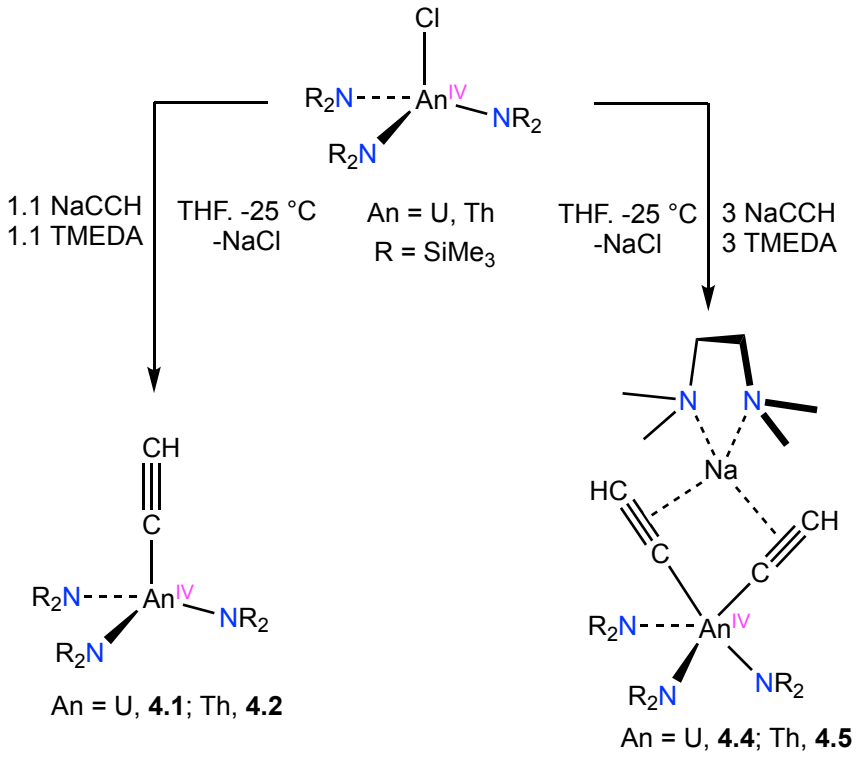

Scheme 4.2. Synthesis of **4.1** from $[U(NR_2)_3]$ and Acetylene Gas

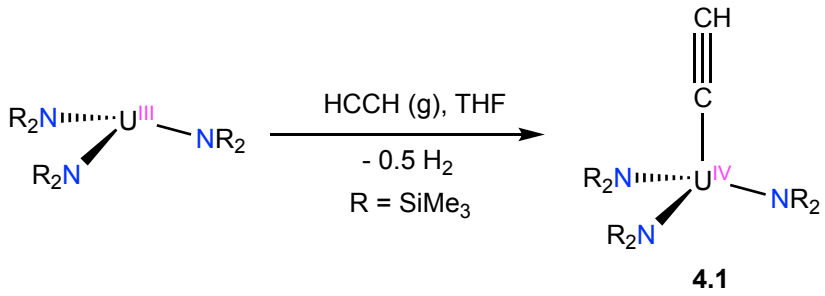

The ^{1}H NMR spectrum of complex **4.1** in C_6D_6 features two paramagnetically-shifted resonances at –1.95 and –5.47 ppm, in a 54:1 ratio, which are assignable the $SiMe_3$ and ethynyl proton environments, respectively (Figure A4.1). Similarly, the ^{1}H NMR spectrum of complex **4.2** in THF-d_8 features resonances at 0.38 and 2.32 ppm, in a 54:1 ratio, assignable to the $SiMe_3$ and ethynyl proton environments, respectively (Figure A4.3). Additionally, the $^{13}C\{^1H\}$ NMR

spectrum of **4.2** in THF-d_8 features resonances at 176.1, 97.3, and 4.7 ppm, assignable to the C_α, C_β, and $SiMe_3$ environments (Figure A4.5). For comparison, the α-acetylide ^{13}C chemical shift for [Th(C≡C-*p*-tolyl)(BIMA)$_3$] (BIMA = MeC(N^{i}Pr)$_2$) is found at 189.2 ppm, whereas the hafnium complex [{Cp*$_2$Hf(C≡CH)$_2$}(μ–C$_2$)] exhibits an C_α ^{13}C chemical shift of 128.29 ppm.[28, 29] I attribute the ~50 ppm downfield shift between [{Cp*$_2$Hf(C≡CH)$_2$}(μ-C$_2$)] and the two Th complexes to the spin orbit induced deshielding of the α-acetylide resonance, which is evidence for 5f involvement in the Th–C bonds (see below for more discussion). The IR spectrum of **4.1** exhibits acetylide C–H and C≡C stretches at 3292 and 1938 cm^{-1}, respectively (Figure A4.16). As seen in Table 4.1, the calculated acetylide C-H and C≡C stretching frequencies agree well with the experimental values. The IR spectrum of **4.2** exhibits nearly identical acetylide C–H and C≡C stretches, at 3278 and 1938 cm^{-1}, respectively (Figure A4.17). For comparison, free acetylene features a C≡C stretch at 1974 cm^{-1},[30] whereas [{Cp*$_2$Hf(C≡CH)$_2$}(μ–C$_2$)] features C≡C and C–H stretches at 1938 and 3280 cm^{-1}, respectively.[28, 29] These values indicate some activation of the C≡C bond in **1** and **2** relative to HCCH.

Table 4.1. Selected IR spectral data for complexes **4.1**, **4.2**, **4.4**, **4.5**, and **4.8**.

Complex	ν(C≡C) (cm^{-1})	ν(C–H) (cm^{-1})
4.1	1938 (1937)[a]	3292 (3328)[a]
4.2	1938	3278
4.4	1913	3255
4.5	1917	3255
4.8	2019	N/A

[a] Calculated [PBE/6-31G(d), scaled by 0.986] frequencies in parentheses.

While complex **4.1** readily crystallized from pentane, all diffraction data collected for this material resisted refinement, despite my best efforts. In contrast, complex **4.2** crystalized nicely from pentane in the monoclinic space group $P2_1/c$ (Figure 4.1). It features a pseudotetrahedral geometry about the thorium center with Th−C and C≡C distances of 2.481(8) and 1.173(12) Å, respectively (Table 4.2). Only a handful of thorium-acetylide complexes have been previously reported, including $[1,3\text{-}(Me_3C)_2C_5H_3]_2Th(C{\equiv}CPh)_2$ and Th(C≡C-*p*-tolyl)$(BIMA)_3$.[31, 32] Their Th–C distances range from 2.461(4) to 2.542(2) Å, whereas their C≡C distances range from 1.197(5) to 1.220(5) Å.[11, 29, 31, 32] The only other structurally characterized actinide parent acetylide complex, $[Cp_3U(C{\equiv}CH)]$, features U−C and C≡C distances of 2.36(3) and 1.29(5) Å, respectively.[26]

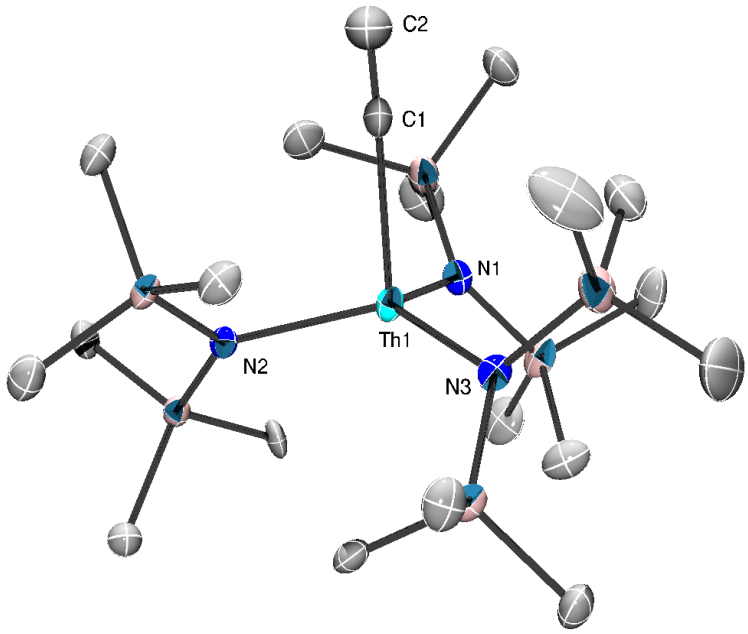

Figure 4.1. Solid-state molecular structure of $[Th(C{\equiv}CH)(NR_2)_3]$ (**4.2**), with 50% probability ellipsoids shown for all atoms. Hydrogen atoms omitted for clarity.

Addition of 2 equiv of KC_8 to a cold stirring solution of **4.1** in THF, followed by filtration and addition of 1 equiv of 2.2.2-cryptand affords [K(2.2.2-cryptand)][U(C≡CH)$(NR_2)_3$] (**4.3**), which can be isolated as deep blue needles in 79% yield after work-up (Scheme 4.3). Complex **4.3** crystallizes as a discrete cation-anion pair in the monoclinic space group $P2_1/n$ and features a pseudotetrahedral geometry about the uranium center (Figure 4.2). Importantly, its structural characterization confirms the connectivity of complex **4.1**. The U−C and C≡C distances in **4.3** are 2.512(8) Å and 1.162(11) Å, respectively (Table 4.2). For comparison, the U(III) acetylide complex, [Tp*2U(C≡CPh)], exhibits a U−C distance of 2.589(9) Å and a C≡C distance of 1.100(11) Å.[33]

Scheme 4.3. Synthesis of Complex **4.3**

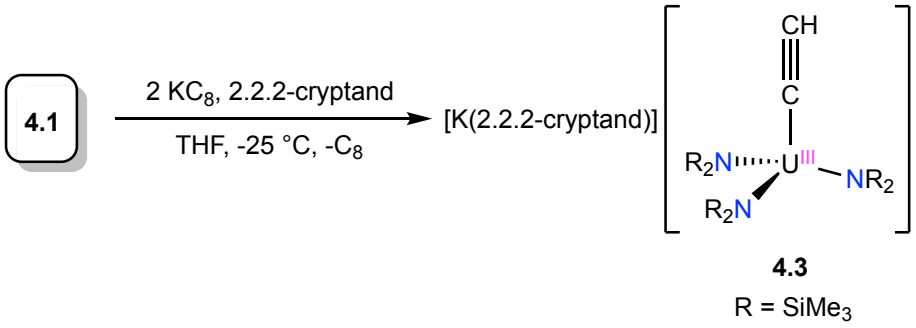

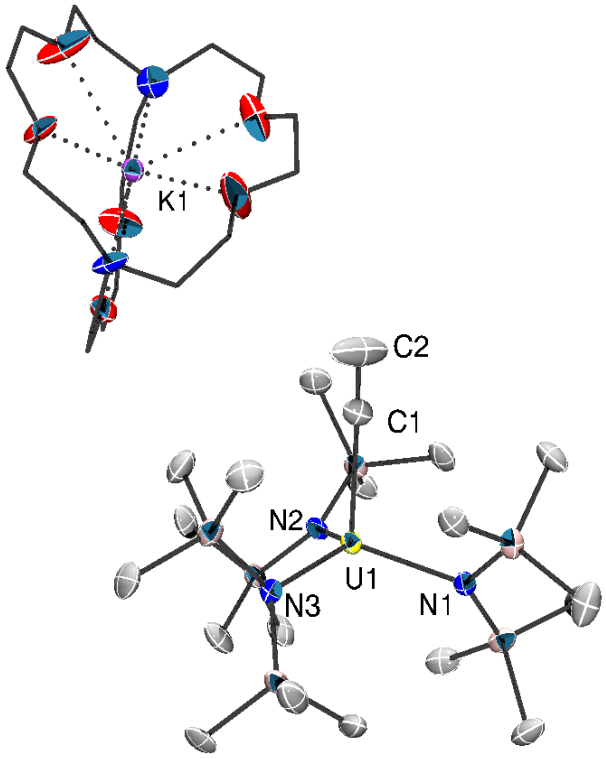

Figure 4.2. Solid-state molecular structure of **4.3** shown with 50% probability ellipsoids shown for all atoms except cryptand carbon atoms, which are shown in wireframe. Hydrogen atoms are removed for clarity.

Addition of 3 equiv of sodium acetylide and 3 equiv of TMEDA to a cold stirring solution of $[UCl(NR_2)_3]$ (R = $SiMe_3$) in THF results in formation of $[Na(TMEDA)][U(C{\equiv}CH)_2(NR_2)_3]$ (**4.4**), which can be isolated in 47% yield as light green blocks after work-up and crystallization (Scheme 4.1). The thorium analogue, $[Na(TMEDA)][Th(C{\equiv}CH)_2(NR_2)_3]$ (**4.5**), can be prepared in a similar fashion in 53% yield as colorless blocks (Scheme 4.1). The highest yields are achieved when an excess of NaCCH is used in the reactions. When a stoichiometric amount of NaCCH is employed instead, mixtures of the bis- and mono-acetylide complexes are generated. The ^{1}H NMR spectrum of **4.4** in THF-d_8 features one paramagnetically-shifted

singlet at 65.79 ppm and one extremely broad singlet centered at –9.66 ppm ($\nu_{1/2}$ = 3100 Hz), which are assignable to the ethynyl and $SiMe_3$ environments, respectively (Figure A4.7). Additionally, resonances at 2.30 and 2.15 ppm, in a 4:12 ratio, are assignable to the TMEDA moiety. The ^{1}H NMR spectrum of **4.5** in THF-d_8 exhibits four singlets at 2.30, 2.15, 1.57 and 0.33 ppm, in an 4:12:2:54 ratio, which are assignable to the two TMEDA environments, the ethynyl proton environment, and the $SiMe_3$ environment, respectively (Figure A4.8). Additionally, the $^{13}C\{^1H\}$ NMR spectrum of **5** in THF-d_8 exhibits diagnostic resonances at 183.9 and 94.5 ppm which correspond to α-acetylide and β-acetylide carbons (Figure A4.9). The IR spectrum of **4.4** exhibits acetylide C–H and C≡C stretches at 3255 and 1913 cm^{-1} (Table 4.1, Figure A4.19), whereas, the IR spectrum of **4.5** exhibits acetylide C–H and C≡C stretches at 3255 and 1917 cm^{-1} (Figure A4.20). For comparison, the U(IV) bis(acetylide), [Li(THF)][(NN'$_3$)U(CCPh)$_2$], exhibits a C≡C stretch at 2044 cm^{-1}.[12] In principle, **4.4** and **4.5** could exhibit symmetric and asymmetric C≡C stretches;[34] however, only one C≡C stretch is observed. Similar spectral behavior was found for the aforementioned [Li(THF)][(NN'$_3$)U(CCPh)$_2$], as well as [(L)An(C≡CR′)$_2$] (L = *trans*-calix[2]benzene[2]pyrrolide; An = Th, U; R′ = $SiMe_3$, Si^iPr_3).[11, 12]

Table 4.2. Selected Metrical Parameters for Complexes **4.2**-**4.5** (Å and deg)

Bond	**4.2**	**4.3**	**4.4**	**4.5**
M–C	2.481(8)	2.512(8)	2.519(5),2.572(5)	2.570(5), 2.642(5)
C≡C	1.173(12)	1.162(11)	1.194(7), 1.190(7)	1.193(7), 1.194(7)
$M–N_{amide}$	2.302(6), 2.302(6) 2.313(5)	2.379(5), 2.382(5), 2.383(5)	2.251(4), 2.280(4), 2.319(4)	2.300(3), 2.329(4), 2.395(4)
$Na–C_{\alpha}$			2.657(5), 2.673(6)	2.649(5), 2.683(6)
$Na–C_{\beta}$			2.522(5), 2.582(5)	2.482(5), 2.572(5)
M–C≡C	176.7(8)	176.5(8)	176.1(4), 171.9(4)	175.9(4), 170.6(4)
N–M–C	97.3(2), 97.6(2), 101.1(2)	99.9(2), 101.6(2), 102.6(2)	78.90(15), 85.07(15), 92.93(14), 109.80(15), 117.23(14), 169.83(13)	78.81(14), 85.60(14), 92.29(13), 110.25(13), 116.94(13), 168.40(12)
C–M–C			76.92(15)	76.13(14)
τ^5			0.75	0.73

Complexes **4.4** and **4.5** crystallize in the monoclinic space group Cc and are isostructural. Both **4.4** and **4.5** crystallize as contact ion pairs and feature distorted trigonal bipyramidal geometries about their metal centers (**4.4**: $\tau^5 = 0.75$; **4.5**: $\tau^5 = 0.73$),[35] wherein one acetylide ligand occupies an axial site and one occupies an equatorial site (Figure 4.3). The sodium counterion is bound to both acetylide ligands via η^2-interactions, as well as to a TMEDA fragment. The axial and equatorial U−C bond lengths in **4.4** are 2.572(5) and 2.519(5) Å, respectively, while the C≡C bond lengths are 1.190(7) and 1.194(7) Å (Table 4.2). For comparison, the axial and equatorial Th−C bond lengths of **4.5** are 2.642(5) and 2.570(5) Å, respectively, while the C≡C bond lengths are 1.193(7) and 1.194(7) Å (Table 4.1). Not surprisingly, the average Th−C distance in **4.5** is longer than the U−C distance in **4.4**, due to the larger ionic radius of Th^{4+} vs U^{4+}.[36]

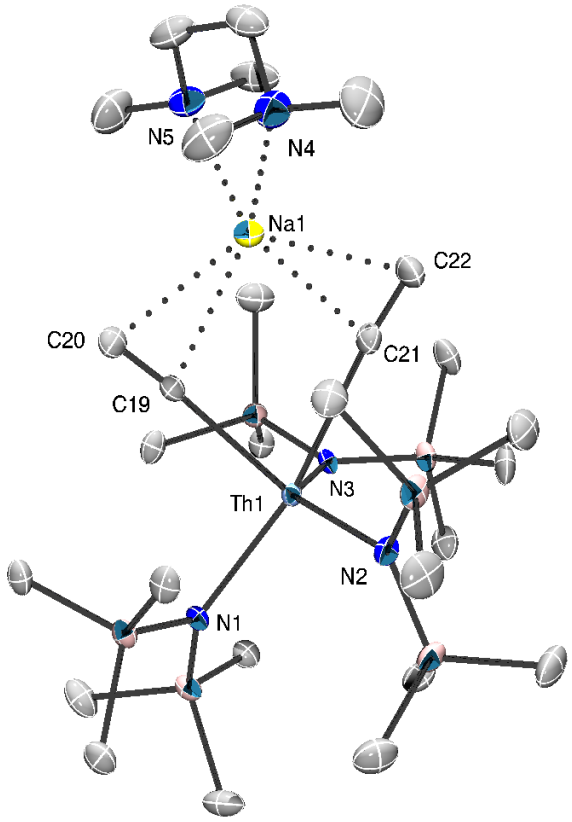

Figure 4.3. Solid-state molecular structure of [Na(TMEDA)][Th(C≡CH)$_2$(NR$_2$)$_3$] (**4.5**) with 50% probability ellipsoids shown for all atoms. Hydrogen atoms omitted for clarity.

I also briefly explored the reactivity of complexes **4.1** and **4.2**. Thus, heating a benzene-d_6 solution of **4.1** at 45 °C for 24 h results in a color change from purple to dark brown. Examination of the ^{1}H NMR spectrum of this solution shows the disappearance of the resonances assignable to **4.1** and the appearance of a single new SiMe$_3$ resonance at –6.29 ppm, assignable to the dicarbide complex, [{U(NR$_2$)$_3$}$_2$(μ,η^1:η^1-C$_2$)] (**4.6**). Similarly, heating a benzene-d_6 solution of **4.2** at 75 °C for 24 h results in formation of a new species with an SiMe$_3$ resonance at 0.54 ppm, according to the ^{1}H NMR spectrum of the reaction mixture. This resonance is assignable to the dicarbide complex, [{Th(NR$_2$)$_3$}$_2$(μ,η^1:η^1-C$_2$)] (**4.7**). I hypothesize that the by-product of these reactions is free HCCH; however, I do not observe

any signals assignable to HCCH in the ^{1}H NMR spectra of either reaction mixture. Complexes **4.6** and **4.7** can be isolated in 77% and 65% yields, respectively, upon work-up (Scheme 4.4). The $^{13}C\{^{1}H\}$ NMR spectrum of **4.7** in THF-d_8 features resonances at 202.7 and 5.4 ppm, assignable to the μ-dicarbide (C_2) and $SiMe_3$ environments, respectively, consistent with the proposed formulation (Figure A4.14). For comparison, [{Cp*$_2$Hf(C≡CH)$_2$}(μ$_2$-C$_2$)] exhibits a resonance at 153.3 ppm assignable to the C_2 ligand,[28] whereas the C_2 resonance of [{(CpMe)$_2$Zr(NH^{t}Bu)$_2$}(μ-CC)] appears at 171.0 ppm.[37] Interestingly, [{Cp$_2$Ti(PMe$_3$)}$_2$(μ-C$_2$)], which is thought to feature some Ti–C multiple bond character, exhibits a C_2 resonance at 258.1 ppm.[38]

Scheme 4.4. Synthesis of Complexes **4.6** and **4.7**.

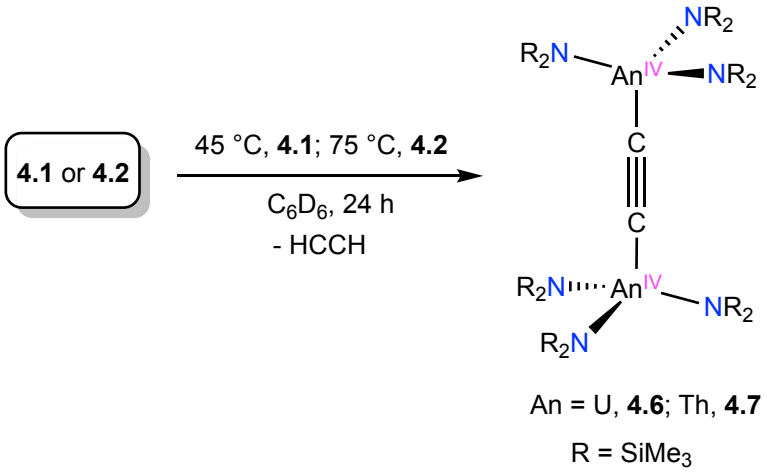

Complexes **4.6** and **4.7** both crystallize in the monoclinic space group P2$_1$/n and are isomorphous. Each metal center features a pseudotetrahedral geometry and a nearly linear μ,η^1:η^1-C$_2$ coordination mode of the dicarbide ligand (**4.6**: M–C≡C = 179.0(6)/179.1(6) Å; **4.7**: M–C≡C 178.5(5)/178.9(5) Å) (Figure 4.4 and Table 4.3). The U−C distances in **4.6** are 2.436(8) and 2.466(7) Å, whereas the Th−C distances in **7** are 2.484(6) and 2.501(6) Å. The

C≡C distances in **4.6** and **4.7** are 1.225(10) and 1.233(8) Å, respectively. For comparison, the closely related diuranium dicarbide complex, $[(\mu,\eta^1{:}\eta^1{-}C_2)\{U(N[t\text{-Bu}]Ar)_3\}_2]$, exhibits U−C and C≡C distances of 2.416(5) and 1.227(10) Å, respectively.[27]

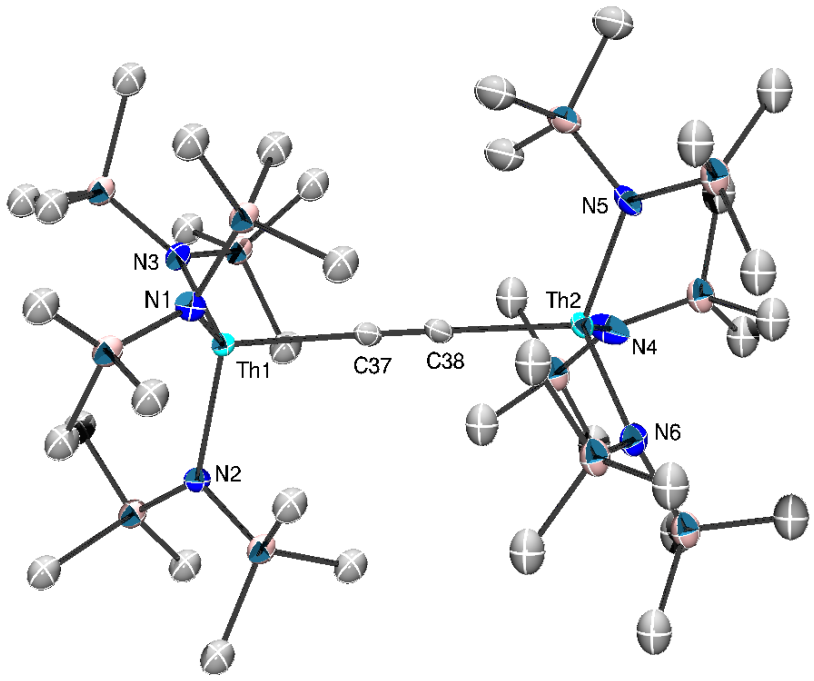

Figure 4.4. Solid-state molecular structure of $[\{Th(NR_2)_3\}_2(\mu,\eta^1{:}\eta^1\text{-}C_2)]$ (**4.7**) with 50% probability ellipsoids shown for all atoms. Hydrogen atoms omitted for clarity.

I next sought to synthesize a mixed-actinide dicarbide complex for comparison to **4.6** and **4.7**. Thus, reaction of equimolar quantities of **4.1** and the thorium metallacycle, $[Th\{N(R)(SiMe_2)CH_2\}(NR_2)_2]$ (R = $SiMe_3$) in C_6D_6 for 24 h results in a color change from purple to pale pink. Monitoring the reaction via ^{1}H NMR spectroscopy reveals the loss of the resonances assignable to $[Th\{N(R)(SiMe_2)CH_2\}(NR_2)_2]$ and **4.1**, contaminant with the observation of two new broad and paramagnetically-shifted peaks at –0.77 and –5.24 ppm, which integrate in a 1:1 ratio, as anticipated (Figure A4.15). Work-up of the reaction mixture,

followed by crystallization affords $[U(NR_2)_3(\mu,\eta^1{:}\eta^1\text{-}C_2)Th(NR_2)_3]$ (**4.8**) as light-pink plates in 52% yield (Scheme 4.5). The IR spectrum of complex **4.8** (KBr mull) features a C≡C stretch at 2019 cm^{-1} (Figure A4.23), which is substantially blue shifted from that observed for $[(\mu,\eta^1{:}\eta^1\text{–}C_2)\{U(N[t\text{-Bu}]Ar)_3\}_2]$ (1904 cm^{-1}).[27] Interestingly, this mode was not observed in the IR spectra of **4.6** and **4.7** because of their inversion symmetry.

Scheme 4.5. Synthesis of Complex **4.8**.

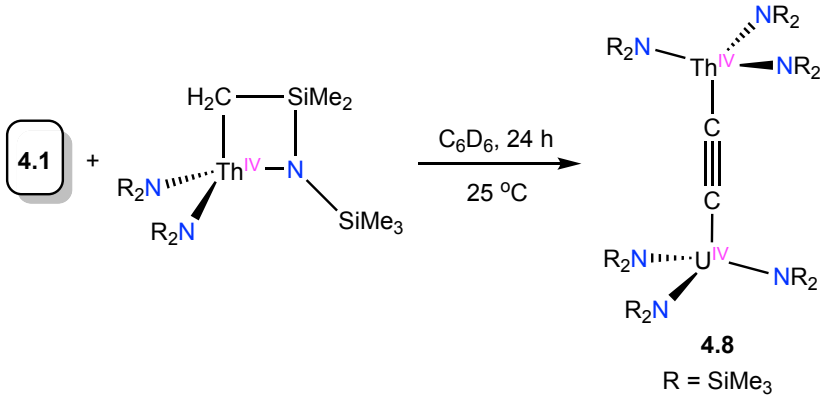

Complex **4.8** is isomorphous with complexes **4.6** and **4.7**. Each metal center in **4.8** features a pseudo tetrahedral geometry and a linear coordination mode of the dicarbide ligand (M–C≡C = 178.8(6)/179.3(6) Å) (Table 4.3). However, the uranium and thorium atoms are disordered evenly over both sites. As a result, the M−C bond lengths (2.450(7) and 2.484(7) Å) are intermediate between those of **4.6** and **4.7**. Finally, the C≡C distance in **4.8** (1.224(9) Å) is identical to those of **4.6** and **4.7**.

Table 4.3. Selected Metrical Parameters for Complexes **4.6**-**4.8** (Å and deg)

Bond	**4.6**	**4.7**	**4.8**
M–C	2.436(8)/ 2.466(7)	2.484(6)/ 2.501(6)	2.450(7)/ 2.484(7)
C≡C	1.225(10)	1.233(8)	1.224(9)
$M–N_{amide}$	2.238(6), 2.239(5), 2.246(5), 2.246(5), 2.249(6), 2.252(5)	2.299(4), 2.300(4), 2.303(4), 2.304(4), 2.305(4), 2.309(5)	2.260(5), 2.266(5), 2.269(5), 2.270(5), 2.270(5), 2.282(5)
M–C≡C	179.0(6), 179.1(6)	178.5(5), 178.9(5)	178.8(6), 179.3(6)
N–M–C	104.3(2), 105.6(2), 105.5(2), 106.3(2), 107.7(2), 112.6(2)	104.04(17), 104.89(17), 105.21(17), 105.71(18), 107.45(17), 111.53(18)	104.6(2), 105.0(2), 105.5(2), 105.6(2), 107.18(19), 112.2(2)

4.2.2 Magnetic Properties

The temperature dependent magnetic susceptibilities of complexes **4.6** and **4.8** were measured using SQUID magnetometry (Figure 4.5). Complex **4.6** exhibits a room temperature $\chi_M T$ value of 1.69 emu K mol^{-1}, whereas **4.8** exhibits a much smaller room temperature $\chi_M T$ value (1.02 emu K mol^{-1}), consistent with the presence of only one paramagnetic U(IV) center (Figure 4.5). The $\chi_M T$ values for **4.6** and **4.8** both trend to zero upon cooling to 2 K, consistent with the non-magnetic $5f^2$ ground state expected for U(IV).[39-42] Similar magnetic susceptibility behavior is observed for $[\{(NN'_3)U\}_2(1,3\text{-}(CC)_2C_6H_4)]$.[12]

To assess the presence of magnetic communication in **4.6**, I applied the subtraction procedure developed by Long and co-workers, using complex **4.8** as the exchange-free control.[43] The resulting data were fit using the exchange Hamiltonian, $\hat{H} = -2J_1\hat{S}_1\cdot\hat{S}_2$. By setting $S_1 = S_2 = 1$, the adjusted $\chi_M T$ data give fit parameters of $J = 1.78$ cm^{-1}, $g_1 = g_2 = 1.76$, and TIP = 428×10^{-6} emu (Figure 4.5). Comparable J values are observed for the uranium(IV)–ethynylbenzene complexes reported by Shores and co-workers. For example, $[\{(NN'_3)U\}_2(1,4\text{-}(CC)_2C_6H_4)]$ features $J = 2.75$ cm^{-1}, despite having a much longer linker.[12]

This comparison suggest that linker length has relatively little effect on the magnitude of magnetic communication in uranium, and that the nature of U-L bond is the principal contributor to their magnetic properties. Indeed, no magnetic communication was observed in [{Tp*$_2$U}$_2$(1,3-(CC)$_2$C$_6$H$_4$)],[13] likely on account of the reduced covalency in the U(III)-ligand bonds. The chalcogenide-bridged U(IV) complexes, [{U(Tren^{TIPS})}$_2$(μ-E)] (E = S, Se, Te; Tren^{TIPS} = N(CH$_2$CH$_2$NSi^{i}Pr$_3$)$_3$) also exhibit no apparent magnetic communication.[44] Interestingly, though, their χ vs. T plots reveal a plateau at ca. 50 K, which the authors argue is due to presence of a singlet ground state.

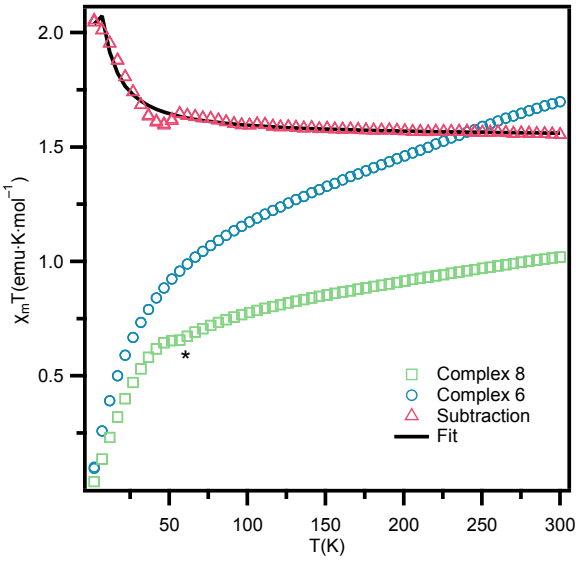

Figure 4.5. Temperature dependent solid-state magnetic susceptibility data (χMT vs. T) for complex **4.6**, complex **4.8**, and data obtained via the subtraction method. The black line is the fit (see text for details). (*) Indicates the antiferromagnetic transition of O_2.

4.2.3 Computational Studies

Relativistic DFT calculations were performed by Dr. Xiaojuan Yu and Prof. Jochen Autschbach at the University of Buffalo on complexes **4.1**, **4.2**, **4.6**, and **4.7** to probe the nature of their An–C bonds. Complete computational details are given in Section 4.4.13. The geometry for complex **4.1** was fully optimized, whereas calculations for complexes **4.2**, **4.6**, and **4.7** were performed using the X-ray crystal structures with hydrogen positions optimized. Natural Localized Molecular Orbital (NLMO) analyses found very similar An–C bonding interactions across all four complexes.[45] These bonding interactions can be represented as two-center two-electron σ(An−C) bonds with 18% total U weight for **4.1** and **4.6** and 17% total Th weight for **4.2** and **4.7**. Within the metal weights, the 5f contributions range from 14% for **4.2** to 19% for **4.6**, respectively. U–Cα Wiberg bond orders (WBOs) are 0.71 in **4.1** and 0.70 in **4.6**, whereas the Th–Cα WBOs for **4.2** and **4.7** are 0.67 and 0.66, respectively. In addition, the calculated natural charges for An, C_α, C_β, and H are 1.66, -0.47, -0.26, and 0.25 for **4.1**, and 1.60, -0.50, -0.23, and 0.24 for **4.2**, respectively. The calculated positive charges for the acetylide hydrogen atoms suggest that they are acidic, consistent with their observed reactivities (Schemes 4.3 and 4.4). Moreover, the greater covalency and increased 5f involvement observed for the uranium analogues is consistent with expected periodic trends.[46-49] Unsurprisingly, though, the degree of 5f orbital participation in **4.1** and **4.6** is significantly less than that observed for the U(VI) acetylide series, $[U(O)(C{\equiv}C{-}C_6H_4{-}p{-}R)\{N(SiMe_3)_2\}_3]$,[14] which exhibit 28-29% total U participation and 60-62% 5f orbital participation in their U–C bonds.

The ^{13}C NMR chemical shifts of the C_α nuclei were calculated for **4.2** and **4.7** using a variety of functionals by Dr. Xiaojuan Yu and Prof. Jochen Autschbach,[50, 51] with and without SO coupling effects (Table 4.4). Good agreement between calculated and experimental shifts was obtained in all cases. As seen in Table 4.4, the calculated chemical shifts are only slightly dependent on the different functionals; for brevity I will focus on the PBE/SO-PBE results. This functional has previously provided reliable chemical shifts in actinide complexes.[23,48] The calculated C_α shift for complex **4.2** is 174.9 ppm (expt. = 176.1 ppm) and includes a 32.2 ppm deshielding contribution due to SO effects. The calculated C_α shift for complex **4.7** is 205.7 ppm (expt. = 202.7 ppm) with 38.9 ppm deshielding due to SO effects. A similar magnitude in SO deshielding was previously found for $[Th(C_6Cl_5)_5]^-$ and $[ThCl_3(C_6Cl_5)_3]^{2-}$, which also exhibit comparable amounts of 5f involvement in their Th-C bonds.[48] In contrast, much stronger SO-induced desheilding was found for $[U(O)(C{\equiv}C{-}C_6H_4{-}p{-}R)\{N(SiMe_3)_2\}_3]$.[14] The magnitude of the SO effects on the ligand shielding in the different complexes is consistent with the varying degrees of 5f orbital participation in the U–C bonds.

Table 4.4. Calculated carbon shielding (σ) and chemical shift (δ) for the Cα nuclei of **4.2** and **4.7**, using various functionals.

Complex	Method	σ_{calc}(ppm)[c]	δ_{calc}(ppm)	Δ_{SO}(ppm)	δ_{expt}(ppm)
4.2	PB86/SO-BP86	45.4 / 14.0	141.5 / 173.8	32.3	
	PBE/SO-PBE	44.8 / 13.5	142.7 / 174.9	32.2	
	PBE0/SO-PBE0 (25%)[a]	51.2 / 18.1	141.0 / 174.9	33.9	176.1
	PBE0/SO-PBE0 (40%)	55.1 / 20.7	139.6 / 174.8	35.2	
4.7[b]	PB86/SO-BP86	20.3 / -17.9	166.6 / 205.7	39.1	
	PBE/SO-PBE	20.7 / -17.3	166.8 / 205.7	38.9	
	PBE0/SO-PBE0 (25%)	23.2 / -18.5	169.0 / 211.5	42.5	202.7
	PBE0/SO-PBE0 (40%)	24.5 / -19.4	170.2 / 214.9	44.7	

[a] Fraction of exact exchange in the functional in parentheses.

[b] Data averaged over equivalent C_α nuclei of complex **4.7**.

[c] The two values are derived from calculations performed without and with the inclusion of spin-orbit coupling, respectively.

4.3 Summary

In summary, I have prepared and characterized a series of actinide parent acetylide and dicarbide complexes, including $[An(C{\equiv}CH)(NR_2)_3]$ and $[\{An(NR_2)_3\}_2(\mu,\eta^1{:}\eta^1\text{-}C_2)]$ (An = U, Th). The ^{13}C NMR chemical shifts of the α-acetylide carbons in the Th derivatives exhibit a characteristic spin-orbit induced downfield shift, due to involvement of the 5f orbitals in the Th–C bonding. In addition, SQUID magnetometry reveals weak ferromagnetic coupling between the U(IV) centers in the dicarbide complex, $[\{U(NR_2)_3\}_2(\mu,\eta^1{:}\eta^1\text{-}C_2)]$. The An–C

bonding within [An(C≡CH)$(NR_2)_3$] and [{An$(NR_2)_3$}$_2$(μ,η^1:η^1-C_2)] was also probed by relativistic DFT calculations by Dr. Xiaojuan Yu and Prof. Jochen Autschbach at the University of Buffalo. Their calculations reveal moderate amounts of An–C covalency, on par with that observed for other An(IV) organometallic complexes, and consistent with the magnitude of the spin-orbit induced deshielding predicted for these species. Overall, these data provide the first detailed picture of the bonding interactions between the parent acetylide and dicarbide ligands and the An^{4+} ions, an interaction which has been underexplored but is of particular importance for a variety of potential material science applications, including the development of magnetic materials and non-linear optical materials.[52-55]

4.4 Experimental

4.4.1 General. All reactions and subsequent manipulations were performed under anaerobic and anhydrous conditions under an atmosphere of dinitrogen. Diethyl ether (Et_2O), pentane, and hexanes were dried using a Vacuum Atmospheres DRI-SOLV Solvent Purification system and stored over 3Å sieves for 24 h prior to use. Tetrahydrofuran (THF) was distilled over calcium hydride followed by distillation over sodium benzophenone, collected, and stored over 3Å sieves for 24 h prior to use. THF-d_8, C_6D_6, and tetramethylethylenediamine (TMEDA) were stored over 3Å sieves for 24 h prior to use. [U$(NR_2)_3$] (R = $SiMe_3$), [UCl$(NR_2)_3$], [ThCl$(NR_2)_3$], and [Th{N(R)$(SiMe_2)CH_2$}$(NR_2)_2$] were synthesized according to previously reported literature procedures.[56-58] Sodium acetylide was purchased from Sigma-Aldrich as an 18% w/w slurry in xylene and used as received.

1D NMR spectra were recorded on a Varian UNITY INOVA 500 spectrometer and 2D NMR spectra were recorded on a Varian Unity Inova AS600 600 MHz spectrometer. ^{1}H and

$^{13}C\{^{1}H\}$ NMR spectra were referenced to external $SiMe_4$ using the residual protio solvent peaks as internal standards.[59, 60] IR spectra were recorded on a Nicolet 6700 FT-IR spectrometer with a NXR FT Raman Module. Elemental analyses were performed by the Microanalytical Laboratory at University of California (Berkeley, CA).

4.4.2 Synthesis of [U(C≡CH)(N(SiMe$_3$)$_2$)$_3$] (4.1). To a stirring, cold (-25 °C), pink solution of [UCl(NR$_2$)$_3$] (800 mg, 1.06 mmol) in THF (7 mL) was added dropwise a cold (-25 °C) slurry of sodium acetylide (304.4 mg of an 18% sodium acetylide slurry in xylenes, 54.8 mg of NaCCH, 1.16 mmol) and TMEDA (135.5 mg, 1.16 mmol) in THF (4 mL). After stirring for 20 min at room temperature, the resulting brown suspension was filtered through a Celite column supported on glass wool (0.5 cm × 2 cm) and the volatiles were removed *in vacuo*. The resulting red-brown powder was extracted into pentane (4 mL), filtered through a Celite column supported on glass wool (0.5 cm × 2 cm) and the volatiles were removed *in vacuo* to provide an analytically-pure, red-purple microcrystalline solid (637 mg, 81%). Crystals were grown by dissolving **4.1** (300 mg) in pentane (2 mL). This solution was transferred to a 4 mL vial, which was then placed inside a 20 mL scintillation vial. Iso-octane (2 mL) was added to the outer vial. Storage of this two-vial system at -25 ºC for 3 d resulted in the deposition of large purple plates (Figure 4.6). Despite my best efforts, however, any diffraction data collected for **4.1** resisted refinement. X-ray parameters: R-3m (no. 166), a = 18.4296 Å, b = 18.4296 Å, c = 17.6631 Å, α = 90, β = 90, γ = 120. Anal. Calcd for $UN_3Si_6C_{20}H_{55}$: C, 32.28; H, 7.45; N, 5.65. Found: C, 32.67; H, 7.56; N, 5.79. ^{1}H NMR (C_6D_6, 298 K, 500 MHz): δ -1.95 (br s, 54H, C*H*$_3$), -5.47 (s, 1H, C≡C*H*). IR (KBr pellet, cm^{-1}): 3292 (w, C*C*-*H*), 2956 (s), 2897 (m), 1938 (m, *C*≡*C*H), 1250 (vs), 1182 (m), 916 (m), 892 (m), 847 (s), 771 (m), 654 (m), 611(m).

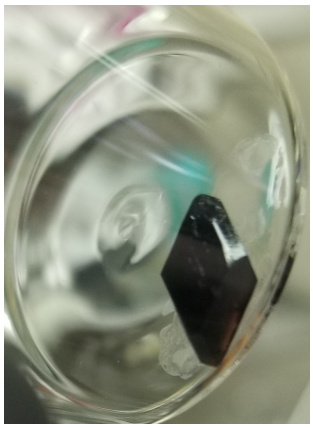

Figure 4.6. Single crystal of **4.1** weighing 76.1 mg.

4.4.3 Synthesis of [U(C≡CH)(N(SiMe$_3$)$_2$)$_3$] (4.1) from acetylene. A 4 mL scintillation vial was charged with [U(N(SiMe$_3$)$_2$)$_3$] (195 mg, 0.271 mmol), Et$_2$O (2 mL), and a small stir bar (Scheme 4.2). This vial was placed within a 20 mL scintillation vial, which had been charged with calcium carbide (700 mg, 10.9 mmol) and Et$_2$O (4 mL). A solution of benzoic acid (600 mg, 4.91 mmol) in Et$_2$O (2 mL) was then quickly added to the outer vial and the two-vial assembly was immediately sealed. The solution in the inner vial was allowed to stir for 5 h. After 5 h, the solution in the inner vial was filtered through a Celite column supported on glass wool (0.5 cm × 2 cm) and the volatiles were removed *in vacu*o. The resulting purple solid was extracted into pentane (2 mL) and the solution was filtered through a Celite column supported on glass wool (0.5 cm × 2 cm). Concentration of the filtrate *in vacuo* followed by storage at -25 °C for 24 h resulted in the deposition of **4.1** as purple plates. Yield: 70.9 mg, 35 %. The ^{1}H NMR spectrum of this solid was identical to that recorded for an authentic sample of **4.1**.

4.4.4 Synthesis of [Th(C≡CH)(N(SiMe$_3$)$_2$)$_3$] (4.2). To a stirring, cold (-25 °C), colorless solution of [ThCl(NR$_2$)$_3$] (375.1 mg, 0.501 mmol) in THF (5 mL) was added dropwise a cold

(-25 °C) slurry of sodium acetylide (143.9 mg of an 18% sodium acetylide slurry in xylenes, 25.9 mg of sodium acetylide, 0.551 mmol) and TMEDA (64.1 mg, 0.551 mmol) in THF (5 mL). After stirring for 20 min at room temperature, the resulting light-yellow suspension was filtered through a Celite column supported on glass wool (0.5 cm × 2 cm), the volatiles were removed *in vacuo,* and the resulting solid was triturated with pentane (3 × 1 mL). The light-yellow solid was then extracted into pentane (4 mL) and the resulting solution filtered through a Celite column supported on glass wool (0.5 cm × 2 cm). The volatiles were removed *in vacuo* to afford a white solid. This white solid was then redissolved in pentane (1 mL). The resulting solution was transferred to a 4 mL vial, which was then placed inside a 20 mL scintillation vial. Iso-octane (2 mL) was added to the outer vial. Storage of this two-vial system at -25 ºC for 3 d resulted in the deposition of large colorless plates. Yield: 288.4 mg, 78 %. Anal. Calcd for $ThN_3Si_6C_{20}H_{55}$: C, 32.54; H, 7.51; N, 5.69. Found: C, 32.81; H, 7.39; N, 5.72. ^{1}H NMR (C_6D_6, 298 K, 500 MHz): δ 2.02 (s, 1H, C≡C*H*), 0.45 (s, 54H, CH_3). ^{1}H NMR (THF-d_8, 298 K, 500 MHz): δ 2.32 (s, 1H, C≡C*H*), 0.38 (s, 54H, CH_3). ^{13}C{^{1}H} NMR (C_6D_6, 298 K, 126 MHz): δ 175.29 (*C*≡CH), 97.36 (C≡*C*H), 4.42 (*C*H_3). ^{13}C{^{1}H} NMR (THF-d_8, 298 K, 126 MHz): δ 176.13 (*C*≡CH), 98.25 (C≡*C*H), 4.69 (*C*H_3). IR (KBr pellet, cm^{-1}): 3278 (w, C*C*-*H*), 2949 (m), 2897 (w), 1938 (m, *C*≡*C*H), 1250 (s), 1182 (w), 930 (m), 849 (m), 833 (m), 771 (m), 615 (m), 609 (s).

4.4.5 Synthesis of [K(2.2.2-Cryptand)][U(C≡CH)(N(SiMe$_3$)$_2$)$_3$] (4.3). To a stirring, cold (-25 °C), red-purple solution of **4.1** (338 mg, 0.454 mmol) in THF (5 mL) was added KC_8 (122.7 mg, 0.908 mmol), which resulted in an immediate color change to dark blue. After stirring for 10 min at room temperature, the suspension was filtered through a Celite column supported on glass wool (0.5 cm × 2 cm). 2.2.2-Cryptand (151 mg, 0.454 mmol) was added

to the dark-blue filtrate, which was then stirred for 10 min. The volatiles were removed *in vacuo* and the resulting dark-blue solid was extracted into Et_2O (3 mL). This dark-blue solution was then filtered through a Celite column supported on glass wool (0.5 cm × 2 cm) and layered with pentane (4 mL). Storage of this solution at -25 ºC for 24 h resulted in the deposition dark blue needles. Yield: 414 mg, 79 %. Anal. Calcd for $UN_5C_{38}H_{91}Si_6O_6K$: C, 39.35; H, 7.91; N, 6.04. Found: C, 39.47; H, 7.76; N, 5.84. ^{1}H NMR (THF-d_8, 298 K, 500 MHz) δ 17.12 (s, 1H, C≡C*H*), 3.31 (m, 24H, cryptand CH_2), 2.32 (t, J = 4.6 Hz, 12H, cryptand CH_2), -5.51 (s, 54H, CH_3). IR (KBr pellet, cm^{-1}): 2900 (s), 2885 (s), 2816 (s), 1477 (m),1458 (w), 1446 (w), 1356 (s), 1300 (m), 1257 (m), 1238 (s), 1149 (w), 1119 (s), 1107 (vs), 984 (m), 951 (s), 931 (m), 864 (m), 831 (s), 768 (w), 752 (m), 687 (w), 663 (m), 598 (m), 525 (w).

4.4.6 Synthesis of [Na(TMEDA)][U(C≡CH)$_2$(N(SiMe$_3$)$_2$)$_3$] (4.4). To a stirring, cold (-25 °C), pink solution of [UCl(NR$_2$)$_3$] (210.3 mg, 0.278 mmol) in THF (2 mL) was added dropwise a cold (-25 °C) slurry of sodium acetylide (218.3 mg of an 18% sodium acetylide slurry in xylenes, 39.3 mg of sodium acetylide, 0.836 mmol) and TMEDA (97.2 mg, 0.836 mmol) in THF (2 mL). After stirring for 2 h at room temperature, the resulting green suspension was filtered through a Celite column supported on glass wool (0.5 cm × 2 cm) and the volatiles were removed *in vacuo*. The resulting yellow-green solid was extracted into pentane (4 mL), filtered through a Celite column supported on glass wool (0.5 cm × 2 cm) and the volatiles were removed *in vacuo*. The yellow-green solid was again extracted into pentane (2 mL) and the resulting solution was filtered through a Celite column supported on glass wool (0.5 cm × 2 cm) and the filtrate was transferred to a 4 mL vial. This vial was then placed inside a 20 mL scintillation vial and iso-octane (2 mL) was added to the outer vial. Storage of this two-vial system at -25 ºC for 3 d resulted in the deposition of light green blocks. Yield: 120 mg, 47.4%.

Anal. Calcd for $UN_5C_{28}H_{72}Si_6Na$: C, 37.02; H, 7.99; N, 7.71. Found: C, 37.11; H, 7.79; N, 7.65. ^{1}H NMR (THF-d_8, 298 K, 500 MHz): δ 65.79 (s, 2H, C≡C*H*), 2.30 (s, 4H, NCH_2), 2.15 (s, 12H, N(CH_3)$_2$), -9.66 (br. s, 54H, CH_3). IR (KBr pellet, cm^{-1}): 3255 (m, C*C*-H), 2956 (m), 2895 (m), 2835 (m), 2798 (m), 1913 (vw, *C*≡*C*H), 1462 (m), 1360 (vw), 1271 (w), 1248 (s), 1180 (m), 1155 (w), 1132 (w), 1040 (w), 1036 (w), 1020 (w), 935 (m), 920 (m), 860 (m), (895) (m), 845 (s), 775 (m), 663 (m), 611 (m).

4.4.7 Synthesis of [Na(TMEDA)][Th(C≡CH)$_2$(N(SiMe$_3$)$_2$)$_3$] (4.5). To a stirring, -25 °C, colorless solution of [ThCl(NR$_2$)$_3$] (324.0 mg, 0.432 mmol) in THF (2 mL) was added slowly a -25 °C slurry of sodium acetylide (338.9 mg of an 18% sodium acetylide slurry in xylenes, 61.0 mg of sodium acetylide, 1.298 mmol) and TMEDA (150.9 mg, 1.298 mmol) in THF (2 mL). After stirring for 2 h at room temperature, the resulting light-yellow suspension was filtered through a Celite column supported on glass wool (0.5 cm × 2 cm) and the volatiles were removed *in vacuo*. The pale yellow solid was extracted into pentane (4 mL), the resulting solution was filtered through a Celite column supported on glass wool (0.5 cm × 2 cm) and the volatiles were removed *in vacuo*. The off-white solid was again extracted into pentane (2 mL), and the resulting solution was filtered through a Celite column supported on glass wool (0.5 cm × 2 cm) and the filtrate was transferred to a 4 mL vial. This vial was placed inside a 20 mL scintillation vial and iso-octane (2 mL) was added to the outer vial. Storage of this two-vial system at -25 ºC for 3 d resulted in the deposition of colorless blocks. Yield: 210 mg, 53%. Anal. Calcd for $ThN_5C_{28}H_{72}Si_6Na$: C, 37.27; H, 8.04; N, 7.76. Found: C, 37.06; H, 7.93; N, 7.62. ^{1}H NMR (THF-d_8, 298 K, 500 MHz): δ 2.30 (s, 4H, NCH_2), 2.15 (s, 12H, N(CH_3)$_2$), 1.57 (s, 2H, C≡C*H*), 0.33 (s, 54H, CH_3). ^{13}C{^{1}H} NMR (THF-d_8, 298 K, 126 MHz): δ 183.91 (*C*≡CH), 94.46 (C≡*C*H), 59.08 (*C*H$_2$), 46.36 (N(*C*H$_3$)$_2$), 5.94 (*C*H$_3$). IR (KBr pellet, cm^{-1}):

3255 (w, C*C-H*), 2954 (m), 2939 (w), 2835 (w), 2800 (w), 1917 (vw, *C*≡*C*H), 1460 (m), 1360 (w), 1271 (w), 1248 (s), 1180 (w), 1132 (w), 1072 (w), 1020 (w), 930 (s), 910 (s), 845 (s), 775 (m), 673 (s), 609 (s).

4.4.8 Synthesis of [{U(NR$_2$)$_3$}$_2$(μ,η^1:η^1-C$_2$)] (4.6). An NMR tube fitted with a J-Young valve was charged with a purple solution of **4.1** (51.9 mg, 0.069 mmol) in C_6D_6 (1 mL). The NMR tube was placed into an oil bath at 45 ºC and heated for 24 h, whereupon the solution changed from purple to dark brown. After 24 h, the NMR tube was removed from the oil bath, brought back into the glovebox, and the solution transferred to a 20 mL vial. The NMR tube was rinsed with pentane (3 × 0.5 mL) and the rinsings were transferred to the vial. The volatiles were removed *in vacuo*. The brown solid was then extracted into pentane (1.5 mL), and the resulting solution was filtered through a Celite column supported on glass wool (0.5 × 2 cm). The brown filtrate was transferred to a 4 mL vial, which was placed inside a 20 mL scintillation vial and iso-octane (2 mL) was added to the outer vial. Storage of this two-vial system at -25 ºC for 2 d resulted in the deposition of large brown-yellow blocks. The crystals were isolated by decanting the supernatant and then dried *in vacuo* (40 mg, 77% yield). Anal. Calcd for $U_2N_6Si_{12}C_{38}H_{108}$: C, 31.21; H, 7.44 N, 5.75. Found: C, 31.40; H, 7.59; N, 5.43. ^{1}H NMR (C_6D_6, 298 K, 500 MHz): δ -6.29 (s, C*H*$_3$). IR (KBr pellet, cm^{-1}): 2954 (m), 2897 (w), 1252 (s), 1182 (w), 1045 (vw), 891 (s), 854 (s), 843 (s), 754 (w), 687 (vw).

4.4.9 Synthesis of [{Th(NR$_2$)$_3$}$_2$(μ,η^1:η^1-C$_2$)] (4.7). An NMR tube fitted with a J-Young valve was charged with a colorless solution of **4.2** (122.9 mg, 0.166 mmol) in C_6D_6 (1 mL). The NMR tube was placed into an oil bath at 75 ºC and heated for 24 h, whereupon the solution changed from colorless to yellow. After 24 h, the NMR tube was removed from the oil bath,

brought back into the glovebox, and the solution transferred to a 20 mL vial. The NMR tube was rinsed with pentane (3 × 1 mL) and the rinsings were transferred to the vial. The volatiles were removed *in vacuo*. The resulting yellow solid was then extracted into pentane (1.5 mL), and the resulting solution was filtered through a Celite column supported on glass wool (0.5 × 2 cm). The light-yellow filtrate was transferred to a 4 mL vial, which was placed inside a 20 mL scintillation vial and iso-octane (2 mL) was added to the outer vial. Storage of this two-vial system at -25 ºC for 3 d resulted in the deposition of large pale-yellow crystalline blocks of **4.7**. The crystals were isolated by decanting of the supernatant followed by drying *in vacuo* (80.0 mg, 65% yield). Anal. Calcd for $Th_2N_6Si_{12}C_{38}H_{108}$: C, 31.47; H, 7.51 N, 5.79. Found: C, 31.26; H, 7.18; N, 5.61. ^{1}H NMR (C_6D_6, 298 K, 500 MHz): δ 0.54 (s, C*H*$_3$). ^{13}C{^{1}H} NMR (C_6D_6, 298 K, 126 MHz) δ 201.97 (*C*≡*C*), 5.08 (*C*H$_3$). ^{1}H NMR (THF-d_8, 298 K, 500 MHz): δ 0.42 (s, C*H*$_3$). ^{13}C{^{1}H} NMR (THF-d_8, 298 K, 126 MHz): δ 202.65 (*C*≡*C*), 5.39 (*C*H$_3$). IR (KBr pellet, cm^{-1}): 2951 (m), 2899 (w), 1400 (w), 1246 (s), 1182 (m), 918 (s), 845 (s), 822 (s), 660 (s), 611 (s).

4.4.10 Synthesis of [U(NR$_2$)$_3$(μ,η^1:η^1-C$_2$)Th(NR$_2$)$_3$] (4.8). An NMR tube fitted with a J-Young valve was charged with a purple solution of **1** (104.6 mg, 0.141 mmol) in C_6D_6 (1 mL). To this NMR tube was added [Th{N(R)(SiMe$_2$)CH$_2$}(NR$_2$)$_2$] (100.2 mg, 0.141 mmol) as a C_6D_6 solution (0.5 mL). The solution turned from purple to light pink in color immediately upon addition. The reaction was allowed to stand at room temperature and monitored intermittently by ^{1}H NMR spectroscopy. After 24 h, the NMR tube was brought back into the glovebox and the solution was transferred to a 20 mL vial. The NMR tube was rinsed with pentane (3 × 1 mL) and the rinsings were transferred to the vial. The volatiles were removed *in vacuo*. The resulting pink solid was then extracted into pentane (1.5 mL), and the resulting

solution was filtered through a Celite column supported on glass wool (0.5 × 2 cm). The light pink filtrate was transferred to a 4 mL vial, which was placed inside a 20 mL scintillation vial and iso-octane (2 mL) was added to the outer vial. Storage of this two-vial system at -25 ºC for 3 d resulted in the deposition of large pale pink blocks of **4.8**. The crystals were isolated by decanting the supernatant followed by drying *in vacuo* (107.1 mg, 52.3% yield). Anal. Calcd for $UThN_6Si_{12}C_{38}H_{108}$: C, 31.34; H, 7.47 N, 5.77. Found: C, 31.04; H, 7.26; N, 5.53. ^{1}H NMR (C_6D_6, 298 K, 500 MHz): δ -0.77 (s, C*H*$_3$), -5.24 (s, C*H*$_3$). IR (KBr pellet, cm^{-1}): 2954 (m), 2899 (w), 2019 (m *C*≡*C*), 1271 (w), 1252 (s), 1182 (w), 933 (s), 843 (s), 771 (m), 768 (m), 660 (w), 611 (m).

4.4.11 X-ray Crystallography. Data for **4.2** - **4.8** were collected on a Bruker KAPPA APEX II diffractometer equipped with an APEX II CCD detector using a TRIUMPH monochromater with a Mo Kα X-ray source (α = 0.71073 Å). The crystals were mounted on a cryoloop under Paratone-N oil, and data were collected at 100(2) K (with the exception of **4.3**, which was collected at 110(2) K) using an Oxford nitrogen gas cryostream system. X-ray data for **4.2**, **4.3**, **4.4**, **4.5**, **4.6**, **4.7** and **4.8** were collected utilizing frame exposures of 2, 5, 5, 2, 10, 5, and 10 seconds, respectively. Data collection and cell parameter determination were conducted using the SMART program.[61] Integration of the data frames and final cell parameter refinement were performed using SAINT software.[62] Absorption corrections of the data were carried out using the multi-scan method SADABS.[63] Subsequent calculations were carried out using SHELXTL.[64] Structure determination was done using direct or Patterson methods and difference Fourier techniques. All hydrogen atom positions were idealized, and rode on the atom of attachment. Structure solution, refinement, graphics, and creation of publication materials were performed using SHELXTL. Further crystallographic details can be found in

Tables S3 and S4. Complexes **4.2**-**4.8** have been deposited in the Cambridge Structural Database (**4.2**: CCDC 2095104; **4.3**: CCDC 2095105; **4.4**: 2095106; **4.5**: 2095107; **4.6**: CCDC 2095108; **4.7**: CCDC 2095109; **4.8**: 2095110).

The trimethylsilyl groups in complexes **4.6**, **4.7**, and **4.8** exhibited positional disorder that was modeled over two positions in 38: 62, 34: 66, and 34: 66 ratios, respectively. Additionally, the carbon and silicon atoms of these trimethylsilyl groups were constrained with the SADI and EADP commands. Complex **4.8** also exhibited positional disorder of the thorium and uranium atoms. As a result, their parameters were averaged using the EXYZ command.

Table 4.5. X-ray Crystallographic Data for Complexes **4.2**, **4.3**, **4.4**, and **4.5**.

	4.2	**4.3**	**4.4**	**4.5**
empirical formula	$C_{20}H_{55}N_3Si_6Th$	$C_{38}H_{91}KN_5O_6Si_6U$	$C_{28}H_{72}N_5NaSi_6U$	$C_{28}H_{72}N_5NaSi_6Th$
Crystal habit, color	Block, Colorless	Needle, Dark-Blue	Block, Light-green	Block, Colorless
crystal size (mm)	0.25 × 0.25 × 0.15	0.3 × 0.1 ×0.1	0.2 × 0.15 × 0.10	0.30 × 0.25 × 0.20
crystal system	Monoclinic	Monoclinic	Monoclinic	Monoclinic
space group	$P2_1/c$	$P2_1/n$	Cc	Cc
vol ($Å^3$)	3477.3(18)	5726.1(10)	4475.4(19)	4475.4(19)
a (Å)	17.587(5)	16.1683(16)	12.355(3)	12.355(3)
b (Å)	12.407(4)	21.814(2)	30.306(7)	30.306(7)
c (Å)	15.963(5)	16.2839(16)	12.443(3)	12.443(3)
α (deg)	90.00	90	90.00	90.00
β (deg)	93.318(4)	94.422(2)	106.152(3)	106.152(3)
γ (deg)	90.00	90	90.00	90.00
Z	4	4	4	4
fw (g/mol)	738.25	1159.82	908.46	902.47
density (calcd) (Mg/m^3)	1.410	1.345	1.348	1.339
abs coeff (mm^{-1})	4.507	3.073	3.820	3.525
F_{000}	1480	2388	1848	1840
Total no. reflections	7808	36803	18218	23446
Unique reflections	7808	12117	5425	8000
R_{int}	0.0586	0.1037	0.0271	0.0347
final R indices [$I > 2\sigma(I)$]	$R_1 = 0.0498$ $wR_2 = 0.0936$	$R_1 = 0.0516$ $wR_2 = 0.0950$	$R_1 = 0.0162$, $wR_2 = 0.0360$	$R_1 = 0.0199$, $wR_2 = 0.0411$
largest diff peak and hole ($e^-Å^{-3}$)	2.358 and -2.727	1.060 and -1.777	0.378 and -0.248	0.526 and -0.298
GOF	1.029	0.974	1.012	0.828

Table 4.6. X-ray Crystallographic Data for Complexes **4.6**, **4.7**, and **4.8**.

	4.6	**4.7**	**4.8**
empirical formula	$C_{38}H_{108}N_6Si_{12}U_2$	$C_{38}H_{108}N_6Si_{12}Th_2$	$C_{38}H_{108}N_6Si_{12}ThU$
Crystal habit, color	Block, Dark-yellow	Block, Light-yellow	Plate, Light-pink
crystal size (mm)	0.30 × 0.25 × 0.20	0.30 × 0.25 × 0.20	0.3 × 0.25 × 0.20
crystal system	Monoclinic	Monoclinic	Monoclinic
space group	$P2_1/n$	$P2_1/n$	$P2_1/n$
vol ($Å^3$)	6685.0(8)	6758.5(5)	6705.8(7)
a (Å)	16.1343(10)	16.1757(8)	16.1339(10)
b (Å)	11.7792(8)	11.8447(5)	11.8136(7)
c (Å)	35.186(2)	35.2874(16)	35.197(2)
α (deg)	90	90.00	90
β (deg)	91.4254(8)	91.548(2)	91.6431(8)
γ (deg)	90	90.00	90
Z	4	4	4
fw (g/mol)	1462.44	1450.46	1456.45
density (calcd) (Mg/m^3)	1.453	1.425	1.443
abs coeff (mm^{-1})	5.083	4.637	4.870
F_{000}	2920	2904	2912
Total no. reflections	70531	27747	47574
Unique reflections	12734	11825	15033
R_{int}	0.0574	0.0190	0.0481
final R indices [$I > 2\sigma(I)$]	$R_1 = 0.0462$, $wR_2 = 0.0916$	$R_1 = 0.0357$, $wR_2 = 0.0747$	$R_1 = 0.0460$, $wR_2 = 0.0918$
largest diff peak and hole ($e^-Å^{-3}$)	3.091 and -2.961	2.253 and -1.919	3.201 and -2.546
GOF	1.031	1.025	1.028

4.4.12 SQUID Magnetometry. The magnetic properties of **4.6** and **4.8** were recorded using a Quantum Design Magnetic Property Measurement System SQUID vibrating sample magnetometer (MPMS3 SQUID-VSM). 10.8 mg and 41.3 mg of polycrystalline **4.6** and **4.8**, respectively, were used for each measurement. Samples were loaded under an inert atmosphere into a glass NMR tube packed with 1 cm of quartz wool on either side of the sample. The samples were flame sealed to prevent exposure to air. The magnetic susceptibilities of **6** and **8** was corrected for the sample diamagnetism (**4.6**: χ_{dia} = -8.039 × 10^{-4} $cm^3 \cdot mol^{-1}$, **4.8**: χ_{dia} = -7.919 × 10^{-4} $cm^3 \cdot mol^{-1}$) using Pascal's constants.[65] Data subtraction to determine coupling between metal centers was done using Eq. S1 and setting $\chi_m T_{s.o.}$ = 1.000389 $emu \cdot K \cdot mol^{-1}$.[43]

$$\chi_M T_{sub} = \chi_M T_{\mathbf{6}} - 2 \cdot \chi_M T_{\mathbf{8}} + 2(\chi_M T_{s.o.}) \quad \text{(Eq. A1)}$$

4.4.13 Computational Details. Density functional calculations for **4.1**, **4.2**, **4.6**, and **4.7** were performed with the Perdew-Burke-Ernzerhof[66] (PBE) exchange-correlation functional. The geometry of complex **4.1** was fully optimized. Calculations for complexes **4.2**, **4.6**, and **4.7** were carried out based on crystal structure coordinates; only the positions of the hydrogen atoms were optimized. Small-core Stuttgart energy-consistent relativistic pseudopotentials, ECP60MWB for Th and U, were utilized with matching valence basis sets.[67] The 6-31G(d) basis set was used for the Si, C, N, and H atoms.[68] Atom-pairwise corrections for dispersion forces were considered via Grimme's D3 model augmented with the Becke-Johnson (BJ) damping.[69] The optimizations and single-point calculations employed the Gaussian 16 package.[70] To identify the compositions of the chemical bond, natural localized molecular orbital (NLMO) analyses were carried out with NBO program, version 6.0.[71]

NMR shielding constants (σ, ppm) for **4.2** and **4.7** were calculated with the NMR module of the ADF package (version 2017),[50, 51, 72] using the scalar relativistic and spin-orbit all electron Zeroth-Order Regular Approximation[73] (ZORA) Hamiltonian, in conjunction with all-electron doubly polarized triple-ζ (TZ2P)[74] Slater-type basis set. The conductor-like screening model (COSMO) was used to describe solvent effect (tetrahydrofuran).[75] For the NMR calculations, the functionals BP86, PBE, PBE0 (25% exact exchange), and PBE0 (40% exact exchange) were used.[50, 51] The ^{13}C chemical shifts (δ, ppm) were obtained by subtracting the C_α nuclear magnetic shielding of interest from the reference compound (Tetramethylsilane, TMS), with the latter calculated at the same level of theory.

Table 4.7. % compositions of the An-C (An = Th, U) bonding NLMOs in **4.1, 4.2, 4.6**, and **4.7**.

Complex	Orbital	Total C	2s	2p	Total An	7s	7p	6d	5f
4.1	σ(U-C)	80	50	50	18	16	1	66	17
4.2	σ(Th-C)	81	46	54	17	18	1	67	14
4.6	σ(U-C)	79	46	54	18	13	0	68	19
4.7	σ(Th-C)	82	47	53	17	13	1	70	16

Table 4.8. Calculated carbon shielding (σ) for the reference (TMS) complex, using various functionals.

Complex	Method	σ_{calc} (ppm)
TMS	BP86/SO-BP86	186.9 / 187.8
	PBE/SO-PBE	187.5 / 188.4
	PBE0/SO-PBE0 (25%)[a]	192.2 / 193.0
	PBE0/SO-PBE0 (40%)	194.7 / 195.5

[a] Numbers in parentheses indicate the fraction of exact exchange in the functional.

4.5 Appendix

4.5.1 NMR Spectra

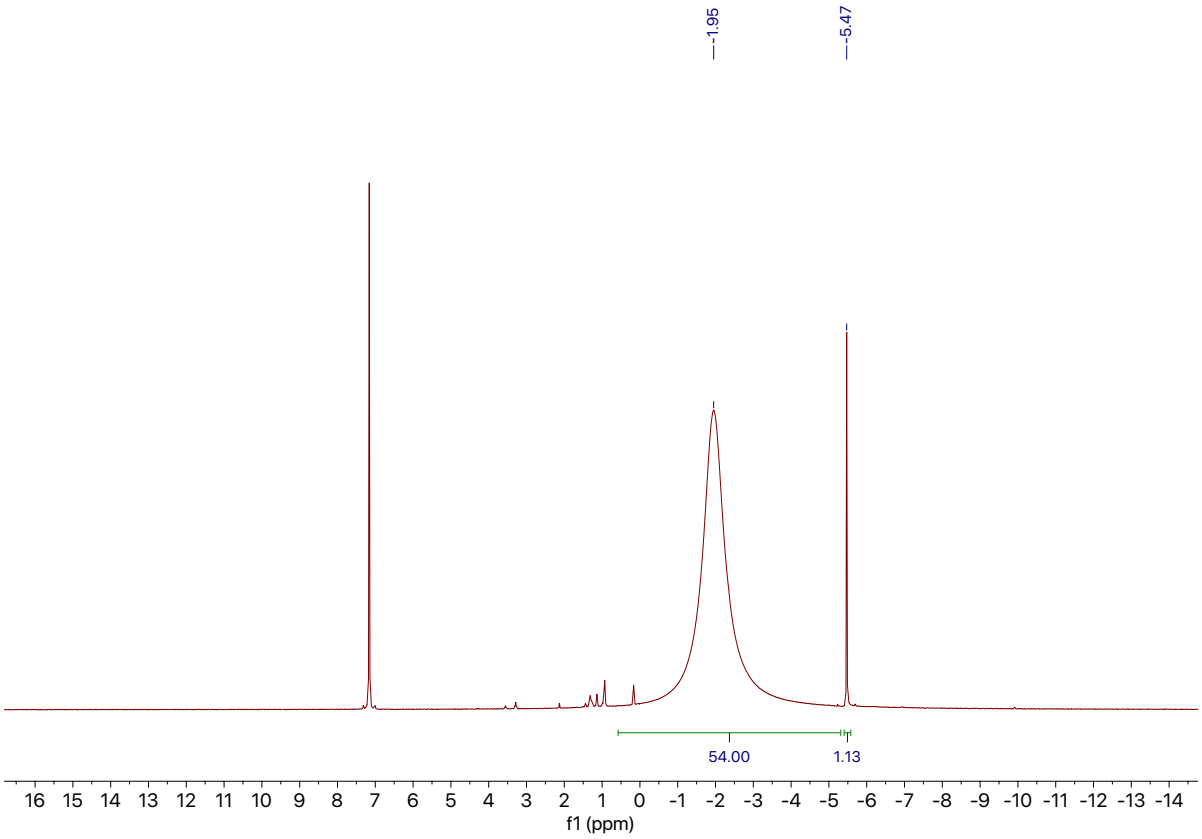

Figure A4.1. ^{1}H NMR spectrum of [U(C≡CH)(N(SiMe$_3$)$_2$)$_3$] (**4.1**) in C_6D_6 at room temperature.

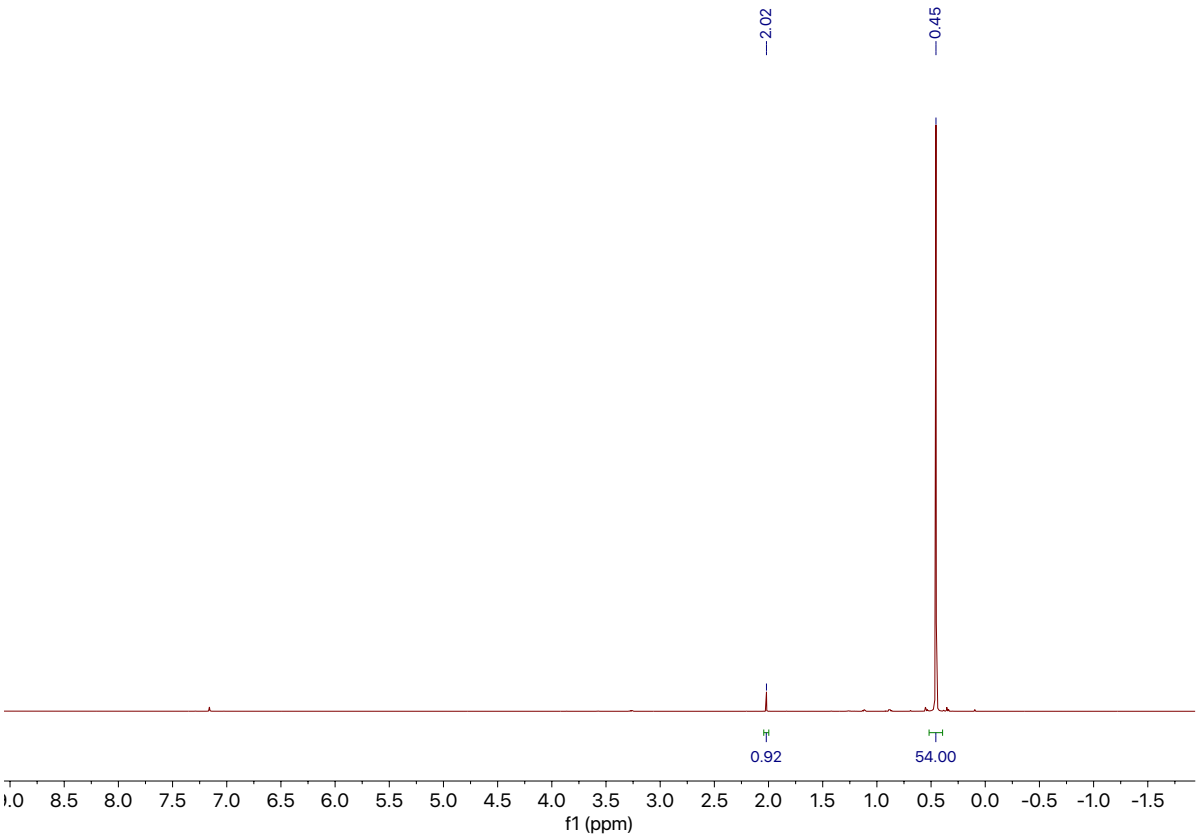

Figure A4.2. ^{1}H NMR spectrum of $[Th(C{\equiv}CH)(N(SiMe_3)_2)_3]$ (**4.2**) in C_6D_6 at room temperature.

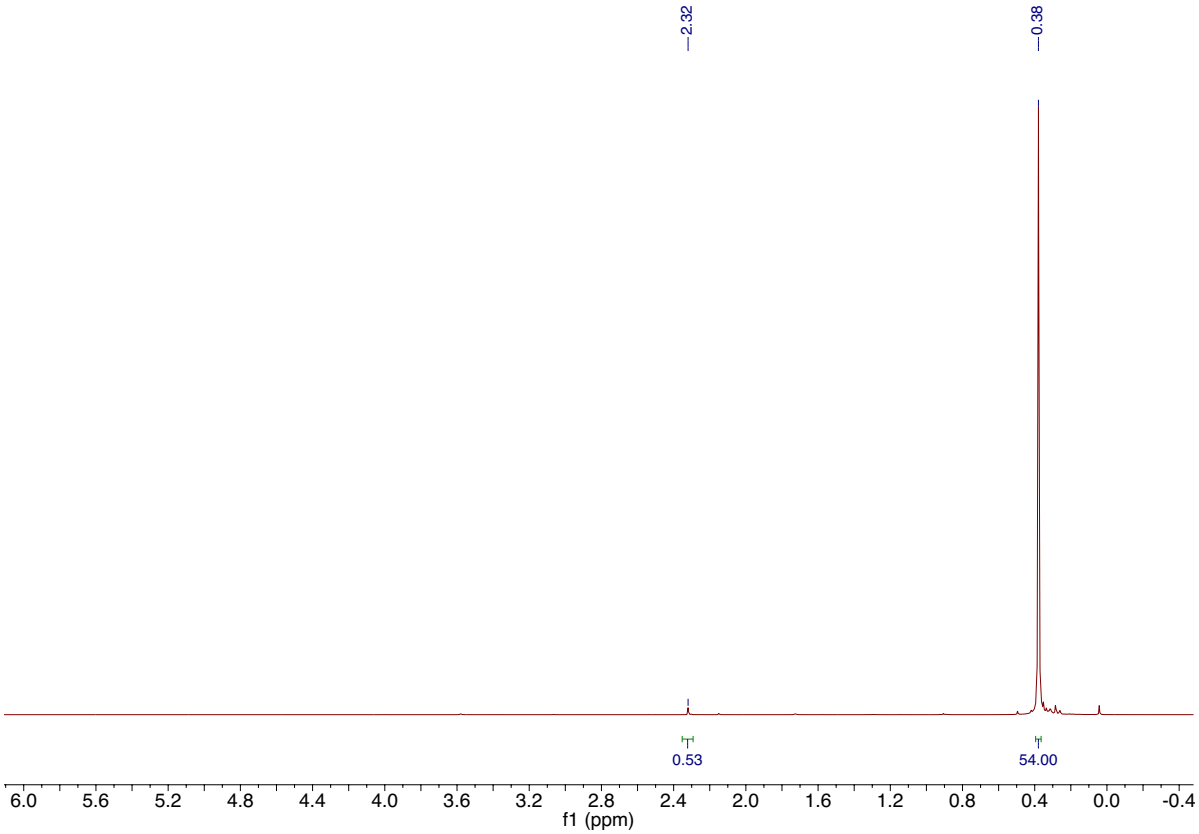

Figure A4.3. ^{1}H NMR spectrum of [Th(C≡CH)(N(SiMe$_3$)$_2$)$_3$] (**4.2**) in THF-d_8 at room temperature.

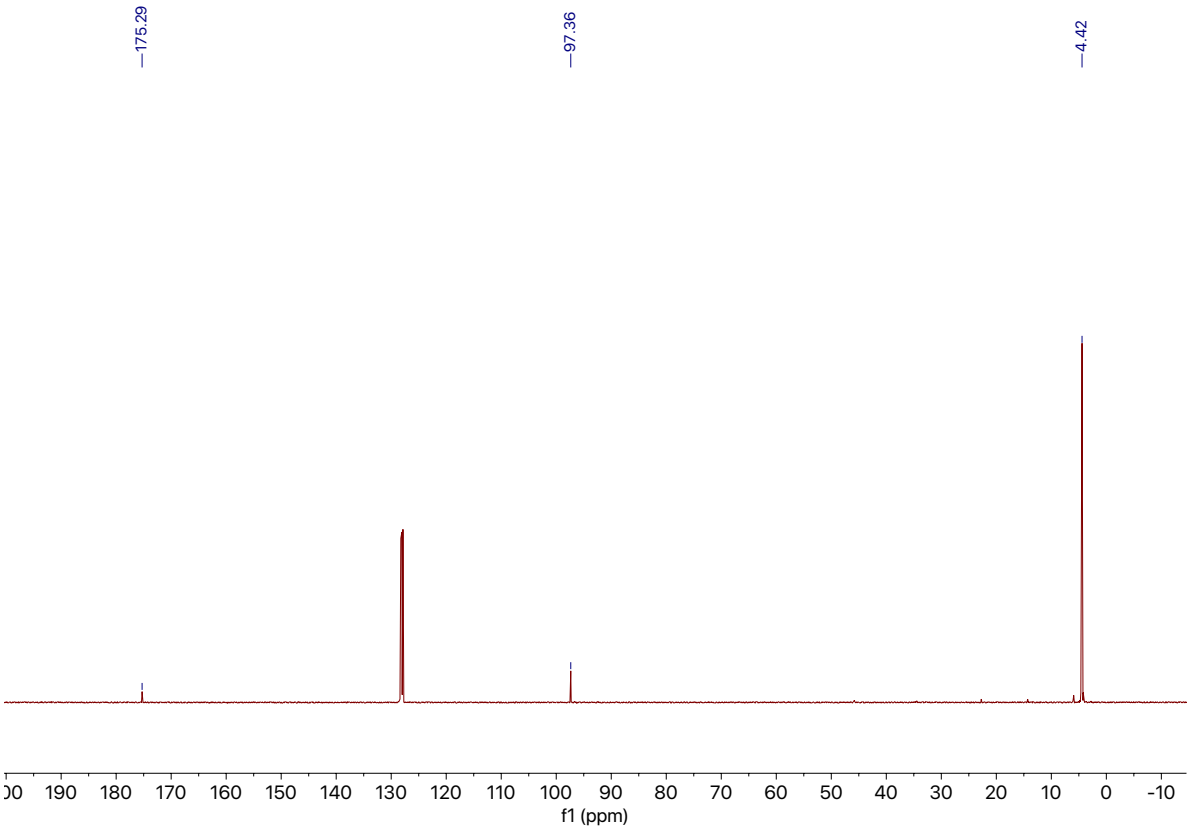

Figure A4.4. $^{13}C\{^{1}H\}$ NMR spectrum of [Th(C≡CH)(N(SiMe$_3$)$_2$)$_3$] (**4.2**) in C_6D_6 at room temperature.

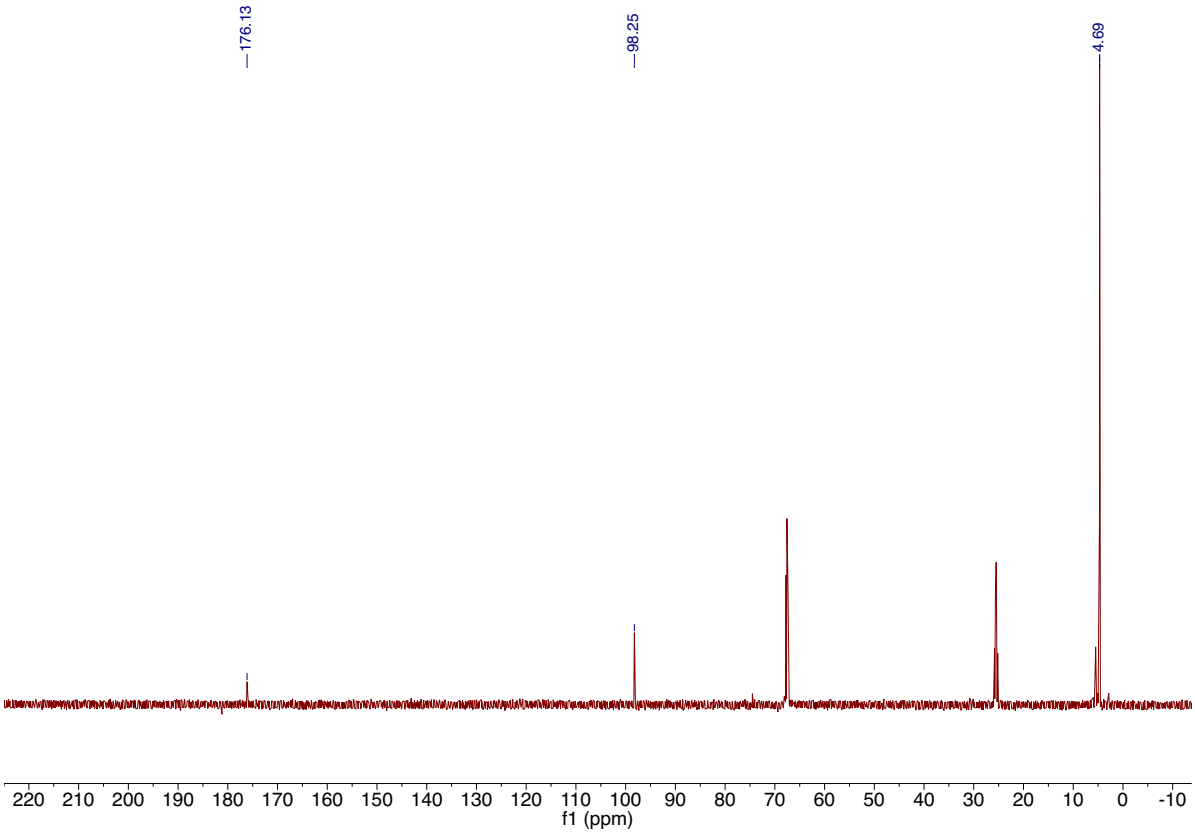

Figure A4.5. $^{13}C\{^{1}H\}$ NMR spectrum of [Th(C≡CH)(N(SiMe$_3$)$_2$)$_3$] (**4.2**) in THF-d_8 at room temperature.

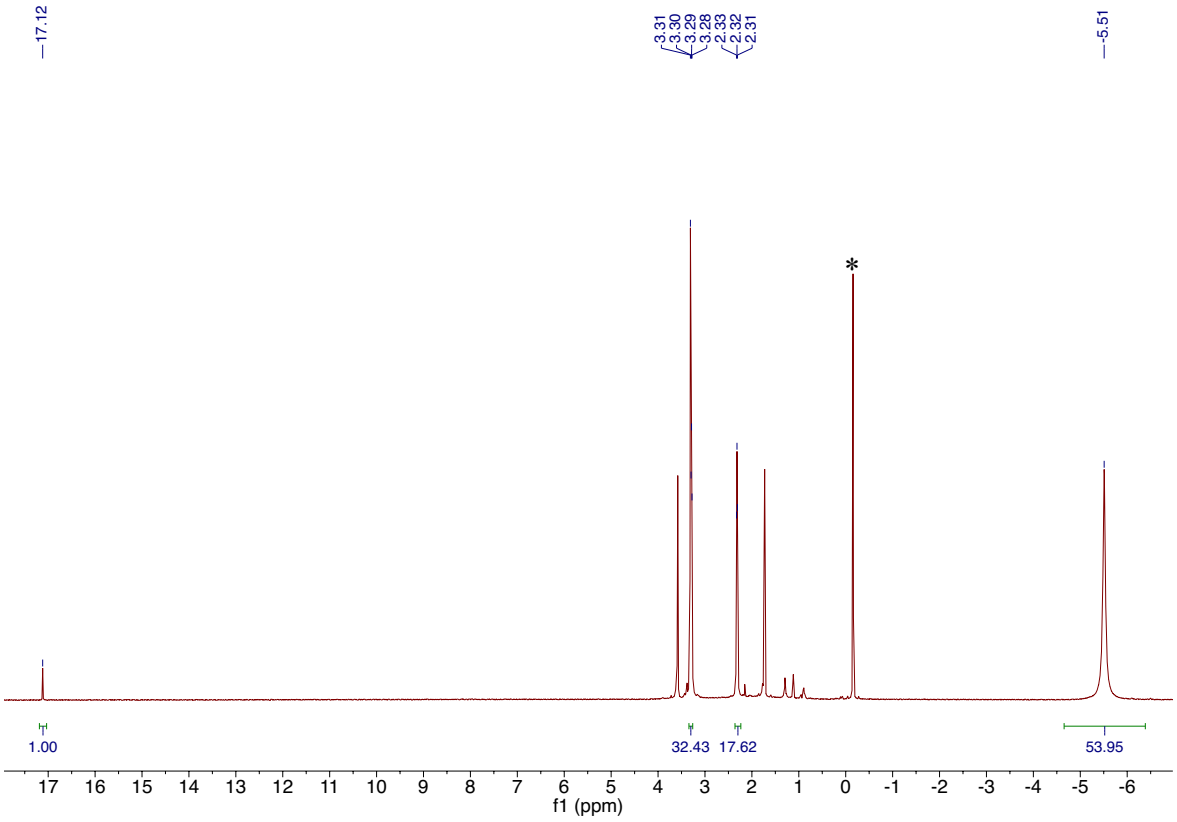

Figure A4.6. ^{1}H NMR spectrum of [K(2.2.2-Cryptand)][U(C≡CH)(N(SiMe$_3$)$_2$)$_3$] (**4.3**) in THF-d_8 at room temperature. (*) indicates free HN(SiMe$_3$)$_2$.

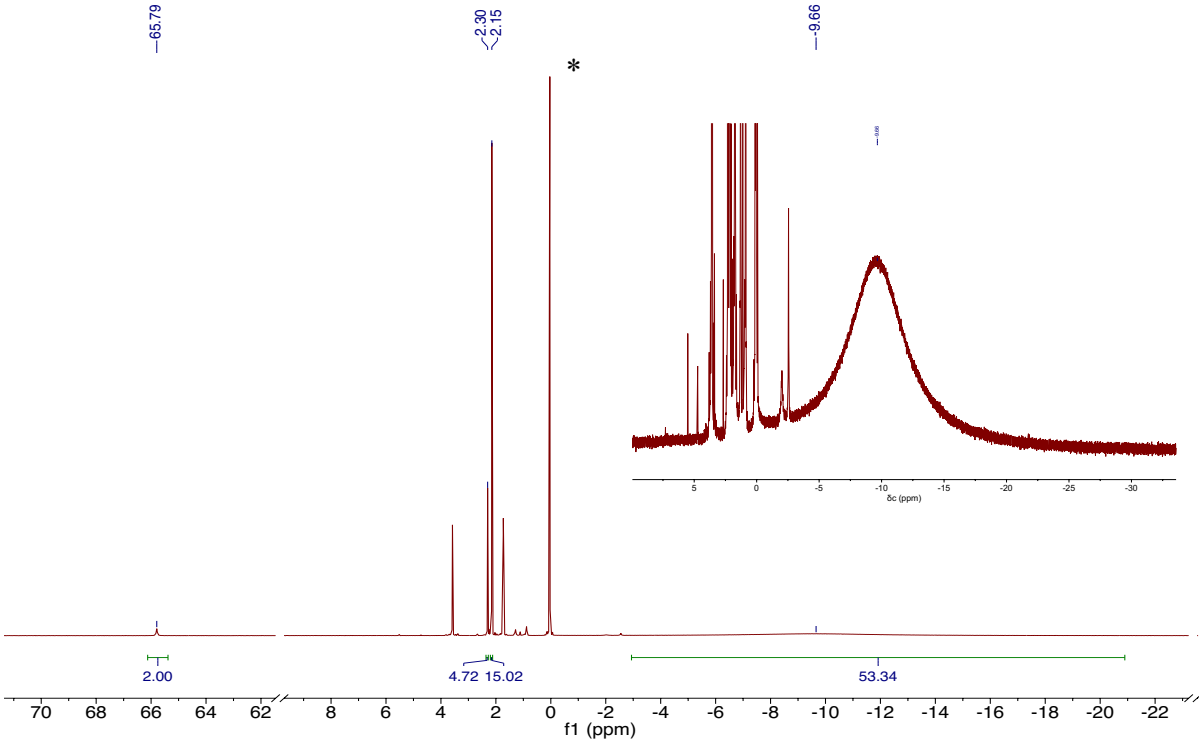

Figure A4.7. ^{1}H NMR spectrum of [Na(TMEDA)][U(C≡CH)$_2$(N(SiMe$_3$)$_2$)$_3$] (**4.4**) in THF-d_8 at room temperature. (*) indicates free HN(SiMe$_3$)$_2$. Inset shows silylamide peak.

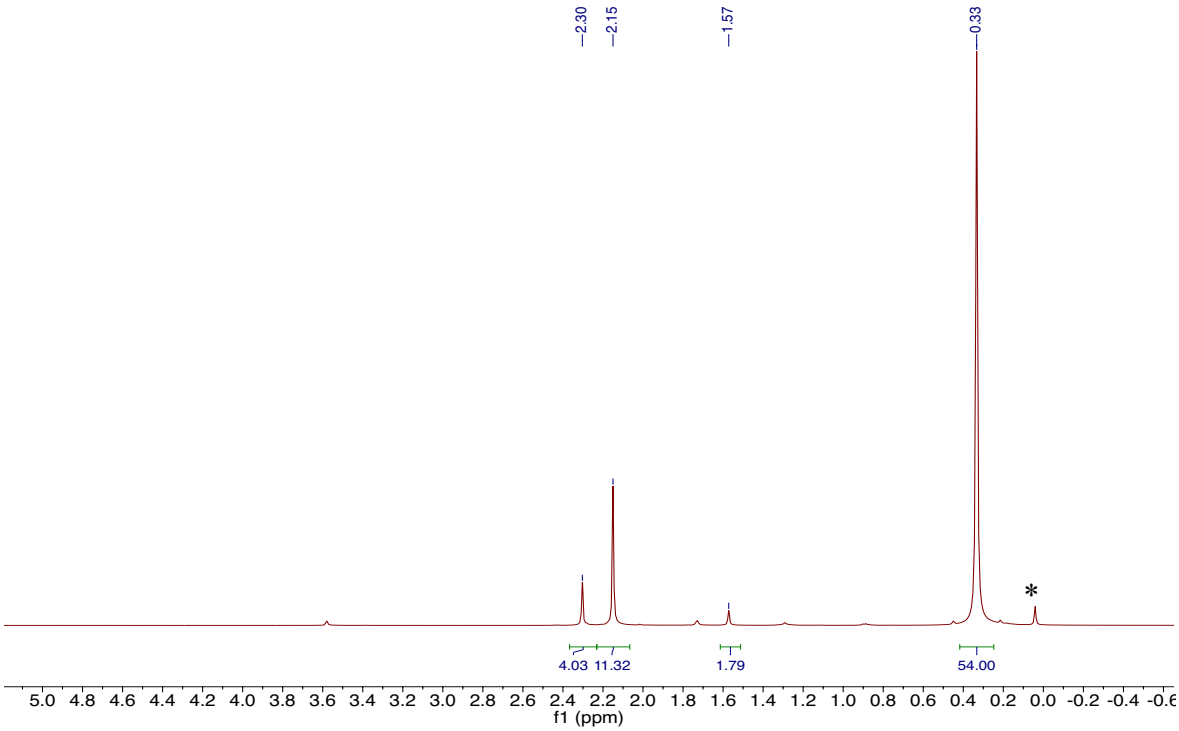

Figure A4.8. ^{1}H NMR spectrum of [Na(TMEDA)][Th(C≡CH)$_2$(N(SiMe$_3$)$_2$)$_3$] (**4.5**) in THF-d_8 at room temperature. (*) indicates free HN(SiMe$_3$)$_2$.

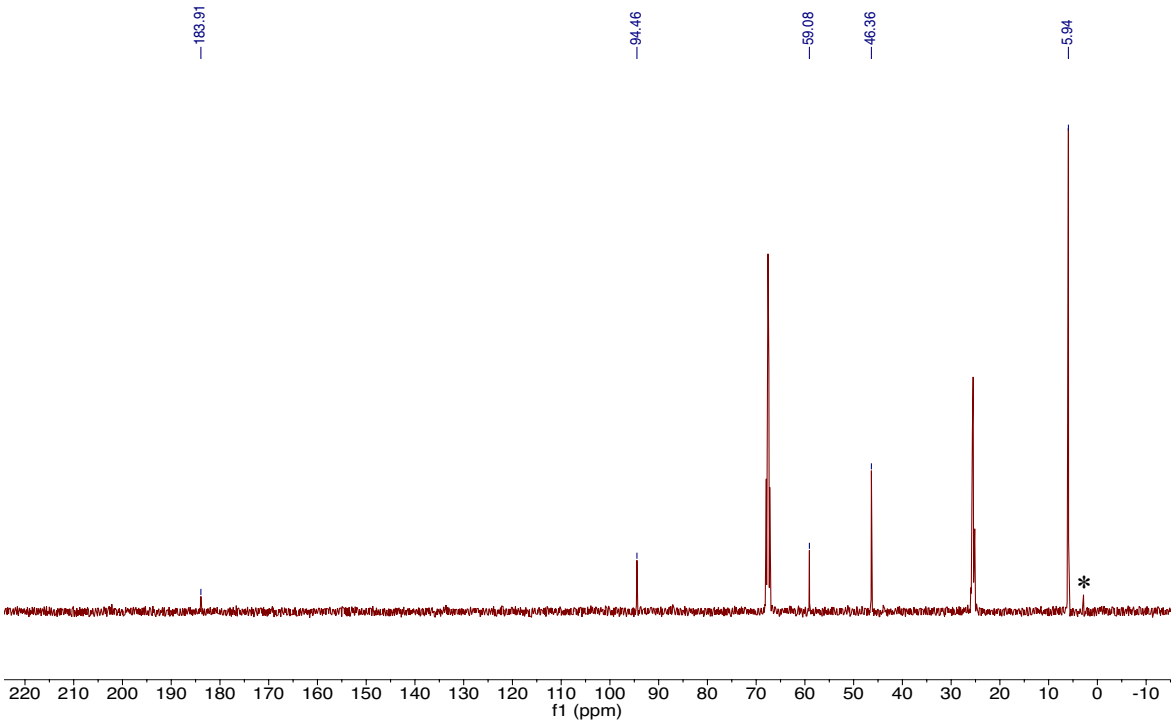

Figure A4.9. $^{13}C\{^{1}H\}$ NMR spectrum of $[Na(TMEDA)][Th(C{\equiv}CH)_2(N(SiMe_3)_2)_3]$ (**4.5**) in THF-d_8 at room temperature. (*) indicates free $HN(SiMe_3)_2$.

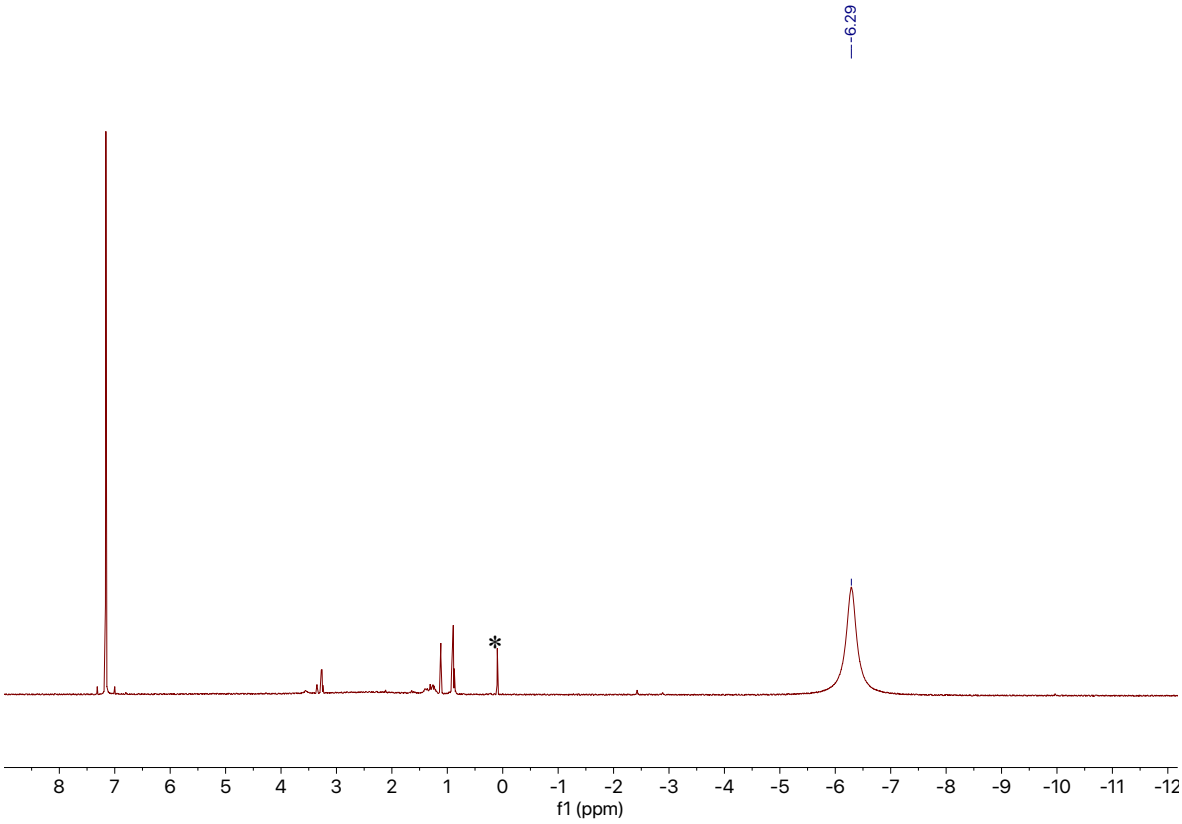

Figure A4.10. ^{1}H NMR spectrum of $[\{U(NR_2)_3\}_2(\mu,\eta^1{:}\eta^1\text{-}C_2)]$ (**4.6**) in C_6D_6 at room temperature. (*) indicates free $HN(SiMe_3)_2$.

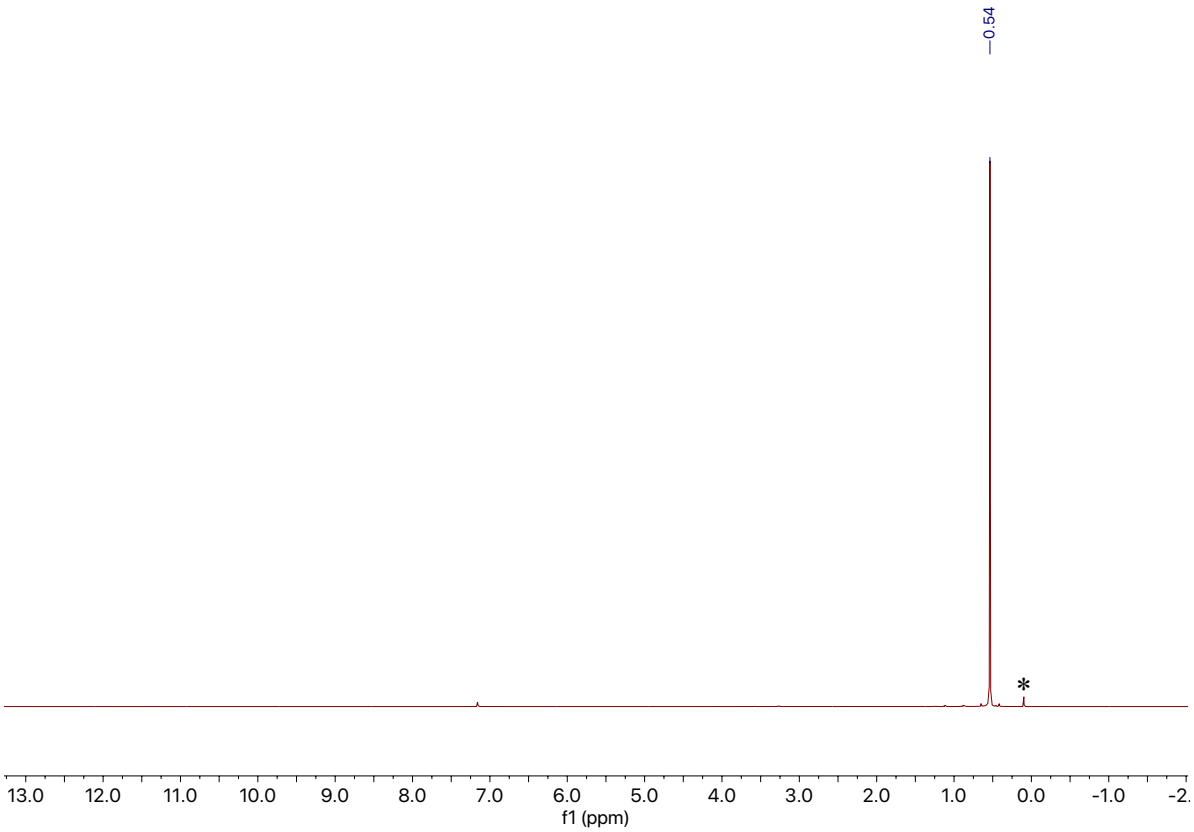

Figure A4.11. ^{1}H NMR spectrum of [{Th(NR$_2$)$_3$}$_2$(μ,η^1:η^1-C$_2$)] (**4.7**) in C_6D_6 at room temperature. (*) indicates free HN(SiMe$_3$)$_2$.

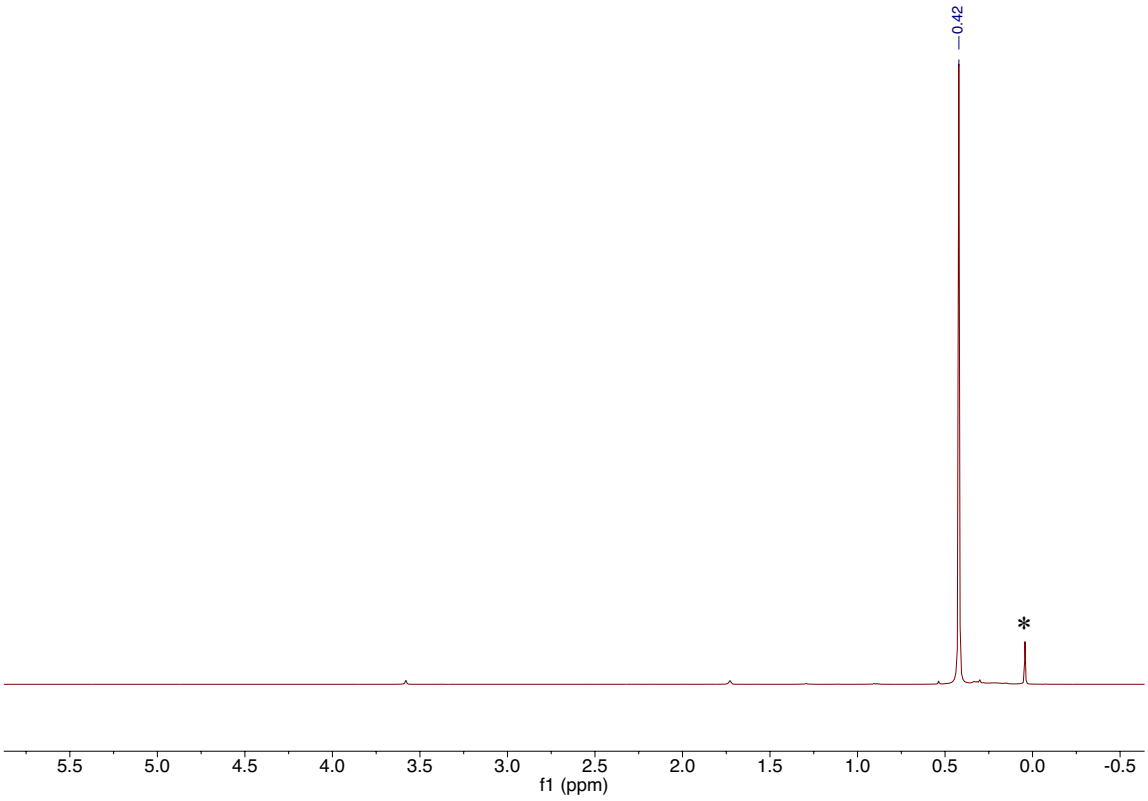

Figure A4.12. ^{1}H NMR spectrum of [{Th(NR$_2$)$_3$}$_2$(μ,η^1:η^1-C$_2$)] (**4.7**) in THF-d_8 at room temperature. (*) indicates free HN(SiMe$_3$)$_2$.

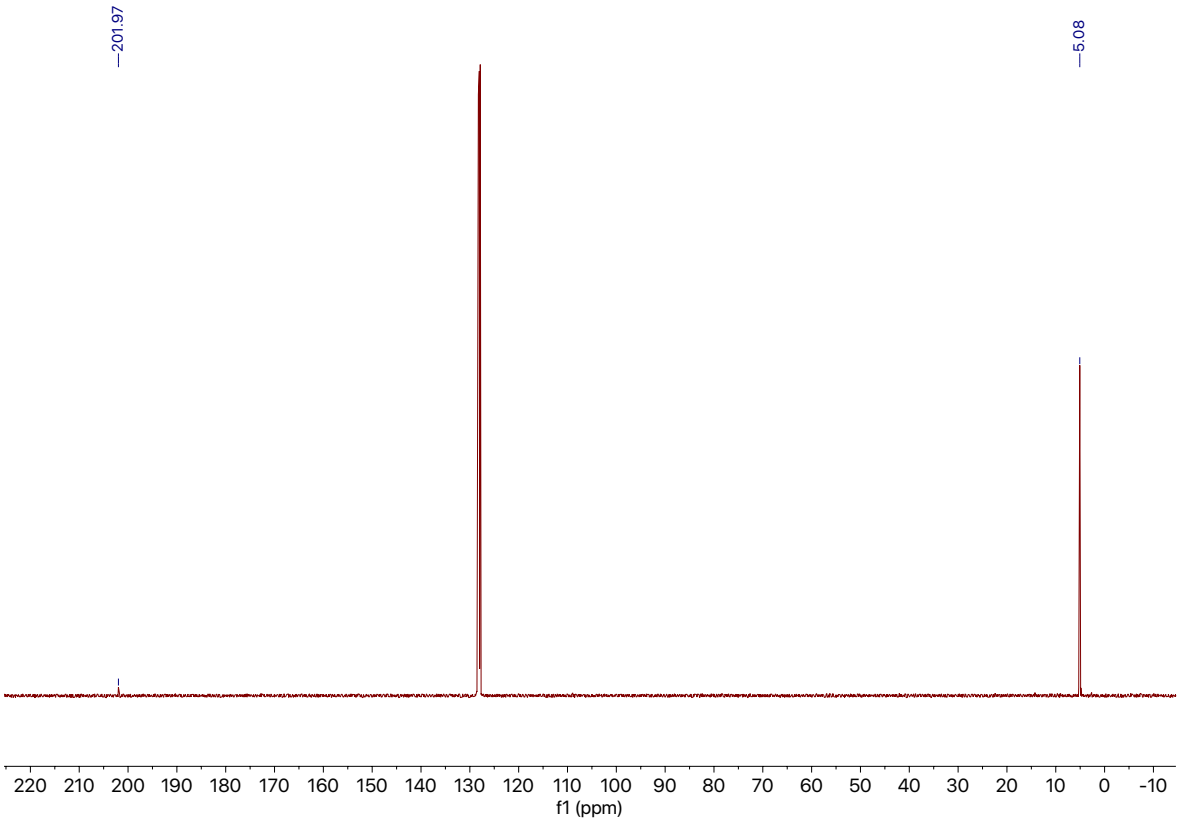

Figure A4.13. $^{13}C\{^{1}H\}$ NMR spectrum of $[\{Th(NR_2)_3\}_2(\mu,\eta^1:\eta^1\text{-}C_2)]$ (**4.7**) in C_6D_6 at room temperature.

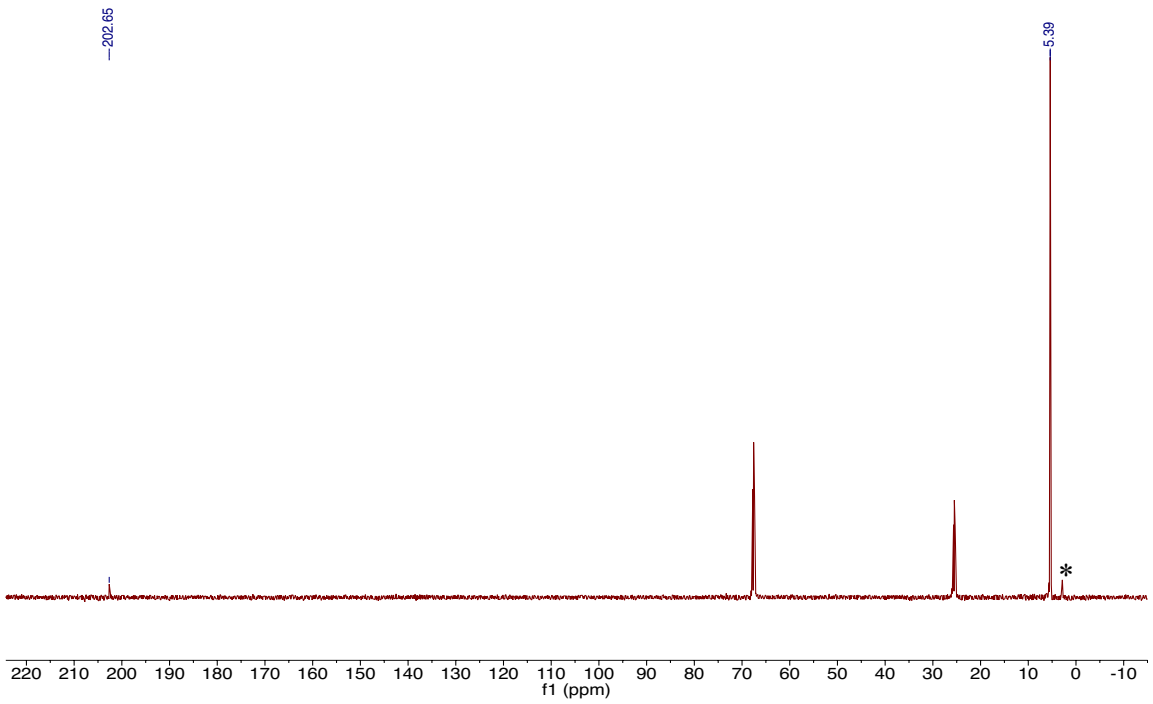

Figure A4.14. $^{13}C\{^{1}H\}$ NMR spectrum of $[\{Th(NR_2)_3\}_2(\mu,\eta^1{:}\eta^1\text{-}C_2)]$ (**4.7**) in THF-d_8 at room temperature. (*) indicates free $HN(SiMe_3)_2$.

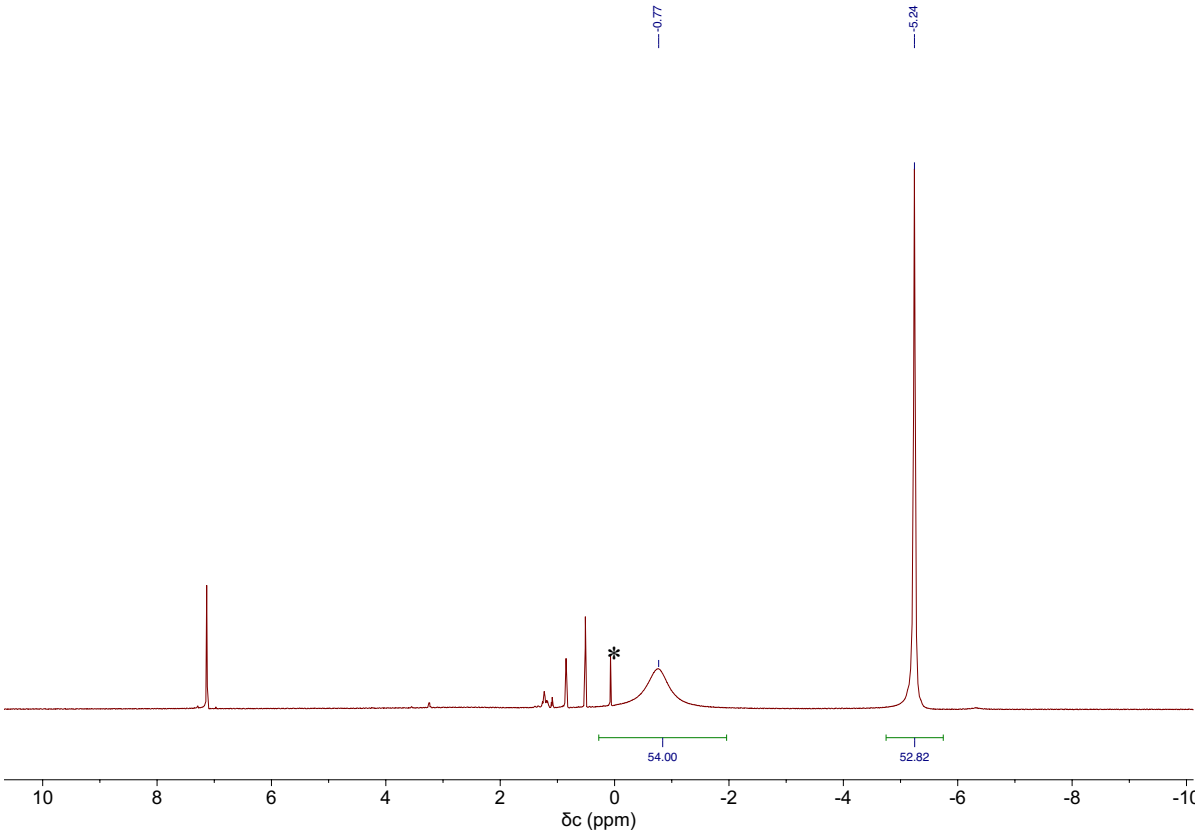

Figure A4.15. ^{1}H NMR spectrum of $[U(NR_2)_3(\mu,\eta^1{:}\eta^1\text{-}C_2)Th(NR_2)_3]$ (**4.8**) in C_6D_6 at room temperature. (*) indicates free $HN(SiMe_3)_2$.

4.5.2 IR Spectra

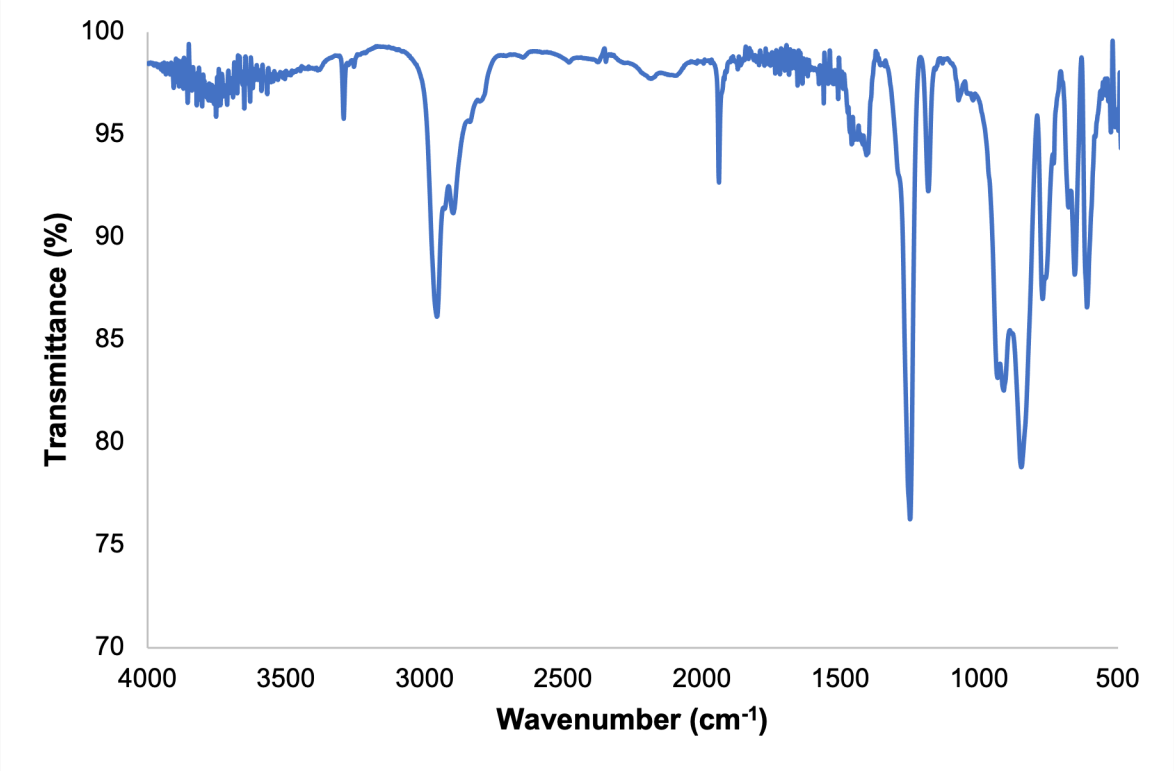

Figure A4.16. IR spectrum of **4.1** (KBr Pellet).

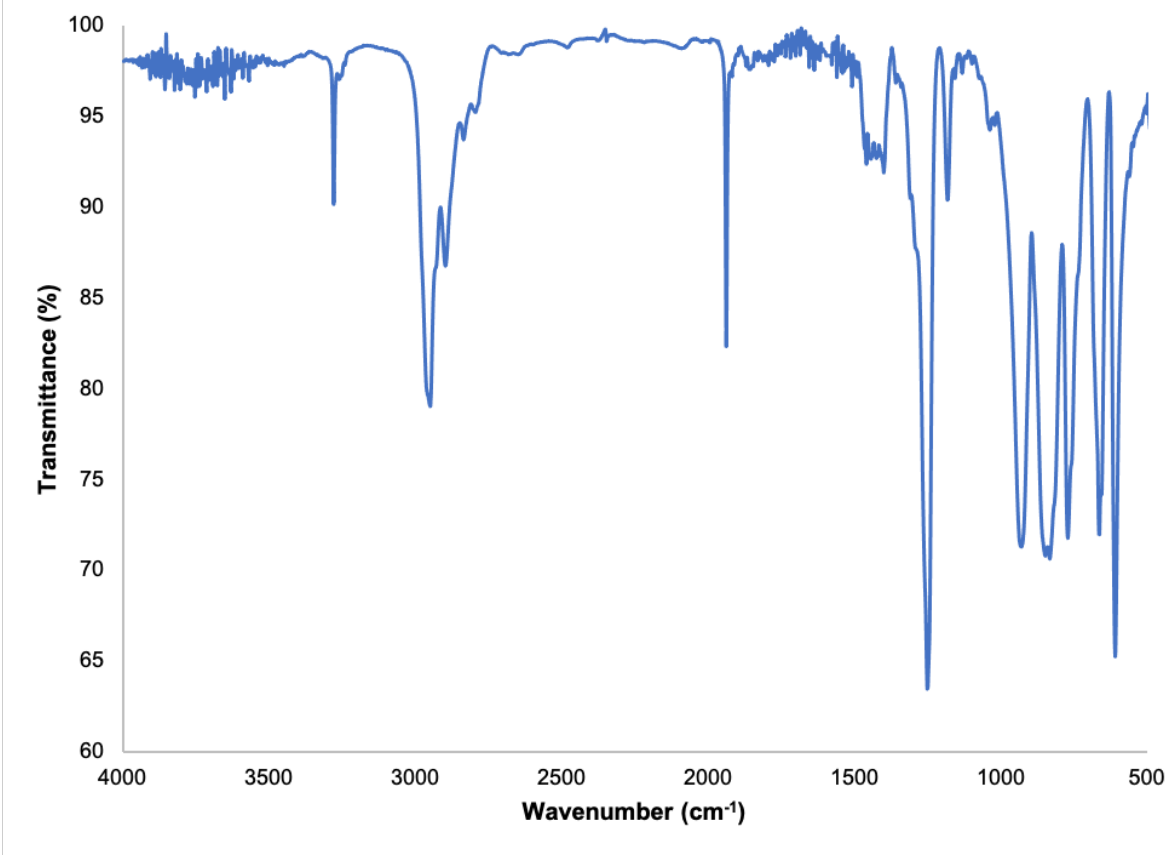

Figure A4.17. IR spectrum of **4.2** (KBr Pellet).

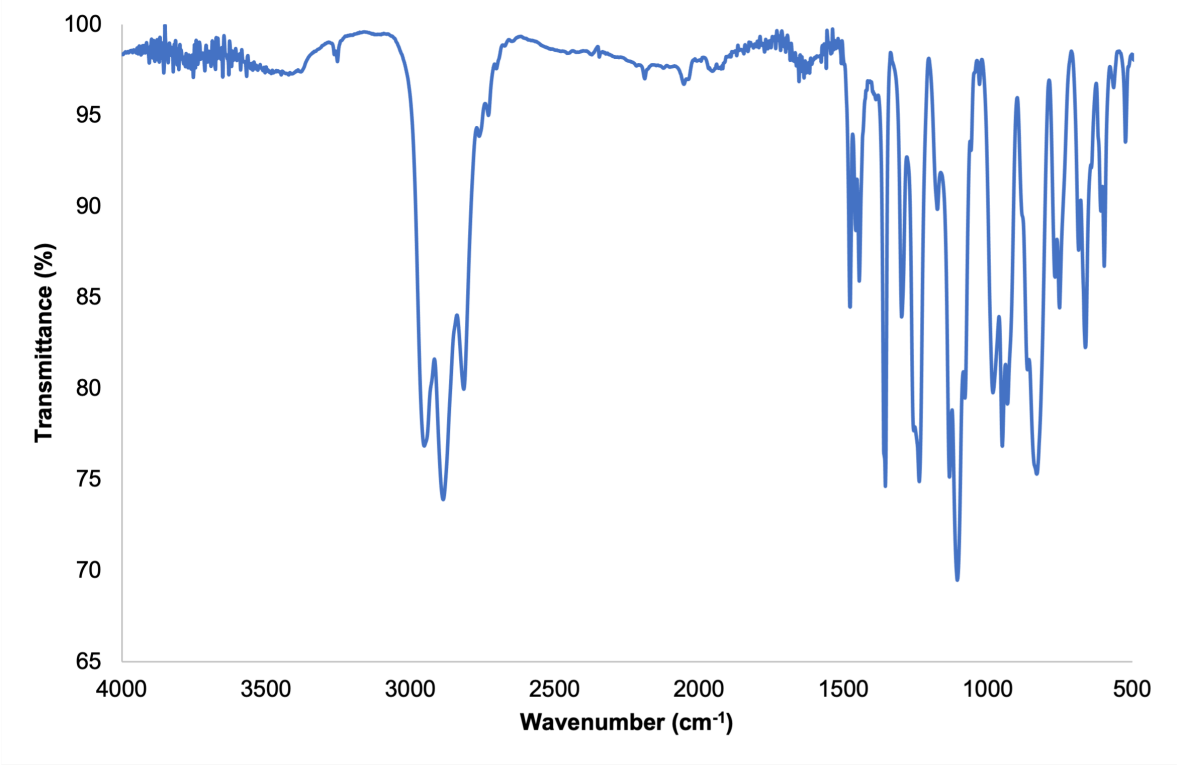

Figure A4.18. IR spectrum of **4.3** (KBr Pellet).

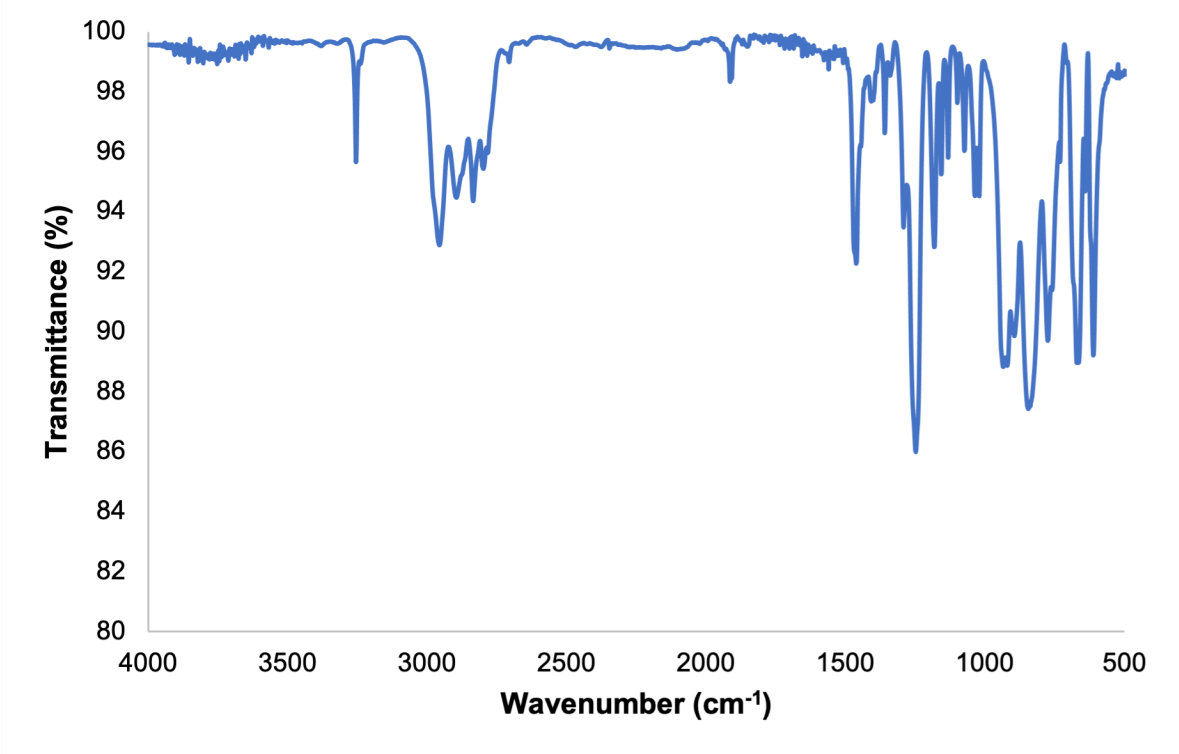

Figure A4.19. IR spectrum of **4.4** (KBr Pellet).

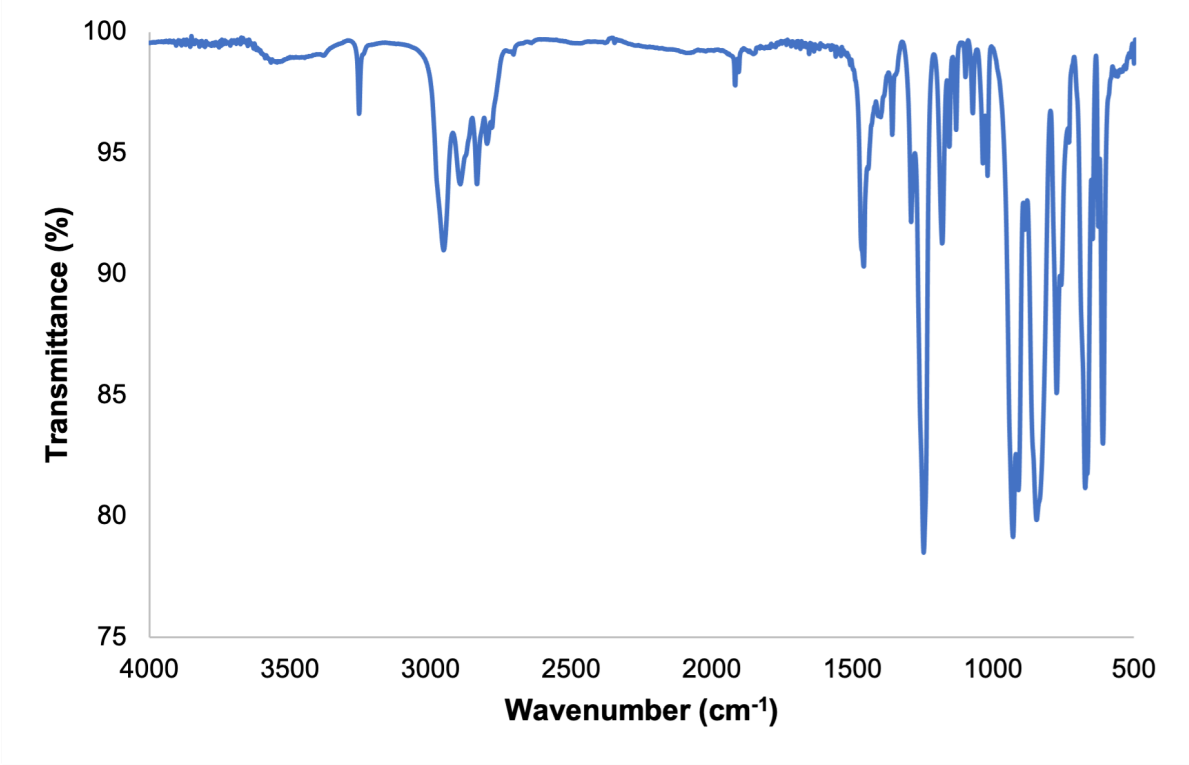

Figure A4.20. IR spectrum of **4.5** (KBr Pellet).

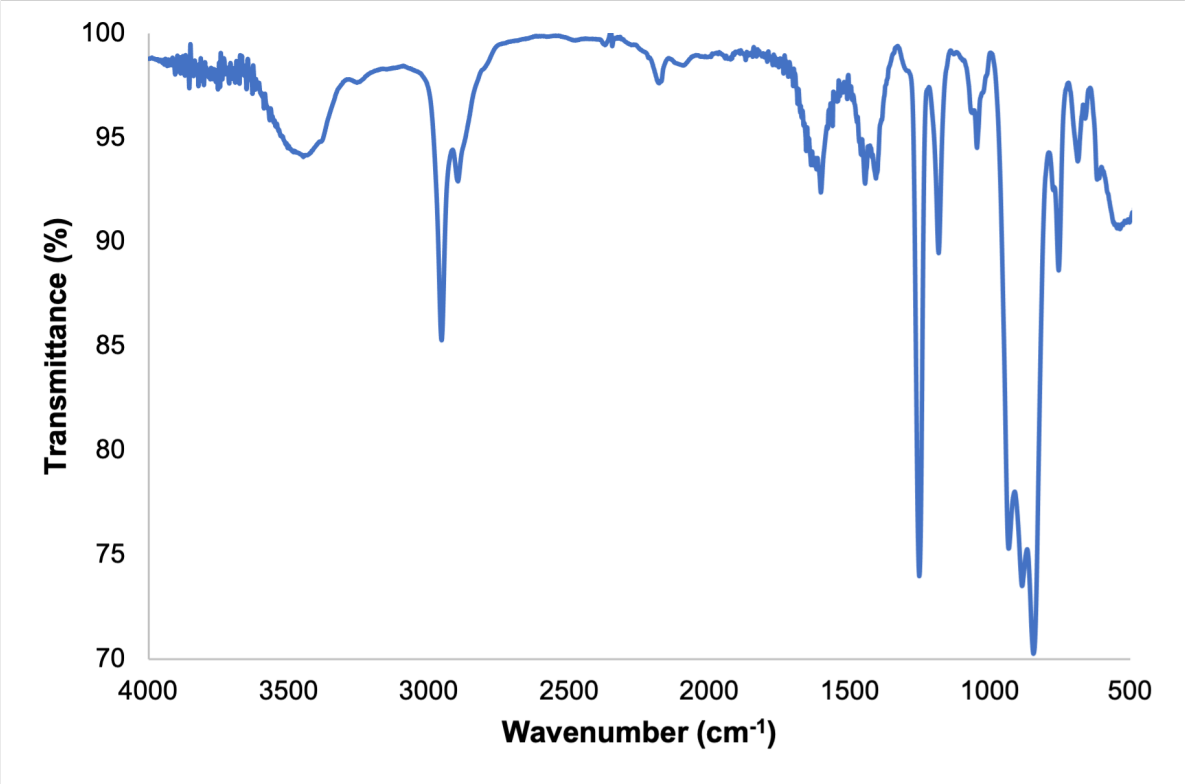

Figure A4.21. IR spectrum of **4.6** (KBr Pellet).

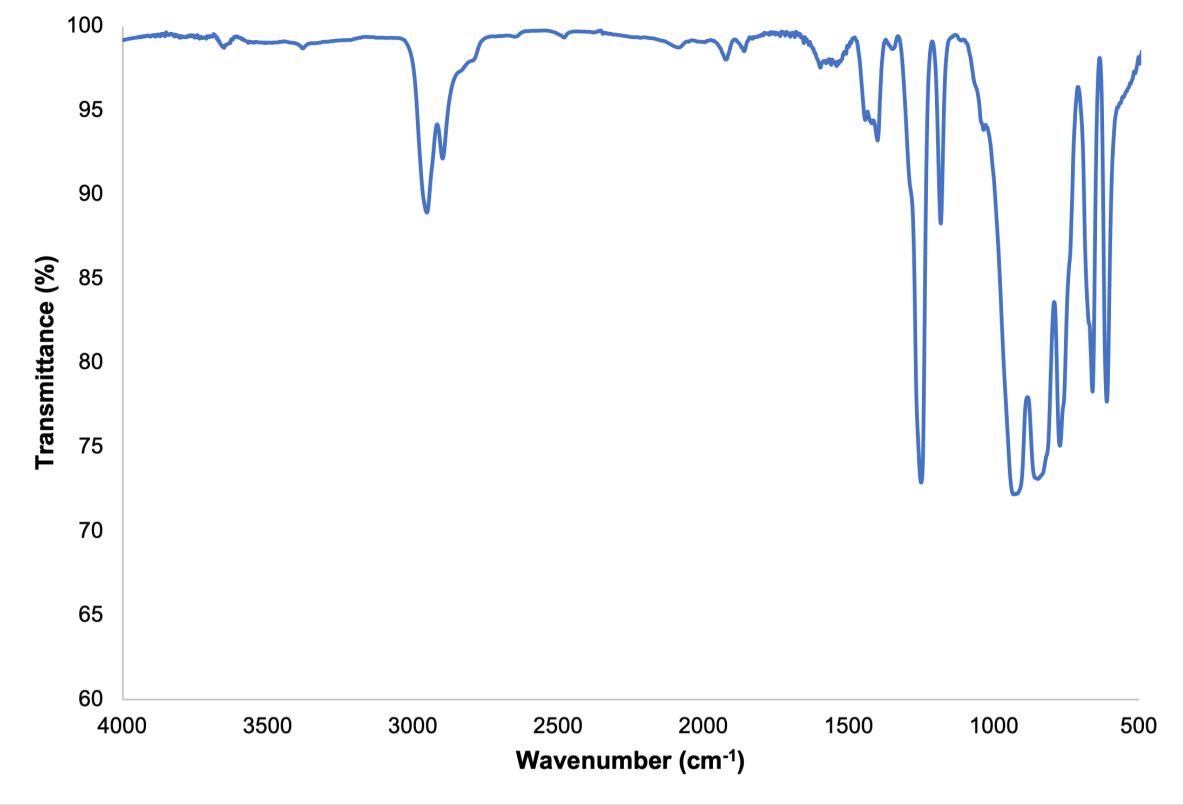

Figure A4.22. IR spectrum of **4.7** (KBr Pellet).

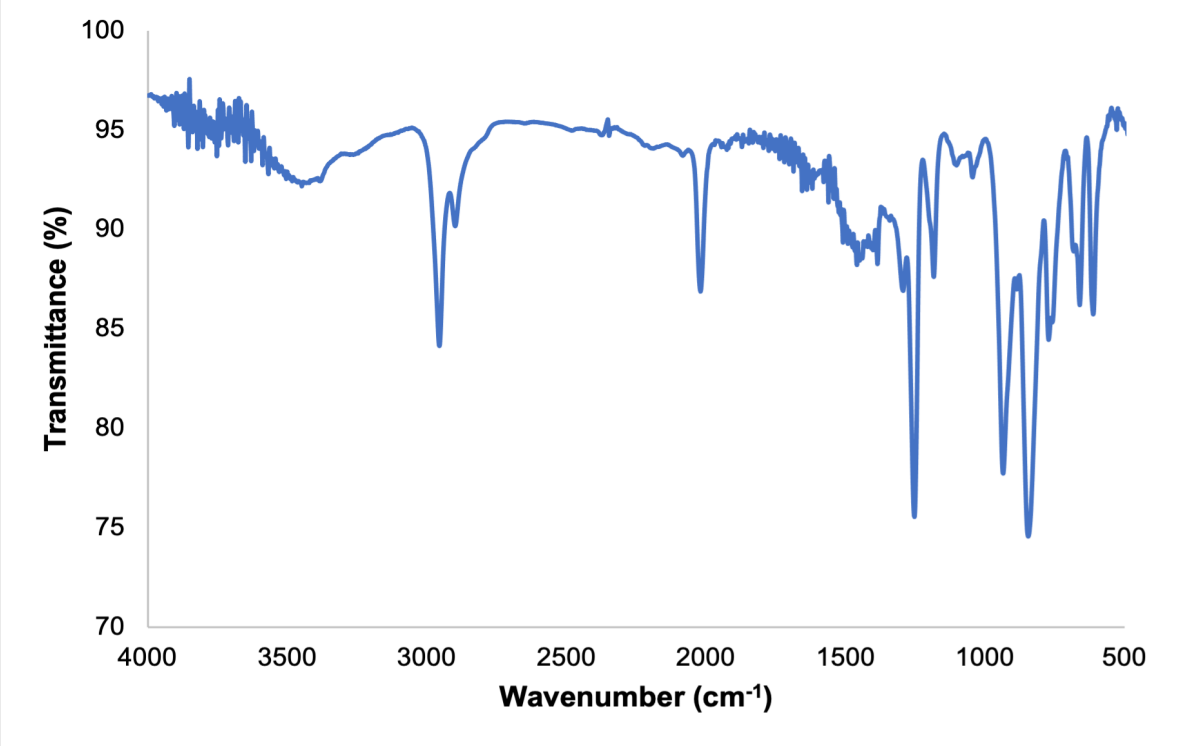

Figure A4.23. IR spectrum of **4.8** (KBr Pellet).

4.6 References

1. Dash, A. K.; Gourevich, I.; Wang, J. Q.; Wang, J.; Kapon, M.; Eisen, M. S., The Catalytic Effect in Opening an Organoactinide Metal Coordination Sphere: Regioselective Dimerization of Terminal Alkynes and Hydrosilylation of Alkynes and Alkenes with $PhSiH_3$ Promoted by $Me_2SiCp'_2Th^nBu_2$. *Organometallics* **2001**, *20*, 5084-5104.

2. Straub, T.; Haskel, A.; Neyroud, T. G.; Kapon, M.; Botoshansky, M.; Eisen, M. S., Intermolecular Hydroamination of Terminal Alkynes Catalyzed by Organoactinide Complexes. Scope and Mechanistic Studies. *Organometallics* **2001**, *20*, 5017-5035.

3. Wang, J.; Kapon, M.; Berthet, J. C.; Ephritikhine, M.; Eisen, M. S., Cross dimerization of terminal alkynes catalyzed by $[(Et_2N)_3U][BPh_4]$. *Inorg. Chim. Acta* **2002**, *334*, 183-192.

4. Dash, A. K.; Gurevizt, Y.; Wang, J. Q.; Wang, J.; Kapon, M.; Eisen, M. S., Organoactinides—novel catalysts for demanding chemical transformations. *J. Alloys Compd.* **2002**, *344*, 65-69.

5. Fox, A. R.; Bart, S. C.; Meyer, K.; Cummins, C. C., Towards uranium catalysts. *Nature* **2008**, *455*, 341-349.

6. Evans, W. J.; Walensky, J. R.; Ziller, J. W.; Rheingold, A. L., Insertion of Carbodiimides and Organic Azides into Actinide−Carbon Bonds. *Organometallics* **2009**, *28*, 3350-3357.

7. Haskel, A.; Straub, T.; Dash, A. K.; Eisen, M. S., Oligomerization and Cross-Oligomerization of Terminal Alkynes Catalyzed by Organoactinide Complexes. *J. Am. Chem. Soc.* **1999**, *121*, 3014-3024.

8. Haskel, A.; Wang, J. Q.; Straub, T.; Neyroud, T. G.; Eisen, M. S., Controlling the Catalytic Oligomerization of Terminal Alkynes Promoted by Organoactinides: A Strategy to Short Oligomers. *J. Am. Chem. Soc.* **1999**, *121*, 3025-3034.

9. Wang, J. Q.; Dash, A. K.; Berthet, J. C.; Ephritikhine, M.; Eisen, M. S., Selective Dimerization of Terminal Alkynes Promoted by the Cationic Actinide Compound $[(Et_2N)_3U][BPh_4]$. Formation of the Alkyne π-Complex $[(Et_2N)_2U(C{\equiv}C^tBu)(\eta_2\text{-}HC{\equiv}C^tBu)][BPh_4]$. *Organometallics* **1999**, *18*, 2407-2409.

10. Batrice, R. J.; McKinven, J.; Arnold, P. L.; Eisen, M. S., Selective Oligomerization and [2 + 2 + 2] Cycloaddition of Terminal Alkynes from Simple Actinide Precatalysts. *Organometallics* **2015**, *34*, 4039-4050.

11. Suvova, M.; O'Brien, K. T. P.; Farnaby, J. H.; Love, J. B.; Kaltsoyannis, N.; Arnold, P. L., Thorium(IV) and Uranium(IV) trans-Calix[2]benzene[2]pyrrolide Alkyl and Alkynyl Complexes: Synthesis, Reactivity, and Electronic Structure. *Organometallics* **2017**, *36*, 4669-4681.

12. Newell, B. S.; Rappé, A. K.; Shores, M. P., Experimental Evidence for Magnetic Exchange in Di- and Trinuclear Uranium(IV) Ethynylbenzene Complexes. *Inorg. Chem.* **2010**, *49*, 1595-1606.

13. Tatebe, C. J.; Kiernicki, J. J.; Higgins, R. F.; Ward, R. J.; Natoli, S. N.; Langford, J. C.; Clark, C. L.; Zeller, M.; Wenthold, P.; Shores, M. P.; Walensky, J. R.; Bart, S. C., Investigation of the Electronic Structure of Aryl-Bridged Dinuclear U(III) and U(IV) Compounds. *Organometallics* **2019**, *38*, 1031-1040.

14. Mullane, K. C.; Hrobárik, P.; Cheisson, T.; Manor, B. C.; Carroll, P. J.; Schelter, E. J., ^{13}C NMR Shifts as an Indicator of U–C Bond Covalency in Uranium(VI) Acetylide Complexes: An Experimental and Computational Study. *Inorg. Chem.* **2019**, *58*, 4152-4163.

15. Lewis, A. J.; Carroll, P. J.; Schelter, E. J., Stable Uranium(VI) Methyl and Acetylide Complexes and the Elucidation of an Inverse Trans Influence Ligand Series. *J. Am. Chem. Soc.* **2013**, *135*, 13185-13192.

16. Smiles, D. E.; Wu, G.; Hrobárik, P.; Hayton, T. W., Use of ^{77}Se and ^{125}Te NMR Spectroscopy to Probe Covalency of the Actinide-Chalcogen Bonding in $[Th(En)\{N(SiMe_3)_2\}_3]^-$ (E = Se, Te; n = 1, 2) and Their Oxo-Uranium(VI) Congeners. *J. Am. Chem. Soc.* **2016**, *138*, 814-825.

17. Staun, S. L.; Sergentu, D.-C.; Wu, G.; Autschbach, J.; Hayton, T. W., Use of ^{15}N NMR spectroscopy to probe covalency in a thorium nitride. *Chem. Sci.* **2019**, *10*, 6431-6436.

18. Sergentu, D.-C.; Kent, G. T.; Staun, S. L.; Yu, X.; Cho, H.; Autschbach, J.; Hayton, T. W., Probing the Electronic Structure of a Thorium Nitride Complex by Solid-State ^{15}N NMR Spectroscopy. *Inorg. Chem.* **2020**, *59*, 10138-10145.

19. Wu, W.; Rehe, D.; Hrobárik, P.; Kornienko, A. Y.; Emge, T. J.; Brennan, J. G., Molecular Thorium Compounds with Dichalcogenide Ligands: Synthesis, Structure, ^{77}Se NMR Study, and Thermolysis. *Inorg. Chem.* **2018**, *57*, 14821-14833.

20. Seaman, L. A.; Hrobárik, P.; Schettini, M. F.; Fortier, S.; Kaupp, M.; Hayton, T. W., A Rare Uranyl(VI)–Alkyl Ate Complex $[Li(DME)_{1.5}]_2[UO_2(CH_2SiMe_3)_4]$ and Its Comparison with a Homoleptic Uranium(VI)–Hexaalkyl. *Angew. Chem. Int. Ed.* **2013**, *52*, 3259-3263.

21. Pedrick, E. A.; Hrobárik, P.; Seaman, L. A.; Wu, G.; Hayton, T. W., Synthesis, structure and bonding of hexaphenyl thorium(iv): observation of a non-octahedral structure. *Chem. Commun.* **2016**, *52*, 689-692.

22. Smiles, D. E.; Wu, G.; Hrobárik, P.; Hayton, T. W., Synthesis, Thermochemistry, Bonding, and 13C NMR Chemical Shift Analysis of a Phosphorano-Stabilized Carbene of Thorium. *Organometallics* **2017**, *36*, 4519-4524.

23. Ordoñez, O.; Yu, X.; Wu, G.; Autschbach, J.; Hayton, T. W., Synthesis and Characterization of Two Uranyl-Aryl "Ate" Complexes. *Chem. Eur. J.* **2020**, *27*, 5885-5889.

24. Panetti, G. B.; Sergentu, D.-C.; Gau, M. R.; Carroll, P. J.; Autschbach, J.; Walsh, P. J.; Schelter, E. J., Isolation and characterization of a covalent CeIV-Aryl complex with an anomalous ^{13}C chemical shift. *Nat. Commun.* **2021**, *12*, 1713.

25. Rungthanaphatsophon, P.; Huang, P.; Walensky, J. R., Phosphorano-Stabilized Carbene Complexes with Short Thorium(IV)– and Uranium(IV)–Carbon Bonds. *Organometallics* **2018**, *37*, 1884-1891.

26. Atwood, J. L.; Tsutsui, M.; Ely, N.; Gebala, A. E., THE CRYSTAL AND MOLECULAR STRUCTURE OF TRICYCLOPENTADIENYLETHYNYLURANIUM(IV). *J. Coord. Chem.* **1976**, *5*, 209-215.

27. Fox, A. R.; Creutz, S. E.; Cummins, C. C., A bimetallic uranium μ-dicarbide complex: synthesis, X-ray crystal structure, and bonding. *Dalton Trans.* **2010**, *39*, 6632-6634.

28. Southard, G. E.; Curtis, M. D.; Kampf, J. W., Synthesis of an Alkyne-Bridged Decamethylhafnocene Dimer and Related Alkyne-Substituted Monomers. *Organometallics* **1996**, *15*, 4667-4668.

29. Settineri, N. S.; Arnold, J., Insertion, protonolysis and photolysis reactivity of a thorium monoalkyl amidinate complex. *Chem. Sci.* **2018**, *9*, 2831-2841.

30. Bell, E. E.; Nielsen, H. H., The Infra-Red Spectrum of Acetylene. *J. Chem. Phys.* **1950**, *18*, 1382-1394.

31. Wang, Y.; Zhang, C.; Zi, G.; Ding, W.; Walter, M. D., Preparation of a potassium chloride bridged thorium phosphinidiide complex and its reactivity towards small organic molecules. *New J. Chem.* **2019**, *43*, 9527-9539.

32. Garner, M. E.; Parker, B. F.; Hohloch, S.; Bergman, R. G.; Arnold, J., Thorium Metallacycle Facilitates Catalytic Alkyne Hydrophosphination. *J. Am. Chem. Soc.* **2017**, *139*, 12935-12938.

33. Matson, E. M.; Fanwick, P. E.; Bart, S. C., Formation of Trivalent U–C, U–N, and U–S Bonds and Their Reactivity toward Carbon Dioxide and Acetone. *Organometallics* **2011**, *30*, 5753-5762.

34. Manna, J.; John, K. D.; Hopkins, M. D., The Bonding of Metal-Alkynyl Complexes. In *Advances in Organometallic Chemistry*, Stone, F. G. A.; West, R., Eds. Academic Press: 1995; Vol. 38, pp 79-154.

35. Addison, A. W.; Rao, T. N.; Reedijk, J.; van Rijn, J.; Verschoor, G. C., Synthesis, structure, and spectroscopic properties of copper(II) compounds containing nitrogen–sulphur donor ligands; the crystal and molecular structure of aqua[1,7-bis(N-methylbenzimidazol-2′-yl)-2,6-dithiaheptane]copper(II) perchlorate. *J. Chem. Soc., Dalton Trans.* **1984**, 1349-1356.

36. Shannon, R., Revised effective ionic radii and systematic studies of interatomic distances in halides and chalcogenides. *Acta Crystallogr., Sect. A: Found. Crystallogr.* **1976**, *32*, 751-767.

37. Harlan, C. J.; Tunge, J. A.; Bridgewater, B. M.; Norton, J. R., Trapping of Acetylene by a Zirconocene Terminal Imido Complex. *Organometallics* **2000**, *19*, 2365-2372.

38. Binger, P.; Müller, P.; Philipps, P.; Gabor, B.; Mynott, R.; Herrmann, A. T.; Langhauser, F.; Krüger, C., Synthese und Struktur eines neuen Bis[(trimethylphosphan)titanocen]-Komplexes mit einer verbrückenden C_2-Einheit. *Chem. Ber.* **1992**, *125*, 2209-2212.

39. Kindra, D. R.; Evans, W. J., Magnetic Susceptibility of Uranium Complexes. *Chem. Rev.* **2014**, *114*, 8865-8882.

40. Castro-Rodríguez, I.; Meyer, K., Small molecule activation at uranium coordination complexes: control of reactivity via molecular architecture. *Chem. Commun.* **2006**, 1353-1368.

41. Rosenzweig, M. W.; Scheurer, A.; Lamsfus, C. A.; Heinemann, F. W.; Maron, L.; Andrez, J.; Mazzanti, M.; Meyer, K., Uranium(iv) terminal hydrosulfido and sulfido complexes: insights into the nature of the uranium–sulfur bond. *Chem. Sci.* **2016**, *7*, 5857-5866.

42. Schelter, E. J.; Yang, P.; Scott, B. L.; Thompson, J. D.; Martin, R. L.; Hay, P. J.; Morris, D. E.; Kiplinger, J. L., Systematic Studies of Early Actinide Complexes: Uranium(IV) Fluoroketimides. *Inorg. Chem.* **2007**, *46*, 7477-7488.

43. Rinehart, J. D.; Bartlett, B. M.; Kozimor, S. A.; Long, J. R., Ferromagnetic exchange coupling in the linear, chloride-bridged cluster (cyclam)$Co^{II}[(\mu\text{-}Cl)U^{IV}(Me_2Pz)_4]_2$. *Inorg. Chem. Acta* **2008**, *361*, 3534-3538.

44. Gardner, B. M.; King, D. M.; Tuna, F.; Wooles, A. J.; Chilton, N. F.; Liddle, S. T., Assessing crystal field and magnetic interactions in diuranium-μ-chalcogenide triamidoamine complexes with U^{IV}–E–U^{IV} cores (E = S, Se, Te): implications for determining the presence or absence of actinide–actinide magnetic exchange. *Chem. Sci.* **2017**, *8*, 6207-6217.

45. Glendening, E. D.; Landis, C. R.; Weinhold, F., Natural bond orbital methods. *WIREs Comput Mol Sci* **2012**, *2*, 1-42.

46. Hayton, T. W., Hydride, Alkyl, Aryl, Acetylide, Carbonyl, and Cyanide Complexes of the Actinides. In *Reference Module in Chemistry, Molecular Sciences and Chemical Engineering*, Elsevier: 2021.

47. Wolford, N. J.; Sergentu, D.-C.; Brennessel, W. W.; Autschbach, J.; Neidig, M. L., Homoleptic Aryl Complexes of Uranium (IV). *Angew. Chem. Int. Ed.* **2019**, *58*, 10266-10270.

48. Ordoñez, O.; Yu, X.; Wu, G.; Autschbach, J.; Hayton, T. W., Homoleptic Perchlorophenyl "Ate" Complexes of Thorium(IV) and Uranium(IV). *Organometallics* **2021**, *Manuscript Submitted*.

49. Seaman, L. A.; Pedrick, E. A.; Tsuchiya, T.; Wu, G.; Jakubikova, E.; Hayton, T. W., Comparison of the Reactivity of 2-Li-$C_6H_4CH_2NMe_2$ with MCl_4 (M=Th, U): Isolation of a Thorium Aryl Complex or a Uranium Benzyne Complex. *Angew. Chem. Int. Ed.* **2013**, *52*, 10589-10592.

50. Autschbach, J.; Zurek, E., Relativistic Density-Functional Computations of the Chemical Shift of ^{129}Xe in $Xe@C_{60}$. *J. Phys. Chem. A* **2003**, *107*, 4967-4972.

51. Autschbach, J.; Zheng, S., Chapter 1 Relativistic Computations of NMR Parameters from First Principles: Theory and Applications. In *Annu. Rep. NMR Spectrosc.*, Webb, G. A., Ed. Academic Press: 2009; Vol. 67, pp 1-95.

52. Powell, C. E.; Cifuentes, M. P.; Morrall, J. P.; Stranger, R.; Humphrey, M. G.; Samoc, M.; Luther-Davies, B.; Heath, G. A., Organometallic Complexes for Nonlinear Optics. 30.[1] Electrochromic Linear and Nonlinear Optical Properties of Alkynylbis(diphosphine)ruthenium Complexes. *J. Am. Chem. Soc.* **2003**, *125*, 602-610.

53. Grelaud, G.; Cifuentes, M. P.; Paul, F.; Humphrey, M. G., Group 8 metal alkynyl complexes for nonlinear optics. *J. Organomet. Chem.* **2014**, *751*, 181-200.

54. Shen, C.; Loas, G. h.; Srebro-Hooper, M.; Vanthuyne, N.; Toupet, L.; Cador, O.; Paul, F.; López Navarrete, J. T.; Ramírez, F. J.; Nieto-Ortega, B.; Casado, J.; Autschbach, J.; Vallet, M.; Crassous, J., Iron Alkynyl Helicenes: Redox-Triggered Chiroptical Tuning in the IR and Near-IR Spectral Regions and Suitable for Telecommunications Applications. *Angew. Chem. Int. Ed.* **2016**, *55*, 8062-8066.

55. Long, N. J.; Williams, C. K., Metal Alkynyl σ Complexes: Synthesis and Materials. *Angew. Chem. Int. Ed.* **2003**, *42*, 2586-2617.

56. Turner, H. W.; Andersen, R. A.; Zalkin, A.; Templeton, D. H., Chloro-, methyl-, and (tetrahydroborato)tris((hexamethyldisilyl)amido)thorium(IV) and uranium(IV). Crystal structure of (tetrahydroborato)tris((hexamethyldisilyl)amido)thorium(IV). *Inorg. Chem.* **1979**, *18*, 1221-1224.

57. Andersen, R. A., Tris ((hexamethyldisilyl) amido) uranium (III): preparation and coordination chemistry. *Inorg. Chem.* **1979**, *18*, 1507-1509.

58. Cantat, T.; Scott, B. L.; Kiplinger, J. L., Convenient access to the anhydrous thorium tetrachloride complexes $ThCl_4(DME)_2$, $ThCl_4(1,4\text{-dioxane})_2$ and $ThCl_4(THF)_{3.5}$ using commercially available and inexpensive starting materials. *Chem. Commun.* **2010**, *46*, 919-921.

59. Harris, R. K.; Becker, E. D.; De Menezes, S. M. C.; Granger, P.; Hoffman, R. E.; Zilm, K. W., Further Conventions for NMR Shielding and Chemical Shifts (IUPAC Recommendations 2008). *Magn. Reson. Chem.* **2008**, *46*, 582-598.

60. Harris, R. K.; Becker, E. D.; Cabral de Menezes, S. M.; Goodfellow, R.; Granger, P., NMR nomenclature: nuclear spin properties and conventions for chemical shifts. IUPAC Recommendations 2001. International Union of Pure and Applied Chemistry. Physical Chemistry Division. Commission on Molecular Structure and Spectroscopy. *Magn. Reson. Chem.* **2002**, *40*, 489-505.

61. *SMART Apex II*, Version 2.1 ed.; Bruker AXS Inc.: Madison WI, 2005.

62. *SAINT Software User's Guide*, Version 7.34a ed.; Bruker AXS Inc.: Madison, WI,

2005.

63. Sheldrick, G. M., *SADABS*, the Siemens Area Detector Absorption Correction; University of Göttingen: Göttingen, Germany, 2005.

64. *SHELXTL PC*, Version 6.12 ed.; Bruker AXS Inc.:Madison, WI, 2005.

65. Bain, G. A.; Berry, J. F., Diamagnetic Corrections and Pascal's Constants. *J. Chem. Educ.* **2008**, *85*, 532.

66. Paier, J.; Hirschl, R.; Marsman, M.; Kresse, G., The Perdew–Burke–Ernzerhof exchange-correlation functional applied to the G2-1 test set using a plane-wave basis set. *J. Chem. Phys.* **2005**, *122*, 234102.

67. Cao, X.; Dolg, M., Valence basis sets for relativistic energy-consistent small-core lanthanide pseudopotentials. *J. Chem. Phys.* **2001**, *115*, 7348-7355.

68. Rassolov, V. A.; Pople, J. A.; Ratner, M. A.; Windus, T. L., 6-31G* basis set for atoms K through Zn. *J. Chem. Phys.* **1998**, *109*, 1223-1229.

69. Grimme, S.; Ehrlich, S.; Goerigk, L., Effect of the damping function in dispersion corrected density functional theory. *J. Comput. Chem.* **2011**, *32*, 1456-1465.

70. Frisch, M.; Trucks, G.; Schlegel, H.; Scuseria, G.; Robb, M.; Cheeseman, J.; Scalmani, G.; Barone, V.; Petersson, G.; Nakatsuji, H., Gaussian 16. Gaussian, Inc. Wallingford, CT: 2016.

71. Glendening, E. D.; Landis, C. R.; Weinhold, F., NBO 6.0: Natural bond orbital analysis program. *J. Comput. Chem.* **2013**, *34*, 1429-1437.

72. Baerends, E. J.; Ziegler, T.; Atkins, A. J.; Autschbach, J.; Baseggio, O.; Bashford, D.; Bérces, A.; Bickelhaupt, F. M.; Bo, C.; Boerrigter, P. M.; Cavallo, L.; Daul, C.; Chong, D. P.; Chulhai, D. V.; Deng, L.; Dickson, R. M.; Dieterich, J. M.; Ellis, D. E.; Faassen, M. v.; Fan, L.; Fischer, T. H.; Guerra, C. F.; Franchini, M.; Ghysels, A.; Giammona, A.; Gisbergen, S. J. A. v.; Goez, A.; Götz, A. W.; Groeneveld, J. A.; Gritsenko, O. V.; Grüning, M.; Gusarov, S.; Harris, F. E.; Hoek, P. v. d.; Hu, Z.; Jacob, C. R.; Jacobsen, H.; Jensen, L.; Joubert, L.; Kaminski, J. W.; Kessel, G. v.; König, C.; Kootstra, F.; Kovalenko, A.; Krykunov, M. V.; Lenthe, E. v.; McCormack, D. A.; Michalak, A.; Mitoraj, M.; Morton, S. M.; Neugebauer, J.; Nicu, V. P.; Noodleman, L.; Osinga, V. P.; Patchkovskii, S.; Pavanello, M.; Peeples, C. A.; Philipsen, P. H. T.; Post, D.; Pye, C. C.; Ramanantoanina, H.; Ramos, P.; Ravenek, W.; Rodríguez, J. I.; Ros, P.; Rüger, R.; Schipper, P. R. T.; Schlüns, D.; Schoot, H. v.; Schreckenbach, G.; Seldenthuis, J. S.; Seth, M.; Snijders, J. G.; Solà, M.; Stener, M.; Swart, M.; Swerhone, D.; Tognetti, V.; Velde, G. t.; Vernooijs, P.; Versluis, L.; Visscher, L.; Visser, O.; Wang, F.; Wesolowski, T. A.; Wezenbeek, E. M. v.; Wiesenekker, G.; Wolff, S. K.; Woo, T. K.; Yakovlev, A. L.: Amsterdam Density Functional. 2017 ed.; SCM, Theoretical Chemistry, Vrije Universiteit Amsterdam, The Netherlands, 2017. .

73. Lenthe, E. v.; Baerends, E. J.; Snijders, J. G., Relativistic regular two-component Hamiltonians. *J. Chem. Phys.* **1993**, *99*, 4597-4610.

74. Weigend, F.; Ahlrichs, R., Balanced basis sets of split valence, triple zeta valence and quadruple zeta valence quality for H to Rn: Design and assessment of accuracy. *Phys. Chem. Chem. Phys.* **2005**, *7*, 3297-3305.

75. Pye, C. C.; Ziegler, T., An implementation of the conductor-like screening model of solvation within the Amsterdam density functional package. *Theor. Chem. Acc.* **1999**, *101*, 396-408.

Chapter 5. Synthesis and Electronic Structure Analysis of the Actinide Allenylidenes, $[\{(NR_2)_3\}An(CCCPh_2)]^-$ (An = U, Th; R = $SiMe_3$)

Portions of this work were published in:

Greggory T. Kent, Xiaojuan Yu, Guang Wu, Jochen Autschbach, Trevor W. Hayton Synthesis and Electronic Structure Analysis of the Actinide Allenylidenes, $[\{(NR_2)_3\}An(CCCPh_2)]^-$ (An = U, Th; R = $SiMe_3$). *Chem. Sci.* **2021**, 12, 14383-14388.

5.1 Introduction

Despite the significant advancements made in actinide-carbene chemistry in the past decade,[1-6] every example reported thus far has relied on ancillary chelators or heteroatom-containing substituents to stabilize the An–C multiple bond.[7-10] For example, the groups of Ephritikhine and Zi employed a pincer-type ligand to form $[U\{C(PPh_2S)_2\}(BH_4)_2(THF)_2]$ and $[Th\{C(PPh_2S)_2\}_2(DME)$, respectively,[11] where two thiophosphinoyl pendant arms support the An-carbene interaction.[12] In addition, Liddle *et al.* isolated the silyl-phosphino-carbene $[Li(2.2.2\text{-cryptand})][U\{C(SiMe_3)(PPh_2)\}(BIPM^{TMS})(Cl)]$ ($BIPM^{TMS}$ = $C(PPh_2NSiMe_3)_2$), whose U=C bond is stabilized by a P(III) substituent.[13] Similarly, the uranium(IV) arsonium carbene complex $[U(Tren^{TIPS})(CHAsPh_3)]$ ($Tren^{TIPS}$ = $N(CH_2CH_2NSiPr^i_3)_3$) features stabilization by an As(V) substituent.[14] These heteroatom substituents help dissipate the negative charge at the carbene carbon caused by the weak An=C π-bond, which itself results from the energetic mismatch between actinide and carbon valence orbitals combined with the relatively small r_{max} of the 5f orbitals.[14] Without these substituents, the An=C bond would likely be too reactive to isolate.

Because of the requirement for heteroatom substituents, no isolable "Schrock-type" actinide alkylidenes, i.e., $An=CR_2$ (R = H, alkyl, aryl), are known,[7, 9, 15] although they have been observed in inert gas matrices.[16-22] Even vinylidene and allenylidene complexes, which should be less reactive than alkylidenes, are unknown, in part due to the lack of viable synthetic routes. Allenylidenes are especially informative in this regard, as they are typically made by H_2O elimination from a propargyl alcohol – a route that is problematic for actinide organometallics given their high sensitivity to water.[23, 24]

Herein, I report the synthesis of the actinide allenyl complexes [{$(NR_2)_3$}An(CH=C=CPh_2)] (An = U, **5.1**; Th, **5.2**), formed via salt metathesis with lithium-3,3-diphenylcyclopropene. Subsequent deprotonation of **5.1** and **5.2** results in the formation of the actinide allenylidene complexes, [Li(2.2.2-cryptand)][{$(NR_2)_3$}An($CCCPh_2$)] (An = U, **5.4**; Th, **5.5**). Significantly, **5.4** and **5.5** represent the first complexes with An–C multiple bonds that do not feature heteroatom stabilization.

5.2 Results and discussion

5.2.1 Synthesis and Characterization

Drawing inspiration from the groups of Hashmi and Binger,[25, 26] I sought to synthesize an An-cyclopropenyl complex, which I hypothesized could undergo thermal ring opening to form an An-allenyl complex. In fact, addition of *in situ* generated lithium-3,3-diphenylcyclopropene to an Et_2O solution of [UCl$(NR_2)_3$] (R = $SiMe_3$) does result in formation of the allenyl complex, **5.1**, which can be isolated as dark-brown blocks in 72% yield after work up (Scheme 5.1).[25] The thorium analogue **5.2** can be prepared in a similar fashion in 62% yield, via the reaction of [ThCl$(NR_2)_3$] with 1 equiv of lithium-3,3-diphenylcyclopropene in Et_2O. I hypothesize that the ring opening occurs after salt metathesis.

Scheme 5.1. Synthesis of complexes **5.1**, **5.2**, **5.4** and **5.5**.

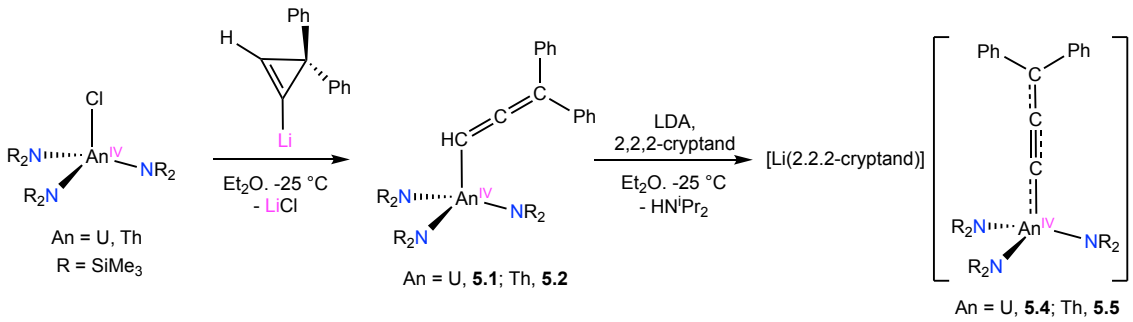

The ^{1}H NMR spectrum of complex **5.1** in C_6D_6/THF-d_8 features a resonance at –174.8 ppm assigned to the proton attached to the C_α carbon (Figure A5.1). The ^{1}H NMR spectrum of **5.2** in C_6D_6/THF-d_8 displays a resonance at 5.77 ppm assigned to same ligand environment (Figure A5.2). Additionally, the $^{13}C\{^{1}H\}$ NMR spectrum of **5.2** features resonances at 139.4, 204.7, and 96.7 ppm assigned to the C_α, C_β, and C_γ environments of the allenyl ligand, respectively (Figure A5.3). For comparison, the C_α and C_β NMR shifts of 1,1-diphenylallene are 78.2 and 210.0 ppm, respectively,[27] whereas the C_α, C_β, and C_γ shifts of $[OsCl_2(NO)(CH{=}C{=}CPh_2)(P^iPr_3)_2]$ are 79.1, 199.1, and 101.0 ppm, respectively.[28] I attribute the large C_α shift of **5.2** to spin-orbit coupling (SOC) effects (see below for more discussion).[4, 29-32 33] Finally, the IR spectra of **5.1** and **5.2** exhibit C_α–C_β and C_β–C_γ stretching modes at 1934/1871 and 1934/1869^{-1} cm^{-1}, respectively (Table 5.1). For comparison, $[OsCl_2(NO)(CH{=}C{=}CPh_2)(P^iPr_3)_2]$ exhibits a single C=C stretch at 1881 cm^{-1} in its IR spectrum.[28]

Table 5.1. Selected IR spectral data for complexes **5.1**, **5.2**, **5.4** and **5.5**.

Complex	$\nu(C_\alpha–C_\beta)$ (cm^{-1})	$\nu(C_\beta–C_\gamma)$ (cm^{-1})
5.1	1934	1871
5.2	1934	1869
5.4	2050	1911
5.5	2044	1921

Complexes **5.1** and **5.2** both crystallize in the triclinic space group P–1 with one and two independent molecules in their asymmetric unit cells, respectively (Figure 5.1). The An–C distances (**5.1**: 2.457(3); **5.2**: 2.529(5), 2.536(5) Å) are consistent with those previously reported for An(IV)–C single bonds.[34-37] Additionally, the longer distances observed for **5.2** reflect the increased ionic radius of Th(IV) vs. U(IV) (Table 5.2).[38] The $C_\alpha–C_\beta$ and $C_\beta–C_\gamma$ distances of the allenyl ligands, along with the $C_\alpha–C_\beta–C_\gamma$ angles, are consistent with those previously reported for transition metal allenyl complexes.[28, 39-42] Furthermore, the $An–C_\alpha–C_\beta$ angles (**5.1**: 133.2(2); **5.2**: 132.0(4), 128.6(4)°) confirm that C_α is sp^2 hybridized, consistent with my proposed formulation. Notably, **5.1** and **5.2** are the first reported f element allenyl complexes.

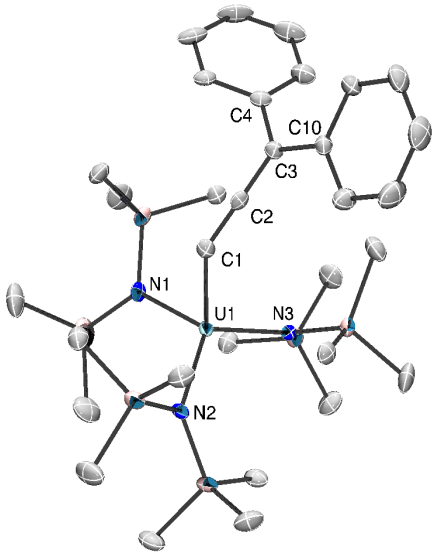

Figure 5.1. Solid-state structure of **5.1** shown with 50% probability ellipsoids. Hydrogen atoms omitted for clarity.

During an attempt to isolate **5.2**, a few crystals of the Th-allenylidene complex $[\{Li(DME)_2\}\{\{(NR_2)_3\}ThCl_2\}][\{Li(DME)\}\{\{(NR_2)_3\}Th(CCCPh_2)\}]_2$ were isolated (**5.3**, Figure 5.2). Complex **5.3** crystallizes in the P–1 space group with two molecules of $[\{Li(DME)\}\{\{(NR_2)_3\}Th(CCCPh_2)\}]$, one anion of $\{(NR_2)_3\}ThCl_2\}^-$, and a $\{Li(DME)_2\}^+$ counterion in its asymmetric unit. The allenylidene anion crystallizes as a contact ion pair with a $[Li(DME)]^+$ counterion, where the Li–C bond distances are shortest at the Li–C_β carbon interaction (2.02(2) and 2.109(17) Å, Table 5.2) and longest at the Li–C_γ interaction (2.40(2) and 2.539(18) Å). The C_α–C_β distances are 1.214(10) and 1.250(11) Å, and resemble the distances seen in a C≡C bond, while the C_β–C_γ distances are similar to a C=C bond (1.409(12) and 1.418(10) Å). Given the short Th–C bond distances in each $[\{Li(DME)\}\{\{(NR_2)_3\}Th(CCCPh_2)\}]$ fragment (2.397(8), 2.439(8) Å), I believed that

complete characterization of a separated ion pair An-allenylidene anion would provide the first example of an non-heteroatom stabilized An=C bond.

Table 5.2. Selected metrical parameters for Complexes **5.1**–**5.5**.

Bond (Å, °)	**5.1**	**5.2**	**5.3**	**5.4**·C_5H_{12}	**5.5**·C_5H_{12}
An–C_α	2.457(3)	2.529(5), 2.536(5)	2.439(8), 2.397(8)	2.305(8)	2.368(16)
C_α–C_β	1.299(4)	1.292(7), 1.288(7)	1.214(10), 1.250(11)	1.221(11)	1.23(2)
C_β–C_γ	1.329(4)	1.327(7), 1.319(7)	1.409(12), 1.418(10)	1.403(11)	1.40(2)
C_γ–C_{ipso}	1.490(4), 1.474(4)	1.492(7), 1.487(7), 1.497(7), 1.488(7)	1.460(13), 1.455(10), 1.484(11), 1.458(13)	1.443(12), 1.468(12)	1.47(2), 1.45(2)
Li–$C_{\alpha/\beta/\gamma}$	N/A	N/A	2.287(18), 2.02(2), 2.40(2)/ 2.265(17), 2.109(17), 2.539(18)	N/A	N/A
An–C_α–C_β	133.2(2)	132.0(4), 128.6(4)	160.0(7), 157.2(8)	173.3(8)	172.0(14)
C_α–C_β–C_γ	176.1(3)	175.5(6), 176.5(6)	171.0(9), 172.1(10)	176.7(9)	174.6(16)
$\Sigma(\angle C_{ipso/\beta}$–$C_\gamma$–$C_{ipso})$	359.0	360.0/359.9	359.8	359.9	359.9

Given the low proton affinity at C_α,[43] it is unsurprising that addition of base to **5.1** or **5.2** would yield an actinide–allenylidene. Thus, addition of 1 equiv of LDA and 2.2.2-cryptand to **5.1** in Et_2O results in the formation of **5.4**, which can be isolated as dark purple blocks in 54% yield after work-up (Scheme 5.1). The thorium analogue **5.5** can be prepared in a similar fashion, via the reaction of **5.2** with 1 equiv of LDA and 2.2.2-cryptand, in 46% yield as deep orange-red solid. Complexes **5.4** and **5.5** are the first reported f-element allenylidenes and are

the first An=C complexes that do not employ heteroatoms or ancillary chelators to stabilize the An=C interaction.

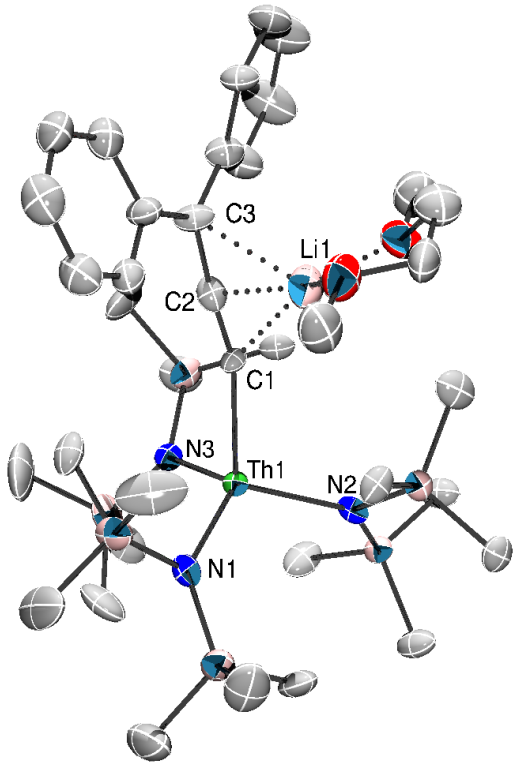

Figure 5.2. Solid-state structure of one molecule of [{Li(DME)}{{$(NR_2)_3$}Th($CCCPh_2$)}] in **5.3** shown with 50% probability ellipsoids. {$(NR_2)_3$}$ThCl_2$}$^-$, {$Li(DME)_2$}$^+$, Hydrogen atoms omitted for clarity.

The ^{1}H NMR spectrum of **5.4** in C_6D_6/THF-d_8 features a broad singlet at –1.60 ppm, assignable to the lone $SiMe_3$ environment (Figure A5.4). The ^{1}H NMR spectrum of **5.5** features a sharp singlet at 0.53 ppm, assignable to its $SiMe_3$ environment (Figure A5.6), whereas its ^{13}C{^{1}H} NMR spectrum exhibits resonances at 205.4, 128.5, and 70.6 ppm. These resonances are assigned to the C_α, C_β, and C_γ environments of the allenylidene ligand, respectively (Figure 5.3). Complexes **5.4** and **5.5** exhibit C_α–C_β and C_β–C_γ stretching modes at

2050/1911 and 2044/1921 cm^{-1}, respectively, in their IR spectra (Table 5.1). These values are blue-shifted from those observed for their respective precursors, suggesting an increase in both the C_α–C_β and C_β–C_γ bond orders upon deprotonation. For further comparison, the Os allenylidene complex, $[Os(CCCPh_2)(CH_3CN)_3(IPr)(P^iPr_3)][BF_4]_2$, features a single C=C band at 1929 cm^{-1} in its IR spectrum.[44] Finally, the UV-vis spectrum of **5.5** in C_6H_6 features intense absorptions at 403 nm ($\varepsilon = 8310\ L \cdot mol^{-1} \cdot cm^{-1}$) and 537 nm ($\varepsilon = 15{,}030\ L \cdot mol^{-1} \cdot cm^{-1}$) (Figure A5.8). The spectrum is qualitatively similar to that recorded for $[CPh_3]^-$,[45] suggesting a similar electronic environment for C_γ (see below for more discussion).

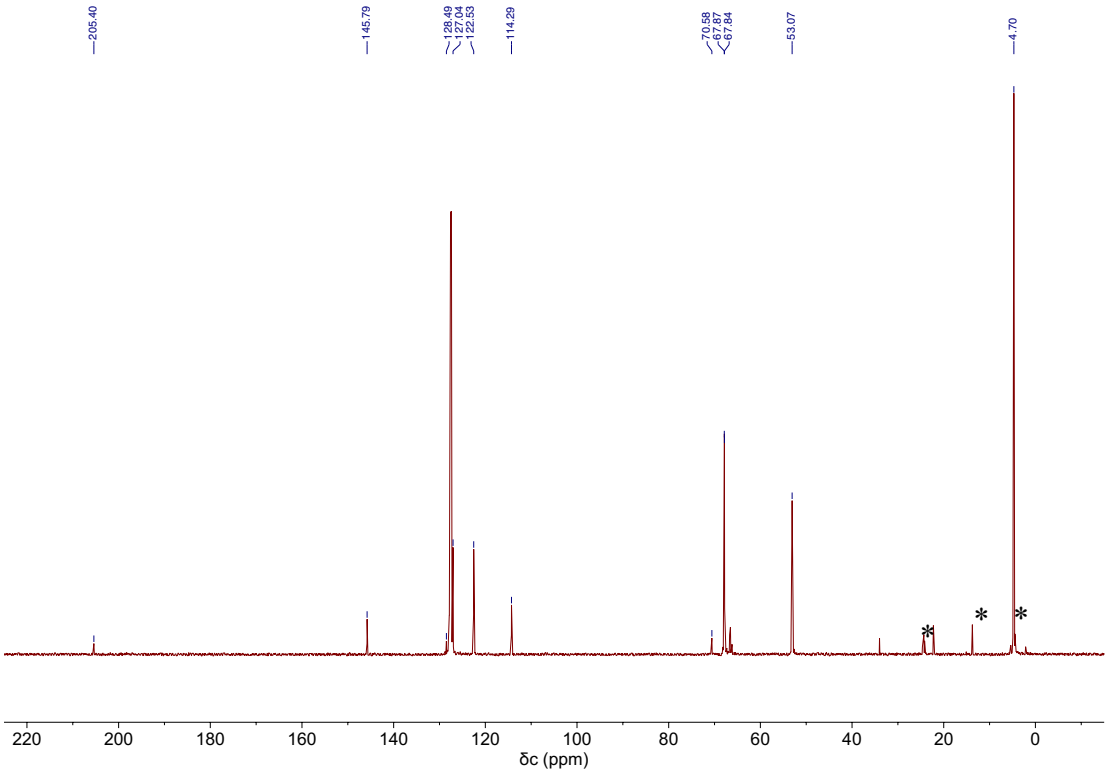

Figure 5.3. $^{13}C\{^1H\}$ NMR spectrum of $[Li(2.2.2\text{-Cryptand})][\{(NR_2)_3\}Th(CCCPh_2)]$ (**5.5**) in a 10:1 mixture of C_6D_6 and THF-d_8 at room temperature. (*) indicates pentane.

Complexes **5.4** and **5.5** crystallize in the monoclinic space group $P2_1$ as the pentane solvates, **5.4**·C_5H_{12} and **5.5**·C_5H_{12}, respectively. They are isomorphous and crystallize as discrete cation-anion pairs (Figure 5.4). The An–C_α distances in **5.4** and **5.5** are 2.305(8) and 2.368(16) Å, respectively (Table 5.2). These distances are among the shortest known An-C distances and suggest the presence of An-C_α multiple bond character. Additionally, these values are shortened by 0.15 Å from the An–C_α distances observed for their respective precursors. For comparison, the U–C_α distances in $Cp_3U{=}CHPMe_3$ and $[U\{C(SiMe_3)(PPh_2)\}(BIPM^{TMS})(DMAP)_2]$ are 2.274(8) and 2.296(5) Å,[46] [13] respectively, whereas the Th–C_α distances in $[(C_5Me_5)_2ThCl(CHPPh_3)]$ and $[Th(CHPPh_3)(NR_2)_3]$ are 2.3235(1) and 2.362(2) Å, respectively.[4, 5]

Scheme 5.2. Available resonance forms to allenylidene complexes.

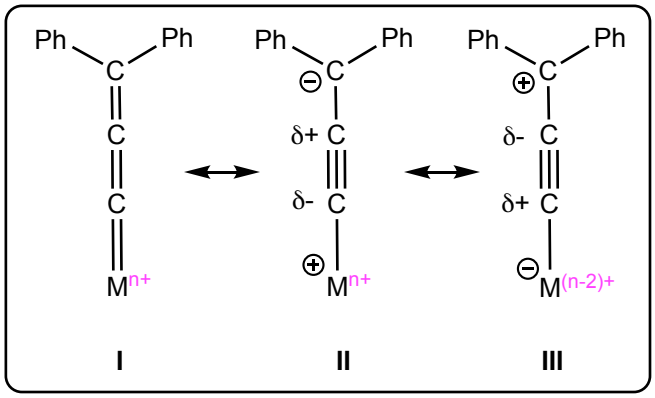

Compared to **5.1** and **5.2**, the C_α–C_β distances in **5.4** and **5.5** are slightly shortened, whereas the C_β–C_γ distances are slightly elongated. The C_α–C_β distances are similar to those observed for the An-acetylide complexes $[Th(C{\equiv}CH)(NR_2)_3]$ (1.173(12) Å) and $[(NN'_3)U(CCPh)]$ (1.212(5) Å, NN'_3 = $[N(CH_2CH_2NSi^tBuMe_2)_3]$). However, the An–C distances in these examples are much longer, at 2.481(8) and 2.480(4) Å, respectively, reflecting their single

bond character.[47, 48] The C_α–C_β–C_γ angles in **5.4** and **5.5** remain unchanged, whereas the An–C_α–C_β angles approach linear. In addition, the sum of angles around C_γ confirms that it is sp^2 hybridized (Table 5.2). These metrical parameters are typical of the allenylidene ligand and can be rationalized by the contribution of resonance forms **I** and **II** to its electronic structure (Scheme 5.2).[49] For comparison, $[Os(CCCPh_2)(CH_3CN)_3(IPr)(P^iPr_3)][BF_4]_2$ features C_α–C_β and C_β–C_γ distances of 1.246(8) and 1.362(9) Å, respectively.[44]

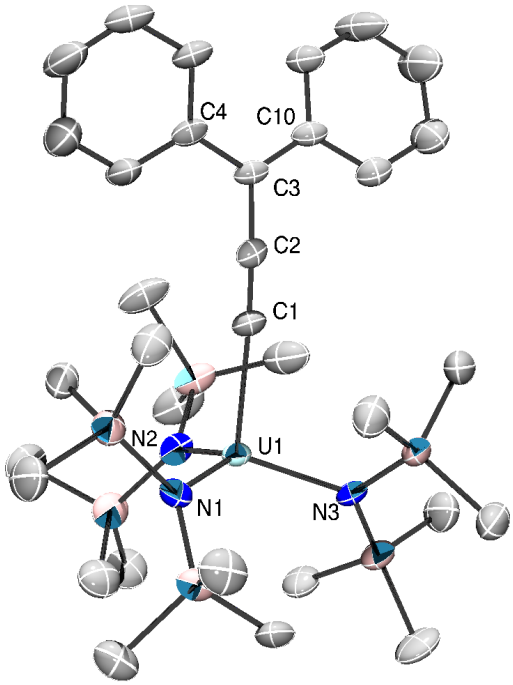

Figure 5.4. Solid-state structure of $[Li(2.2.2\text{-cryptand})][\{(NR_2)_3\}U(CCCPh_2)]$ (**5.4**) shown with 50% probability ellipsoids. Hydrogen atoms, [Li(2.2.2-cryptand)], and pentane solvate omitted for clarity.

5.2.2 Electronic Structure Analysis

The An-allenylidene interaction in complexes **5.4** and **5.5** was analyzed via relativistic density functional theory (DFT) by Dr. Xiaojuan Yu and Prof. Jochen Autschbach at the University of Buffalo.[50-53] Complete computational details and results are provided in the SI. Based on Natural Localized Molecular Orbital (NLMO) analyses, complexes **5.4** and **5.5** exhibit strong π-delocalization (Figure 5.3). Taking **5.5** as an example, the NLMO picture indicates triple bond character between C_α and C_β, corresponding to resonance structure (RS) **II** in Scheme 5.2. However, three-center character involving thorium, C_α, and C_β, denoted as π(Th–C) in Table 5.3 (in section 5.4.6), also reveals an important contribution from RS **I**. The calculated natural charges for Th, C_α, C_β, and C_γ are 1.52, –0.67, 0.05 and –0.22, respectively, whereas the averaged natural charge for three N atoms bound to Th is -1.65. The NLMO representing the lone pair (and negative charge) at C_γ is π-LP(C_γ), and is strongly delocalized over the phenyl groups, C_β, and even C_α and Th. This delocalization further confirms that RS **I** contributes to the overall electronic structure. In addition, for complex **5.4**, the Mulliken spin population of U is 2.3 (excess alpha over beta spin), beyond the two unpaired spins expected for the f^2 configuration, indicating preferential alpha spin electron donation from ligand to metal. The spin populations for C_α, C_β, and C_γ are -0.08, 0.02, -0.10, respectively; the remaining spin density in the ligand is further delocalized.

Table 5.3. % compositions of the An-C (An = Th, U) bonding NLMOs in **5.1-5.5**.

Complex	Orbital	Total C_α	2s	2p	Total C_β	2s	2p	Total An	7s	7p	6d	5f
5.1	σ(U-C)	75	31	69	4	0	100	16	12	1	69	18
	π(U-C)	50	0	100	44	0	100	4	0	0	53	47
5.2	σ(Th-C)	77	30	70	5	0	100	14	13	1	73	13
	π(Th-C)	50	0	100	44	0	100	4	0	0	53	47
5.4	σ(U-C)	78	47	53	0	0	0	20	16	1	67	16
	π(U-C)	47	0	100	47	0	100	5	0	0	55	45
	π(U-C)	31	0	100	28	0	100	11	0	0	32	68
5.5	σ(Th-C)	80	47	53	0	0	0	18	16	1	71	12
	π(Th-C)	48	0	100	45	0	100	5	0	0	60	40
	π(Th-C)	53	0	100	37	0	100	7	0	0	62	38

An NLMO representing the π-component of a An=C double bond is clearly seen for both **5.4** and **5.5** (Figure 5.3). This NLMO features multi-center character (**5.4**: 31% C_α, 28% C_β, and 11% U; **5.5**: 53% C_α, 37% C_β, and 7% Th), and indicates that RS **I** is an important contributor to the overall electronic structure of both complexes, more so for **5.4** than for **5.5**; although the metal weight in **5.5** is still significant. The other π–bonding NLMO in either complex has only 5% metal weight. Finally, the σ(An−C) bonds of **5.4** and **5.5** are represented by two-center two electron NLMOs with 20% and 18% total An weight for **5.4** and for **5.5**, respectively (Figure 5.3). These results are similar to the weights found in the uranium methanediide complex, $[\{C(PPh_2S)_2\}U(BH_4)_2(THF)_2]$.[12]

As seen in Table 5.4, the Wiberg Bond Order (WBO) analyses are consistent with the conclusions drawn from the NLMO picture. For example, the An–C_α, C_α–C_β, and C_β–C_γ WBOs are 0.91, 2.36, and 1.31, respectively, for **5.5**, and 0.98, 2.40, and 1.28, respectively, for **5.4**, further suggesting RS **I** is more important for **5.4** than for **5.5**. Interestingly, the An–

C_α WBOs in **5.4** and **5.5** are notably larger than those of **5.1** (0.60) and **5.2** (0.57). The An–C_α WBOs in **5.4** and **5.5** are also larger than those of the An(IV) parent acetylides, [An(C≡CH)$(NR_2)_3$] (An = Th, WBO = 0.67; U, WBO = 0.71).[48] Thus, the larger An-C_α WBOs evident in **5.4** and **5.5** vs. [{$(NR_2)_3$}An(CH=C=CPh_2)] vs. [An(C≡CH)$(NR_2)_3$] also supports the importance of resonance form **I** for these species, and confirms that they can be properly described as actinide carbenes.

Table 5.4. The Wiberg Bond Orders for the selected bonds in **5.1-5.5** and [An(C≡CH)$(NR_2)_3$] (An = U or Th) complexes.

Complexes	An-C_α	C_α-C_β	C_β-Cγ
5.1	0.597	2.005	1.638
5.2	0.565	2.003	1.634
5.4	0.983	2.401	1.281
5.5	0.912	2.355	1.305
[U(C≡CH)$(NR_2)_3$][48]	0.709		
[Th(C≡CH)$(NR_2)_3$][48]	0.674		

An alternative way to examine the bonding in complexes **5.4** and **5.5** is offered by the quantum theory of atoms in molecules (QTAIM). This theory utilizes a variety of descriptors based on the topology of the electron density at a bond critical point (BCP).[54] QTAIM data (Table 5.6) suggest that the An-C bonds in **5.4** and **5.5** are polarised toward the ligand but possess covalent character, and, for **5.4**, the results are nearly identical to the data reported for [U(BIPM^{Mes})$Cl_2(THF)_2$] (BIPM^{Mes}={C(PPh_2NMes)$_2$}).[3] Furthermore, the QTAIM data suggest that Th-C bond in **5.5** is somewhat less covalent than the U-C bond in **5.4**, consistent with the NLMO analysis.

5.2.3 ^{13}C Chemical Shift Analysis

An NLMO analysis of the ^{13}C NMR shielding for complexes **5.2** and **5.5** was also performed by Dr. Xiaojuan Yu and Prof. Jochen Autschbach at the University of Buffalo using the computational methods reported in References [50-52, 55-57]. Data reported here are from the SR-PBE and SO-PBE levels of theory. Additional data provided show that the calculated shifts do not vary strongly with the functional used in the calculations (Table 5.5). A shielding analysis of allene ($H_2C=C=CH_2$) was also performed,[58] for comparison with complex **5.2**. For all compounds, the diamagnetic and paramagnetic contributions to the shieldings were combined. Dr. Xiaojuan Yu and Prof. Jochen Autschbach confirmed that the observed variations in the carbon shielding and chemical shift come from the (usually negative) paramagnetic shielding mechanism, involving magnetic coupling between occupied and unoccupied orbitals,[59] along with SO effects. The diamagnetic shielding per carbon is essentially constant, as usual.

Table 5.5. Calculated carbon shielding (σ) and chemical shift (δ) for TMS, Allene, Acetylene, and the C_α, C_β, and C_γ nuclei of **5.2** and **5.5** using various functionals.

Complex	Method	σ_{calc}(ppm)	δ_{calc}(ppm)	Δ_{SO}(ppm)	δ_{expt}(ppm)
TMS	PB86/SO-BP86	186.9 / 187.8			
	PBE/SO-PBE	187.5 / 188.4			
	PBE0/SO-PBE0 (25%)[a]	192.2 / 193.0			
	PBE0/SO-PBE0 (40%)	194.7 / 195.5			
Allene	PBE/SO-PBE	107.9, -41.1, 107.9 / 108.5, -40.4, 108.5	79.6, 228.6, 79.6 / 79.9, 228.8, 79.9	0.3, 0.2, 0.3	
	MPW1PW91	109, -41, 109[b]			73.9, 208.5, 73.9[c]
Acetylene	PBE/SO-PBE	108.3 / 108.9	79.2 / 79.5	0.3	
5.2[d]	PB86/SO-BP86	69.9, -23.4, 82.2 / 43.7, -26.2, 82.8	117.0, 210.3, 104.7 / 144.1, 214.0, 105.0	27.1, 3.7, 0.3	139.4, 204.7, 96.7
	PBE/SO-PBE	70.4, -22.9, 82.8 / 44.5, -25.7, 83.4	117.1, 210.4, 104.7 / 143.9, 214.1, 105.0	26.8, 3.7, 0.3	
	PBE0/SO-PBE0 (25%)	75.3, -26.5, 88.7 / 46.2, -28.8, 89.1	116.9, 218.7, 103.6 / 146.8, 221.8, 103.9	29.9, 3.1, 0.3	
	PBE0/SO-PBE0 (40%)	78.5, -27.5, 91.8 / 47.2, -29.4, 92.0	116.2, 222.2, 102.9 148.3, 224.9, 103.5	32.1, 2.7, 0.6	
5.5	PB86/SO-BP86	12.3, 59.3, 104.3 / -23.2, 51.2, 105.2	174.6, 127.6, 82.6 / 211.0, 136.6, 82.0	36.4, 9.0, 0.0	205.4, 128.5, 70.6
	PBE/SO-PBE	12.6, 59.6, 104.8 / -22.7, 51.4, 105.8	174.9, 127.9, 82.7 / 211.1, 137.0, 82.6	36.2, 9.1, -0.1	
	PBE0/SO-PBE0 (25%)	19.4, 62.8, 115.1 / -19.3, 55.1, 115.5	172.8, 129.4, 77.1/ 212.3, 137.9, 77.5	39.5, 8.5, 0.4	
	PBE0/SO-PBE0 (40%)	23.7, 65.0, 120.4/ -16.8, 57.4, 120.6	171.0, 129.7, 74.3/ 212.3, 138.1, 74.9	41.3, 8.4, 0.6	

[a] Fraction of exact exchange in the functional in parentheses.

[b] Values taken from Ref [58].

[c] Values taken from Ref [81].

[d] The shielding and chemical shifts are averaged from two experimental geometries.

The calculated shielding constants for allene agree well with those reported by Wiberg *at al.* who analyzed the system in great detail (Table 5.7 in section 5.4.6).[58] Effects from spin-orbit coupling (SOC) are very minor, as expected for an organic molecule without a heavy element. C_β is strongly deshielded, by almost 150 ppm, relative to the methylene carbons. The primary reason for this difference is a strong paramagnetic deshielding from both π(C–C) NLMOs for C_β (Table 5.7 in section 5.4.6). Although, the σ-bond NLMOs also contribute somewhat to the large shielding difference between the central and terminal carbons.

The calculated chemical shifts for complex **5.2** agree reasonably well with the experimental data (Tables 5.5 and table 5.8 in section 5.4.6). For example, the calculated C_α shift for **5.2** is 144 ppm (expt. = 139.4 ppm). The replacement of $C_\gamma H_2$ in allene by $C_\gamma Ph_2$ in **5.2** and the bonding of C_α to Th has a noticeable effect on most of the NLMO shielding contributions, leading to an overall decrease of the C_α and C_γ shielding, relative to allene, and a modest increase (13–17 ppm) of the C_β shielding. The shielding patterns and contributions remain allene-like, however. This conclusion is further buttressed by the WBOs for C_α–C_β (2.0) for C_β–C_γ (1.6). The former value corresponds exactly to the expected bond order, whereas the latter reflects the aforementioned delocalization of π(C_β–C_γ) onto C_{ipso}. The main difference to allene is the inequivalency of C_α and C_γ. The shielding difference is –13 ppm in the calculations without SOC, and is primarily caused by more negative contributions from σ(C_α–Th) and σ(C_α–H) to the C_α shielding versus the σ(C_γ–C_{ipso}) contributions to the C_γ shielding, and a more negative contribution of σ(C_α–C_β) to the C_α shielding vs. σ(C_β–C_γ) contributing to the C_γ shielding. These differences are partially counteracted by a more positive allene-like C_α shielding from π(C_α–C_β) compared to the C_γ shielding from π(C_β–C_γ) (Table 5.8 in section 5.4.6). The delocalization onto C_{ipso} evidently enhances the C_γ paramagnetic deshielding

relative to allene. With SOC effects included, the difference between the C_α and C_γ shielding becomes –39 ppm, as a result of the Th 5f (and 6d) AO contributions in $\sigma(C_\alpha–Th)$ and an associated SOC deshielding in the C_α core. The situation is reminiscent of the SOC effects on the shielding of nitrogen atoms bound to Th that was identified recently.[60, 61]

The calculated ^{13}C chemical shifts for complex **5.5** (Table 5.5 and table 5.9 in section 5.4.6) also agree reasonably well with the experimental data. For example, the calculated C_α shift for complex **5.5** is 211 ppm (expt. = 205.4 ppm). This value includes a 36 ppm deshielding contribution due to SOC, which is about 10 ppm larger in magnitude than that calculated for C_α in complex **5.2** as a result of the stronger $\sigma(An–C)$ covalency in **5.5**. The calculations also reproduce the experimentally assigned chemical shift ordering $C_\alpha > C_\beta > C_\gamma$, in **5.5**, which is different from complex **5.2**, for which the shifts are $C_\beta > C_\gamma > C_\alpha$. The increased C_β shielding (smaller chemical shift) in **5.5** compared to **5.2** partially reflects the formal $C_\alpha–C_\beta$ triple bond, according to RS **II**. However, C_β in **5.5** is still substantially deshielded relative to C_β in an authentic alkyne, such as PhCCH (77.2 ppm chemical shift),[62] consistent with delocalization according to RS **I**. The different ordering is the result of two effects: (1) C_β in **5.5** has triple bond character with a concomitant increase in magnetic shielding; and (2) The stronger $C_\alpha–Th$ covalency lowers the shielding of C_α in **5.5**, compared to **5.2**, via the combined effects of greater paramagnetic deshielding due to stronger Th–C bonding, and a stronger SOC deshielding (Tables 5.8 and 5.9 in section 5.4.6). Finally, the SOC induced deshielding for C_β in **5.5** (–9 ppm) is much larger than that calculated for complex **5.2** (–4 ppm), which shows independently from the NLMO analysis that the delocalization involves Th, where most of the SOC originates.

5.3 Summary

In summary, reaction of [AnCl$(NR_2)_3$] with *in situ* generated lithium-3,3-diphenylcyclopropene affords the first actinide-allenyl complexes, [{$(NR_2)_3$}An(CH=C=CPh_2)] (An = U, Th). Subsequent treatment with LDA and 2.2.2-cryptand results in the formation of the actinide-allenylidene complexes, [Li(2.2.2-cryptand)][{$(NR_2)_3$}An(CCCPh_2)] (An = U, Th), which represent the first non-heteroatom supported carbene complexes of the actinides. Importantly, their isolation suggests that other actinide cumulenylidene complexes could be isolable, provided a viable synthetic route is available. Quantum chemical calculations give a detailed picture of the actinide-allenylidene interaction, which features partial An=C double bond character. Additionally, the C_α chemical shift in the two Th complexes exhibit SOC-induced deshielding due to 5f orbital participation in the Th–C bonds. The larger deshielding in the allenylidene complex vs. the allenyl is consistent with its greater σ(Th−C) covalency.

Going forward, I plan to explore the reactivity of my actinide allenylidene for comparison with the late transition metal allenylidenes, which will provide further insight into their electronic structure and potentially uncover new modes of allenylidene reactivity. The latter point is significant because the polarity of the carbon atoms within the actinide allenylidene unit is reversed relative to that observed in the late transition metals (e.g., resonance form **III**, Scheme 5.2).[23, 24, 63]

5.4 Experimental

5.4.1 General. All reactions and subsequent manipulations were performed under anaerobic and anhydrous conditions under an atmosphere of dinitrogen. Diethyl ether (Et_2O), pentane and hexanes were dried using a Vacuum Atmospheres DRI-SOLV Solvent Purification system and stored over 3Å sieves for 24 h prior to use. Tetrahydrofuran (THF) was distilled over calcium hydride then distilled over sodium benzophenone, collected, and stored over 3Å sieves for 24 h prior to use. Isooctane was distilled over sodium benzophenone, collected, and stored over 3Å sieves for 24 h prior to use. THF-d_8 and C_6D_6 were stored over 3Å sieves for 24 h prior to use. $[UCl(NR_2)_3]$ (R = $SiMe_3$), $[ThCl(NR_2)_3]$, LDA, and 3,3-diphenylcyclopropene were synthesized according to previously reported literature procedures.[64-67] All other reagents were purchased from commercial vendors and used as received.

^1H, $^{13}C\{^1H\}$, and $^7Li\{^1H\}$ NMR spectra were recorded on a Varian UNITY INOVA 400 MHz or a Varian UNITY INOVA 500 MHz spectrometer. ^1H and $^{13}C\{^1H\}$ NMR spectra were referenced to external $SiMe_4$ using the residual protio solvent peaks as internal standards.[68, 69] $^7Li\{^1H\}$ spectra were referenced to a saturated LiCl solution in D_2O. IR spectra were recorded on a Nicolet 6700 FT-IR spectrometer with a NXR FT Raman Module. Electronic absorption spectra were recorded on a Shimadzu UV3600 UV-NIR Spectrometer. Elemental analyses were performed by the Microanalytical Laboratory at University of California (Berkeley, CA).

5.4.2 Synthesis of $[\{(NR_2)_3\}U(CH{=}C{=}CPh_2)]$ (5.1). To a cold (-25 °C), colorless Et_2O solution (0.5 mL) of 3,3-diphenylcyclopropene (42.1 mg, 0.0.219 mmol) was added quickly a cold (-25 °C), colorless Et_2O solution (0.5 mL) of LDA (22.3 mg, 0.208 mmol). Immediately,

the solution turned light yellow. This solution was then added drop wise to a cold (-25 °C) stirring pink slurry of [$UCl(NR_2)_3$] (157.2 mg, 0.208 mmol) in Et_2O (3 mL). The stirring solution immediately turned red-brown concomitant with the deposition of a light tan precipitate. After stirring for 45 min the resulting brown solution was filtered through a Celite column supported on glass wool (0.5 cm × 2 cm) and the volatiles were removed from the filtrate *in vacuo*. The resulting brown oil was extracted into pentane (4 mL), filtered through a Celite column supported on glass wool (0.5 cm × 2 cm) and the volatiles were removed from the filtrate *in vacuo*, yielding a brown solid. The resulting brown powder was extracted again into pentane (2 mL), filtered through a Celite column supported on glass wool (0.5 cm × 2 cm) and transferred to a 4 mL scintillation vial. This vial was placed into a 20 mL scintillation vial and the solution was concentrated to 0.5 mL. Isooctane (2 mL) was added to the outer vial and storage of this two-vial system at -25 ºC for 24 h resulted in the deposition of brown blocks. Decanting the supernatant, rinsing the crystals with cold (-25 °C) pentane (2 mL), and drying *in vacuo* afforded **5.1** (137.3 mg, 72.4 % yield) Anal. Calcd for $UN_3Si_6C_{33}H_{65}$: C, 43.53; H, 7.20; N, 4.62. Found: C, 43.34; H, 7.03; N, 4.68. ^{1}H NMR (C_6D_6/THF-d_8, 298 K, 500 MHz): δ 3.34 (t, J = 7.1 Hz, 4H, *m*-CH), 3.03 (t, J = 7.2 Hz, 2H, *p*-CH), -1.84 (br. s, 54H, C*H*3), -9.13 (d, J = 7.1 Hz, 4H, *o*-CH), -174.80 (s, 1H, α-C*H*). IR (KBr pellet, cm^{-1}): 2954 (m), 2897 (w), 1936 (w, C_α–C_β stretch), 1871 (w, C_β–C_γ stretch), 1400 (w), 1250 (s), 1182 (w), 904 (s), 847 (s), 769 (m), 681 (w), 656 (w), 611 (m).

5.4.3 Synthesis of [{$(NR_2)_3$}Th(CH=C=CPh_2)] (5.2). To a cold (-25 °C), colorless Et_2O solution (0.5 mL) of 3,3-diphenylcyclopropene (40.5 mg, 0.211 mmol) was added quickly a cold (-25 °C), colorless Et_2O solution (0.5 mL) of LDA (21.4 mg, 0.200 mmol). Immediately, the solution turned light yellow. This solution was then added drop wise to a cold (-25 °C)

stirring colorless slurry of [Th(Cl)(NR_2)$_3$] (150.2 mg, 0.200 mmol) in Et_2O (3 mL). The stirring solution immediately turned yellow-orange concomitant with the deposition of a light tan precipitate. After stirring for 45 min the resulting orange suspension was filtered through a Celite column supported on glass wool (0.5 cm × 2 cm) and the volatiles were removed from the filtrate *in vacuo*. The resulting orange oil was extracted into pentane (4 mL), filtered through a Celite column supported on glass wool (0.5 cm × 2 cm) and the volatiles were removed from the filtrate *in vacuo*, yielding a brown solid. The resulting orange oil was extracted again into pentane (2 mL), filtered through a Celite column supported on glass wool (0.5 cm × 2 cm) and transferred to a 4 mL scintillation vial. This vial was placed into a 20 mL scintillation vial and the solution was concentrated to 0.5 mL. Isooctane (2 mL) was added to the outer vial and storage of this two-vial system at -25 ºC for 24 h resulted in the deposition of off-white blocks. Decanting the supernatant, rinsing the crystals with cold (-25 °C) pentane (2 mL), and drying *in vacuo* afforded **5.2** (112.0 mg, 61.7 % yield) Anal. Calcd for $ThN_3Si_6C_{33}H_{65}$: C, 43.82; H, 7.24; N, 4.65. Found: C, 43.71; H, 7.03; N, 4.57. ^{1}H NMR (C_6D_6/THF-d_8, 298 K, 500 MHz): δ = 7.42 (d, *J* = 7.3 Hz, 4H, *o*-CH), 7.17 (t, *J* = 7.7 Hz, 4H, *m*-CH), 6.96 (d, *J* = 7.4 Hz, 2H, *p*-CH), 5.77 (s, 1H, α-C*H*), 0.27 (s, 54H, C*H*3). ^{13}C{^{1}H} NMR (C_6D_6/THF-d_8, 298 K, 126 MHz) δ 204.67 (C_β), 150.63 (C_{ipso}), 139.38 (C_α), 128.89 (C_{ortho}), 128.39 (C_{meta}), 125.63 (C_{para}), 96.72 (C_γ), 4.57. IR (KBr pellet, cm^{-1}): 2953 (m), 2895 (w), 1934 (w, C_α–C_β stretch), 1869 (m, C_β–C_γ stretch), 1597 (m), 1491 (m), 1450 (m), 1252 (s), 1182 (m), 1113 (w), 1072 (w), 1030 (w), 931 (s), 847 (s), 768 (s), 696 (s), 658 (w), 640 (w), 609 (m).

5.4.4 Synthesis of [Li(2.2.2-Cryptand)][{(NR_2)$_3$}U(CCCPh_2)] (5.4). To a cold (-25 °C), dark brown Et_2O solution (3 mL) of **5.1** (65.8 mg, 0.072 mmol) and 2.2.2-cryptand (27.2 mg,

0.072 mmol) was added dropwise a cold (-25 °C), colorless Et_2O solution (0.5 mL) of LDA (7.74 mg, 0.072 mmol). Upon addition, the solution turned dark purple-red. After 2 min, the solution was concentrated *in vacuo* to 0.5 mL and filtered through a Celite column supported on glass wool (0.5 cm × 2 cm) into a 4 mL scintillation vial. This vial was placed into a 20 mL scintillation vial and isooctane (2 mL) was added to the outer vial. Storage of this two-vial system at -25 ºC for 48 h resulted in the deposition of dark purple solid. Decanting off the supernatant, rinsing with pentane (2 mL), and drying *in vacuo* afforded **5.4** as an analytically pure dark purple solid (50.0 mg, 53.5 % yield). X-ray quality crystals of **5.4** were grown by dissolving 40 mg of this material in THF:pentane (0.25:2.5 mL). Storage of this solution at -25 ºC for 24 h resulted in the deposition of dark purple needles. Anal. Calcd for $C_{51}H_{100}LiN_5O_6Si_6U$: C, 47.38; H, 7.80; N, 5.42. Found: C, 47.33; H, 7.59; N, 5.04. ^{1}H NMR (C_6D_6/THF-d_8, 298 K, 500 MHz,) δ 2.78 (br s, 12H, CH_2), 2.59 (br s, 12H, CH_2), 2.07 (t, J = 8.3 Hz, 4H, *m*-CH), 1.86 (br s, 12H, CH_2), -1.60 (br s, 54H, CH_3), -1.74 (t, J = 8.3 Hz, 2H, *p*-CH), -12.89 (d, J = 8.8 Hz, 4H, *o*-CH). ^{7}Li{^{1}H} NMR (C_6D_6/THF-d_8, 25 °C, 155 MHz): δ –1.59. IR (KBr pellet, cm^{-1}): 2954 (m), 2887 (m), 2862 (w), 2050 (w, C_α–C_β stretch), 1911 (w, C_β–C_γ stretch), 1514 (w), 1477 (m), 1385 (m), 1356 (s), 1263 (m), 1255 (s), 1136 (m), 1101 (s), 1088 (w), 933 (s), 862 (w), 841 (s), 894 (w), 694 (w).

5.4.5 Synthesis of [Li(2.2.2-cryptand)][{(NR$_2$)$_3$}Th(CCCPh$_2$)] (5.5). To a cold (-25 °C), dark brown Et_2O solution (3 mL) of **5.2** (82.1 mg, 0.091 mmol) and 2.2.2-cryptand (29.0 mg, 0.091 mmol) was added dropwise a cold (-25 °C), colorless Et_2O solution (0.5 mL) of LDA (9.7 mg, 0.091 mmol). Upon addition, the solution turned dark red-orange. After 2 min, the solution was concentrated *in vacuo* to 0.5 mL and filtered through a Celite column supported on glass wool (0.5 cm × 2 cm) into a 4 mL scintillation vial. This vial was placed into a 20 mL

scintillation vial and isooctane (2 mL) was added to the outer vial. Storage of this two-vial system at -25 ºC for 48 h resulted in the deposition of dark orange blocks. Decanting off the supernatant, rinsing with pentane (2 mL), and drying *in vacuo* afforded **5.5** as an analytically pure dark orange solid (53.4 mg, 45.7 % yield). X-ray quality crystals of **5.5** were grown by dissolving 36 mg of this material into THF:pentane (0.25:2.5 mL). Storage of this vial at -25 ºC for 24 h resulted in the deposition of orange needles. Anal. Calcd for $C_{51}H_{100}LiN_5O_6Si_6Th$: C, 47.60; H, 7.83; N, 5.44. Found: C, 47.30; H, 7.46; N, 5.14. ^{1}H NMR (C_6D_6/THF-d_8, 298 K, 500 MHz): δ 7.85 (d, J = 8.3 Hz, 4H, *o*-CH), 7.09 (t, J = 7.7 Hz, 4H, *m*-CH), 6.45 (t, J = 7.0 Hz, 2H, *p*-CH), 3.08 (m, 12H, CH_2), 3.03 (t, J = 5.0 Hz, 12H, CH_2), 2.08 (t, J = 5.0 Hz, 12H, CH_2), 0.53 (s, 54H, CH_3). ^{7}Li{^{1}H} NMR (C_6D_6/THF-d_8, 25 °C, 155 MHz): δ –1.81. ^{13}C{^{1}H} NMR (C_6D_6/THF-d_8, 298 K, 126 MHz) δ: 205.40 (C_α), 145.79 (C_{ipso}), 128.49 (C_β), 127.04 (C_{ortho}), 122.53 (C_{meta}), 114.29 (C_{para}), 70.58 (C_γ), 67.87 ($C_{cryptand}$), 67.84 ($C_{cryptand}$), 53.07 ($C_{cryptand}$), 4.70 (CH_3). UV-Vis/NIR (C_6H_6, 0.263 mM, 25 °C, L·mol^{-1}·cm^{-1}): 403 nm (ε = 8310) 537 nm (ε = 15,030). IR (KBr pellet, cm^{-1}): 2954 (m), 2883 (m), 2816 (w), 2044 (m, C_α–C_β stretch), 1921 (s, C_β–C_γ stretch), 1585(w), 1479 (m), 1444 (w), 1356 (m), 1296 (w), 1250 (s), 1144 (w), 1115 (m), 1101 (s), 933 (s), 837 (s), 771 (m), 696 (w), 663 (w), 607 (w).

5.4.6 Computational Details. Kohn-Sham density functional calculations were employed for **5.1**-**5.5** with the Gaussian 16 package.[70] The crystal structure coordinates were optimized for hydrogen positions using the Perdew-Burke-Ernzerhof (PBE) exchange-correlation functional.[71] Small-core Stuttgart energy-consistent relativistic pseudopotentials, ECP60MWB for Th and U, were utilized with matching valence basis sets.[72] The 6-31G(d) basis set was used for the Si, C, N, and H atoms.[73] Atom-pairwise corrections for dispersion forces were considered via Grimme's D3 model augmented with the Becke-Johnson (BJ) damping.[74] To quantify the compositions of the chemical bonds of interest, natural localized molecular orbital (NLMO) analyses were carried out with the NBO program, version 6.0.[75] The quantum theory of atoms in molecules (QTAIM) analysis was performed with Multiwfn 3.6.[76]

NMR shielding constants (σ, ppm) for **5.2** and **5.5** were calculated with the NMR module of the ADF package (version 2017),[77] using the scalar relativistic and spin-orbit all electron Zeroth-Order Regular Approximation (ZORA) Hamiltonian,[78] in conjunction with all-electron doubly polarized triple-ξ (TZ2P)[79] Slater-type basis set. The conductor-like screening model (COSMO) was used to describe solvent effect (tetrahydrofuran).[80] Functionals used for the NMR calculations were BP86, PBE, PBE0 (25% exact exchange), and PBE0 (40% exact exchange) The ^{13}C chemical shifts (δ, ppm) were obtained by subtracting the C_α, C_β, C_γ nuclear magnetic shielding of interest from the reference compound (Tetramethylsilane, TMS), with the latter calculated at the same level of theory. The localized molecular orbital (LMO) analysis of the NMR shielding and the character of specific chemical bonds quantified on the basis of orbital localizations were described elsewhere.[55, 56] It helps to provide useful information on how spin-orbit coupling affects the chemical shifts. Note that the NLMOs produced from

ECP60MWB valence basis set and Slater-type basis set (TZ2P) are qualitatively comparable to each other.

Table 5.6. QTAIM analysis of the complexes **5.4** and **5.5**.

Complex	BCP[a]	$\rho(r)$[b]	$\nabla^2\rho(r)$[c]	$H(r)$[d]	$\varepsilon(r)$[e]
5.4	U-C_α	0.102	0.147	-0.038	0.300
	C_α-C_β	0.399	0.939	-0.693	0.026
	C_β-C_γ	0.295	0.751	-0.293	0.201
5.5	Th-C_α	0.093	0.116	-0.033	0.193
	C_α-C_β	0.388	0.958	-0.662	0.012
	C_β-C_γ	0.292	0.739	-0.293	0.229

[a] The bond critical points.

[b] The electron density ($\rho(\boldsymbol{r})$, au).

[c] Laplacian of electron density ($\nabla^2\rho(\boldsymbol{r})$, au).

[d] Total electronic energy density ($H(\boldsymbol{r})$, au).

[e] Ellipticity of electron density ($\varepsilon(\boldsymbol{r})$, au).

Table 5.7 Localized Molecular Orbital(LMO) Analysis of NMR Shielding for allene.

LMO type	**SR/ C_α(L+NL)**	**SOC/ C_α(L+NL)**	**SR/ C_β(L+NL)**	**SOC/ C_β(L+NL)**	**SR/ C_γ(L+NL)**	**SOC/ C_γ(L+NL)**
$\sigma(C_\alpha\text{-}C_\beta)$	-57.9	-57.9	-77.1	-77.1	-6.3	-6.3
$\pi(C_\alpha\text{-}C_\beta)$	32.2	32.2	-40.7	-40.8	2.0	2.0
$\sigma(C_\alpha\text{-}H_1)$	-32.1	-32.1	-2.0	-2.0	-0.6	-0.5
$\sigma(C_\alpha\text{-}H_2)$	-32.1	-32.1	-2.0	-2.0	-0.6	-0.5
$\sigma(C_\beta\text{-}C_\gamma)$	-6.3	-6.3	-77.1	-77.1	-57.9	-57.9
$\pi(C_\beta\text{-}C_\gamma)$	2.0	2.0	-40.7	-40.7	32.2	32.2
C_α(core)	203.4	204.1	-0.6	-0.6	-0.1	-0.1
C_β(core)	-0.1	-0.1	203.6	204.4	-0.1	-0.1
C_γ(core)	-0.1	-0.1	-0.6	-0.6	203.4	204.1
$\sigma(C_\alpha\text{-}H_3)$	-0.6	-0.5	-2.0	-2.0	-32.1	-32.1
$\sigma(C_\alpha\text{-}H_4)$	-0.6	-0.5	-2.0	-2.0	-32.1	-32.1
$\sum$other	0.0	-0.2	0.0	0.1	0.0	-0.2
Total calc.	**107.9**	**108.5**	**-41.1**	**-40.4**	**107.9**	**108.5**

Table 5.8. Localized Molecular Orbital(LMO) Analysis of NMR Shielding for complex **5.2**.

LMO type	**SR/ C_α(L+NL)**	**SOC/ C_α(L+NL)**	**Δ^{SO}/ C_α**	**SR/ C_β(L+NL)**	**SOC/ C_β(L+NL)**	**Δ^{SO}/ C_β**	**SR/ C_γ(L+NL)**	**SOC/ C_γ(L+NL)**	**Δ^{SO}/ C_γ**
$\sigma(C_\alpha$-$C_\beta)$	-49.2	-48.3	0.9	-85.8	-86.3	-0.5	-6.0	-6.0	0.0
$\pi(C_\alpha$-$C_\beta)$/ π(Th-C)	26.3	26.4	0.1	-15.7	-15.8	-0.1	1.6	1.6	0.0
$\sigma(C_\alpha$-H)	-48.1	-46.9	1.2	-4.2	-4.1	0.1	0.4	0.4	0.0
$\sigma(C_\beta$-$C_\gamma)$	-6.6	-6.6	0.0	-89.6	-89.7	-0.1	-37.3	-37.3	0.0
$\pi(C_\beta$-$C_\gamma)$	0.2	0.2	0.0	-29.9	-29.8	0.1	5.6	5.5	-0.1
$\sigma(C_\gamma$-$C_{ipso1})$	-0.3	-0.3	0.0	1.0	1.1	0.1	-38.1	-38.1	0.0
$\sigma(C_\gamma$-$C_{ipso2})$	-0.3	-0.3	0.0	0.5	0.5	0.0	-35.4	-35.4	0.0
C_α(core)	203.6	189.5	-14.1	-0.5	-0.5	0.0	-0.1	-0.1	0.0
C_β(core)	-0.3	-0.3	0.0	203.7	203.1	-0.6	0.0	0.0	0.0
C_γ(core)	-0.2	-0.2	0.0	-1.0	-1.0	0.0	203.3	204.0	0.7
σ(Th-C_α)	-50.1	-61.0	-10.9	2.7	1.5	-1.2	2.0	2.0	0.0
Th(core)	-1.9	-3.9	-2.0	-0.4	-0.3	0.1	-0.1	-0.1	0.0
∑other	-3.1	-3.5	-0.4	-5.4	-6.1	-0.7	-13.1	-13.1	0.0
Total calc.	**70.0**	**44.8**	**-25.2**	**-24.6**	**-27.4**	**-2.8**	**82.8**	**83.4**	**0.6**

Table 5.9. Localized Molecular Orbital(LMO) Analysis of NMR Shielding for complex **5.5**.

LMO type	**SR/ C_α(L+NL)**	**SOC/ C_α(L+NL)**	**Δ^{SO}/ C_α**	**SR/ C_β(L+NL)**	**SOC/ C_β(L+NL)**	**Δ^{SO}/ C_β**	**SR/ C_γ(L+NL)**	**SOC/ C_γ(L+NL)**	**Δ^{SO}/ C_γ**
$\sigma(C_\alpha$-$C_\beta)$	-69.2	-68.0	1.2	-68.5	-69.1	-0.6	-2.6	-2.7	-0.1
$\pi(C_\alpha$-$C_\beta)$	-2.2	-1.8	0.4	13.4	13.0	-0.4	1.7	1.7	0.0
$\pi(C_\alpha$-$C_\beta)$	-12.5	-12.3	0.2	37.6	37.5	-0.1	-0.4	-0.5	-0.1
$\sigma(C_\beta$-$C_\gamma)$	-7.7	-8.0	-0.3	-72.1	-72.6	-0.5	-26.5	-26.4	0.1
$\sigma(C_\gamma$-$C_{ipso1})$	-1.0	-1.0	0.0	0.5	0.5	0.0	-37.7	-37.8	-0.1
$\sigma(C_\gamma$-$C_{ipso2})$	-0.9	-0.9	0.0	0.1	0.0	-0.1	-37.6	-37.8	-0.2
C_α(core)	203.7	183.4	-20.3	-0.5	-0.4	0.1	-0.1	-0.1	0.0
C_β(core)	-0.7	-0.6	0.0	203.6	201.1	-2.5	0.2	0.2	0.0
C_γ(core)	-0.2	-0.2	0.0	-0.7	-0.7	0.0	203.3	204.1	0.8
σ(Th-C_α)	-81.4	-95.2	-13.8	-12.9	-15.9	-3.0	2.0	2.0	0.0
C_γ LP	-7.6	-7.6	0.0	-27.9	-28.1	-0.2	17.9	18.2	0.3
Th(core)	-4.5	-6.9	-2.4	-1.2	-1.6	-0.4	-0.3	-0.2	0.1
∑other	-3.2	-3.6	-0.4	-11.8	-12.3	-0.5	-15.1	-14.9	0.2
Total calc.	**12.6**	**-22.7**	**-35.3**	**59.6**	**51.4**	**-8.2**	**104.8**	**105.8**	**1.0**

5.4.7 X-ray Crystallography. Data for complexes **5.1**-**5.5**·C_5H_{12} were collected on a Bruker KAPPA APEX II diffractometer equipped with an APEX II CCD detector using a TRIUMPH monochromater with a Mo Kα X-ray source (α = 0.71073 Å). The crystals were mounted on a cryoloop under Paratone-N oil, and data were collected at 110(2) K using an Oxford nitrogen gas cryostream system. X-ray data for **5.1**, **5.2**, **5.3**, **5.4**·C_5H_{12}, and **5.5**·C_5H_{12} were collected utilizing frame exposures of 5, 10, 10, 20, and 20 s, respectively. Data collection and cell parameter determination were conducted using the SMART program.[82] Integration of the data frames and final cell parameter refinement were performed using SAINT software.[83] Absorption corrections of the data were carried out using the multi-scan method SADABS.[84] Subsequent calculations were carried out using SHELXTL.[85] Structure determination was done using direct or Patterson methods and difference Fourier techniques. All hydrogen atom positions were idealized, and rode on the atom of attachment. Structure solution, refinement, graphics, and creation of publication materials were performed using SHELXTL.[85]

The pentane solvate molecule in **5.4**·C_5H_{12} exhibited positional disorder, as a result the pentane carbon atoms were constrained using the SADI and EADP commands and refined isotopically. The cryptand ligand in **5.4**·C_5H_{12} also contained slight positional disorder and as a result the temperature factors of the carbon and nitrogen atoms were constrained using the EADP command. The pentane solvate in **5.5**·C_5H_{12} contained more severe disorder, as a result it was constrained using the SADI and EADP commands, refined isotopically and hydrogen atoms were not assigned. The cryptand moiety in **5.5**·C_5H_{12} contained unresolved positional disorder, as a result carbon and oxygen atom temperature factors were constrained using the EADP command, and the lithium and nitrogen atoms were refined isotopically. Bond distances

on the cryptand moiety were constrained using SADI command and three hydrogen-hydrogen distances were constrained, using the DFIX command, to a distance of 1.99 Å.

Further crystallographic details can be found in Tables 5.8. Complexes **5.1**-**5.4** have been deposited in the Cambridge Structural Database (**5.1**: CCDC 2098903; **5.2**: CCDC 2098904; **5.3**·C_5H_{12}: CCDC 2098905; **5.4**·C_5H_{12}: CCDC 2098906).

Table 5.10. X-ray Crystallographic Data for Complexes **5.1**, **5.2**.

	5.1	**5.2**
empirical formula	$C_{33}H_{65}N_3Si_6U$	$C_{33}H_{65}N_3Si_6Th$
Crystal habit, color	Block, Brown	Block, Colorless
crystal size (mm)	0.30 × 0.20 × 0.10	0.30 × 0.20 × 0.10
crystal system	Triclinic	Triclinic
space group	P–1	P–1
vol (Å^3)	2162.2(9)	4339.3(18)
a (Å)	11.486(3)	11.816(3)
b (Å)	11.561(3)	19.383(5)
c (Å)	18.978(5)	19.538(5)
α (deg)	77.340(4)	97.533(3)
β (deg)	80.647(4)	101.555(3)
γ (deg)	61.820(4)	91.603(3)
Z	2	4
fw (g/mol)	910.45	904.46
density (calcd) (Mg/m^3)	1.398	1.384
abs coeff (mm^{-1})	3.944	3.626
F_{000}	920	1832
Total no. reflections	23271	43276
Unique reflections	9281	18382
R_{int}	0.0399	0.0376
final R indices [$I > 2\sigma(I)$]	R_1 = 0.0237 wR_2 = 0.0556	R_1 = 0.0381 wR_2 = 0.0810
largest diff peak and hole (e$^-$Å^{-3})	1.235 and -0.448	6.071and -1.692
GOF	1.149	1.005

Table 5.11. X-ray Crystallographic Data for Complexes **5.3**, **5.4**·C_5H_{12}, and **5.5**·C_5H_{12}.

	5.3	**5.4**·C_5H_{12}	**5.3**·C_5H_{12}
empirical formula	$C_{100}H_{222}Cl_2Li_3N_9Si_{18}Th$	$C_{56}H_{112}LiN_5O_6Si_6U$	$C_{56}H_{112}LiN_5O_6Si_6Th$
Crystal habit, color	Plate, Yellow	Needle, Dark-purple	Needle, Orange
crystal size (mm)	0.20 × 0.20 × 0.10	0.40 × 0.10 × 0.05	0.40 × 0.10 × 0.05
crystal system	Triclinic	Monoclinic	Monoclinic
space group	P–1	$P2_1$	$P2_1$
vol (Å^3)	7267(3)	3449.1(13)	3520.1(16)
a (Å)	13.967(4)	12.471(3)	12.595(3)
b (Å)	19.169(5)	10.829(2)	10.892(3)
c (Å)	27.846(7)	25.657(6)	25.756(7)
α (deg)	93.197(4)	90.00	90.00
β (deg)	96.007(4)	95.484(3)	94.977(4)
γ (deg)	100.600(4)	90.00	90.00
Z	2	2	2
fw (g/mol)	2972.31	1365.01	1359.02
density (calcd) (Mg/m^3)	1.358	1.314	1.282
abs coeff (mm^{-1})	3.294	2.503	2.265
F_{000}	3028	1420	1416
Total no. reflections	60075	36346	28848
Unique reflections	29682	14410	14458
R_{int}	0.0899	0.0343	0.0444
final R indices [$I > 2\sigma(I)$]	R_1 = 0.0657 wR_2 = 0.0899	R_1 = 0.0404, wR_2 = 0.1001	R_1 = 0.0623, wR_2 = 0.1615
largest diff peak and hole (e$^-$Å^{-3})	4.495 and -2.852	1.180 and -0.840	1.859 and -1.978
GOF	1.138	1.012	1.049

5.5 Appendix

5.5.1 NMR Spectra

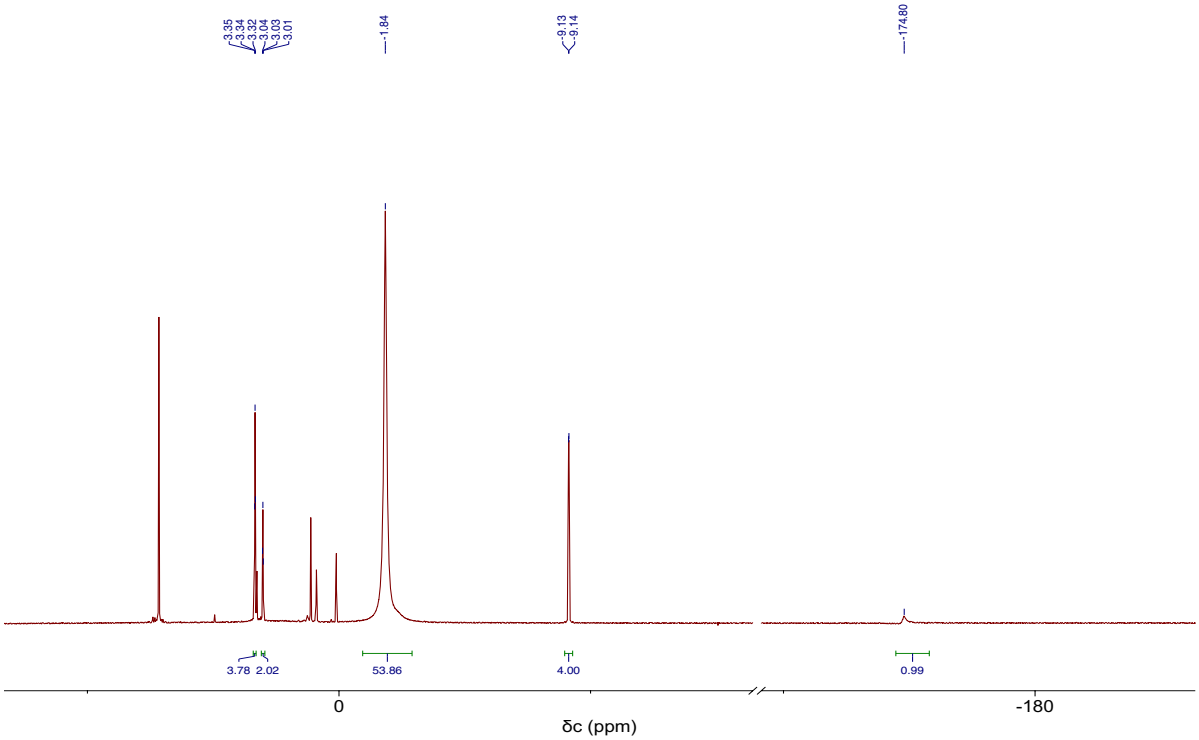

Figure A5.1. ^{1}H NMR spectrum of [{$(NR_2)_3$}U(CH=C=CPh_2)] (**5.1**) in a 10:1 mixture of C_6D_6 and THF-d_8 at room temperature.

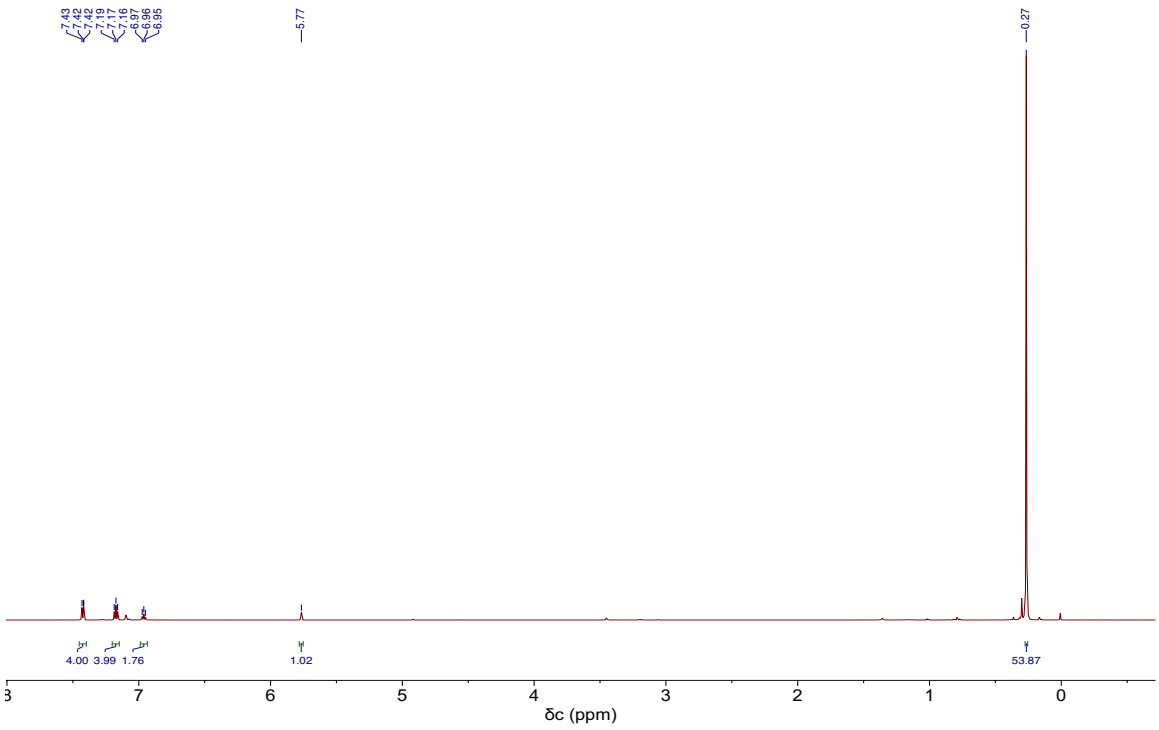

Figure A5.2. ^{1}H NMR spectrum of [{$(NR_2)_3$}Th(CH=C=CPh_2)] (**5.2**) in a 10:1 mixture of C_6D_6 and THF-d_8 at room temperature.

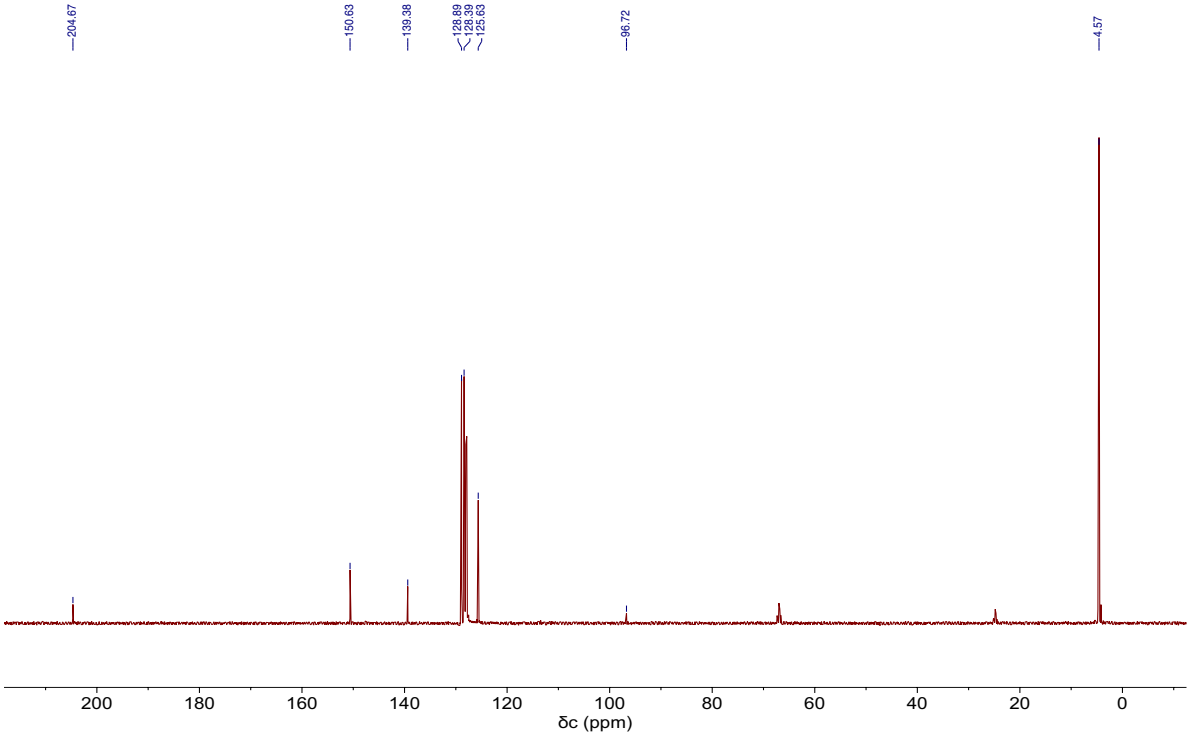

Figure A5.3. $^{13}C\{^{1}H\}$ NMR spectrum of [{$(NR_2)_3$}Th(CH=C=CPh_2)] (**5.2**) in a 10:1 mixture of C_6D_6 and THF-d_8 at room temperature.

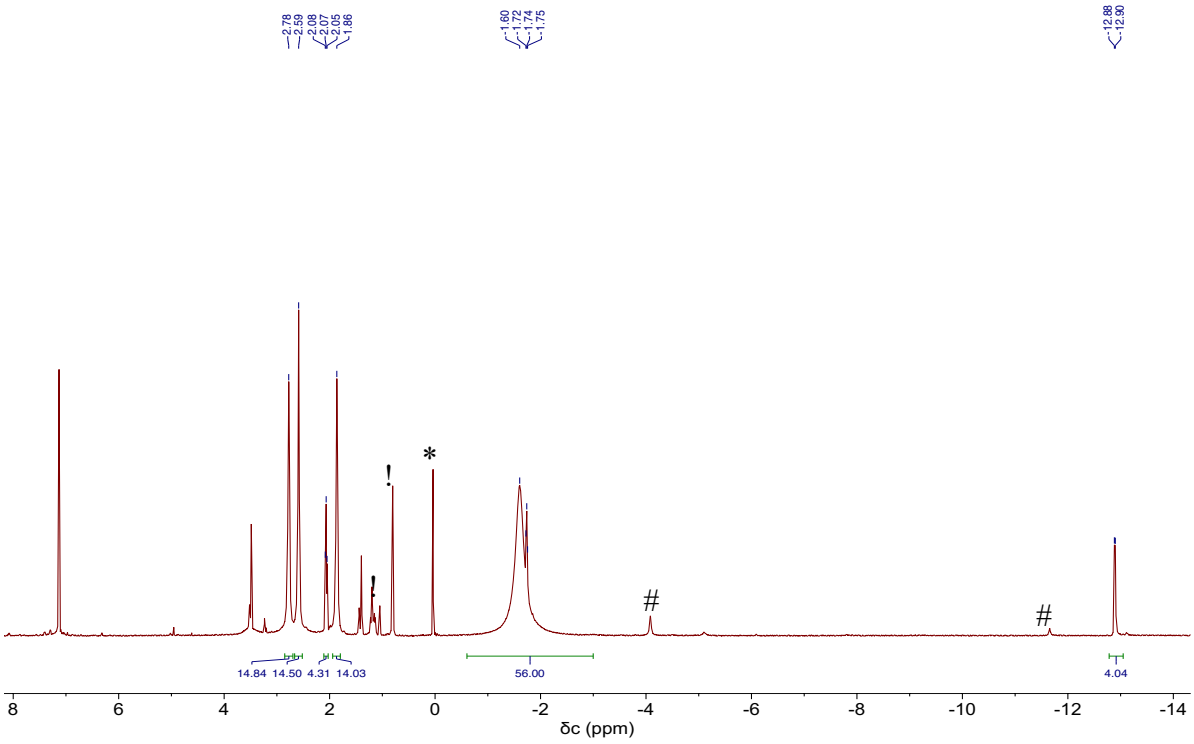

Figure A5.4. ^{1}H NMR spectrum of [Li(2.2.2-Cryptand)][{$(NR_2)_3$}U(CCCPh$_2$)] (**5.4**) in a 10:1 mixture of C_6D_6 and THF-d_8 at room temperature. (*) indicates free $HN(SiMe_3)_2$, (#) indicates an unidentified impurity. (!) indicates pentane.

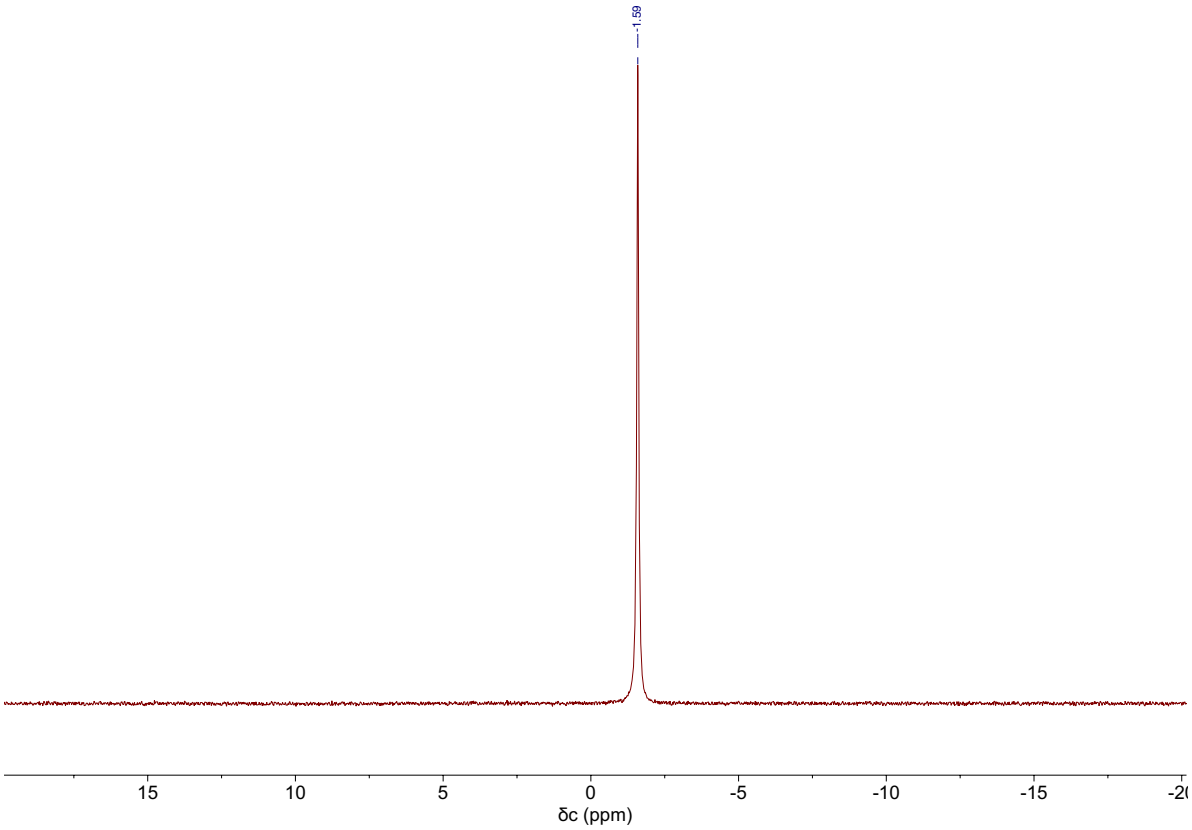

Figure A5.5. $^{7}Li\{^{1}H\}$ NMR spectrum of [Li(2.2.2-Cryptand)][{$(NR_2)_3$}U(CCCPh$_2$)] (**5.4**) in a 10:1 mixture of C_6D_6 and THF-d_8 at room temperature.

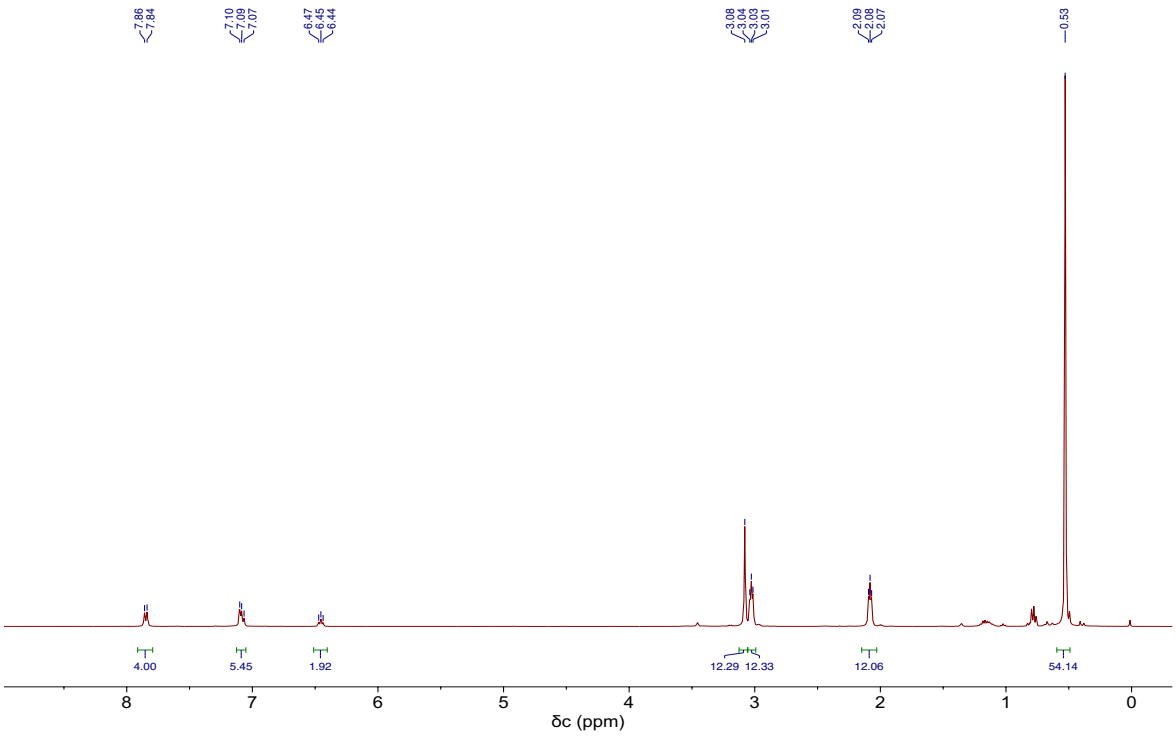

Figure A5.6. ^{1}H NMR spectrum of [Li(2.2.2-Cryptand)][{$(NR_2)_3$}Th($CCCPh_2$)] (**5.5**) in a 10:1 mixture of C_6D_6 and THF-d_8 at room temperature.

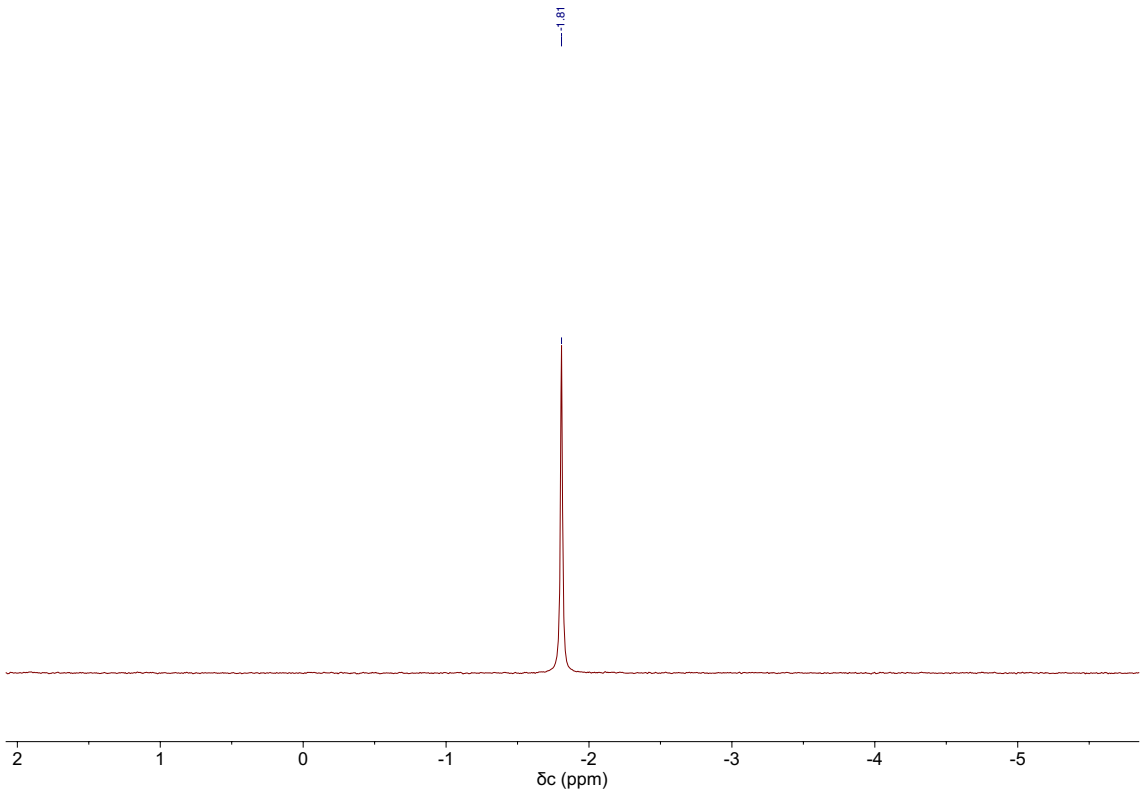

Figure A5.7. $^{7}Li\{^{1}H\}$ NMR spectrum of [Li(2.2.2-Cryptand)][{$(NR_2)_3$}Th($CCCPh_2$)] (**5.5**) in a 10:1 mixture of C_6D_6 and THF-d_8 at room temperature.

5.5.2 UV-Vis Spectra

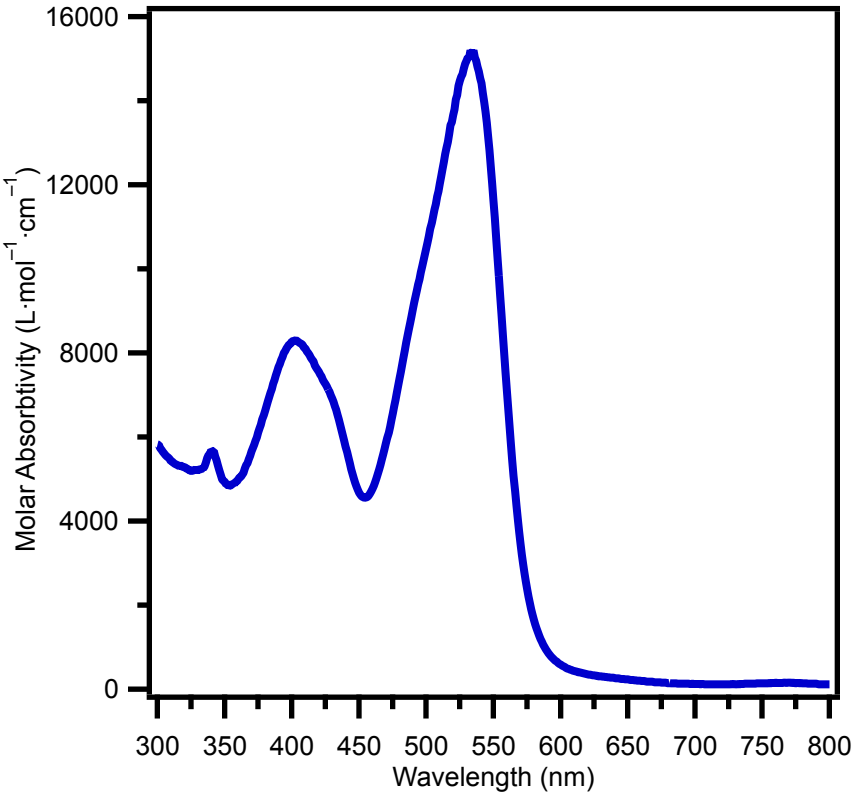

Figure A5.8. UV-Vis spectra of **5.5** (0.263 mM) in C_6H_6.

5.5.3 IR Spectra

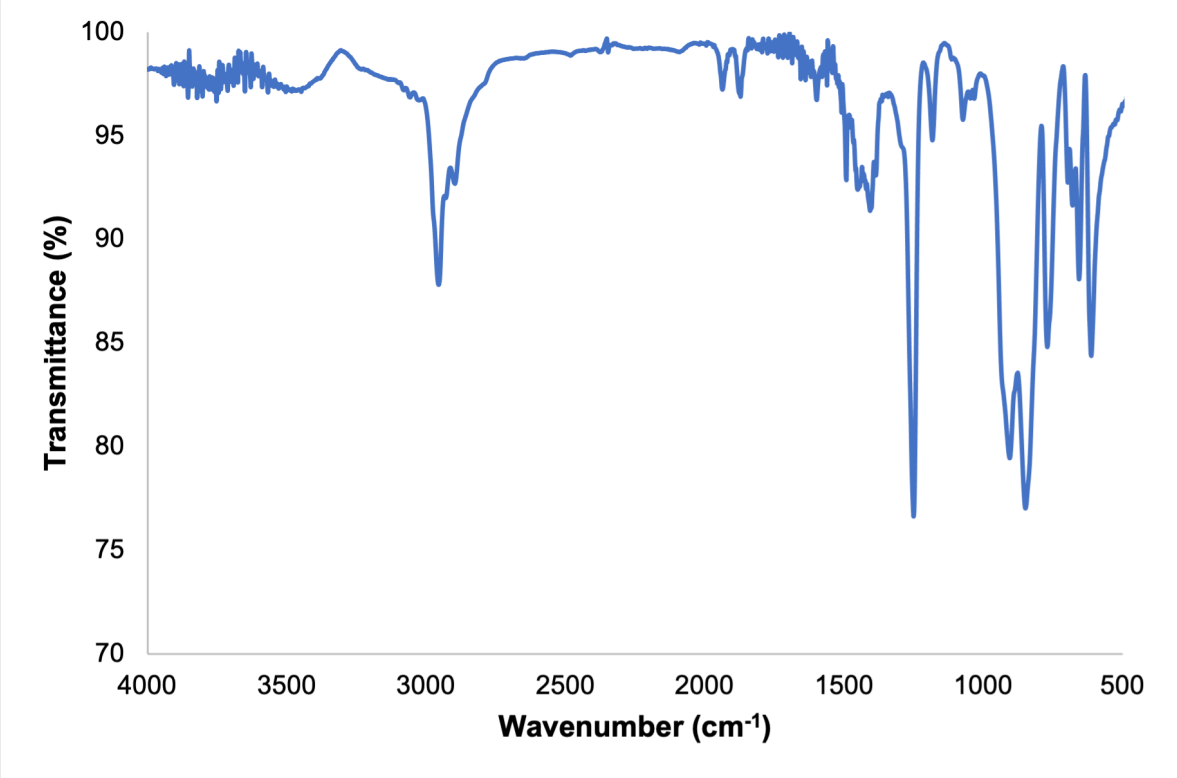

Figure A5.9. IR spectrum of **5.1** (KBr Pellet).

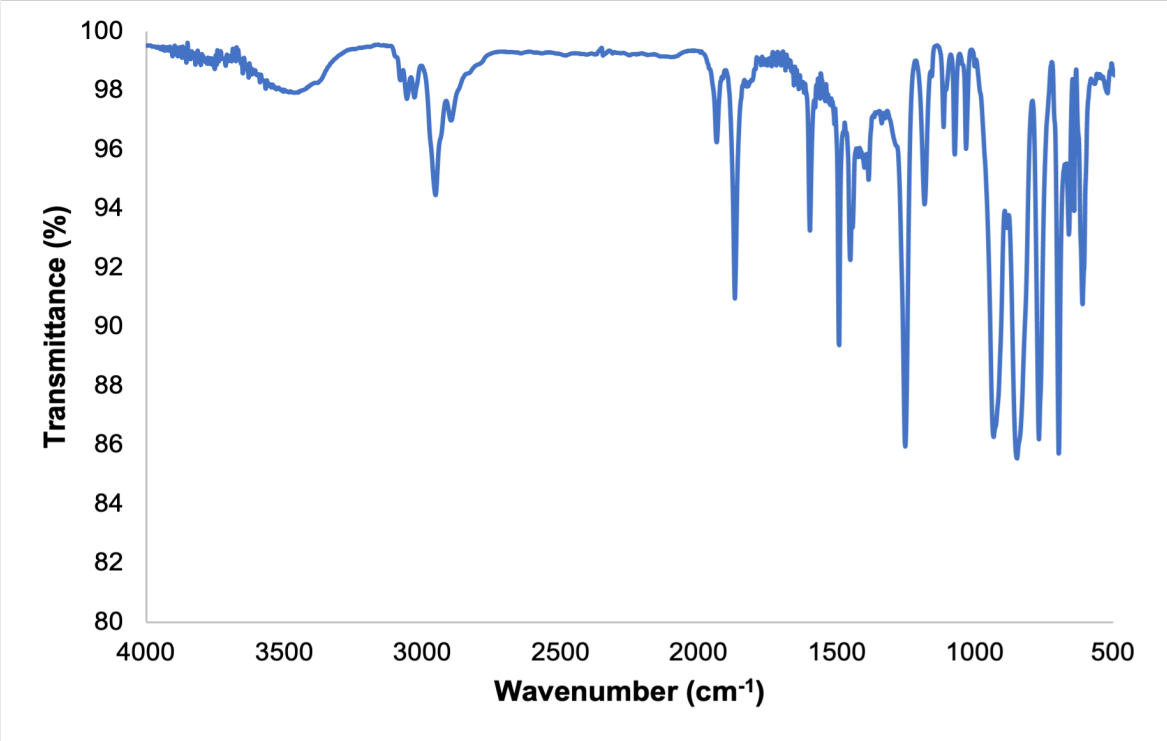

Figure A5.10. IR spectrum of **5.2** (KBr Pellet).

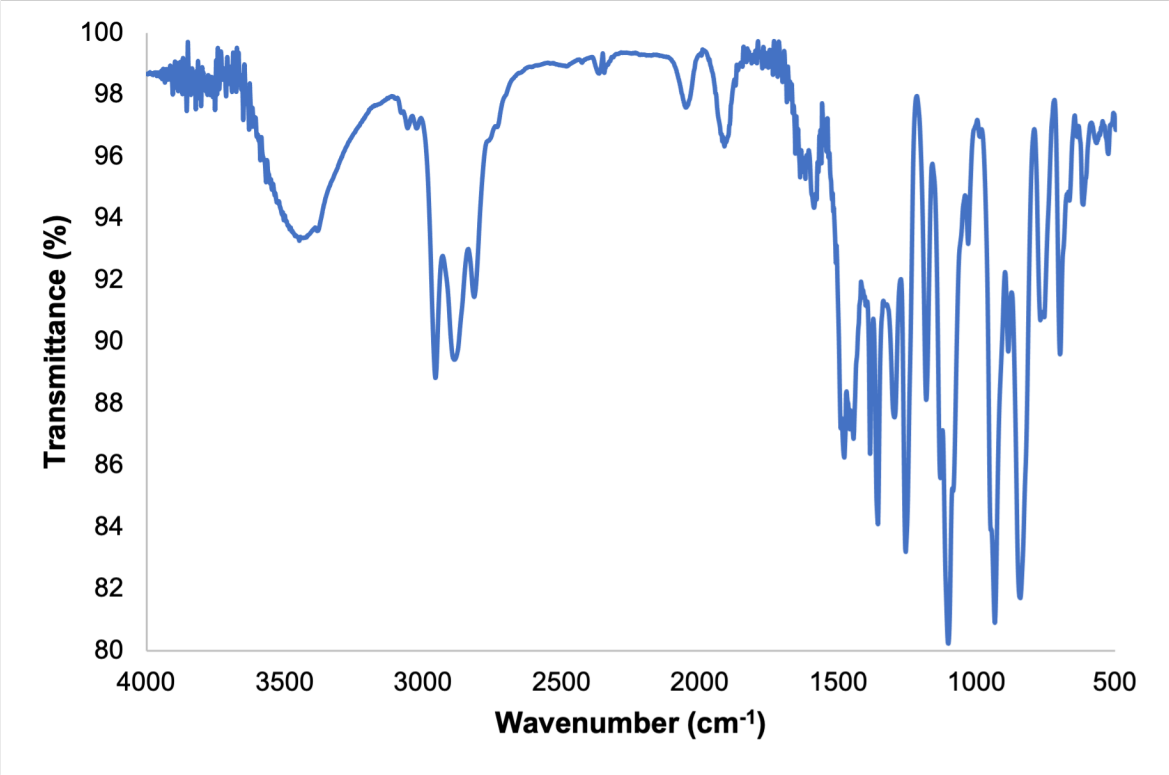

Figure A5.11. IR spectrum of **5.4** (KBr Pellet).

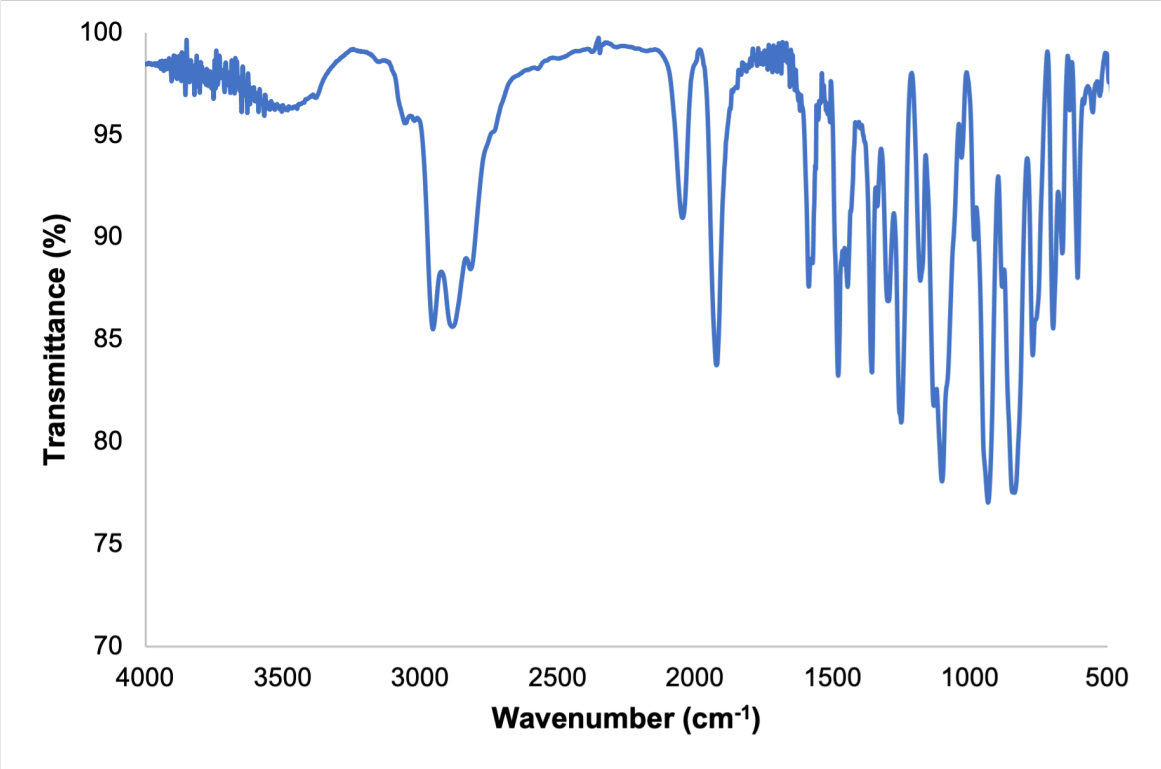

Figure A5.12. IR spectrum of **5.5** (KBr Pellet).

5.6 References

1. Fortier, S.; Walensky, J. R.; Wu, G.; Hayton, T. W., Synthesis of a Phosphorano-Stabilized U(IV)-Carbene via One-Electron Oxidation of a U(III)-Ylide Adduct. *J. Am. Chem. Soc.* **2011**, *133*, 6894-6897.

2. Cooper, O. J.; Mills, D. P.; McMaster, J.; Moro, F.; Davies, E. S.; Lewis, W.; Blake, A. J.; Liddle, S. T., Uranium–Carbon Multiple Bonding: Facile Access to the Pentavalent Uranium Carbene [U{C(PPh_2NSiMe_3)$_2$}$(Cl)_2(I)$] and Comparison of U^{V}=C and U^{IV}=C Bonds. *Angew. Chem. Int. Ed.* **2011**, *50*, 2383-2386.

3. Cooper, O. J.; Mills, D. P.; McMaster, J.; Tuna, F.; McInnes, E. J. L.; Lewis, W.; Blake, A. J.; Liddle, S. T., The Nature of the U=C Double Bond: Pushing the Stability of High-Oxidation-State Uranium Carbenes to the Limit. *Chem. Eur. J.* **2013**, *19*, 7071-7083.

4. Smiles, D. E.; Wu, G.; Hrobárik, P.; Hayton, T. W., Synthesis, Thermochemistry, Bonding, and ^{13}C NMR Chemical Shift Analysis of a Phosphorano-Stabilized Carbene of Thorium. *Organometallics* **2017**, *36*, 4519-4524.

5. Rungthanaphatsophon, P.; Huang, P.; Walensky, J. R., Phosphorano-Stabilized Carbene Complexes with Short Thorium(IV)– and Uranium(IV)–Carbon Bonds. *Organometallics* **2018**, *37*, 1884-1891.

6. Rungthanaphatsophon, P.; Bathelier, A.; Castro, L.; Behrle, A. C.; Barnes, C. L.; Maron, L.; Walensky, J. R., Formation of Methane versus Benzene in the Reactions of $(C_5Me_5)_2Th(CH_3)_2$ with $[CH_3PPh_3]X$ (X=Cl, Br, I) Yielding Thorium-Carbene or Thorium-Ylide Complexes. *Angew. Chem. Int. Ed.* **2017**, *56*, 12925-12929.

7. Liddle, S. T., The Renaissance of Non-Aqueous Uranium Chemistry. *Angew. Chem. Int. Ed.* **2015**, *54*, 8604-8641.

8. Gregson, M.; Wooles, A. J.; Cooper, O. J.; Liddle, S. T., Covalent Uranium Carbene Chemistry. *Comments Inorg. Chem.* **2015**, *35*, 262-294.

9. Hayton, T. W., Metal–ligand multiple bonding in uranium: structure and reactivity. *Dalton Trans.* **2010**, *39*, 1145-1158.

10. Boronski, J. T.; Seed, J. A.; Wooles, A. J.; Liddle, S. T., Fragmentation, catenation, and direct functionalisation of white phosphorus by a uranium(IV)–silyl–phosphino–carbene complex. *Chem. Commun.* **2021**, *57*, 5090-5093.

11. Ren, W.; Deng, X.; Zi, G.; Fang, D.-C., The Th=C double bond: an experimental and computational study of thorium poly-carbene complexes. *Dalton Trans.* **2011**, *40*, 9662-9664.

12. Cantat, T.; Arliguie, T.; Noël, A.; Thuéry, P.; Ephritikhine, M.; Floch, P. L.; Mézailles, N., The U=C Double Bond: Synthesis and Study of Uranium Nucleophilic Carbene Complexes. *J. Am. Chem. Soc.* **2009**, *131*, 963-972.

13. Lu, E.; Boronski, J. T.; Gregson, M.; Wooles, A. J.; Liddle, S. T., Silyl-Phosphino-Carbene Complexes of Uranium(IV). *Angew. Chem. Int. Ed.* **2018**, *57*, 5506-5511.

14. Seed, J. A.; Sharpe, H. R.; Futcher, H. J.; Wooles, A. J.; Liddle, S. T., Nature of the Arsonium-Ylide $Ph_3As=CH_2$ and a Uranium(IV) Arsonium–Carbene Complex. *Angew. Chem. Int. Ed.* **2020**, *59*, 15870-15874.

15. Jones, M. B.; Gaunt, A. J., Recent Developments in Synthesis and Structural Chemistry of Nonaqueous Actinide Complexes. *Chem. Rev.* **2013**, *113*, 1137-1198.

16. Lyon, J. T.; Andrews, L., Formation and Characterization of Thorium Methylidene CH_2=ThHX Complexes. *Inorg. Chem.* **2005**, *44*, 8610-8616.

17. Lyon, J. T.; Andrews, L., Formation and Characterization of the Uranium Methylidene Complexes CH_2=UHX (X = F, Cl, and Br). *Inorg. Chem.* **2006**, *45*, 1847-1852.

18. Li, J.; Hu, H.-S.; Lyon, J. T.; Andrews, L., Chirality, Agostic Interactions, and Pyramidality in Actinide Methylidene Complexes. *Angew. Chem. Int. Ed.* **2007**, *46*, 9045-9049.

19. Roos, B. O.; Lindh, R.; Cho, H.-G.; Andrews, L., Agostic Interaction in the Methylidene Metal Dihydride Complexes H_2MCH_2 (M = Y, Zr, Nb, Mo, Ru, Th, or U). *J. Phys. Chem. A* **2007**, *111*, 6420-6424.

20. Lyon, J. T.; Andrews, L.; Malmqvist, P.-Å.; Roos, B. O.; Yang, T.; Bursten, B. E., Infrared Spectrum and Bonding in Uranium Methylidene Dihydride, CH_2=UH_2. *Inorg. Chem.* **2007**, *46*, 4917-4925.

21. Cho, H.-G.; Lyon, J. T.; Andrews, L., Reactions of Actinide Metal Atoms with Ethane: Computation and Observation of New Th and U Ethylidene Dihydride, Metallacyclopropane Dihydride, and Vinyl Metal Trihydride Complexes. *J. Phys. Chem. A* **2008**, *112*, 6902-6907.

22. Lyon, J. T.; Andrews, L.; Hu, H.-S.; Li, J., Infrared Spectra and Electronic Structures of Agostic Uranium Methylidene Molecules. *Inorg. Chem.* **2008**, *47*, 1435-1442.

23. Bruce, M. I., Transition Metal Complexes Containing Allenylidene, Cumulenylidene, and Related Ligands. *Chem. Rev.* **1998**, *98*, 2797-2858.

24. Cadierno, V.; Gimeno, J., Allenylidene and Higher Cumulenylidene Complexes. *Chem. Rev.* **2009**, *109*, 3512-3560.

25. Mulks, F. F.; Antoni, P. W.; Rominger, F.; Hashmi, A. S. K., Cyclopropenylgold(I) Complexes as Aurated Carbenoids or Quasi-Carbenes. *Adv. Synth. Catal.* **2018**, *360*, 1810-1821.

26. Binger, P.; Müller, P.; Wenz, R.; Mynott, R., (3,3-Diphenylallenylidene)trimethylphosphanetitanocene: The First Titanocene Carbene Complex with Three Cumulative Double Bonds. *Angew. Chem. Int. Ed.* **1990**, *29*, 1037-1038.

27. Wang, J.-S.; Yao, L.; Ying, J.; Luo, X.; Wu, X.-F., Palladium-catalyzed directing group assisted and regioselectivity reversed cyclocarbonylation of arylallenes with 2-iodoanilines. *Org. Chem. Front.* **2021**, *8*, 792-798.

28. Werner, H.; Fluegel, R.; Windmueller, B.; Michenfelder, A.; Wolf, J., Synthesis and Reactions of Stable 16-Electron Osmium(0) Complexes [OsCl(NO)$(PR3)_2$] Including the

X-ray Crystal Structure of $[OsCl_2(NO)(\eta^1\text{-}CH{=}C{=}CPh_2)(P\text{-}i\text{-}Pr_3)_2]$. *Organometallics* **1995**, *14*, 612-618.

29. Pedrick, E. A.; Hrobárik, P.; Seaman, L. A.; Wu, G.; Hayton, T. W., Synthesis, structure and bonding of hexaphenyl thorium(IV): observation of a non-octahedral structure. *Chem. Commun.* **2016**, *52*, 689-692.

30. Lewis, A. J.; Carroll, P. J.; Schelter, E. J., Stable Uranium(VI) Methyl and Acetylide Complexes and the Elucidation of an Inverse Trans Influence Ligand Series. *J. Am. Chem. Soc.* **2013**, *135*, 13185-13192.

31. Mullane, K. C.; Hrobárik, P.; Cheisson, T.; Manor, B. C.; Carroll, P. J.; Schelter, E. J., 13C NMR Shifts as an Indicator of U–C Bond Covalency in Uranium(VI) Acetylide Complexes: An Experimental and Computational Study. *Inorg. Chem.* **2019**, *58*, 4152-4163.

32. Panetti, G. B.; Sergentu, D.-C.; Gau, M. R.; Carroll, P. J.; Autschbach, J.; Walsh, P. J.; Schelter, E. J., Isolation and characterization of a covalent Ce^{IV}-Aryl complex with an anomalous ^{13}C chemical shift. *Nat Commun* **2021**, *12*, 1713.

33. Seaman, L. A.; Hrobárik, P.; Schettini, M. F.; Fortier, S.; Kaupp, M.; Hayton, T. W., A Rare Uranyl(VI)–Alkyl Ate Complex $[Li(DME)_{1.5}]_2[UO_2(CH_2SiMe_3)_4]$ and Its Comparison with a Homoleptic Uranium(VI)–Hexaalkyl. *Angew. Chem. Int. Ed.* **2013**, *52*, 3259-3263.

34. Settineri, N. S.; Garner, M. E.; Arnold, J., A Thorium Chalcogenolate Series Generated by Atom Insertion into Thorium–Carbon Bonds. *J. Am. Chem. Soc.* **2017**, *139*, 6261-6269.

35. Fortier, S.; Melot, B. C.; Wu, G.; Hayton, T. W., Homoleptic Uranium(IV) Alkyl Complexes: Synthesis and Characterization. *J. Am. Chem. Soc.* **2009**, *131*, 15512-15521.

36. Seaman, L. A.; Walensky, J. R.; Wu, G.; Hayton, T. W., In Pursuit of Homoleptic Actinide Alkyl Complexes. *Inorg. Chem.* **2013**, *52*, 3556-3564.

37. Behrle, A. C.; Myers, A. J.; Rungthanaphatsophon, P.; Lukens, W. W.; Barnes, C. L.; Walensky, J. R., Uranium(III) and thorium(IV) alkyl complexes as potential starting materials. *Chem. Commun.* **2016**, *52*, 14373-14375.

38. Shannon, R., Revised effective ionic radii and systematic studies of interatomic distances in halides and chalcogenides. *Acta Crystallogr., Sect. A: Found. Crystallogr.* **1976**, *32*, 751-767.

39. Elsevier, C. J.; Kleijn, H.; Boersma, J.; Vermeer, P., Synthesis, structure and reactivity of some (σ-allenyl)- and (σ-prop-2-ynyl)palladium(II) complexes. *Organometallics* **1986**, *5*, 716-720.

40. Keng, R. S.; Lin, Y. C., Preparation and chemical reactivities of the tungsten allenyl complex $CpW(CO)_3CH{=}C{=}CH_2$. *Organometallics* **1990**, *9*, 289-291.

41. Wojcicki, A.; Shuchart, C. E., Transition-metal-propargyl complexes: versatile reagents in synthesis. *Coord. Chem. Rev.* **1990**, *105*, 35-60.

42. Shuchart, C. E.; Willis, R. R.; Wojcicki, A., Propargyl complexes of ruthenium. *J. Organomet. Chem.* **1992**, *424*, 185-198.

43. Alabugin, I. V., Stereoelectronic Effects with Donor and Acceptor Separated by a Vinyl Bridge. In *Stereoelectronic Effects*, 2016; pp 183-213.

44. Castarlenas, R.; Esteruelas, M. A.; Lalrempuia, R.; Oliván, M.; Oñate, E., Osmium−Allenylidene Complexes Containing an N-Heterocyclic Carbene Ligand. *Organometallics* **2008**, *27*, 795-798.

45. Buncel, E.; Menon, B., Carbanion mechanisms. 9. Spectrophotometric study of triphenylmethyl alkali metal salts. Contact and solvent-separated ion pairs in ethereal solvents. *J. Org. Chem.* **1979**, *44*, 317-320.

46. Cramer, R. E.; Bruck, M. A.; Edelmann, F.; Afzal, D.; Gilje, J. W.; Schmidbaur, H., Synthesis and structure of $Cp_3U{=}CHPMe_3$: A compound with a U=C multiple bond. *Chem. Ber.* **1988**, *121*, 417-420.

47. Newell, B. S.; Rappé, A. K.; Shores, M. P., Experimental Evidence for Magnetic Exchange in Di- and Trinuclear Uranium(IV) Ethynylbenzene Complexes. *Inorg. Chem.* **2010**, *49*, 1595-1606.

48. Kent, G. T.; Yu, X.; Wu, G.; Autschbach, J.; Hayton, T. W., Synthesis of Parent Acetylide and Dicarbide Complexes of Thorium and Uranium and an Examination of Their Electronic Structures. *Inorg. Chem.* **2021**, *Accepted*.

49. Coletti, C.; Marrone, A.; Re, N., Metal Complexes Containing Allenylidene and Higher Cumulenylidene Ligands: A Theoretical Perspective. *Acc. Chem. Res.* **2012**, *45*, 139-149.

50. Autschbach, J.; Zurek, E., Relativistic Density-Functional Computations of the Chemical Shift of ^{129}Xe in $Xe@C_{60}$. *J. Phys. Chem. A* **2003**, *107*, 4967-4972.

51. Glendening, E. D.; Landis, C. R.; Weinhold, F., Natural bond orbital methods. *WIREs Comput Mol Sci* **2012**, *2*, 1-42.

52. Wolff, S. K.; Ziegler, T.; Lenthe, E. v.; Baerends, E. J., Density functional calculations of nuclear magnetic shieldings using the zeroth-order regular approximation (ZORA) for relativistic effects: ZORA nuclear magnetic resonance. *J. Chem. Phys.* **1999**, *110*, 7689-7698.

53. Velde, G. t.; Bickelhaupt, F. M.; Baerends, E. J.; Guerra, C. F.; Gisbergen, S. J. A. v.; Snijders, J. G.; Ziegler, T., Chemistry with ADF. *J. Comput. Chem.* **2001**, *22*, 931–967.

54. Bader, R. F. W.; Slee, T. S.; Cremer, D.; Kraka, E., Description of conjugation and hyperconjugation in terms of electron distributions. *J. Am. Chem. Soc.* **1983**, *105*, 5061-5068.

55. Autschbach, J., Analyzing NMR shielding tensors calculated with two-component relativistic methods using spin-free localized molecular orbitals. *J. Chem. Phys.* **2008**, *128*, 164112.

56. Autschbach, J.; Zheng, S., Analyzing Pt chemical shifts calculated from relativistic density functional theory using localized orbitals: The role of Pt 5d lone pairs. *Magn. Reson. Chem.* **2008**, *46*, S45-S55.

57. Baerends, E. J.; Ziegler, T.; Autschbach, J.; Bashford, D.; Bérces, A.; Bickelhaupt, F.; Bo, C.; Boerrigter, P.; Cavallo, L.; Chong, D., ADF2017, SCM, Theoretical Chemistry, Vrije Universiteit, Amsterdam, The Netherlands. *URL: http://www. scm. com* **2014**.

58. Wiberg, K. B.; Hammer, J. D.; Zilm, K. W.; Cheeseman, J. R., NMR Chemical Shifts. 3. A Comparison of Acetylene, Allene, and the Higher Cumulenes. *J. Org. Chem.* **1999**, *64*, 6394-6400.

59. Viesser, R. V.; Ducati, L. C.; Tormena, C. F.; Autschbach, J., The unexpected roles of σ and π orbitals in electron donor and acceptor group effects on the ^{13}C NMR chemical shifts in substituted benzenes. *Chem. Sci.* **2017**, *8*, 6570-6576.

60. Staun, S. L.; Sergentu, D.-C.; Wu, G.; Autschbach, J.; Hayton, T. W., Use of ^{15}N NMR spectroscopy to probe covalency in a thorium nitride. *Chem. Sci.* **2019**, *10*, 6431-6436.

61. Sergentu, D.-C.; Kent, G. T.; Staun, S. L.; Yu, X.; Cho, H.; Autschbach, J.; Hayton, T. W., Probing the Electronic Structure of a Thorium Nitride Complex by Solid-State ^{15}N NMR Spectroscopy. *Inorg. Chem.* **2020**, *59*, 10138-10145.

62. Wrackmeyer, B.; Horchler, K., NMR parameters of alkynes. *Prog. Nucl. Magn. Reson. Spectrosc.* **1990**, *22*, 209-253.

63. Roh, S. W.; Choi, K.; Lee, C., Transition Metal Vinylidene- and Allenylidene-Mediated Catalysis in Organic Synthesis. *Chem. Rev.* **2019**, *119*, 4293-4356.

64. Turner, H. W.; Andersen, R. A.; Zalkin, A.; Templeton, D. H., Chloro-, methyl-, and (tetrahydroborato)tris((hexamethyldisilyl)amido)thorium(IV) and uranium(IV). Crystal structure of (tetrahydroborato)tris((hexamethyldisilyl)amido)thorium(IV). *Inorg. Chem.* **1979**, *18*, 1221-1224.

65. Andersen, R. A., Tris ((hexamethyldisilyl) amido) uranium (III): preparation and coordination chemistry. *Inorg. Chem.* **1979**, *18*, 1507-1509.

66. Huang, J.-H.; Lee, T.-Y.; Swenson, D. C.; Messerle, L., An alkylidene-tethered tantallanorbornadiene from reduction of a tantalum(phenylalkenyl)alkylidene derived from 3,3-diphenylcyclopropene ring opening by $(\eta\text{-}C_5Me_4R)_2Ta_2(\mu\text{-}X)_4$ (Ta=Ta). *Inorg. Chim. Acta* **2003**, *345*, 209-215.

67. Barnett, N. D. R.; Mulvey, R. E.; Clegg, W.; O'Neil, P. A., Crystal structure of lithium diisopropylamide (LDA): an infinite helical arrangement composed of near-linear nitrogen-lithium-nitrogen units with four units per turn of helix. *J. Am. Chem. Soc.* **1991**, *113*, 8187-8188.

68. Harris, R. K.; Becker, E. D.; De Menezes, S. M. C.; Granger, P.; Hoffman, R. E.; Zilm, K. W., Further Conventions for NMR Shielding and Chemical Shifts (IUPAC Recommendations 2008). *Magn. Reson. Chem.* **2008**, *46*, 582-598.

69. Harris, R. K.; Becker, E. D.; Cabral de Menezes, S. M.; Goodfellow, R.; Granger, P., NMR nomenclature: nuclear spin properties and conventions for chemical shifts. IUPAC Recommendations 2001. International Union of Pure and Applied Chemistry. Physical Chemistry Division. Commission on Molecular Structure and Spectroscopy. *Magn. Reson. Chem.* **2002**, *40*, 489-505.

70. Frisch, M.; Trucks, G.; Schlegel, H.; Scuseria, G.; Robb, M.; Cheeseman, J.; Scalmani, G.; Barone, V.; Petersson, G.; Nakatsuji, H., Gaussian 16. Gaussian, Inc. Wallingford, CT: 2016.

71. Paier, J.; Hirschl, R.; Marsman, M.; Kresse, G., The Perdew–Burke–Ernzerhof exchange-correlation functional applied to the G2-1 test set using a plane-wave basis set. *J. Chem. Phys.* **2005**, *122*, 234102.

72. Cao, X.; Dolg, M., Valence basis sets for relativistic energy-consistent small-core lanthanide pseudopotentials. *J. Chem. Phys.* **2001**, *115*, 7348-7355.

73. Rassolov, V. A.; Pople, J. A.; Ratner, M. A.; Windus, T. L., 6-31G* basis set for atoms K through Zn. *J. Chem. Phys.* **1998**, *109*, 1223-1229.

74. Grimme, S.; Ehrlich, S.; Goerigk, L., Effect of the damping function in dispersion corrected density functional theory. *J. Comput. Chem.* **2011**, *32*, 1456-1465.

75. Glendening, E. D.; Landis, C. R.; Weinhold, F., NBO 6.0: Natural bond orbital analysis program. *J. Comput. Chem.* **2013**, *34*, 1429-1437.

76. Lu, T.; Chen, F., Multiwfn: A multifunctional wavefunction analyzer. *J. Comput. Chem.* **2012**, *33*, 580-592.

77. Baerends, E. J.; Ziegler, T.; Atkins, A. J.; Autschbach, J.; Baseggio, O.; Bashford, D.; Bérces, A.; Bickelhaupt, F. M.; Bo, C.; Boerrigter, P. M.; Cavallo, L.; Daul, C.; Chong, D. P.; Chulhai, D. V.; Deng, L.; Dickson, R. M.; Dieterich, J. M.; Ellis, D. E.; Faassen, M. v.; Fan, L.; Fischer, T. H.; Guerra, C. F.; Franchini, M.; Ghysels, A.; Giammona, A.; Gisbergen, S. J. A. v.; Goez, A.; Götz, A. W. G., J. A.; Gritsenko, O. V.; Grüning, M.; Gusarov, S.; Harris, F. E.; Hoek, P. v. d.; Hu, Z.; Jacob, C. R.; Jacobsen, H.; Jensen, L.; Joubert, L.; Kaminski, J. W.; Kessel, G. v.; König, C.; Kootstra, F.; Kovalenko, A.; Krykunov, M. V.; Lenthe, E. v.; McCormack, D. A.; Michalak, A.; Mitoraj, M.; Morton, S. M.; Neugebauer, J.; Nicu, V. P.; Noodleman, L.; Osinga, V. P.; Patchkovskii, S.; Pavanello, M.; Peeples, C. A.; Philipsen, P. H. T.; Post, D.; Pye, C. C.; Ramanantoanina, H.; Ramos, P.; Ravenek, W.; Rodríguez, J. I.; Ros, P.; Rüger, R.; Schipper, P. R. T.; Schlüns, D.; Schoot, H. v.; Schreckenbach, G.; Seldenthuis, J. S.; Seth, M.; Snijders, J. G.; Solà, M.; Stener, M.; Swart, M.; Swerhone, D.; Tognetti, V.; Velde, G. t.; Vernooijs, P.; Versluis, L.; Visscher, L.; Visser, O.; Wang, F.; Wesolowski, T. A.; Wezenbeek, E. M. v.; Wiesenekker, G.; Wolff, S. K.; Woo, T. K.; Yakovlev, A. L.: , Amsterdam Density Functional. 2017 ed.; SCM, Theoretical Chemistry, Vrije Universiteit Amsterdam, The Netherlands,. . **2017**.

78. Lenthe, E. v.; Baerends, E. J.; Snijders, J. G., Relativistic regular two-component Hamiltonians. *J. Chem. Phys.* **1993**, *99*, 4597-4610.

79. Weigend, F.; Ahlrichs, R., Balanced basis sets of split valence, triple zeta valence and quadruple zeta valence quality for H to Rn: Design and assessment of accuracy. *Phys. Chem. Chem. Phys.* **2005**, *7*, 3297-3305.

80. Pye, C. C.; Ziegler, T., An implementation of the conductor-like screening model of solvation within the Amsterdam density functional package. *Theor. Chem. Acc.* **1999**, *101*, 396-408.

81. van Dongen, J. P. C. M.; van Dijkman, H. W. D.; de Bie, M. J. A., Characteristic 13C chemical shifts and 13C–H coupling constants in organolithium compounds. *Recl. Trav. Chim. Pays-Bas* **1974**, *93*, 29-32.

82. *SMART Apex II*, Version 2.1 ed.; Bruker AXS Inc.: Madison WI, 2005.

83. *SAINT Software User's Guide*, Version 7.34a ed.; Bruker AXS Inc.: Madison, WI, 2005.

84. Sheldrick, G. M., *SADABS*, the Siemens Area Detector Absorption Correction; University of Göttingen: Göttingen, Germany, 2005.

85. *SHELXTL PC*, Version 6.12 ed.; Bruker AXS Inc.:Madison, WI, 2005.

Chapter 6. Reactivity of [$M(NR_2)_3$] (M = Ce, U; R = $SiMe_3$) with the Prospective Carbon Atom Transfer Reagent Bis(diisopropylamino)cyclopropenylidene (BAC)

Portions of this work were published in:

Greggory T. Kent, Selena L. Staun, Guang Wu, Trevor W. Hayton Reactivity of [$Ce(NR_2)_3$] (R = $SiMe_3$) with Prospective Carbon Atom Transfer Reagents. *Organometallics* **2020**, 39, 2375–2382

6.1 Introduction

While f-element N-heterocyclic carbene (NHC) complexes are now relatively common,[1-4] f-element complexes containing unsupported Schrock- or Fischer-type carbenes are essentially unknown. Likewise, f-element carbides and alkylidynes are also unknown. That said, some progress has been made toward the generation of An/Ln-C multiple bonds in recent years. For example, Liddle and co-workers have reported the synthesis of the cerium methanediide complexes, $[Ce(BIPM^{TMS})(ODipp)_2]$ and $[Ce(BIPM^{TMS})_2]$ ($BIPM^{TMS} = [C(PPh_2NR)_2]^{2-}$, R = $SiMe_3$; Dipp = 2,6-diisopropylphenyl).[5-8] More recently, Zhu and co-workers ligated the carbodiphosphorane, $C(PPh_3)_2$, to Ce(III),[9, 10] forming $[BrCe(CDP)_2][BPh_4]_2$. DFT calculations revealed that the Ce-C bond in this complex consisted of a strong σ-interaction and a weak π-interaction. In contrast, a significant number of heteroatom-stabilized actinide carbene complexes have been reported in recent years,[6, 11-16] including $[U(Tren^{TIPS})(CHAsPh_3)]$ ($Tren^{TIPS} = N(CH_2CH_2NSiPr^i_3)_3$),[17] $[U\{C(SiMe_3)(PPh_2)\}(BIPM^{TMS})(Cl)]^-$ ($BIPM^{TMS} = C(PPh_2NSiMe_3)_2$),[18] and $[An(CHPPh_3)(NR_2)_3]$ (An = Th, U; R = $SiMe_3$).[19, 20] Additionally, in Chapter 5 I described the synthesis of the actinide allenylidenes $[\{(NR_2)_3\}An(CCCPh_2)]^-$ (An = U, **5.3**; Th, **5.4**), which were also the first reported An carbenes that contain no heteroatom stabilization.[21]

In the past few years, a number of carbon-atom transfers reagents have been identified, which could, in principle, be employed to generate an elusive unsupported Ln/An-C multiple bond. For example, Smith and co-workers demonstrated that bis(diisopropylamino)cyclopropenylidene (BAC) can transfer a carbon atom to the iron(IV) nitride, $[\{PhB(^iPr_2Im)_3\}Fe(N)]$ ($^iPr_2Im$ = 1,2-diisopropylimidazolylidene), resulting in

formation of a cyanide complex concomitant with loss of bis(diisopropylamino)acetylene (Scheme 6.1a).[22] Additionally, Agapie and coworkers showed in 2021 that reaction of $[Tp^*M(\mu^3\text{-}S)_3Fe_3Cl(BAC)_3][BPh_4]$ (Tp* = hydrotris(3,5-dimethylpyrazolyl)borate, M = W or Mo) with excess KC_8 results in ring opening of one BAC ligand to form the Fe_3-μ^3-carbyne complex $[Tp^*M(\mu^3\text{-}S)_3Fe_3(\mu^3\text{-}C\text{-}(C(^iPr)=C(^iPr))(BAC)_2]$ (Scheme 6.1b).[23]

Scheme 6.1. Previously reported reactivity of BAC.

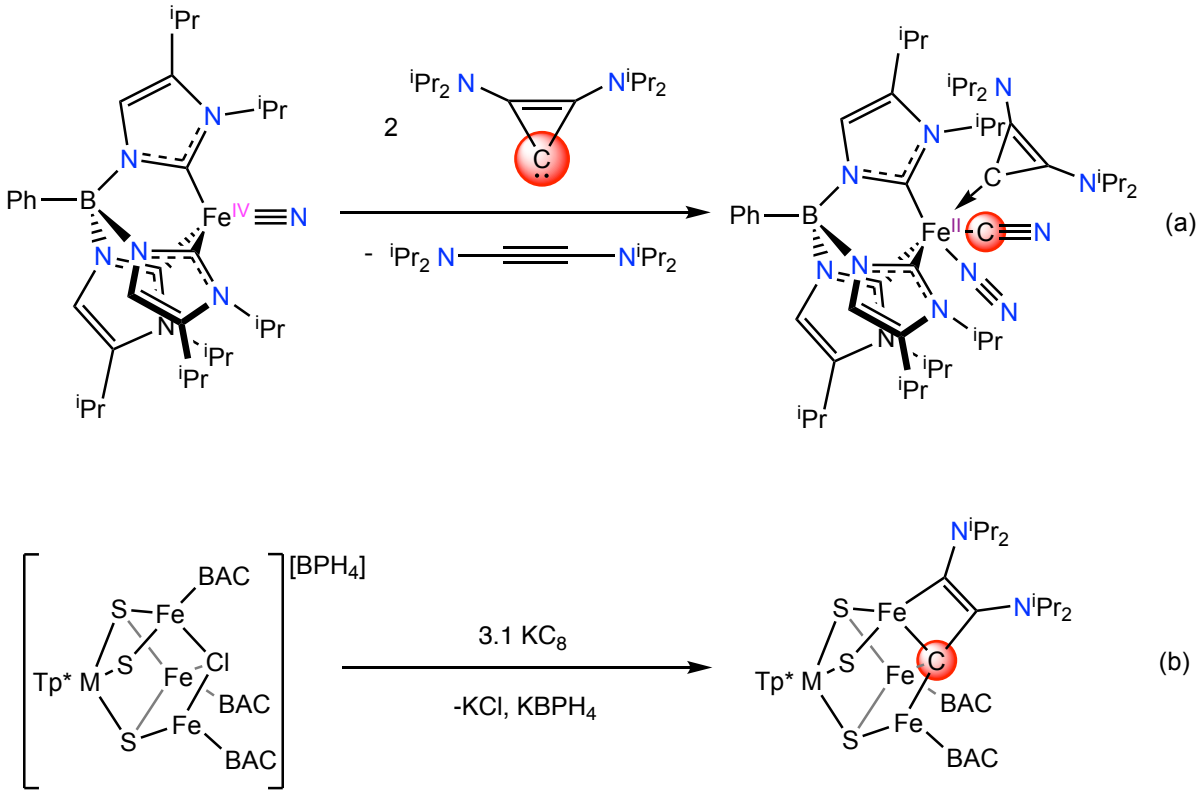

Generally speaking, the use of these carbon-atom transfer reagents requires reducing conditions to effect C-atom transfer.[22, 23] While uranium(III) is strongly reducing and can be easily oxidized to U(IV), U(V), or U(VI),[19, 24, 25] depending on the conditions, cerium(III) is not usually considered to be a good reductant, as it prefers the 3+ oxidation state;[26, 27] however, it has recently been shown that photolysis of cerium(III) results in the generation of a

substantially more reducing metal center.[28] For example, Schelter and co-workers reported that photolysis of $[Ce(NR_2)_3]$ (R = $SiMe_3$) resulted in formation of a relatively long-lived excited state.[29, 30] This excited state species is strongly reducing, and can elicit homolytic cleavage of the C-Cl bond in $PhCH_2Cl$, resulting in formation of $[Ce(Cl)(NR_2)_3]$ and bibenzyl.[29] Since then, Ce(III) has been shown to facilitate a variety of photo-mediated transformations, including aryl coupling and borylation reactions.[30-33] In addition, Dr. Mikiyas Assefa previously reported that photolysis of a cerium nitrate complex, [Li(2,2,2-cryptand)][Ce(κ^2-O_2NO)$(NR_2)_3$], resulted in formation of the terminal Ce=O complex, [Li(2,2,2-cryptand)][Ce(O)$(NR_2)_3$], via formal loss of NO_2.[34] Motivated by these past results, I hypothesized that ligation of a carbon-atom transfer reagent to cerium(III) or uranium(III), followed by photolysis or thermolysis, respectively, could induce either partial or complete carbon atom transfer and allow access to novel Ce(IV) and U(V/VI) organometallics.

Herein, I describe the ligation of the prospective carbon-atom transfer reagent and bis(diisopropylamino)cyclopropenylidene (BAC), to the well-known f-element (III) tris(amide) complexes, $[M(NR_2)_3]$ (M = Ce, U), along with an investigation of their photolytic or thermolytic chemistry, respectively. While carbon-atom transfer from BAC is nominally a $4e^-$ redox process,[22] and each Ce(III) and U(III) center can provide only one electron and three electrons, respectively, I envisioned that cooperative reactivity of multiple M(III) (M = Ce, U) centers could give rise to unique alkylidene- or carbide-containing complexes or clusters.

6.2 Results and discussion

6.2.1 Synthesis and Characterization of BAC Adducts 6.1 and 6.2

Scheme 6.2. Synthesis of BAC adducts **6.1** and **6.2**.

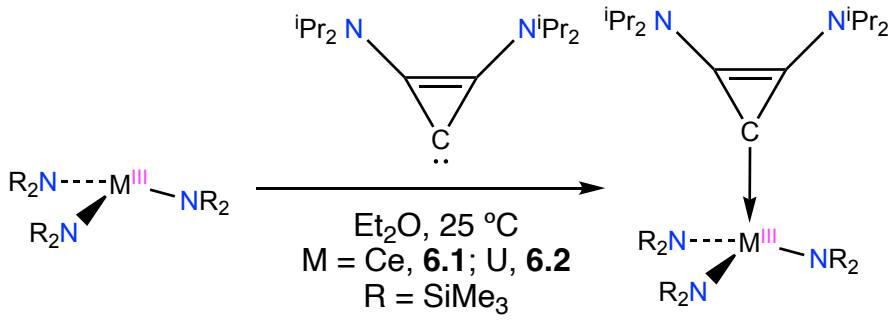

Reaction of $[Ce(NR_2)_3]$ with 1 equiv of bis(diisopropylamino)cyclopropenylidene (BAC) in Et_2O results in a rapid color change from deep yellow to orange (Scheme 6.2). Work up of the reaction mixture, followed by crystallization from pentane/hexamethyldisiloxane (HMDSO), results in the isolation of $[(NR_2)_3Ce(BAC)]$ (**6.1**) as yellow blocks in 60% yield. The uranium analog **6.2** can be prepared in a similar manner in 62% yield from the reaction of $[U(NR_2)_3]$ with 1 equiv BAC in Et_2O. The ^1H NMR spectrum of **6.1** exhibits broad resonances at 3.12, 0.81, and 0.01 ppm, which are assignable to a BAC methine environment and two BAC isopropyl methyl environments, respectively. In addition, a broad singlet at -2.25 ppm is assignable to the $SiMe_3$ proton environment. The chemical shift of the $SiMe_3$ groups, along with a broadening of all resonances, is consistent with the presence of a paramagnetic Ce(III) metal center. The ^1H NMR spectrum of **6.2** exhibits broad resonances at -2.60, -6.43, and -9.88, which are assignable to BAC isopropyl methyl, $SiMe_3$ groups and BAC Methine environments, respectively.

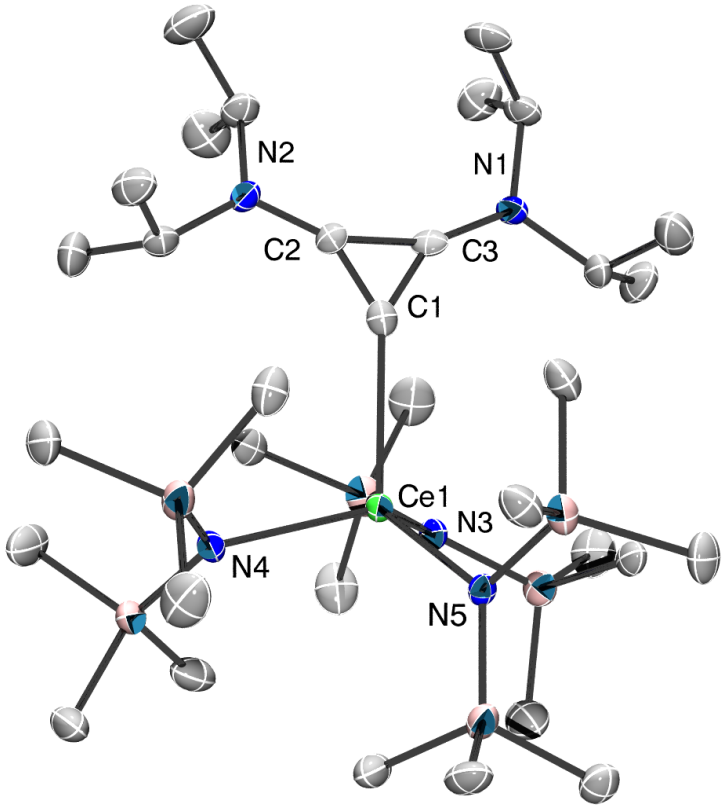

Figure 6.1. Solid-state molecular structure of **6.1**, shown with 50% probability ellipsoids. Hydrogen atoms removed for clarity. Selected bond lengths (Å) and angles (°): **6.1**: Ce1-N3 = 2.371(3), Ce1-N4 = 2.380(3), Ce1-N5 = 2.384(3), Ce1-C1 = 2.669(4), C1-C2 = 1.380(5), C1-C3 = 1.393(5), C2-C3 = 1.365(5), N3-Ce1-N4 = 121.1(1), N3-Ce1-N5 = 113.7(1), N4-Ce1-N5 = 104.1(1). **6.2**: U1-N3 = 2.366(3), U1-N4 = 2.378(3), U1-N5 = 2.353(3), U1-C1 = 2.614(4), C1-C2 = 1.389(5), C1-C3 = 1.404(5), C2-C3 = 1.361(5), N3-U1-N4 = 104.1(1), N3-U1-N5 = 119.9(1), N4-U1-N5 = 113.3(1).

Complex **6.1** crystalizes in the monoclinic space group $P2_1/c$ and features a pseudo-tetrahedral geometry about the cerium(III) center (Figure 6.1). The Ce-N_{amide} distances (av. Ce-N = 2.38 Å) are similar to Ce-N distances reported for other cerium(III) amide complexes,[34-38] while the Ce-C_{BAC} bond length (2.669(4) Å) is slightly longer than those

reported for other Ce(III)-NHC adducts.[4] The C1-C2 and C1-C3 distances are 1.380(5) and 1.393(5) Å, respectively, which are comparable to those of the free ligand (1.405(3) Å).[39] The C2-C3 distances in complex **6.1** (1.365(5) Å) and free ligand (1.344(3) Å) are also comparable. Complex **6.2** is isomorphous to **6.1** and features a pseudo-tetrahedral geometry about the uranium(III) center (Figure 6.1). The U-N_{amide} distances (av. U-N = 2.36 Å) are similar to U-N distances reported for other uranium(III) amide complexes,[19, 20, 40-42] while the U-C_{BAC} bond length (2.614(4) Å) is somewhat shorter than those reported for other U(III)-NHC adducts.[4, 43] The C1-C2 and C1-C3 distances are 1.389(5) and 1.404(5) Å, respectively, which are comparable to those of **6.1** and the free ligand (1.405(3) Å).[39] The C2-C3 distances in complex **6.2** (1.361(5) Å), **6.1**, and free ligand are also comparable.

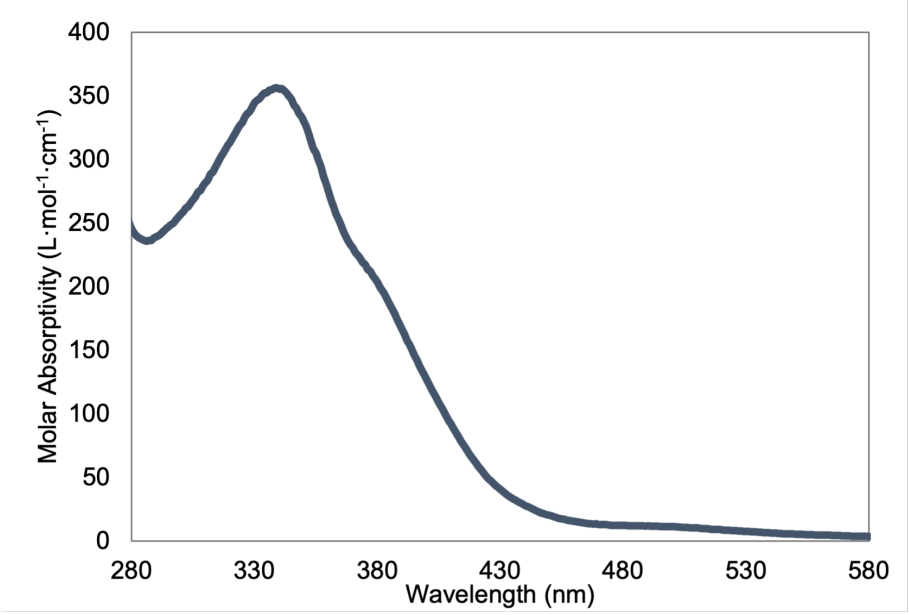

Figure 6.2. UV-vis spectrum of complex **6.1** (0.49 mM, λ_{max} = 343 nm, ε = 352 $L \cdot mol^{-1} \cdot cm^{-1}$) in benzene.

The UV-vis spectrum of **6.1** in benzene features a broad absorption at 343 nm (ε = 352 $M^{-1}cm^{-1}$), along with a prominent shoulder at ca. 380 nm (Figure 6.2), which I have assigned to the 4f $\rightarrow$ $5d_{xz/yz}$ and 4f $\rightarrow$ $5d_z^2$ transitions, respectively. The latter assignment is significantly blue shifted with respect to that reported for $[Ce(NR_2)_3]$,[29] a consequence of donation from the strongly-donating BAC ligand to the $5d_z^2$ orbital.

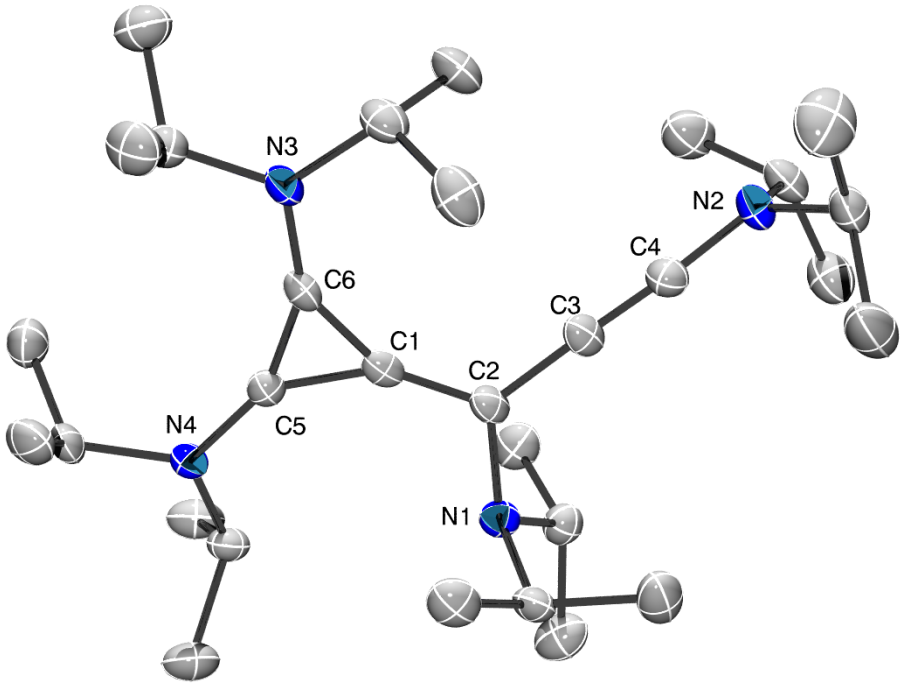

Figure 6.3. Solid-state molecular structure of **6.3**, shown with 50% probability ellipsoids. Hydrogen atoms removed for clarity. Selected bond lengths (Å) and angles (°): C1-C2 = 1.370(3), C1-C5 = 1.408(3), C1-C6 = 1.418(3), C2-C3 = 1.403(3), C6-C5 = 1.359(3), C6-N3 = 1.363(3), C5-N4 = 1.358(3), C2-N1 = 1.478(3), C4-N2 = 1.355(3), C3-C4 = 1.211(3), C6-C1-C2 = 153.6(2), C5-C1-C6 = 57.5(2), C5-C1-C2 = 148.9(3) C4-N2-C22 = 118.4(2), C4-N2-C21 = 116.8(2), C22-N2-C21 = 117.5(2).

6.2.2 Photochemical Reactivity of 6.1

Given the similar optical properties of **6.1** and [Ce(NR$_2$)$_3$], I hypothesized that photolysis of **6.1** would also generate a highly reducing photo-excited state, which could initiate a *C*-atom transfer to the Ce center. Photolysis of a benzene-d_6 solution of **6.1**, in an NMR tube equipped with a J-Young valve, using a 365 nm LED lightstrip slowly generated a new diamagnetic product, according to the ^{1}H NMR spectrum. This spectrum features four new magnetically inequivalent diisopropylamino groups, as evidenced by septets at 4.37, 3.61, 3.59, and 3.00 ppm. Also present in this spectrum is free [Ce(NR$_2$)$_3$], as evidenced by a broad singlet at -3.38 ppm (Scheme 6.3 and Figure A6.3). The new diamagnetic product was identified as the methylenecyclopropeneyne, [(^{i}Pr$_2$N)$_2$C$_3$C(N^{i}Pr$_2$)(CCN^{i}Pr$_2$)] (**6.3**), by X-ray crystallography, which is evidently formed by a photo-induced dimerization of the BAC ligand.

Scheme 6.3. Synthesis of [(^{i}Pr$_2$N)$_2$C$_3$C(N^{i}Pr$_2$)(CCN^{i}Pr$_2$)] (**6.3**).

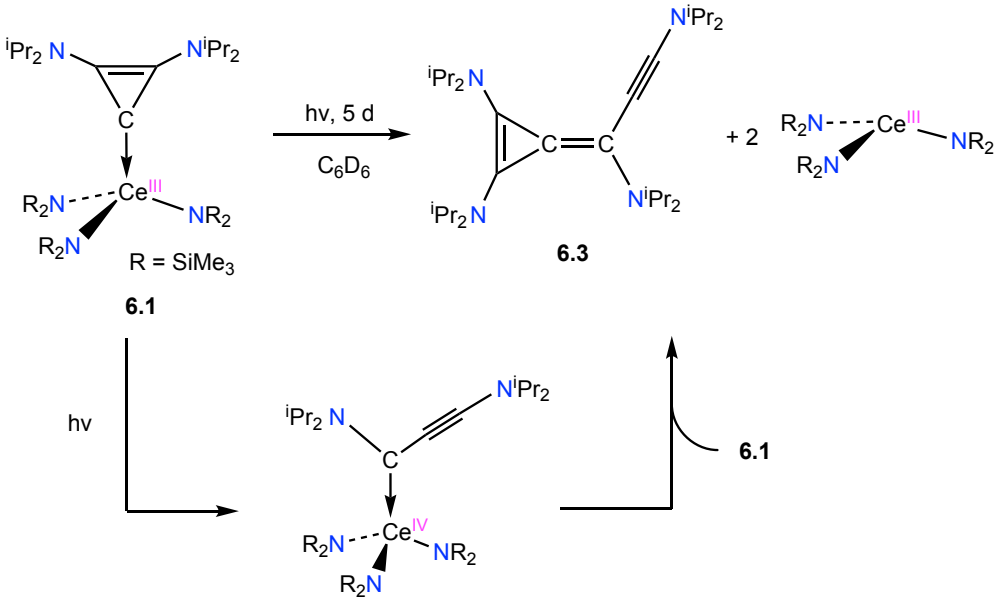

Compound **6.3** crystalizes in the monoclinic space group $P2_1/c$ (Figure 6.3). The C1-C2 (1.370(3) Å) and C6-C5 (1.359(3) Å) distances are somewhat longer than those expected for a C-C double bond, whereas the C1-C5 (1.408(3) Å) and C1-C6 (1.418(3) Å) distances are shorter than those expected for a C-C single bond (Figure 6.4). Overall, these metrical parameters are evidence of mesoionic character in **6.3**. For comparison, the metrical parameters of the methylenecyclopropene unit in **6.3** are essentially identical with those previously reported for 4,4-dicyano-2,3-diphenyltriafulvene (Figure 6.4),[44] which was also thought to feature considerable mesoionic character.[45]

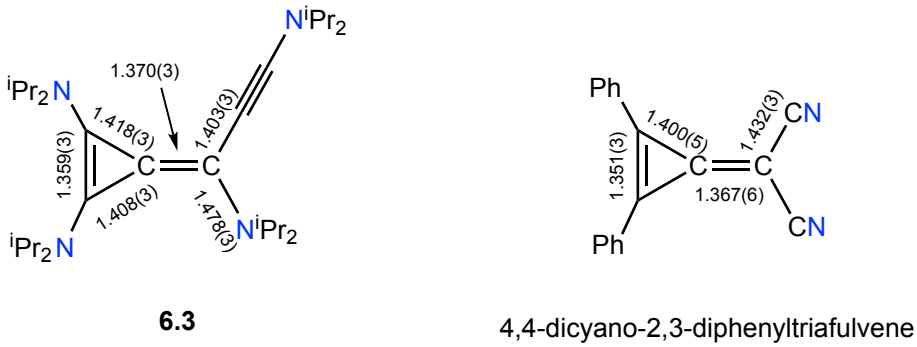

Figure 6.4. Comparison of the metrical parameters of **6.3** and 4,4-dicyano-2,3-diphenyltriafulvene.[44] Bond lengths are reported in Å.

The unsubstituted methylenecyclopropene fragment is highly reactive and has only been observed at low temperatures (ca. -95 °C).[46-49] Alkyl-substituted methylenecyclopropenes are somewhat more stable, but still decompose quickly at ambient temperatures.[50] In contrast, **6.3** shows no evidence of decomposition at room temperature even over the course of several weeks. No doubt, the enhanced thermal stability of **6.3** is due to its strongly donating diisopropylamino substituents. Similar thermal stability is seen with Bertrand's tetra(amino)-substituted methylenecyclopropene, likely for similar reasons.[51] That said, **6.3** is still highly

reactive. For instance, attempts to isolate and purify **6.3** using an aqueous work-up result in its complete decomposition, which is likely initiated by protonation at C2. Because of this reactivity, and its similar solubility with [$Ce(NR_2)_3$], I was unable to isolate analytically pure samples of **6.3**.

To rationalize the formation of **6.3**, I hypothesized that photolysis of **6.1** results in a redox-mediated ring opening of the BAC fragment, followed by a 1,2-nitrogen shift to generate a transient Ce(III) amino alkynyl carbene, [$Ce(^iPr_2NCC{\equiv}CN^iPr_2)(NR_2)_3$], which subsequently reacts with the BAC fragment in unreacted **6.1** to form the cross-coupled product **6.3** and regenerate [$Ce(NR_2)_3$] (Scheme 6.3). In support of this proposed mechanism, I note that Bertrand has previously observed coupling of the highly nucleophilic BAC to both cyclic alkyl(amino) carbenes (CAACs) and six- and seven-membered diamido carbenes (DACs).[51] In addition, Bertrand has also reported the ring opening of BAC fragment.[51, 52]

The reformation of [$Ce(NR_2)_3$] during the photolysis of **6.1** suggests that **6.3** could be generated in a catalytic manner. To test this hypothesis, I photolyzed a C_6D_6 solution of BAC in the presence of 10 mol% [$Ce(NR_2)_3$] (eq 6.1). Exposure of this mixture to blue light from a 365 nm LED lightstrip, over the course of 6 d, resulted in 90% conversion of BAC to **6.3** (Figure A6.4). Control experiments reveal that the formation of **6.3** is, in fact, catalyzed by [$Ce(NR_2)_3$]. For instance, photolysis of a benzene-d_6 solution of BAC alone for 20 h resulted in partial decomposition of the BAC starting material, according to ^{1}H NMR spectroscopy (Figure A6.7), but no formation of **6.3**. Likewise, thermolysis of **6.1** at 50 °C for 2 d, in the absence of light, resulted in partial decomposition of **6.1**, but no formation of **6.3**, according to the ^{1}H NMR spectrum of the reaction mixture (Figure A6.6).

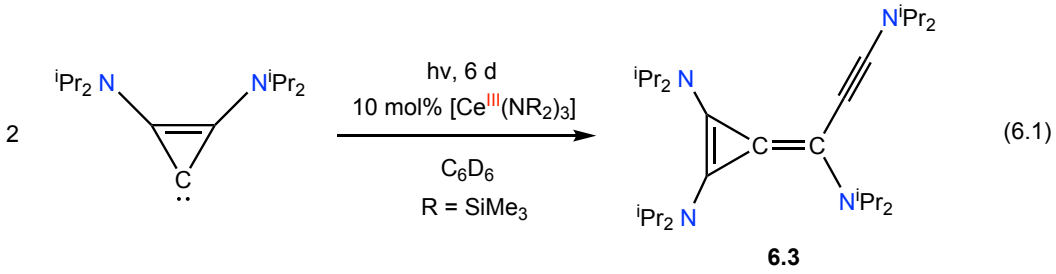

(6.1)

6.2.3 Thermolytic Reactivity of 6.2

To explore the reactivity of the uranium(III) BAC adduct, I heated a benzene-d_6 solution of **6.2**, in an NMR tube equipped with a J-Young valve, and slowly observed the generation of a new paramagnetic product, as well the uranium metallacycle, $[U\{N(R)(SiMe_2)CH_2\}(NR_2)_2]$,[53] in a 1:0.75 ratio, respectively, according to the ^{1}H NMR spectrum (Scheme 6.4, Figure A6.9). Work up of this reaction mixture followed by slow evaporation of a concentrated pentane solution affords a mixture of $[U\{N(R)(SiMe_2)CH_2\}(NR_2)_2]$, as yellow needles and $[(NR_2)_2U\{N(R)(SiMe_2)(2,3\text{-}(N^iPr_2)\text{-}C(H)C{=}CC(H))\}]$ (**6.4**), as yellow plates. The ^{1}H NMR spectrum of **6.4** in benzene-d_6 shows a complex NMR spectrum with four inequivalent $SiMe_3$ environments, at 19.92, 7.65, -19.65 and -24.80 ppm, as well as nine isopropyl methyl environments located at 21.61, 9.27, 7.32, -0.91, -3.92, -5.27, 6.46, -16.36, and -17.95 ppm, suggestive of C_1 symmetry in solution (Figure A6.8). It should be noted that one $SiMe_3$ environment, the isopropyl methine proton environments, and the dienyl proton resonances could not be located in the ^{1}H NMR spectrum, while resonances assignable to $[U\{N(R)(SiMe_2)CH_2\}(NR_2)_2]$ are also still present. Unfortunately, due to the low yields and high solubility of complex **6.4** in non-polar solvents (including pentane, HMDSO, hexanes and isooctane), the isolation analytically pure samples eluded me and I was unable to complete the characterization of this material.

Scheme 6.4. Synthesis of Complex **6.4**.

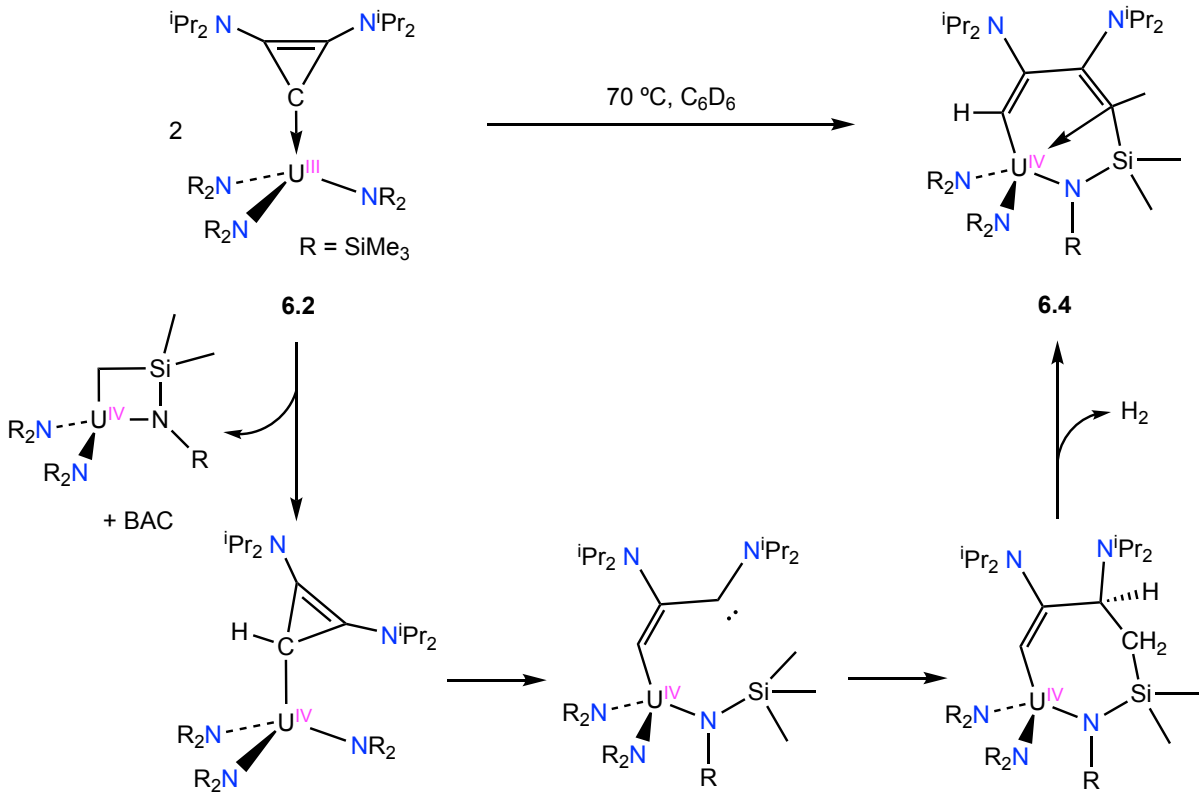

The connectivity of **6.4** was, however, confirmed by X-ray crystallography. Complex **6.4** crystalizes in the monoclinic space group $P2_1/n$ (Figure 6.5). The U-C_α bond distance is 2.401(4) Å and is somewhat shorter than the previously reported U(IV)-vinyl complexes [{((^{Ad}ArO)$_3$N)U^{IV}}$_2$(μ–η^2:η^1-1,2-(CH)$_2$-cyclohexane)] (2.511(5), 2.434(5) Å) and [{((^{Ad}ArO)$_3$N)U^{IV}}$_2$(μ–η^2:η^1-1,2-(CH)$_2$-cyclopentane)] (2.549(4), 2.503(5) Å), likely on account of reduced steric interactions between the dienyl ligand and silylamide co-ligands in **6.4**.[54] For further comparison, the U-C_α bond distance in **6.4** is slightly shorter than that seen for the U-allenyl complex **5.1** (2.457(3) Å). Complex **6.4** also exhibits a weak interaction between the uranium center and C4 (2.894(5) Å). The C1-C2 and C3-C4 bond distances

(1.356(6) and 1.384(6) Å, respectively) and C2-C3 bond distance (1.503(6) Å) are consistent with the formation of a metallacyclic dienyl moiety.

To account for the formation of **6.4**, I propose that the reaction proceeds via an initial hydrogen atom abstraction from 0.5 equiv of **6.2**, resulting in loss of 0.5 equiv BAC and [U{N(R)($SiMe_2$)CH_2}(NR_2)$_2$] (Scheme 6.4). Subsequent cyclopropenyl ring opening results in generation of a transient carbene, which can then insert undergo C–H insertion into a $SiMe_3$ methyl group and H_2 elimination to afford the final product, **6.4**. To support the proposed mechanism, I note the near 1:1 formation of [U{N(R)($SiMe_2$)CH_2}(NR_2)$_2$] and **6.4** in crude mixtures (Figure A6.9). While I would also expect to observe the formation of free BAC, the instability of this molecule likely results in its decomposition over the course of the reaction. Furthermore [U(NR_2)$_3$] has been previously shown to act as an efficient H-atom donor.[55, 56]

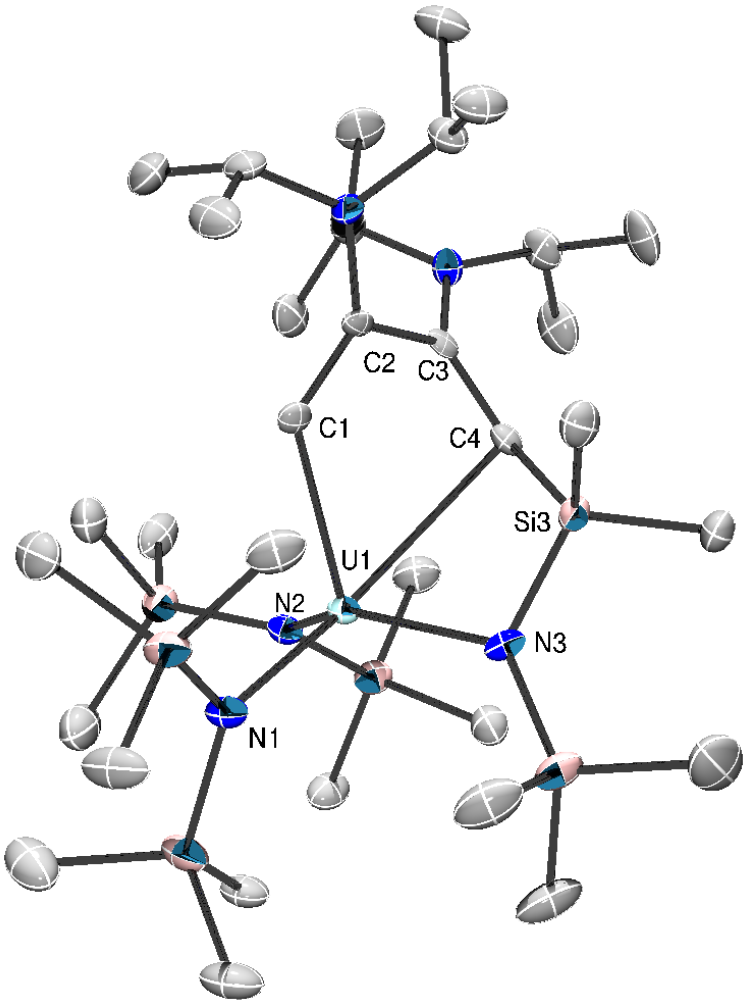

Figure 6.5. Solid-state molecular structure of **6.4**, shown with 50% probability ellipsoids. Hydrogen atoms removed for clarity. Selected bond lengths (Å) and angles (°): U1-N1 = 2.292(4), U1-N2 = 2.293(4), U1-N3 = 2.274(4), U1-C1 = 2.401(4), U1-C4 = 2.894(5), C1-C2 = 1.356(6), C2-C3 = 1.503(6), C3-C4 = 1.384(6), Si3-C4 = 1.868(5), N1-U1-N2 = 108.3(1), N1-U1-N3 = 98.0 (1), N2-U1-N3 = 136.3(1), U1-C1-C2 = 123.7(3).

6.3 Summary

In summary, I have explored the coordination chemistry of $[M(NR_2)_3]$ (M = Ce, U) with bis(diisopropylamino)cyclopropenylidene (BAC). Photolysis of $[(NR_2)_3Ce(BAC)]$ (**6.1**) or

thermolysis of $[(NR_2)_3U(BAC)]$ **6.2**, does not result in the originally envisioned carbon-atom transfer, but instead results in ligand rearrangement. In the case of $[(NR_2)_3Ce(BAC)]$, I isolate the methylenecyclopropene species, $[(^iPr_2N)_2C_3C(N^iPr_2)(CCN^iPr_2)]$ (**6.3**), which is generated by the formal dimerization and rearrangement of two BAC fragments. While in the case of $[(NR_2)_3U(BAC)]$, I isolate the ring opened and dienyl product, $[(NR_2)_2U\{N(R)(SiMe_2)(2,3\text{-}(N^iPr_2)\text{-}C(H)C{=}CC(H))\}]$ (**6.4**), along with $[U\{N(R)(SiMe_2)CH_2\}(NR_2)_2]$. While ultimately unsuccessful in my efforts to generate either a carbide or alkylidene complex, this work expands the scope of Ce(III)-mediated photochemistry, which is an emerging area of photocatalysis. In addition, I have discovered a new synthetic pathway to the highly reactive methylenecyclopropene fragment, which is of interest for its insights into aromaticity, as well as its use as a precursor to spiro-compounds.[57-61]

6.4 Experimental

6.4.1 General. All reactions and subsequent manipulations were performed under anaerobic and anhydrous conditions under an atmosphere of nitrogen. Hexanes, Et_2O, and toluene were dried using a Vacuum Atmospheres DRI-SOLV Solvent Purification system and stored over 3Å sieves for 24 h prior to use. THF was dried by distillation from sodium/ benzophenone, and stored over 3Å sieves for 24 h prior to use. Benzene-d_6 and THF-d_8 were dried over 3Å molecular sieves for 24 h prior to use. $[Ce(N(SiMe_3)_2)_3]$, $CNNPPh_3$, and BAC were synthesized according to the previously reported procedures.[34, 39, 62] All other reagents were purchased from commercial suppliers and used as received.

NMR spectra were recorded on an Agilent Technologies 400-MR DD2 400 MHz Spectrometer or a Varian UNITY INOVA 500 spectrometer. ^1H NMR spectra were referenced

to external tetramethylsilane (TMS) using the residual protio solvent peaks as internal standards. $^{13}C\{^{1}H\}$ and $^{31}P\{^{1}H\}$ NMR spectra were referenced indirectly with the ^{1}H resonance of TMS at 0.0 ppm, according to IUPAC standard,[63, 64] using the residual solvent peaks as internal standards. Lumcrissy 12V flexible LED Lightstrips, emitting at 380 nm, and Waveform lighting 12V flexible LED Lighstrips, emitting at 365 nm, were used for photolyses. IR spectra were recorded on a Nicolet 6700 FT-IR spectrometer with a NXR FT Raman Module. Electronic absorption spectra were recorded on a Shimadzu UV3600 UV-NIR Spectrometer. Elemental analyses were performed by the Micro-Analytical Facility at the University of California, Berkeley.

6.4.2 Synthesis of $[(NR_2)_3Ce(BAC)]$ (6.1). To a stirring deep yellow solution of $[Ce(N(SiMe_3)_2)_3]$ (120.6 mg, 0.194 mmol) in diethyl ether (2 mL) was added a light-yellow solution of BAC (45.9 mg, 0.194 mmol) in diethyl ether (2 mL). After stirring for 30 min the volatiles were removed *in vacuo* to yield a dark yellow solid. The solid was then extracted into pentane (5 mL) and the yellow orange solution was filtered through a Celite column supported on glass wool (0.5 × 2 cm). The yellow filtrate was concentrated *in vacuo* to 2 mL and layered onto HMDSO (4 mL). Storage of this solution for 24 h at -25 ºC resulted in the deposition of X-ray quality pale yellow plates. The crystals were isolated by decanting the supernatant and then dried *in vacuo* to afford **6.1**. Yield: 0.098 g, 60% yield. Anal. Calcd for $CeN_5Si_6C_{33}H_{69}$: C, 46.93; H, 8.23; N, 8.23. Found: C, 46.39; H, 9.78; N, 8.00. ^{1}H NMR (400 MHz, 25 °C, C_6D_6): δ -2.25 (s, 54H, SiC*H*$_3$), 0.01 (br s, 12H, CHC*H*$_3$), 0.81 (br s, 12H, CHC*H*$_3$), 3.12 (br s, 4H, C*H*CH$_3$). UV-Vis/NIR (C_6H_6, 0.49 mM, 25 °C, L·mol^{-1}·cm^{-1}): 343 nm (ε = 352), 380 (sh). IR (KBr pellet, cm^{-1}): 538(w), 597(s), 665(s), 674(m), 752(s), 767(s), 825(vs), 935(m), 977(s),

1114(m), 1182(w), 1245(s), 1322 (w), 1363(w), 1370(m), 1470(s), 1521(w), 1614(w), 1625(w), 1828(s), 2898(m), 2956(s).

6.4.3 Synthesis of [(NR$_2$)$_3$U(BAC)] (6.2). To a stirring deep purple solution of [U(N(SiMe$_3$)$_2$)$_3$] (122.0 mg, 0.170 mmol) in diethyl ether (2 mL) was added a light-yellow solution of BAC (40.1 mg, 0.170 mmol) in diethyl ether (2 mL). After stirring for 30 min the volatiles were removed *in vacuo* to yield a dark green solid. The solid was then extracted into pentane (5 mL) and the green solution was filtered through a Celite column supported on glass wool (0.5 × 2 cm). The green filtrate was concentrated *in vacuo* to 2 mL and layered onto HMDSO (4 mL). Storage of this solution for 24 h at -25 ºC resulted in the deposition of X-ray quality dark green-blue plates. The crystals were isolated by decanting the supernatant and then dried *in vacuo* to afford **6.2**. Yield: 0.100 g, 62% yield. ^{1}H NMR (400 MHz, 25 °C, THF-d_8): δ -2.60 (br s, 24 H, CHC*H*$_3$), -6.43 (s, 54H, SiC*H*$_3$), -9.88 (br s, 4 H, C*H*CH$_3$).

6.4.4 Synthesis of [(^{i}Pr$_2$N)$_2$C$_3$C(N^{i}Pr$_2$)(CCN^{i}Pr$_2$)] (6.3). An NMR tube fitted with a J-Young valve was charged with a light-yellow solution of BAC (25.0 mg, 0.106 mmol), [Ce(N(SiMe$_3$)$_2$)$_3$] (65.7 mg, 0.106 mmol), and C$_6$D$_6$ (1 mL). A ^{1}H NMR spectrum was then recorded (Figure A6.3). ^{1}H NMR (400 MHz, 25 °C, C$_6$D$_6$): δ -2.25 (s, 54H, SiC*H*$_3$), 0.01 (br s, 12H, CHC*H*$_3$), 0.81 (br s, 12H, CHC*H*$_3$), 3.12 (br s, 4H, C*H*CH$_3$). This mixture was then placed into an aluminum foil-wrapped beaker with a 4 ft (0.7 watts/ ft), 365 nm LED strip lining the inside. The internal temperature of the beaker was determined to be 50 °C during photolysis. After 5 d of photolysis, the NMR tube was brought back into the glove box, where the solution was transferred to a 20 mL scintillation vial and the volatiles were removed *in vacuo* to afford a dark orange oil. The oil was extracted into pentane (2 mL) and the resulting

orange solution was filtered through a Celite column supported on glass wool (0.5 × 2 cm). The orange filtrate was concentrated *in vacuo* to 1 mL and stored at -25 ºC for 24 h, which resulted in the deposition of yellow needles of [Ce(N(SiMe$_3$)$_2$)$_3$], whose identity was confirmed by comparison of its ^{1}H NMR spectrum and unit cell to the literature values.[1, 11] The supernatant was decanted away and the volatiles were removed *in vacuo* to afford a dark orange oil. This oil was then stored at -25 ºC for 24 h, which resulted in the deposition of a few colorless X-ray quality crystals of **6.3** on the vial walls. It should be noted that these crystals quickly melt when taken out of the freezer.

6.4.5 Catalytic Synthesis of 6.3. An NMR tube fitted with a J-Young valve was charged with a light-yellow solution of BAC (30 mg, 0.127 mmol) and [Ce(N(SiMe$_3$)$_2$)$_3$] (10 mol%, 7.9 mg, 0.012 mmol) in C_6D_6 (1 mL). A ^{1}H NMR spectrum was then recorded (Figure A6.4). ^{1}H NMR (500 MHz, 25 °C, C_6D_6): δ -2.26 (s, 54H, SiC*H*$_3$), 1.24 (br s, 24h, C*H*$_3$), 3.47 (br s, 4H, C*H*). This mixture was then placed into an aluminum foil-wrapped beaker with a 4 ft (0.7 watts/ft), 365 nm LED strip lining the inside. The photolysis was monitored intermittently by ^{1}H NMR spectroscopy. After 6 d of photolysis, hexamethylbenzene (HMB) (1.0 mg, 0.006 mmol) was added to the NMR tube as an internal standard, and the conversion was determined to be 90%. The NMR tube was brought back into the glove box, the solution was transferred to a 20 mL scintillation vial, and the volatiles were removed *in vacuo* to afford a dark orange oil (35.8 mg). ^{1}H NMR (500 MHz, 25 °C, benzene-d_6) δ: 4.37 (septet, J = 6.8 Hz, 2H, (C*H*(CH$_3$)$_2$)$_2$), 3.61 (septet, J = 6.8 Hz, 2H, (C*H*(CH$_3$)$_2$)$_2$), 3.59 (septet, J = 6.8 Hz, 2H, (C*H*(CH$_3$)$_2$)$_2$), 3.00 (septet, J = 6.8 Hz, 2H, (C*H*(CH$_3$)$_2$)$_2$), 2.13 (s, 18H, HMB), 1.40 (d, J = 6.8 Hz, 6H, (CH(C*H*$_3$)$_2$)$_2$), 1.38 (d, J = 6.8 Hz, 6H, (CH(C*H*$_3$)$_2$)$_2$), 1.32 (d, J = 6.8 Hz, 12H, (CH(C*H*$_3$)$_2$)$_2$), 1.28 (d, J = 6.8 Hz, 12H, (CH(C*H*$_3$)$_2$)$_2$), 1.12 (d, J = 6.8 Hz, 12H, (CH(C*H*$_3$)$_2$)$_2$),

-2.22 (s, N(Si(CH_3)$_3$)$_2$). ^{13}C{^{1}H} NMR (126 MHz, 25 °C, benzene-d_6) δ: 123.91 (N*C*=CN), 115.24 (NC=*C*N), 107.76 (*C*=C-C≡C-N(CH(CH$_3$)$_2$)$_2$), 90.13 (C=C-*C*≡C-N(CH(CH$_3$)$_2$)$_2$), 73.69 (C=C-C≡*C*-N(CH(CH$_3$)$_2$)$_2$), 71.14 (C=*C*-C≡C-N(CH(CH$_3$)$_2$)$_2$), 52.97 (*C*H(CH$_3$)$_2$), 49.14 (*C*H(CH$_3$)$_2$), 49.11 (*C*H(CH$_3$)$_2$), 48.68 (*C*H(CH$_3$)$_2$), 21.98 (CH(*C*H$_3$)$_2$), 21.92 (CH(*C*H$_3$)$_2$), 21.89 (CH(*C*H$_3$)$_2$), 21.22 (CH(*C*H$_3$)$_2$).

6.4.6 Thermolysis of 6.1. An NMR tube fitted with a J-Young valve was charged with a light-yellow solution of BAC (5.7 mg, 0.024 mmol) and [Ce(N(SiMe$_3$)$_2$)$_3$] (15.1 mg, 0.024 mmol) in C_6D_6 (1 mL). A ^{1}H NMR spectrum was then recorded (Figure A6.6). ^{1}H NMR (400 MHz, 25 °C, C_6D_6): δ -2.25 (s, 54H, SiC*H*$_3$), 0.01 (br s, 12H, CHC*H*$_3$), 0.81 (br s, 12H, CHC*H*$_3$), 3.12 (br s, 4H, C*H*CH$_3$). This mixture was then wrapped in aluminum foil and heated to 50 °C. After 2 d, a ^{1}H NMR spectrum was re-recorded, which revealed the absence of **6.3**, along with the formation of several unidentified decomposition products. Complex **6.1** had decomposed by approximately 15%, according to the integration of its silylmethyl resonances against the solvent peak before and after thermolysis (Figure A6.6).

6.4.7 Photolysis of BAC. An NMR tube fitted with a J-Young valve was charged with a light-yellow solution of BAC (3.6 mg, 0.015 mmol) in C_6D_6 (0.5 mL) and exposed to blue light in an aluminum foil-wrapped beaker with a 4 ft (0.7 watts/ft) 365 nm LED strip lining the inside. A ^{1}H NMR spectrum was recorded after 20 h, which revealed the absence of **6.1**, along with the formation of several unidentified decomposition products. The BAC had decomposed by approximately 20%, according to the integration of its isopropyl resonances against the solvent peak before and after thermolysis (Figure A6.7).

6.4.8 Synthesis of [$(NR_2)_2U\{N(R)(SiMe_2)(2,3\text{-}(N^iPr_2)\text{-}C(H)C{=}CC(H))\}$] (6.4). An NMR tube fitted with a J-Young valve was charged with a green-blue solution of BAC (35.5 mg, 0.151 mmol), [$U(N(SiMe_3)_2)_3$] (108.6 mg, 0.151 mmol), and C_6D_6 (1 mL) and heated for 3 d at 50 ºC. After heating for 3d the conversion to **6.4** was confirmed via ^{1}H NMR spectroscopy. The NMR tube was brought back into the glove box, the solution was transferred to a 20 mL scintillation vial, and the volatiles were removed *in vacuo* to afford a dark brown oil. The oil was extracted into pentane (1 mL) and the resulting brown solution was filtered through a Celite column supported on glass wool (0.5 × 2 cm) and transferred to a 4 mL scintillation vial. This vial was placed into a 20 mL scintillation vial and the solution was concentrated to 0.5 mL. Isooctane (2 mL) was added to the outer vial and storage of this two-vial system at -25 ºC for 1 w resulted in the deposition of yellow-brown plates. Decanting the supernatant and drying *in vacuo* afforded **6.4** ^{1}H NMR (600 MHz, Benzene-d_6) δ 21.61 (s, 3H, ^{i}PrMe), 19.92 (s, 9H, $SiMe_3$), 9.27 (s, 3H, ^{i}PrMe), 7.65 (s, 9H, $SiMe_3$), 7.32 (s, 3H, ^{i}PrMe), -0.91 (s, 3H, ^{i}PrMe), -3.92 (s, 3H, ^{i}PrMe), -5.27 (s, 3H, ^{i}PrMe), -6.46 (s, 3H, ^{i}PrMe), -16.36 (s, 3H, ^{i}PrMe), -17.95 (s, 3H, ^{i}PrMe), -19.65 (s, 9H, $SiMe_3$), -24.80 (s, 9H, $SiMe_3$).

6.4.9 X-ray Crystallography. Data for **6.1**, **6.2**, **6.3**, and **6.4** were collected on a Bruker KAPPA APEX II diffractometer equipped with an APEX II CCD detector using a TRIUMPH monochromator with a Mo Kα X-ray source (α = 0.71073 Å). The crystals were mounted on a cryoloop under Paratone-N oil. Complexes **6.1**, **6.2**, **6.3** and **6.4** were collected at 100(2) K, 110(2) K, 123(2) K, and 113(2) K, respectively, using an Oxford nitrogen gas cryostream. Data were collected using ω scans with 0.5° frame widths. Frame exposures of 15, 10, 20, and 20 seconds were used for **6.1**, **6.2**, **6.3**, and **6.4**, respectively. Data collection and cell parameter determinations were conducted using the SMART program.[65] Integration of the data frames and final cell parameter refinements were performed using SAINT software.[66] Absorption corrections of the data were carried out using the multi-scan method SADABS for **6.2**-**4**, and TWINABS for **6.1**.[67,9] Subsequent calculations were carried out using SHELXTL.[10] Structure determination was done using direct or Patterson methods and difference Fourier techniques. All hydrogen atom positions were idealized, and rode on the atom of attachment. Structure solution, refinement, graphics, and creation of publication materials were performed using SHELXTL.[68] Further crystallographic details can be found in Table 6.1.

Table 6.1. X-ray Crystallographic Data for **6.1**, **6.2**, **6.3** and **6.4**.

	6.1	**6.2**	**6.3**	**6.4**
empirical formula	$C_{33}H_{82}N_5Si_6Ce$	$C_{33}H_{82}N_5Si_6U$	$C_{30}H_{56}N_4$	$C_{33}H_{81}UN_5Si_6$
crystal habit, color	Block, Yellow	Plate, Dark Green	Block, Colorless	Plate, yellow
crystal size (mm)	0.2 × 0.15 × 0.15	0.25 × 0.10 × 0.05	0.2 × 0.2 × 0.1	0.2 × 0.1 × 0.05
space group	$P2_1/c$	$P2_1/c$	$P2_1/c$	$P2_1/n$
volume (Å^3)	4858.5(10)	4853.6(4)	3139.1(11)	4688.2(7)
a (Å)	19.658(2)	19.7027(8)	12.507(2)	10.8501(9)
b (Å)	12.588(2)	12.5449(5)	11.416(2)	18.2485(14)
c (Å)	19.736(2)	19.7335(9)	22.608(5)	24.039(2)
α (deg)	90	90	90	90
β (deg)	95.823(3)	95.679(3)	103.476(9)	99.941(2)
γ (deg)	90	90	90	90
Z	4	4	4	4
formula weight (g/mol)	857.69	955.60	472.78	954.59
density (calculated) (Mg/m^3)	1.173	1.308	1.000	1.352
absorption coefficient (mm^{-1})	1.111	3.518	0.058	3.642
F_{000}	1828	1964	1056	1960
total no. reflections	36544	30801	11063	21322
unique reflections	12437	11743	5596	9610
Final R Indices	$R_1 = 0.0526$	$R_1 = 0.0362$	$R_1 = 0.0621$	$R_1 = 0.0331$
(I >2σ(I)]	$wR_2 = 0.0658$	$wR_2 = 0.0556$	$wR_2 = 0.0745$	$wR_2 = 0.0622$
largest diff. peak and hole (e$^-$ A^{-3})	0.890 and 0.834	0.706 and -0.736	0.258 and -0.196	1.784 and -0.912
GOF	1.043	0.986	1.220	0.849

6.5 Appendix

6.5.1 NMR Spectra

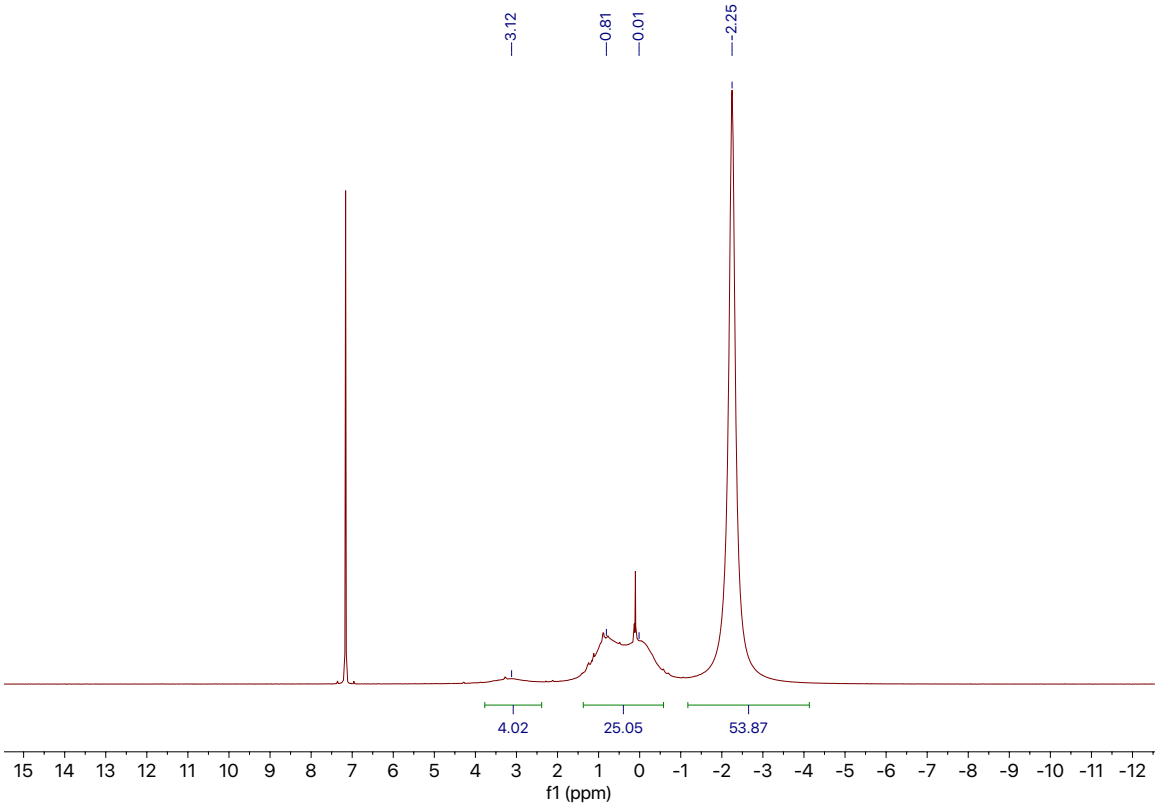

Figure A6.1. ^{1}H NMR spectrum of [$(NR_2)_3$Ce(BAC)] (**6.1**) in C_6D_6.

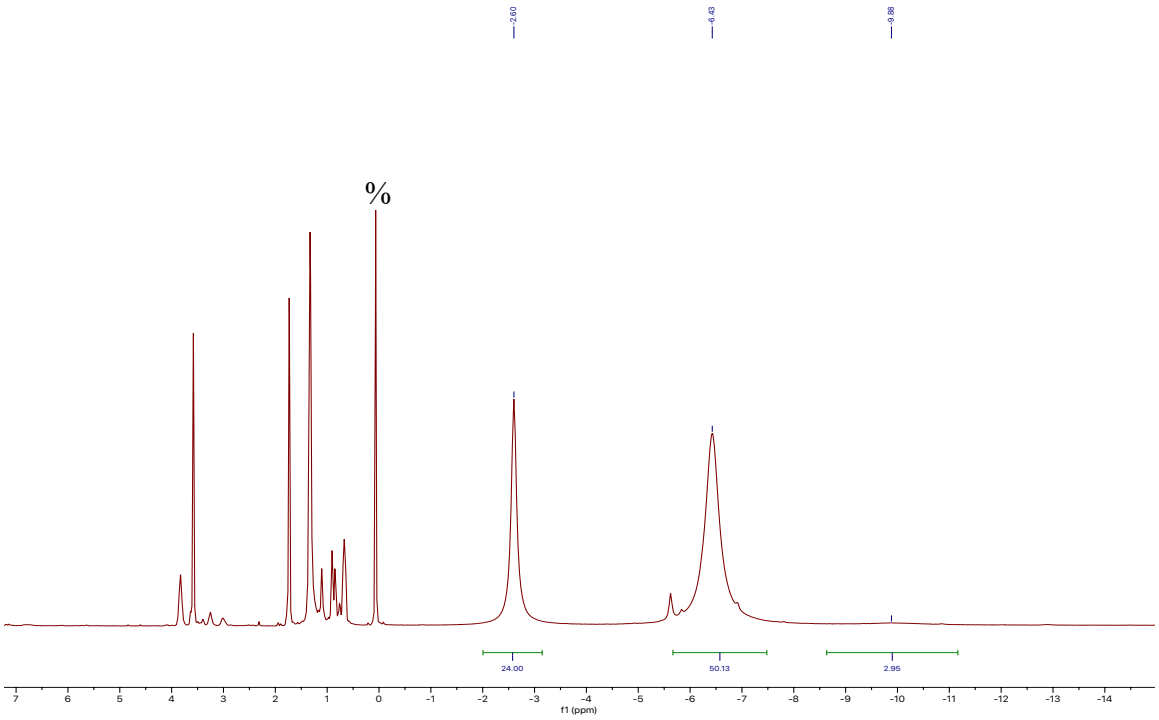

Figure A6.2. ^{1}H NMR spectrum of [$(NR_2)_3U(BAC)$] (**6.2**) in THF-d_8. (%) indicates the presence of free $HN(SiMe_3)_2$.

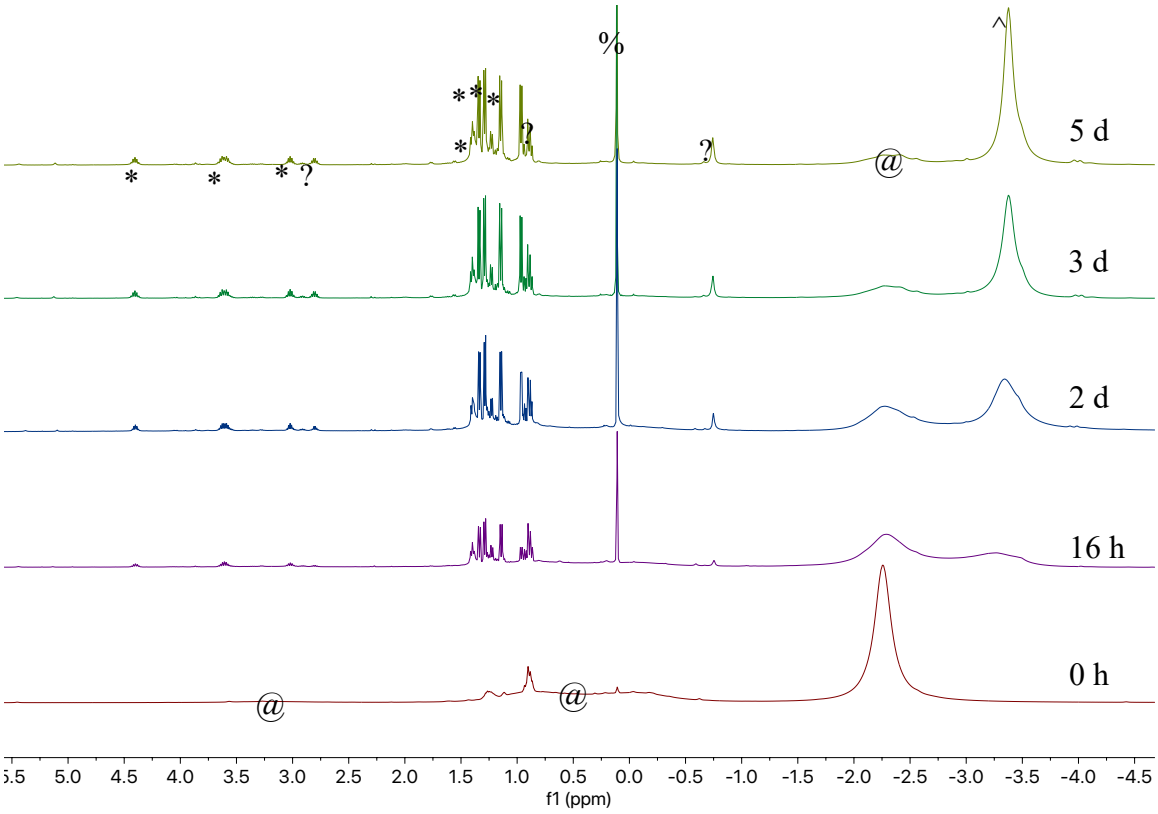

Figure A6.3. Partial ^{1}H NMR spectra of the photolysis of **6.1** in C_6D_6 over 5 days. (*) indicates **6.3**, (@) indicates **6.1**, (^) indicates [Ce(N(SiMe$_3$)$_2$)$_3$], (%) indicates the presence of free HN(SiMe$_3$)$_2$, and (?) indicates an unidentified by-product.

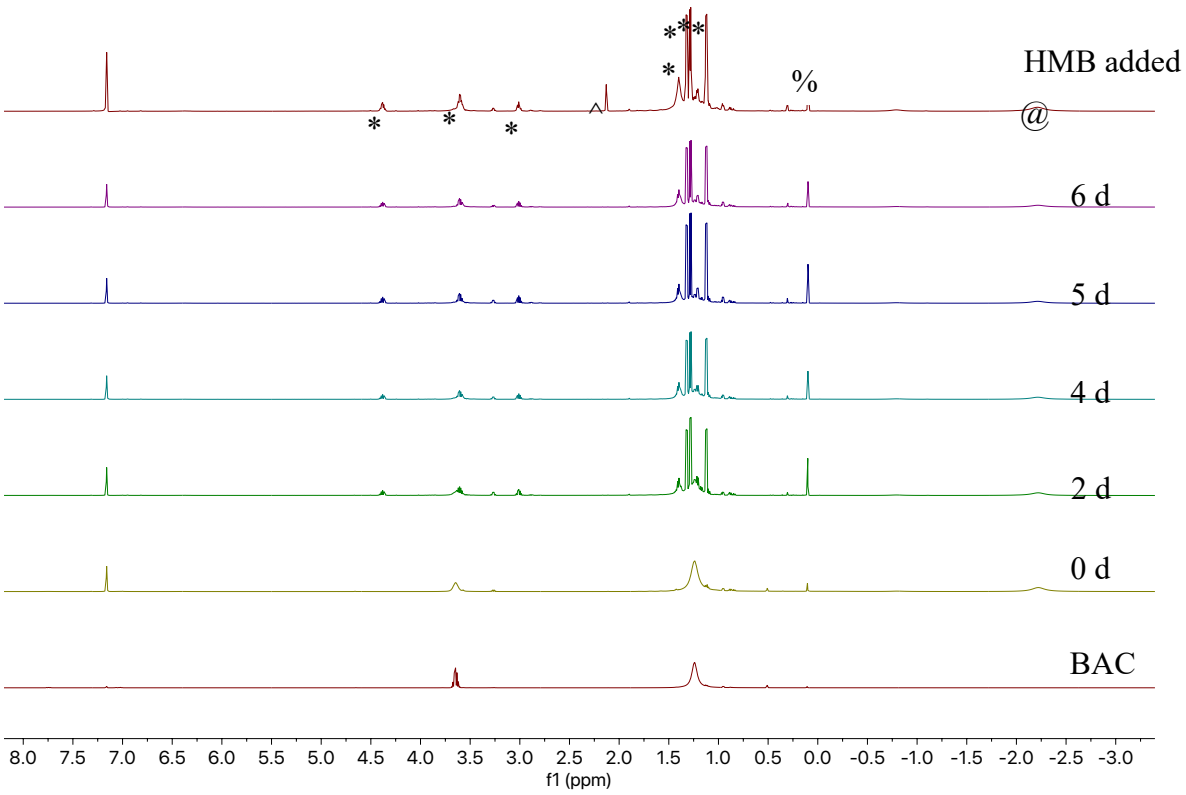

Figure A6.4. ^{1}H NMR spectra of the photocatalytic generation of **6.3**, in the presence of 10 mol% of $[Ce(N(SiMe_3)_2)_3]$, over the course of 6 d in C_6D_6. (*) indicates **6.3**, (@) indicates **6.1**, (^) indicates hexamethylbenzene (HMB), (%) indicates the presence of free $HN(SiMe_3)_2$.

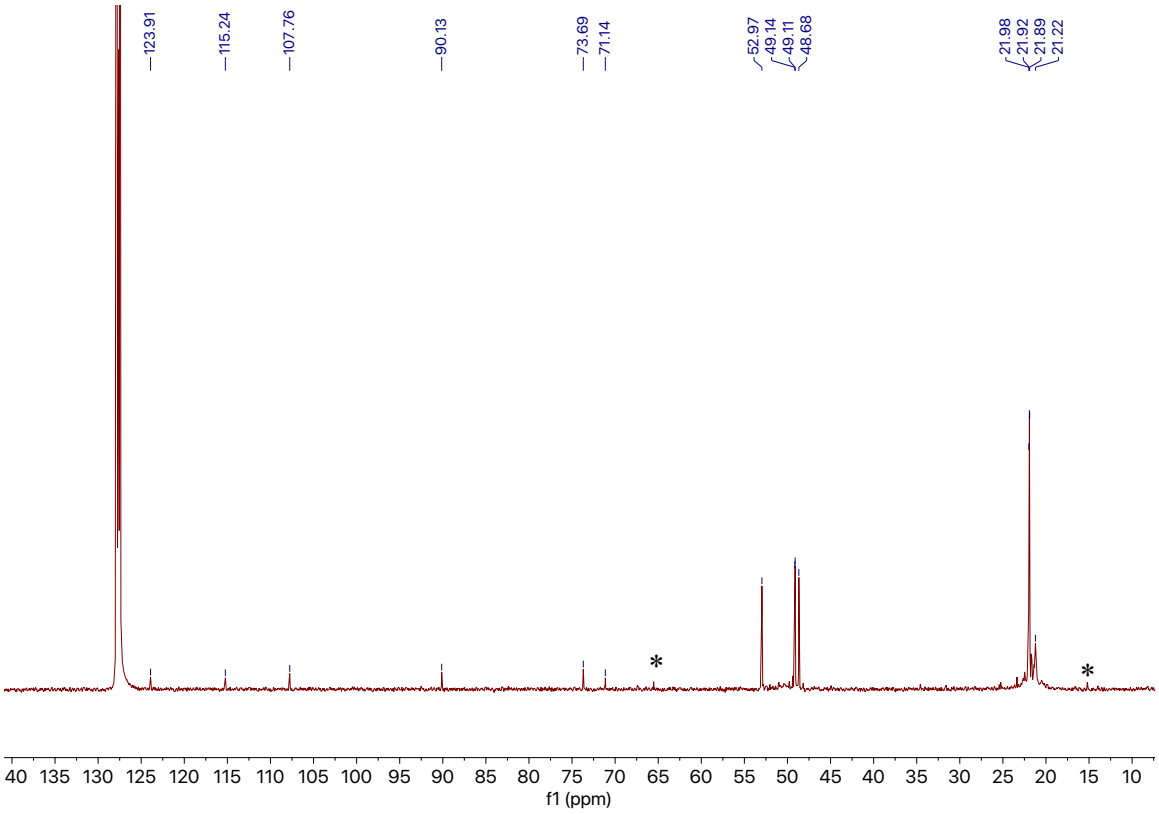

Figure A6.5. $^{13}C\{^{1}H\}$ NMR spectrum of the photocatalytic generation of **6.3**, in the presence of 10 mol% of $[Ce(N(SiMe_3)_2)_3]$, after 6 d in C_6D_6. (*) indicates Et_2O.

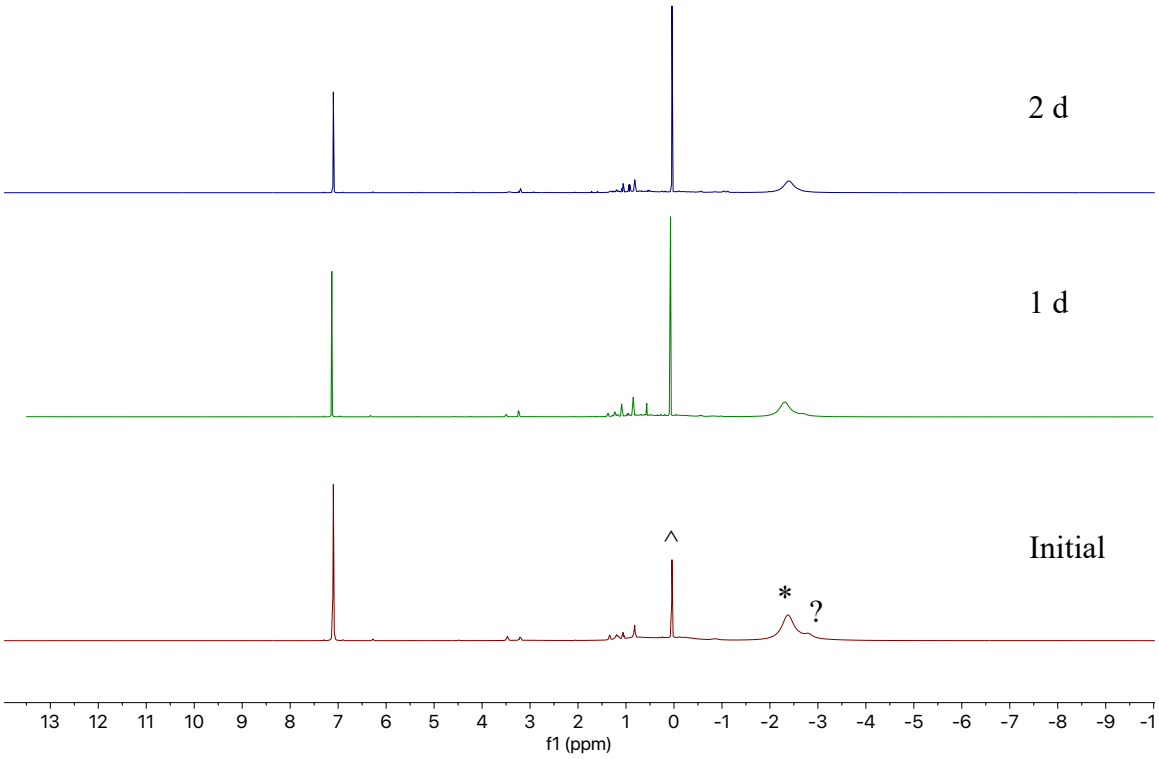

Figure A6.6. ^{1}H NMR spectra of the thermolysis of **6.1** at 50 ºC in C_6D_6. (*) indicates **6.1**, (^) indicates free $HN(SiMe_3)_2$, and (?) indicates an unidentified Ce(III) complex.

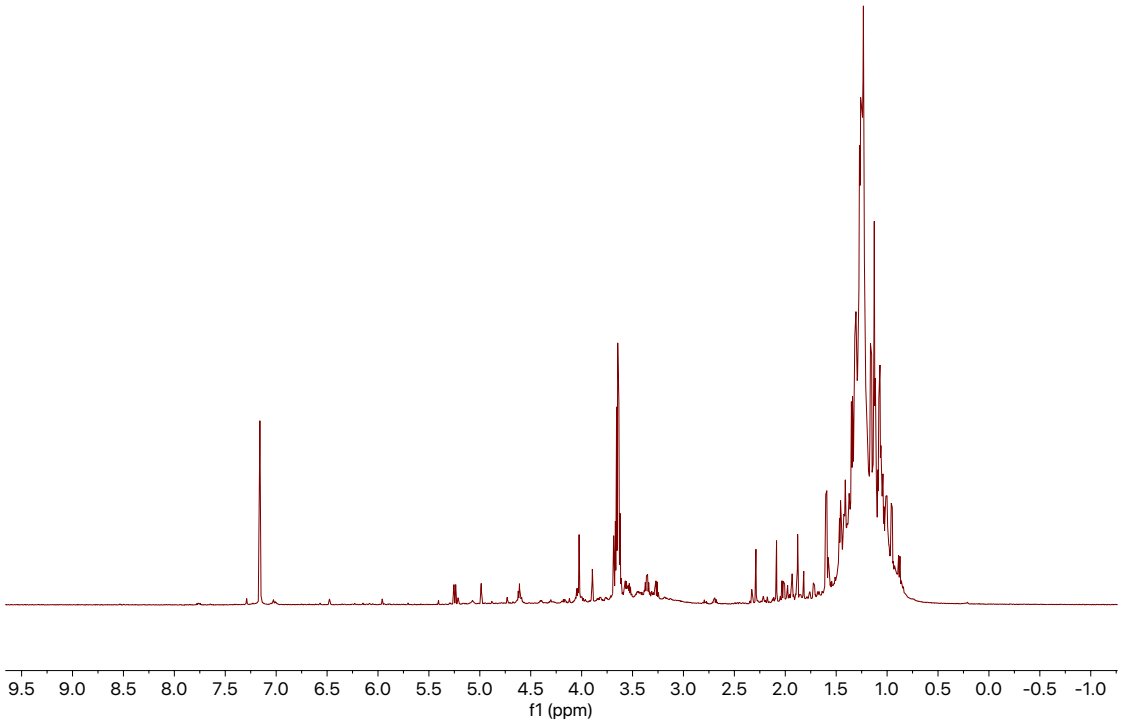

Figure A6.7. ^{1}H NMR spectrum of the BAC ligand after 20 h of photolysis @ 365 nm in C_6D_6.

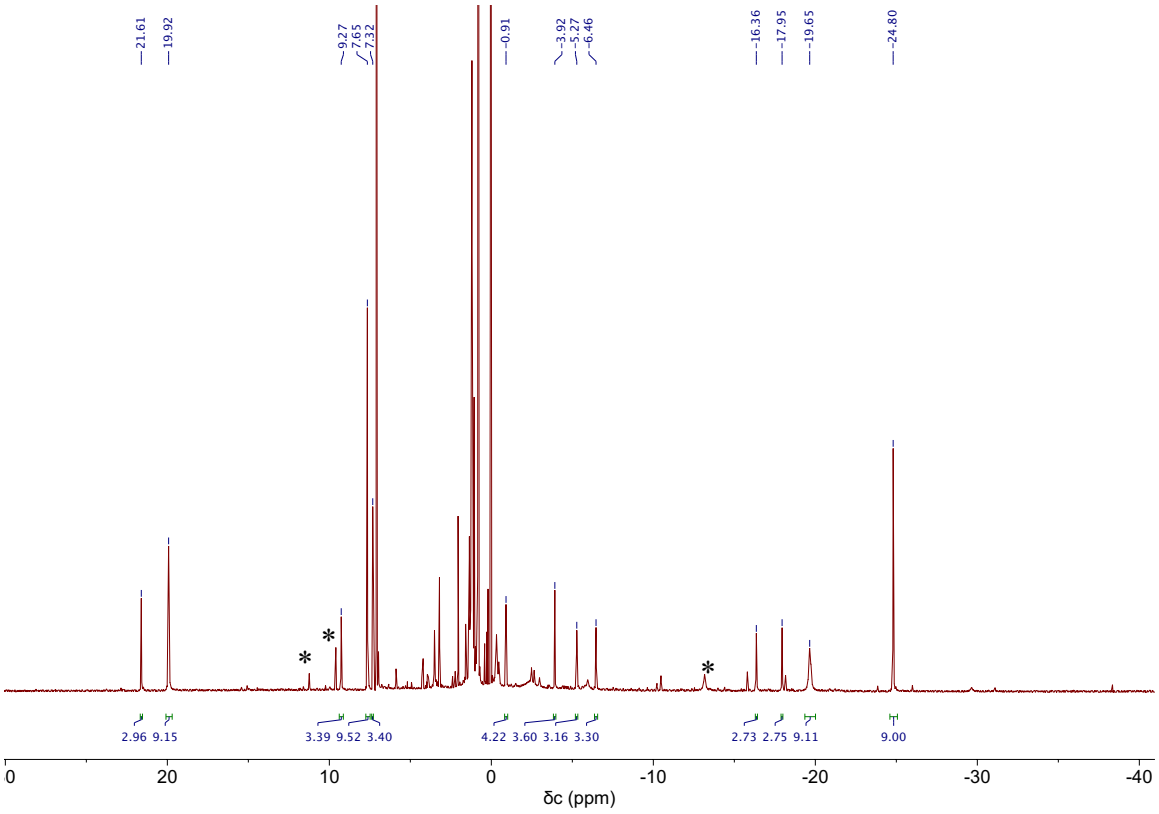

Figure A6.8. Tentative NMR of crystals of complex **6.4** in C_6D_6. (*) indicates $[U\{N(R)(SiMe_2)CH_2\}(NR_2)_2]$.

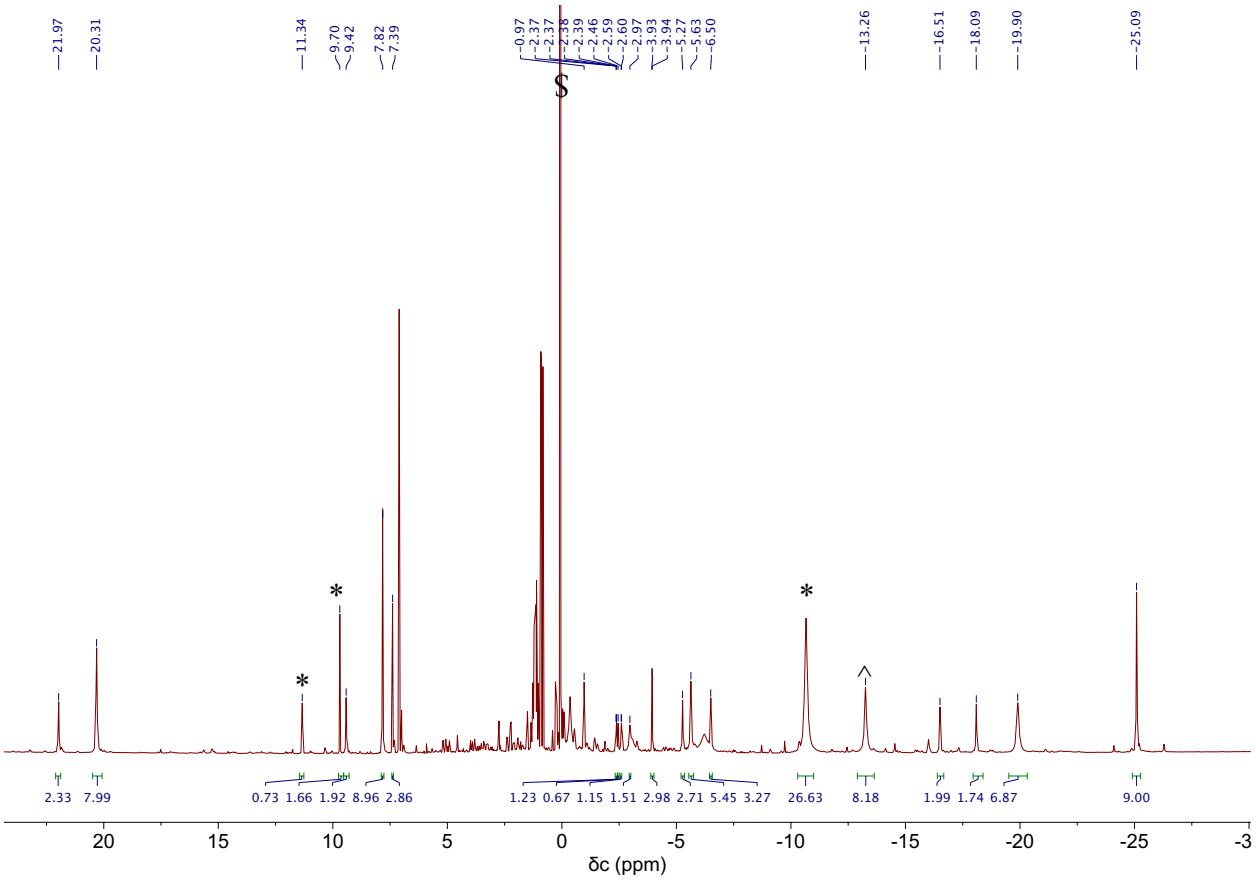

Figure A6.9. ^{1}H NMR spectrum of a crude reaction mixture of **6.4** in C_6D_6. (*) indicates [U{N(R)(SiMe$_2$)CH$_2$}(NR$_2$)$_2$]. (^) indicates free [U(NR$_2$)$_3$]. ($) indicates free HN(SiMe$_3$)$_2$.

6.5.2 IR Spectra

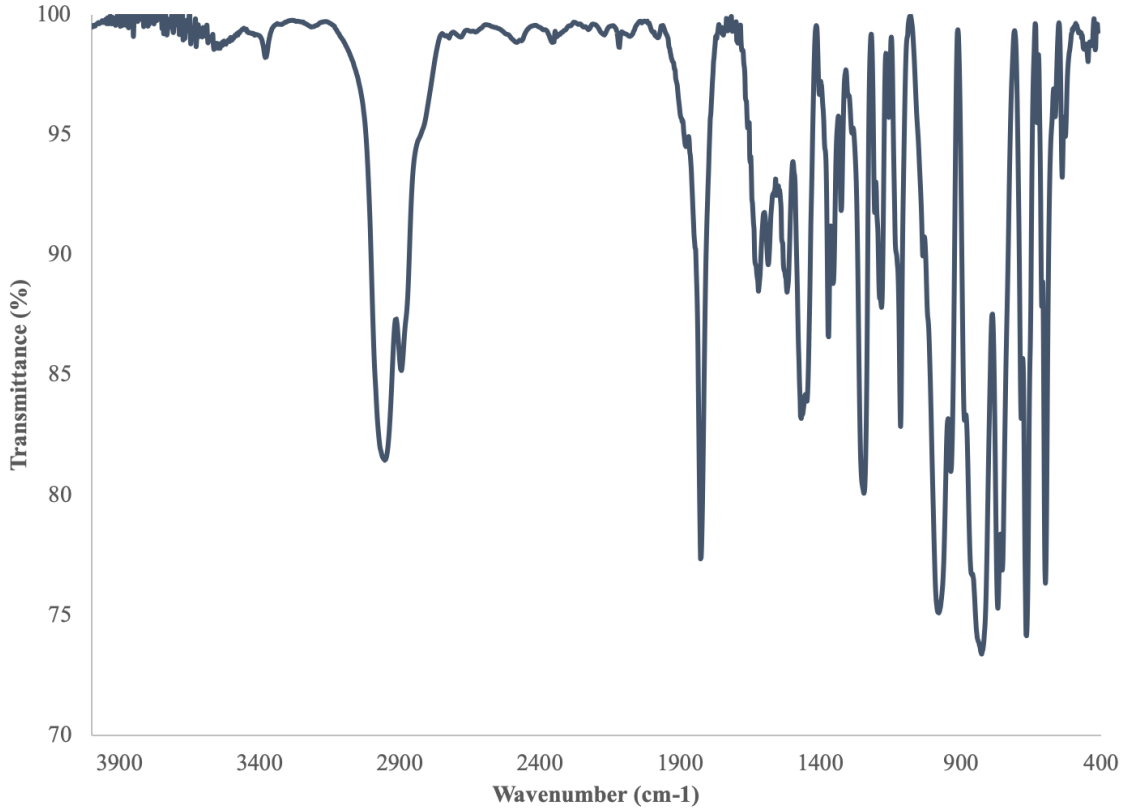

Figure A6.10. IR spectrum of $[(NR_2)_3Ce(BAC)]$ (**6.1**) (KBr pellet).

6.6 References

1. Casely, I. J.; Liddle, S. T.; Blake, A. J.; Wilson, C.; Arnold, P. L., Tetravalent cerium carbene complexes. *Chem. Commun.* **2007**, 5037-5039.

2. Liddle, S. T.; Arnold, P. L., Synthesis of Heteroleptic Cerium(III) Anionic Amido-Tethered N-Heterocyclic Carbene Complexes. *Organometallics* **2005**, *24*, 2597-2605.

3. Arnold, P. L.; Casely, I. J., F-Block N-Heterocyclic Carbene Complexes. *Chem. Rev.* **2009**, *109*, 3599-3611.

4. Mehdoui, T.; Berthet, J.-C.; Thuéry, P.; Ephritikhine, M., The remarkable efficiency of N-heterocyclic carbenes in lanthanide(III)/actinide(III) differentiation. *Chem. Commun.* **2005**, 2860-2862.

5. Gregson, M.; Lu, E.; McMaster, J.; Lewis, W.; Blake, A. J.; Liddle, S. T., A Cerium(IV)–Carbon Multiple Bond. *Angew. Chem. Int. Ed.* **2013**, *52*, 13016-13019.

6. Gregson, M.; Lu, E.; Mills, D. P.; Tuna, F.; McInnes, E. J. L.; Hennig, C.; Scheinost, A. C.; McMaster, J.; Lewis, W.; Blake, A. J.; Kerridge, A.; Liddle, S. T., The inverse-trans-influence in tetravalent lanthanide and actinide bis(carbene) complexes. *Nat. Commun.* **2017**, *8*, 14137.

7. Marshall, G.; Wooles, A. J.; Mills, D. P.; Lewis, W.; Blake, A. J.; Liddle, S. T., Synthesis and Characterisation of Lanthanide N-Trimethylsilyl and -Mesityl Functionalised Bis(iminophosphorano)methanides and -Methanediides. *Inorganics* **2013**, *1*, 46-69.

8. Wooles, A. J.; Mills, D. P.; Lewis, W.; Blake, A. J.; Liddle, S. T., Lanthanide tri-benzyl complexes: structural variations and useful precursors to phosphorus-stabilised lanthanide carbenes. *Dalton Trans.* **2010**, *39*, 500-510.

9. Su, W.; Pan, S.; Sun, X.; Zhao, L.; Frenking, G.; Zhu, C., Cerium–carbon dative interactions supported by carbodiphosphorane. *Dalton Trans.* **2019**, *48*, 16108-16114.

10. Su, W.; Pan, S.; Sun, X.; Wang, S.; Zhao, L.; Frenking, G.; Zhu, C., Double dative bond between divalent carbon(0) and uranium. *Nat. Commun.* **2018**, *9*, 4997.

11. Ren, W.; Zhou, E.; Fang, B.; Hou, G.; Zi, G.; Fang, D.-C.; Walter, M. D., Experimental and Computational Studies on the Reactivity of a Terminal Thorium Imidometallocene towards Organic Azides and Diazoalkanes. *Angew. Chem. Int. Ed.* **2014**, *53*, 11310-11314.

12. Rungthanaphatsophon, P.; Bathelier, A.; Castro, L.; Behrle, A. C.; Barnes, C. L.; Maron, L.; Walensky, J. R., Formation of Methane versus Benzene in the Reactions of $(C_5Me_5)_2Th(CH_3)_2$ with $[CH_3PPh_3]X$ (X=Cl, Br, I) Yielding Thorium-Carbene or Thorium-Ylide Complexes. *Angew. Chem. Int. Ed.* **2017**, *56*, 12925-12929.

13. Rungthanaphatsophon, P.; Huang, P.; Walensky, J. R., Phosphorano-Stabilized Carbene Complexes with Short Thorium(IV)– and Uranium(IV)–Carbon Bonds. *Organometallics* **2018**, *37*, 1884-1891.

14. Cantat, T.; Arliguie, T.; Noël, A.; Thuéry, P.; Ephritikhine, M.; Floch, P. L.; Mézailles, N., The U=C Double Bond: Synthesis and Study of Uranium Nucleophilic Carbene Complexes. *J. Am. Chem. Soc.* **2009**, *131*, 963-972.

15. Gregson, M.; Wooles, A. J.; Cooper, O. J.; Liddle, S. T., Covalent Uranium Carbene Chemistry. *Comments Inorg. Chem.* **2015**, *35*, 262-294.

16. Ma, G.; Ferguson, M. J.; McDonald, R.; Cavell, R. G., Actinide Metals with Multiple Bonds to Carbon: Synthesis, Characterization, and Reactivity of U(IV) and Th(IV) Bis(iminophosphorano)methandiide Pincer Carbene Complexes. *Inorg. Chem.* **2011**, *50*, 6500-6508.

17. Seed, J. A.; Sharpe, H. R.; Futcher, H. J.; Wooles, A. J.; Liddle, S. T., Nature of the Arsonium-Ylide $Ph_3As{=}CH_2$ and a Uranium(IV) Arsonium–Carbene Complex. *Angew. Chem. Int. Ed.* **2020**, *59*, 15870-15874.

18. Lu, E.; Boronski, J. T.; Gregson, M.; Wooles, A. J.; Liddle, S. T., Silyl-Phosphino-Carbene Complexes of Uranium(IV). *Angew. Chem. Int. Ed.* **2018**, *57*, 5506-5511.

19. Fortier, S.; Walensky, J. R.; Wu, G.; Hayton, T. W., Synthesis of a Phosphorano-Stabilized U(IV)-Carbene via One-Electron Oxidation of a U(III)-Ylide Adduct. *J. Am. Chem. Soc.* **2011**, *133*, 6894-6897.

20. Smiles, D. E.; Wu, G.; Hrobárik, P.; Hayton, T. W., Synthesis, Thermochemistry, Bonding, and ^{13}C NMR Chemical Shift Analysis of a Phosphorano-Stabilized Carbene of Thorium. *Organometallics* **2017**, *36*, 4519-4524.

21. Kent, G. T.; Yu, X.; Wu, G.; Autschbach, J.; Hayton, T. W., Synthesis and electronic structure analysis of the actinide allenylidenes, $[\{(NR_2)_3\}An(CCCPh_2)]^-$ (An = U, Th; R = SiMe3). *Chem. Sci.* **2021**, *12*, 14383-14388.

22. Martinez, J. L.; Lin, H.-J.; Lee, W.-T.; Pink, M.; Chen, C.-H.; Gao, X.; Dickie, D. A.; Smith, J. M., Cyanide Ligand Assembly by Carbon Atom Transfer to an Iron Nitride. *J. Am. Chem. Soc.* **2017**, *139*, 14037-14040.

23. Le, L. N. V.; Bailey, G. A.; Scott, A. G.; Agapie, T., Partial synthetic models of FeMoco with sulfide and carbyne ligands: Effect of interstitial atom in nitrogenase active site. *Proc. Natl. Acad. Sci.* **2021**, *118*, e2109241118.

24. Lewis, A. J.; Carroll, P. J.; Schelter, E. J., Stable Uranium(VI) Methyl and Acetylide Complexes and the Elucidation of an Inverse Trans Influence Ligand Series. *J. Am. Chem. Soc.* **2013**, *135*, 13185-13192.

25. Settineri, N. S.; Shiau, A. A.; Arnold, J., Two-electron oxidation of a homoleptic U(iii) guanidinate complex by diphenyldiazomethane. *Chem. Commun.* **2018**, *54*, 10913-10916.

26. Cotton, S., *Lanthanide and Actinide Chemistry*. John Wiley and Sons: West Sussex, U.K., 2006.

27. Piro, N. A.; Robinson, J. R.; Walsh, P. J.; Schelter, E. J., The electrochemical behavior of cerium(III/IV) complexes: Thermodynamics, kinetics and applications in synthesis. *Coord. Chem. Rev.* **2014**, *260*, 21-36.

28. Qiao, Y.; Schelter, E. J., Lanthanide Photocatalysis. *Acc. Chem. Res.* **2018**, *51*, 2926-2936.

29. Yin, H.; Carroll, P. J.; Anna, J. M.; Schelter, E. J., Luminescent Ce(III) Complexes as Stoichiometric and Catalytic Photoreductants for Halogen Atom Abstraction Reactions. *J. Am. Chem. Soc.* **2015**, *137*, 9234-9237.

30. Yin, H.; Jin, Y.; Hertzog, J. E.; Mullane, K. C.; Carroll, P. J.; Manor, B. C.; Anna, J. M.; Schelter, E. J., The Hexachlorocerate(III) Anion: A Potent, Benchtop Stable, and Readily Available Ultraviolet A Photosensitizer for Aryl Chlorides. *J. Am. Chem. Soc.* **2016**, *138*, 16266-16273.

31. Qiao, Y.; Yang, Q.; Schelter, E. J., Photoinduced Miyaura Borylation by a Rare-Earth-Metal Photoreductant: The Hexachlorocerate(III) Anion. *Angew. Chem. Int. Ed.* **2018**, *57*, 10999-11003.

32. Yin, H.; Carroll, P. J.; Manor, B. C.; Anna, J. M.; Schelter, E. J., Cerium Photosensitizers: Structure–Function Relationships and Applications in Photocatalytic Aryl Coupling Reactions. *J. Am. Chem. Soc.* **2016**, *138*, 5984-5993.

33. Qiao, Y.; Cheisson, T.; Manor, B. C.; Carroll, P. J.; Schelter, E. J., A strategy to improve the performance of cerium(III) photocatalysts. *Chem. Commun.* **2019**, *55*, 4067-4070.

34. Assefa, M. K.; Wu, G.; Hayton, T. W., Synthesis of a terminal Ce(IV) oxo complex by photolysis of a Ce(III) nitrate complex. *Chem. Sci.* **2017**, *8*, 7873-7878.

35. Daniel, S. D.; Lehn, J.-S. M.; Korp, J. D.; Hoffman, D. M., Syntheses and X-ray structures of cerium amide complexes. *Polyhedron* **2006**, *25*, 205-210.

36. Hitchcock, P. B.; Hulkes, A. G.; Lappert, M. F., Oxidation in Nonclassical Organolanthanide Chemistry: Synthesis, Characterization, and X-ray Crystal Structures of Cerium(III) and -(IV) Amides. *Inorg. Chem.* **2004**, *43*, 1031-1038.

37. Hitchcock, P. B.; Lappert, M. F.; Protchenko, A. V., Facile formation of a homoleptic Ce(IV) amide via aerobic oxidation. *Chem. Commun.* **2006**, 3546-3548.

38. Schneider, D.; Spallek, T.; Maichle-Mössmer, C.; Törnroos, K. W.; Anwander, R., Cerium tetrakis(diisopropylamide) – a useful precursor for cerium(IV) chemistry. *Chem. Commun.* **2014**, *50*, 14763-14766.

39. Lavallo, V.; Canac, Y.; Donnadieu, B.; Schoeller, W. W.; Bertrand, G., Cyclopropenylidenes: From Interstellar Space to an Isolated Derivative in the Laboratory. *Science* **2006**, *312*, 722.

40. Smiles, D. E.; Wu, G.; Hrobárik, P.; Hayton, T. W., Use of 77Se and 125Te NMR Spectroscopy to Probe Covalency of the Actinide-Chalcogen Bonding in [Th(En){N(SiMe3)2}3]− (E = Se, Te; n = 1, 2) and Their Oxo-Uranium(VI) Congeners. *J. Am. Chem. Soc.* **2016**, *138*, 814-825.

41. Staun, S. L.; Sergentu, D.-C.; Wu, G.; Autschbach, J.; Hayton, T. W., Use of ^{15}N NMR spectroscopy to probe covalency in a thorium nitride. *Chem. Sci.* **2019**, *10*, 6431-6436.

42. Kent, G. T.; Wu, G.; Hayton, T. W., Synthesis and Crystallographic Characterization of the Tetravalent Actinide-DOTA Complexes [An^{IV}(κ^8-DOTA)(DMSO)] (An = Th, U). *Inorg. Chem.* **2019**, *58*, 8253-8256.

43. Nakai, H.; Hu, X.; Zakharov, L. N.; Rheingold, A. L.; Meyer, K., Synthesis and Characterization of N-Heterocyclic Carbene Complexes of Uranium(III). *Inorg. Chem.* **2004**, *43*, 855-857.

44. Ammon, H. L., Structures of, and charge separation in, 2,3-diphenyl-4,4-dicyanotriafulvene and 2,3-diphenylcyclopropenone. *J. Am. Chem. Soc.* **1973**, *95*, 7093-7101.

45. Pahor, N. B.; Calligaris, M.; Randaccio, L.; Lenarda, M., Structure and bonding of 4,4-dicyano-2,3-diphenyltriafulvene. *J. Chem. Soc., Perkin Trans. 2* **1979**, 130-132.

46. Albers, R.; Sander, W., Photolysis of Diazo(3-thienyl)methane: A Simple Synthesis of a Methylenecyclopropene. *J. Org. Chem.* **1997**, *62*, 761-764.

47. Billups, W. E.; Lin, L.-J., Uses of adsorbed reagents in the synthesis of reactive molecules via elimination reactions. *Tetrahedron* **1986**, *42*, 1575-1579.

48. Billups, W. E.; Lin, L. J.; Casserly, E. W., Synthesis of methylenecyclopropene. *J. Am. Chem. Soc.* **1984**, *106*, 3698-3699.

49. Staley, S. W.; Norden, T. D., Synthesis and direct observation of methylenecyclopropane. *J. Am. Chem. Soc.* **1984**, *106*, 3699-3700.

50. Billups, W. E.; Lin, L.-J., 1,4-di-tert-butylmethylenecyclopropene. *Tetrahedron Lett.* **1983**, *24*, 1683-1686.

51. Weinstein, C. M.; Martin, C. D.; Liu, L.; Bertrand, G., Cross-Coupling Reactions between Stable Carbenes. *Angew. Chem. Int. Ed.* **2014**, *53*, 6550-6553.

52. Kuchenbeiser, G.; Soleilhavoup, M.; Donnadieu, B.; Bertrand, G., Reactivity of Cyclic (Alkyl)(amino)carbenes (CAACs) and Bis(amino)cyclopropenylidenes (BACs) with Heteroallenes: Comparisons with their N-Heterocyclic Carbene (NHCs) Counterparts. *Chem. - Asian J.* **2009**, *4*, 1745-1750.

53. Simpson, S. J.; Turner, H. W.; Andersen, R. A., Preparation and hydrogen-deuterium exchange of alkyl and hydride bis(trimethylsilyl)amido derivatives of the actinide elements. *Inorg. Chem.* **1981**, *20*, 2991-2995.

54. Kosog, B.; Kefalidis, C. E.; Heinemann, F. W.; Maron, L.; Meyer, K., Uranium(III)-Mediated C–C-Coupling of Terminal Alkynes: Formation of Dinuclear Uranium(IV) Vinyl Complexes. *J. Am. Chem. Soc.* **2012**, *134*, 12792-12797.

55. Stewart, J. L. Tris (bis (trimethylsilyl) amido); uranium: Compounds with tri-, tetra-, and penta-valent uranium. University of California, Berkeley, 1988.

56. Wedal, J. C.; Bekoe, S.; Ziller, J. W.; Furche, F.; Evans, W. J., C–H Bond Activation via U(II) in the Reduction of Heteroleptic Bis(trimethylsilyl)amide U(III) Complexes. *Organometallics* **2020**, *39*, 3425-3432.

57. Otohiko, T.; Minoru, T.; Hiroshi, S.; Shuji, K., Reactions of 2-Methylenebenzothiazolines with Methylenecyclopropenes. *Bull. Chem. Soc. Jpn.* **1983**, *56*, 1688-1693.

58. Billups, W. E.; Moorehead, A. W., Cyclopropenyl Compounds. In *The Chemistry of the Cyclopropyl Group*, Rappoport, Z., Ed. 1987; Vol. 1, pp 1533-1574.

59. Swan, E.; Platts, K.; Blencowe, A., An overview of the cycloaddition chemistry of fulvenes and emerging applications. *Beilstein J. Org. Chem.* **2019**, *15*, 2113-2132.

60. Racine, J.; Touadjine, M. A.; Rahmouni, A.; Humbel, S., Methylenecyclopropene: local vision of the first $^1B_2$ excited state. *J Mol Model* **2017**, *23*, 22.

61. Möllerstedt, H.; Piqueras, M. C.; Crespo, R.; Ottosson, H., Fulvenes, Fulvalenes, and Azulene: Are They Aromatic Chameleons? *J. Am. Chem. Soc.* **2004**, *126*, 13938-13939.

62. Stolzenberg, H.; Weinberger, B.; Fehlhammer, W. P.; Pühlhofer, F. G.; Weiss, R., Free and Metal-Coordinated (N-Isocyanimino)triphenylphosphorane: X-ray Structures and Selected Reactions. *Eur. J. Inorg. Chem.* **2005**, *2005*, 4263-4271.

63. Harris, R. K.; Becker, E. D.; Cabral de Menezes, S. M.; Goodfellow, R.; Granger, P., NMR nomenclature: nuclear spin properties and conventions for chemical shifts. IUPAC Recommendations 2001. International Union of Pure and Applied Chemistry. Physical Chemistry Division. Commission on Molecular Structure and Spectroscopy. *Magn. Reson. Chem.* **2002**, *40*, 489-505.

64. Harris, R. K.; Becker, E. D.; De Menezes, S. M. C.; Granger, P.; Hoffman, R. E.; Zilm, K. W., Further Conventions for NMR Shielding and Chemical Shifts (IUPAC Recommendations 2008). *Magn. Reson. Chem.* **2008**, *46*, 582-598.

65. Alder, R. W.; Blake, M. E.; Chaker, L.; Harvey, J. N.; Paolini, F.; Schütz, J., When and How Do Diaminocarbenes Dimerize? *Angew. Chem. Int. Ed.* **2004**, *43*, 5896-5911.

66. *SAINT Software User's Guide*, Version 7.34a ed.; Bruker AXS Inc.: Madison, WI, 2005.

67. Sheldrick, G. M., *SADABS*, the Siemens Area Detector Absorption Correction; University of Göttingen: Göttingen, Germany, 2005.

68. *SHELXTL PC*, Version 6.12 ed.; Bruker AXS Inc.:Madison, WI, 2005.

Chapter 7. Diverging Reactivity of 1-Li-3,3-Diphenylcylopropene with [Cp_3AnCl] (An = Th, U) and Reactivity of [$Cp_3U(THF)$] with 3,3-Diphenylcylopropene

Portions of this work were published in: Greggory T. Kent, Xiaojuan Yu, Guang Wu, Jochen Autschbach, Trevor W. Hayton Ring-opening of a Thorium Cyclopropenyl Complex Generates a Transient Thorium-bound Carbene. *Chem. Commun.* **2022** *In Press.*

7.1 Introduction

A large number of heteroatom-stabilized actinide carbene complexes have been reported in recent years,[1-7] including [U(Tren^{TIPS})(CHAsPh$_3$)] (Tren^{TIPS} = N(CH$_2$CH$_2$NSiPr$^i_3$)$_3$),[8] [U{C(SiMe$_3$)(PPh$_2$)}(BIPM^{TMS})(Cl)]$^-$ (BIPM^{TMS} = C(PPh$_2$NSiMe$_3$)$_2$),[9] and [An(CHPPh$_3$)(NR$_2$)$_3$] (An = Th, U; R = SiMe$_3$).[10, 11] Yet, an isolable "Schrock-type" actinide alkylidene, which features no heteroatom stabilization, remains elusive. Their scarcity is likely due to a number of factors, but the high reactivity of the An=C linkage, a consequence of the weak An-C π bond, plays a significant role.[8] Another important factor is the dearth of viable synthetic routes.[12-14] For instance, in a seminal contribution, Kiplinger and co-workers found that reaction of [Cp*$_2$U(NAr)] (Ar = 2,4,6-^{t}Bu$_3$C$_6$H$_2$) with diphenyldiazoalkane did not result in N$_2$ elimination and carbene formation, but instead resulted in generation of the U(VI) hydrazonato complex, [Cp*$_2$U(NAr)(N$_2$CPh$_2$)].[15] Several other groups have reported similar diazoalkane reactivity with the actinides.[1, 16-19]

In an effort to find new routes to an actinide alkylidene, we turned our attention to 3,3-diphenylcyclopropene and its derivatives. This reagent has been successfully employed by Binger,[20, 21] and others,[22-26] to generate transition metal vinyl carbenes and allenylidenes.[27-29] For example, reaction of [Cp$_2$Ti(PMe$_3$)$_2$] with 3,3-diphenylcyclopropene results in ring opening and formation of the vinyl carbene complex, [Cp$_2$Ti(=C(H)C(H)=CPh$_2$)(PMe$_3$)].[20] Similarly, reaction of [RuCl$_2$(PPh$_3$)$_4$] with 3,3-diphenylcyclopropene results in formation of [Ru(=C(H)C(H)=CPh$_2$)Cl$_2$(PPh$_3$)$_2$].[28, 30]

Drawing inspiration from this work, as well as recent results from Hashmi and co-workers,[31] we began exploring the reactivity of 3,3-diphenylcyclopropene with the actinides.

In particular, we found that reaction of 1-lithium-3,3-diphenylcyclopropene with [$AnCl(NR_2)_3$] (An = Th, U; R = $SiMe_3$) resulted in the formation of the An-allenyl complexes [$\{(NR_2)_3\}An(CH{=}C{=}CPh_2)$] (An = U, **5.1**; Th, **5.2**).[32] Subsequent deprotonation resulted in the formation of the first An allenylidenes, $[\{(NR_2)_3\}An(CCCPh_2)]^-$ (An = U, **5.4**; Th, **5.5**), which were also the first reported An carbenes that contain no heteroatom stabilization. These results were reported and discussed in Chapter 5.

Given the rarity of An carbenes, and the promise of this new synthetic protocol for generating An=C bonds, we wanted to explore the generality of this approach. Herein I describe the synthesis and characterization of [Cp_3Th(3,3-diphenylcyclopropenyl)] (**7.1**), which was formed by reaction of [Cp_3ThCl] with 1-lithium-3,3-diphenylcyclopropene. This complex isomerizes to [Cp_3Th(3-phenyl-1H-inden-1-yl)] (**7.3**) upon thermolysis. I propose that this transformation proceeds via a transient carbene intermediate. I also describe the reactivity of [Cp_3UCl] with 1-lithium-3,3-diphenylcyclopropene, which instead forms [Cp_2U{1-phenyl-2-diphenyl-ethylene}] (**7.4**) after salt metathesis. I propose that the formation of **7.4** proceeds by an unobserved U(VI) carbyne. Finally, I report the synthesis of [$Cp_3U\{\eta^1$-2,2-diphenylcylopropane}] (**7.5**), which can be formed by reaction of 3,3-diphenylcyclopropene with [$Cp_3U(THF)$].

7.2 Results and discussion

7.2.1 Synthesis and Characterization

Scheme 7.1. Synthesis of complexes **7.1**-**7.3**.

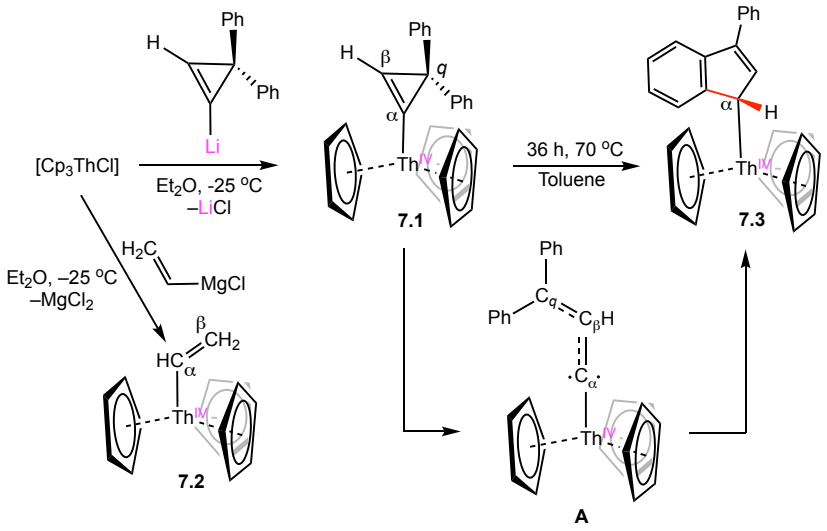

Addition of *in situ* generated 1-lithium-3,3-diphenylcyclopropene to an Et_2O solution of [Cp_3ThCl] results in the formation of the cyclopropenyl complex, [Cp_3Th(3,3-diphenylcyclopropenyl)] (**7.1**), which was isolated as colourless plates in 75% yield after work-up (Scheme 7.1). The ^{1}H NMR spectrum of **1** in THF-d_8 features diagnostic resonances at 6.17 ppm and 7.62 ppm, which are assignable to the Cp and H_β environments, respectively. The peaks are present in a 15:1 ratio, consistent with the proposed formulation. Additionally, the $^{13}C\{^1H\}$ NMR spectrum of **7.1** features three cyclopropenyl environments at 177.4, 127.2, and 39.5 ppm, which are assignable to the C_α, C_β, and C_q (q = quaternary) positions, respectively (Figures 7.2 and A7.2). Complex **7.1** crystallizes in the orthorhombic space group *P*bca and confirms the connectivity of the diphenylcyclopropenyl ligand (Figure 1). The Th–C bond distance is 2.52(1) Å and is within error of those reported for thorium allenyl or vinylic complexes, including [{$(NR_2)_3$}Th(CH=C=CPh_2)] (R = $SiMe_3$, 2.529(5)/2.536(5) Å) and [η^5-

1,2,4-$^{t}Bu_3C_5H_2$][η^5-1,2-$^{t}Bu_2$-4-(CH_2CMe_2)C_5H_2]Th[C(Ph)=CH(C_6H_{11})] (2.480(6) Å).[32-34] The C_α–C_β distance is 1.28(1) Å, consistent with its double bond character, whereas the C_α–C_q (1.47(1) Å) and C_β–C_q (1.56(1) Å) distances are assignable to C–C single bonds. Interestingly, the two C–C single bonds differ by ca. 0.1 Å, suggesting activation of the cyclopropenyl ring (see below). Hashmi and co-workers observed a similar level of activation in [(IPr)Au(3,3-diphenylcyclopropenyl)] complex (IPr = 1,3-bis-(2,6-diisopropylphenyl)imidazole-2-ylidene).[31] Finally, the isolation of **7.1** supports our hypothesis that the ring opening required to form [{(NR_2)$_3$}An(CH=C=CPh_2)] (An = U, **5.4**; Th, **5.5**) occurs after salt metathesis (see Chapter 5).[32]

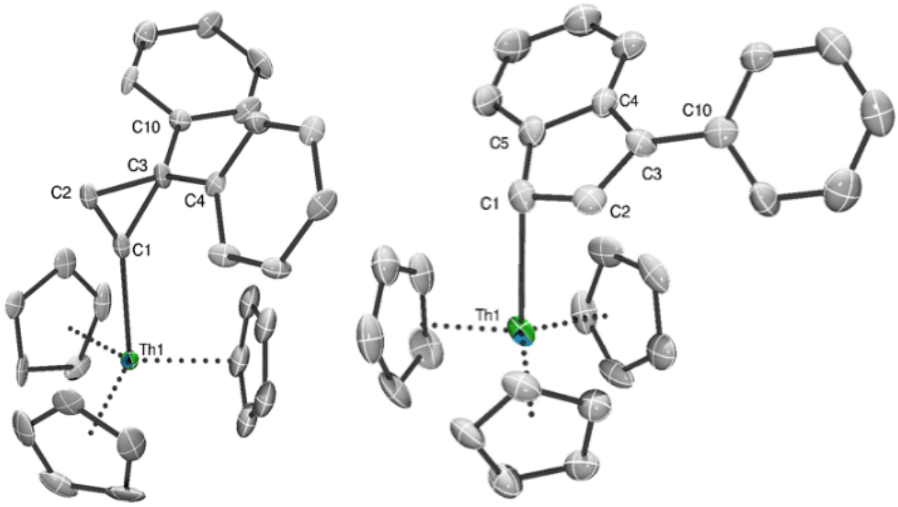

Figure 7.1. Solid-state molecular structures of **7.1** (left) and **7.3** (right); thermal ellipsoids set at 50% probability and hydrogen atoms are omitted for clarity. Selected bond lengths [Å] and angles [deg]: **1**: Th1–C1 = 2.523(11), C1–C2 = 1.278(14), C1–C3 = 1.559(14), C2–C3 = 1.467(13), Th1–C1–C2 = 153.6(8), Th1–C1–C3 = 145.1(7), C2–C1–C3 = 61.3(7). **3**: Th1–C1 = 2.674(6), C1–C2 = 1.429(9), C1–C5 = 1.451(10), C2–C3 = 1.399(9), C3–C4 = 1.438(10), C4–C5 = 1.422(9), Th1–C1–C2 = 104.0(4), Th1–C1–C5 = 112.3(4), C1–C2–C3 = 109.7(7).

For further spectroscopic and structural comparison we independently synthesized and characterized the parent thorium vinyl complex [$Cp_3Th(C(H)=CH_2)$] (**7.2**) via reaction of [Cp_3ThCl] with [$ClMg(C(H)=CH_2)$] in Et_2O (Scheme 7.1). Complex **7.2** can be isolated in 80% yield as white needles after work-up. It represents the first reported thorium parent vinyl complex.[33-35] The ^1H NMR spectrum of **7.2** in C_6D_6 exhibits three vinyl environments at 8.19, 7.00, and 6.21 ppm, and one Cp environment at 5.96 ppm (Figure A7.3). These resonances are present in a 1:1:1:15 ratio. The $^{13}C\{^1H\}$ NMR spectrum of **7.2** in C_6D_6 features resonances at 199.6, 134.3, and 116.7 ppm, which are assignable to the C_α, C_β, and Cp environments, respectively (Figures 7.2 and A7.4).

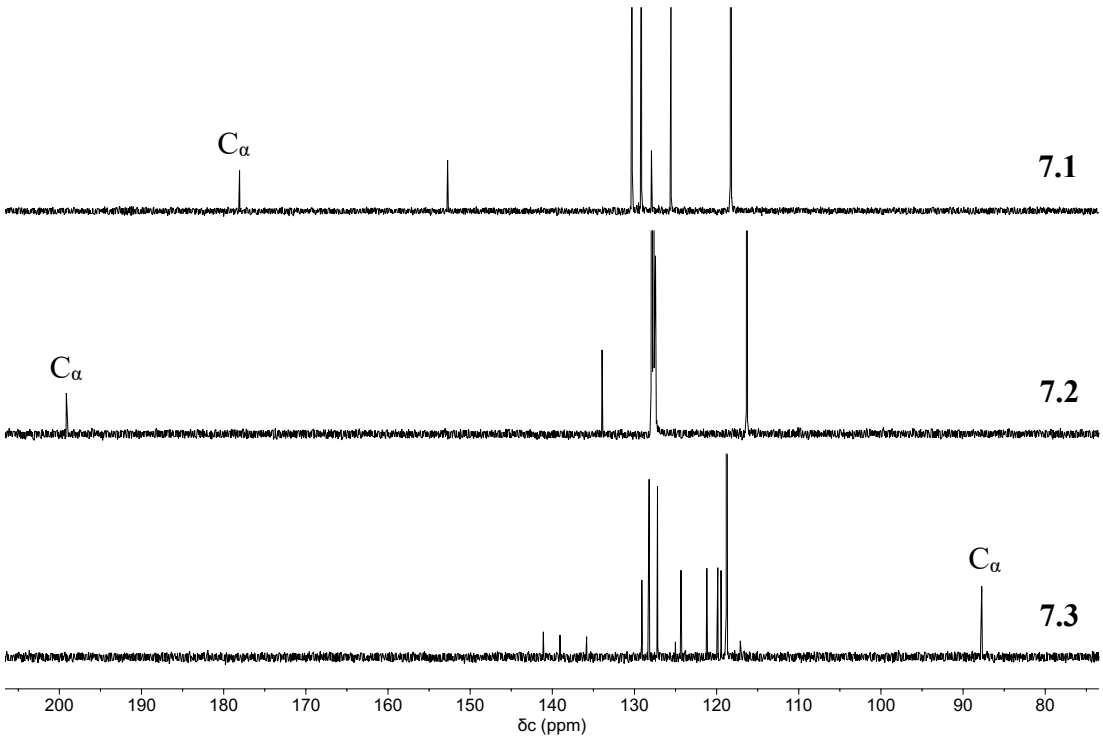

Figure 7.2. Partial $^{13}C\{^1H\}$ NMR spectra overlay of complexes **7.1** (top), **7.2** (middle), and **7.3** (bottom), with labelled C_α resonances.

The connectivity of **7.2** was further confirmed by X-ray crystallography (Figure 7.3). Complex **7.2** crystallized in the orthorhombic space group $Pna2_1$. Its Th–C bond distances are 2.52(3) and 2.52(2) Å and are consistent with previously report Th–C single bonds.[32, 36, 37] The vinyl C–C distances (1.32(3) and 1.24(3) Å) are also consistent with the expected C=C double bond, while the Th–C_α–C_β angles (134(2) and 139.1(19)º) confirms the sp^2 hybridization at C_α.

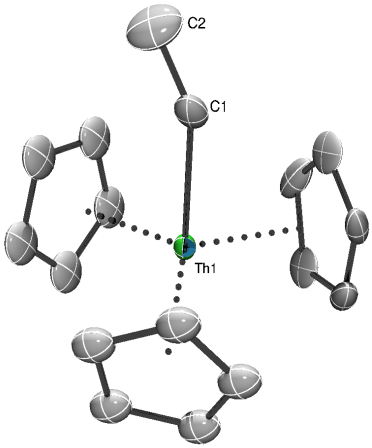

Figure 7.3. Solid state molecular structure of **7.2**, shown with thermal ellipsoids set at 50% probability. A second molecule in the asymmetric unit and hydrogen atoms are omitted for clarity. Selected bond lengths [Å] and angles [deg]: Th1–C1= 2.52(3), Th2–C33 = 2.52(2), C1–C2 = 1.32(3), C33–C34 = 1.24(3), Th1–C1–C2 = 139.1(19), Th2–C33–C34= 134(2).

In an effort to effect ring-opening, we heated a toluene solution of **7.1** for 36 h. Work-up of the resulting yellow-orange solution resulted in the isolation of the thorium indenyl complex, [Cp_3Th(3-phenyl-1H-inden-1-yl)] (**7.3**), in a 60% yield. The ^{1}H NMR spectrum of complex **7.3** in THF-d_8 features doublets at 7.57 (J_{HH} = 2.1 Hz) and 5.35 ppm (J_{HH} = 2.1 Hz), which are assignable to the H_α and H_β environments of the indenyl ring (Figure A7.5). The $^{13}C\{^1H\}$ NMR spectrum of **7.3** in THF-d_8 features 14 resonances, consistent with the proposed

structure. Notably, the C_α resonance (88.9 ppm) is downfield (less shielded) in comparison to the equivalent carbon resonance of 3-phenylindene, primarily due to metalation (Figures 7.2 and A7.6).[38, 39]

Complex **7.3** crystallizes in the monoclinic space group $P2_1/n$ and its solid-state structure confirms the connectivity of the indenyl ligand (Figure 7.1). The Th–C distance is 2.674(6) Å, which is elongated in comparison to that of **7.1** on account of the weaker σ-donating ability of the indenyl ligand. The sum of angles around C_α (325.7º) also confirm that that C_α is sp^3 hybridized. Furthermore, the range of the intra-ring distances (1.399(9)-1.451(10) Å) falls between the expected C–C single and double bond distances, and suggests that the cyclopentene ring is aromatic.

Scheme 7.2. Diverging reactivity of the ring-opened carbene **A**.

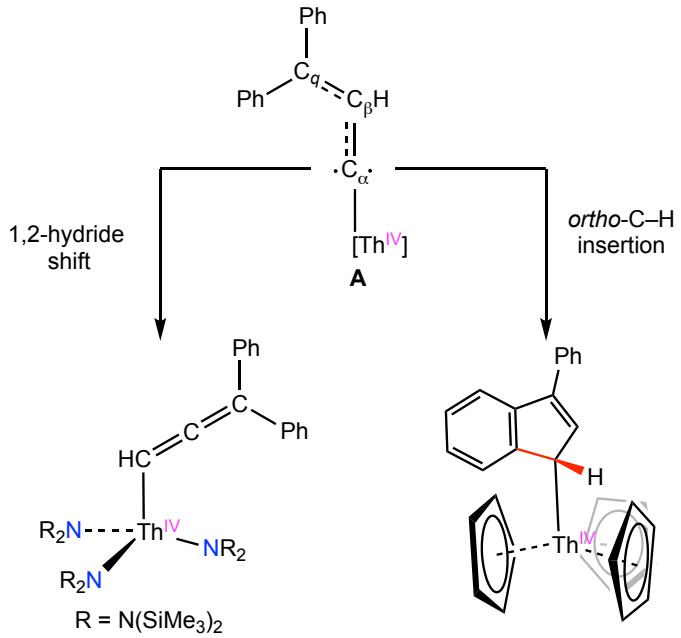

To account for the formation of **7.3**, we propose that thermolysis of **7.1** results in ring opening, forming a transient carbene intermediate **A** (Scheme 7.2), which activates an *ortho*

C-H bond to form **7.3**. A similar transformation was observed by Hashmi upon thermolysis of [(IPr)Au(3,3-diphenylcyclopropenyl)].[31] Curiously, reaction of [ThCl(NR$_2$)$_3$] with 1-lithium-3,3-diphenylcyclopropene does not generate the analogous indenyl complex, and instead results in isolation of [{(NR$_2$)$_3$}Th(CH=C=CPh$_2$)] (**5.2**), presumably via a 1,2-H-shift from an analogous carbenoid intermediate (Scheme 7.2). Steric maps of the [{(NR$_2$)$_3$}Th]$^+$ and [ThCp$_3$]$^+$ fragments (Figure 7.4) demonstrate that the former is substantially more bulky than the latter,[40] suggesting that the *ortho* C–H bonds cannot approach the C$_\alpha$ carbenoid center in [{(NR$_2$)$_3$}Th(CC(H)=CPh$_2$)], leaving the 1,2-H-shift as the next best pathway for isomerization.

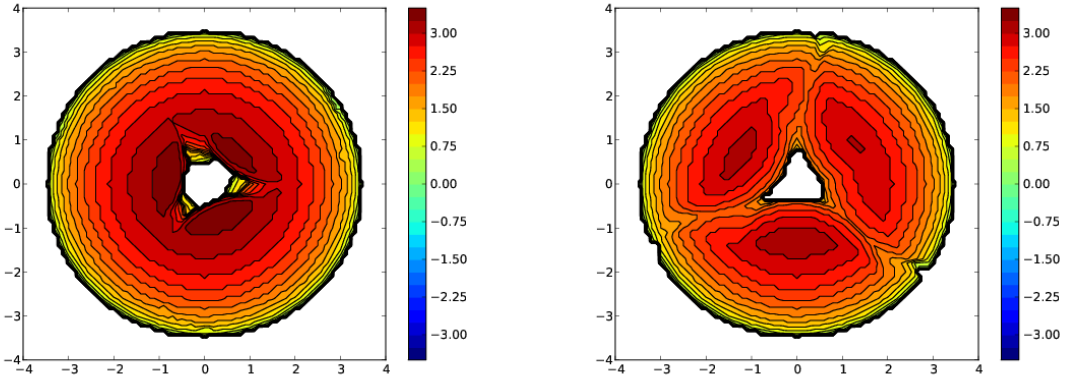

Figure 7.4. Steric profile maps of [Th(N(SiMe$_3$)$_2$)$_3$]$^+$ (left) and [ThCp$_3$]$^+$ (right).[40]

Having investigated the reactivity of 1-lithium-3,3-diphenylcyclopropene with [Cp$_3$ThCl], I next endeavored to examine its reactivity with [Cp$_3$UCl]. Addition of *in situ* generated 1-lithium-3,3-diphenylcyclopropene to an Et$_2$O solution of [Cp$_3$UCl] instead results isolation of the triphenylethylene complex, [Cp$_2$U(η^2-triphenylethylene)] (**7.4**), which is evidently formed by opening of the cyclopropenyl ring and insertion into a Cp ligand. The crude ^{1}H NMR spectrum of **7.4** shows two inequivalent Cp environments at 10.91 and –10.54 ppm which are

present in a 1:1 ratio, nine aryl environments and a single H_α resonance at –136.86 ppm (Figure A7.7). Complexes **7.4** is very temperature sensitive and degrades in solution, even at –25 ºC, thus I was only able to isolate **7.4** in a 5% yield. Consequently, analytically pure samples eluded me and I was unable to complete the characterization of this material. To isolate a more stable derivative of complex **7.4,** I also attempted to react ^{t}Bu-isocyanide with a crude reaction mixture of **7.4**. Unfortunately, the ^{1}H NMR spectrum of this reaction mixture seemed to suggest that the triphenylethylene ligand dissociated from the metal center, as only a U(III) species containing resonances assignable Cp (–14.73 ppm) and ^{t}Bu-isocyanide(–2.36 ppm) could be located in its ^{1}H NMR spectrum. I also attempted to isolate a more stable derivative of complex **7.4** by reacting the crude reaction mixture with an additional equivalent of diphenyl cyclopropene. Interestingly this reaction results in the formation of the uranium(IV)-cyclopropyl complex [Cp_3U(3,3-diphenylcyclopropyl)] as the major product (**7.5**, see below for more details).

Scheme 7.3. Synthesis of complex **7.4**.

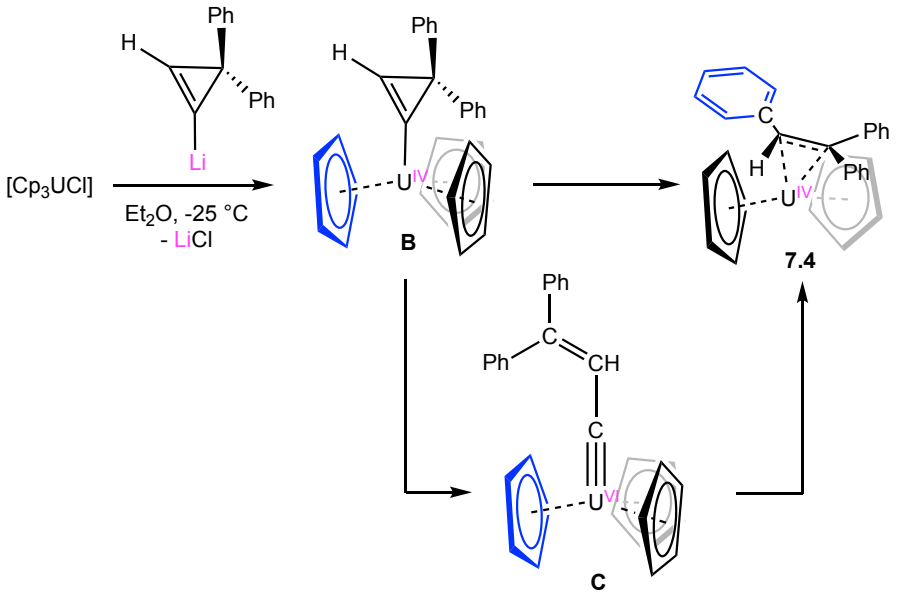

I was, however, able to grow single crystals of complex **7.4** via slow mixing of a toluene solution of **7.4** with hexanes. Complex **7.4** crystalizes in the triclinic space group P–1 (Figure 7.5) and confirms the ring opening and insertion of the diphenylcyclopropene ring into a Cp ligand to yield a η^2-triphenylethylene ligand. The U–C2 and U–C3 distances are 2.512(12) and 2.603(12) Å, respectively, and are slightly elongated in comparison to most U–C single bonds. This elongation likely stems from the approach of the triphenylethylene ligand plane to the Cp rings. For comparison, Walter and co-workers previously reported the Cp-linked metallacyclopropane complex [(η^5-C_5Me_5)U(η^5-$C_5Me_4CH_2C(Ph)=C(Ph)C(Ph)CHPh$)] which shows similar U–C bond distances of 2.528(3) and 2.498(4) Å.[41] Walter and co-workers also reported [(η^5-C_5Me_5)$_2$U(η^2-$C_2(SiMe_3)_2$)], which can be viewed as an unsaturated analog to[(η^5-C_5Me_5)$_2$U(η^2-$C_2(SiMe_3)_2$)] and **7.4**. This compound displays slightly shorter U–C bond distances (2.315(9) and 2.350(9) Å) where the shortening is likely due to the greater σ-donating ability of sp^2-hybridized carbon atoms and the π-interaction from the U-(η^2-C=C) moiety. Furthermore, the C2–C3 bond distance (1.497(15) Å) is indicative of a C–C single bond and confirms the η^2-triphenylethylene ligand as a dianion coordinated to the uranium(IV) metal center as a metallacyclopropane complex. Drs. Pedrick and Seaman of the Hayton group previously reported the dibenzyne, [Li]$_2$[U(2,3-$C_6H_3CH_2NMe_2$)$_2$(2-$C_6H_4CH_2NMe_2$)$_2$], which can be described as a metallacyclopropene complex. Interestingly, its U–C bond distances are substantially shorter (2.409(3) and 2.432(3) Å) than those found in **7.4**, in line with the greater σ-donating ability of its sp^2-hybridized carbon atoms.[42]

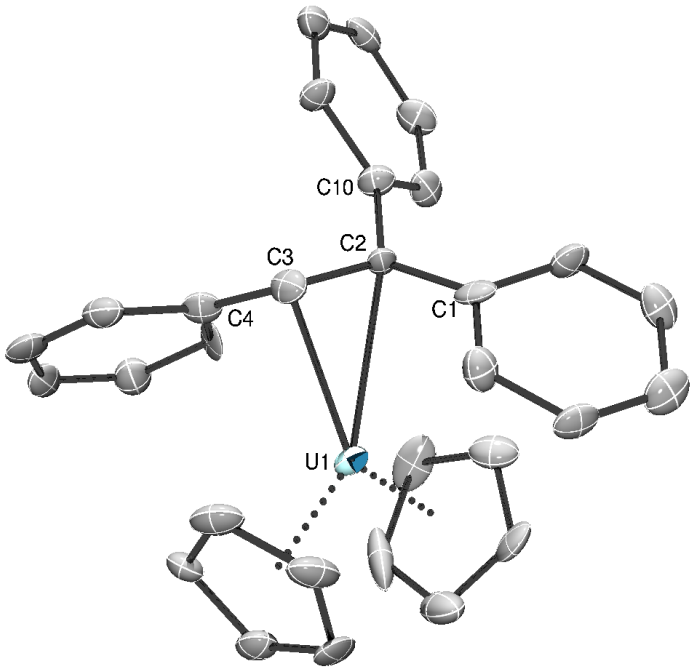

Figure 7.5. Solid state molecular structure of **7.4**, shown with thermal ellipsoids set at 50% probability. A second molecule in the asymmetric unit and hydrogen atoms are omitted for clarity. Selected bond lengths [Å] and angles [deg]: U–C2 = 2.512(12), U–C3 = 2.603(12), C3–C2 = 1.497(15), C4–C3 = 1.436(17), C2–C10 = 1.524(15), C1–C2 = 1.460(16), C1–C2–C3 = 115.8(10), C3–C2–C10 = 117.9(9), C1–C2–C10 = 122.9(10), C4–C3–C2 = 119.4(11).

To account for the formation of **7.4**, I hypothesize that upon formation of intermediate **B** spontaneous ring opening occurs. This is likely due to the smaller ionic radii of U(IV), in comparison to Th(IV), which results in stronger steric interactions between $[Cp_3U]^+$ and the cyclopropenyl ligand (Scheme 7.3).[45] The spontaneous ring opening then results in the formation of the transient uranium(VI) carbyne **C**. Intermediate **C** would be extremely unstable and quickly react with a neighboring Cp ligand to form **7.4** (Scheme 7.3). While rare, cyclopentadienide ring expansions are not unknown. For instance Messerle and Deboer reported that reduction of $[(C_5Me_5)Ta(COCH_2CMe_3)Cl_3]$ with excess magnesium metal results

in ring expansion of $(C_5Me_5)^-$ and liberation of $C_6Me_5(CH_2CMe_3)$, via formal carbyne transfer (Scheme 7.4a).[43] In another example of deoxygenative acyl insertion, de With and de Boer found that reaction of $[(C_5Me_5)_2TiC(O)Me]$ with 0.5 equiv $[CpMo(CO)_3]_2$ resulted in formation of hexamethylbenzene via insertion of a "MeC" carbyne fragment into $(C_5Me_5)^-$ (Scheme 7.4b).[44]

Scheme 7.4. Some previous examples of Cp ring expansion, data taken from refs 43 (a) and 44 (b).

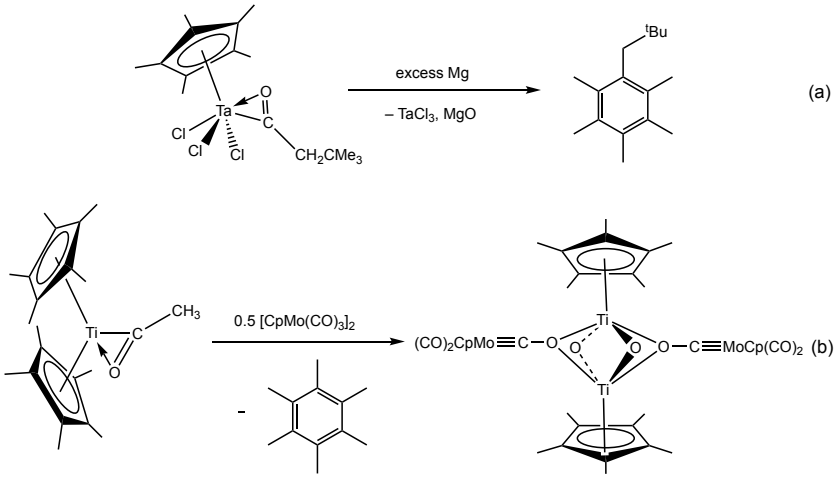

Finally, I believe that the inherent instability of **7.4** stems from the unfavorable steric interactions between the $[Cp_2U]^{2+}$ fragment and the bulky triphenylethylene ligand, which promotes dissociation of the triphenylethylene ligand, resulting in the formation of the $[Cp_2U(II)]$ and triphenylethylene. To support this hypothesis, I do observe a diagnotsic singlet at 6.41 ppm in the crude ^1H NMR spectra which is assignable to triphenylethylene. Furthermore, there is precident for synthesis of U(II) cylcopentadienyl sandwich complexes.[46-50] For instance, Layfield and co-workers showed that potassium graphite reduction of the uranium(III) metallocene $[(\eta^5\text{-}C_5{}^iPr_5)_2UI]$ resulted in the isolation of $[(\eta^5\text{-}C_5{}^iPr_5)_2U]$.[48] While

[(η^5-$C_5{}^iPr_5$)$_2$U], was shown to decompose in aliphatic solvents over the course of several weeks at –40 ºC, [$Cp_2U(II)$] would be even more reactive, due to the lack of bulky supporting substituents on the Cp rings, and be expected to rapidly decompose in a reaction mixture.

In my continued efforts to synthesize a uranium-alkylidene complex using 3,3-diphenylcyclopropene, I also explored the reactivity of diphenylcyclopropene with [$Cp_3U(THF)$]. Reaction of 2 equiv. of diphenylcylopropene with [$Cp_3U(THF)$] in Et_2O for 16 h results in the formation of [Cp_3U(3,3-diphenylcyclopropyl)] (**7.5**, Scheme 7.5), which can be isolated as brown plates in 55% yield, after work-up. The ^{1}H NMR spectrum of **7.5** in THF-d_8 features one Cp environment located at –3.04 ppm, six diastereotopic aryl proton environments, and three diastereotopic cyclopropyl proton environments, where the H_α chemical shift can be located at –171.94 ppm (Figure A7.8).

Scheme 7.5. Synthesis of complex **7.5** from diphenylcyclopropene.

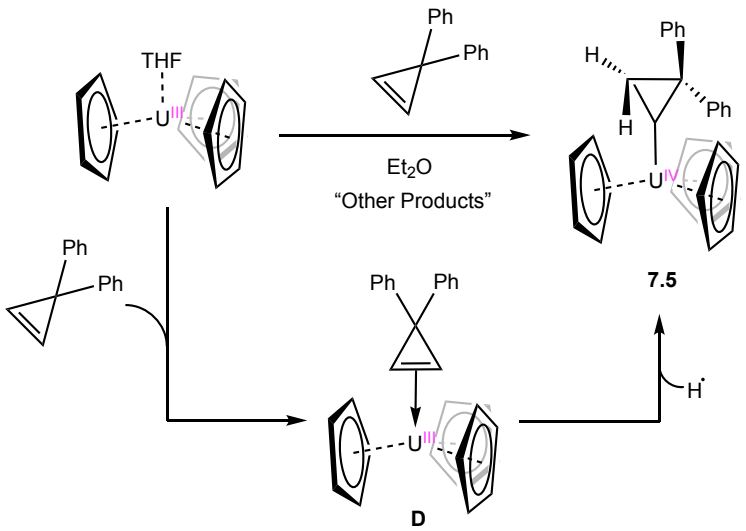

Alternatively, Complex **7.5** can also be synthesized via reaction of [Cp_3UCl] with in *situ* generated 1-lithium-3,3-diphenylcyclopropyl in Et_2O. Under these conditions complex **7.5** can

be isolated in 63% yield and its isolation by this route confirms the formation of **7.5** in the reaction between [$Cp_3U(THF)$] and 3,3-diphenylcyclopropene (Scheme 7.5). The thorium analog can be prepared in a similar manner, whereby addition of an Et_2O solution of *in situ* generated 1-lithium-3,3-diphenylcyclopropyl to an Et_2O solution of [Cp_3ThCl] affords [Cp_3Th(3,3-diphenylcyclopropyl)] (**7.6**) in 82% yield, after work-up (Scheme 7.6). The ^1H NMR spectrum of **7.6** in benzene-d_6 features one Cp environment located at 5.83 ppm, six diastereotopic aryl proton environments, and three diastereotopic cyclopropyl proton environments, where the H_α chemical shift can be located at 0.85 ppm as an overlapping doublet of doublets (Figure A7.9). The $^{13}C\{^1H\}$ NMR spectrum of **7.6** in benzene-d_6 exhibits the expected 12 resonances and features three cyclopropyl environments at 66.1, 42.8, and 28.4 ppm, which are assignable to the C_α, C_q, and C_β (q = quaternary) positions, respectively (Figure A7.10). I was also able to grow crystals of complexes **7.5** and **7.6**; both crystallize in the orthorhombic space group *C*mca and confirm the connectivity of the 3.3-diphenylcyclopropyl ligand. Complexes **7.5** and **7.6** exhibit disorder of their Cp and 3,3-diphenylcyclopropyl ligands over two orientations and as a result the metrical parameters are subject to large errors, which makes analysis uninformative (Figure 7.6).

Scheme 7.6. Synthesis of complexes **7.5** and **7.6**.

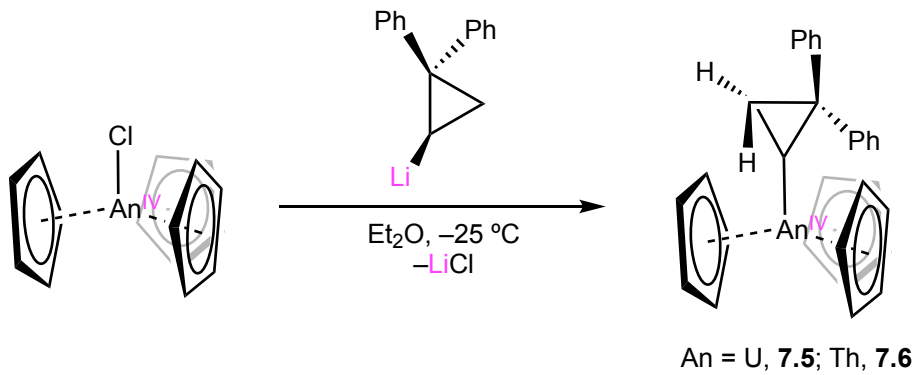

An = U, **7.5**; Th, **7.6**

To rationalize the generation of complex **7.5** from 3,3-diphenylcyclopropene and [$Cp_3U(THF)$], I hypothesize that a highly reactive π-complex between 3,3-diphenylcyclopropene and [$Cp_3U(THF)$], namely **D**, is initially formed. Intermediate **D** can then abstract a hydrogen atom from another equivalent of 3,3-diphenylcyclopropene or solvent and form **7.5**. In support of this mehcanism, I note that in benzene-d_6 2 equiv 3,3-diphenylcyclopropene was required for complete conversion to **7.5**, where 1 equiv of 3,3-diphenylcyclopropene is acting as a hydrogen atom source. However, when the reaction is carried out in a hydrogen atom donor solvent, such as THF or diethyl ether, conversion to **7.5** does apparently not require excess 3,3-diphenylcyclopropene. I also observe the formation of another $[Cp_3U]^+$ containing product in crude reaction mixtures, when the reaction is carried out in benzene-d_6, further supporting my proposed mechanism and the need for hydrogen atom transfer to occur. Unfourtunatly, I was unable to isolate and characterize this product. In an attempt to provide an alternative hydrogen atom donor, reaction of 3,3-diphenylcyclopropene with [$Cp_3U(THF)$] and excess 1,4-cyclohexadiene in toluene-d_8 results in the formation of benzene. However, it appears that donation of a hydrogen atom by 1,4-cyclohexadiene or 3,3-

diphenylcyclopropene is competitive as the same unidentified $[Cp_3U]^+$ containing product is still observed.

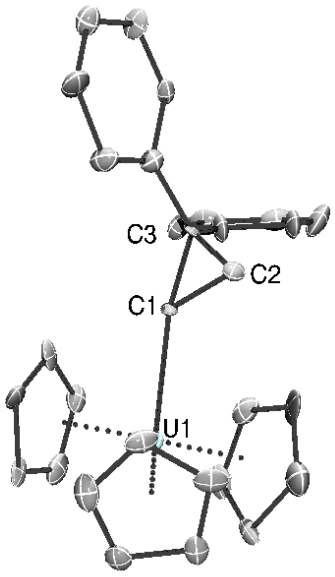

Figure 7.6. Solid state molecular structure of **7.5**, shown with thermal ellipsoids set at 50% probability. A second molecule in the asymmetric unit and hydrogen atoms are omitted for clarity. Selected bond lengths [Å] and angles [deg] **7.5**: U–C1 = 2.435(14), C1–C2 = 1.49(2), C1–C3 = 1.525(19), C2–C3 = 1.56(4), U–C1–C2 = 128.6(10), U–C1–C3 = 142.8(12). **7.6**: Th–C1 = 2.48(3), C1–C2 = 1.59(4), C1–C3 = 1.59(4), C2–C3 = 1.56(4), Th–C1–C2 = 130.2(18), Th–C1–C3 = 139(2).

7.2.2 Electronic Structure Analysis

To better understand the nature of the Th-C interactions in complexes **7.1**-**7.3**, as well as intermediate **A**, Dr. Xiaojuan Yu and Prof. Jochen Autschbach at the University of Buffalo analyzed their electronic structures by relativistic density functional theory with different functionals. Natural localized molecular orbital (NLMO)[51] analysis of **7.1** is indicative of a

two-center two-electron σ(Th–C) bond with 22% total thorium weight (8% 7s; 76% 6d; 16% 5f). The polarization toward C is typical, and reflective of the dative character of the bond (Table 1). The An-C interaction in **7.2** is similar to that of **7.1**, with 23% total thorium weight (7% 7s; 79% 6d; 14% 5f). The NLMO analysis of complex **7.3** shows donation bonding via a delocalized π orbital evincing the conjugation between the 5- and 6-membered rings of the ligand. The total Th contribution in this orbital is only 10%, indicating weaker donation bonding, which is consistent the relatively long Th-C bond observed for this complex. The Th–C_α Wiberg bond orders (WBOs) are 0.68, 0.72, and 0.39 for **7.1**, **7.2**, and **7.3**, respectively, supporting the visual analysis of the orbitals (Table 2). The combined Th-C WBOs for all carbons in the 5-membered ring of **7.3** is 0.59, which is still much below the WBOs of **7.1** and **7.2** and consistent with the increased distance. The total thorium weights calculated for **7.1** and **7.2** are slightly larger (ca. 5% points) than those calculated for [Th{NR_2}$_3$(CCH)] and [Th{NR_2}$_3$(CH=C=CPh_2)] (**4.2** and **5.2**),[32, 37] but comparable overall. The DFT optimized structure of **A** is indicative of a triplet ground state for the carbene, which is lower by 4.9 kcal/mol than the singlet state. Most of its spin density resides on C_α (1.26 electron spin population), with the remainder delocalized toward C_q and Th, the former arising from the π delocalization across C_α, C_β, and C_q as revealed by NLMO analysis. The Th-C bond in **A** also has some, albeit weak, π-character.

Table 1. % compositions of the Th-C bonding NLMOs in complexes **7.1**-**7.3**.

Complex	Orbital	Total C_α	2s	2p	Total C_β	2s	2p	Total An	7s	7p	6d	5f
7.1	σ(Th-C)	77	47	53	/	/	/	22	8	0	76	16
	π(Th-C)	45	0	100	49	0	100	2	0	0	38	62
7.2	σ(Th-C)	74	33	67	/	/	/	23	7	0	79	14
	π(Th-C)	47	0	100	51	0	100	3	0	0	42	58
7.3	σ(Th-C)	56	6	94	/	/	/	10	5	0	80	15

Table 2. The Wiberg Bond Orders for the selected bonds in complexes **7.1**-**7.3**.

Complex	Th-C_α	C_α-C_β
7.1	0.678	1.873
7.2	0.721	1.995
7.3	0.392	/

7.2.3 ^{13}C Chemical Shift Analysis

The ^{13}C NMR chemical shifts of the α-carbon nuclei were also calculated by Dr. Xiaojuan Yu and Prof. Jochen Autschbach at the University of Buffalo for complexes **7.1**-**7.3** using a variety of functionals, with and without SO coupling effects.[52-54] The Hayton group, others, and myself (see chapters 4 and 5) have previously used ^{13}C NMR chemical shifts to assess the covalency of An-C and Ln-C bonds.[11, 36, 55-60] The calculated chemical shifts are not strongly functional dependent; for convenience, I only discuss the PBE0/SO-PBE0 results (Table 3, in Section 7.4.9). The calculated α-carbon shift for **7.1** is 179.9 ppm (expt. = 177.4 ppm) and includes a 20.8 ppm deshielding contribution due to SO effects. Complex **7.2** also exhibits good agreement between calculated (200.8 ppm) and experimental (199.6 ppm) α-carbon shifts, with 18.7 ppm deshielding due to SO effects. Complex **7.3** exhibits almost no SO effects on the calculated α-carbon shielding (4.7 ppm), likely for two reasons. First, the donation bonding is weaker, and second the relevant orbital is of local π symmetry at the carbon atoms, which does not support the effective transmission of isotropic SO effects to the ligand. The

SO contributions observed for **7.1** and **7.2** are clear evidence of the covalent nature of the Th—C interactions, but they are smaller than those reported for other thorium organometallics,[37, 59] even after controlling for the carbon 2s character and despite comparable bond orders and 5f contributions from Th. Because shielding is a magnetic response property, changes to the ancillary ligands at Th will modulate the magnitude of the spin density induced by the SO coupling and the external field, which in turn modulates the SO shielding effect. Therefore, care must be taken when comparing SO contributions between complexes with disparate ligand environments.

7.3 Summary

In summary, reaction of [Cp_3ThCl] with *in situ* generated lithium-3,3-diphenylcyclopropene results in the formation of [Cp_3Th(3,3-diphenylcyclopropenyl)]. This species undergoes ring opening upon thermolysis to generate the *ortho* C–H activated product, [Cp_3Th(3-phenyl-1H-inden-1-yl)]. I propose that this transformation proceeds via a transient triplet carbene intermediate. In the case of [Cp_3UCl] I instead isolate [Cp_2U(1-phenyl-2,2-diphenyl-triphenyletheylenyl)] which is the product of cyclopropene ring-opening and insertion into a Cp ligand. I propose that this transformation instead proceeds via a transient U(VI) carbyne intermediate. I also investigated the reaction of [Cp_3U(THF)] with diphenylcyclopropene and instead of ring opening observe the formation of the cyclopropyl complex [Cp_3U(3,3-diphenylcyclopropyl)]. Finally, I am able to isolate [Cp_3U(3,3-diphenylcyclopropyl)] and its thorium analog via salt metathesis of [Cp_3AnCl] (An = U, Th) with *in situ* generated lithium-3,3-diphenylcyclopropane. Importantly, this work uncovers multiple new modes of reactivity of 3,3-diphenylcyclopropene with the actinides, improving

our ability to use this reagent as a carbene source. Moving forward, the Hayton group will continue to explore the reactivity of 3,3-diphenylcyclopropene, and its derivatives, with common actinide fragments in an effort to generate an elusive actinide shrock-carbene.

7.4 Experimental

7.4.1 General. All reactions and subsequent manipulations were performed under anaerobic and anhydrous conditions under an atmosphere of dinitrogen. Diethyl ether (Et2O), pentane, and hexanes were dried using a Vacuum Atmospheres DRI-SOLV Solvent Purification system and stored over 3Å sieves for 24 h prior to use. Tetrahydrofuran (THF) was distilled over calcium hydride then distilled over sodium benzophenone, collected, and stored over 3Å sieves for 24 h prior to use. Isooctane was distilled over sodium benzophenone, collected, and stored over 3Å sieves for 24 h prior to use. THF-d8 and C6D6 were stored over 3Å sieves for 24 h prior to use. [Cp3AnCl], lithium diisopropylamide (LDA), 1-bromo-3,3-diphenylcyclopropane, and 3,3-diphenylcyclopropene were synthesized according to previously reported literature procedures.61-63 All other reagents were purchased from commercial vendors and used as received.

1H, 13C{1H}, and 2D NMR spectra were recorded on a Varian UNITY INOVA 500 MHz or a Varian Unity Inova AS600 600 MHz spectrometer. 1H and 13C{1H} NMR spectra were referenced to external SiMe4 using the residual protio solvent peaks as internal standards.64, 65 IR spectra were recorded on a Nicolet 6700 FT-IR spectrometer with a NXR FT Raman Module. Electronic absorption spectra were recorded on a Shimadzu UV3600 UV-NIR Spectrometer. Elemental analyses were performed by the Microanalytical Laboratory at University of California (Berkeley, CA).

7.4.2 Synthesis of [Cp_3Th(3,3-diphenylcyclopropenyl)] (7.1). To a cold (-25 °C), colorless Et_2O solution (0.5 mL) of 3,3-diphenylcyclopropene (69.0 mg, 0.358 mmol) was added quickly a cold (–25 °C), colorless Et_2O solution (0.5 mL) of LDA (36.6 mg, 0.342 mmol). The solution immediately turned pale yellow. This solution was then added drop wise to a cold (–25 °C) stirring white slurry of [Cp_3ThCl] (158.3 mg, 0.342 mmol) in Et_2O (3 mL). The stirring solution immediately turned pale yellow concomitant with the deposition of a pale grey precipitate. After stirring for 25 min the volatiles were removed *in vacuo* and the resulting grey solid was triturated with pentane (3 × 1 mL). The grey solid was then extracted into toluene (6 mL), and the resulting pale yellow solution was filtered through a Celite column supported on glass wool (0.5 cm × 2 cm) and the filtrate was layered with hexanes (6 mL). Storage of this solution at -25 ºC for 24 h resulted in the deposition of colorless plates. Decanting the supernatant, rinsing the crystals with cold (–25 °C) pentane (2 mL), and drying *in vacuo* afforded **1** as white plates (158.7 mg, 75 % yield). Anal. Calcd for $ThC_{30}H_{26}$: C, 58.25; H, 4.25. Found: C, 58.25; H, 4.35. ^{1}H NMR (500 MHz, 25 ºC, THF-d_8): δ 7.62 (s, 1H, α-C*H*), 7.39 (d, J = 6.8 Hz, 4H, *o*-CH), 7.27 (t, J = 7.6 Hz, 4H, *m*-CH), 7.06 (t, J = 7.3 Hz, 2H, *p*-CH), 6.17 (s, 15H, Cp). ^{13}C NMR (126 MHz, 25 ºC, THF-d_8): δ 177.37 (C_α), 152.04 (C_{ipso}), 129.59 (*o*-C), 128.46 (*m*-C), 127.23 (C_β), 124.86 (*p*-C), 117.58 (Cp), 39.49 (C_q). IR (KBr pellet, cm^{-1}): 3095 (w), 3076 (w), 3024 (w), 1603 (w), 1593 (w), 1574 (w), 1489 (m), 1439 (m), 1284 (w), 1196 (w), 1173 (w), 1120 (w), 1095 (w), 1076 (w), 1012 (m), 991 (w), 895 (m), 808 (s), 783 (s), 731 (s), 698 (s), 669 (s), 561 (m), 544 (w).

7.4.3 Synthesis of [$Cp_3Th(C(H)=CH_2)$] (7.2). To a stirring colorless slurry of [Cp_3ThCl] (114.5 mg, 0.247 mmol) in cold (–25 ºC) Et_2O (3 mL) was added vinyl magnesium chloride dropwise as a cold (–25 ºC) 1.6 M THF solution (155 μL, 0.247 mmol). The stirring solution

immediately turned pale yellow, concomitant with the deposition of a dark-grey precipitate. After stirring for 25 min the volatiles were removed *in vacuo* and the resulting grey solid was triturated with pentane (3 × 1 mL). The grey solid was then extracted into toluene (1.5 mL), and the resulting pale yellow solution was filtered through a Celite column supported on glass wool (0.5 cm × 2 cm) and the filtrate was layered with hexanes (6 mL). Storage of this solution at -25 ºC for 24 h resulted in the deposition of colorless needles. Decanting the supernatant, rinsing the crystals with cold (–25 °C) pentane (2 mL), and drying *in vacuo* afforded **2** as white needles (90.1 mg, 80 % yield). Anal. Calcd for $ThC_{17}H_{18}$: C, 44.94; H, 3.99. Found: C, 44.88; H, 3.97. ^{1}H NMR (500 MHz, 25 ºC, Benzene-d_6): δ 8.19 (dd, J = 21.1, 16.4 Hz, 1H, $C_\alpha H$), 7.00 (dd, J = 16.4, 5.2 Hz, 1H, $C_\beta H$), 6.21 (dd, J = 21.1, 5.2 Hz, 1H, $C_\beta H$), 5.96 (s, 15H, Cp). ^{13}C NMR (126 MHz, 25 ºC, Benzene-d_6): δ 199.55 (C_α), 134.34 (C_β), 116.73 (Cp). IR (KBr pellet, cm^{-1}): 3088 (w), 2983 (w), 2929 (w), 2891 (w), 2830 (w), 2810 (w), 2713 (w), 1547 (w), 1439 (m), 1383 (w), 1240 (w), 1122 (w), 1063 (w), 1011 (s), 922 (m), 787 (s), 640 (m), 609 (w).

7.4.4 Synthesis of [Cp$_3$Th(3-phenyl-1H-inden-1-yl)] (7.3). A 25 mL Schlenk flask equipped with the teflon rotoflow valve was charged with a magnetic stir bar, **7.1** (100.1 mg, 0.162 mmol), and toluene (5 mL). The flask was removed from the glovebox and heated to 70 ºC with stirring, which resulted in a colour change to yellow-orange. After 36 h, the solution was cooled to room temperature, which resulted in the deposition of yellow-orange crystals on the walls of the reaction vessel. The reaction mixture was brought inside the glovebox and the solution and crystals were transferred to a 20 mL scintillation vial. Decanting the supernatant, rinsing the crystals with cold (–25 °C) pentane (2 × 1 mL), and drying *in vacuo* afforded **3** as yellow-orange blocks (45 mg, 45 % yield). The supernatant was concentrated in vacuo to 3 mL

and layered with hexane (5 mL). Storage of this solution at −25 °C for 48 h led to the deposition of more crystals (15 mg), which were isolated by decanting off the supernatant, rinsing the crystals with cold (–25 °C) pentane (2 × 1 mL), and drying *in vacuo* (combined yield: 60 mg, 60%). Anal. Calcd for $ThC_{30}H_{26}$: C, 58.25; H, 4.25. Found: C, 57.89; H, 4.27. ^{1}H NMR (500 MHz, 25 ºC, THF-d_8): δ 8.00 (d, J = 8.1 Hz, 1H, **5/8**), 7.85 (d, J = 8.0 Hz, 1H, **5/8**), 7.81 (d, J = 8.2 Hz, 2H, *o*-H), 7.57 (d, J = 2.1 Hz, 1H, **2**), 7.41 (t, J = 7.7 Hz, 2H, *m*-H), 7.15 (t, J = 7.4 Hz, 1H, *p*-H), 7.11 (t, J = 7.5 Hz, 1H, **6/7**), 7.04 (t, J = 7.5 Hz, 1H, **6/7**), 6.20 (s, 15H, Cp), 5.35 (d, J = 2.1 Hz, 1H, **1**). ^{13}C NMR (126 MHz, 25 ºC, THF-d_8): δ 142.26 (**4/3**/C_{ipso}), 140.23 (**4/3**/C_{ipso}), 136.99 (**4/3**/C_{ipso}), 130.28 (**2**), 129.39 (*m*-C), 128.37 (*o*-C), 126.19 (**9**), 125.51 (*p*-C), 122.36 (**5/8**), 121.1 (**5/8**), 121.03 (**6/7**), 120.64 (**6/7**), 119.97 (**Cp**), 88.90 (**1**). UV-Vis/NIR (C_6H_6, 0.60 mM, 25 °C, L·mol^{-1}·cm^{-1}): 369 nm (ε = 2200). IR (KBr pellet, cm^{-1}): 3082 (vw), 3024 (vw), 1595 (w), 1514 (w), 1439 (w), 1333 (w), 1306 (w), 1227 (vw), 1186 (w), 1142 (w), 1072 (vw), 1072 (m), 1009 (s), 941 (w), 910 (vw), 816 (s), 793 (s), 789 (s), 773 (s), 741 (s), 700 (s), 683 (m), 650 (m), 638 (m), 611 (w), 577 (w), 513 (w).

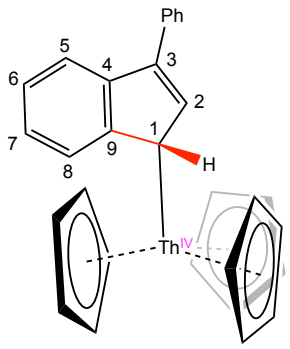

7.4.5 Synthesis of [Cp$_2$U(1-phenyl-2,2-diphenyl-triphenyletheylenyl)] (7.4). To a cold (-25 °C), colorless toluene solution (0.5 mL) of 3,3-diphenylcyclopropene (36.1 mg, 0.188 mmol) was added quickly a cold (–25 °C), colorless Et_2O solution (0.25 mL) of LDA (20.1

mg, 0.188 mmol). Immediately, the solution turned light yellow and was let stir for 2 min. This solution was then added drop wise to a cold (–25 °C) stirring brown slurry of [Cp_3UCl] (83.9 mg, 0.180 mmol) in toluene (2 mL). The stirring solution immediately turned black-green concomitant with the deposition of a dark grey precipitate. After stirring for 30 s the solution was concentrated *in vacuo* to 2 mL and filtered through a Celite column supported on glass wool (0.5 cm × 2 cm). Layering with hexanes (6 mL) and storage of this solution at –25 ºC for 24 h resulted in the deposition of black-green blocks. Decanting the supernatant, rinsing the crystals with cold (–25 °C) pentane (2 mL), and drying *in vacuo* afforded **1** as black-green blocks (5 mg, 4.5 % yield). ^{1}H NMR (500 MHz, Benzene-d_6) δ 87.98 (s, 1H, H_{aryl}), 28.45 (s, 1H, H_{aryl}), 11.86 (m, 2H, H_{aryl}), 11.67 (m, 2H, H_{aryl}), 10.91 (s, 5H, Cp), 7.85(s, 1H, H_{aryl}), 0.23 (s, 1H, H_{aryl}), -10.54 (s, 5H, Cp), -26.95 (m, 1H, H_{aryl}), -26.98 (m, 1H, H_{aryl}), -39.19 (s, 1H, H_{aryl}) , -136.86 (s, 1H, ethylene H).

7.4.6 Synthesis of [Cp_3U(3,3-diphenylcyclopropyl)] (7.5). To a cold (-25 °C), colorless Et_2O solution (0.5 mL) of 1-bromo-3,3-diphenylcyclopropane (139.2 mg, 0.510 mmol) was added dropwise a cold (-25 °C), colorless pentane solution of 1.5 M ^{t}BuLi (0.3 mL, 0.510 mmol). Immediately, the solution turned light yellow. This solution was then added drop wise to a cold (-25 °C) stirring brown slurry of [Cp_3UCl] (159.3 mg, 0.340 mmol) in Et_2O (3 mL). The stirring solution immediately turned red-brown concomitant with the deposition of a red-brown precipitate. After stirring for 45 min the volatiles were removed from the filtrate *in vacuo*. The red-brown powder was then extracted into toluene (3 mL) and filtered through a Celite column supported on glass wool (0.5 cm × 2 cm) leaving behind a tan precipitate on the celite column. Layering this solution with hexanes (5 mL) and storage of this vial at -25 ºC for 24 h resulted in the deposition of brown plates. Decanting the supernatant, rinsing the crystals

with cold (-25 °C) pentane (2 mL), and drying *in vacuo* afforded **7.5** (142.7 mg, 62.6 % yield) Anal. Calcd for $UN_3Si_6C_{33}H_{65}$: C, 57.51; H, 4.50. Found: C, 57.35; H, 4.50. ^{1}H NMR (600 MHz, THF-d_8) δ 7.86 (m, 1H, *p*-H), 6.87 (m, 2H, *m*-H), 2.23 (m, 1H, *p*-H), 1.54 (m, 2H, *m*-H), -3.04 (s, 15H, Cp), -4.69 (s, 2H, *o*-H), -9.30 (d, J = 6.9 Hz, 2H, *o*-H), -17.43 (s, 1H, H_β), -23.55 (s, 1H, H_β), -171.94 (s, 1H, H_α). IR (KBr pellet, cm^{-1}): 3026 (w), 2960 (w), 2873 (w), 1595 (w), 1491 (w), 1441 (w), 1124 (w), 1065 (w), 1011 (m), 924 (w), 891 (w), 781 (s), 758 (s), 696 (m), 592 (w), 540 (w).

7.4.7 Isolation of [Cp$_3$U(3,3-diphenylcyclopropyl)] (7.5). To a stirring brown Et_2O (5 mL) slurry of [$Cp_3U(THF)$] (107.6 mg, 0.213) was added 3,3-diphenylcyclopropene (81.8, 0.426) as colorless Et_2O (1 mL) solution. After stirring for 16 h the volatiles were removed *in vacuo*. The brown residue was then extracted into toluene (4 mL) and filtered through a Celite column supported on glass wool (0.5 cm × 2 cm). Layering this brown solution with hexanes (5 mL) and storage of this vial at –25 ºC for 24 h resulted in the deposition of brown plates. Decanting the supernatant, rinsing the crystals with cold (-25 °C) pentane (2 mL), and drying *in vacuo* afforded **7.5** (73.2 mg, 55 % yield) The ^{1}H NMR spectrum of this solid was identical to that recorded for an authentic sample of **7.5**.

7.4.8 Synthesis of [Cp$_3$Th(3,3-diphenylcyclopropyl)] (7.6). To a cold (-25 °C), colorless Et_2O solution (0.5 mL) of 1-bromo-3,3-diphenylcyclopropane (81.0 mg, 0.297 mmol) was added dropwise a cold (-25 °C), colorless pentane solution of 1.5 M ^{t}BuLi (0.174 mL, 0.297 mmol). Immediately, the solution turned light yellow. This solution was then added drop wise to a cold (-25 °C) stirring colorless slurry of [Cp_3ThCl] (91.5 mg, 0.198 mmol) in Et_2O (3 mL). The stirring solution immediately turned grey concomitant with the deposition of a grey

precipitate. After stirring for 45 min the volatiles were removed from the filtrate *in vacuo*. The colorless powder was then extracted into toluene (3 mL) and filtered through a Celite column supported on glass wool (0.5 cm × 2 cm) leaving behind a grey precipitate on the celite column. Layering this solution with hexanes (5 mL) and storage of this vial at -25 ºC for 24 h resulted in the deposition of colorless plates. Decanting the supernatant, rinsing the crystals with cold (-25 °C) pentane (2 mL), and drying *in vacuo* afforded **7.6** (100.2 mg, 81.7 % yield) Anal. Calcd for $UN_3Si_6C_{33}H_{65}$: C, 58.06; H, 4.55. Found: C, 57.79; H, 4.61. ^{1}H NMR (500 MHz, Benzene-d_6) δ 7.65 (d, 2H, H_o), 7.45 (d, 2H, H_o), 7.22 (t, 2H, H_m), 7.21 (t, 2H, H_m) 7.10 (t, 1H, H_p), 7.03 (t, 1H, H_p), 5.83 (s, 13H), 1.90 (dd, J = 9.6, 2.8 Hz, 1H, H_β), 1.80 (dd, J = 10.8, 2.8 Hz, 1H, H_β), 0.85 (t, J = 10.2 Hz, 1H, H_α). ^{13}C NMR (126 MHz, Benzene-d_6) δ 151.74 (C_{ipso}), 148.36 (C_{ipso}), 131.47 ($C_{m/o}$), 128.05 ($C_{m/o}$), 128.00 ($C_{m/o}$), 126.84 ($C_{m/o}$), 125.77 (C_p), 124.80 (C_p), 116.50 (Cp), 66.13 (C_α), 42.79 (C_q), 28.43 (C_β). IR (KBr pellet, cm^{-1}): 3026 (w), 2960 (w), 2873 (w), 1595 (m), 1491 (m), 1441 (m), 1319 (w), 1124 (w), 1065 (w), 1011 (s), 924 (w), 883 (m), 802 (s), 698 (m), 648 (w), 592 (m), 540 (w).

7.4.9 Computational Details. Kohn-Sham density functional calculations were performed for **7.1**-**7.3** with the 2017 release of the Amsterdam Density Functional (ADF) suite.[10] The crystal structure coordinates were optimized for hydrogen positions using the Perdew-Burke-Ernzerhof[11] (PBE) exchange-correlation functional, the all-electron scalar-relativistic Zeroth-Order Regular Approximation[12] (ZORA) Hamiltonian, and Slater-type atomic orbital (STO) basis sets of triple-ζ doubly polarized (TZ2P)[13] quality for all atoms. An atom-pairwise correction for dispersion forces were considered via Grimme's D3 model augmented with the Becke-Johnson (BJ) damping.[14] The conductor-like screening model (COSMO) was used to describe solvent effect.[15] To quantify the compositions of the chemical bonds, natural localized molecular orbital (NLMO) analyses were carried out with the NBO program, version 6.0, as interfaced with ADF.[16]

The computations of the NMR shielding tensors (σ, ppm) for **7.1**-**7.3** were performed with the NMR module of ADF 2017, using both the scalar relativistic and spin-orbit all electron ZORA Hamiltonian.[17] Functionals used for the NMR calculations were BP86, PBE, PBE0 (25% exact exchange), and PBE0 (40% exact exchange). The ^{13}C chemical shifts (δ, ppm) were obtained by subtracting the α-carbon nuclear magnetic shielding of interest from the reference compound (Tetramethylsilane, TMS), with the latter calculated at the same level of theory.

Table 3. Calculated carbon shielding (σ) and chemical shift (δ) for TMS and the C_α, C_β, C_q nuclei of **7.1**-**7.3** using various functionals.

Complex	Method	σ_{calc}(ppm)	δ_{calc}(ppm)	Δ_{SO} (ppm)	δ_{expt}(ppm)
TMS	BP86/SO-BP86	186.9 / 187.8	/	/	
	PBE/SO-PBE	187.5 / 188.4	/	/	
	PBE0/SO-PBE0 (25%) [a]	192.2 / 193.0	/	/	
	PBE0/SO-PBE0 (40%)	194.7 / 195.5	/	/	
7.1	BP86/SO-BP86	26.6, 59.7, 132.8/ 8.0, 58.9, 133.4	160.3, 127.2, 54.1/ 179.8, 128.9, 54.4	19.5, 1.7, 0.3	177.4, 127.2, 39.5
	PBE/SO-PBE	26.7, 60.3, 133.4/ 8.2, 59.4, 134.0	160.8, 127.2, 54.1/ 180.2, 129.0, 54.4	19.4, 1.8, 0.3	
	PBE0/SO-PBE0 (25%)	33.1, 61.9, 145.3/ 13.1, 61.2, 145.7	159.1, 130.3, 46.9/ 179.9, 131.8, 47.3	20.8, 1.5, 0.4	
	PBE0/SO-PBE0 (40%)	36.9, 63.5, 151.6/ 16.3, 62.9, 151.9	157.8, 131.2, 43.1/ 179.2, 132.6, 43.6	21.4, 1.4, 0.5	
7.2	BP86/SO-BP86	3.7, 59.4/ -12.6, 56.4	183.2, 127.5 / 200.4, 131.4	17.2, 3.9	199.6, 134.3
	PBE/SO-PBE	3.3, 59.9/ -13.0, 57.0	184.2, 127.6/ 201.4, 131.0	17.2, 3.8	
	PBE0/SO-PBE0 (25%)	10.1, 62.2/ -7.8, 59.8	182.1, 130.1/ 200.8, 133.2	18.7, 3.2	
	PBE0/SO-PBE0 (40%)	14.4, 64.0/ -4.4, 62.0	180.3, 130.7/ 199.9, 133.5	19.6, 2.8	
7.3	BP86/SO-BP86	90.6 / 88.1	96.3 / 99.7	3.4	88.9
	PBE/SO-PBE	91.3 / 88.8	96.2 / 99.6	3.4	
	PBE0/SO-PBE0 (25%)	101.9 / 98.0	90.3 / 95.0	4.7	
	PBE0/SO-PBE0 (40%)	107.8 / 103.0	86.9 / 92.5	5.6	

[a] Fraction of exact exchange in the functional in parentheses.

7.4.10 X-ray Crystallography. Data for complexes **7.1**-**7.6** were collected on a Bruker KAPPA APEX II diffractometer equipped with an APEX II CCD detector using a TRIUMPH monochromater with a Mo Kα X-ray source (α = 0.71073 Å). The crystals were mounted on a cryoloop under Paratone-N oil. Data for complexes **7.1** and **7.3**were collected at 110(2) K, whereas data for **7.2** and **7.4**-**7.6** were collected at 100(2) K using an Oxford nitrogen gas cryostream system. X-ray data for **7.1**, **7.2**, **7.3, 7.4, 7.5** and **7.6** were collected utilizing frame exposures of 30, 15, 40, 30, 20 and 60 s, respectively. Data collection and cell parameter determination were conducted using the SMART program.[66] Integration of the data frames and final cell parameter refinement were performed using SAINT software.[67] Absorption corrections of the data were carried out using the multi-scan method SADABS.[68] Subsequent calculations were carried out using SHELXTL.[69] Structure determination was done using direct or Patterson methods and difference Fourier techniques. All hydrogen atom positions were idealized, and rode on the atom of attachment. Structure solution, refinement, graphics, and creation of publication materials were performed using SHELXTL.[69]

Table 4. X-ray Crystallographic Data for Complexes **7.1**, **7.2**, and **7.3**.

	1	**2**	**3**
empirical formula	$C_{30}H_{26}Th$	$C_{17}H_{18}Th$	$C_{30}H_{26}Th$
Crystal habit, color	Plate, Colorless	Needle, Colorless	Block, Yellow-Orange
crystal size (mm)	0.20 × 0.15 × 0.10	0.25 × 0.15 × 0.10	0.25 × 0.15 × 0.10
crystal system	Orthorhombic	Orthorhombic	Monoclinic
space group	Pbca	$Pna2_1$	$P2_1/n$
vol ($Å^3$)	4577.5(8)	2948.8(9)	2265.8(11)
a (Å)	8.4047(8)	24.971(6)	11.148(3)
b (Å)	20.089(2)	8.4506(11)	11.719(3)
c (Å)	27.111(2)	13.974(3)	18.069(5)
α (deg)	90.00	90.00	90.00
β (deg)	90.00	90.00	106.281(6)
γ (deg)	90.00	90.00	90.00
Z	8	8	4
fw (g/mol)	618.55	454.35	618.55
density (calcd) (Mg/m^3)	1.795	2.047	1.813
abs coeff (mm^{-1})	6.530	10.094	6.596
F_{000}	2368	1680	1184
Total no. reflections	17950	17268	13039
Unique reflections	4686	6206	4792
R_{int}	0.1436	0.0985	0.0652
final R indices [$I > 2\sigma(I)$]	$R_1 = 0.0504$ $wR_2 = 0.0868$	$R_1 = 0.0539$, $wR_2 = 0.0742$	$R_1 = 0.0416$ $wR_2 = 0.0680$
largest diff peak and hole ($e^-Å^{-3}$)	1.360 and -1.790	1.748 and -1.401	1.524 and -1.248
GOF	0.982	1.063	0.977

Table 5. X-ray Crystallographic Data for Complexes **7.4**, **7.5**, and **7.6**.

	7.4	**7.5**	**7.6**
empirical formula	$C_{30}H_{26}U$	$C_{30}H_{28}U$	$C_{30}H_{28}Th$
Crystal habit, color	Plate, Black	Plate, Brown	Plate, Colorless
crystal size (mm)	0.20 × 0.10 × 0.05	0.15 × 0.10 × 0.05	0.20 × 0.10 × 0.05
crystal system	Triclinic	Orthorhombic	Orthorhombic
space group	P–1	Cmca	Cmca
vol ($Å^3$)		4543(4)	4625.0(19)
a (Å)	9.023(19)	8.066(4)	8.0925(19)
b (Å)	9.86(2)	28.094(15)	28.423(6)
c (Å)	12.91(3)	20.048(11)	20.107(5)
α (deg)	85.95(6)	90.00	90.00
β (deg)	82.85(5)	90.00	90.00
γ (deg)	83.92(12)	90.00	90.00
Z	2	8	8
fw (g/mol)	624.54	626.57	620.55
density (calcd) (Mg/m^3)	1.833	2.101	1.788
abs coeff (mm^{-1})	7.188	7.177	6.463
F_{000}	596	2656	2400
Total no. reflections	8103	30855	7821
Unique reflections	4441	2831	2057
R_{int}	0.0777	0.0985	0.1383
final R indices [$I > 2\sigma(I)$]	$R_1 = 0.0610$ $wR_2 = 0.1283$	$R_1 = 0.0414$, $wR_2 = 0.1626$	$R_1 = 0.0613$ $wR_2 = 0.1433$
largest diff peak and hole ($e^-Å^{-3}$)	2.315 and -3.918	1.430 and -3.621	1.659 and -2.612
GOF	0.971	1.394	1.037

7.5 Appendix

7.5.1 NMR Spectra

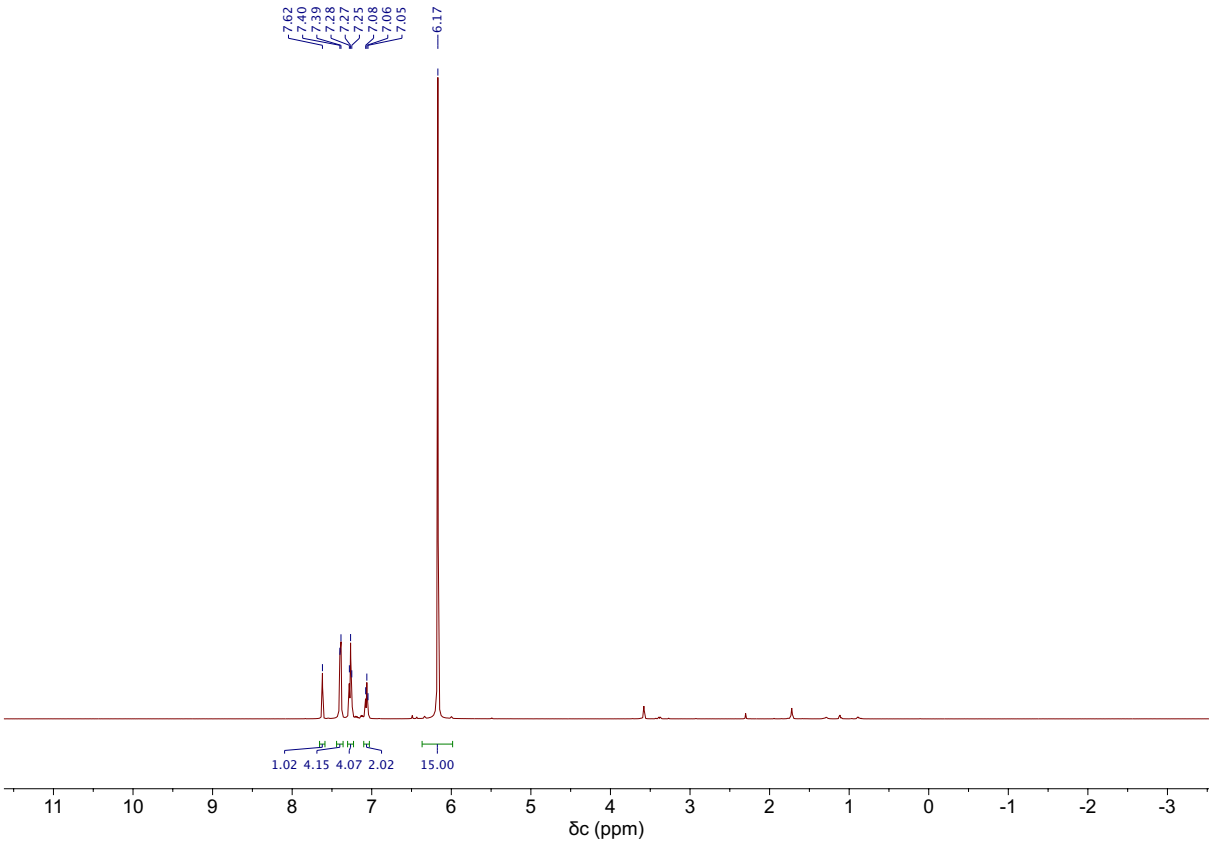

Figure A7.1. ^{1}H NMR spectrum of [Cp_3Th(3,3-diphenylcyclopropenyl)] (**7.1**) in THF-d_8 at room temperature.

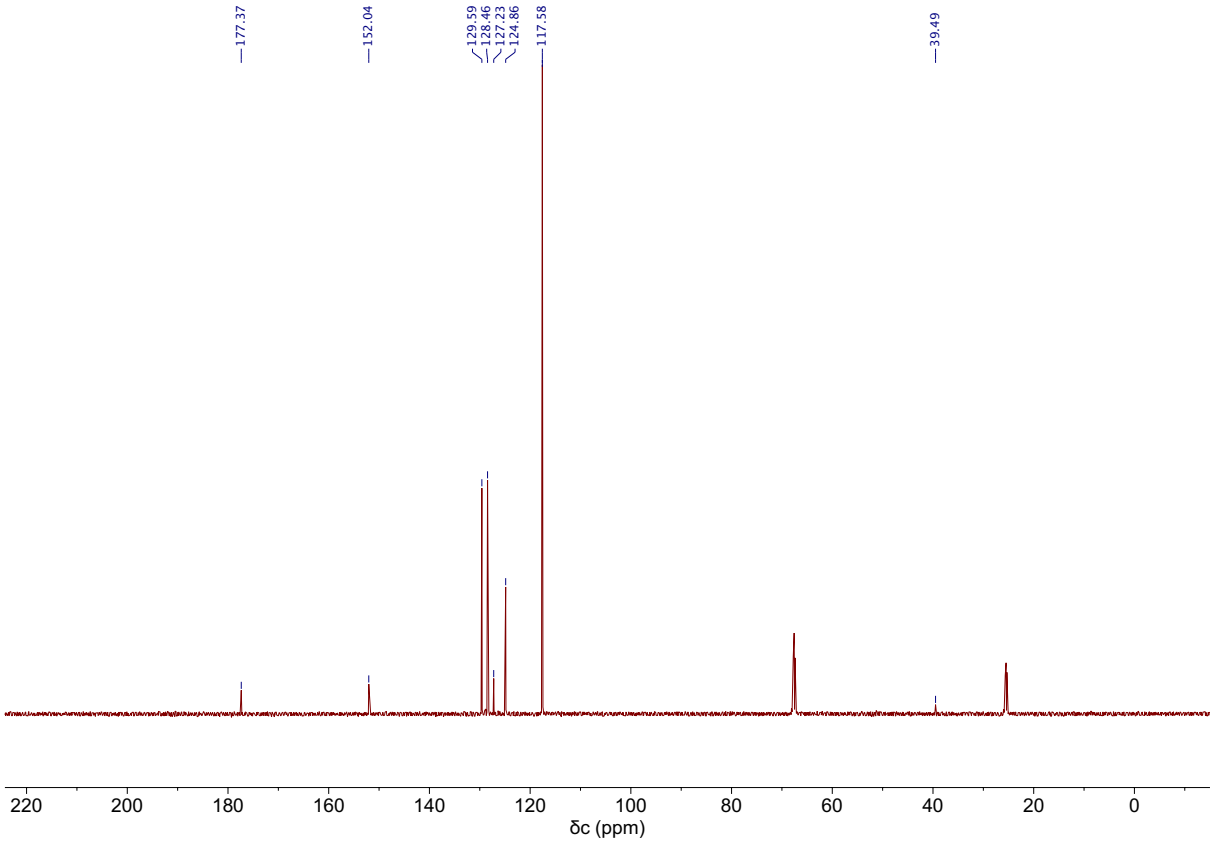

Figure A7.2. $^{13}C\{^{1}H\}$ NMR spectrum of [Cp_3Th(3,3-diphenylcyclopropenyl)] (**7.1**) in THF-d_8 at room temperature.

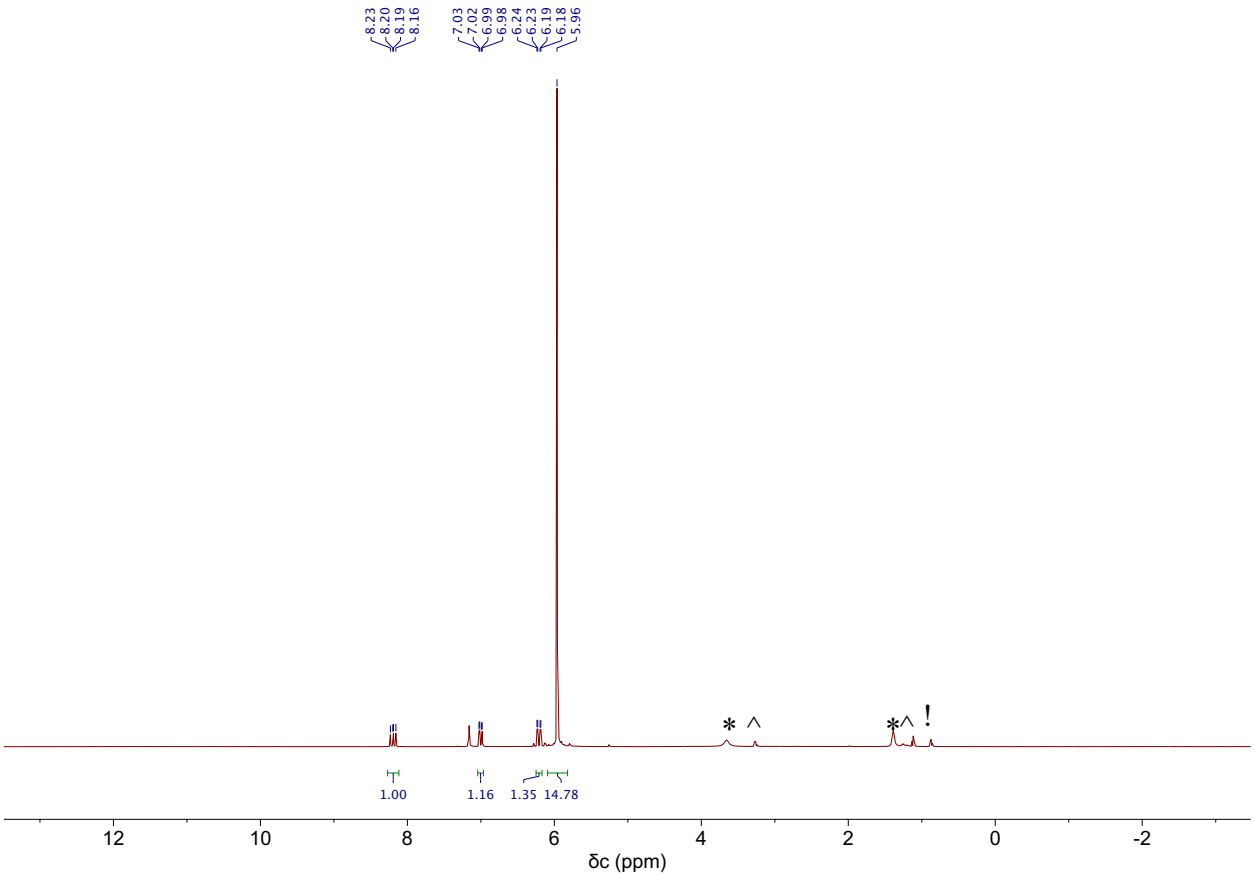

Figure A7.3. ^{1}H NMR spectrum of [$Cp_3Th(C(H)=CH_2)$] (**7.2**) in C_6D_6 at room temperature, (*) denotes THF, (^) denotes Et_2O, and (!) denotes pentane.

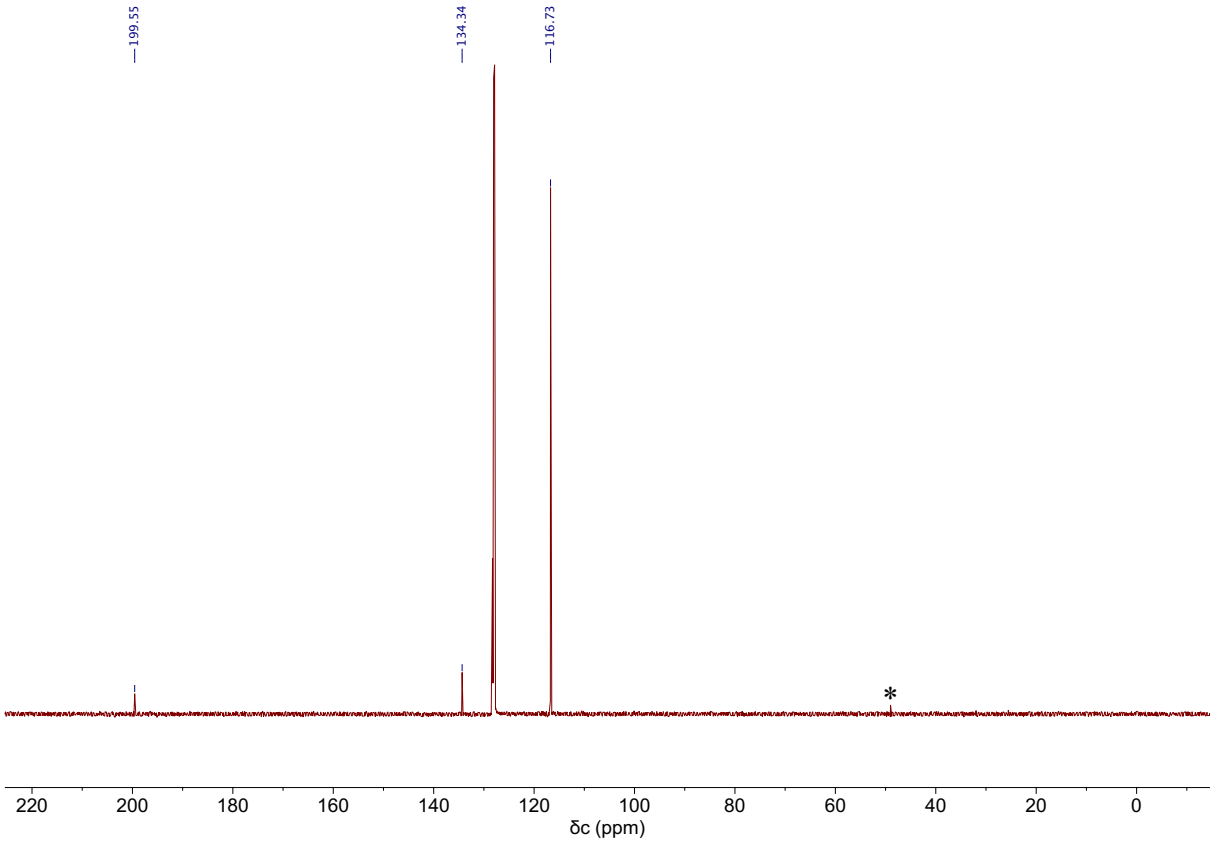

Figure A7.4. $^{13}C\{^{1}H\}$ NMR spectrum of $[Cp_3Th(C(H)=CH_2)]$ (**7.2**) in C_6D_6 at room temperature, (*) denotes a spectrometer artifact.

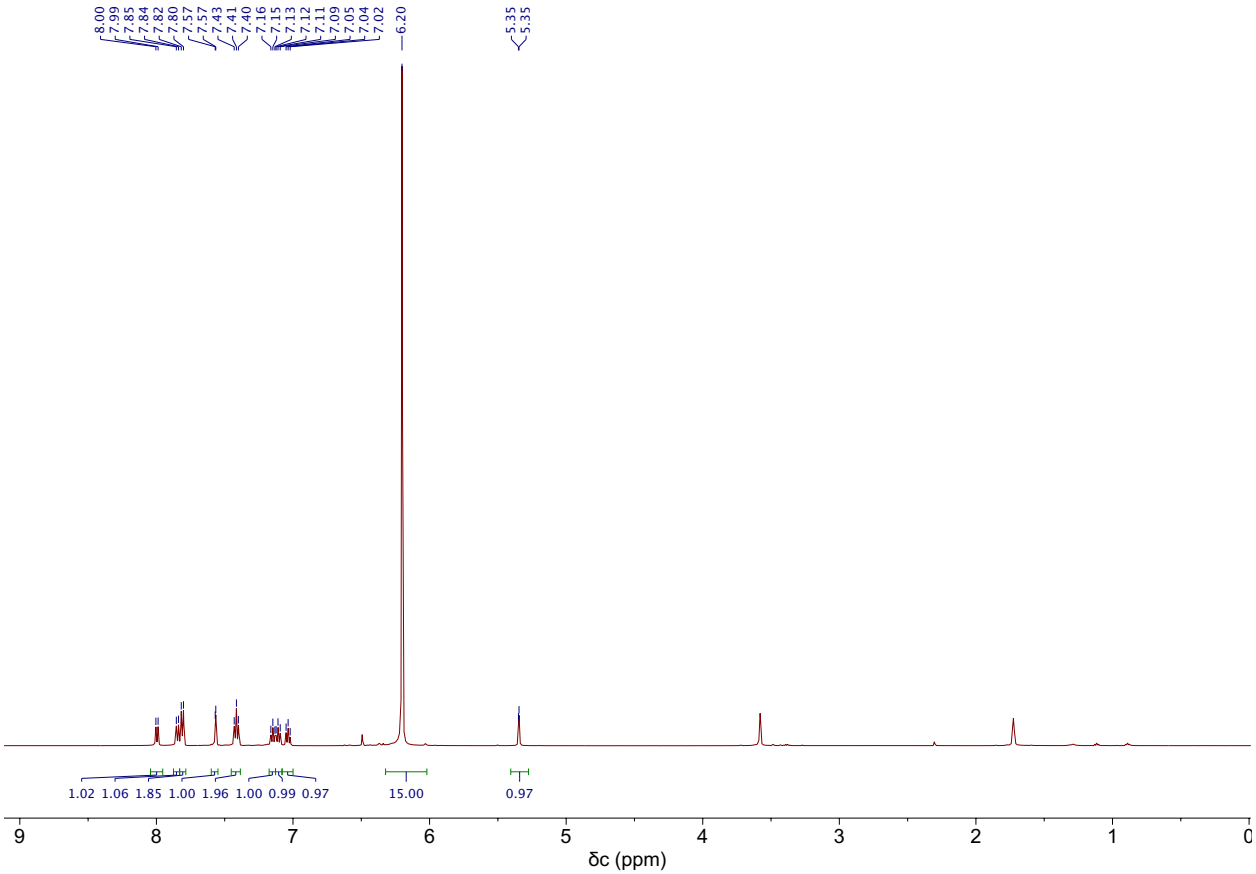

Figure A7.5. ^{1}H NMR spectrum of [Cp_3Th(3-phenyl-1H-inden-1-yl)] (**7.3**) in THF-d_8 at room temperature.

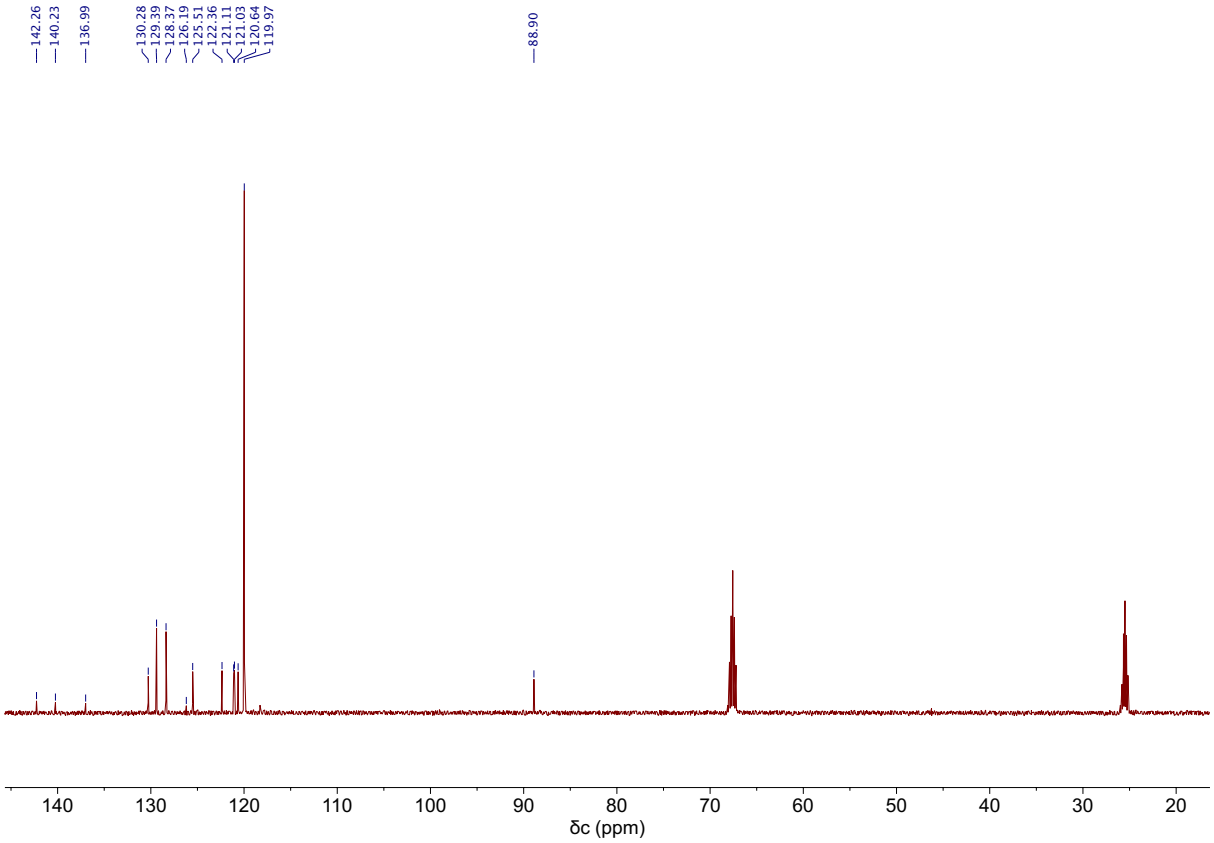

Figure A7.6. $^{13}C\{^{1}H\}$ NMR spectrum of [Cp_3Th(3-phenyl-1H-inden-1-yl)] (**7.3**) in THF-d_8 at room temperature.

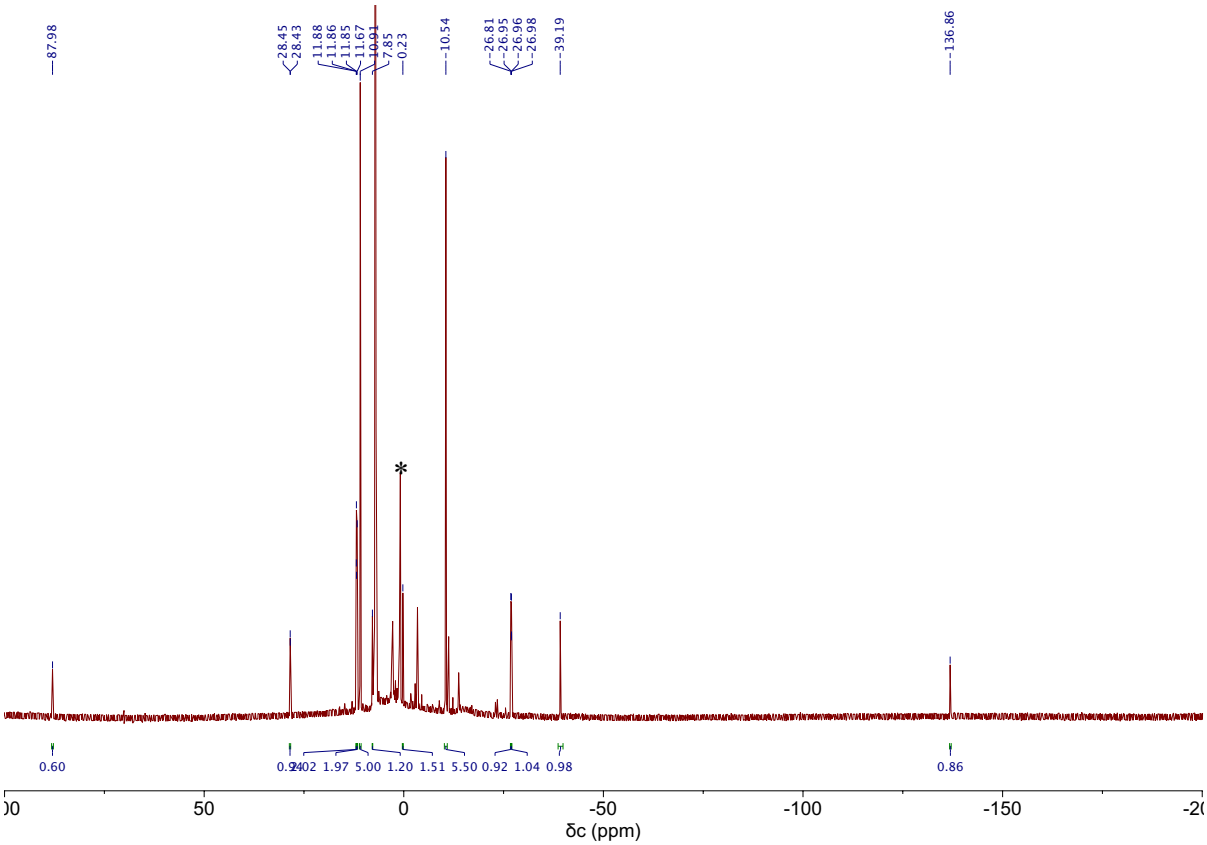

Figure A7.7. ^{1}H NMR spectrum of [Cp_2U(1-phenyl-2,2-diphenyl-triphenyletheylenyl)] (**7.4**) in C_6D_6 at room temperature, (*) denotes pentane.

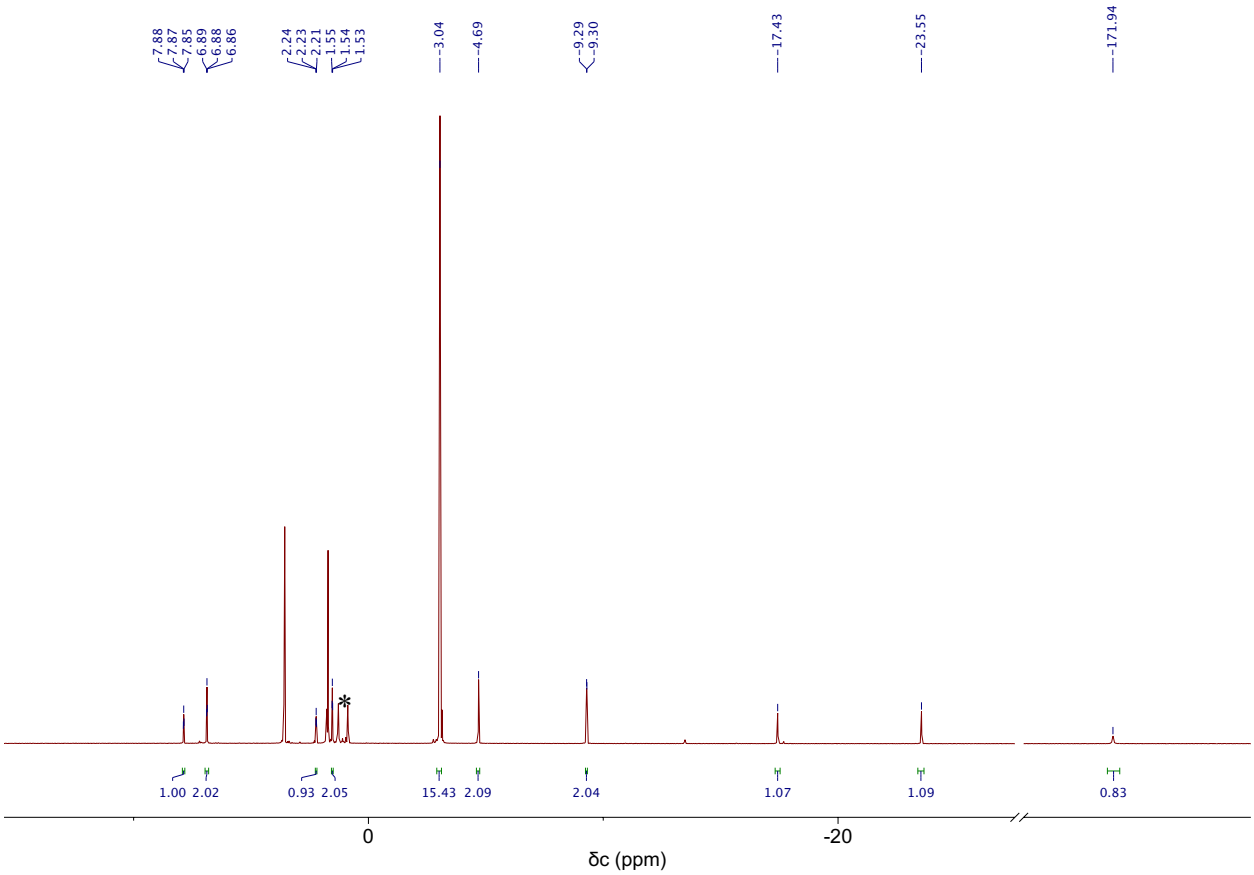

Figure A7.8. ^{1}H NMR spectrum of [Cp_3U(3,3-diphenylcyclopropyl)] (**7.5**) in THF-d_8 at room temperature, (*) denotes pentane.

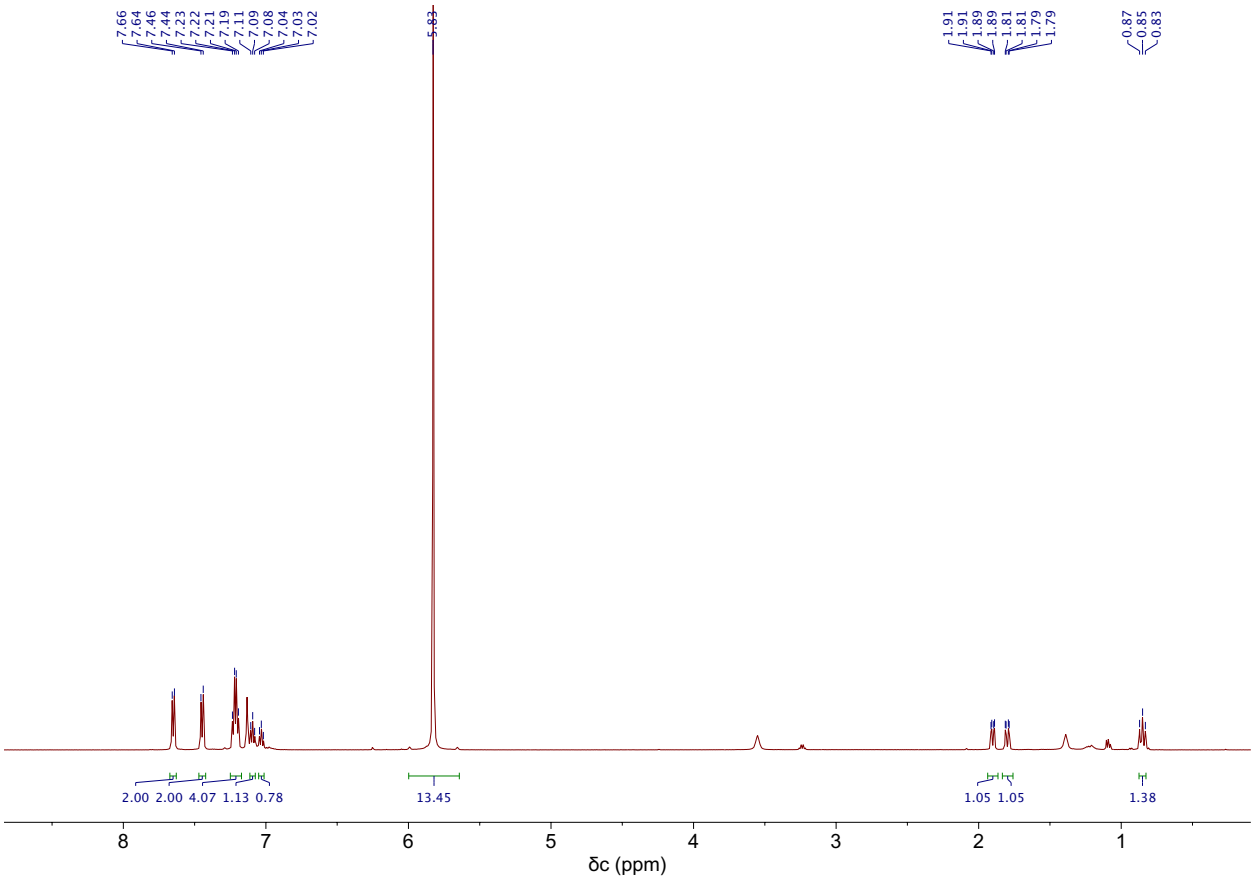

Figure A7.9. ^{1}H NMR spectrum of [Cp_3Th(3,3-diphenylcyclopropyl)] (**7.6**) in C_6D_6 at room temperature, (*) denotes pentane.

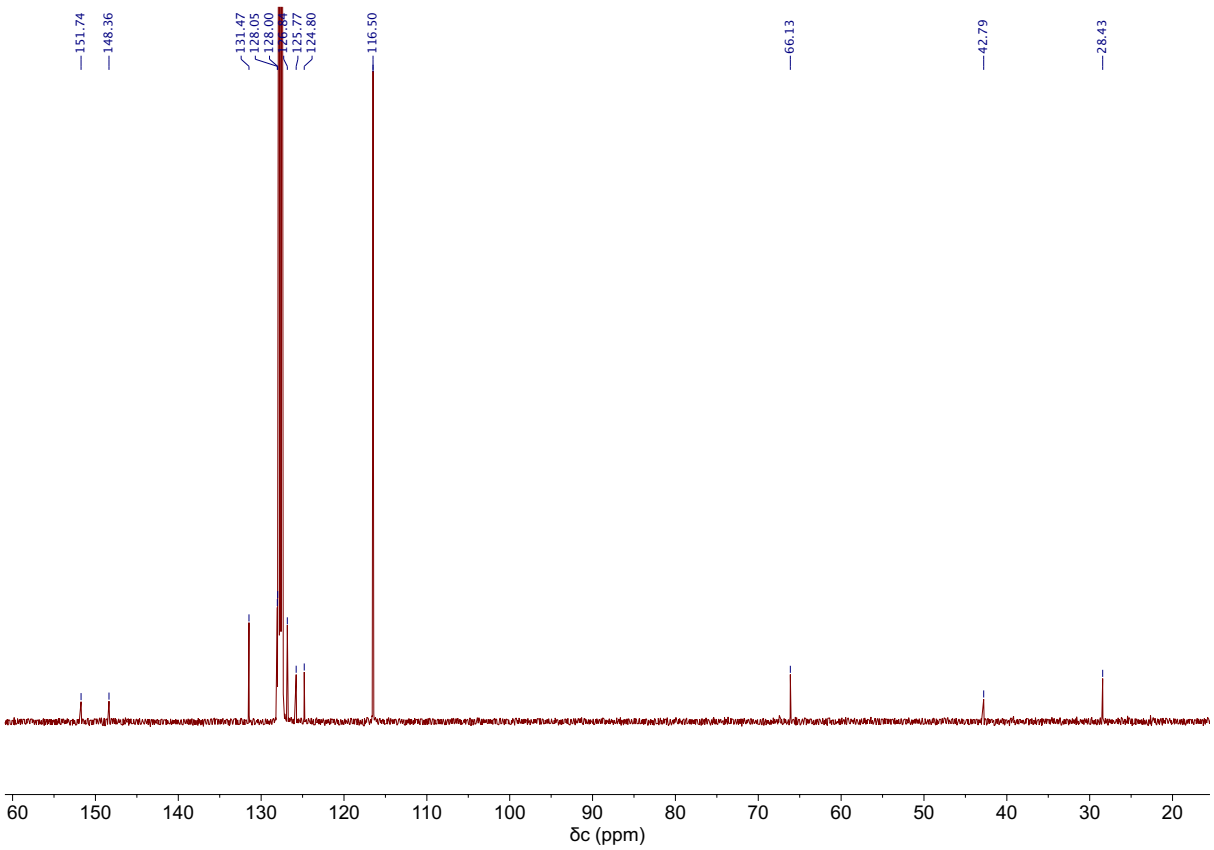

Figure A7.10. $^{13}C\{^{1}H\}$ NMR spectrum of [Cp_3Th(3,3-diphenylcyclopropyl)] (**7.6**) in THF-d_8 at room temperature.

7.5.2 UV-Vis Spectra

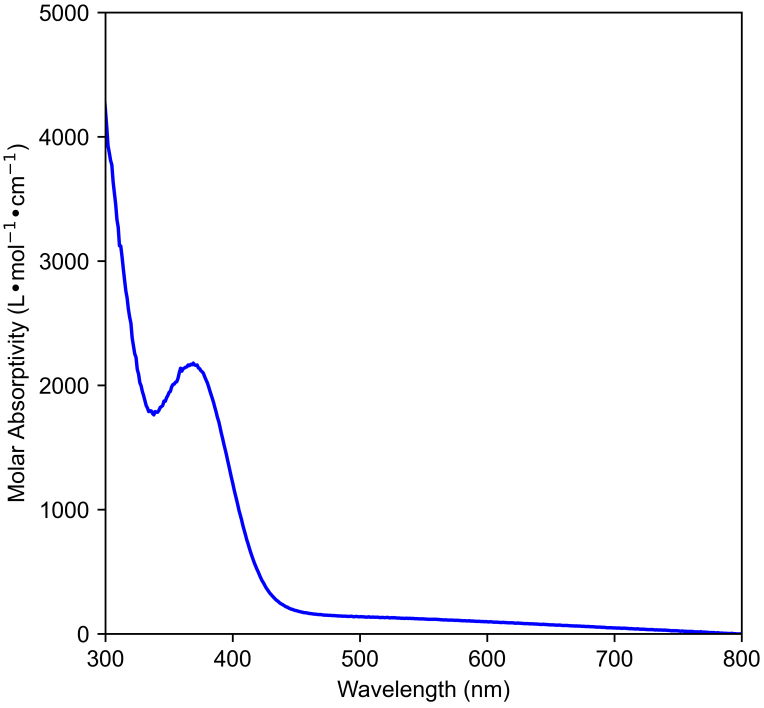

Figure A7.11. UV–Vis spectra of **7.3** (0.60 mM) in C_6H_6.

7.5.3 IR Spectra

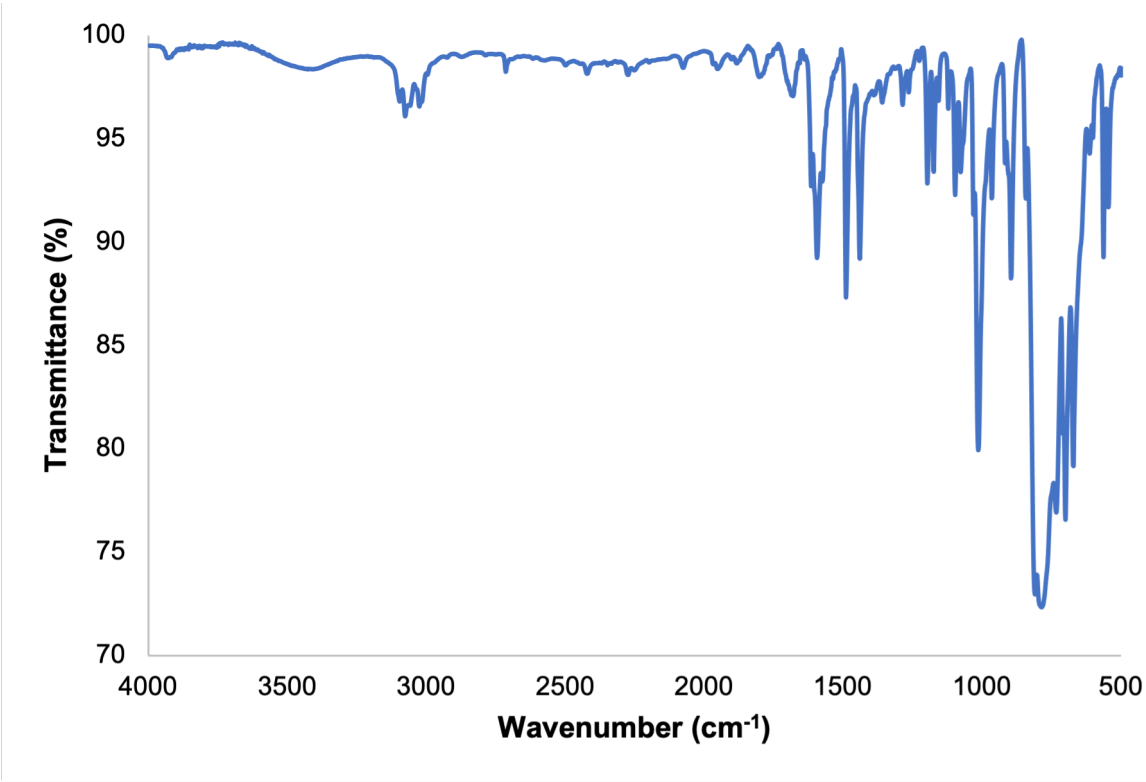

Figure A7.12. IR spectrum of **7.1** (KBr Pellet).

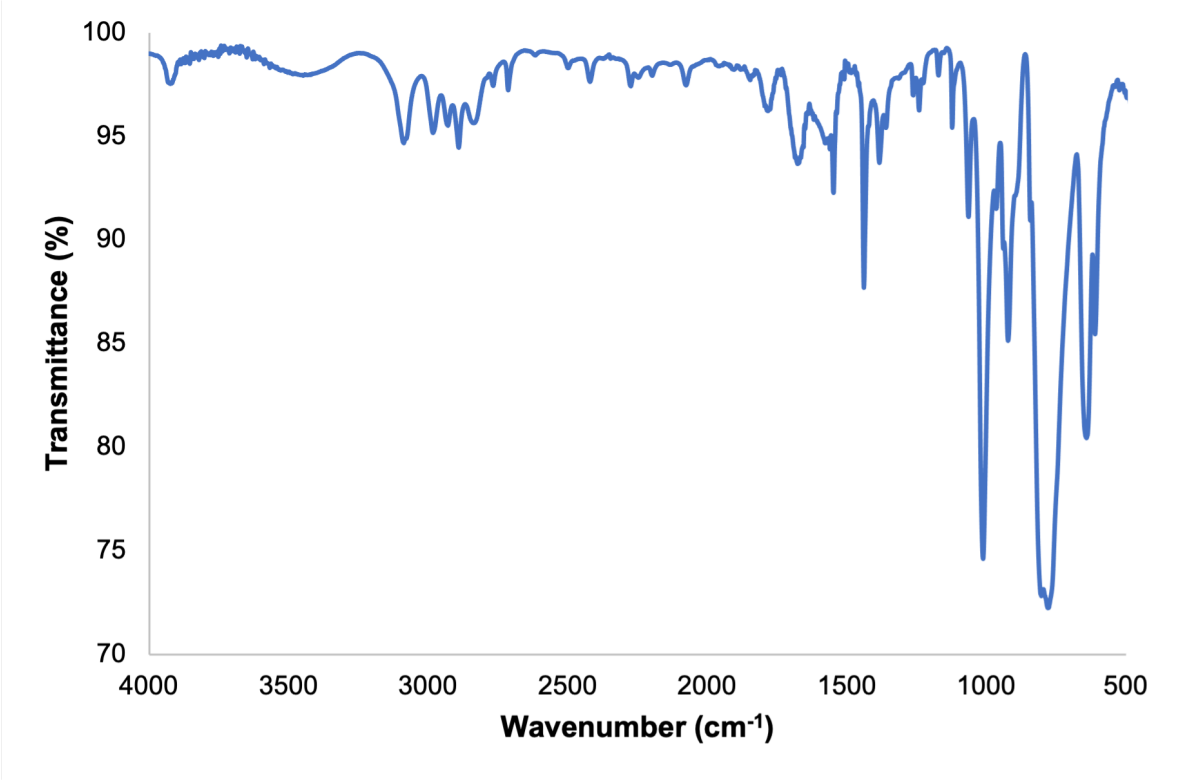

Figure A7.13. IR spectrum of **7.2** (KBr Pellet).

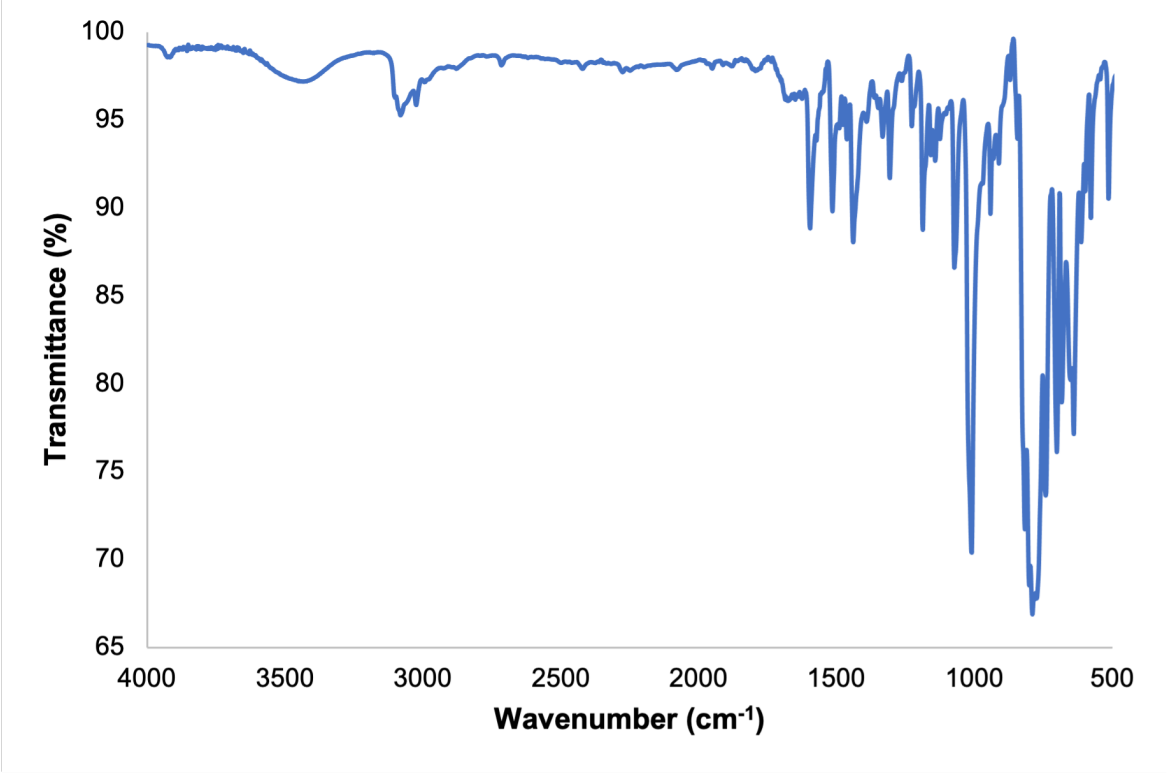

Figure A7.14. IR spectrum of **7.3** (KBr Pellet).

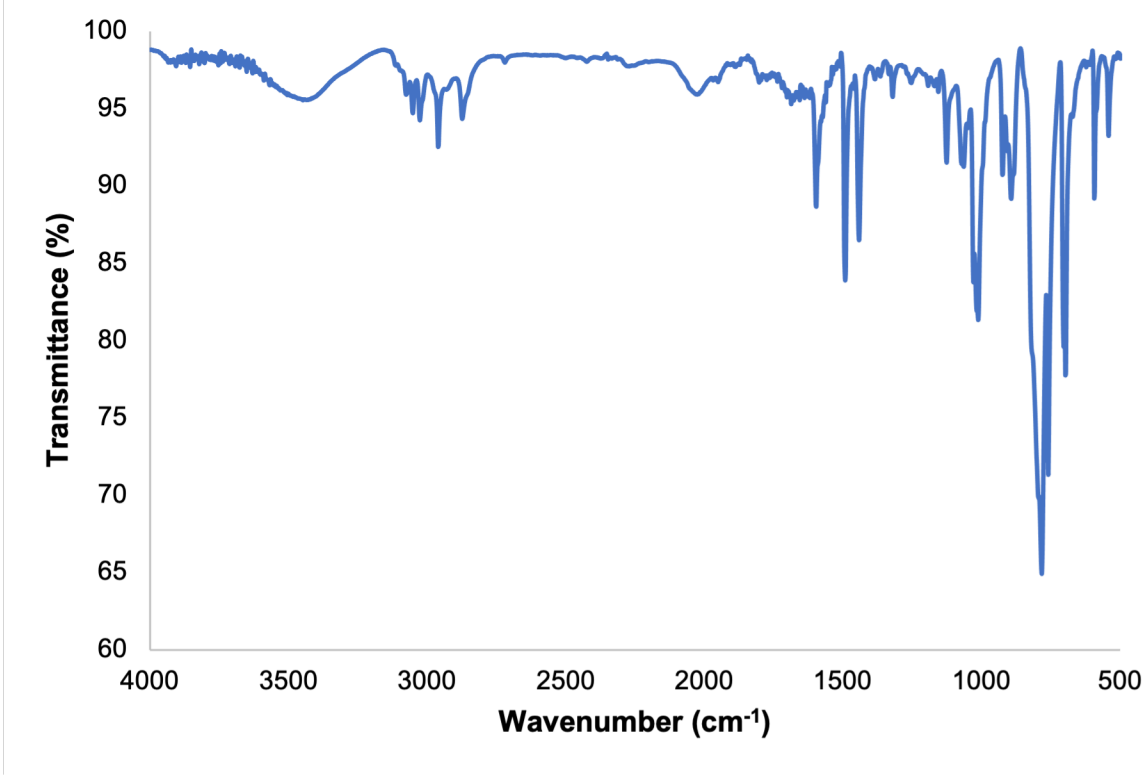

Figure A7.15. IR spectrum of **7.5** (KBr Pellet).

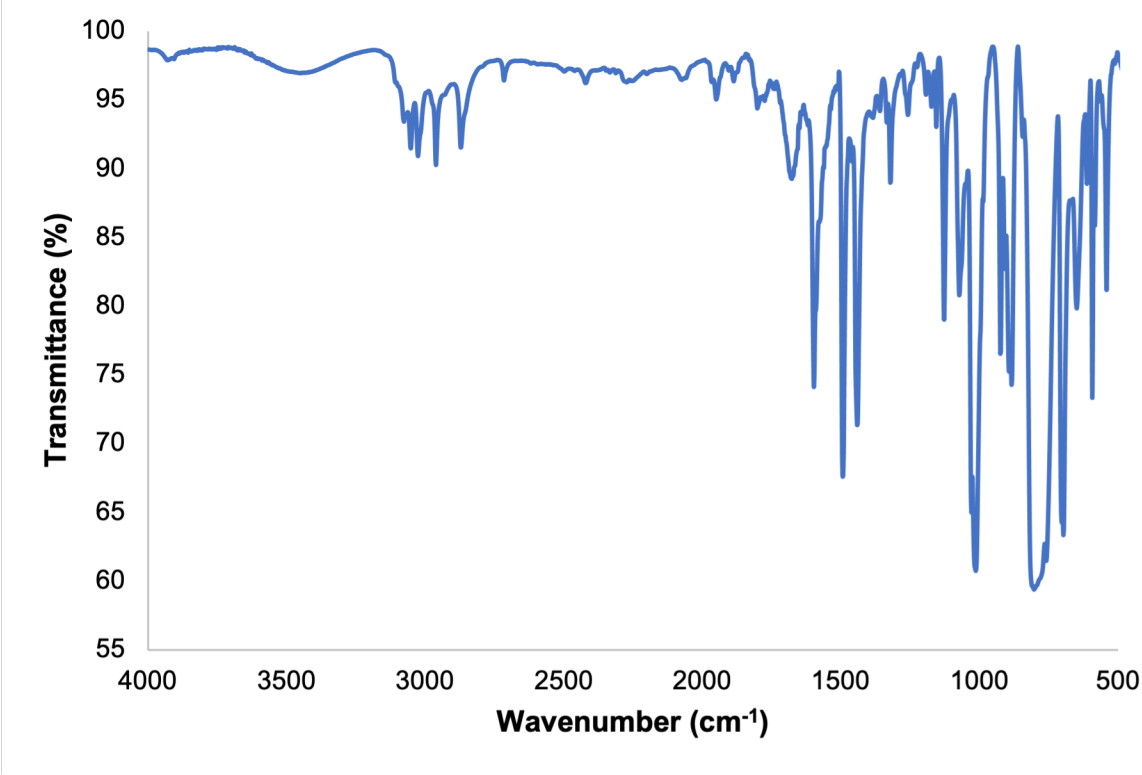

Figure A7.16. IR spectrum of **7.6** (KBr Pellet).

7.6 References

1. Ren, W.; Zhou, E.; Fang, B.; Hou, G.; Zi, G.; Fang, D.-C.; Walter, M. D., Experimental and Computational Studies on the Reactivity of a Terminal Thorium Imidometallocene towards Organic Azides and Diazoalkanes. *Angew. Chem. Int. Ed.* **2014**, *53*, 11310-11314.

2. Rungthanaphatsophon, P.; Bathelier, A.; Castro, L.; Behrle, A. C.; Barnes, C. L.; Maron, L.; Walensky, J. R., Formation of Methane versus Benzene in the Reactions of $(C_5Me_5)_2Th(CH_3)_2$ with $[CH_3PPh_3]X$ (X=Cl, Br, I) Yielding Thorium-Carbene or Thorium-Ylide Complexes. *Angew. Chem. Int. Ed.* **2017**, *56*, 12925-12929.

3. Rungthanaphatsophon, P.; Huang, P.; Walensky, J. R., Phosphorano-Stabilized Carbene Complexes with Short Thorium(IV)– and Uranium(IV)–Carbon Bonds. *Organometallics* **2018**, *37*, 1884-1891.

4. Cantat, T.; Arliguie, T.; Noël, A.; Thuéry, P.; Ephritikhine, M.; Floch, P. L.; Mézailles, N., The U=C Double Bond: Synthesis and Study of Uranium Nucleophilic Carbene Complexes. *J. Am. Chem. Soc.* **2009**, *131*, 963-972.

5. Gregson, M.; Wooles, A. J.; Cooper, O. J.; Liddle, S. T., Covalent Uranium Carbene Chemistry. *Comments Inorg. Chem.* **2015**, *35*, 262-294.

6. Ma, G.; Ferguson, M. J.; McDonald, R.; Cavell, R. G., Actinide Metals with Multiple Bonds to Carbon: Synthesis, Characterization, and Reactivity of U(IV) and Th(IV) Bis(iminophosphorano)methandiide Pincer Carbene Complexes. *Inorg. Chem.* **2011**, *50*, 6500-6508.

7. Gregson, M.; Lu, E.; Mills, D. P.; Tuna, F.; McInnes, E. J. L.; Hennig, C.; Scheinost, A. C.; McMaster, J.; Lewis, W.; Blake, A. J.; Kerridge, A.; Liddle, S. T., The inverse-trans-influence in tetravalent lanthanide and actinide bis(carbene) complexes. *Nat. Commun.* **2017**, *8*, 14137.

8. Seed, J. A.; Sharpe, H. R.; Futcher, H. J.; Wooles, A. J.; Liddle, S. T., Nature of the Arsonium-Ylide $Ph_3As{=}CH_2$ and a Uranium(IV) Arsonium–Carbene Complex. *Angew. Chem. Int. Ed.* **2020**, *59*, 15870-15874.

9. Lu, E.; Boronski, J. T.; Gregson, M.; Wooles, A. J.; Liddle, S. T., Silyl-Phosphino-Carbene Complexes of Uranium(IV). *Angew. Chem. Int. Ed.* **2018**, *57*, 5506-5511.

10. Fortier, S.; Walensky, J. R.; Wu, G.; Hayton, T. W., Synthesis of a Phosphorano-Stabilized U(IV)-Carbene via One-Electron Oxidation of a U(III)-Ylide Adduct. *J. Am. Chem. Soc.* **2011**, *133*, 6894-6897.

11. Smiles, D. E.; Wu, G.; Hrobárik, P.; Hayton, T. W., Synthesis, Thermochemistry, Bonding, and ^{13}C NMR Chemical Shift Analysis of a Phosphorano-Stabilized Carbene of Thorium. *Organometallics* **2017**, *36*, 4519-4524.

12. Hayton, T. W., Metal–ligand multiple bonding in uranium: structure and reactivity. *Dalton Trans.* **2010**, *39*, 1145-1158.

13. Liddle, S. T., The Renaissance of Non-Aqueous Uranium Chemistry. *Angew. Chem. Int. Ed.* **2015**, *54*, 8604-8641.

14. Farnaby, J. H.; Chowdhury, T.; Horsewill, S. J.; Wilson, B.; Jaroschik, F., Lanthanides and actinides: Annual survey of their organometallic chemistry covering the year 2019. *Coord. Chem. Rev.* **2021**, *437*, 213830.

15. Kiplinger, J. L.; Morris, D. E.; Scott, B. L.; Burns, C. J., Enhancing the reactivity of uranium(vi) organoimido complexes with diazoalkanes. *Chem. Commun.* **2002**, 30-31.

16. Matson, E. M.; Fanwick, P. E.; Bart, S. C., Diazoalkane Reduction for the Synthesis of Uranium Hydrazonido Complexes. *Eur. J. Inorg. Chem.* **2012**, *2012*, 5471-5478.

17. Lam, O. P.; Feng, P. L.; Heinemann, F. W.; O'Connor, J. M.; Meyer, K., Charge-Separation in Uranium Diazomethane Complexes Leading to C−H Activation and Chemical Transformation. *J. Am. Chem. Soc.* **2008**, *130*, 2806-2816.

18. Settineri, N. S.; Shiau, A. A.; Arnold, J., Two-electron oxidation of a homoleptic U(III) guanidinate complex by diphenyldiazomethane. *Chem. Commun.* **2018**, *54*, 10913-10916.

19. Cantat, T.; Graves, C. R.; Scott, B. L.; Kiplinger, J. L., Challenging the Metallocene Dominance in Actinide Chemistry with a Soft PNP Pincer Ligand: New Uranium Structures and Reactivity Patterns. *Angew. Chem. Int. Ed.* **2009**, *48*, 3681-3684.

20. Binger, P.; Müller, P.; Benn, R.; Mynott, R., Vinylcarbene Complexes of Titanocene. *Angew. Chem. Int. Ed. Engl.* **1989**, *28*, 610-611.

21. Binger, P.; Müller, P.; Langhauser, F.; Sandmeyer, F.; Philipps, P.; Gabor, B.; Mynott, R., Metallabicyclo[3.1.0]hexene und deren Umlagerung zu Vinylmetallacyclobutenen (M=Ti, Zr). *Chem. Ber.* **1993**, *126*, 1541-1550.

22. Johnson, L. K.; Grubbs, R. H.; Ziller, J. W., Synthesis of tungsten vinyl alkylidene complexes via the reactions of $WCl_2(NAr)(PX_3)_3$ (X = R, OMe) precursors with 3,3-disubstituted cyclopropenes. *J. Am. Chem. Soc.* **1993**, *115*, 8130-8145.

23. Flatt, B. T.; Grubbs, R. H.; Blanski, R. L.; Calabrese, J. C.; Feldman, J., Synthesis, Structure, and Reactivity of a Rhenium Oxo-Vinylalkylidene Complex. *Organometallics* **1994**, *13*, 2728-2732.

24. de la Mata, F. J.; Grubbs, R. H., Synthesis and Reactions of Tungsten Oxo Vinylalkylidene Complexes: Reactions of $WCl_2(O)(PX_3)$ (X = OMe, R) Precursors with 3,3-Diphenylcyclopropene. *Organometallics* **1996**, *15*, 577-584.

25. Fujimura, O.; de la Mata, F. J.; Grubbs, R. H., Synthesis of New Chiral Ligands and Their Group VI Metal Alkylidene Complexes. *Organometallics* **1996**, *15*, 1865-1871.

26. Huang, J.-H.; Lee, T.-Y.; Swenson, D. C.; Messerle, L., An alkylidene-tethered tantallanorbornadiene from reduction of a tantalum(phenylalkenyl)alkylidene derived from 3,3-diphenylcyclopropene ring opening by $(\eta\text{-}C_5Me_4R)_2Ta_2(\mu\text{-}X)_4$ (Ta=Ta). *Inorganica Chimica Acta* **2003**, *345*, 209-215.

27. Rubin, M.; Rubina, M.; Gevorgyan, V., Transition Metal Chemistry of Cyclopropenes and Cyclopropanes. *Chem. Rev.* **2007**, *107*, 3117-3179.

28. Nguyen, S. T.; Johnson, L. K.; Grubbs, R. H.; Ziller, J. W., Ring-opening metathesis polymerization (ROMP) of norbornene by a Group VIII carbene complex in protic media. *J. Am. Chem. Soc.* **1992**, *114*, 3974-3975.

29. Binger, P.; Müller, P.; Wenz, R.; Mynott, R., (3,3-Diphenylallenylidene)trimethylphosphanetitanocene: The First Titanocene Carbene Complex with Three Cumulative Double Bonds. *Angew. Chem. Int. Ed. Engl.* **1990**, *29*, 1037-1038.

30. Nguyen, S. T.; Grubbs, R. H.; Ziller, J. W., Syntheses and activities of new single-component, ruthenium-based olefin metathesis catalysts. *J. Am. Chem. Soc.* **1993**, *115*, 9858-9859.

31. Mulks, F. F.; Antoni, P. W.; Rominger, F.; Hashmi, A. S. K., Cyclopropenylgold(I) Complexes as Aurated Carbenoids or Quasi-Carbenes. *Adv. Synth. Catal.* **2018**, *360*, 1810-1821.

32. Kent, G. T.; Yu, X.; Wu, G.; Autschbach, J.; Hayton, T. W., Synthesis and electronic structure analysis of the actinide allenylidenes, $[\{(NR_2)_3\}An(CCCPh_2)]^-$ (An = U, Th; R = $SiMe_3$). *Chem. Sci.* **2021**, *12*, 14383-14388.

33. Fang, B.; Zhang, L.; Hou, G.; Zi, G.; Fang, D.-C.; Walter, M. D., C–H bond activation induced by thorium metallacyclopropene complexes: a combined experimental and computational study. *Chem. Sci.* **2015**, *6*, 4897-4906.

34. Fang, B.; Hou, G.; Zi, G.; Ding, W.; Walter, M. D., Steric and Electronic Influences of Internal Alkynes on the Formation of Thorium Metallacycles: A Combined Experimental and Computational Study. *Organometallics* **2016**, *35*, 1384-1391.

35. Schock, L. E.; Seyam, A. M.; Sabat, M.; Marks, T. J., A new approach to measuring absolute metal—ligand bond disruption enthalpies in organometallic compounds. The $[(CH_3)_3SiC_5H_4]_3$ U-system. *Polyhedron* **1988**, *7*, 1517-1529.

36. Pedrick, E. A.; Hrobárik, P.; Seaman, L. A.; Wu, G.; Hayton, T. W., Synthesis, structure and bonding of hexaphenyl thorium(iv): observation of a non-octahedral structure. *Chem. Commun.* **2016**, *52*, 689-692.

37. Kent, G. T.; Yu, X.; Pauly, C.; Wu, G.; Autschbach, J.; Hayton, T. W., Synthesis of Parent Acetylide and Dicarbide Complexes of Thorium and Uranium and an Examination of Their Electronic Structures. *Inorg. Chem.* **2021**, *60*, 15413-15420.

38. Taylor, G. A.; Rakita, P. E., Studies in organometallic rearrangements IV—proton and carbon nuclear magnetic resonance spectra of group IVA substituted indenes and indenyl anions. *Org. Magn. Reson.* **1974**, *6*, 644-647.

39. Nakano, T.; Endo, K.; Ukaji, Y., Silver-Catalyzed Allylation of Ketones and Intramolecular Cyclization through Carbene Intermediates from Cyclopropenes Under Ambient Conditions. *Chem. Asian J.* **2016**, *11*, 713-721.

40. Falivene, L.; Cao, Z.; Petta, A.; Serra, L.; Poater, A.; Oliva, R.; Scarano, V.; Cavallo, L., Towards the online computer-aided design of catalytic pockets. *Nat. Chem.* **2019**, *11*, 872-879.

41. Zhang, L.; Hou, G.; Zi, G.; Ding, W.; Walter, M. D., Influence of the 5f Orbitals on the Bonding and Reactivity in Organoactinides: Experimental and Computational Studies on a Uranium Metallacyclopropene. *J. Am. Chem. Soc.* **2016**, *138*, 5130-5142.

42. Pedrick, E. A.; Seaman, L. A.; Scott, J. C.; Griego, L.; Wu, G.; Hayton, T. W., Synthesis and Reactivity of a U(IV) Dibenzyne Complex. *Organometallics* **2016**, *35*, 494-502.

43. Meyer, T. Y.; Messerle, L., Reduction of an electronically unsaturated transition-metal η^2-acyl complex. Arene formation from deoxygenative acyl coupling with a cyclopentadienyl ligand. *J. Am. Chem. Soc.* **1990**, *112*, 4564-4565.

44. de Boer, E. J. M.; de With, J., Acyl C=O bond cleavage in Cp^*_2TiCOR compounds: formation of benzene derivatives by Cp*-ring expansion involving incorporation of the acyl carbon atom ($Cp^* = \eta^5$-C_5Me_5). *J. Organomet. Chem.* **1987**, *320*, 289-293.

45. Shannon, R., Revised effective ionic radii and systematic studies of interatomic distances in halides and chalcogenides. *Acta Crystallogr., Sect. A: Found. Crystallogr.* **1976**, *32*, 751-767.

46. La Pierre, H. S.; Scheurer, A.; Heinemann, F. W.; Hieringer, W.; Meyer, K., Synthesis and Characterization of a Uranium(II) Monoarene Complex Supported by δ Backbonding. *Angew. Chem. Int. Ed.* **2014**, *53*, 7158-7162.

47. Billow, B. S.; Livesay, B. N.; Mokhtarzadeh, C. C.; McCracken, J.; Shores, M. P.; Boncella, J. M.; Odom, A. L., Synthesis and Characterization of a Neutral U(II) Arene Sandwich Complex. *J. Am. Chem. Soc.* **2018**, *140*, 17369-17373.

48. Guo, F.-S.; Tsoureas, N.; Huang, G.-Z.; Tong, M.-L.; Mansikkamäki, A.; Layfield, R. A., Isolation of a Perfectly Linear Uranium(II) Metallocene. *Angew. Chem. Int. Ed.* **2020**, *59*, 2299-2303.

49. Windorff, C. J.; MacDonald, M. R.; Meihaus, K. R.; Ziller, J. W.; Long, J. R.; Evans, W. J., Expanding the Chemistry of Molecular U^{2+} Complexes: Synthesis, Characterization, and Reactivity of the $\{[C_5H_3(SiMe_3)_2]_3U\}^-$ Anion. *Chem. Eur. J.* **2016**, *22*, 772-782.

50. MacDonald, M. R.; Fieser, M. E.; Bates, J. E.; Ziller, J. W.; Furche, F.; Evans, W. J., Identification of the +2 Oxidation State for Uranium in a Crystalline Molecular Complex, $[K(2.2.2\text{-Cryptand})][(C_5H_4SiMe_3)_3U]$. *J. Am. Chem. Soc.* **2013**, *135*, 13310-13313.

51. Glendening, E. D.; Landis, C. R.; Weinhold, F., Natural bond orbital methods. *WIREs Comput Mol Sci* **2012**, *2*, 1-42.

52. Autschbach, J.; Zurek, E., Relativistic Density-Functional Computations of the Chemical Shift of ^{129}Xe in $Xe@C_{60}$. *J. Phys. Chem. A* **2003**, *107*, 4967-4972.

53. Autschbach, J., The role of the exchange-correlation response kernel and scaling corrections in relativistic density functional nuclear magnetic shielding calculations with the zeroth-order regular approximation. *Mol. Phys.* **2013**, *111*, 2544-2554.

54. Wolff, S. K.; Ziegler, T.; Lenthe, E. v.; Baerends, E. J., Density functional calculations of nuclear magnetic shieldings using the zeroth-order regular approximation

(ZORA) for relativistic effects: ZORA nuclear magnetic resonance. *J. Chem. Phys.* **1999**, *110*, 7689-7698.

55. Lewis, A. J.; Carroll, P. J.; Schelter, E. J., Stable Uranium(VI) Methyl and Acetylide Complexes and the Elucidation of an Inverse Trans Influence Ligand Series. *J. Am. Chem. Soc.* **2013**, *135*, 13185-13192.

56. Mullane, K. C.; Hrobárik, P.; Cheisson, T.; Manor, B. C.; Carroll, P. J.; Schelter, E. J., ^{13}C NMR Shifts as an Indicator of U–C Bond Covalency in Uranium(VI) Acetylide Complexes: An Experimental and Computational Study. *Inorg. Chem.* **2019**, *58*, 4152-4163.

57. Seaman, L. A.; Hrobárik, P.; Schettini, M. F.; Fortier, S.; Kaupp, M.; Hayton, T. W., A Rare Uranyl(VI)–Alkyl Ate Complex $[Li(DME)_{1.5}]_2[UO_2(CH_2SiMe_3)_4]$ and Its Comparison with a Homoleptic Uranium(VI)–Hexaalkyl. *Angew. Chem. Int. Ed.* **2013**, *52*, 3259-3263.

58. Panetti, G. B.; Sergentu, D.-C.; Gau, M. R.; Carroll, P. J.; Autschbach, J.; Walsh, P. J.; Schelter, E. J., Isolation and characterization of a covalent Ce^{IV}-Aryl complex with an anomalous ^{13}C chemical shift. *Nat. Commun.* **2021**, *12*, 1713.

59. Ordoñez, O.; Yu, X.; Wu, G.; Autschbach, J.; Hayton, T. W., Homoleptic Perchlorophenyl "Ate" Complexes of Thorium(IV) and Uranium(IV). *Inorg. Chem.* **2021**, *60*, 12436-12444.

60. Ordoñez, O.; Yu, X.; Wu, G.; Autschbach, J.; Hayton, T. W., Synthesis and Characterization of Two Uranyl-Aryl "Ate" Complexes. *Chem. Eur. J.* **2021**, *27*, 5885-5889.

61. Marks, T. J.; Seyam, A. M.; Wachter, W. A.; Halstead, G. W.; Raymond, K. N., Chlorotris(η-Cyclopentadienyl)Complexes of Uranium(IV) and Thorium(IV). In *Inorganic Syntheses*, 1976; pp 147-151.

62. Barnett, N. D. R.; Mulvey, R. E.; Clegg, W.; O'Neil, P. A., Crystal structure of lithium diisopropylamide (LDA): an infinite helical arrangement composed of near-linear nitrogen-lithium-nitrogen units with four units per turn of helix. *J. Am. Chem. Soc.* **1991**, *113*, 8187-8188.

63. Huang, J.-H.; Lee, T.-Y.; Swenson, D. C.; Messerle, L., An alkylidene-tethered tantallanorbornadiene from reduction of a tantalum(phenylalkenyl)alkylidene derived from 3,3-diphenylcyclopropene ring opening by $(\eta\text{-}C_5Me_4R)_2Ta_2(\mu\text{-}X)_4$ (Ta=Ta). *Inorg. Chim. Acta* **2003**, *345*, 209-215.

64. Harris, R. K.; Becker, E. D.; De Menezes, S. M. C.; Granger, P.; Hoffman, R. E.; Zilm, K. W., Further Conventions for NMR Shielding and Chemical Shifts (IUPAC Recommendations 2008). *Magn. Reson. Chem.* **2008**, *46*, 582-598.

65. Harris, R. K.; Becker, E. D.; Cabral de Menezes, S. M.; Goodfellow, R.; Granger, P., NMR nomenclature: nuclear spin properties and conventions for chemical shifts. IUPAC Recommendations 2001. International Union of Pure and Applied Chemistry. Physical Chemistry Division. Commission on Molecular Structure and Spectroscopy. *Magn. Reson. Chem.* **2002**, *40*, 489-505.

66. *SMART Apex II*, Version 2.1 ed.; Bruker AXS Inc.: Madison WI, 2005.

67. *SAINT Software User's Guide*, Version 7.34a ed.; Bruker AXS Inc.: Madison, WI,

2005.

68. Sheldrick, G. M., *SADABS*, the Siemens Area Detector Absorption Correction; University of Göttingen: Göttingen, Germany, 2005.

69. *SHELXTL PC*, Version 6.12 ed.; Bruker AXS Inc.:Madison, WI, 2005.